

ISSN: 2349-6495(P) | 2456-1908 (O)



International Journal of Advanced Engineering Research and Science

(IJAERS)

An Open Access International Journal



Journal DOI: 10.22161/ijaers

Issue DOI: 10.22161/ijaers.4.4

AI PUBLICATIONS

Vol.- 4 | Issue - 4 | April, 2017
editor@ijaers.com | <http://www.ijaers.com/>

Editorial Board

Dr. C.M. Singh

*BE., MS(USA), PhD(USA), Post-Doctoral fellow at NASA (USA)
Professor, Department of Electrical & Electronics Engineering, INDIA*

Dr. Ram Karan Singh

*BE.(Civil Engineering), M.Tech.(Hydraulics Engineering), PhD(Hydraulics & Water Resources Engineering), BITS- Pilani
Professor, Department of Civil Engineering, King Khalid University, Saudi Arabia.*

Dr.Asheesh Kumar Shah

*IIM Calcutta, Wharton School of Business, DAVV INDORE, SGSITS, Indore
Country Head at CrafsOL Technology Pvt.Ltd, Country Coordinator at French Embassy, Project Coordinator at IIT Delhi, INDIA*

Dr.Swapnesh Taterh

*Ph.d with Specialization in Information System Security
Associate Professor, Department of Computer Science Engineering
Amity University, INDIA*

Dr.Ebrahim Nohani

Ph.D.(hydraulic Structures), Department of hydraulic Structures, Islamic Azad University, Dezful, IRAN.

Dr.Dinh Tran Ngoc Huy

*Specialization Banking and Finance, Professor, Department Banking and Finance
Viet Nam*

Dr.Sameh El-Sayed Mohamed Yehia

*Assistant Professor, Civil Engineering(Structural), Higher Institute of Engineering -El-Shorouk Academy,
Cairo, Egypt*

Dr.Ahmadad Nabih Zaki Rashed

*Specialization Optical Communication System, Professor, Department of Electronic Engineering,
Menoufia University*

Dr. Alok Kumar Bharadwaj

BE(AMU), ME(IIT, Roorkee), Ph.D (AMU), Professor, Department of Electrical Engineering, INDIA

Dr. M. Kannan

*Specialization in Software Engineering and Data mining
Ph.D, Professor, Computer Science, SCSVMV University, Kanchipuram, India*

Dr.Sambit Kumar Mishra

*Specialization Database Management Systems
BE, ME, Ph.D, Professor, Computer Science Engineering
Gandhi Institute for Education and Technology, Baniatangi, Khordha, India*

Dr. M. Venkata Ramana

*Specialization in Nano Crystal Technology
Ph.D, Professor, Physics, Andhara Pradesh, INDIA*

DR. C. M. Velu

Prof. & HOD, CSE, Datta Kala Group of Institutions, Pune, India

Dr. Rabindra Kayastha

*Associate Professor, Department of Natural Sciences
School of Science, Kathmandu University, Nepal*

Dr. P. Suresh

Specialization in Grid Computing and Networking, Associate Professor, Department of Information Technology, Engineering College, Erode, Tamil Nadu, INDIA

Dr. Uma Choudhary

Specialization in Software Engineering Associate Professor, Department of Computer Science Mody University, Lakshmanagarh, India

Dr. Varun Gupta

Network Engineer, National Informatics Center, Delhi, India

Dr. Hanuman Prasad Agrawal

Specialization in Power Systems Engineering Department of Electrical Engineering, JK Lakshmi Pat University, Jaipur, India

Dr. Hou, Cheng-I

Specialization in Software Engineering, Artificial Intelligence, Wisdom Tourism, Leisure Agriculture and Farm Planning, Associate Professor, Department of Tourism and MICE, Chung Hua University, Hsinchu Taiwan

Dr. Anil Trimbakrao Gaikwad

Associate Professor at Bharati Vidyapeeth University, Institute of Management, Kolhapur, India

Dr. Ahmed Kadhim Hussein

Department of Mechanical Engineering, College of Engineering, University of Babylon, Republic of Iraq

Dr. Gamal Abd El-Nasser Ahmed Mohamed Said

Computer Lecturer, Department of Computer and Information Technology, Port Training Institute (PTI), Arab Academy For Science, Technology and Maritime Transport, Egypt









Mr. T. Rajkiran Reddy









*Specialization in Networking and Telecom
Research Database Specialist, Quantile Analytics, India*

M. Hadi Amini


Carnegie Mellon University, USA

Vol-4, Issue-4, April 2017



Sr No.	Details with DOI
1	<p><u>Eco-Efficiency of Drinking Water Treatment</u> Author: M. Farhaoui  DOI: 10.22161/ijaers.4.4.1</p> <p style="text-align: right;"><i>Page No: 001-008</i></p>
2	<p><u>Transmission Line Fault Monitoring and Identification System by Using Internet of Things</u> Author: S.Suresh, R.Nagarajan, L.Sakthivel, V.Logesh, C.Mohandass, G.Tamilselvan  DOI: 10.22161/ijaers.4.4.2</p> <p style="text-align: right;"><i>Page No: 009-014</i></p>
3	<p><u>Research on Multiple Complex Data Processing Methods Based on OpenStack Cloud Platform</u> Author: Huansong Yang, Mengyuan Wang, Jiaping Wu  DOI: 10.22161/ijaers.4.4.3</p> <p style="text-align: right;"><i>Page No: 015-020</i></p>
4	<p><u>Power Quality Issues of Electric Arc Furnace and their Mitigations -A Review</u> Author: Amarjeet Singh, Ravindra Kumar Singh, Asheesh Kumar Singh  DOI: 10.22161/ijaers.4.4.4</p> <p style="text-align: right;"><i>Page No: 022-041</i></p>
5	<p><u>Energy Audit for an educational building which operates in Middle East climatic conditions</u> Author: Salim R K, Dr Sudhir CV  DOI: 10.22161/ijaers.4.4.5</p> <p style="text-align: right;"><i>Page No: 042-048</i></p>
6	<p><u>Energy and Exergy Analysis on Si Engine by Blend of Ethanol with Petrol</u> Author: Kuntesh A Mithaiwal, Ashish J Modi, Dipak C Gosai  DOI: 10.22161/ijaers.4.4.6</p> <p style="text-align: right;"><i>Page No: 049-061</i></p>
7	<p><u>Seismic Risk Assessment of Existing School Buildings in Egypt</u> Author: Islam M. Ezz El-Arab  DOI: 10.22161/ijaers.4.4.7</p> <p style="text-align: right;"><i>Page No: 062-070</i></p>
8	<p><u>ITIL Implementation in a Moroccan Stat Organization: The case of incident management process</u> Author: Mourad EL Baz, Malik Motii Armand, Collins Anong, Belaissaoui Mustapha  DOI: 10.22161/ijaers.4.4.8</p> <p style="text-align: right;"><i>Page No: 071-078</i></p>

9	<p><u>Design and Study of Swirl Injector of Pulse Detonation Engine</u> Author: Navdeep Banga, Kanika  DOI: 10.22161/ijaers.4.4.9</p>	<i>Page No: 079-082</i>
10	<p><u>Performance Analysis of LEACH, SEP and ZSEP under the Influence of Energy</u> Author: Sulekha Kumari  DOI: 10.22161/ijaers.4.4.10</p>	<i>Page No: 083-088</i>
11	<p><u>Students Learning Evaluation Using Learning Analytics</u> Author: Prof. U. M. Kalshetti, Keyur Kulkarni, Deepenkumar Patel, Sharang Nimbalkar  DOI: 10.22161/ijaers.4.4.11</p>	<i>Page No: 089-092</i>
12	<p><u>Smart Waste Management System using IoT</u> Author: Prof. S.A. Mahajan, Akshay Kokane, Apoorva Shewale, Mrunaya Shinde , Shivani Ingale,  DOI: 10.22161/ijaers.4.4.12</p>	<i>Page No: 093-095</i>
13	<p><u>On r-Dynamic Chromatic Number of the Corronation of Path and Several Graphs</u> Author: Arika Indah Kristiana, Dafik, M. Imam Utoyo, Ika Hesti Agustin  DOI: 10.22161/ijaers.4.4.13</p>	<i>Page No: 096-101</i>
14	<p><u>Determinants of Stock Prices of Joint - Stock Companies in Industrial Sector Listed On Hcm City Stock Exchange</u> Author: Vuong Quoc Duy, Le Long Hau, Nguyen Huu Dang  DOI: 10.22161/ijaers.4.4.14</p>	<i>Page No: 102-108</i>
15	<p><u>Efficiency and Performance analysis of routing protocols in WSN</u> Author: Kaysar Ahmed Bhuiyan , Md Whaiduzzaman, Mostofa Kamal Nasir  DOI: 10.22161/ijaers.4.4.15</p>	<i>Page No: 109-118</i>
16	<p><u>Study of Electron Transport in Fullerene (C60) Quantum Confined Channel Layer Based Field Effect Transistor</u> Author: Cyril Robinson Azariah John Chelliah, Barbara Szymanik, Rajesh Swaminathan  DOI: 10.22161/ijaers.4.4.16</p>	<i>Page No: 119-125</i>
17	<p><u>Low Power and Low Voltage Double Tail Dynamic Latch Comparator using 180nm Technology</u> Author: Balayan Sapna, Gupta Anshu  DOI: 10.22161/ijaers.4.4.17</p>	<i>Page No: 126-135</i>

18	<p><u>Enhancement of Analytical OBR (Out of Band Radiation) and BER Calculation for Digital Audio-Video Broadcasting in Companded OFDM System using Non-Symmetric QAM/QPSK Techniques</u></p> <p>Author: Santosh, Prof. Piyush Vyas, Prof. K. K. Arora</p> <p>DOI: 10.22161/ijaers.4.4.18</p> <p style="text-align: right;"><i>Page No: 136-141</i></p>
19	<p><u>Review of Dehumidifier with Association to Solar Circular Collector for Close Water Open Air System (CWOA) Humidification & Dehumidification Process</u></p> <p>Author: Anilkumar Motiram Patel</p> <p>DOI: 10.22161/ijaers.4.4.19</p> <p style="text-align: right;"><i>Page No: 142-149</i></p>
20	<p><u>An Empirical Estimation of CSS Cognitive Radio Network Performance under Spectrum Sensing Data Falsification Attack</u></p> <p>Author: Rajesh D. Kadu, Dr. Pravin P. Karde, Dr. V. M. Thakare</p> <p>DOI: 10.22161/ijaers.4.4.20</p> <p style="text-align: right;"><i>Page No: 150-154</i></p>
21	<p><u>High quality techniques for Multiple Sequences Alignment</u></p> <p>Author: Shalini Mehra</p> <p>DOI: 10.22161/ijaers.4.4.21</p> <p style="text-align: right;"><i>Page No: 155-158</i></p>
22	<p><u>Design of High Performance and Energy Efficient Explicit Pulsed Sense Amplifier Based Flip-Flop</u></p> <p>Author: Priyanka Sharma</p> <p>DOI: 10.22161/ijaers.4.4.22</p> <p style="text-align: right;"><i>Page No: 159-164</i></p>
23	<p><u>Effects of Refinery Processes on the Quality of Various Water Samples from Kaduna Refinery and Petrochemical Company (KRPC) Limited</u></p> <p>Author: C.T.Onyema, J.J. Ilebaye</p> <p>DOI: 10.22161/ijaers.4.4.23</p> <p style="text-align: right;"><i>Page No: 165-170</i></p>
24	<p><u>Implementation & Comparative Analysis of CMOS vs GDI for 8T SRAM Functionality under Power, Delay over Performance</u></p> <p>Author: T. Vasudeva Reddy, Dr B. K. Madhavi</p> <p>DOI: 10.22161/ijaers.4.4.24</p> <p style="text-align: right;"><i>Page No: 171-175</i></p>
25	<p><u>Comparison of Measured and Predicted Performance and the Emission Characteristics of Single Cylinder CI Engine using Pongamia Pinnata based Bio-Diesel</u></p> <p>Author: A. Yazharsu, T. Rajagopal, U. Karthick, V.P. Srinivasan</p> <p>DOI: 10.22161/ijaers.4.4.25</p> <p style="text-align: right;"><i>Page No: 176-183</i></p>

26	<p><u>A Phenomenon of Low-Alloy Steel Distribution Transformation Parameters at Cyclic Loading in Low-Cyclic Area</u> Author: Shipachev A., Nazarova M.  DOI: 10.22161/ijaers.4.4.26</p>	<i>Page No: 184-187</i>
27	<p><u>Forecasting Particulate Matter Concentrations: Use of Unorganized Machines</u> Author: Yara de Souza Tadano, Hugo Valadares Siqueira, Thiago Antonini Alves, Manoel Henrique de Nobrega Marinho  DOI: 10.22161/ijaers.4.4.27</p>	<i>Page No: 188-191</i>
28	<p><u>Separation of Sediment Contents and Water from Crude Oil of Khurmala and Guwayer Oil Fields in Kurdistan Region by using Centrifuge Method</u> Author: Saima Jadoon, Arif Malik  DOI: 10.22161/ijaers.4.4.28</p>	<i>Page No: 192-194</i>
29	<p><u>Call Blocking Probabilities Reduction of Channel Assignment in Mobile Communication Systems</u> Author: Mohamed Abdelghader Morsi, Dr. Amin Babkir A.Alnabi, Dr. Ashraf Gasim Alsid  DOI: 10.22161/ijaers.4.4.29</p>	<i>Page No: 195-200</i>
30	<p><u>Notion, Essence and Evaluation of the use of Information Technologies in the Economy of Metallurgical Industry</u> Author: Ghomrani Mohammed El Amine, Pavel B. Boldyrevskii  DOI: 10.22161/ijaers.4.4.30</p>	<i>Page No: 201-203</i>
31	<p><u>Performance Evaluation and Study of Routing Protocols: MANET vs VANET</u> Author: Annu, Ms. Reema  DOI: 10.22161/ijaers.4.4.31</p>	<i>Page No: 204-208</i>
32	<p><u>Power Factor Correction Using Bridgeless Boost Topology</u> Author: Sachin Saini, Piyush Sharma, Dheeraj Kumar Dhakad, Love Kumar Tripathi  DOI: 10.22161/ijaers.4.4.32</p>	<i>Page No: 209-215</i>
33	<p><u>Boundary Detection in 2-D and 3-D Wireless Sensor Networks</u> Author: Aditi Pandey, Ranjana Thalore  DOI: 10.22161/ijaers.4.4.33</p>	<i>Page No: 216-220</i>

34	<p><u>A Review of Various Routing Protocols in VANET</u> Author: Rajashree Dutta, Ranjana Thalore  DOI: 10.22161/ijaers.4.4.34</p>	<i>Page No: 221-224</i>
35	<p><u>Assessment of Quality of Groundwater in Certain Villages nearby Krishna River, Krishna District, Andhra Pradesh, India</u> Author: V. Rajesh, R. L. N. Charyulu, B. V. Ravi Kumar, B. Prasanna Kumar  DOI: 10.22161/ijaers.4.4.35</p>	<i>Page No: 225-230</i>
36	<p><u>Experimental Study on Pervious Concrete: An Eco Friendly Concrete Pavement</u> Author: Yogesh N. Sonawane  DOI: 10.22161/ijaers.4.4.36</p>	<i>Page No: 231-233</i>
37	<p><u>Optical and Thermal Performance Analysis of a Steady Spherical Collector with a Crescent-shaped Rotating Absorber</u> Author: Thierry S. M. Ky, Boureima Dianda, Moktar Ousmane, Magloire Pakouzou, Sie Kam, Dieudonne J. Bathiebo  DOI: 10.22161/ijaers.4.4.37</p>	<i>Page No: 234-245</i>
38	<p><u>Susceptibility Gene Prediction in Hereditary Disease Retinoblastoma</u> Author: S. Sumathi, Dr. R. Dhaya, Dr. R. Kanthavel  DOI: 10.22161/ijaers.4.4.38</p>	<i>Page No: 246-250</i>
39	<p><u>Development of Automated Room Security System</u> Author: Saksham Rastogi, Rahul Das, Kriti  DOI: 10.22161/ijaers.4.4.39</p>	<i>Page No: 251-254</i>
40	<p><u>Advanced Image Processing Technique for Failure Analysis</u> Author: Smt. Maya. V. Lakha, Dr. S. P. RajaManohar, Dr. K. ChennaKeshava Reddy, Dr .Abdul Sattar  DOI: 10.22161/ijaers.4.4.40</p>	<i>Page No: 255-258</i>
41	<p><u>Electro-synthesized Conjugated Salen Polymer-Glassy Carbon as Hydrochromic Reflective Filter for Humidity Detection: Introduction of Humidity Optical Sensor</u> Author: Mohammad Mahdi Doroodmand, Sina Owji  DOI: 10.22161/ijaers.4.4.41</p>	<i>Page No: 259-272</i>

42	<p><u>Energy Efficient MAC Protocols with Adaptive Duty Cycle for Wireless Sensor Networks</u> Author: Kaushik Ghosh, Prashansa Choudhary  DOI: <u>10.22161/ijaers.4.4.42</u> <i>Page No: 273-280</i></p>
43	<p><u>The Relationship between Cost-Volume Profit Management and Profitability in Private Organizations</u> Author: Dr. Ghassan Farouk Ghandour  DOI: <u>10.22161/ijaers.4.4.43</u> <i>Page No: 281-288</i></p>

Eco-Efficiency of Drinking Water Treatment

M. Farhaoui

National Office of Electricity and Drinking Water, Meknes, Morocco

Abstract— Problem statement: In the water treatment processes, the chemicals (aluminum sulfate AS, chlorine, and polyelectrolyte) are required in the different steps of treatment (coagulation, flocculation, settling, disinfection...). The chemicals residues can affect the human healthy and the environment. The treatment process produces sludge according to the level of the water turbidity. However, the sludge management increases the monitoring expenses. Moreover, this water treatment sub-product constitutes a threat for the environment and the downstream water users. **Approach:** In this study, the effectiveness of chemicals uses and sludge reuse was evaluated in order to find optimal operational conditions and reduce its residues. The influence of the chemicals consumption on the cost of treated water was also studied. A set of jar test experiments was conducted to find the sludge and aluminum sulfate dosages in order to improve the produced water quality for different turbidity levels. **Results:** Results demonstrated that the consumption of chemicals could be reduced by 10 to 15%. The sludge reuse improve the water quality and decrease the AS consumption by 50 to 60%. The turbidity removal is increasing and the aluminum residues is decreasing by 50%. **Conclusions/Recommendations:** Results show that the sludge reuse plays a very important role in reducing the aluminum sulfate dosage, improving the treated water quality and reducing water cost. The AS control and modeling reduce the chemicals consumption. This approach contributes in preserving the environment and opens income-earning opportunities for local population by promoting local products made from water treatment sludge.

Keywords— Efficiency, water treatment, water quality, chemicals residues, sludge, environment, beneficiaries.

I. INTRODUCTION

The demand on water supply is increasing over the last century due to improved lifestyle, industrial development and population growth. This increased demand is facing a paradox to produce treated water with high quality at lower cost. In order to reduce the water cost, it is very important to optimize the operating expenses in the water treatment plant (power, chemicals, operator's expenses...) and many measures should be taken in this vision [1].

The treatment of drinking water comprises the aeration, coagulation, sedimentation, filtration and disinfection of raw water produced by the springs. During the rainfall period, the water's turbidity increases, colloidal particles are separated in the treatment plant by means of a chemical coagulation process: consisting in the charge destabilization of the suspended particles by adding coagulant. The coagulant used is aluminum sulfate; it is the most widely used coagulant in Morocco as well as many other countries in the drinking water industry. It is mainly used because of its effectiveness, accessibility and low price. As a common practice, aluminum sulfate is applied according to the jars test results. The main difficulty is how to reduce the treated water cost and improve the water quality in the same time. Also, the sludge management is a real problem in water treatment plant, it is increasing the both investment and operating costs. optimize the aluminum sulfate dosage related to raw water characteristics by using other cheaper products. Some attempts have been made to improve the effectiveness of the aluminum sulfate or to substitute this coagulant by another natural, available and cheaper [2]. Finding of various coagulation processes have been reported in literature. Some of these include; studying the effect of using the bentonite, Moringa Oleifera, Date seeds, Pollen Sheath, Mesquite Bean and Cactus Latifariaon the coagulation in the treatment of low turbidity [3],[4],[5]. Those natural products have coagulating activity in the treatment of turbid water and can be used as coagulant or as coagulant aid with other synthetic and industrial coagulants (aluminum sulfate...) in order to reduce the coagulant consumption in the water treatment plant. However, Studies have demonstrated that sludge produced by the water treatment plant can improve the coagulation process and reduce the aluminum sulfate consumption [6].

This paper addresses the problem of improving water quality by decreasing the chemicals use in water treatment plant and the possibility to reuse sludge in the water production chain. This paper is organized as follows. After an introduction of the objective of this study, the experimental section is described in section II, also, the methodology used to assess the approach impacts is explained. In section III, the results are presented and discussed.

II. EXPERIMENTAL SECTION

a) Water treatment operation

This study was developed in a water treatment plant located in Meknes in the middle of Moroccan Kingdom, whose source is two big springs Bittit (630 l/s) and Ribaa (400l/s). The quality of water produced by the springs changes according to the rainfall in the region.

Sometimes, it can be affected by the snow in the Atlas Mountain. The treatment water plant, as part of other water resources, water to more than 700.000 inhabitants of Meknes city, Morocco and has a nominal capacity of 600 l/s of treated water. Figure 1 presents a schematic overview of the various operations necessary to treat the water.

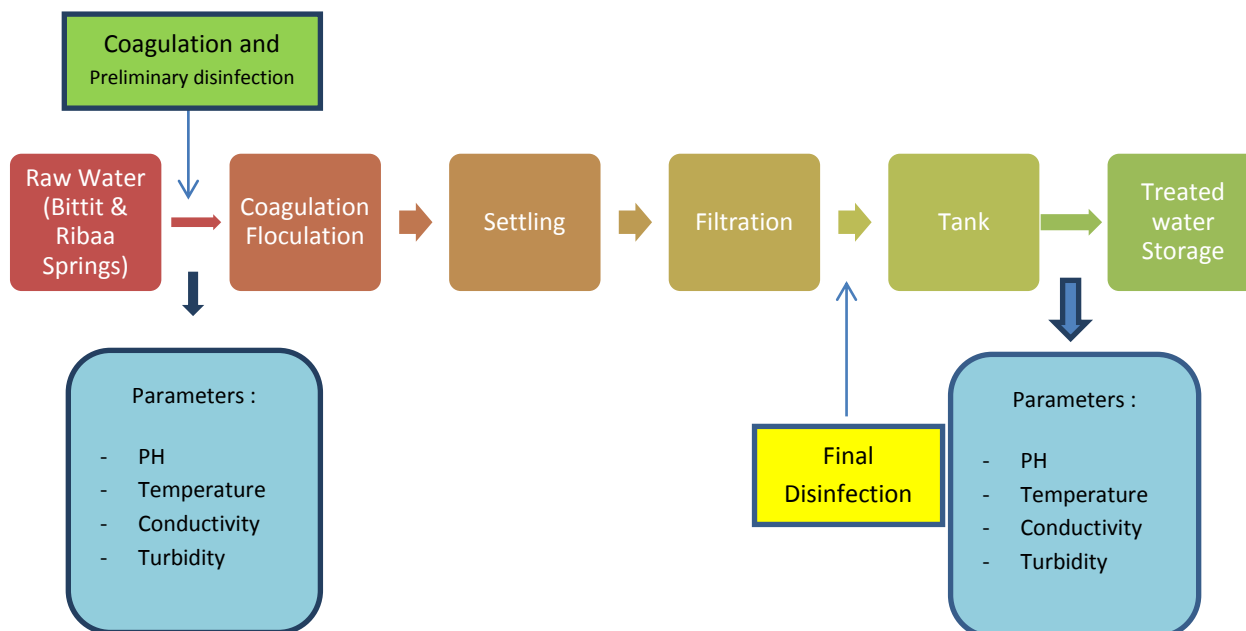


Fig.1: simplified synopsis of the water treatment plant.

Many measurements of variables such as turbidity level, PH, conductivity, temperature is needed to carry out the jars test in order to determine the optimal dose of the aluminum sulfate. The raw water variables used in this study present the following variation intervals:

Table.1: statistical summary of raw water conditions from 01/01/2013 to 31/12/2016 (ONEE, 2016)

Variables	Min	Max
Turbidity: Bittit (NTU)	1.7	850
Turbidity: Ribaa (NTU)	1.62	960
PH	6.80	7.74
Temperature: (°C)	14	24.70
Conductivity micro s/cm	509	624

In the rainfall period, the turbidity of raw water changes from time to time as shown in the figure 2:

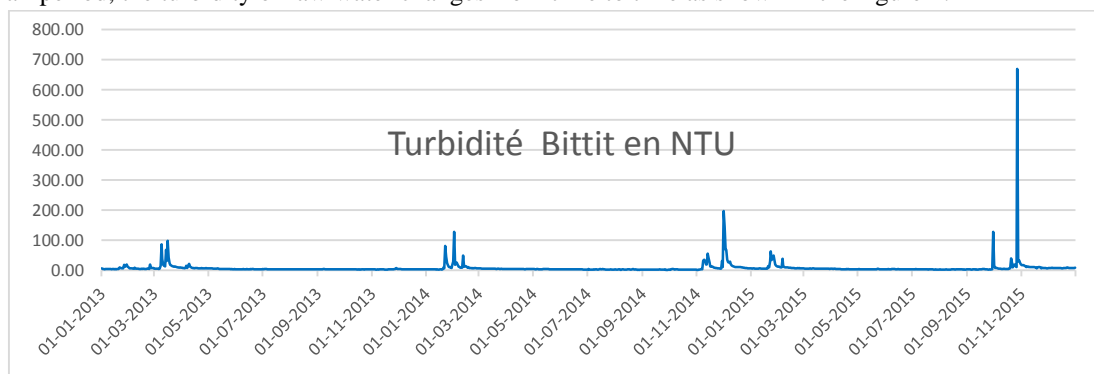


Fig.2: statistical data of turbidity level of the spring's water from 01/01/2013 to 31/12/2015 (ONEE, 2016).

The chemicals used in the water treatment process consume about 50% the total operating expenses of the water treatment. The energy cost is between 10 to 15% related to the total cost in 2013, 2014 and 2015 as shown in the Figure 3.

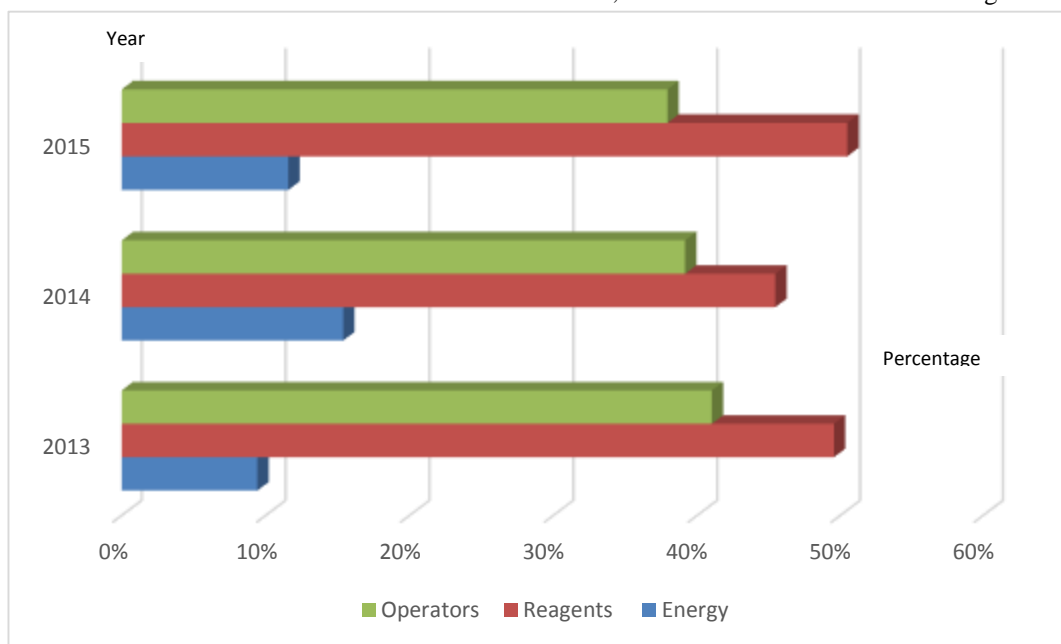


Fig.3: Operations expenses of the water treatment plant in 2013, 2014 and 2015 (National Office of Electricity and Drinking Water ONEE, 2015).

In addition, used as coagulant, the aluminum sulfate (Alum) consumption is more than 70% of the total chemicals consumption in the water treatment plant. Le polyelectrolyte (Poly) consumption is less than 10% and the chlorine is between 16 and 26% of the total chemicals used in the water treatment plant according to the water quality as shown by the figure below:

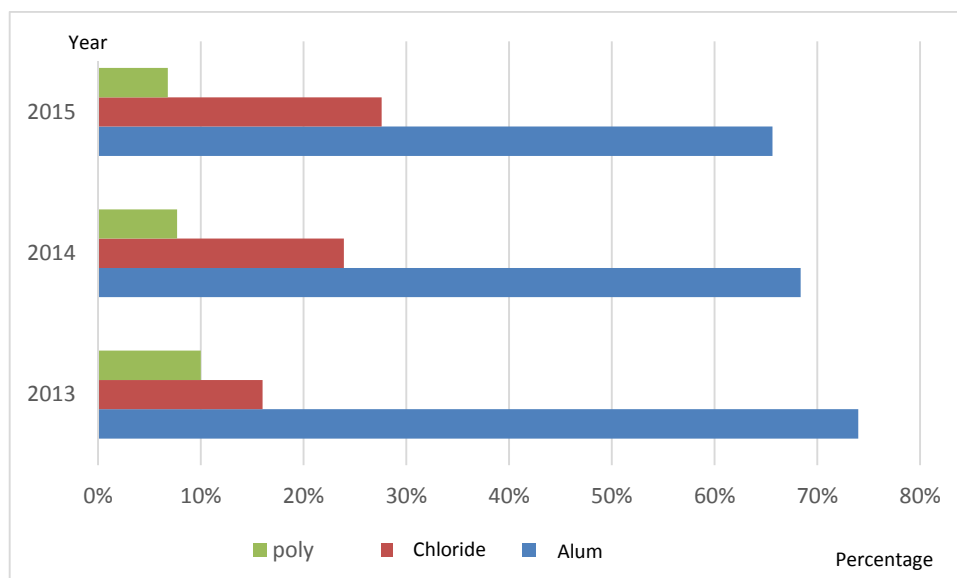


Fig.4: Percentage of chemicals expenses consumed by the water treatment plant in 2013, 2014 and 2015 (National Office of Electricity and Drinking Water ONEE, 2015).

The table 2 show the volume of the treated water and sludge produced by the water treatment plant between 2013 and 2015.

Table.2: Volume of treated water and sludge produced by the WTP in 2013, 2014 and 2015 per month (National Office of Electricity and Drinking Water ONEE, 2016)

Year	Volume of treated water (m ³)	Consumption of aluminum sulfate (kg)	Volume of sludge produced in the WTP (m ³)
2013	15098736	242850	9559
2014	15508924	203820	14021
2015	15214486	149330	10810

b) Materials and methods

b.1 Modeling of the aluminum sulfate dose:

The prediction of optimal coagulant dose from raw water characteristics is a nonlinear regression problem. The identification aims at modeling and parameter estimation. It consists of constructing a mathematical model that can describe the behavior "-Input-output" of the system [17]. The problem is to determine the model parameters from input and output data. The analysis of experimental data

for different periods of the year in the water treatment plant allow obtain mathematical models describing the changes in dose of Alum based on the input parameters of the raw water using Statgraphics software [7].

The model to develop will be based on the data available in the plant from 01/06/2014 to 31/12/2015 (495 data). The data validation, processing and modeling of the coagulant dosage rate are the main steps to construct the model as presented by the figure 5.

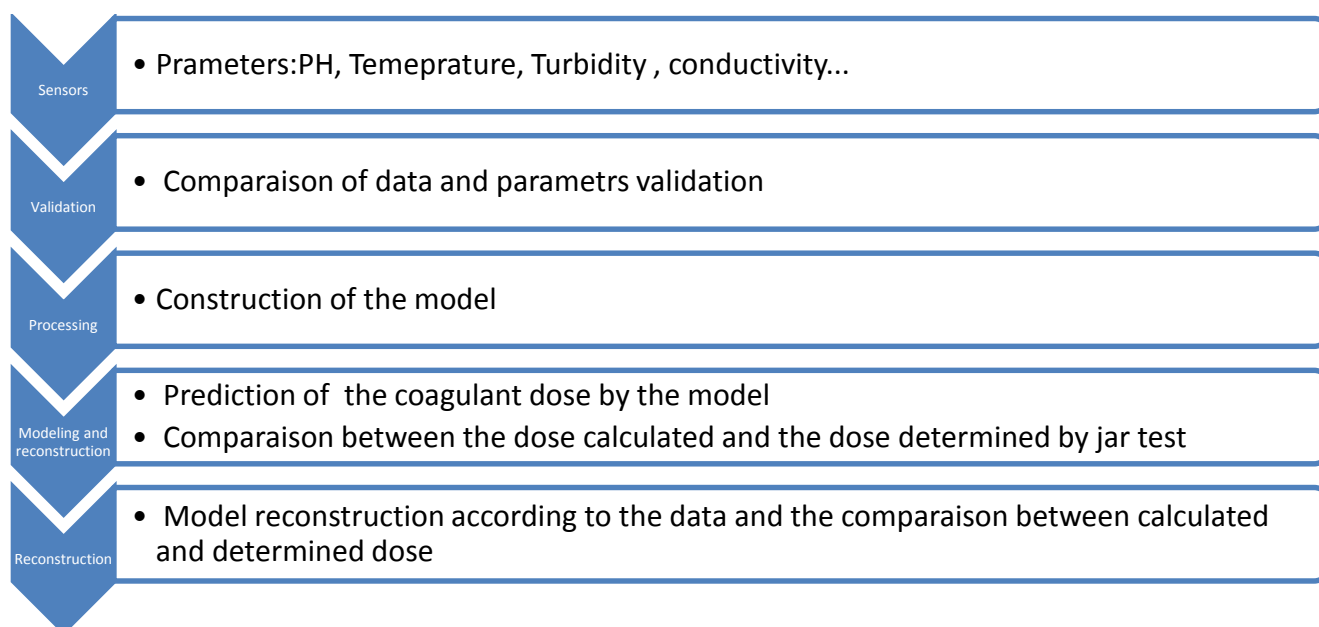


Fig.5: structure of the model for the prediction of the coagulant dosage rate.

According to the data recorded in the water treatment plant, many models are identified and analyzed using Statgraphics software which indicates the relationship between the Aluminum doses measured and calculated by different models. Only eleven models from the simplest to a complex one are examined below regarding to the output (aluminum sulfate dose calculated).

After the construction of the models, they are compared each one to the other. Two statistical tests are performed on models in order to choose the model fitted with the observed data. First, an ANOVA test is performed on models to determine if there is a significant difference between models and observed data. Finally, the Euclidian distance method is applied to models in order to choose the more representative of the observed data.

b.2 Reusing sludge in the water treatment process:

1/ Preparation of synthetic turbid water:

The turbid water is prepared by adding different weights of sludge in mg into 1 liter of raw water from the spring for the medium (20 NTU) and high (40 NTU) turbidity levels. However, the low turbidity (10 NTU) water is obtained directly from the spring.

2/ Preparation of Aluminum solution:

The Aluminum solution was prepared by dissolving 1 g of AS (Al₂(SO₄)₃) in distilled water (PH = 7 ± 0.1) and the solution volume is increased to 1 liter. Each 1 ml of prepared stock solution is equal to 10 mg/l when it is added to 1 liter of turbid water to be tested.

3/ Preparation of sludge solution:

The sludge produced in the settling step of the treatment process is used to prepare the sludge solution. A certain volume of raw water is added to the blend and stirred for 5 minutes at 300 rpm using magnetic stirrer. The volume of obtained suspension is increased to 1 liter and the gravity filtered through a 1um filter paper to separate residual particles from the prepared solution. The filtrate solution is referred to a sludge coagulant in this study.

4/Research methodology:

A standard jar test apparatus equipped with six paddles rotating in a set of six beakers is used to simulate coagulation, flocculation and sedimentation processes. At the first, Control experiments for coagulation tests are performed in order to determine the optimal dose of the

aluminum sulfate in normal conditions. The selected level of turbid water (1L) is filled into the beakers and various doses in the range from 10 to 100 mg/l of sludge and the aluminum sulfate according to the results of the first jar test determining the optimal dose of the inorganic coagulant in normal conditions are separately added in the beakers and mixed rapidly (300 rpm) for one minute. The mixing speed was then reduced to 40 rpm for 20 minutes. Then the stirrer is turned off and the suspensions are allowed to settle for different periods of time ranging from 30 to 120 minutes under quiescent conditions. After each period of settling time, supernatant samples of each beaker in the jar test is withdrawn from located 10 cm below the water level and residual turbidity is measured.

III. RESULTS AND DISCUSSIONS

3.1. Evaluation of experiments impacts:

1/ Modeling of the aluminum sulfate dose:

According to this study, the coagulant dose modeling can reduce the aluminum sulfate consumption by 10 to 15% [7].

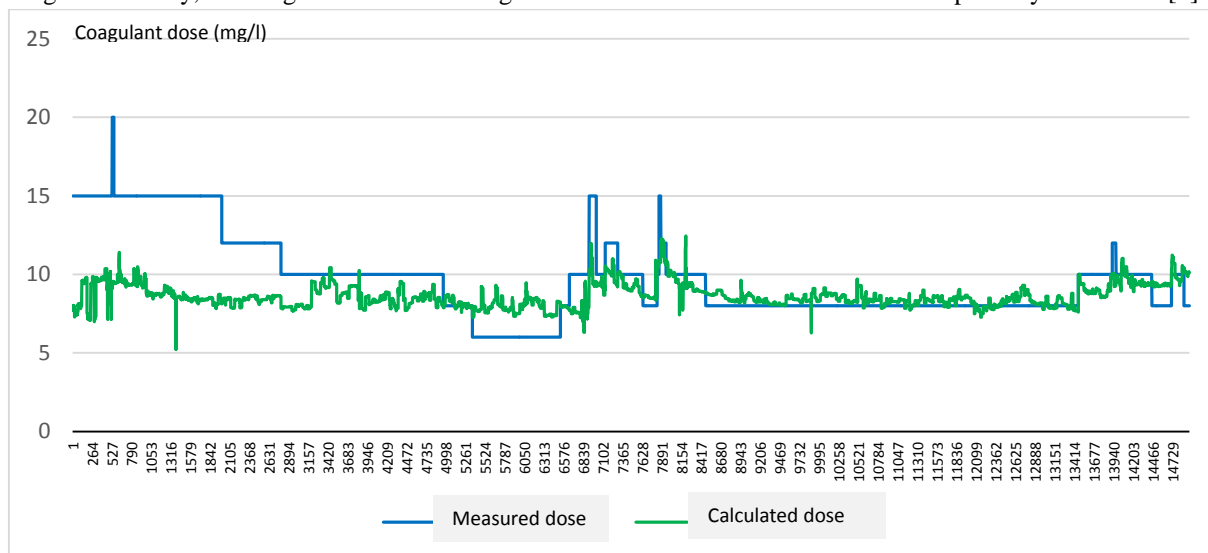


Fig.6: Comparison between the calculated and measured dose of the coagulant.

2/ Sludge reusing:

According to the jar test experiments, the sludge can play a very interesting role the improvement of settling activities in the water treatment process. The sludge reusing can reduce the aluminum sulfate consumption by 40 to 50% according to the water turbidity level [6].

The table 3 shows the results of coagulant consumption reduction after using sludge as aid coagulant with aluminum sulfate:

Table.3: AS consumption reduction for different levels of turbidity using AS and sludge

	Low Turbidity	Medium turbidity	High turbidity
Initial turbidity	9.34	21	39.4
Optimal dose of Aluminum sulfate (mg/l) (1)	10	20	20
Optimal dose of sludge (mg/l) used within AS (2)	35	50	60
Dose of AS (mg/l) proposed to be used with optimal dose of sludge (3).	6	10	12
% of AS reduction	40%	50%	40%

3.2. Evaluation of operational impacts:

1/ Improvement of water quality:

Both modeling of coagulant dose and reusing of sludge in coagulation process improve the water quality produced by the water treatment plant. Concerning the dose modeling, the calculated dose based on real time parameters is just the dose that the process requires and many problems of over or under dose are avoid. Thus, the

quality of water is improved. In addition, the sludge reusing improves the water quality by increasing the turbidity removal.

The table 4 shows the results of turbidity removal percentage using aluminum sulfate only, optimal dose of AS and sludge and the optimal dose of sludge and the proposed dose of AS :

Table.4: Turbidity removal percentage for different levels of turbidity using AS and sludge

	Low Turbidity	Medium turbidity	High turbidity
Initial turbidity	9.34	21	39.4
Turbidity removal percentage using only AS (1)	96.71%	98.05%	98.98%
Turbidity removal percentage using AS and sludge as coagulant aid (1)+(2)	97.14%	98.33%	99.34%
Turbidity removal percentage using optimal dose of sludge and AS (2)+(3)	97.56%	98.96%	99.47%

The results show that the sludge used as coagulant aid with the AS improves not only the water quality produced by the treatment plant (turbidity removal percentage from 96.71 to 97.56%, from 98.05 to 98.96% and from 98.98 to 99.47% for low, medium and high turbid water

respectively).In addition, it can be used to reduce the AS dose in the coagulation process.

Furthermore, the sludge reuse in coagulation process decrease the aluminum residues in produced water. The figure 7 show the aluminum residues before and after reusing sludge in water treatment process.

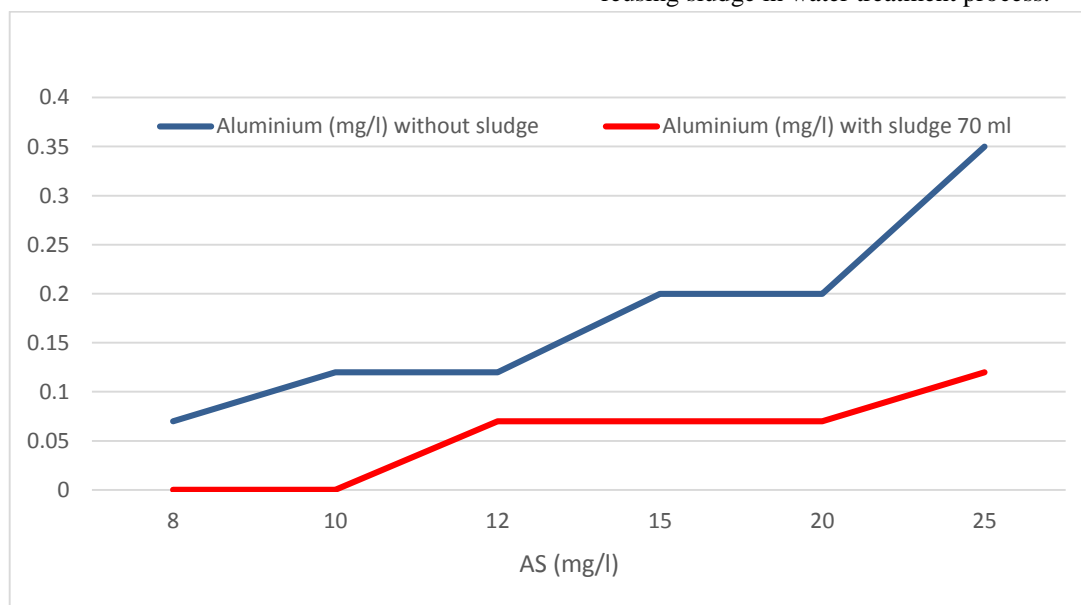


Fig.7: Impact of sludge reusing on aluminum residues in treated water.

2/ Reduction of waste streams:

The sludge reusing in the coagulation process reduce the volume of waste streams and plays a great role in the environment preservation. Properties of the sludge produced by the water treatment plant depends on the raw water quality and the WTP process [8]. Moreover, the

sludge can play very interesting role in removing phosphorus as various species of phosphate by means of its aluminum components [9].A model has been elaborated to predict the sludge volume [10]. The model contributes to master the sub-products produced by the WTP in order to manage the plant performances.

3/Improvement of the local population income:

Several studies have been performed in order to treasure the sludge produced by both drinking water treatment plants (WTP) and wastewater treatment plants (WWTP) [11]. Although the reuse of sludge from WWTP is of crucial importance according to the organic matter it contain. In fact, the reuse of sludge have been studied in different sectors especially in the field of construction and civil engineering.

As in construction field, WTP sludge is very important in the pottery sector. Indeed, the use of a mixture consisting of sludge (85%) and sand (silicon dioxide) 15% in pottery manufacturing is proposed [12]. Then, sludge produced by the water treatment plant contributes in the development of handcraft activities in the region. It can create more than 10000 handcraft items (each item needs 1.5 kg of sludge and costs more than five \$). Thus, the sludge will become an asset for the local population not an obstacle for WTP managers.

3.3. Evaluation of approach impacts:

The approach based on modeling of the coagulant dose and the sludge reusing in water treatment plant can be widespread. The relevance of these approach findings for the challenge is appreciated at three levels:

1/ The environmental level:

The application of this approach contributes to enhance and protect the environment and improve the water quality. The treated water quality is improved by increasing the turbidity removal percentage and decreasing the aluminium residues. However, the rejected water quality is improved by decreasing all of the chemicals residues. In addition, this approach play a very important role in reducing waste streams (sludge). Thus, the agricultural activities in the plant downstream are not affected by the WTP streams.

2/ The economic level:

The application of this approach contributes:

- Reduce operating costs by mastering the coagulant dose determined by the automatic method instead of manual method and reducing the coagulant consumption after reusing sludge as aid coagulant.
- Improve operator productivity and efficiency and increase operator profits by decreasing the operating expenses. The sludge reusing and modelling contributes to decrease both the investment and operating costs [10].
- Optimize life-cycle economic performance: this approach improve the performances facilities.

3/ The Social level:

The application of this approach contributes to enhance population health and comfort by improving

water quality. It can contribute to the socio-economic development of the region by opening income earning opportunities and promoting local products. Thus, the water plant management enhance local livelihood.

IV. CONCLUSIONS

This paper has presented some results concerning the improvement of the water treatment efficiency and the reduction of its impacts on the environment. It is based on systemic approach that include environmental, economic and social issues and touches all the stakeholders. An innovative solution that reduce environmental impact, optimize water use efficiency and improve the competitiveness of the water supply company. This approach gets the water treatment process more efficient by reducing waste and increasing sub-products recycling and recovery. The study findings show that the water quality is improved while the chemicals consumption is reduced. Thus, the treated water cost is reducing. In addition, this approach touches the social issues, it is based on the idea that improve the local population income and engage the rural community in sustainable economy activities (craft, fertilizers...). Finally, the approach can be generalized for water treatment plants all over the world.

REFERENCES

- [1] Farhaoui, M. and Derraz, M. (2016), Review on Optimization of Drinking Water Treatment Process. *Journal of Water Resource and Protection*, Vol.8, pp.777-786.
<http://dx.doi.org/10.4236/jwarp.2016.88063>
- [2] Shen, Y.H., Treatment of low turbidity water by sweep coagulation using bentonite. *J. Chem. Technol. Biot.*, 2005, 80: 581-586.
- [3] Mukheled A. A Novel Water Pretreatment Approach for Turbidity Removal Using Date Seeds and Pollen Sheath. *Journal of Water Resource and Protection*, 2012, 4, 79-92
- [4] N. A. Eman, A. M. Suleyman, M. S. Hamzah, Md. A. Zahangir and M. R. M. Salleh, Production of Natural Coagulant from Moringa Oleifera Seed for Application in Treatment of Low Turbidity Water, *Journal of Water Resource and Protection*, Vol. 2, 2010, No. 3, pp. 259- 266.
- [5] Aho, I. M. and Lagasi, J.E., A new water treatment system using Moringa Oleifera seed", *American Journal of Scientific and Industrial Research*, 3 (6), pp. 487-492. doi:10.5251/ajsir.2012.3.6.487.492.
- [6] Farhaoui M. & Derraz M., (2016), Optimizing coagulation process by using sludge produced in the water treatment plant, *Journal of Chemical and Pharmaceutical Research*, V.8(4), pp.749-756.

- [7] Farhaoui M., Hasnaoui L., Derraz M., (2016), Optimization of Drinking Water Treatment Process by Modeling the Aluminum Sulfate Dose, *British Journal of Applied Science & Technology*, Vol.17(1), pp.1-14. DOI: 10.9734/BJAST/2016/26840.
- [8] Kyncl M., 2008, Opportunities for water treatment sludge reuse, *Geo Science Engineering*, Vol. LIV 2, No. 1, pp. 11- 22.
- [9] Graham-Jones A., 2014, Evaluating reuse of sludge from water treatment for wastewater treatment, An assesment of effects of spent alum sludges on wastewater treatment in Gothenburg, Sweden, MEng degree thesis submitted in Civil and Environmental Engineering with European Studies at the School of Engineering, University of Aberdeen, Sweden, Pp. 67.
- [10] Farhaoui M., (2017), "Managing and modeling of the drinking water treatment sludge." *International Journal of Research - Granthaalayah*, 5(2), 168-179. <https://doi.org/10.5281/zenodo.345636>
- [11] Aeslina Binti Abdul Kadir, Ahmad Shayuti Bin Abdul Rahim, An Overview of Sludge Utilization into Fired Clay Brick, *World Academy of Science, Engineering and Technology, International Journal of Environmental, Chemical, Ecological, Geological and Geophysical Engineering* Vol:8, No:8, 2014.
- [12] Faris Gorashi Faris, ChoongChoe Earn, A New Approach to Reuse Alum Sludge in Pottery Manufacturing Using Silica and Thermal Curing, *International Journal of Chemical, environmental & Biological Sciences (IJCEBS)* Volume 2, Issue 3 (2014).

Transmission Line Fault Monitoring and Identification System by Using Internet of Things

S.Suresh¹, R.Nagarajan², L.Sakthivel³, V.Logesh⁴, C.Mohandass⁵, G.Tamilselvan⁶

¹Asst. Professor, Department of Electrical and Electronics Engineering, Gnanamani College of Technology, Namakkal, India.

²Professor, Department of Electrical and Electronics Engineering, Gnanamani College of Technology, Namakkal, India.

³⁻⁶ U.G. Students, Department of Electrical and Electronics Engineering, Gnanamani College of Technology, Namakkal, India.

Abstract — *The fault location detection has been a goal of power system engineers, since the creation of distribution and transmission systems. Quick fault detection can help protect the equipment by allowing the disconnection of faulted lines before any significant damage of the equipment. The accurate fault location can help utility personnel remove persistent of the faults and locate the areas where the faults regularly occur, thus reducing the occurrence of fault and minimize the time of power outages. As a result, while the fault location detection schemes have been developed in the past, a variety of algorithms continue to be developed to perform this task more accurately and more effectively. The detection and location of faults on power transmission lines is essential to the protection and maintenance of a power system. Most methods of fault detection and location relate to the measurements of electrical quantities provided by current and voltage transformers. These transformers can be expensive and require physical contact with the monitored high voltage equipment.*

Keywords— *IoT, Relay, PIC Microcontroller, Transmitter, Receiver.*

I. INTRODUCTION

CURRENTLY, the electric power infrastructure is highly vulnerable against many forms of natural and malicious physical events [1], which can adversely affect the overall performance and stability of the grid. Additionally, there is an impending need to equip the age old transmission line infrastructure with a high performance data communication network, that supports future operational requirements like real time monitoring and control necessary for smart grid integration [2], [3]. Many electric power transmission companies have primarily relied on circuit indicators to detect faulty sections of their transmission lines. However there are still challenges in detecting the exact location of these faults. Although fault indicator technology has provided a reliable means to locate permanent faults, the technical crew and patrol teams still has to physically patrol

and inspect the devices for longer hours to detect faulty sections of their transmission lines. Wireless sensor based monitoring of transmission lines provides a solution for several of these concerns like real time structural awareness, faster fault localization, accurate fault diagnosis by identification and differentiation of electrical faults from the mechanical faults, cost reduction due to condition based maintenance rather than periodic maintenance, etc.. These applications specify stringent requirements such as fast delivery of enormous amount of highly reliable data. The success of these applications depends on the design of cost effective and reliable network architecture with a fast response time. The network must be able to transport sensitive data such as current state of the transmission line and control information to and from the transmission grid. This research provides a cost optimized framework to design a real time data transmission network. To monitor the status of the power system in real time, sensors are put in various components in the power network. These sensors are capable of taking fine grained measurements of a variety of physical or electrical parameters and generate a lot of information. Delivering this information to the control centre in a cost efficient and timely manner is a critical challenge to be addressed in order to build an intelligent smart grid. Network design is a critical aspect of sensor based transmission line monitoring due to the large scale, vast terrain, uncommon topology, and critical timing requirements. Mechanical faults, cost reduction due to condition based maintenance rather than periodic maintenance, etc. The use of sensor networks has been proposed for several applications like mechanical state processing and dynamic transmission line rating applications [4]-[6]. To monitor the status of the power system in real time, sensors are put in various components in the power network [7]-[10].

The hierarchical model proposed in, offers a very expensive solution with the idea of deploying cellular transceivers on every tower. While such a network can provide extremely low latency data transmission, this model is highly cost inefficient as it incurs huge installation and subscription

costs. The only work that addresses the problem of finding optimal locations of cellular transceivers is presented [11], [12]. The paper presents a digital fault locator by dynamic system parameter estimation for a double end fed transmission line. The authors of [13] and [14] were the first to propose a two level model specifically for supporting the overhead transmission line monitoring applications. But considering the topological constraints posed by the transmission lines, the low band-width, low data rate wireless nodes would fail to transmit huge amount of data in a multi hop manner.

In these works, the goal is to deploy multiple different sensors in critical and vulnerable locations of the transmission line to sense mechanical properties of its various components and transmit the sensed data through a suitable wireless network to the control center. However, most of these works address this theme at a very high level of abstraction. Small scale real world deployments of wireless sensors include tension monitoring using load cells [15]-[17], and power conductor surface temperature monitoring, sago meter, etc. This paper deals with the application of artificial neural networks (ANNs) to fault detection and location in extra high voltage (EHV) transmission lines for high speed protection using terminal line data. The proposed neural fault detector and locator were trained using various sets of data available from a selected power network model and simulating different fault scenarios (fault types, fault locations, fault resistances and fault inception angles) and different power system data (source capacities, source voltages, source angles, time constants of the sources) [18], [19].

II. BLOCK DIAGRAM

In Fig. 1 shows the block diagram of wireless networking system. The transmission line infrastructure, wireless networking presents a feasible and cost effective solution for transmission line monitoring such as voltage and current. The several works and propose to improve the state of the art in transmission line monitoring by harnessing the power of wireless sensor networks for real time monitoring and control GSM is a cellular network, which means that mobile phones connect to it by searching for cells in the immediate vicinity. The GSM networks operate in four different frequency ranges. Most GSM networks operate in the 900 MHz or 1800 MHz bands. Some countries in the Americas (including Canada and the United States) use the 850 MHz and 1900 MHz bands because the 900 and 1800 MHz frequency bands were already allocated GSM has used a variety of voice codices to squeeze 3.1 kHz audio into between 5.6 and 13 kbps.

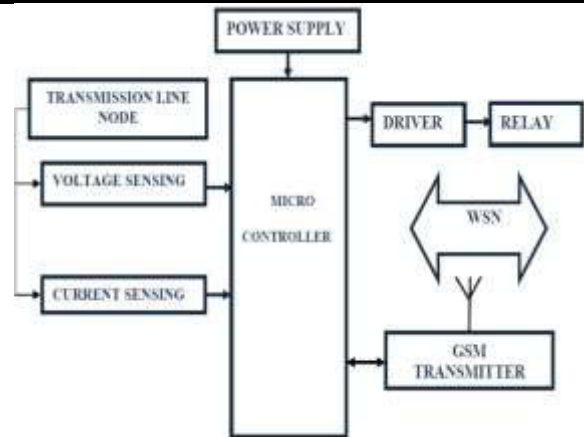


Fig.1: Block diagram

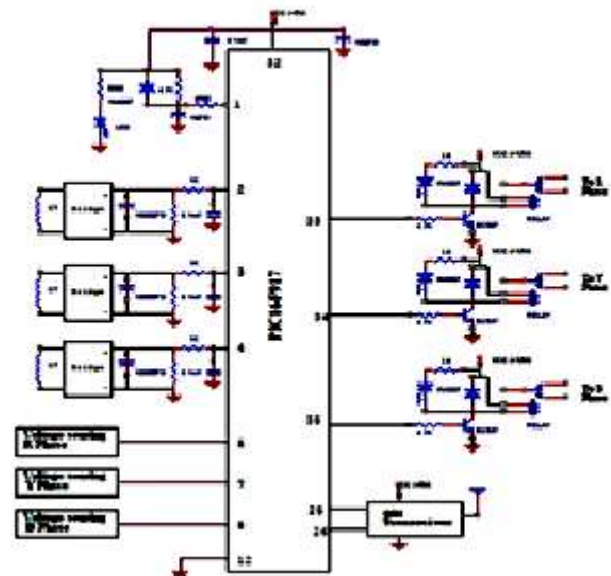


Fig.2: Circuit diagram

Originally, two codes, named after the types of data channel they were allocated, were used, called Half Rate (5.6 kbps) and Full Rate (13 kbps). These used a system based upon linear predictive coding (LPC). In addition to being efficient with bitrates, these codes also made it easier to identify more important parts of the audio, allowing the air interface layer to prioritize and better protect these parts of the signal installation and subscription costs.[20], [21]. In Fig. 2 shows the circuit diagram of wireless networking system.

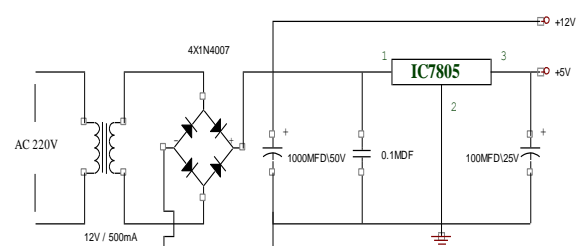


Fig.3: Power supply circuit

In this circuits need two power supplies. The 78XX ICs are worked on regulated DC power 5V with GND. Relay driver worked on DC 12V with GND. This unit consists of transformer, rectifier, filter and regulator. The AC voltage typically 230v RMS is connected to a transformer which steps that AC voltage down to the level of the desired AC voltage. The Diode rectifier then provides a bridge rectified voltage that is initially filtered by a simple capacitor filter to produce a DC voltage. This resulting DC voltage usually has some ripple or AC voltage variations. A regulator circuit can use this DC input to provide DC voltage that not only has much less ripple voltage but also remains the same DC value even the DC voltage varies somewhat, or the load connected to the output DC voltages changes [22], [23].

III. INTERNET OF THINGS



Fig.4: Internet of things

In Fig.4 shows the IoT. The user interface is through web pages that are created on the client-side, using HTML. JavaScript is used for validity checks of the information entered by the users. The client's browser parses the URL into a number of separate parts, including address, path name and protocol. A Domain Name Server (DNS) translates the domain name the user has entered into its IP address, a numeric combination that represents the site's true address on the Internet (a domain name is merely a "front" to make site addresses easier to remember). The browser now determines which protocol (the language client machines use to communicate with servers) should be used. Examples of protocols include FTP (File Transfer Protocol), and HTTP (Hyper Text Transfer Protocol). The browser sends a GET request to the Web server to retrieve the address it has been given. For example, when a user types `http://www.example.com/1.jpg`, the browser sends a GET 1.jpg command to example.com and waits for a response. The server now responds to the browser's requests. It finds the necessary files, runs the appropriate scripts, exchanges cookies if necessary, and returns the results back to the browser. If it cannot locate the file, the server sends an error message to the client. The browser, after receiving the HTML file, displays the web page to the user.[24].

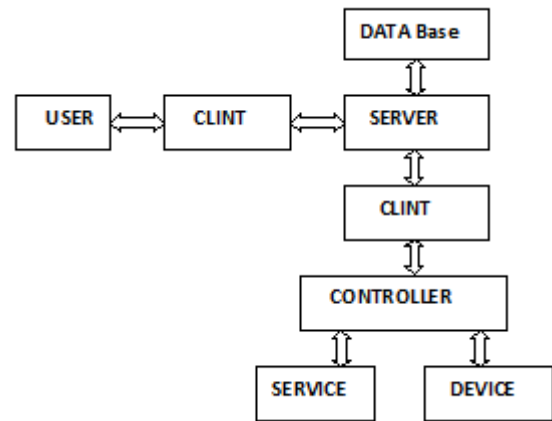


Fig.5: Client server architecture

The Internet is basically a client server system. In the retrieval of information that can be accessed using the internet, there are two important components: client, which requests the information and server, which stores it. Each side requires a piece of software to negotiate the exchange of data. During web page retrieval, at the client side, a browser like Netscape or internet explorer is used. The server side software performs the task of negotiating data transfers between clients and servers via hypertext transfer protocol (HTTP), the communications protocol of the Web. The different server software are available for various operating systems such as Microsoft Internet information Server (IIS) for Windows NT and the Apache web server for Unix platform. The Fig.5 shows the client server architecture. The welcome page has a short form that will enable the user to log in to the system. The form has text fields for username and password entry. The user has to specify his/her username and password obeying the following rules. The Fig.6 shows the welcome pages of the IoT.

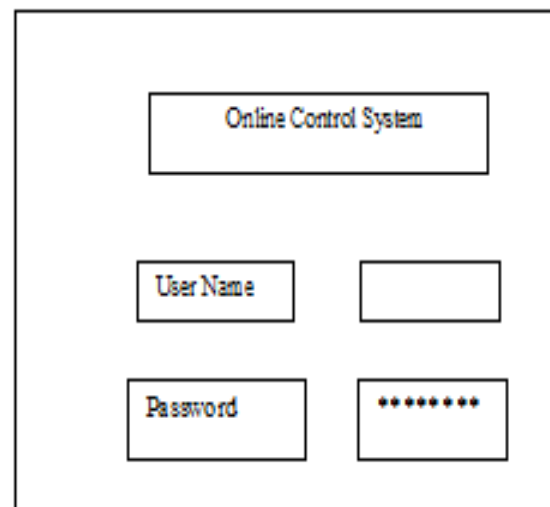


Fig.6: Welcome pages

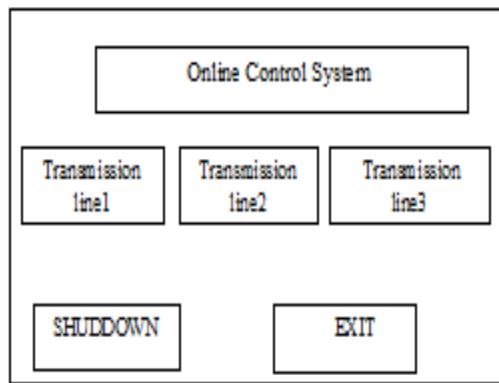


Fig.7: Control pages

In Fig.7 shows the Control pages of the IoT. The menu page displays various buttons where he/she can select from a list of available menus provided by the system. On the menu page, the user can select DEVICE, SHUDDOWN and EXIT. On selecting device, the user can choose among devices to control. SHUDDOWN menu is provided to emergency off regarding the procedure to be followed. EXIT menu is provided to log out of the system. By sensing the voltage and current in this circuit, the short circuit is having the output in the range of high voltage and low current and the open circuit having the output in the range of low voltage and high current range.

IV. EMBEDDED SYSTEM

An embedded system is a combination of computer hardware, software and additional mechanical parts, designed to perform a specific function. An embedded system is designed to do a specific task within a given time frame, repeatedly, without human interaction. Embedded system do not need a complete operating system, but only the basic functionalities of an operating system in a real-time environment, that is, a real time operating system (RTOS). Frequently, embedded system does not have a user interface. PIC (Peripheral Interface Controller) is the IC which was developed to control the peripheral device, dispersing the function of the main CPU. When comparing to the human being, the brain is the main CPU and the PIC shares the part of which is equivalent to the automatic. However, the through out, the memory capacity is not big. It depends on the kind of PIC but the maximum operation clock frequency is about 29 MHz and the memory capacity to write the program is about 1k to 4k words. It is possible to make the compact circuit when using PIC [25], [26].

V. CONCLUSION

In this paper, present an optimal formulation for a cost optimized wireless network capable of transmission of time sensitive sensor data through the transmission line

network in the presence of delay and bandwidth constraints. Our analysis shows that a transmission line monitoring framework using WSN is indeed feasible using available technologies. The proposed method with formulation is generic and en-compasses variation in several factors such as asymmetric data generation at towers, wireless link reliabilities, link utilization dependent costs, non-uniform cellular coverage characteristics and requirements for cost optimized incremental deployment. The evaluation studies show that the main bottleneck in cost minimization is wireless link bandwidth. Further, in cases of increasing flow bandwidth, the limited wireless link bandwidth leads to a feasible but expensive design due to increased dependence on cellular network to satisfy constraints.

REFERENCES

- [1] H.Li, G.W.Rosenwald, J.Jung, and C. Liu, "Strategic power infra-structure defense," Proc. IEEE, vol. 93, no. 5, pp. 918–933, May 2005.
- [2] G. Vidhya Krishnan, R.Nagarajan, T. Durka, M.Kalaiselvi, M.Pushpa and S. Shanmuga priya, "Vehicle Communication System Using Li-Fi Technology," International Journal of Engineering And Computer Science (IJECS), Volume 6, Issue 3, pp. 20651-20657, March 2017.
- [3] J.Chandramohan, R.Nagarajan, K.Satheeshkumar, N.Ajithkumar, P.A.Gopinath and S.Ranjithkumar, "Intelligent Smart Home Automation and Security System Using Arduino and Wi-fi," International Journal of Engineering And Computer Science (IJECS), Volume 6, Issue 3, pp. 20694-20698, March 2017.
- [4] V. C. Gungor and F. C. Lambert, "A survey on communication net-works for electric system automation," Comput. Netw. vol. 50, no.7, pp.877–897, May 2006.
- [5] P. Ramachandran, V. Vittal, and G. T. Heydt, "Mechanical state estimation for overhead transmission lines with level spans," IEEE Trans. Power Syst., vol. 23, no. 3, pp. 908–915, Aug. 2008.
- [6] R.Nagarajan and S.Sathishkumar, K.Balasubramani, C.Boobalan, S.Naveen and N.Sridhar. "Chopper Fed Speed Control of DC Motor Using PI Controller," IOSR- Journal of Electrical and Electronics Engineering (IOSR-JEEE), Volume 11, Issue 3, Ver. I, pp. 65-69, May – Jun. 2016.
- [7] P. Zhang, F. Li, and N. Bhatt, "Next-generation monitoring, analysis, and control for the future smart control center," IEEE Trans. Smart Grid, vol. 1, no. 2, pp. 186–192, Sep. 2010.
- [8] J. Ausen, B. F. Fitzgerald, E. A. Gust, D. C. Lawry, J. P. Lazar, and R. L. Oye, "Dynamic thermal rating

- system relieves transmission con-straint,” in Proc. IEEE 11th Int. Conf. Transmission. Distribution. Construction, Oper, Live-Line Maintenance (ESMO), Oct. 15–19, 2006.
- [9] V.C.Gungor, L.Bin, and G. P. Hancke, “Opportunities and challenges of wireless sensor networks in smart grid,” IEEE Trans. Ind. Electron., vol. 57, no. 10, pp. 3557–3564, Oct. 2010.
- [10] R.Nagarajan and M,Saravanan. “Performance Analysis of a Novel Reduced Switch Cascaded Multilevel Inverter,” Journal of Power Electronics, Vol.14, No.1, pp. 48-60. Jan.2014.
- [11] S. Chandrasekar and Gian Carlo Montanari, “Analysis of Partial Discharge Characteristics of Natural Esters as Dielectric Fluid for Electric Power Apparatus Applications,” IEEE Transactions on Dielectrics and Electrical Insulation Vol. 21, No. 3, pp.1251-1259 June 2014.
- [12] S. Ullo, A. Vaccaro, and G. Velotto, “The role of pervasive and coop-erative sensor networks in smart grids communication,” in Proc. 15th IEEE Mediterranean Electro tech. Conf. (MELECON), Apr. 26–28, 2010, pp. 443–447.
- [13] S. Malhara and V. Vittal, “Mechanical state estimation of overhead transmission lines using tilt sensors,” IEEE Trans. Power Syst., vol. 25, no. 3, pp. 1282–1290, Aug. 2010.
- [14] A. Bose, “Smart transmission grid applications and their supporting infrastructure,” IEEE Trans. Smart Grid, vol. 1, no. 1, pp. 11–19, Jun. 2010.
- [15] R.Nagarajan and M,Saravanan “Staircase Multicarrier SPWM Technique for Nine Level Cascaded Inverter,” Proceedings of the International Conference on Power, Energy and Control, IEEE Press, pp-668-675. 2013.
- [16] K. Moslehi and R. Kumar, “A reliability perspective of the smart grid,” IEEE Trans. Smart Grid, vol. 1, no. 1, pp. 57–64, Jun. 2010.
- [17] K. S. Hung, W. K. Lee, V. O. K. Li, K. S. Lui, P. W. T. Pong, K. K. Y. Wong, G. H. Yang, and J. Zhong, “On wireless sensors communication for overhead transmission line monitoring in power delivery systems,” in Proc. 1st IEEE Int. Conf. Smart Grid Commun. (Smart GridComm.), Oct. 4–6, 2010, pp. 309–314.
- [18] Y. C. Wu, L. F. Cheung, K. S. Lui, and P. W. T. Pong, “Efficient communication of sensors monitoring overhead transmission lines,” IEEE Trans. Smart Grid, vol. 3, no. 3, pp. 1130–1136, Sep. 2012.
- [19] R.Nagarajan, S.Sathishkumar, S.Deepika,G.Keerthana,J.K.Kiruthika and R.Nandhini, "Implementation of Chopper Fed Speed Control of Separately Excited DC Motor Using PI Controller", International Journal of Engineering And Computer Science (IJECS), Volume 6, Issue 3, pp. 20629-20633, March 2017.
- [20] J. Chen, S. Kher, and A. K. Somani, “Energy efficient model for data gathering in structured multi clustered wireless sensor network,” in Proc. 25th IEEE Int. Perform., Computed, Commune. Conf. (IPCCC), Apr. 10–12, 2006, pp. 8–388.
- [21] Y. Yang, F. Lambert, and D. Divan, “A survey on technologies for implementing sensor networks for power delivery systems,” in Proc. IEEE Power Eng. Soc. Gen. Meet., Jun. 24–28, 2007, pp. 1–8, vol., no.,
- [22] Y. Yang, D. Divan, R. G. Harley, and T. G. Habetler, “Design and implementation of power line sensor net for overhead transmission lines,” in Proc. IEEE Power Energy Soc. Gen. Meet. (PES), Jul. 26–30, 2009.
- [23] R. G. Olsen and K. S. Edwards, “A new method for real-time monitoring of high-voltage transmission-line conductor sag,” IEEE Trans. Power Del., vol. 17, no. 4, pp. 1142–1152, Oct. 2002.
- [24] S.Gumbo and H. N. Muyingi, “Performance investigation of wireless sensor network for long distance overhead power lines; mica 2 motes, a case study,” in Proc. 3rd Int. Conf. Broadband Commun., Inf. Technol. Biomed. Appl., Nov. 23–26, 2008, pp. 443–450.
- [25] R.Nagarajan, R.Yuvaraj, V.Hemalatha, S.Logapiya, A.Mekala and S.Priyanga," Implementation of PV - Based Boost Converter Using PI Controller with PSO Algorithm, "International Journal of Engineering And Computer Science (IJECS), Volume 6, Issue 3, pp. 20477-20484, March 2017.
- [26] J. G. Proakis, Digital Communications, 4th ed. New York: McGraw-Hill, 2000



S. Suresh received his B.E. in Electrical and Electronics Engineering from Anna University Chennai, India, in 2010. He received his M.E. in Applied Electronics from Anna University, Chennai, India, in 2012. He is currently working toward his Ph.D. in High Voltage Engineering and Communication System at Anna University Chennai, India. He is currently working as a Assistant Professor of Electrical and Electronics Engineering at Gnanamani College of Technology, Namakkal, Tamilnadu, India. His current research interest includes High Voltage Engineering.



R. Nagarajan received his B.E. in Electrical and Electronics Engineering from Madurai Kamarajar University, Madurai, India, in 1997. He received his M.E. in Power Electronics and Drives from Anna University, Chennai, India, in 2008. He received his Ph.D in Electrical Engineering from Anna University, Chennai, India, in 2014. He has worked in the industry as an Electrical Engineer. He is currently working as Professor of Electrical and Electronics Engineering at Gnanamani College of Technology, Namakkal, Tamilnadu, India. His current research interest includes Power Electronics, Power System, Soft Computing Techniques and Renewable Energy Sources.

Research on Multiple Complex Data Processing Methods Based on OpenStack Cloud Platform

Huansong Yang¹, Mengyuan Wang², Jiaping Wu³

¹The Institute for Education Data Hangzhou Normal University, China
Email: hzjyhs@163.com

²The Institute for Education Data Hangzhou Normal University, China
Email: 488533346@qq.com

³The Institute for Education Data Hangzhou Normal University, China
Email: 746780335@qq.com

Abstract—OpenStack is an open source cloud computing management platform project that supports almost all types of cloud environment. It can achieve data processing services among the interactive information storages, and it can also be stored in the virtual machine of cloud computing platform in various services. When performing complex data combination processing, each service cooperates with other services according to the interaction information, and finally completes the processing of complex data.

Keywords— OpenStack, Complex data processing, Cloud computing, Service

I. INTRODUCTION

OpenStack is an open source cloud computing management platform project that supports almost all types of cloud environments and helps service providers and enterprises implement infrastructure as a service (IaaS) similar to Amazon EC2 and S3. The OpenStack cloud platform contains several key projects, including Compute, Identity Service, Networking, Image Service, Block Storage, Object Storage, Telemetry, Orchestration and Database, which can be installed independently and deployed on demand. People can install any of these projects independently, provide independent services through configuration, or communicate with other projects to form a feature-rich and powerful cloud service system.

II. DESIGN OF MULTIPLE COMPLEX DATA PROCESSING

After the study of OpenStack, OpenStack can be achieved based on a number of complex data processing methods, as follows, as shown in Figure 1.

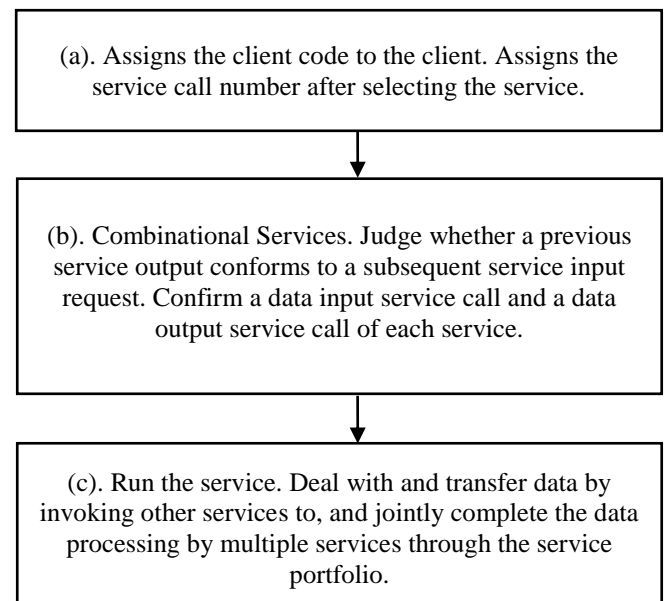


Fig.1: OpenStack based on multiple complex data processing flow chart

(a) Assign a client number to the client. Select the desired service from the service library, and then assign a service call number to this selection for the service.

(b) Combination of selected services. If the former of two services connected to is the data output service call, the latter is for the data input service call, which contains the following process:

(b1) Using the data matching judgment unit to estimate whether the two service output types and the input requirements match, if succeed, then (b3), otherwise the combination is not successful;

(b2) For data output service calls, insert a row of data in the service composition structure database, including: customer number (number of customers assigned for this service composition function), service call number (number of data output service calls, uniquely identifying the service), the next service address (the service address of the data input service call, exposing the service to other

customers or services using the address in the form of a network application interface (WEB API)), the next service call number (number of data entry service calls).

(c) Run the service. Complete the data processing through the way of service combination. For any one of the running of service, it includes the following specific process:

(c1) Receive the data of the previous service, including the next service call number, the customer number parameter, and the data to be processed;

(c2) Processing the received data, completing the data processing function of the service, and outputting the processed data;

(c3) Find the customer number obtained by the Customer Number field in (c1) through the Service Structure database, the service call number field is the line of the next service call number obtained in (c1), To obtain the service after the next service call number and service address, through the service address call the next service, the transfer of the service data, but also includes the customer number, the service after the next service call number.

III. SOLUTION OF MULTIPLE COMPLEX DATA PROCESSING

(a) Assign unique client number C_i to the client, and assign a service call number S_{j,C_i} for each service selected by the client;

Where C_i is the number assigned by the i -th client, S_{j,C_i} is the service call number assigned to the j -th service assigned by the client with the client number C_i , the corresponding service for the sensor data after processing to get the final road traffic data in the process of a sub-processing process;

(b) During the process of selecting a combination, invoke S_{j,C_i} and S_{j+1,C_i} for any two associated connected services respectively correspond to two data processing sub-processes in the traffic data processing process. Among them, comparing with S_{j+1,C_i} , S_{j,C_i} processes output service call for data, and requirement of the output type is $T_{-}S_{j,C_i}(oarg_1, oarg_2, oarg_3, \dots, m)$. Comparing with S_{j,C_i} , S_{j+1,C_i} processes input service call for data, and requirement of the input type is $R_{-}S_{j+1,C_i}(inreq_1, inreq_2, inreq_3, \dots, n)$. The data matching judgment unit is used to tell whether $T_{-}S_{j,C_i}(oarg_1, oarg_2, oarg_3, \dots, m)$ and $R_{-}S_{j+1,C_i}(inreq_1, inreq_2, inreq_3, \dots, n)$ match or not. If the

match succeed, the service invokes the row of data in the service composition database of the server where the S_{j,C_i} is located, including the customer number C_i , the data output service call number S_{j,C_i} , the data input service call address $URL(S_{j+1,C_i})$, and the data input service call number S_{j+1,C_i} .

Where the $T_{-}S_{j,C_i}(oarg_1, oarg_2, oarg_3, \dots, m)$ is the type of the K parameter of the service call TT for the service, m is the number of parameters, and $inreq_t (t = 1, 2, 3, \dots, t \in n)$ is the type of the t -th input parameter of the S_{j+1,C_i} call for the service in the $R_{-}S_{j+1,C_i}(inreq_1, inreq_2, inreq_3, \dots, n)$; $URL(S_{j+1,C_i})$ call the remote service program used by the address for the use of network application program technology.

(c) Run the service. Through the method of service portfolio, jointly complete the massive data processing with the combination of services. The process is shown as follow.

(c1) For any service call number S_{j,C_i} for the service operation, people need to receive the previous service call S_{j-1,C_i} data. The data includes the service call number S_{j,C_i} , the customer number C_i and the data to be processed $Data$. And then process data to complete the service data processing function, obtaining the processed data $RS(Data)$.

(c2) Find the customer number C_i via the service structure database service call number field S_{j,C_i} , so that to obtain the service after the next service call number S_{j+1,C_i} and service address $URL(S_{j+1,C_i})$. Then call the next service through the service address $URL(S_{j+1,C_i})$, and pass S_{j,C_i} processing Data $RS(Data)$, customer number C_i and next service call number S_{j+1,C_i} .

Further, in the step (b), the process of the data matching is: firstly, judging whether m or n satisfies $m = n$. If it is not satisfied, the matching does not succeed. Otherwise, secondly judging whether $oarg_k, inreq_k (k = t, \text{and } k, t = 1, 2, 3, \dots)$ satisfies the condition $oarg_k = inreq_k$ or not. If it satisfies, the match succeeds. Otherwise the match does not succeed.

IV. METHODS OF MULTIPLE COMPLEX DATA PROCESSING

Multiple complex data processing process implementation methods based on OpenStack are as follows:

1. (1) Pick a number of required services from the service list and assign call code to each selected service. For example, s_x ($x=1, 2, 3\dots$) is the service number, $call_id_y$ ($y = 1, 2, 3\dots$) is the service call number. If two or more service numbers are the same service, the input data source and the output destination service processed in the combination are different. There will be the same service number, but different service call number. It is shown in Figure 2.

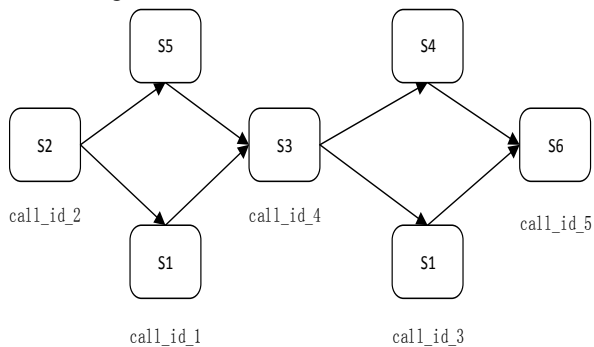


Fig.2: Service call

As shown in Figure 2, s1 is the case. Call the s1 service with the number call_id_1 whose data input source is the s2 service calling the call_id_2, the data output is the s3 service calling the call_id_4 number. And call the s1 service with the number call_id_3, the input data source is called s3 service with the number call_id_4, and the data output is called s6 service with the number call_id_5. These two identical s1 service calls have the same functionality, but belong to different service calls, so the service call number is different.

(2) Assign the customer number $user_id_z$ ($z = 1, 2, 3\dots$), in the service where the server, a service can be used by multiple customers can also be used by the same customer several times, resulting in different service calls. When customer selects a service, the service call number is independent. When different customers choose a service the service numbers may be the same. Therefore, in the server, when different customers call the same service, people can distinguish different service calls through the combination of the customer number and service call number.

For example, s2 is used three times by two clients ($user1_id, user2_id$): the user with the number $user1_id$ is used twice to form two service calls calling call_id_1 and call_id_2. The number of $user2_id$ customers used once, forming a call number call_id_1 service call. At this point, s2 of two service call numbers are call_id_1. But

they belong to different service calls for different clients, so these two different service calls are distinguished by $user1_id + call_id_1$ and $user2_id + call_id_1$.

2. The service side of each service needs to maintain a database of a service composition structure. The database has four fields: $user_id$, $call_id$, $next_call_id$ and $next_service_url$:

User_id: Call the customer number of the service, along with the call_id field, is used to distinguish the service calls to which the service belongs;

Call_id: A service call number for this service, used in conjunction with the user_id field to distinguish service calls to which the service belongs;

Next_call_id: After the end of this service, you need to call the next service call number, in the next service, is used with the user_id to distinguish the next service call

Post service_url: The address of the next service call, after the end of this service, the network application

program interface is used to call the next service;

In the service portfolio structure database, complete the above data modification and insert operation during the process of customer combination. In the $s1 \rightarrow s2 \rightarrow s3$ service composition process, each service composition client has a number. Assume that the current client assigns the number: $user1_id$, S1 service call number is call_id_1, service number is s1_id; S2 service call number is call_id_2, service number is s2_id; S3 service call number is call_id_3, service number is s3_id.

(1) When s1 and s2 are combined, the following events are triggered:

Through the s1 service number s1_id query service library to obtain s1 input data requirements s1_input_type, Output data type s1_output_type, service address s1_url;

Through the s2 service number s2_id query service library to obtain s2 input data requirements s2_input_type, Output data type s2_output_type, service address s2_url;

The data matching judgment unit judges whether the data output type of the S1 and the data input type of the s2 match, and if matched, the following operation is performed:

For the s1 service structure database, insert a row of data, among them, the user_id field is user1_id, the call_id field is call_id_1, the next_call_id field is call_id_2, and the next_service_url field is s2_url.

If not, the combination of s1 and s2 fails.

(2) When using s2 and s3 combination, the trigger event is as follows:

Through the s2 service number s2_id query service library to obtain s2 input data requirements

s2_input_type, Output data type s2_output_type, service address s2_url.

Through the s3 service number s3_id query service library to obtain s3 input data requirements s3_input_type, Output data type s3_output_type, service address s3_url.

The data matching judgment unit judges whether the data output type of the S1 and the data input type of the s2 match, and if matched, the following operation is performed:

For the s2 service structure database, insert a row of data, among them, the user_id field is user1_id, the call_id field is call_id_2, the next_call_id field is call_id_3, and the next_service_url field is s3_url.

If not, the combination of s2 and s3 fails.

Three basic combinations of services and the operation of the process:

Single input single output form, as shown in Figure 3:



Fig.3: Single-input single-output form of service portfolio

Service structure database where service s2 the server maintenance has a row of records, indicating that service output invoked by service invocation is only s3. Assume that the current client assigns an id of: user1_id, s1 service call id is call_id_1, s2 service call id is call_id_2, and s3 service call id is call_id_3.

S2 server in the service structure of the database has a record as shown in Table 1:

Table.1: Structure data record table

user_id	call_id	next_call_id	next_service_url
user1_id	call_id_2	call_id_3	s3_url

The entire calls are as follows:

S1 at the end of data processing, send s1's next service service call number call_id_2, customer number user1_id and source data data1 to the service side of service s2;

S1 accept the original data s2 sent over, and s1 service of the next service call number call_id_2, client number user1_id, s2 processing data1 to get the processed data data2;

Service s2 to find its server-side service structure database, find the call_id for call_id_2, user_id for all user1_id, so as to obtain a call URL for s3_url, and a service call number call_id_3, and through service to address s3_url, call s3 in the form of WEB API, and send data data2 and user number user1_id, the next service call number call_id_3.

Single input multiple output form is shown in Figure 4.

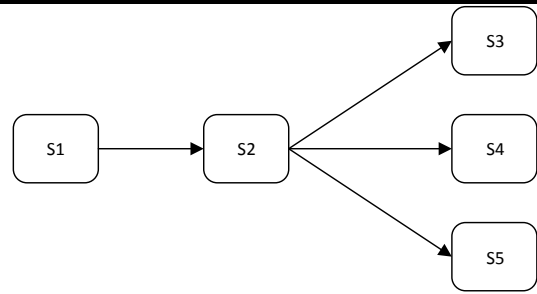


Fig.4: Single-input multi-output form of service portfolio

Service s2 where the service side of the server to maintain the service structure of the database has multiple lines of records, indicating that the service call has multiple calls to the service output. Assume that the current client assigns the number: user1_id. The service call number for s1 is call_id_1. The service call number for s2 is call_id_2. The service call number for s3 is call_id_3. The service call number for s4 is call_id_4. The service call number for s5 is call_id_5.

S2 server in the service structure of the database is shown in Table 2.

Table.2: Service structure data records

user_id	call_id	next_call_id	next_service_url
user1_id	call_id_2	call_id_3	s3_url
user1_id	call_id_2	call_id_4	s4_url
user1_id	call_id_2	call_id_5	s5_url

The entire calls are as follows:

S1 at the end of data processing, send s1's next service call number call_id_2, customer number user1_id and source data data1 to the service side of service s2;

S1 accepts raw data sent by s2, and s1 service of the next service call number call_id_2, client number user1_id, s2 processing data1 to get the processed data data2;

Service s2 to find its server-side service structure database, find the call_id for call_id_2, user_id for all user1_id, so as to obtain a call URL for s3_url, s4_url and s5_url. As well as the corresponding service call number call_id_3, call_id_4, call_id_5, through the service address s3_url, s4_url, s5_url, in the form of network application program interface (web api), respectively call the service s3, s4, s5 and send data data2 and customer number user1_id, and The corresponding next service call number.

Multi-input single output form is shown in Figure 5:

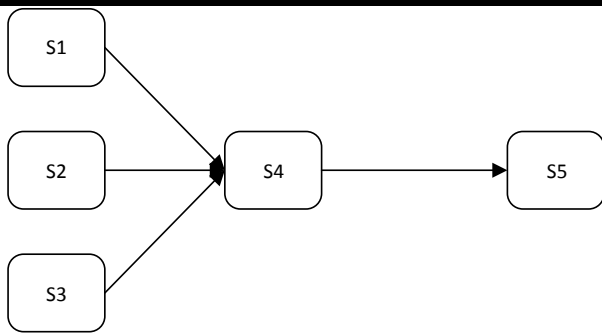


Fig.5: Multi-input single-output form of service portfolio

The service structure database maintained by the S2 server has multiple lines of records, but the output service call is only one. Assume that the current client assigns the number: user1_id, call the S1 service call number call_id_1, S2 service call number call_id_2, S3 service call number call_id_3, S4 service call number call_id_4, S5 service call number is call_id_5.

S2 server in the service structure of the database shown in Table 3:

Table.3: Service structure data records

user_id	call_id	next_call_id	next_service_url
user1_id	call_id_4	call_id_5	s5_url

The entire call processes are as follows:

S3 at the end of the data processing, the next service call number is call_id_4. The client number user1_id and the source data datax are passed to the server of the service s4. (x = 1, 2, 3);

S4 accepts raw data sent by sx., and sx service of the next service call number call_id_4, client number user4_id, s4 processing datax to get the processed data data4; (x = 1, 2, 3);

Service s4 to find its server-side service structure database, find the call_id for call_id_4, user_id for all user4_id, so as to obtain a call url for s5_url, and a service call number call_id_5, and through service to address s5_url, call s5 in the form of WEB API, and send data data4 and user number user1_id, the next service call number call_id_5.

Because the input data of the service is passed through the call of the previous service, all the input sources of the service are single input. The operation of the s4 service is not running under s1, s2, s3, but by s1, s2, s3 call each, so this multi-input single-input mode is equivalent to s1 → s4 → s5, s2 → s4 → s5 and s3 → s4 → s5 combination. Other forms of combination are formed by the above basic combination. And the final data processing is jointly completed by multiple service combinations.

V. CONCLUSION

The above-mentioned OpenStack complex data processing solution can realize the interactive information

storage between data processing services and can be stored in the virtual machine of cloud computing platform where each service is located. When the complex data combination processing is performed, each service in accordance with the interaction of information and other services to coordinate, and ultimately together to complete the processing of complex data. As a client, the required resources can be quickly obtained and the services can be quickly deployed and provided to other users in the form of services. Other users can use the service composition technology to complete the complex data processing process.

ACKNOWLEDGEMENTS

This research was Industry-University Cooperative Education project of Ministry of Education of the People's Republic of China by 2016 and Hangzhou Normal University education reform program and think tank, Program. No.201602034006.

REFERENCES

- [1] Beijing University of Aeronautics and Astronautics. A Method of Constructing Portfolio Path for Cloud - Oriented Manufacturing: China, 10011043, [P].2015-01-13.
- [2] Y. Xia, M. Zhu. Power-aware small world topology in ad hoc networks. Journal of Computers,7(1), Jan. 2012.
- [3] M. Sharma, P. Bedi, K. Chaturvedi, V. Singh, Predicting the priority of a reported bug using machine learning techniques and cross project validation, in: Proceedings of the 12th International Conference on Intelligent Systems Design and Applications, ISDA '12, 2012, pp. 539-545.
- [4] Y. Tian, D. Lo, C. Sun, Drone: Predicting priority of reported bugs by multi-factor analysis, in: Proceedings of the 29th IEEE International Conference on Software Maintenance, ICSM '13, 2013, pp. 200-209.
- [5] Y.Xia, Y.Liu, Z.Ye, W.Wu, M.Zhu. Quadtree-based domain decomposition for parallel map matching on GPS data. Proceeding of 15th IEEE Intelligent Transportation Systems Conference (ITSC 2012), Anchorage, AK, Sep. 2012.
- [6] Liao Jun, Tan Hao, Liu JinDe. Describing and Verifying Web Service Using Pi Calculus[J]. Journal of Computer Science, 2005, 28(4): 635-643.
- [7] OpenStack is the open alternative to proprietary cloud platforms and lock-in , <http://www.rackspace.com/cloud/openstack/>
- [8] XCP Home Page [EB/ OL]. <http://www.xen.org/products/cloudxen.html>, 2011.

- [9] Eucalyptus project [EB/ OL]. Eucalyptus Administrator's Guide, 2011.
- [10] OpenStack Nova Architecture, <http://ken.pepple.info/openstack/2011/04/22/openstack-nova-architecture/>
- [11] Dynamic service composition: state of the art and research directions[R], Department of Computer Science and Electrical Engineering, University of Maryland, USA, <http://www.cs.umbc.edu/~dchakr1/papers/techrepo-rtcomposition.ps>, 2001.
- [12] Xiaolong Wen; Genqiang Gu; Qingchun Li; Yun Gao; Xuejie Zhang. Comparison of open-source cloud management platforms: OpenStack and OpenNebula. *Fuzzy Systems and Knowledge Discovery (FSKD)*, 2012, 9(2457 – 2461).
- [13] F. Wuhib, R. Stadler, and M. Spreitzer, “A gossip protocol for dynamic resource management in large cloud environments,” *Network and Service Management*, IEEE Transactions on, 2014.

Power Quality Issues of Electric Arc Furnace and their Mitigations -A Review

Amarjeet Singh, Ravindra Kumar Singh, Asheesh Kumar Singh

Dept. of Electrical Engineering MNNIT Allahabad, India

Abstract— Electrical Power quality is used to determine the health of the electrical power system that connects the consumer's devices. It is concerned with voltage quality, current quality, reliability of service, quality of power supply etc. Actually the power quality refers to maintaining the sinusoidal waveform of power distribution bus voltage at rated voltage magnitude and frequency. Voltage flicker and harmonics are the main types of power quality problems that are very common to the power system containing electric arc furnace (EAF). Utilities connecting electrical arc furnaces are highly concerned regarding these disturbances and try as far as possible to minimize them. In this paper, EAF is presented for the study of power quality problems and their mitigation. Analysis regarding power quality indices related to both AC and DC type arc furnace has been presented.

Keywords— Electric Arc Furnace (EAF), Flicker Harmonics, Melting and Refining, Power quality.

I. INTRODUCTION

In the past few decades, the use of electric arc furnace has been increased for the production of steel and its alloy throughout the world. Steel production by electric arc furnace route in 2007 was 36% of the total steel production and this share is expected to be increased up to 50 % by 2030. The reason behind is increased use is due its reduced capital cost and less energy required for the production of the steel. The electric arc furnace is either AC or DC operated. It transfers the electric energy to thermal energy (electric arc) to melt the scrap material held by the furnace. The arc produced between the electrodes low voltage and high current supplied by the furnace transformer.

The operation of electric arc furnace can be divided in into intervals namely melting and refining periods. The refining period is further divided in several stages. During the melting stage, the electrode is lowered through a hydraulic actuator system to maintain the stable arc. The furnace draws active power in this condition. More and more buckets of scrap material are added into the furnace during the melting stages. During the refining stage, a long arc is

established. The factors involved during the operation of the furnace are electrode position, electrode arm control scheme, supply voltage, operating reactance and the materials used for melting and refining. The installations of both AC and DC electric arc furnace [1] have been shown in figure 1(a) and figure 1(b) respectively as shown.

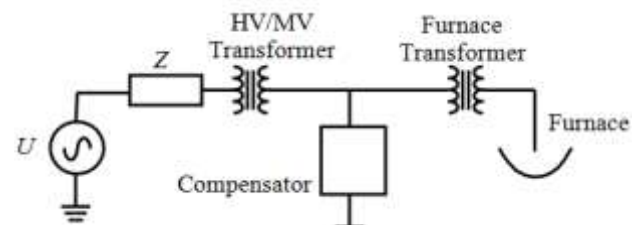


Fig:1(a)

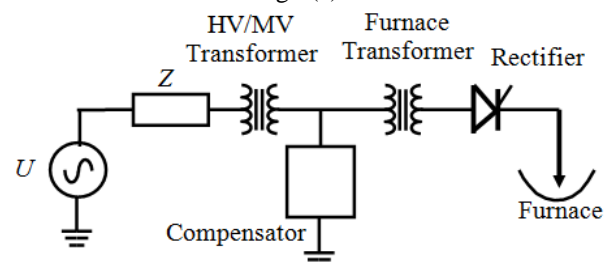


Fig: 1(b)

Fig.1: Installation of Electric Arc Furnace Arc Furnace (a) Installation of AC Arc Furnace (b) Installation of DC Arc Furnace

II. COMMERCIAL USE OF ELECTRIC ARC FURNACE

The electric arc furnace with its high thermal efficiency is suitable for melting down scrap. The electric arc furnace uses about 30% less energy for the same process that the blast furnace and the basic oxygen steelmaking plant. More over in the electric arc furnace scrap can be replaced up to 100% by unreduced iron ore (sponge iron). Electric arc furnace accounts for 51% of the total span of the three basic raw materials (scrap, pig iron and sponge iron), while open hearth furnace take about 17% and basic oxygen converters take about 9%.The growing availability of sponge iron

increases the economics significance of the electric arc furnace. Electric arc furnaces are extremely flexible and can be used in changing circumstances and production levels. It can be used as smelting and refining mode. The electric power can be used in controlled way as per the demand. The electric arc furnace also can be combined with oxygen fuel burner when making special steels.

III. POWER CONVERSION – ELECTRICAL TO HEAT ENERGY

The AC arc furnace is either single phase system or three phase system fed by ac supply system with relatively high reactance. When electrodes are lowered, an arc is produced by high current from electrodes to the scarp held by the furnace. The heat generated by the arc at the temperature up to 3000°C is utilized for melting and refining the scrap held by the furnace.

A DC arc furnace typically consists of graphite electrode (cathode) vertically mounted through an opening in the middle of the furnace roof. The anode connection is in the hearth of the furnace. The anode is in the direct contact of the scrap material to melt. The arc is generated between the tip of the cathode and the upper layer of the scrap held in the furnace. A very high temperature (1500 °C) is generated which is utilized to melt and refine the scrap.

IV. PRINCIPLE OF ARC FURNACE OPERATION

A transformer directly energizes furnace electrodes in a high current circuit in AC arc furnaces, whereas dc furnaces employ a controlled rectifier to supply dc to the furnace electrodes. Arc furnace operation may be classified into stages, depending on the status of the melt and the time lapse from the initial energization of the unit. During the melting period, pieces of steel create momentary short circuits on the secondary side of the furnace transformer. These load changes affect the arc characteristics, causing fluctuations of current. The current fluctuations cause variations in reactive power, which cause a momentary voltage drop or flicker, both at the supply bus and at nearby buses in the interconnected system. The arc currents are more uniform during the refining period and result in less impact on the power quality of the system. Arc furnaces also create harmonic load currents and asynchronous spectral components. Harmonics represent an important power quality issue, because they may cause undesirable operating conditions.

V. DEFINITION OF POWER QUALITY

According to IEEE 1100 standard [2], the power quality is “the concept of powering and grounding sensitive electronic equipment in manner that is suitable to the operation of that equipment and compatible with the premise wiring system and the other connected equipment.” It also understands for the supply reliability, service quality, voltage quality, current quality, quality of supply and the quality of utilizing the electrical power. There are kinds of classifications power quality issues. A few of them classify the events as “steady state” and non steady state phenomena. Duration of the event is the most important factor in ANSI C84.1 standard. IEEE-519 USES the wave shape (duration and magnitude) of each event to categorize the power quality problems. IEC-61000-2-5 standard use the frequency range of the event for the classification of the power quality. As per IEEE-1159 classification, there are three different types of short duration events namely instantaneous, momentary and temporary. Further each category is divided into interruption, sag and swell. Categories and Characteristics of Electromagnetic Phenomena in Power System as defined by IEEE-1159 standard have been shown in appendix.

VI. COMMON DISTURBANCES IN POWER SYSTEMS

The common disturbances in an electrical power system [3] are

- a. Voltage sag
- b. Voltage swell
- c. Momentary interruptions
- d. Transients
- e. Voltage unbalance
- f. Harmonics
- g. Flickers
- g. Voltage fluctuation

VII. ARC FURNACE POWER QUALITY PROBLEMS AND ITS MITIGATION – A REVIEW

J. D. Lavers *et al* [4] describes the detail performance including the harmonic analysis by using a method of data acquisition and analysis of an electric arc furnace. The above method suggested by the author was implemented on a single user minicomputer (a PDP 11/40) and on a large mainframe (IBM 3033). The author proposed harmonic method of analysis by using two software package namely FURNC (create furnace data) and FURNA (analyze furnace data). FURNC utilizes fast Fourier transform methods to compute the current and voltage harmonics. The harmonics produced by FURNC are processed by FURNA to analyze

the specific parameter. The author in his paper presents the two arc furnaces supplied by 33 kV supply by individual 65 MVA on load tap changer furnace transformer. Each arc furnace is fitted with 65 MVA SVC along with filter circuit (2nd, 3rd, 4th, 5th, and 7th). The results are obtained by the furnace during the operation the furnace current harmonics were found to be to the order of one to five percent with second, third and fifth dominating. The harmonic components were found negligible during pellet operation.

Aurelio García-Cerrada et al [5] has compared the performance of TCR based and VSI based flicker compensation experimentally from the arc furnace installation. An electrical arc furnace is a stochastic non linear load [6]. The author has proposed a model for an arc furnace by assuming that whenever there is current, the voltage drop is constant for fixed for fixed arc length.

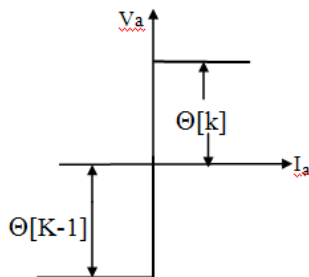


Fig.2: Electric arc I-V characteristic curve

In an arc furnace, the arc length varies with time due to the movement of the electrode and simultaneously the movement of scrap under the electrode. The time varying arc length of the arc length can be modeled as the stochastic process and consequently the proposed arc furnace model is

$$V_a(I_a, \Theta[k]) = \Theta[k] * \text{sign}(I_a) \quad (1)$$

where V_a and I_a are the voltage and current in the arc and $\Theta[k]$ is the parameter directly related to the arc length. The parameter $\Theta[k]$ take different value every time when the electric arc is started that is every time I_a crosses zero. The index k is the counter of the discrete time signal $\Theta[k]$ whose sampling period is $T_s = 0.01$ sec which is the time of half cycle of 50 Hz system. Such a stochastic model of electric arc furnace generates harmonic voltage in the distribution system. The voltage fluctuation of the fundamental component is the origin of flickers [1] in the system. Flicker is due to the variations of the voltage as low as 0.3% and frequencies around 8%. The author used the data collected from the primary of the furnace transformer. The strategy of using TCR and its comparison with PWM-VSI control for flicker compensation was evaluated and it was found that PWM-VSI was superior.

Z. Zhang et al [7] has explained how to measure the flickers produced by the arc furnace and its compensation. The author explained the first Static VAR Generator (SVG) made by the EPRI and Westinghouse in 1986. The performance of SVG was investigated for flicker compensation due to its fast response. SVG has been taken into the circuit to replace the conventional SVC (Static Voltage Compensator) due to its long response time, costly and large in size. It was developed in late 1960s for the compensation of large fluctuating industrial loads. The working of SVG is different from the working of SVC. The SVC can operate selectively connecting passive element with the power line but the SVG is a controlled ac voltage connected to the power line by a reactor. For an arc furnace the response time of SVG is 1ms and for the SVC it is 4-5 ms. The flicker reduction by SVG is 90% whereas by using SVC is of the order of 75%. Harmonic compensation is better for SVG with the same capacity. Size of SVG is reduced by 50% as compared to SVC.

C. S. Chena et al [8] has explained the voltage fluctuation problem and proposed the mitigation of such voltage fluctuation by using SVC. The SVC consists of passive harmonic filter to provide the required amount of reactive power and one TCR for susceptance control. The voltage fluctuation is a big problem during the steel production and for the other industrial customer. The voltage fluctuation problems are generated in the industrial power system containing electric arc furnace due to transient current absorbed by the arc furnace during its early stages of operation. To mitigate the voltage fluctuation, the author proposed the installation of SVC. It is found that the voltage fluctuation is reduced by 0.8% to 0.21% by using SVC.

Omer Ozgun et al [9] has explained that the voltage flickers and harmonic load current are the examples of adverse effects produced by the arc furnace while in operation especially in early stages. The impact of such highly non linear time varying load needs to be investigated. The author proposed to present an arc furnace model in two stages: Dynamic and multivalve voltage – current characteristics of the electrical arc in the first part and generation of low frequency chaotic signal by the simulation of Chua circuit to obtain the voltage fluctuation in the latter part.

The differential equation which represents the dynamics of arc model is based on principle of energy conversion. The following differential equation is given as [10].

$$k_1 r^n + k_2 r \frac{dr}{dt} = \frac{k_3}{r^{m+2}} i^2 \quad (1)$$

Here “r” stands for the arc radius which is chosen as the state variable instead of the arc resistance or the arc conductance. The arc voltage is given as

$$v = \frac{i}{g} \quad (2)$$

where “g” the arc conductance and is given by

$$g = \frac{r^{m+2}}{k_3} \quad (3)$$

The parameters are chosen as $m = 0$ and $n = 2$ for refining stage in the electric arc furnace. The second part of the electric arc furnace is to generate the chaotic signal of the arc voltage. The chaotic component of the arc furnace voltage is supplied from chaotic circuit of Chua [11], [12] which is implemented in Power System Block sets of MATLAB.

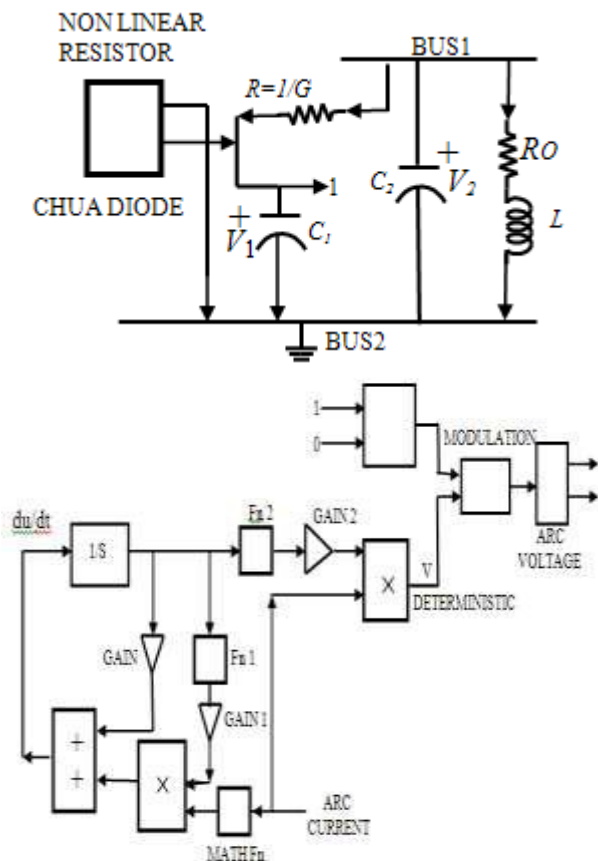


Fig.3: Matlab Implementation of Proposed Arc Furnace

The flicker generated by the simulated voltage waveform at the PCC is calculated by using flicker meter which is presented in IEC 1000-4-15 International Standard [13].

The model of IEC Flicker meter is implemented digitally in MATLAB which basically consists of five blocks as shown in the figure 4. The block 5 executes the online statistical analysis of the statistical analysis of the instantaneous flicker level. In this block, both the short term and long term flicker severity level indices are calculated and the results are displayed.

The output of this block is divided into 64 subclasses according to the instantaneous flicker level.

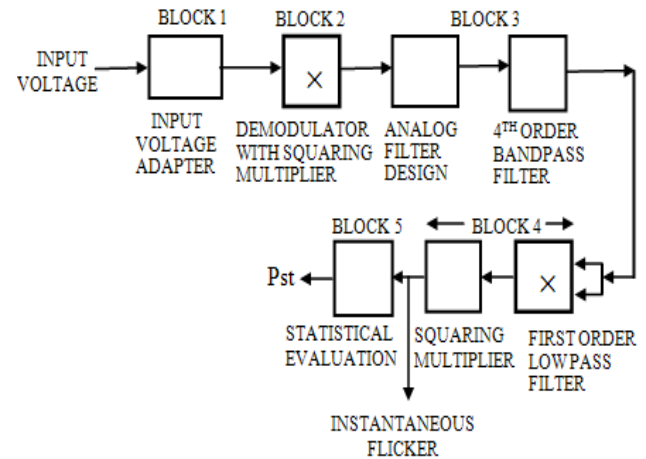


Fig.4: IEC Flicker meter model

Initially the probability distribution function (PDF) is formed by accumulating the number of elements at each level of flicker the cumulative probability function (CPF) can be formed by integrating flicker distribution over the flicker range. The short term flicker P_{st} can be calculated by using the following expression

$$P_{st} = \sqrt{\sum_{i=1}^n k_i P_i} \quad (4)$$

Where k_i is the weighing coefficient and P_i the flicker level these P_i are taken from cumulative distribution curve.

$$P_i = CPF(\eta_i) \quad (5)$$

Where η_i is the particular percent of the observation period. At least five points are normally taken while evaluating short term flicker severity. The short term flicker P_{st} is found to be 1.377 which is a value exceeding 1.00 which indicate that the customer complaint is likely to register.

M.Pamiani et al [14] has presented the benefits of the dynamic reactive shunt compensation by SVC in steel factory. Higher efficiency is the prime importance for the steel industries and to improve the efficiency of the system,

the custom devices such as SVC or STATCOM are used. The author investigated the simulated result of the SVC which eliminates the supply reactance. Additional active power is delivered to the arc furnace when the SVC is in the circuit. Voltage variation is also observed to be low as compared to without SVC in the circuit. Flicker severity level is also calculated by using flicker meter of UIE/IEC type (The Pst is a 10 min integrated value)

$$P_{st99\%} = K_{st} \times \frac{S_{SC EAF}}{S_{SC PCC}} \tag{6}$$

Where Kst is the characteristic emission coefficient for Pst and its value is in between 45-85. SscEAF is the short circuit power at the tip of arc furnace electrode and SscPCC is the short circuit power at PCC. The author also proposed the oversized transformer or use of more transformers which reduces the short circuit impedance between the EAF and network. Pst99% increases at the PCC as the short circuit power increases at the PCC. In this condition the SVC at the arc furnace is the solution. In this condition, the maximum active power transferred is increased but the voltage variation from no load to full load remains the same.

Tongxin Zheng *et al* [15] has proposed an adaptive arc furnace model of arc furnace. According to the author the model is considered to be flexible and accurate. The difference between the proposed model and the existing model is that the control system is included in the model proposed which has been shown in the figure 5.

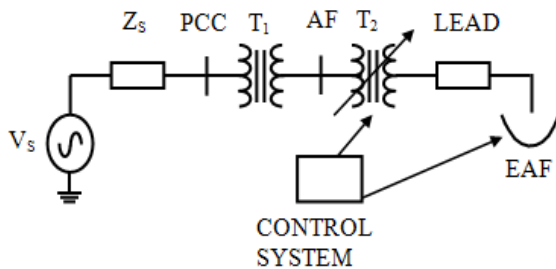


Fig.5: Arc furnace system configuration

As per the author, the adaptive arc furnace model is composed of two parts, the non linear arc model and the controller model. The arc is represented by a non linear current controller resistor. The pattern of the arc generated is determined by the arc length which is controlled by the controller.

The interaction among three components namely supply system, the arc furnace load and the control system constitutes the adaptive arc furnace model. The figure 6

shows the analysis scheme of the adaptive model of the electric arc furnace.

The supply system is assumed to be balanced, the furnace transformer assumed to be an ideal transformer with ratio tp:1 with zero phase shift and the arc furnace load is considered to be operated in balanced condition. Three phase arc voltage are identical with 120° phase shift.

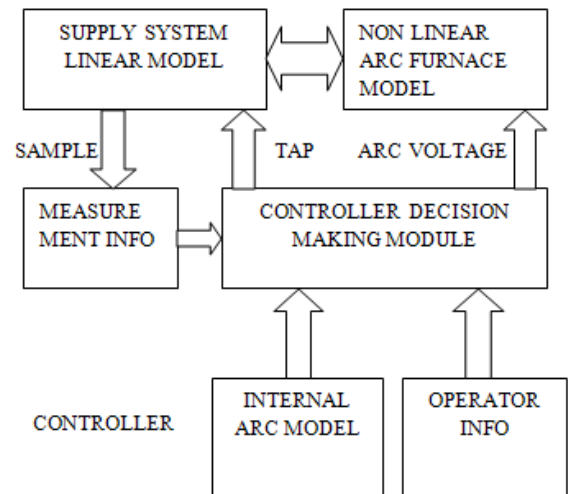


Fig. 6: Adaptive arc furnace model

The arc melting process can be divided into three periods. In the first period the arc begins to reignite from extinction, the arc is established and in the third period the arc begins to extinguish. The arc furnace control basically monitors the electrical and thermal parameters to make the arc furnace operation safe and efficient. The proposed controller is different from the actual controller. Some assumptions are made for the proposed controller.

- (i) Only electrical parameters such as current, voltage and active power are monitored instead of thermal parameters.
- (ii) The controller is assumed as an ideal controller without time delay and response dynamics.
- (iii) The control scheme generates its output every cycle that is every 16.67ms while in actual control system the response time is normally in seconds.

The author has presented only fifth, seventh and eleventh component of harmonics are produced. The current harmonics shows the different characterizations in melting and refining stages. It is found that the contribution of harmonics increases more during melting and reduced in refining stages. The fifth component of harmonic is the greatest component of harmonic and changes with the power input. The voltage harmonic components are found more during refining stage. There is no big change for 5th, 7th and 11th harmonics during refining stage. In first case

the white noise is added to the operating parameter to realize the flicker and in the next case it is observed that the random movement of melting material may change the electrode position which contributes the dynamic phenomena like voltage flicker. The harmonic components of each case are summarized in the Table2.

Table.2: Harmonic component of each four cases

	Harmonics	Case 0	Case1	Case2	Case3
Arc voltage	Fund	275.01	274.62	268.19	273.82
	3rd	N/A	33.33	32.65	32.63
	5th	N/A	20.00	18.83	18.75
	7 th	N/A	14.29	12.44	12.28
	9 th	N/A	11.11	8.92	8.75
	11th	N/A	9.09	6.60	6.42
Arc current	RMS (KA)	62.84	64.38	64.69	62.81
	Fund (KA)	62.75	64.28	64.60	62.71
	5th	4.70	4.67	4.86	5.07
	7 th	2.36	2.39	1.82	1.89
	11 th	N/A	0.97	0.80	0.82
Voltage at AF	RMS (V)	379.00	378.08	376.36	377.14
	Fund	378.00	378.08	376.36	377.14
	5th	N/A	1.89	1.41	1.48
	7 th	N/A	1.28	0.69	0.71
	11 th	N/A	0.89	0.75	0.74

G. Chang *et al* [16] explained that due to the uncontrolled nature of the steel melting process, current harmonics are produced by the arc furnace in a random and unpredictable manner. During melting process in the arc furnace, the arc length (the gap between tip of the electrode and scrap) varies. When the arc length is increased, the oscillation begins to occur due to rapid procession of arc jet around the attachment point on the electrode surface. As the arc length increases further, the arc current produces another transition in temporal behavior from regular oscillation to random and unpredictable motion of the arc. The author has described the power system of electric arc furnace in which the source reactance is small. The utility transformer HV/MV connects the high voltage bus to the medium voltage bus. The furnace transformer MV/LV connects the medium voltage bus to the arc furnace electrodes. An arc furnace produces wide range of harmonics due to current chopping and ignition in each half cycle of ac supply. It is observed that the interharmonics are also produced besides the integer harmonics. The author proposes to install SVC or filter near the arc furnace to reduce 3rd, 5th and higher order harmonics.

Ahmad Esfandiari *et al* [17] discussed the use of Unified Power Quality Conditioner (UPQC) to improve the power quality of the power system connected with electric arc furnace. Series capacitor, series inductor, SVC, passive filter and custom devices such as DVR or DSTATCOM are few compensating devices to improve the power quality of the power system. These devices are having their limitation in their performance. The UPQC consists of series and shunt active filters on a common DC link.

It is used to mitigate the voltage disturbance and compensate the reactive power, harmonics and interharmonics. Since voltages at the point of common coupling (PCC) contain low frequency interharmonics, conventional methods cannot be used for extracting voltage reference signals. The real simulation on a three phase arc furnace of capacity 60 MVA by using UPQC. Voltages found at the PCC before the compensation by using UPQC for 10Hz and 110Hz were found 0.13% and 1.12% whereas after compensation they were found to be reduced by 0.01% and 0.009% respectively.

C. Sharmeela *et al* [18] explained that the voltage flicker is generated in the industrial power system due to large and rapid industrial fluctuating load. Power quality in the electrical power system is affected by the voltage and current harmonics, voltage fluctuation and power factor. Harmonics are generated due to the use of power electronics devices and voltage fluctuation due to the presence of large nonlinear loads such as arc furnace. The author presents the effect of 11kV/0.566 kV, 4Ton AC EAF by installing SVC near the arc furnace. The harmonics and voltage flicker are evaluated with and without the installation of SVC and recorded.

Table.3: Total Harmonic Distortion Voltage and Total Harmonic Distortion Current with Operating Power Factor

	THD-V	THD-I	Power Factor
Without SVC	4.78%	4.975%	0.656
With SVC	2.21%	4.954%	0.857

The voltage flicker at the PCC without SVC is found to be 2% which is more than the permissible limit. After connecting the SVC, the voltage variation is 0.005%. The result shows that there is significant decrease in the voltage variation when the SVC is installed.

M.P. Donsión *et al* [19] has presented the measurement of flicker and its mitigation with SVC on a iron and steel industry containing an AC arc furnace of 83MW (173Ton) with a furnace transformer 120MVA connected by 220 Volt line with power substation where there are other network connected with industrial and domestic consumer. In this paper, arc furnace is considered as an unbalanced, time varying and non linear load which produces many power quality problems such as harmonics, flicker and unbalance in the power system. During the arc furnace operation, the random behavior property of arc melting and its control cause serious power quality problem with the supply system.

Wang Yongning *et al* [20] presented the model of an improved time variant, non linear, three phase electric arc furnace which is based on the stochastic characteristics of arc length and real arc furnace condition. The actual arc furnace installation is not fitted with compensation devices. The arc furnace is a typical load in the power system which injects numbers of harmonic components in the power system whose magnitude changes with the varying loads. The author proposed the system identification technique to estimate the stochastic characteristic. The dynamic arc current and the wave form of bus bar current are obtained which are 22.7% for Ph-A; 12.7 for Ph –B and 21.0% for Ph-C. The total Harmonic Current Distortion at 110kV bus was also found to be 15.9%.

J. Sousa *et al* [21] presented in his paper the guide lines for the estimation for harmonics and flickers produced by the electric arc furnace. Disturbance in form of harmonics and voltage flickers namely are propagated into the distribution system when the electric arc furnace is operated. The cause of components of harmonics are due to the non linear behavior of the current voltage of the electrical arc and the voltage flicker is due the fact that arc length changes during the melting of the scrapes. The author presents 80MW electric arc furnace connected with 30kV/1.1kV, 120MVA furnace transformer, delta star transformer which is connected with utility transformer rated 230kV/30kV, 120MVA. In this paper, the author has evaluated harmonic distortion by using a distributed constant parameter model where as the voltage flicker simulation, nominal pie model is proposed. The voltage THD at PCC and arc furnace bus are obtained as 0.25% and 35.23% respectively and the current THD at PCC and arc furnace bus are found to be 2.08% and 13.26% respectively. The flicker severity index (Pst) at the PCC and arc furnace bus are 2.1 and 4.7 respectively.

I. Vervenne *et al* [22] has shown that the arc furnace converts electrical energy into thermal energy in form of an electrical arc which is used to melt the scrap material held in the furnace. The arc produced between the electrode and the material kept in the melting bath is characterize by the low voltage and high current delivered by the furnace transformer. The author has proposed an arc furnace model based on the power quality point of view. Since the electric arc furnace is responsible to propagate the disturbance in the high voltage network due to its dynamic behavior in melting stage of the operation. Hence such model was required to evaluate the harmonics and the flicker which are the most pronounced and major power quality problems in the power system. The perturbation produced by the arc furnace is of the random nature whether the furnace is supplied by AC or DC. The flicker produced by the arc furnace is variable from one cycle to another and especially during the melting stage the flickers are of high peaks. The flickers are dependent on quantity and quality of scrap, amount of oxygen used during the melting and the crumbling of scrap during melting.

Due to the variable arc length, harmonics are produced. The third harmonic is predominantly produced in such furnace during early stage of the melting. Upper limits of such generated harmonics are given table below.

Table.4: Upper limits of generated harmonics

Harmonics	Melting	Refining
2 nd	5	2
3 rd	20	10
4 th	3	2
5 th	10	10
6 th	1.5	1.5
7 th	6	6
8 th	1	1
9 th	3	3
11 th	2	2
13 th	1	1

DC arc furnace has totally different impact on the power system grid. These furnaces have considerably less flicker. The use of power electronic converter compile with the non linear characteristic DC load produces the harmonics.

E. O'Neill-Carrillo *et al* [23] presented the chaotic dynamics to explain the operation of electric arc furnace which is a non linear load in the power system. The author in this paper has shown the chaotic behavior in the arc furnace current. The Lyapunov Exponent which is the measure of chaotic behavior has been proposed in this

paper. The Lyapunov Exponents are the measure of the rate of divergence (convergence) of state trajectories whose initial conditions are infinitesimally close together. A positive Lyapunov Exponent indicates a net average divergence from initial conditions. This shows the sensitive dependence on the initial conditions and presence of the chaos.

In general there are k Lyapunov Exponents associated with a dynamic process in a k dimensional phase space. The k^{th} exponent is defined as

$$\lambda_k = \ln \left[\lim_{n \rightarrow \infty} (s_{n,k})^{\frac{1}{n}} \right] \quad (1)$$

Whenever the limit exists, $s_{n,k}$ can be regarded as the length of the k^{th} semi axis of the n^{th} iterate of an infinitesimally small ellipsoid of initial condition. The magnitude of largest positive Lyapunov exponent determines the time scale over which the system dynamics becomes unpredictable.

The largest positive Lyapunov exponent λ_1 can be estimated by using Wolf's algorithm [24] and is given by

$$\lambda_1 = \frac{1}{t_M - t_O} \sum_{k=1}^M \log_2 \frac{L'(t_k)}{L'(t_k - 1)} \quad (2)$$

Simulated data was compared with actual arc furnace data to validate the model. The author suggests two perspectives of chaotic dynamics of the arc furnace. The first one explains the detection problems [25] in which the operating level of the EAF is determined by the time series management of the load signals. The second perspective suggests with the modeling of the arc furnace that deals another dynamics of the arc furnace. The author experimentally identified the chaos during the operation single phase electric arc furnace. The Lyapunov Exponent (LE) was used to study the arc furnace data. Table 5 presents the calculation of the currents in the arc furnace. An arc furnace of the capacity 60MVA which is connected with 13.8kV bus is under the consideration and in each case the largest computed exponent is positive between 8 and 12bits/ seconds depending upon the parameters used in Wolf's algorithm.

Table.5: Lyapunov Exponent for 60 MVA EAF

Dimension	Delay (No. of Steps)	Lyapunov Exponent (bits/sec)
4	24	10.78
5	24	10.96

6	24	11.55
7	24	8.53

Table.6: Power Quality Indices for Actual and Modeled data

Index	Actual	Model
THD%	14.11	11.05
K-Factor	1.060	1.061
Zero Peak Flicker factor	0.714	0.646
Crest Factor	1.605	1.578
Lyapunov Exponent	16.89	15.26

Pedro E. Issouribehere *et al* [26] presented the power quality at PCC where an electric arc furnace supplied with alternating current. The quantities measured are current and voltage harmonic, power factor, active power, reactive power and flicker. The power quality is evaluated by comparing the contemporary International and Argentinean standard. Electric arc furnace produces serious electrical disturbances in the power system. Flicker and harmonics are the major power quality issues observed with an arc furnace of 75MW for steel melting was connected at 132kV voltage in the transmission system in Argentina. As per Argentinean regulation, the utility or the power system operator have got the responsibility to ensure the electromagnetic compatibility of the whole system and equipments connected to it. A summary of Flicker Compatibility for LV, MV and HV network [27] is given in the table 7.

Table.7: IEC Flicker Standard

Standard		IEC 61000-3-7 ^[28]	IEC61000-3-7 ^[29]
Purpose		Planning level for controlling emission	Compatibility level for MV network
Objectives at MV	Pst	0.9	1
	Plt	0.7	0.8
Objectives At HV-EHV	Pst	0.8	NA
	Plt	0.6	NA

The minimum required period for assessment is suggested one week and the Pst99% and Plt99% values resulting from the measurement is compared with the allowed 99% or 95% emission limits. The following relationship is considered.

$$Pst99\% = 1.25 Pst95\%$$

$$Plt99\% = 0.84 Plt95\%$$

The Pst measurement summary is given in the Table 8. Flicker level as per the Argentinean regulation is recorded in Table 9.

Table.8: Pst measurement summary

	MV Network	LV Network	HV Network
Scs MVA	905	2800	-----
Flicker Level Pst95%	7.83	2.58	2.01

Table.9: Flicker level as per the Argentinean regulation

MV& HV (1<U≤220Kv) K2=S _l /S _{sc}	Individual Emission Limit
K2≤0.005	0.37
0.005<K2≤0.01	0.46
0.01<K2≤0.02	0.58
0.02<K2≤0.03	0.67
0.03<K2≤0.04	0.74
0.04<K2	0.79

Reference level of voltage harmonic and current harmonic according to ENRE and IEEE and measured and recorded in Table 10 and Table 11 respectively..

Table.10: Reference level of voltage harmonic according to ENRE and IEEE and measured voltage harmonics

	THD	H3	H4	H5	H7	H11	H13
ENRE limit	3	1.5	1	2	1.5	1.5	1.5
IEEE limit	2.5	1.5	1.5	1.5	1.5	1.5	1.5
Pst95 %	1.72	.69	.30	.70	.30	.24	.19

Table.11: Reference level of current harmonic according to ENRE and IEEE and measured current harmonics

	THD	H3	H4	H5	H7	H11	H13
ENRE limit	12	7.5	3.8	6	5.1	2.9	2.2
IEEE limit	4	3.5	0.9	3.5	3.5	1.75	1.75
Pst95 %	4.12	2.1	.88	.86	.46	.27	.25

Table.12: The result of harmonic content of arc furnace current at by IEEE 519 and the result obtained from the measurement

Furnace condition		Harmonic current				
		I ₂	I ₃	I ₄	I ₅	I ₇
Initial melting	Theoretical	7.7	5.8	2.5	4.2	3.1
	Measured	8	7	2.8	3.8	1.4
Refining	Theoretical	--	2.0	--	2.1	--
	Measured	4	2.2	1.2	1	0.5

The flicker level measured in the steel factory is high and more than the reference level at the PCC.

Alfonso Alzate Gomez *et al* [30] presented an arc furnace model based on V-I characteristics which is obtained by the differential equation [31]

Some studies have been suggested to simulate the arc furnace which is based on deterministic [32], [33], Stochastic [34], [35] and chaotic assumptions [36], [37], [38].

The deterministic model of the arc furnace is proposed by modulating the arc radius with sinusoidal signal in form of equation (1)

$$r_s = r[1 + m_s \cdot \sin(\omega t)] \tag{1}$$

Where r_s is the arc radius for the deterministic mode of the arc furnace, r is the arc radius, modulation factor m_s . At a constant frequency of 10Hz and if the value of m_s is 0.025, Pst is close to 1 at PCC.

In stochastic model, the arc length is close to Gaussian distribution and therefore a random signal with such a distribution is used to modulate the magnitude of the arc radius r_s as obtained from equation (1) is presented in (2)

$$r_g = r_s [1 + m_g \cdot \zeta_n] \tag{2}$$

where ζ is the standard deviation from the mean value of a Gaussian distribution which is modulated with factor m_g . For standard distribution values (20%-30%) for each phase and m_g being 0.16, the Pst is 1.0 at the PCC.

In chaotic assumption of the arc furnace model, the magnitude modulation of r_g (a random dynamic) of arc radius with chaotic signal C_h is presented as

$$r_d = r_g \cdot [1 + m_c \cdot C_h] \tag{3}$$

Where the term m_c is the modulation index and C_h is the chaotic normalized signal with low frequency. When m_c is equal to 0.08, the Pst is 1.0 for the voltage at PCC.

Table.13: Harmonic Analysis of the arc furnace current

Component	Peak(%)		
	Ph-A	Ph-B	Ph-C
Fund	100	100	100
2nd	8.02	7.37	6.36
3rd	7.36	6.71	7.74
4th	8.37	7.46	8.15
5th	4.67	4.47	4.29
THD	13.47	11.82	11.37

Table.14: Pst Comparison between real and simulated values

Component	Ph-A	Ph-B	Ph-C
Modeled	1.75	1.57	1.70
Pst99%	1.72	1.78	1.64

The author suggests that this model of electric arc furnace is helpful in the planning stage of new arc furnace on the new distribution system.

G.C. Lazaroiu *et al* [39] presented the power quality problems in a DC arc furnace on a real case application. The author proposed and implemented an ac dc converter control system for power quality improvement by considering flicker and harmonics at the point of common coupling. Two different models of DC furnace are considered in this paper: The deterministic model with sinusoidal disturbance of 10Hz and the random model with a white noise behavior of the disturbance. Proportional Integral Controller is used to minimize the impact of power quality in the AC network. The PCC is maintained at 220 kV line to line, short circuit power is 3500 MVA and the rated power of the DC furnace. The author introduced different power quality indices as follows.

$$THD_I = \sqrt{\sum_{K=2}^{40} \left(\frac{I_K}{I_1}\right)^2} \times 100$$

$$THD_V = \sqrt{\sum_{K=2}^{40} \left(\frac{V_K}{V_1}\right)^2} \times 100$$

$$TIHD_I = \sqrt{\sum_{K=2}^{40} \left(\frac{I_i}{I_1}\right)^2} \times 100 \quad TIHD_V = \sqrt{\sum_{K=2}^{40} \left(\frac{V_i}{V_1}\right)^2} \times 100$$

$$TD_I = \sqrt{THD_I^2 + TIHD_I^2} \quad TD_V = \sqrt{THD_V^2 + TIHD_V^2}$$

where V_1, I_1 are the fundamental value of RMS value of the voltage and current and V_K, I_K are the voltage and current on k_{th} harmonic order. V_i, I_i are the voltage and current on i -th interharmonic order. Without the optimized control the Total Harmonic Voltage Distortion is 8.28% and Total Harmonic Current Distortion is 41.06%. The Pst (50%) is 3.72%.

Tongxin Zhang *et al* [40] presented that the fundamental component of the current drawn by the electric arc furnace produces the fluctuation of the voltage in the local substation. These fluctuations are the responsible for the generation of flicker. The voltage varies as much as 0.3-1% with the frequencies between 2 and 8 Hz. The author proposes the SVC with TCR as the compensating device for the improvement of power quality. The controller of SVC is based on controlling of shunt susceptance which is controlled by changing the firing angle of the thyristor. The presence of controller is to maintain the desired voltage at the bus. In the steady state, the SVC provides steady state voltage to maintain the high voltage bus at the predetermined level. However in case of sudden increase of the load, the voltage of the bus begins to fall below its set point. In such a condition the SVC injects the reactive power into the bus to maintain the voltage of the bus at the desired level. The electrical circuit of the arc furnace supply from substation is shown in the figure 6.

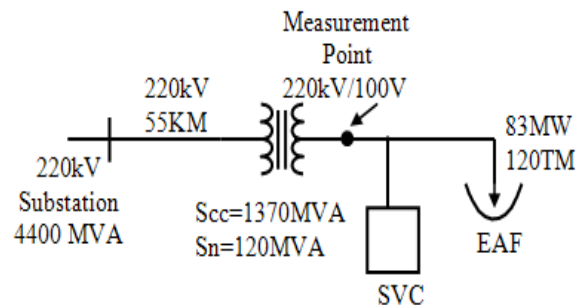


Fig.7: Electrical circuit of the arc furnace supply from Substation

A summary of measured flicker Pst95% at the Steel factory transmitted to substation 55 KM away with and without SVC is presented in the tables given below

A. Flicker measurements without SVC

Table.A.1: Flickers Pst95% at the measurement point

Date	D9	D10	D11	D12	D13
Phase1	0.125	6.031	6.313	6.031	5.938
Phase2	0.156	5.750	6.313	6.375	5.781
Phase3	0.125	5.688	5.625	5.688	5.188

Table.A.2: Pst95% Flicker transmitted to substation

Date	D9	D10	D11	D12	D13
Phase1	0.039	1.878	1.965	1.878	1.849
Phase2	0.049	1.775	1.965	1.985	1.800
Phase3	0.039	1.771	1.751	1.771	1.615

B. Flicker measurements with SVC

Table.B.1: Flickers Pst95% at the measurement point

Date	D16	D17	D18	D19	D20
Phase1	0.156	2.906	3.281	3.313	3.280
Phase2	0.156	2.844	3.281	3.313	3.219
Phase3	0.188	2.750	3.031	3.156	3.094

Table.B.2: Pst95% Flicker transmitted to substation

Date	D16	D17	D18	D19	D20
Phase1	0.049	0.905	1.022	1.031	1.021
Phase2	0.049	0.885	1.022	1.031	1.002
Phase3	0.058	0.856	0.944	0.983	0.963

J. L. Guan et al [41] has presented in this paper that the criteria to estimate the severity of EAF voltage flicker are Maximum Reactive Power Fluctuation Method (MRPFM) [42], [43]. The voltage flicker is calculated by two methods round the world when electric arc furnace AC or DC is operated in the power system. The first flicker meter of IEC standard and established by UIE and the other is ΔV_{10} meter which is established by Japanese Technical Committee. ΔV_{10} method is used by Taiwan Power Company (TPC). The degree of voltage flicker, namely Short Term Flicker Severity (Pst) and 10 Hz equivalent value ΔV_{10} are measured conventionally to characterized the severity of flicker. The investigation carried on AC and DC furnaces reveals that the estimated value of ΔV_{10} measured by conventional method is significantly lower than the surveyed value [44], [45]. The difference between the estimated value and the actual value is quite large.

The author proposed in this paper the maximum complex apparent power fluctuation method (MCAPFM) to overcome the disadvantages of the conventional method. The revised method is based on the fact that the estimated value of ΔV_{10} cannot ignore the effect of active power variation. This method yield more accurate value of ΔV_{10} than the traditional method. During one of the case in a factory, the ΔV_{10} value is in between 0.073% ~ 5.71%

while the ΔV is in between 0.107% ~ 12.543% in the primary side of the furnace transformer at 34.96Kv. In an another case, the ΔV_{10} value is in between 0.138% ~ 6.767% while the ΔV is in between 0.315% ~ 17.081% in the primary side of the furnace transformer.

Douglas Andrews et al [46] has explained that when the electric power is maximized, it affects the productivity of the electric arc furnace operation. Due to the non linear property of electric arc, the significant amount of harmonic current flows in the utility power system. These harmonic current in the power system results the voltage distortion. The author proposed an analytical technique to correct the power factor in a steel factory by field measurement, harmonic analysis and filter design to minimize the harmonic distortion. Power system harmonic was carried out in North Star Steel plant Beaumont, Texas at 13.8kV and 34.5kV voltage level in the power system. Scrap metal and Ladle furnace harmonics have been shown in Table 19.

Table.19: Typical scrap-metal and ladle furnace harmonics

Harmonics	Scrap Furnace	Ladle Furnace
2 nd	5%	2.0%
3 rd	20%	10.0%
4 th	3%	2.0%
5 th	10%	10.0%
6 th	1.5%	1.5%
7 th	6%	6.0%
8 th	1%	1.0%
9 th	3%	3.0%
11 th	2%	2.0%
13 th	1%	1.0%

The voltage THD was found 1.51-8.17% at 13.8% and the current THD in the range of 3.45-9.86%. The voltage THD was found in the range of 0.53- 6.30% during the operation. During extreme sporadic condition of arc furnace, the voltage THD was found to be 19.18%. The current THD was in the range of 3.14-16.08%. The harmonic analysis was carried out by installing the line reactor and 4.7th harmonic filter and it was found that the voltage THD and current THD were 2.63% and 3.83% respectively.

G. W. Chang et al [47] presented the classic and advance models of AC electric arc furnace which is based on the actual recorded data. Electric arc furnace, now days are designed for very large power and due to erratic as well as non linear nature of electric arc, harmonics, flickers and interharmonics are injected in the supply system. Therefore, an accurate model is required for the effective solution of

PQ problem in the power system. The author reviewed two classic models of electric arc furnace such as harmonic current injection model (HCIM) and Harmonic Voltage Source Model (HVSM) and Fast Fourier Transform (FFT) is used to calculate the harmonic component of EAF voltage and EAF current. Due to certain drawback, two advance models of electric arc furnace are proposed by the author namely Cubic Spline Interpolation Method (CSIM) and an improved neural network based method. CSIM is fit to explain the dynamic behavior of the EAF where as the RBFM not only is the accurate model but also describe the dynamic characteristics of the EAF loads.

Arash Dehestani Kolagar *et al* [48] presented the advantages of multiphase transformer in DC arc furnace power supply instead of three phase transformer. By utilizing multi phase transformer, power quality is improved. The transformer has three phases at the primary and multi-phases at secondary. The following Tables 20 and Tables 21 are for three and five phase system and Case-1, Case-2, Case-3 and Case-4 denote the thyristor based power supply with constant current control, DC–DC converter based power supply with constant current control, thyristor based power supply with constant power control and DC–DC converter based power supply with constant power control respectively.

Tables.20: Line current THD values in three phase systems

Feeding Topology	Variable	Min	Max	Mean
Case-1	THDa	0.02025	0.4766	0.2439
	THDb	0.1936	0.4952	0.2218
	THDc	0.1641	0.4807	0.1942
	ITHD	0.1899	0.4842	0.2177
Case-2	THDa	0.1151	0.3108	0.1325
	THDb	0.1151	0.3221	0.1331
	THDc	0.1149	0.3012	0.1321
	ITHD	0.1150	0.3115	0.1326
Case-3	THDa	0.2115	0.5187	0.2554
	THDb	0.2063	0.5325	0.2464
	THDc	0.1805	0.5173	0.2226
	ITHD	0.2008	0.5229	0.2419
Case-4	THDa	0.1069	0.3310	0.1190
	THDb	0.1060	0.3359	0.1187
	THDc	0.1051	0.3073	0.1177
	ITHD	0.1063	0.3250	0.1185

Tables.21: Line current THD values in five phase system

Feeding Topology	Variable	Min	Max	Mean
Case-1	THDa	0.1233	0.4514	0.1588
	THDb	0.1252	0.4551	0.1578
	THDc	0.1173	0.4491	0.1442
	ITHD	0.1225	0.4519	0.1538
Case-2	THDa	0.0381	0.2809	0.0561
	THDb	0.0379	0.2944	0.0570
	THDc	0.0377	0.2715	0.0560
	ITHD	0.0379	0.2824	0.0564
Case3	THDa	0.1351	0.4995	0.1865
	THDb	0.1332	0.4939	0.1818
	THDc	0.1270	0.4950	0.1732
	ITHD	0.1320	0.4961	0.1807
Case4	THDa	0.0403	0.3106	0.0609
	THDb	0.0406	0.3262	0.0615
	THDc	0.0401	0.2935	0.0599
	ITHD	0.0403	0.3104	0.0608

From the above result it is clear that level of harmonic distortion from DC- DC converter based power supply are significantly less than the thyristor power supply.

G. Carpinelli *et al* [49] discussed the problems of the compensation of disturbance of produced by the DC arc furnace while in operation. In previous years, the DC arc furnace is used for the scrap melting and it is replacing the traditional AC arc furnace. The unstable arc causes very rapid change in power absorbed with voltage fluctuation which is responsible for the voltage flicker even if the control system is present. Several compensating devices for the power quality improvement are adopted. The author proposed the active filter, the decoupled compensator and STATCOM are used to comply power quality limit. The following global indices related to power quality in the power system have been considered.

- THD_I And THD_V are the total harmonic distortion factors of current and voltage.
- $THDI_I$ And $THDI_V$ are the total interharmonic distortion factors of current and voltage.
- K-factor
- Pst

Power Quality Indices without and with compensators have been shown in Table 22 and Table 23.

Table.22: Power Quality Indices without compensators.

Power quality indices (%)	Without compensators
THD I	8.45
THD V	11.43
THDI _I	4.10
THDI _V	4.34
K-factor	2.02
Pst	2.07

Table.23: Power Quality Indices with compensators

Power quality indices (%)	Active Filter	stat com	Active Filter& stat com	Decoupled Compen sator
THD I	1.41	6.76	3.08	1.41
THD V	2.07	9.42	3.96	2.51
THDI _I	2.86	3.28	2.05	1.87
THDI _V	1.48	4.43	2.19	1.06
K-factor	1.04	1.97	1.16	1.07
Pst	2.53	0.89	0.66	0.37

From the result obtained in Table 23, it is found that active filter is capable to compensate the waveform distortion and STATCOM is efficient for voltage fluctuation. The decoupled compensator reduces all the power quality indices effectively.

Chi-Jui Wu et al [50] has presented the load characteristics of a DC arc furnace steel factory in which the variation of active power and reactive power is high. The author has proposed the statistical method to understand the load characteristics of DC arc furnace steel factory in Taiwan. The furnace is supplied by a 161kV line. There are three main transformers and the 100MVA transformer supplies the 12 pulse rectifier for 50 Ton DC arc furnace. Four numbers of harmonic filters are at the furnace bus at 33kV. Out of four filters, two are single tune filter and the other two are C- type high pass filter. 2.5% and 97.5% cumulative probability are taken as the maximum and minimum value respectively. The degree of voltage unbalance is the ratio of negative sequence voltage and positive sequence voltage. It is found that the apparent power is in between 60.47~115.27MVA, active power in between 37.95~109.04MW, reactive power between - 47.41~38.43MVAR, voltage between 156~163.25 kV, current between 215.76~426.19 Ampere, Voltage flicker between 0.212~0.941%, total voltage harmonic distortion 0.741~1.09% and the voltage imbalance V^-/V^+ between 0.590~1.06%.

Horia Andrei et al [51] described the electric arc furnace which is used for melting and refining iron metal in steel factory. AC and DC arc furnaces are the most disturbing load in the sub transmission and transmission electric power system. These arc furnaces are characterized by violent change in power that happens during initial stage of melting. The voltage and current characteristics of the electric arc is non linear which results in harmonic current in the power system. The author proposed to use the three phase power analyzer for the power quality analysis and the following quantities are important to be measured such as voltage , current , flicker (IEC 68, IEC 61000-4-15-P_{ST} and P_{LT}), wave shots , THD and harmonics up to the order of 64. Total Harmonic Distortion of voltage and current during melting and refining are presented in Table 24 and Table 25.

Table.24: Harmonic analysis of voltage during melting

	Phase A	Phase B	Phase C
THD V(%)	3.01	2.0	2.92
THD I (%)	10.01	10.73	10.07

Table.25: Harmonic analysis of voltage during refining

	Phase A	Phase B	Phase C
THD V(%)	1.72	1.83	2.0
THD I (%)	4.40	4.74	4.66

In different stages of operation of electrical arc furnace, the THD-I vary between 1-21% for the current and 1-6% for the THD-V. Comparing the value with the international standard; it is observed that the arc furnace does not match with either national or international standard.

H.M. Petersen et al [52] presented that the two models of the electric arc furnace to simulate the arc furnace flicker which is one of the power quality problem in the electric power system. The flicker is severe particularly during the initial bore down period [53]. The above two models present the stochastic values of arc resistance and arc voltage based on the assumption that the arc parameter are closely Gaussian [54].The author also suggested the compensation arrangement such as SVC and synchronous machine.

These are arc voltage and other is the arc resistance and are modeled by using probability technique. The arc voltage depends mainly on the arc length and is given by

$$V_{arc} = \bar{E} + \sigma \left(\sqrt{-2 \ln(\text{rand}1)} \right) \cos(2\pi \text{rand}2) \quad (1)$$

Where rand 1 and rand2 are the uniformly distributed numbers between 0 and 1.

The arc resistance model of the electric arc furnace can be given by

$$R_{arc} = R' + \sigma \left(\sqrt{-2 \ln(\text{rand}1)} \right) \cos(2\pi \text{rand}2) \quad (2)$$

Where the σ is the variance and R be the mean resistance. The author has investigated 33kV arc furnace installation. The furnace is supplied from 275 kV utility networks by two transformers. At 132 kV PCC a HV/MV transformer feeds the furnace transformer which is delta connected secondary from 229 V to 426 V (tap 13). The furnace is simulated for the both the models at the highest tap during bore down period. Measured and Simulated values Flicker without compensation and with compensation are presented in Table 26 and Table 27.

Table.26: Measured and Simulated Flicker values without compensation

Model	Pst Measured	Pst Simulated
Arc Voltage	1.30	1.36
Arc Resistance	1.30	1.33

Table.27: Simulated Flicker values with compensation

Device	Pst Simulated	Reduction Factor/%
40MVA SVC	0.81	1.68/40%
40 MVA Sync. Machine	0.96	1.38/28%
25MVASync. Machine	1.04	1.26/22%

A. Khalik *et al* [55] presented that the electric arc furnace causes the disturbance in the distribution power system due to the distortion in voltage and current due to generated harmonics, flickers, voltage fluctuation and unbalance of voltages. The electric arc furnace suffers from unequalization of three phases due to unbalance arc resistance and inductance of feeding conductors. The author introduced an 80MVA, 20kV/22.5kV/22.5kV, Y/Y/ Δ , main transformer that supplies two electric furnaces of a steel factory through 0.5km cable for Arab Company for special steel. The voltage and current harmonic value were measured for the both the transformers on low and high side during 8 days. Two filters are installed at 22.5kV bus of 12.81MVAR and 15.88 MVAR respectively. Also the TCR of 0.28MVAR is also installed at the bus. The voltage odd harmonic and current odd harmonic value at PCC without filter are tabulated in Table 28 and Table 29. The phase voltage THD and phase current THD at the bus are presented in Table 30 and Table 31.

Table.28: The voltage odd harmonic value at PCC without filter

Odd Harmonic	Max Fund (%)	IEEE-519-992 Max. Limit	Even Harmonic	Max Fund (%)	IEEE-519-992 Max. Limit
3	1.37	3.0	2	1.15	1.5
5	1.73		4	0.50	
7	1.29		6	0.43	
9	0.37		8	0.31	
11	0.66		10	0.30	
13	0.54		12	0.31	
15	0.43		14	0.21	
17	0.50		16	0.20	
19	0.4		18	0.19	
21	0.28		20	0.17	
23	0.27		22	0.19	
25	0.35		24	0.18	

Table.29: The current Odd harmonic value at PCC without filter

Odd Harmonic	Max Fund (%)	IEEE-519-992 Max. Limit	Even Harmonic	Max Fund (%)	IEEE-519-992 Max. Limit
3	58.19	12	2	38.19	3
5	135.12	12	4	12.34	3
7	54.85	12	6	5.56	3
9	4.4	12	8	2.75	3
11	3.32	5.5	10	2.5	3
13	11.36	5.5	12	2.23	1.375
15	1.97	5.5	14	1.91	1.375
17	8.87	5	16	1.4	1.375
19	5.25	5	18	1.24	1.25
21	1.87	5	20	1.28	1.25
23	2.46	2	22	1.45	1.25
25	3.92	2	24	1.41	0.5

Table.30: The phase voltage THD at the bus

Phase	Max THD %	Min THD %	IEEE 519 Max permitted THD %
R	3.7	0.8	5.0
S	3.9	0.8	5.0
T	4.0	0.7	5.0

Table.31: The phase current THD at the bus

Phase	Max THD %	Min THD %	IEEE 519 Max permitted THD %
R	130	1.2	5.0
S	127	1.4	5.0
T	120	1.4	5.0

The author suggests that for the improvement of power quality due to the arc furnace load, a new 5th tuned filter should be connected in addition of already installed 2nd and 3rd filter.

Le Tang *et al* [56] has proposed to develop an EMTP based arc furnace model regarding the generation of flicker in a large steel plant with one or two arc furnace in operation . The dynamic arc presentation is proposed by the author in the initial stage of the melting which is the worst condition of the flicker generation. The author introduces Bayou Steel Company which is supplied by Entergy’s Little Gypsy 230kV switchyard through a 2.5 mile 230 kV transmission line. Initially the company has only one 57 MW arc furnace and in the second phase the company has started another 57MW arc furnace. Due to this proposal the equivalent system strength is reduced from the present 21576-18015 MVA to 13568-10196 MVA. Flicker was measured with one furnace and found to be 0.2 to 0.3%. The author presents the report of the flicker when both the furnaces were put in operation. The prediction of flicker for a single furnace as per the supply system in Europe [57].

The flicker for the single furnace as per Europe [57] is given by

$$P_{st(99)} = \frac{60}{SCR} \tag{1}$$

Where $P_{st(99)}$ is the P_{st} level that exceeds 1% of the time. SCR is the short circuit ratio at the point of common coupling. For more than one furnace, equivalent P_{st} level may be given by

$$P_{st\ total} = \alpha \sqrt{\sum_i P_{sti}^\alpha} \tag{2}$$

Where $\alpha = 3$; $P_{st\ total}$ is total P_{st} resulting from all the furnaces; P_{sti} is due to i^{th} furnace. As per the empirical relationship, for the same size of the electric arc furnace the flicker level for both the furnace must be 26% more than the flicker level of the single furnace. Summary of simulated flicker level at the

Little Gypsy 230 kV bus is presented in Table 32

Table.32: Summary of simulated flicker level at the Little Gypsy 230 kV bus

Fault MVA	One Furnace		Two Furnace	
	$\Delta V/V$ (%)	Unweighted rms Flicker (%)	$\Delta V/V$ (%)	Unweighted rms Flicker (%)
21576	0.28	0.28	0.36	0.43
18015	0.26	0.29	0.41	0.49
15664	0.30	0.33	0.47	0.57
13568	0.35	0.39	0.60	0.75
12203	0.38	0.43	0.68	0.75
10196	0.45	0.52	0.76	0.92

The calculated value of the flicker level at the Little Gypsy (PCC) has been presented in two categories. First in the peak value of the $\Delta V/V$ and the other in unweighted RMS flicker. The maximum value of the acceptable unweighted RMS flicker is 0.5%.

E. A. Cano Plata *et al* [58] has proposed the new idea to present the electrical behavior of the electric arc furnace by the measurement of electric power in stationary and transient imbalance. The new technique adopted in characterizing the behavior the arc furnace is by using time frequency domain. The actual measurement made in the iron and steel company was compared by the electromagnetic transients ATPDraw. Voltage harmonics produced by the arc furnace is recorded in Table 33 below

Table.33: EAF voltage harmonics

Harmonic	Worst Case % Fundamental	Typical% Fundamental
2	17.0	5.0
3	29.0	20.0
4	7.5	3.0
5	10.0	10.0
6	3.5	1.5
7	8.0	3.0
8	2.5	1.0
9	5.0	3.0

The author in this paper presents an power quality indices namely Total Demand Distortion (TDD) of the current which is the ratio of short circuit current (I_{sc}) and load current I_L and is accepted by IEEE- 519 standard. Total Demand Distortion of the current (ITDD) is recorded in Table 34. Total Voltage Harmonic Distortion flicker propagation in different position (actual conditions) are recorded in Table 35 and Table 36.

Table.34: Total Demand Distortion of the current (ITDD)

Indicator	THD Ia	THD Ia3	THD Ia5	THD Ia7
Average	8.40%	0.86%	7.18%	4.05%
Std Deviation	3.52%	0.36%	3.49%	1.67%
Min Value	2.02%	0.18%	0.80%	0.61%
Max. Value	12.58 %	4.19%	24.02%	13.45%
Acceptable THD	15%	12%		

Table.35: Total Voltage Harmonic Distortion

Indicator	THD Va	THD Va 3	THD Va 5	THD Va 7
Average	1.1%	0.3%	0.7%	0.5%
Std Deviation	4.6%	0.1%	0.3%	0.2%
Min Value	0.3%	0.1%	0.1%	0.1%
Max. Value	6.1%	0.7%	1.8%	0.9%
Acceptable THD	5%	3%		

Table.36: Summary of flicker propagation in different position (actual conditions)

Measurement Point	Pst	Plt
Arc Furnace	13.59	12.0
EVOLIS Substation	1.7929	1.9
115kV ACASA Substation	1.2566	1.2
La Enea Substation	1.1548	1.1

Warsaw BROCIK *et al* [59] presented the model of three phase arc furnace considering that the arc is non linear and non linearity that also appears in the windings of the furnace transformer. Voltage and Current distortion is the crucial parameter that describes the power quality. The voltage and current harmonics and the total harmonic distortion in the primary and secondary sides of the arc furnace transformer 30/0.75 kV are evaluated. The utility is at 110 kV and fault MVA level is 500MVA. The PCC is at 30 kV at the fault MVA is 200MVA. The furnace is connected with 30/0.75kV, 75MVA furnace transformer. The values of the current harmonics at PCC, the values of the current harmonics in secondary winding of furnace transformer, the values of the current harmonics at electrodes, the values of the voltage harmonics at PCC, The values of the voltage harmonics in secondary winding of

furnace transformer and the values of the voltage harmonics at electrodes are recorded in Table 37, 38, 39, 40, 41 and 42 respectively.

Table.37: The values of the current harmonics at PCC

Harmonic order	Primary Winding		
	Phase A	Phase A	Phase A
1	1129	1713	1825
3	422	218	211
5	89	236	211
7	22	30	46
9	74	36	82
11	16	62	53
13	10	13	13
15	17	21	36
17	6	14	15
19	8	10	15
21	3	10	14
23	4	5	9

Table.38: The values of the current harmonics in secondary winding of furnace transformer

Harmonic order	Secondary Winding		
	Phase AB	Phase BC	Phase CA
1	18812	28545	30414
3	7037	3640	3519
5	1334	3935	3523
7	364	501	773
9	1234	607	1358
11	267	1037	891
13	170	212	211
15	284	355	606
17	95	231	255
19	139	172	258
21	57	174	230
23	68	70	144

Table.39: The values of the current harmonics at electrodes

Harmonic order	Electrode		
	Phase A	Phase B	Phase C
1	41750	37582	55909
3	10515	10637	1324
5	3592	4702	7342
7	1100	411	1252
9	2523	1392	1705

11	808	1226	1915
13	319	321	388
15	878	213	925
17	308	244	477
19	377	176	416
21	287	118	404
23	211	170	210

Table.40: The values of the voltage harmonics at PCC

Harmonic order	Primary Winding		
	Phase A	Phase A	Phase A
1	23849	24277	23377
3	1593	824	796
5	503	824	796
7	192	265	408
9	837	412	922
11	222	860	739
13	167	208	207
15	321	401	686
17	122	296	327
19	199	264	369
21	90	275	365
23	118	132	249

Table.41: The values of the voltage harmonics in secondary winding of furnace transformer

Harmonic order	Secondary Winding		
	Phase AB	Phase BC	Phase CA
1	1412	1428	1373
3	96	50	48
5	30	89	80
7	12	16	25
9	50	25	55
11	13	52	44
13	10	12	12
15	19	24	41
17	18	20	17
19	15	22	7
21	5	17	22
23	7	8	15

Table.42: The values of the voltage harmonics at electrodes

Harmonic order	Electrode		
	Phase A	Phase B	Phase C
1	789	968	693
3	159	67	116
5	37	24	110
7	29	18	17
9	67	31	55
11	26	18	47
13	11	12	21
15	23	9	28
17	17	12	10
19	7	8	21
21	9	4	13
23	11	4	6

The results obtained for the harmonics estimation determine the propagation of voltage and current in the electric power system.

VIII. CONCLUSION

The associate problems and the issues related to the Power Quality in an electric power system that a customer encounter depends how the wave form of the voltage and current are distorted. There are numbers of power quality problems mentioned the review above namely voltage and current harmonics, flickers, voltage imbalance, transients, interharmonics, sag, swells etc. Among them harmonics and flickers are the most important power quality issues are found in the power system containing electric arc furnace. Major power quality indices are found to be more than the standard limit set by recognized international standard agencies especially during the melting stage of the operation. The information of the power quality indices related to the arc furnace obtained will be helpful to understand the mitigation technique.

REFERENCES

- [1] Reuben F. Burch IV, Senior Member, IEEE “Thoughts on Improving the Electric Arc Furnace Model”
- [2] IEEE 100, The Authoritative Dictionary of IEEE Standard Terms, seventh edition, 2000, p. 234.
- [3] E.R.”Randy” Collins, J.R. PhD, PE Chair, Working Group of Monitoring Eledftric Power Quality.onitoring Electric Power Quality. IEEE Standard 1159: Recommended Practices for Monitoring Electric Power Quality – A Status Updates

- [4] J. D. LAVERS, Member, IEEE, Behnam Danai, P. P. Biringer, Fellow, IEEE, and Donald J. Chia-Ling, Member, IEEE “A Method of Examining in Detail Electric Arc Furnace Performance” IEEE transactions on industry applications, vol. ia-21, no. 1, January/February 1985
- [5] Aurelio García-Cerrada, Member, IEEE, Pablo García-González, Rafael Collantes, Tomás Gomez, Member, IEEE, and Javier Anzola “Comparison of Thyristor Controlled Reactors and Voltage-Source Inverters for Compensation of Flicker Caused by Arc Furnaces” IEEE transactions on power delivery, vol. 15, no. 4, October 2000
- [6] Rafael Collantes-Bellido, Tomas Gomez, Member, IEEE “Identification and Modeling of a Three Phase Arc Furnace for Voltage Disturbation Simulation. IEEE Transactions on Power Delivery, Vol. 12, No. 4, October 1997
- [7] Z. Zhang, student, N. R. Fahmi, MIEE CEng., W. T. Norris, MIEE “Flicker Analysis and Methods for Electric Arc Furnace Flicker (EAF) Mitigation (A Survey)”
- [8] C. S. Chena, H. J. Chuanga, T. Hsu, S. M. Tseng “mitigation of voltage fluctuation for an industrial customer with arc furnace”
- [9] Omer Ozgun and Ali Abur “Flicker Study Using a Novel Arc Furnace Model” IEEE transactions on power delivery, vol. 17, no. 4, October 2002
- [10] E. Acha, A. Semlyen, and N. Rajakovic, “A harmonic domain computational package for nonlinear problems and its application to electric arcs,” IEEE Trans. Power Delivery, vol. 5, pp. 1390–1397, July 1990.
- [11] M. P. Kennedy, “Three steps to chaos, Part 1: Evolution,” IEEE Trans. Circuit Syst. I, vol. 40, no. 10, pp. 640–656, October 1993.
- [12] “Three steps to chaos, Part 2: A Chua’s circuit primer,” IEEE Trans. Circuits Syst. I, vol. 40, pp. 657–674, Oct. 1993.
- [13] “Flickermeter-Functional and Testing Specifications,” CEI, IEC Publ. 61 000-4-15, 1997.
- [14] M. Pamiani, Assistant professor, H. Mokhtari, Assistant professor, M. Hejri, Graduate Student “Effects of Dynamic Reactive Compensation in Arc Furnace Operation Characteristics and its Economic Benefits”
- [15] Tongxin Zheng, Student Member, IEEE, and Elham B. Makram, Senior Member, IEEE “An Adaptive Arc Furnace Model” IEEE transactions on power delivery, vol. 15, no. 3, July 2000
- [16] G. Chang (chair), C. Hatziadoniu (vice chair), W. Xu (past chair), P. Ribeiro (past vice chair), R. Burch, W. M. Grady, M. Halpin, Y. Liu, S. Ranade, D. Ruthman, N. Watson, T. Ortmeier, J. Wikston, A. Medina, A. Testa, R. Gardinier, V. Dinavahi, F. Acram and P. Lehn. “Modeling Devices with Nonlinear Voltage-Current. Task Force on Harmonics Modeling and Simulation Characteristics for Harmonic Studies” IEEE transactions on power delivery, vol. 19, no. 4, October 2004.
- [17] Ahmad Esfandiari, Mustafa Parniani and Hussein Mokhtari “Mitigation of Electric Arc Furnace Disturbances Using the Unified Power Quality Conditioner” The 3Mh Annual Conference of the IEEE Industrial Electronics Society, November 2 - 6, 2004, Busan, Korea
- [18] C. Sharmeela, G. Uma, M.R. Mohan and K. Karthikeyan “Voltage Flicker Analysis and Mitigation-Case Study in AC Electric Arc Furnace Using PSCAD/EMTDC” 2004 International Conference on Power System Technology - POWERCON 2004 Singapore, 21-24 November 2004
- [19] M.P. Donsión, F. Oliveira “AC Arc Furnaces Flicker Measurement without and with a SVC System Connected”
- [20] Wang Yongning, Li Heming, Xu Boqiang, Member, IEEE, Sun Lilhg, Student Member, IEEE “Simulation Research of Harmonics in Electric System of Arc Furnace” 2004 International Conference on Power System Technology - POWERCON 2004, Singapore, 21-24 November 2004
- [21] J. Sousa, M.T. Correia de Barros M. Covas A. Simões “Harmonics and Flicker Analysis in Arc Furnace Power Systems”
- [22] I. Vervenne, Student Member, IEEE, K. Van Reusel and R. Belmans, Fellow, IEEE “Electric Arc Furnace Modeling from a “Power Quality” Point of View” 3rd IEEE Benelux young researchers symposium in electrical power engineering 27-28 April 2006, Ghent, Belgium
- [23] E. O’Neill-Carrillo G.T. Heydt E.J. Kostelich S.S. Venkata A. Sundaram “Nonlinear Deterministic Modeling of Highly Varying Loads” IEEE Transactions on Power Delivery, Vol. 14, No. 2, April 1999
- [24] A. Wolf, J. Swift, H. Swinney, J. Vastano, “Determining Lyapunov Exponents from a Time Series,” *Physica D*, vol. 16, 1985, pp. 285-317.
- [25] G. T. Heydt, E. O’Neill-Carrillo, R. Y. Zhao., “The Modeling of Nonlinear Loads as Chaotic Systems in Electric Power Engineering,” Proceedings of the 1996

- IEEE PES International Conference on Harmonics and Quality of Power, Las Vegas, Oct. 1996, pp. 704-711.
- [26] Pedro E. Issouribehe, Juan C. Barbero, Fernando Issouribehe, IEEE Member, and Gustavo A. Barbera "Power quality measurements in a steel industry with electric arc furnaces"
- [27] Joint Working Group CIGRÉ C4.07/CIRED. Power Quality Indices and Objectives. Final WG Report. January 2004.
- [28] IEC 61000-3-7:1996-Assessment of Emission Limits for Fluctuating Loads in MV and HV Power Systems, technical report type 3.
- [29] IEC 61000-2-12:2003-04: Electromagnetic Compatibility (EMC)-Part 2- 12: Compatibility levels for low-frequency conducted disturbances and signaling in public medium-voltage power supply systems.
- [30] Alfonso Alzate Gomez, Jessor J. Marulanda Durango, Andres Escobar Mejia "Electric Arc Furnace Modeling for Power Quality Analysis
- [31] E. Acha, A. Semlyen and N. Rajakovic, "A harmonic domain computational package for nonlinear problems and its applications to electric arcs", IEEE Trans. Power Delivery, vol. 5, pp. 1390-1397, Jul. 1990
- [32] G. C. Montanari, M. Loggini, A. Cavallani and D. Zaninelli, "Arc furnace model for the study of flicker compensation in electrical networks," IEEE Trans. Power Delivery, vol. 9, pp. 2026-2036, Oct. 1994.
- [33] R. Horton, T. Haskew and R. F. Burch "A time domain AC electric arc furnace model for flicker planning studies," IEEE Trans. Power Delivery, vol. 24, pp. 1450-1457, July. 2009.
- [34] G. Manchur and C.C. Even, "Development of a model for predicting flicker from arc furnaces," IEEE Trans. Power Delivery, vol. 7, pp. 416- 426, Jan. 1992.
- [35] V. Srinivas, B. Elham and A. Adly , "A New Time Domain Voltage Source Model for an Arc Furnace using EMTP", IEEE Transactions on Power Delivery, Vol 11, No. 3, July 1996.
- [36] O. Ozgun and A. Abur, "Development of an arc furnace model for power quality studies," Proc. IEEE -PES Summer Meeting 1999, vol. 1, pp. 507-511, 1999.
- [37] E. O'Neill-Carrillo, G. Heydt, E. J. Kostelich, S. S. Venkata, and A Sundaram "Nonlinear deterministic modeling of highly varying loads," IEEE Trans. Power Delivery, vol. 14, pp. 537-542, Apr. 1999.
- [38] G. Carpinelli, F. Iacovone, A. Russo and P. Varilone, "Chaos-based modeling of dc arc furnace for power quality issues", IEEE Trans. Power Delivery, vol. 19, pp. 1869-1876, Oct. 2004.
- [39] G.C. Lazaroiu, D. Zaninelli "A control system for dc arc furnaces for power quality improvements" journal homepage: www.elsevier.com/locate/epsr; Electric Power Systems Research 80 (2010) 1498–1505
- [40] Tongxin Zhang, Eltham B. Makram, "An Adaptative Arc Furnace Model", IEEE Trans. Power Delivery, Vol.15, pp. 931-939, July 2000.
- [41] J. L. Guan, J. C. Gu, M. T. Yang, and H. H. Chang "New Assessment and Prediction for Arc Furnace Flicker".
- [42] New trend in supply problems of arc furnace for steel plants, Japanese: Elect. Eng. Soc., 1978, vol.2, no.72, pp.3-26.
- [43] The Survey of DC Arc Furnace, Japanese: Nihon Kou-Kan Co., NKK, Technical Report, 1989.
- [44] J. C. Gu, C. J. Wu, and J. C. Chiang, "Effects of High Voltage Side Voltage Flicker Sources on Low Voltage Side Customers," Power Research Institute, Taiwan Power Company, 1994.
- [45] C. J. Wu and J. C. Gu, "Measurement and Analysis of Voltage Flicker," Power Research Institute, Energy Commission, Ministry of Economic Affairs, Technical Report, 2000
- [46] Douglas Andrews, Member, IEEE, Martin T. Bishop, Senior Member, IEEE, and John F. Witte, Member, IEEE "Harmonic Measurements, Analysis, and Power Factor Correction in a Modern Steel Manufacturing Facility"
- [47] G. W. Chang, Senior Member, IEEE, Y. J. Liu, and C. I Chen, Student Members, IEEE "Modeling Voltage-Current Characteristics of an Electric Arc Furnace Based on Actual Recorded Data: A Comparison of Classic and Advanced Models"
- [48] Arash Dehestani Kolagar, Abbas Shoulaie "Power Quality Improvement in DC Electric Arc Furnace Plants Utilizing Multiphase Transformer. ISBN: 978-1-4673-0113-8/12/2012IEEE
- [49] G. Carpinelli, member, IEEE, and A. Russo, member, IEEE "Comparison of some of active devices for the compensation of DC arc furnace".
- [50] Chi-Jui Wu, member, Tsu-Hsun Fu, You-Jen Chen "Load Characteristics and harmonic Analysis of DC arc furnace"
- [51] Horia Andrei, Costin Cepisca and Sorin Grigorescu "Power Quality and Electrical Arc Furnaces"
- [52] H.M. Petersen, R.G. Koch, P.H. Swart, R. van Heerden "Modeling Arc Furnace Flicker and Investigating Compensation Techniques"

[53] Manchur, G., Erven, C.C.: 'Development of a Model for Predicting Flicker from Electrical Arc Furnaces', IEEE Transactions on Power Delivery, Vol. 7, No.1, January 1992.

[54] Lavers, D., Danai, B.: 'Computer Evaluation of Electrical Arc Furnace Disturbances', Paper No. 83143 IEEC, 1983.

[55] H.A. Khalik, M. A. Aziz, and E. Farouk "Improvement of Power System Distribution Quality Due to Using Dc-Converter Loads and Electric Arc Furnaces" New York Science Journal, 2011;4(12)

[56] Le Tang Member, IEEE, Sharma Kolluri, Senior Member, IEEE, Mark F. McGranaghan, Member, IEEE "voltage flicker prediction for two simultaneously operated ac arc furnaces"

[57] A. Robert and M. Couvreur, "Arc Furnace Flicker Assessment and Prediction," 12th International Conference on Electricity Distribution (CIRED), Paper 2.02, Birmingham, England, May 17-21, 1993.

[58] E. A. Cano Plata, Member, IEEE, A. J. Ustariz Farfan, Member, IEEE, O. J. Soto Marin, Member, IEEE "Electric Arc Furnace Model in Distribution Systems. 978-1-4799-2288-8/14 © 2014 IEEE

[59] Wiesław BROCIĘK1, Robert WILANOWICZ2, "Estimation of voltage and current distortions in the power system supplying the AC arc furnace"

2.2.3 Swell		30 cycles–3s
2.3.1 Interruption		
2.3.2 Sag		3 s–1 min
2.3.3 Swell		3 s–1 min
3.0 Long-duration variations		
3.1 Interruption, sustained		>1 min
3.2 Under voltages		>1 min
3.3 Overvoltage		>1 min
4.0 Voltage imbalance		Steady state
5.0 Waveform distortion		Steady state
5.1 Dc offset		
5.2 Harmonics	0–100 Hz	
5.3 Interharmonics	0–6 kHz	
5.4 Notching		
5.5 Noise Broadband		
6.0 Voltage fluctuations	>25 Hz	Intermittent
7.0 Power frequency variations		<10 s

APPENDIX

Categories	Typical Spectral Content	Typical Duration
1.0 Transients		
1.1 Impulsive		
1.1.1 Nanosecond	5 ns rise	<50 ns
1.1.2 Microsecond	1 μs rise	50 ns–1 ms
1.1.3 Millisecond	0.1 ms rise	>1 ms
1.2 Oscillatory		
1.2.1 Low Frequency	<5 kHz	0.3–50 ms
1.2.2 Medium Frequency	5–500 kHz	20 μs
1.2.3 High Frequency	0.5–5 MHz	5 μs
2.0 Short-duration variations		
2.1 Instantaneous		
2.1.1 Sag		0.5–30 cycles
2.1.2 Swell		0.5–30 cycles
2.2 Momentary		
2.2.1 Interruption		0.5–30 cycles
2.2.2 Sag		30 cycles–3s

Energy Audit for an educational building which operates in Middle East climatic conditions

Salim R K, Dr Sudhir CV

Caledonian College of Engineering, P.O. Box 2322, CPO 111 Seeb, Muscat, Sultanate of Oman

Abstract— The Energy Audit done for an educational building which is working for last 20 years in the Middle East region. This region has extreme climatic conditions for both summer and winter. In summer the temperature reaches up to 48^oc or 49^oc. The energy consumption comes high at summer season. The audit conducted for electric energy consumed largely for air conditioning as well as other uses like lighting and teaching accessories. Important results getting with retrofitting the building envelop and change of lightings to LEDs. Simple payback period got as 5.49 years. A considerable savings in carbon emission is also accounted as a result of this retrofitting.

Keywords— Energy audit, Building envelop, Energy Conservation Measures, Energy load profile, Simple payback period.

I. INTRODUCTION

Energy usage and its audit is a crucial business for any establishment. The financial benefits through the energy savings are not negligible and more important in the present energy scenario. On the other hand, the energy savings is the savings for the better environment. Auditing the energy usage and finding ways to reduce the expenses in energy utilization plays a vital role for any business establishment. The energy audit encompasses analysis of energy usage for each and every usage points within the building.[1] This audit will give out the measures to improve energy efficiency of all the equipment or facilities which uses the energy. These measures should not affect any normal performance of the building or the establishment. The ultimate aim of the energy audit is reducing the energy usage without any negative impact for the establishment and provides better savings on the long run.

Objectives of energy audit may vary according to the asset management policy. Usually it aims to understand how energy is used within the system and to find efficient measures for improvement of energy efficiency [2]. The energy audit is being done as per the type of industry or asset, functions, size of the industry and the depth of energy utilization etc. Mainly the energy audit can categorized in to two such as preliminary audit or walk through audit and the detailed audit or diagnosis audit.

Tailored rating observations are followed in this audit. The aim of the tailored rating observation is the simulation of the real conditions and behavior of the building in order to the specific requirement during the operations [3]. This approach gives an accurate results and evaluations.

Making an inventory of all electrical loads aims to answer two important questions: where the electricity is used? How much and how fast is electricity used in each category of load? By analyzing these two questions, the prioritization of the electricity-saving opportunities can be done [4]. Magnitude of energy loads is also monitored.

II. ENERGY AUDIT PREPARATION FOR THE SELECTED BUILDING

Initially the audit criteria to be defined for an effective energy audit benefits. For the selected building, following criteria has taken in to consideration. The building chosen for this energy audit is the one from a leading engineering college in Muscat, Oman. The campus includes several buildings for academic and administration uses. The building selected is centrally located which includes an assembly hall in first floor and some lecture halls on the ground floor. An IT server room is also operates from the energy connectivity of this building. The building includes common utility spaces and two store cases. All the interiors of the building are equipped with air conditions and the lightings provided throughout the spaces. The building operates minimum 12 hours per day and five days a week.

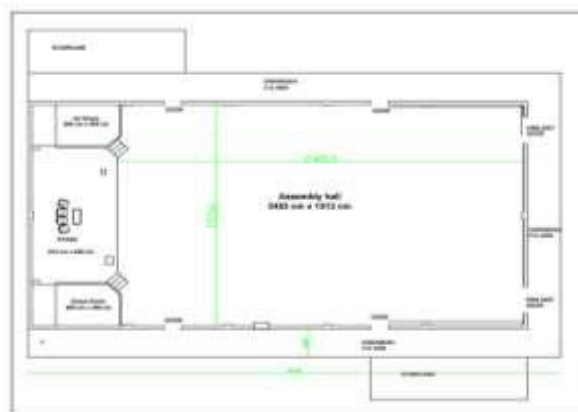


Fig.1: Lay out of Assembly Hall building

The audit plan aims to bring out the energy usage profile for the building and detailed analysis of Air Conditioning and lighting systems. Since the building particularly includes an assembly hall, the air conditioning and lighting have to be assessed for the best performance in minimum energy usage. Assembly hall meant for gathering group of people and the comfort level is of course very important. If the optimum conditions for comfort and energy usages are not achieved, higher difference in consumption will happen. Preliminary audit or walks through audit have to be done at the beginning for an overall observation of the functions of the building. This will brought out the frequency and period of usage of all the functions of the building. The detailed audit or diagnosis audit performed for each system wise analysis of the existing usage.[5]

III. METHODOLOGY

The building uses only electricity energy from the government grid. The electricity connection already isolated from the other buildings in campus. The energy bills and energy meter readings collected from the central services of the college. They recorded energy meter readings daily basis. The peak summer usages are avoided since the assumptions and the estimates may be deviated from the root cause. The Muscat region comes high summer temperatures and excessive usage of air conditioning systems. That season to be studied separately.

The energy meter gives directly the kWh readings. The reading gives only the total usage, since the energy meter is connected to input of the electric panel. The smart WiFi energy meter used to find the individual usage of the systems particularly air conditioners for detailed diagnosis.

IV. ANALYSIS OF ENERGY USAGE

4.1 monthly bills

Analysis of energy usage can be best utilized the regularly provided electricity bills. When considering the electricity bills it has to be considered for the different components of the unit charges. The electricity charge includes only charges for used energy units. Bill charges for 1 kWh is OMR 0.020. The municipal dues as 0.02% of the energy usage charge. There is no extra slab for quantum of usage or peak period usage. The classification provided only about commercial or domestic. In both the cases the electricity charges are well subsidized.

Table.1: Energy meter readings and effect days for the selected period of operations in OMR

#	Month	Bill date	Current reading	Previous reading	Units Consumed	No of Days	Charges	Municipal dues	Total Charges
1	42656	21/10/2013	541140	520619	20521	29	410.420	8.208	418.628
2	42687	24/11/2013	562589	541140	21449	34	428.980	8.580	437.560
3	42717	22/12/2013	576081	562589	13492	28	269.840	5.397	275.237
4	42383	31/01/2014	593025	576081	16944	36	338.880	6.778	345.658
5	42414	28/02/2014	605779	593025	12754	28	255.080	5.102	260.182
6	42443	31/03/2014	631313	605779	25534	31	510.680	10.214	520.894
7	42474	30/04/2014	648678	631313	17365	30	347.300	6.946	354.246
8	42504	31/05/2014	668937	648678	20259	31	405.180	8.104	413.284
9	42535	30/06/2014	680393	668937	11456	30	229.120	4.582	233.702
10	42565	16/07/2014	695954	680393	15561	16	311.220	6.224	317.444
11	42596	27/08/2014	721804	695954	25850	42	517.000	10.340	527.340
12	42627	23/09/2014	743387	721804	21583	27	431.660	8.633	440.293
13	42657	22/10/2014	761496	743387	18109	29	362.180	7.244	369.424
14	42688	18/11/2014	777765	761496	16269	27	325.380	6.508	331.888
15	42718	23/12/2014	797032	777765	19267	35	385.340	7.707	393.047
16	42384	22/01/2015	810223	797032	13191	30	263.820	5.276	269.096
17	42415	17/02/2015	820393	810223	10170	26	203.400	4.068	207.468
18	42444	15/03/2015	834419	820393	14026	26	280.520	5.610	286.130
19	42475	19/04/2015	858874	834419	24455	35	489.100	9.782	498.882
20	42505	19/05/2015	884535	858874	25661	30	513.220	10.264	523.484

4.2 Lighting

Florescent tube lights are using for the entire lighting except the stage lighting in the hall. Each fluorescent lighting units carries four tubes of 18w capacity. The main hall is using only on demand and the other lecture hall are using for regular teaching activities. On all this usages lights are in full use for the time period. A detailed data is available for Assembly hall usage for two years. From that data the average usage for the Assembly hall per month is 63 hours. The Table.2 provided here is the observation from the walk through survey. In lecture hall usage per day is 10 hrs and weekly 5 days. I took 23 work days per month for finding monthly usage. Common passage lightings are using on all evening of work days. Passage lights are using daily at least 3 hours and a support usage found with nominal lighting throughout the night.

Table.2: Survey on lighting inventory

#	Area	Type of lighting	Number of units	Energy load in kW	Average usage per	Monthly Energy in kWh
1	Assembly hall	Florescent tubes 4 x 18 = 72w	60	4.32	63	272.16
2	Stage&green room	LED units 14 w	14	0.196	63	12.348
3	Lecture hall 1	Florescent tubes 4 x 18 = 72w	18	1.296	230	298.08
4	Lecture hall 2	Florescent tubes 4 x 18 = 72w	18	1.296	230	298.08
5	Lecture hall 3	Florescent tubes 4 x 18 = 72w	18	1.296	230	298.08
6	Lecture hall 4	Florescent tubes 4 x 18 = 72w	18	1.296	230	298.08
7	Lecture hall 5	Florescent tubes 4 x 18 = 72w	18	1.296	230	298.08
8	Lecture hall 6	Florescent tubes 4 x 18 = 72w	18	1.296	230	298.08
9	Passages	Florescent tubes 4 x 18 = 72w	80	5.76	93	535.68
			Total	262	18.052	2608.67

4.3 Teaching accessories

In all the rooms there are some teaching accessories which are having moderate usage while the functioning of the halls.

Table.3: Survey on teaching aids in lecturer halls

#	Description	Type	Quantity	Power rating
1	Lecture hall 1	Projector	1	300 w
		Sound System	1	30 w
2	Lecture hall 2	Projector	1	300 w
		Sound system	1	30 w
3	Lecture hall 3	Projector	1	300 w
		Sound system	1	30 w
4	Lecture hall 4	Projector	1	300 w
		Sound system	1	30 w
5	Lecture hall 5	Projector	1	300 w
		Sound system	1	30 w
6	Lecture hall 6	Projector	1	300 w
		Sound system	1	30 w
7	Assembly Hall	Projector	1	300 w
		Sound system	1	1000 w
		Mixer	1	550 w
		Focus Lights	6	120 w
Total			21	3651 w

4.4 IT server room

The building includes an IT server room which operates in full swing throughout the day and every day. IT sever room which draws 10 kW constant for all the time. Energy usage per hour for the IT server room comes as 10kW.

4.5 Air conditioning units.

The main hall provided with five HVAC packaging units of the capacity of 5 tonnage. All other lecturer hall and rooms are provided 2 Tonnagecapacity.

- The total energy demand is as follows
- Total lighting load = 17.856 kW
- Total teaching accessories load = 3.651 kW
- IT Server room = 10.000 kW
- Air conditioning Load = 94.110 kW
- Total connected Energy Load=125.617 kW

Table.4: Air Conditioning units installed in the building

#	Description	Room No	Type	Qty	Power rating	Total Power
1	Classroom	A001	AGT-2T	4	2.400 kW	9.600 kW
2	Classroom	A002	AGT-2T	4	2.400 kW	9.600 kW
3	Classroom	A003	AGT-2T	4	2.400 kW	9.600 kW
4	Classroom	A004	AGT-2T	4	2.400 kW	9.600 kW
5	Classroom	A005	AGT-2T	4	2.400 kW	9.600 kW
6	Classroom	A006	AGT-2T	4	2.400 kW	7.200 kW
			Dai-2T	1	2.410 kW	2.410 kW
7	Assembly Hall	A101	Cooline-Package-11.5T	5	7.300 kW	36.500 kW
Total						94.110 kW

V. DETAILED DIAGNOSIS ANALYSIS OF ENERGY USAGE

Assembly hall

Monthly usage of main assembly hall is provides major contribution in electricity bills. But this hall is not a regular usage point. As per the separate requirements, the assembly hall is using for that time period. So this is

to be considered separately. TheFig.2 shows the monthly usage of assembly hall in hours.

The average usage per month for the period is 44 hrs.The energy usage for Assembly hall per hour
 = AC load + Lighting Load + Hall accessories load
 = 36.5 + 4.32 + 1.97 = 42.79 kW

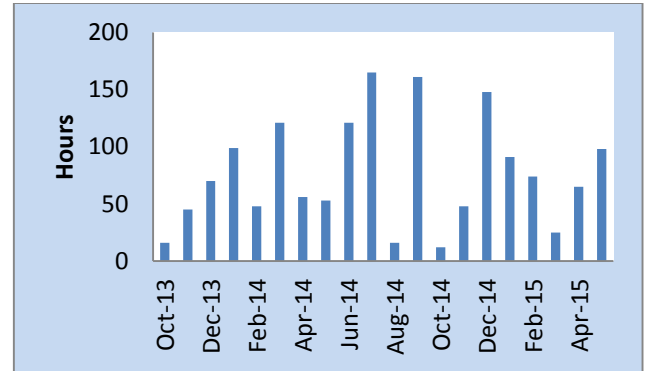


Fig.2: Usage of Assembly hall in hours

Lecturer Halls

Average usage of lecture halls per day (8 am to 8 pm) is observed as 6.5hrs per day. On an average, working days in a month has taken as 22 days. So monthly usage estimated as 6 x 22 = 132hrs per month.Energy usage for 6 lecturer hall per hour

= 6 x (AC Load + lighting load + teaching accessories load)
 = 6 x (9.6 + 1.296 + 0.33) = 67.356 kW

IT Server Room

Usage of IT server room is continuous throughout the day and it is rated as 10 kW. There are some other equipment in IT server room including AC but not connected to this building lines.

Passage lights

Apart from this core usage common passage lighting is using daily.Passage lights are using 3 hours per day in all week days.

Energy usage for passage lights per hour = number of light units x power rating x time
 = 80 x 72 x 1= 5760 W = 5.76 kW

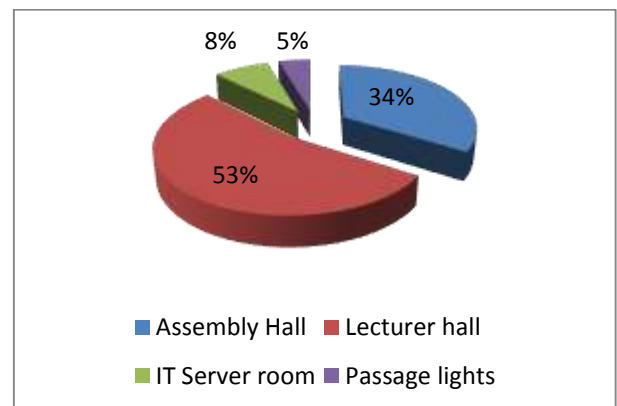


Fig.3 : Energy consumption pattern location wise

VI. ESTIMATED CONSUMPTION AND ACTUAL CONSUMPTION

Comparing connected load and Consumed Energy, a difference of 4.79% coming which is negligible. Energy consumption per month as per the energy meter readings is 18195.800 kWh while the estimated usage of energy with the connected load is 19112.108 kWh. For taking an average, 20 months considered.

Table.5: Comparative statement for Actual and estimated consumption

#	Location	Connected load in kW	Usage time / month in Hours	Consumption per month in kWh
1	Assembly Hall	42.790	44	1882.760
2	Lecturer Halls	67.356	143	9631.908
3	IT Server room	10.000	720	7200.000
4	Passage lighting	5.760	69	397.440
5	Estimated consumption per month			19112.108
6	Average consumption per month taken by Energy meters			18195.800
7	Percentage difference in actual and Estimation			4.79

VII. LOAD FACTOR

It is the ratio of energy consumed over a period of time in kWh to the energy which would have been consumed for the maximum demand [4]. It is normally taken in percentage.

Load Factor

$$= \frac{\text{Energy used during a period in kWh} \times 100}{\text{Maximum demand} \times \text{time under consideration}}$$

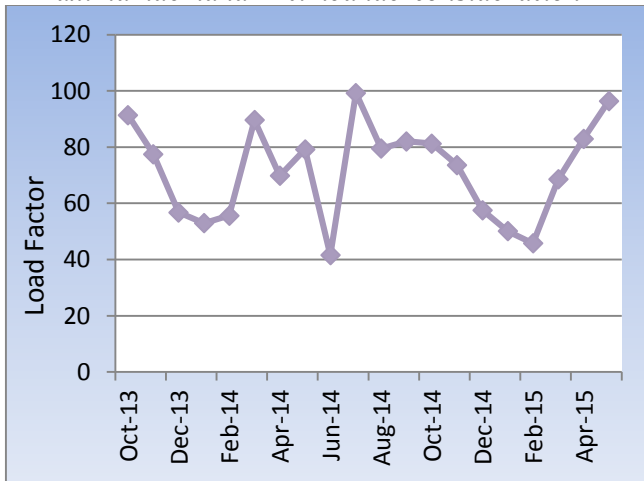


Fig.4: Load Factor plot for the seasonal variations

Load factor gets very low in December, January and February months. The reason might be the winter season of the region. Usage of the air conditioning for these months will be very less. In July 2014 the load factor reaches close to the 100% since the peak summer period. In June 2014 marked as very low Load factor. The reason investigated and found that the month Ramzan fasting was observing in the region so the building usage was less.

VIII. LOAD PROFILE

Load profile is the analysis for the energy usage for a particular day and this pattern gives a good observation about the loading of the system. Here it is providing a load profile for the day 4th January 2016. The building has 5 Distribution Boards for all the systems. An ideal DB selected which is having a moderate usage throughout the day.

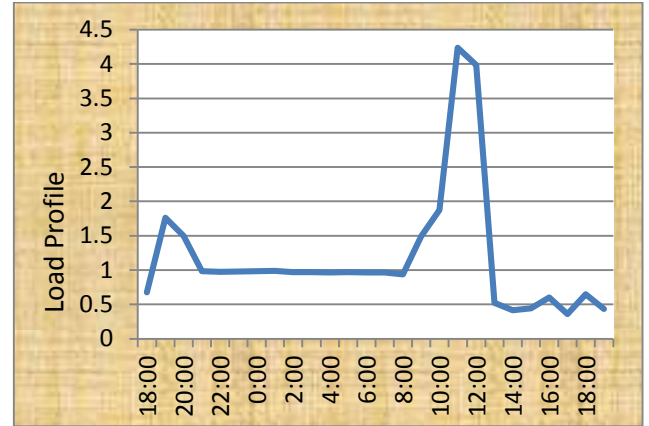


Fig.5 : Load profile for a typical day

IX. IDENTIFYING ENERGY EFFICIENCY AND COST REDUCTION OPPORTUNITIES

The energy efficiency opportunities can trace out by close monitoring of load factor performance and periodic Load Profile performances. For identifying cost reduction opportunities, initially the energy demand control to be reviewed and analyze thoroughly[6]. The second step is the analysis of equipment effectiveness or performance with a standard benchmark. Tracing out the operational and maintenance sequences schedules to be reviewed. Finally the better or modern alternative to the equipment or its accessories can bring out more energy efficient measures to the system.

X. DIAGNOSTIC ANALYSIS FOR IMPROVEMENTS IN LIGHTING

The existing lighting units are florescent tubes and one unit includes 4 tubes of 18 watts. So, one unit requires 72 watts power. Moderate illumination is getting with the help of reflectors but this can improve further with the modern LED lights. For achieving same illumination, less number of LED lightings is enough. Calculations provided with the same number of light units. More switching controls can save excess light usage over the demanded level. At present single switches operates many lighting units at once. Automatic Switching controls can also be used for passage lightings.

10.1 Power savings through the led installations

Table.6: Table of retrofitting on lighting energy

#	Area	Type of lighting	Number of units	Energy load in kW	Average usage per month in hours	Energy in kWh
1	Assembly hall	LED units - 14 w	60	0.84	63	52.92
2	Stage and green room	LED units - 14 w	14	0.196	63	12.348
3	Lecture hall 1	LED units - 14 w	18	0.252	230	57.96
4	Lecture hall 2	LED units - 14 w	18	0.252	230	57.96
5	Lecture hall 3	LED units - 14 w	18	0.252	230	57.96
6	Lecture hall 4	LED units - 14 w	18	0.252	230	57.96
7	Lecture hall 5	LED units - 14 w	18	0.252	230	57.96
8	Lecture hall 6	LED units - 14 w	18	0.252	230	57.96
9	Passages	LED units - 14 w	80	1.12	93	104.16
Total			262	3.668		517.188

Existing power consumption for light units= 72 watts

Power of LED unit for equal illumination (or 10% better)
 = 14 watts

Existing monthly energy consumption for lighting
 = 12872.9 kWh

Usage of LED lights instead of florescent lamps
 = 517.188 kWh

Savings in energyfor lighting = 2608.668 – 517.188 =
 2091.48 kWh

Savings in energy cost = 2091.48 x 0.02
 = 41.829 OMR per month

10.2Diagnostic analysis for improvements in air conditioning

Assembly Hall area to be conditioned is very large as the height of the hall is about 6 meter. Reduction in this volume by decreasing the ceiling height will save AC usages for the Assembly hall. Thermal leakage of the ceiling recorded as shown inFig.6

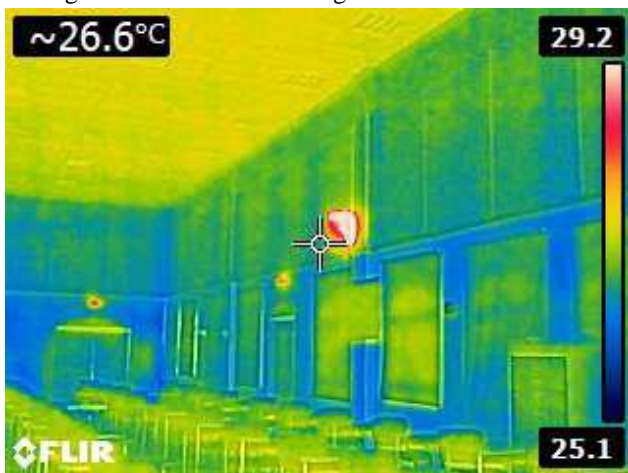


Fig.6: Thermo graphic image of heat gain through ceiling of Hall

Another point of thermal leakage is through window blinds. That can analyze through the figure captured as shown inFig.7. Dark blinds are using but the window glasses are plain and the blinds are insufficient size. These images captured during a winter season (06/01/2016). So on summer season thermal leakage

impact will be more and the air conditioning load increases.

Building envelops to retrofit with the usage of less heat conductive materials in interiors. All the curtain blinds used in the lecture hall is of split leaf type and doesn't work good to protect heat radiation from outside.

Temperature controls for all the AC systems are separate for each one. So that ACs are in unbalanced loading in majority of the time. Common control for room temperature for avoiding individual system overloading and balanced operations can maintain throughout the usage.

Savings in energy for air conditioning need to get from the lecture hall since more energy is utilizing for this areas. Usage hours are more for Lecturer halls. Also the split AC systems are provided for all the lecture halls which draw more power. As per the investment concerns, the change of systems is not economical. More concentrated operational and maintenance attentions can put in place to reduce AC loads.

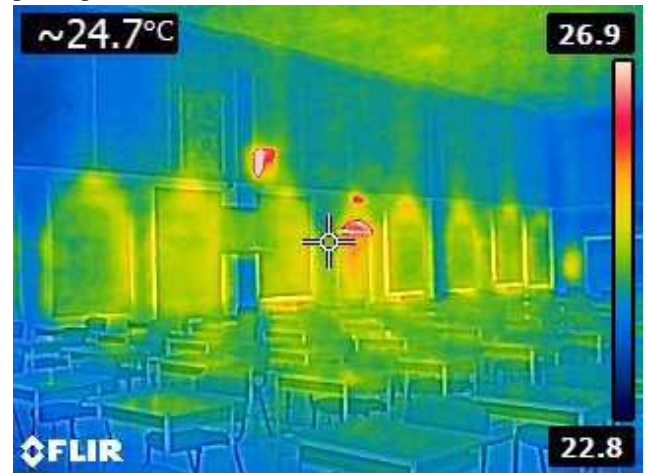


Fig.7: Thermo graphic image of heat gain through window blinds

On estimation, 8% AC load can reduce through the above said recommendations. That is 8 % of 94.11 kW is 7.52 kW.

Monthly ACs are functioning 1443 hrs average
 So, savings in energy units is
 = 7.52x1443 = 10851.36 kWh

Cost savings through reduction in energy usage
 = 217.027 OMRper month

XI. IMPLEMENTATION OF ENERGY EFFICIENCY MEASURES

The action points for implementing energy efficiency measures for lightings are as follows

In the previous sections the light energy comparisons made with LED fittings which are the latest technology in the field. From online portals, one LED light of 14w and

60x60 size costs 35 OMR. Number of units to be replaced is 248 nos.

Purchase cost for LED lights= 248x35= 8680 OMR
 Fitting charges = 600 OMR
 Scarp value for the existing fittings = 200 OMR
 Net cost for the LED replacement
 = 8680+600-200 = **9080 OMR**

The action points for implementing energy efficiency measures for ACs are as follows

- Implement proper maintenance procedures for AC systems, since the package units are not in regular use. It requires proper check for energy effectiveness
- Rework on thermal insulation for Main hall and all the lecture halls
- Windows and blinds are focal points to maintain thermal effectiveness
- Ceiling of Assembly hall is another weak point of thermal insulation. Need to be maintained properly and reduction in ceiling height will improve the comfort level of hall
- Synchronized temperature control for each hall will improve system efficiency and energy savings

Estimated cost for the recommendations=**8000 OMR**
 (Provided by a local contractor who is attending similar projects)

XII. COST BENEFIT ANALYSIS FOR IDENTIFIED OPPORTUNITIES OF IMPROVEMENT

As detailed in the previous sessions, the total savings in energy bills is

Table.7: Savings in energy expenditure and expenses for retrofitting

Category	Savings		Expenses
	Monthly	Yearly	
Lighting	41.829	501.948	9080
Air conditioning	217.027	2604.324	8000
Total		OMR 3106.272	OMR 17080.000

XIII. SIMPLE PAYBACK PERIOD ANALYSIS

Simple Payback Period analysis gives a one shot result for a financial investment. It gives the time period for covering the initial investment through annual returns.[7] SPP doesn't consider any other recurring costs and the discount value. Here it is chose SPP because the life expectancy for all these recommendations cannot be judged without further investigation

$$SPP = \frac{\text{Initial investment}}{\text{annual returns}}$$

$$SPP = \frac{17080}{3106.272} = 5.49 \text{ years}$$

Here the SPP is getting as 5.49 years. In the above sections the savings per month is calculated for the expected load factor of 100%. Only at one month the Load Factor achieved near to 100%. So, further investigations are required to find more accurate estimations. Energy billing has come less for some of the months than the energy savings found. The reason could be the lower load factor values.

XIV. CONCLUSION

The information about the energy usage of this building brings out the connected load usage is not utilizing to the optimum. The load factor comes to the desired value of 100% only once in the investigating period. The reason could be the importance of the building such as the assembly hall is a vital point of the campus and the IT server is also connected to the same building.

The energy reading shows high fluctuations from February 2014 to August 2014. This period requires much detail investigation for both the energy readings and usage data. Like this fluctuations needed to be avoided.

5.49 years of payback period is not much economical but the future benefits will be generating revenue further. More over the reduction in carbon emissions and benefits to the nature is the real impact with this investment. Savings in energy usage is the savings for nature and the nation [8].

REFERENCES

- [1] Definitions.uslegal.com, "Energy Conservation Measure - ECM Law & Legal Definition," 2016. [Online]. Available: <http://definitions.uslegal.com/e/energy-conservation-measure-ecm/>. [Accessed 12 April 2016].
- [2] S. Doty and W. C. Turner, Energy Management Hand Book, 8th ed., Lilburn, GA 30047: The Fairmont Press Inc, 2013.
- [3] M. Dongellini, C. Marinosci and G. L. Morini, "Energy audit of an industrial site: a case study," *Science Direct*, vol. 45, no. 1, pp. 424-433, 2014.
- [4] A. Hasanbeigi and L. Price, October 2010. [Online]. Available: https://china.lbl.gov/sitesall/files/guidebooks/Industrial_Energy_Audit_Guidebook_EN.pdf.
- [5] C. Beggs, Energy Management Supply and Conservation, 2nd Edition ed., London: Routledge, 2009.
- [6] S. U. Kulkarni and K. Patil, "Energy Audit of an Industrial Unit- A Case Study," *International*

Journal of Emerging Science and Engineering (JSESE), vol. 2, no. 1, pp. 22-26, 2013.

- [7] D. Diwan and M. Yaqoot, "Overview of Alternate Energy Resources," in *Energy Management*, 1st Edition ed., P. Diwan and M. Yaqoot, Eds., New Delhi, Pentagon Energy Press, 2010, pp. 292-322.
- [8] K. Frank and G. D.Yogi, "Wind Energy Conversion," in *Hand Book of Energy Efficiency and Renewable Energy*, F. Kreith and D. Y. Goswami, Eds., New York, CRC Press, 2007, pp. 22.1-22.30.

Energy and Exergy Analysis on Si Engine by Blend of Ethanol with Petrol

Kuntesh A Mithaiwal, Ashish j Modi, Dipak c Gosai

Abstract— Need to use renewable energy in the form of ethanol fuel derived using agriculture waste to reduce load on petrol derived from crude oil, which is available in limited quantity. This is mostly due to stock of petroleum product are depleting day by day, hence more use of renewable fuels gets attraction in developing country like India. In recent years, Considerable efforts made to develop and introduce alternative renewable fuel, to replace conventional petroleum-base fuels. The main objective of the current work id to investigate influences of blends of ethanol-petrol blend used in IC engine performance using energy and exergy analysis. Here, experimental work divided into mainly two parts. In first part, Engine performance carried out using E0, E25, E40 and E100 blends of ethanol-petrol blends. In other part, exergy analysis carried out. Experimental test set-up developed in laboratory. The stationary petrol engine was run in laboratory at a medium speed, variable load condition experienced in most urban driving conditions and various measurements like fuel flow, exhaust temperature, exhaust emission measurement and exhaust smoke test were carried out. The fuel properties of biodiesel such as kinematic viscosity, calorific value, flash point, carbon residue and specific gravity investigated. Heat balance sheet and availability calculated for different condition like E0, E25, E40 and E100 blends of ethanol-petrol blends.

Keyword— ethanol, SI engine, exergy, energy.

I. INTRODUCTION

Energy flows and energy efficiencies in the operation of a modern automobile expressed in terms of simple relations. One purpose is to convert any internal combustion engine energy into useful work. The overall energy use depends on two factors, vehicle load and power train efficiency. The former depends on speed, acceleration, and key vehicle characteristics such as mass. The latter depends on internal combustion engine thermodynamic efficiency, and engine and transmission frictions.

Energy conservation and efficiency have been the quest of engineers concerned with internal combustion engines. From the heat, energy of the fuel offered by diesel engine goes one third to the coolant, one-third to exhaust and leaving only about one-third as useful power output. Theoretically, if the

heat rejected could reduce, then the thermal efficiency would be improved. Low Heat Rejection engines aim to do this by reducing the heat lost to the coolant.

Reason for Alternate fuels

IC engines are the major consumer of the fossil fuels. Petrol and diesel will become very costly. It is also that there will be emissions of gases like CO₂ NO_x and HC. Require to reduce emissions from engines by different fossil fuel. Due to these reason Alternate fuels are require. Alkali base renewable fuels more prefer to of alternative fuels because of the possibilities of cleaner combustion. The use of new, alternative, and clean-burning fuels as primary energy resources in internal combustion (IC) engines. Main reason behind to use of alternative fuel is to achieve lower pollutant emissions and higher fuel economy and low content of Sulphur. The compression ignition (CI) engine of the dual fuel type has employed to utilize various alternative renewable fuels resources in place of conventional petrol engine.

Ethanol is better alternative of fossil fuel

- Ethanol has high octane number, low flame temperature, high density, and high latent heat of vaporization.
- Ethanol can reduce country's dependence on fossil fuel, it should foreign supplies be interrupted.
- The ethanol is improving quality of the environment. It reduced Carbon monoxide emissions, lead and other carcinogens (cancer causing agents) which removed from gasoline.
- Ethanol-blended fuels can clean the fuel system also absorb moisture

Energy and Exergy in Engines:

Energy is physical quantity. It is a state of thermodynamics. Energy is present in various forms such as electrical, mechanical, chemical magnetic energy etc. Energy conversion from one form to another. The machine, which is use to energy conversion, known as engine. In general, engines have efficiencies of about 35% and about 50% of fuel energy is lost in cooling water and exhaust gases.

Exergy defined as the maximum theoretical useful work obtained from a system. Exergy is not stored as energy but destroyed in the system. Exergy destroyed whenever an irreversible process occurs.

An Energy analysis is based on first law of thermodynamics. From the 1st law analysis we can find the energy transformations and there losses.

An Exergy analysis based on the second law of thermodynamics. It can removes the limitations of an energy-based analysis. Exergy analysis is a detail analysis of energy transformations and there losses. This provides useful information to improve the overall efficiency and cost effectiveness of a system.

II. LITERATURE SURVEY

Paolo Iodice et al. [2016] [1] is investigated that the Effect of ethanol–gasoline blends on CO and HC emissions in last generation four stork SI engines within the cold-start transient. Which work with ethanol-gasoline mixture by 10%, 20%, and 30% by volume called G10, G20, and G30 . This paper is reducing the CO and HC emission at cold-start transient commercial gasoline, with the 20% v/v ethanol blend achieving the highest emission reduction. **Golmohammad Khoobbakht et al. [2016] [2]** worked on Optimization of operating factors and blended levels of diesel, biodiesel and ethanol fuels to minimize exhaust emissions of diesel engine using response surface methodology. Aim of this paper investigated on operating of engine speed and load as well as different level of blends of ethanol in biodiesel. It is work on the diesel engine. This experiment is work on the statistical tool known as Design of Experiments (DoE) based on central composite rotatable design (CCRD) of response surface methodology (RSM). Surface methodology is also use to predict the amount of fuel emission like CO, HC, NOX, and THC. This paper indicated that the amount of CO and HC is reducing at the end of experiment. When the amount CO₂ is increasing at the end of the experiment but adding diesel fuel blend in ethanol is reducing the amount of CO₂. An engine load of 80% of full load bar, speed of 2800 rpm and a blend of 26% biodiesel, 11% ethanol and 63% diesel were found to be optimal values with a high desirability of 74% for the test engine having 0.013% of CO, 41 ppm of HC, 643 ppm of NO_x, 12% of smoke opacity and 7.3% of CO₂.

W.M. Ambrós et al. [2016] [3] worked on Experimental analysis and Modeling of internal combustion engine operating with wet ethanol. In this paper using ethanol with different mixture of different percentage of ethanol and water and improving the efficiency of SI and di engine. The

experiment take place based on first law of thermodynamic. The trials and the results found confirm that the engine is capable of operating with mixtures of wet ethanol up to 40% by volume of water. E70W30 blend showed the best values of power, torque, efficiency and specific consumption. **N. M. Al-Najem et al [1992] [4]** is worked on energy-exergy analysis of diesel engine. This analysis is based on 1st and 2nd law of thermodynamic. Exergy analysis is based on 2nd law of thermodynamic. Using this law, we can find the availability of energy, losses of energy in diesel engine. 2nd law indicated different between high-grade energy and low-grade energy. 1st law indicated some lost energy due to the process. 1st and 2nd law combined indicated the datum (zero level) of energy and exergy. At that level, we find the enthalpy losses and other losses, which take place at near of datum. Diesel engines have efficiencies of about 35% and about 50% of the input fuel energy is lost in cooling water and exhaust gases. The wasted energy in the cooling water usually considered useless due to its low temperature level. In this paper, we focused on the exhaust gas. The present analysis is to illustrate the capability of the exergy analysis to provide a systematic approach to pinpoint the waste and lost energy within diesel engines.

A.Vamshikrishna Reddy et al. [2014] [5] is worked on diesel engine by using dual fuel mode. Biogas and diesel used for the dual fuel mode and find the fuel consumption, brake thermal efficiency, exergy efficiency and different availabilities with the varying load. Biogas used as alternative renewable fuel in diesel engine, find the performance of diesel engine. The performance of the engine check on the bases of the 1st and 2nd law of thermodynamic. 1st low of thermodynamic gives the energy analysis and 2nd law of thermodynamic give the exergy analysis of dual fuel mode. **Chongqing Feng et al [2016] [6]** is worked on Availability analysis of using is-octane/n-butanol blends in spark ignition engine. This is representing a detailed energy and exergy analysis of an iso-octane/n-butanol blend-fueled spark-ignition (SI) engine, investigate exergy loss mechanisms and understand how the exergy destruction changes with different iso-octane/n-butanol blend fuels. **Rakhi Maheta et al [2012] [7]** have experimentally investigated that the alcohol like ethanol and butanol properties compare with diesel and experimental analysis of ethanol-diesel blend or butanol-diesel bland use as fuel. This paper is show the different characteristics of both ethanol and butanol compare with diesel as per ASTM standards. The ethanol shows properties like calorific value, density, flash point, cetane number with pure diesel. There is only flashpoint reduce due to alcohol blend. **Alvydas Pikunas et**

al [2015] [8] have to investigate experimentally and compare the engine performance and pollutant emission of a SI engine using ethanol–gasoline blended fuel and pure gasoline. The results showed that when ethanol added, the heating value of the blended fuel decreases, while the octane number of the blended fuel increases. The results of the engine test indicated that when ethanol–gasoline blended fuel is used, the engine power and specific fuel consumption of the engine slightly increase; CO emission decreases dramatically because of the leaning effect caused by the ethanol addition; HC emission decreases in some engine working conditions; and CO₂ emission increases because of the improved combustion. Using ethanol–gasoline blend, CO emission may reduce 10–30%, while CO₂ emission increases by 5–10% depending on engine conditions. The engine power and specific fuel consumption increase approximately by 5% and 2–3%, respectively, in all working conditions. **Dattatray Bapu et al. [2014] [9]** have worked about injection timing on which ethanol blend run the engine. The blends tested are D70/E20/B10 (blend A), D50/E30/B20 (blend B) D50/E40/B10 (blend C), and Diesel (D100). The blends are prepared to get maximum percentage of oxygen content but keeping important properties such as density, viscosity and Cetane index within acceptable limits. Experiments conducted on a multi cylinder, DI diesel engine, whose original injection timing was 13° BTDC. The engine did not run on blends B and C at this injection timing and it was required to advance timing to 18° and 21° BTDC to enable the use of blends B and C Respectively However advancing injection timing almost doubled the NO emissions and increased peak firing pressure. Smoke reduced remarkably for blends especially at medium and high loads of both speeds and all injection timings. Maximum reduction is about 60% to 70% at higher loads for respective high ethanol content blend at all injection timing and speeds. Advancing injection timing reduced the smoke for all blends and diesel fuel at both speeds. Significant reduction in smoke observed for high ethanol content blends; however, reduction in smoke does not indicate the reduction in particulate matter in same proportion.

Objectives

- 1) To blend ethanol with petrol fuel and observe the performance of I.C. Engine and improve performance of engine.
- 2) To do the analysis of the Ethanol on various parameters like input parameter like load, output parameter like specific fuel consumption, brake power, and brake thermal efficiency.

- 3) Experimental energy and exergy analysis on SI engine by ethanol-petrol blend(E0, E25, E40,E100)

Table.1: Properties of ethanol and blends of petrol

Properties	E0	E25	E40	E100
Specific Gravity 25° C gm/cc	0.765	0.7792	0.7792	0.789
Calorific Value (KJ/Kg)	48000	38809	37160	26900
Octane number	88	97	97	118
Flash point	-43 ° C	-13.5 ° C	-13.5 ° C	-12.5 ° C
Auto Ignition Temp.	246° C	294° C	294° C	365° C

III. EXPERIMENTAL SETUP AND PROCEDURES

Experimental set up

The single cylinder, four-stroke petrol engine connected with an electrical load bank. The engine set-up developed to measure the parameters like fuel consumption, cooling water temperature, and inlet air and exhaust gas temperature.

The test carried out with variation in engine load from low to high load conditions. At each operating stage, the observations of various parameters taken for both ethanol blend with petrol and base fuel as petrol.

Apparatus specifications

Table.2: Engine Specification

Type	Honda,4-Stroke, Side valve, One Cylinder
Dynamometer	Self-Exciting, two Pole, Rotating Field Type
Displacement	76 Cm ³
Bore X Stroke	46x46 Mm
Max Horse Power	1.6HP @ 3600 Rpm
Compression Ratio	6.0:1
Fuel Consumption	0.53/5
Cooling System	Forced Air
Lubricating System	Splash
Oil Capacity	0.35 Liter
Fuel Tank Capacity	2.8 Liter
Oil	SAE10W-40

Measurement

- a) Calibrated burette for fuel intake measurement.

- b) Orifice meter - Fitted to the air inlet tank with water manometer for air intake measurement.
- c) Lesser Gun used to measure temperature at various points.
- d) Exhaust gas calorimeter to measure heat carried away by exhaust gas.

- e) Measure the water flow rate of engine jacket and calorimeter.

At each operating condition, the dynamometer load, speed, fuel, and airflow recorded after allowing time for the engine to stabilize.

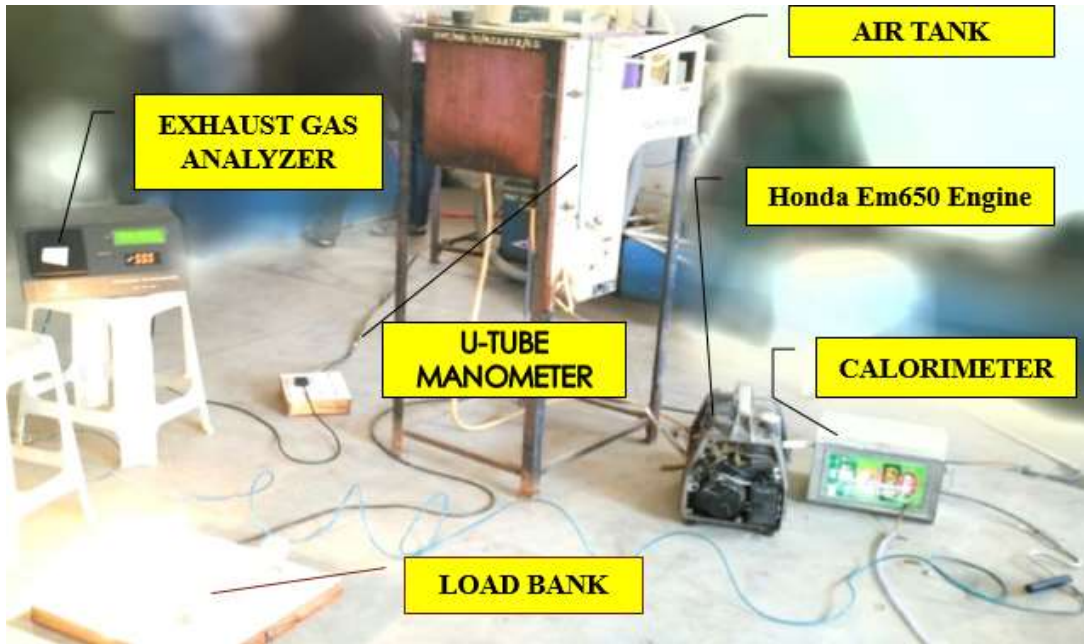


Fig.1: Experimental set-up

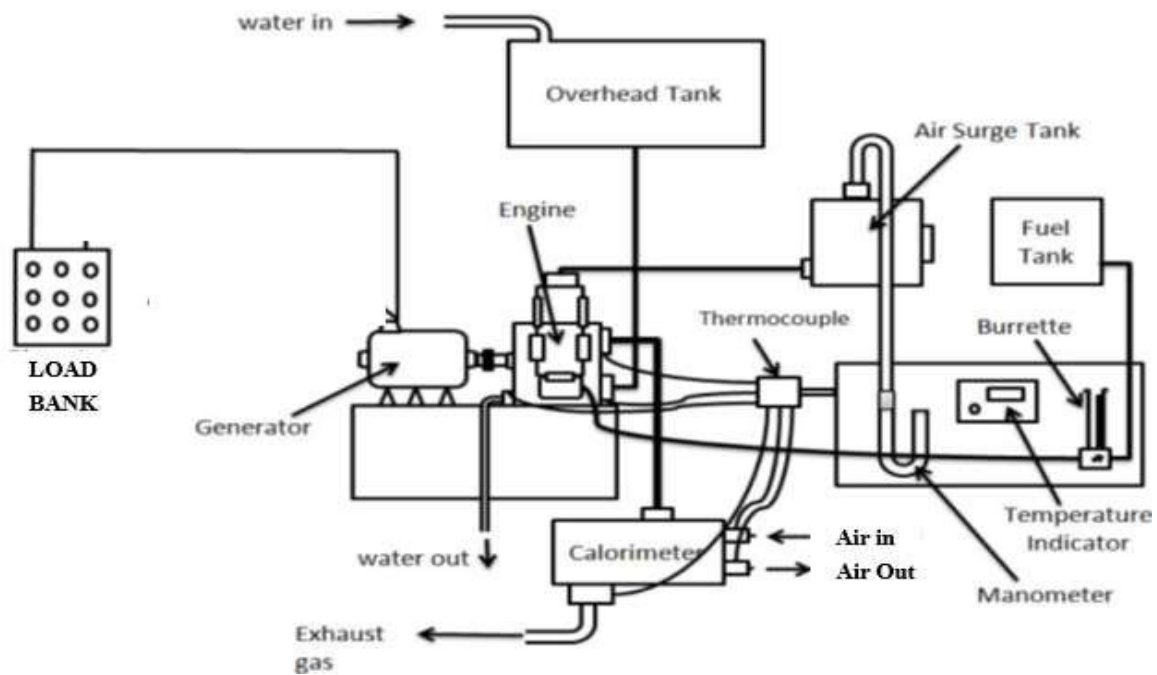


Fig.2: Block diagram of the experimental setup

Energy Analysis

(1) Fuel energy supplied per unit time ,

$$Q_{in} = m_f * LCV , \text{ kW}$$

Where m_f = mass of fuel consume per unit time

LCV= lower calorific value of fuel

(2) Energy in exhaust gas per unit time,

$$Q_e = (m_a + m_f) * C_{pe} * (T_{e1} - T_{e2}) , \text{ kW}$$

$$A_{in} = [m_f * LCV] * [1.0401 + 0.1728(O/C) + 0.0432(O/C) + 0.2169(S/C) \{1 - 0.2689(H/C)\}] Q$$

Where H, C, O, S are mass fraction of hydrogen,

carbon, oxygen, Sulphur

(2) Shaft power availability,

A_s = brake power of engine, kW

(3) Exhaust gas availability,

$$A_e = Q_e + [(m_a + m_f) * T_{amb} * \{c_{pe} \ln(T_{amb}/T_{e1})\}] - R_e * \ln(P_{amb})$$

(4) Colling water and destructed availability,

$$A_d = \{A_{in} - (A_s + A_w + A_e)\}$$

(5) The exergy efficiency

$$\eta_{II} = 1 - (A_{destroyed} / A_{in})$$

IV. RESULTS AND DISCUSSION

From the dual fuel mode viewpoint, it is very essential to have the knowledge of available fuel energy losses or destroys whereabouts in the engine operations. Therefore, in this chapter, the first and second law coupled in order to get a clear view of the dual fuel operation of Ethanol.

Therefore, in this chapter the effect of load and pilot fuel variation in the energy and exergy balances of the dual fuel operations evaluated and compared to that of the baseline petrol mode.

Specific fuel consumption (SFC)

Where T_{e1} , T_{e2} are exhaust gas inlet and outlet temperature

C_{pe} is the specific heat of exhaust gases

m_a is mass of intake air

(3) Energy in cooling water and Unaccounted per unit time

$$Q_{colling+unaccountable} = Q_{in} - (Q_s + Q_e) , \text{ kW}$$

Exergy Analysis

(1) Input availability,

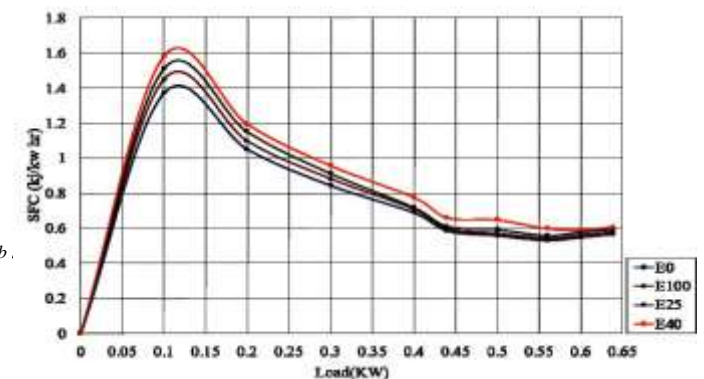


Fig.3: Variation of SFC with varying loads

Ethanol addition reduces the heating value of the petrol-ethanol blends, therefore, more fuel is needed (by mass) to obtain same power when blended fuels are used instead of petrol. However, as mentioned previously, ethanol addition to petrol makes the engine operation leaner and improves engine combustion and performance, as shown in fig 5.1 SFC measured for different loadings

It can be seen in fig 3, at low load (0 to 0.2 kW), SFC increases with increase in load by 5%, 9%, and 15% for E100, E25, E40 respectively compare to E0. At medium load (0.2 to 0.5 kW), SFC consumption is increasing by 2%, 4%, and 12% for E100, E25, E40 respectively compare to E0. At High load (0.5 to 0.65 kW), SFC is increasing by 2%, 5%, and 7% for E100, E25, E40 respectively compare to E0.

Brake Thermal Efficiency

Presence of oxygen in ethanol composition allow better combustion product, complete combustion results in high temperature and pressure inside cylinder thus results in higher power output.

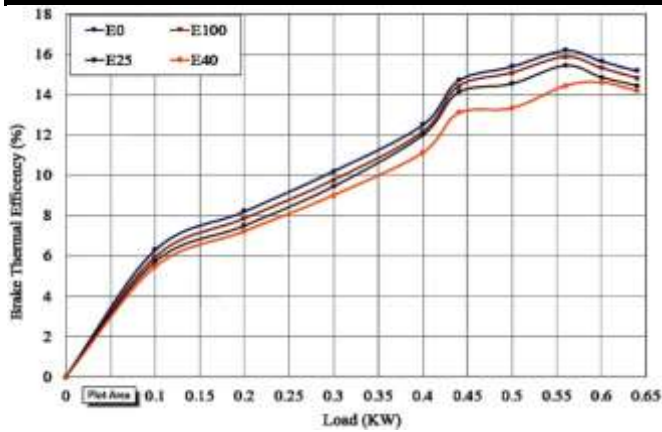


Fig.4: Variation of brake thermal efficiency with load

Fig 4 Shows variation of brake thermal efficiency with varying loads. As increase in load, brake thermal efficiency of engine reduces for Fuel blend. The vaporization of fuel continues increasing during the intake and compression stroke. This tends to decrease the temperature of the working charge, which reduces compression work of engine at high engine speed there is less time for completion of combustion, which takes place in later stage of cycle, which increase thermal efficiency.

When the latent heat of the fuel used is low, as in the case of Petrol, the effect of cooling is not sufficient to overcome the effect of additional vapor. Increasing the latent heat of the fuel blend used by increasing the ethanol percentage increases the effect of cooling, which results in increase thermal efficiency thus higher engine power output.

It can be seen in fig 5.2 at low load (0 to 0.2 kW), BTE is reducing with increases in load by 5%, 9%, and 13% for E100, E25, E40 respectively compare to E0. At medium load (0.2 to 0.5 kW) BTE is reducing by 2%, 4%, and 11% for E100, E25, E40 respectively compare to E0. At High load (0.5 to 0.65 kW), BTE is reducing by 3%, 5%, and 7% for E100, E25, E40 respectively compare to E0.

Heat balance sheet:

Heat balance sheet (E0)

Heat balance sheet of petrol and Ethanol show in fig 5 to fig 8. This balance sheet is represent the total amount of heat and how many heat utilized by shaft power, exhaust gas, and Colling water at different load. At low load, the amount of exhaust energy is low and cooling water energy is high. When load is increases, the exhaust gas energy increases rapidly with decrease with cooling water energy as shown in fig 5 to fig 8.

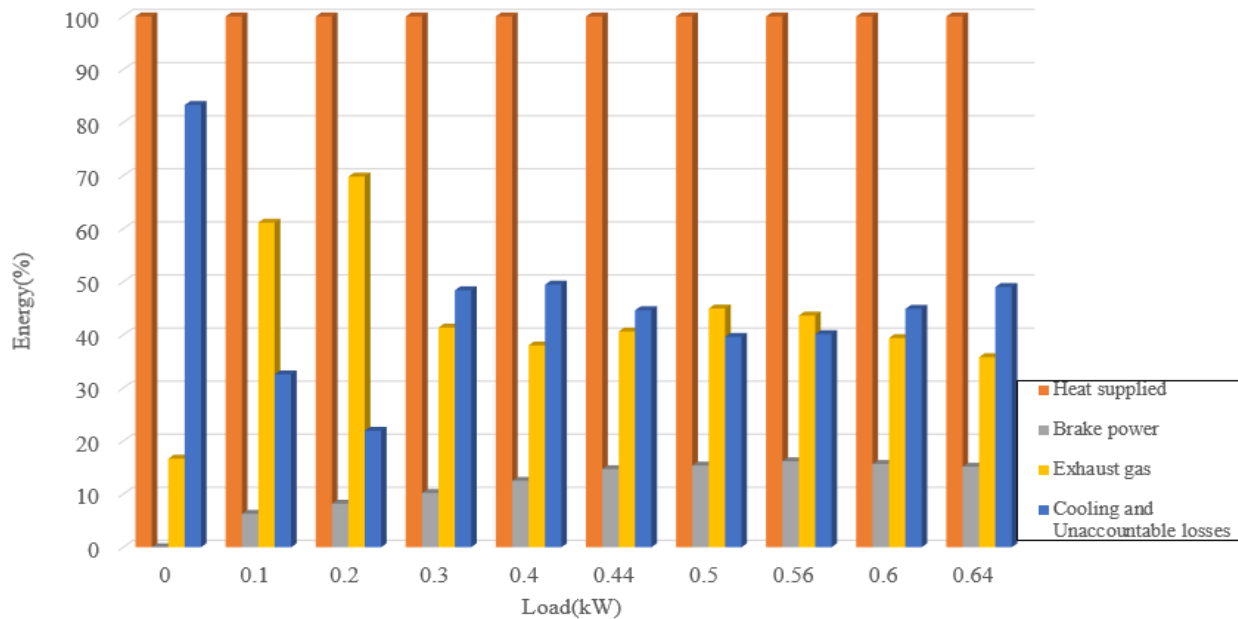


Fig.5: Heat Balance sheet for - E0

Fig 5 represents the heat balance sheet of E0. At low load (0 to 0.2 kW), out of total power generated the brake power of the engine varies 6% to 10%, heat carried out by the exhaust gas is varies 60% to 70% and heat carried out by the Colling

water varies 20% to 35%. Similarly for lower load (0.2 to 0.5 kW) out of total power generated 15%, 45% 40% energy carried by brake power, exhaust gas and Colling water. In addition, at higher load (0.5 to 0.65 kW) out of total power

generated 15%, 35%, 50% energy carried by brake power, exhaust gas and Colling water.

Heat balance sheet (E25)

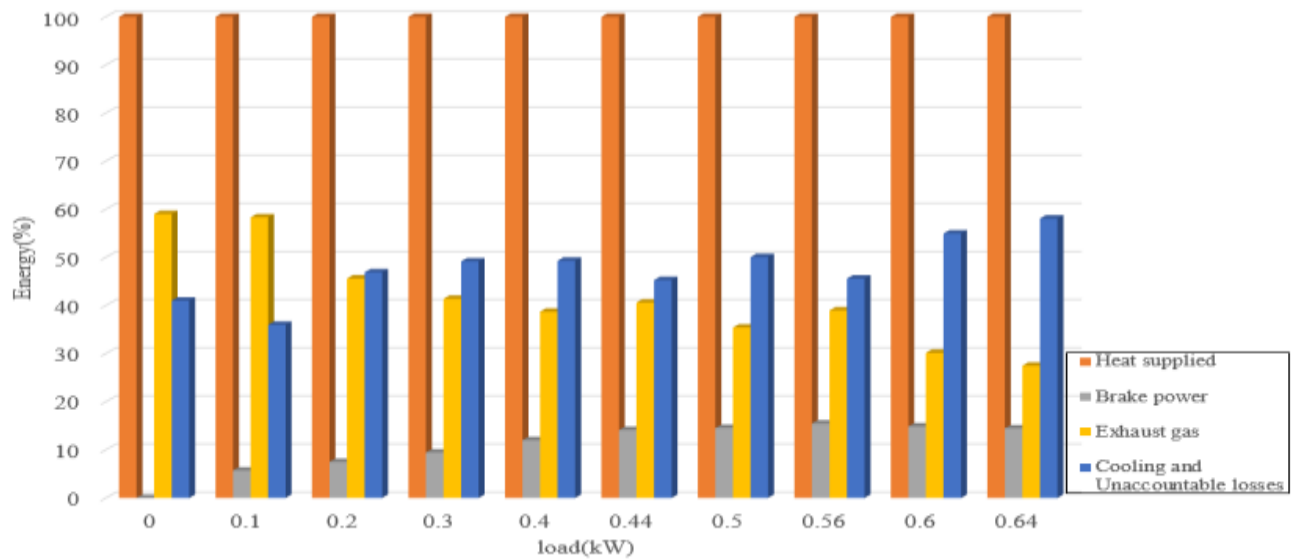


Fig.6: Heat balance sheet for – E25

Fig 6 represents the heat balance sheet of E-25. At low load (0 to 0.2 kW) and Medium load (0.2 to 0.5 kW) out of total power generated brake power, exhaust gas and Colling water energy is same compare to E0 respectively. However, for

higher load (0.5 to 0.65 kW) out of total power generated brake, power is same but exhaust gas energy is reducing 10% and Colling water energy increases 10% to E0 respectively.

Heat balance sheet (E40)

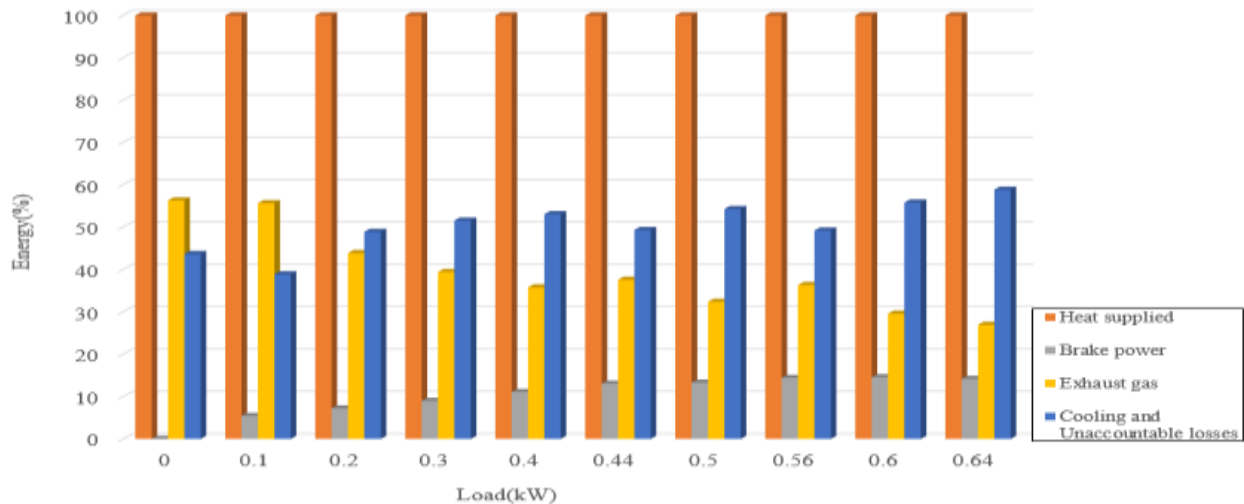


Fig.7: Heat Balance sheet for – E40

Fig 7 represents the heat balance sheet of E-25. At low load (0 to 0.2 kW) and Medium load (0.2 to 0.5 kW) out of total power generated brake power, exhaust gas and Colling water energy is same compare to E0. However, for higher load (0.5

to 0.65 kW) out of total power generated brake power is same but, exhaust gas energy is reducing 15% and Colling water energy increases 15% to E0 respectively.

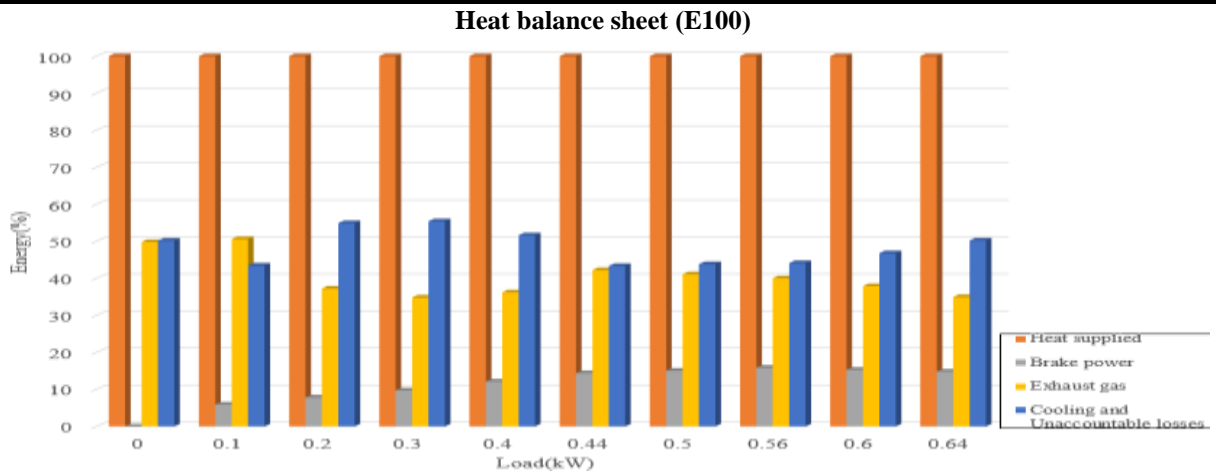


Fig.8: Heat Balance sheet for – E100

Fig 8 represents the heat balance sheet of E-100. At low load (0 to 0.2 kW) out of total power generated brake power of the engine reduces 2%, heat carried out by the exhaust gas reduces between 15% and heat carried out by the Colling

water reduces 20% respectively compare to E0. Similarly, for medium load (0.2 to 0.5 kW) and higher load (0.5 to 0.65 kW) out of total power generated brake power, exhaust gas and Colling water energy is same compare to E0.

Availability Analysis:

Availability Analysis (E0)

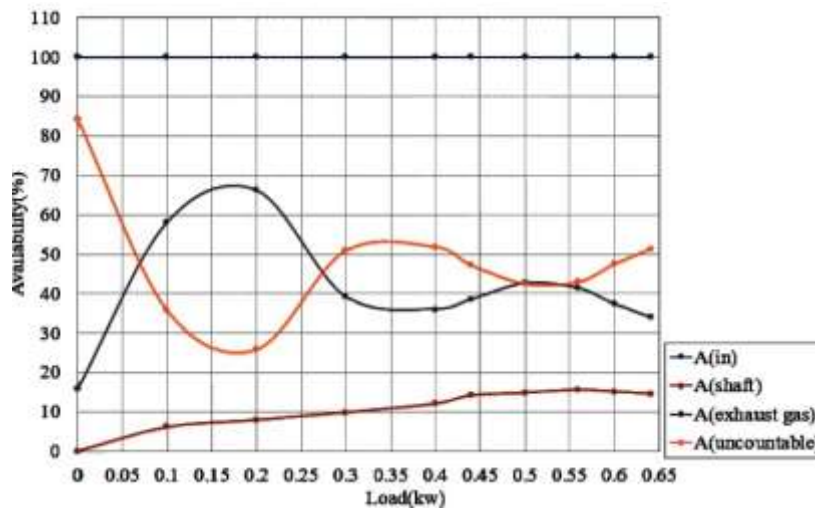


Fig.8: Availability input VS load (E0)

Fig 8 represents the availability of the E0. At low load (0 to 0.2 kW), available energy of shaft increases 0% to 9% with increases in load, exhaust gas availability increases to 15% to 67% with increases in load, but uncountable available energy is reduces 85% to 25% with increases in load respectively compare to the E0. At medium load (0.2 to 0.5 kW) available energy of shaft increases 9% to 13% increases with load, exhaust gas availability increases to 39% to 45% with increases in load, but uncountable available energy is reducing 51% to 42% with increases in load respectively compare to the E0. At higher load (0.5 to 0.65 kW), available

energy of shaft is increases 13% to 15% increases with load, exhaust gas availability reduces to 41% to 35% with increases in load, but uncountable available energy increases 35% to 41% with increases in load respectively compare to the E0.

Availability Analysis (E25)

Fig 9 represents the availability of the E25. When we saw that at low load (0 to 0.2 kW) available energy of shaft is equal to the E0 respectively, exhaust gas availability reduces to 12% to 16% compare to E0 respectively. but uncountable

available energy increases 15% to 18% respectively compare to E0. At medium load (0.2 to 0.5 kW) available energy of shaft is equal to the E0 respectively, exhaust gas availability reduces to 5% to 10% respectively compare to E0. However, uncountable available energy increases 9% to 11%

respectively compare to E0. At higher load (0.5 to 0.65 kW) available energy of shaft, exhaust gas availability reduces to 5% to 10% respectively compare to E0, but uncountable available energy increases 9% to 11% respectively compare to E0.

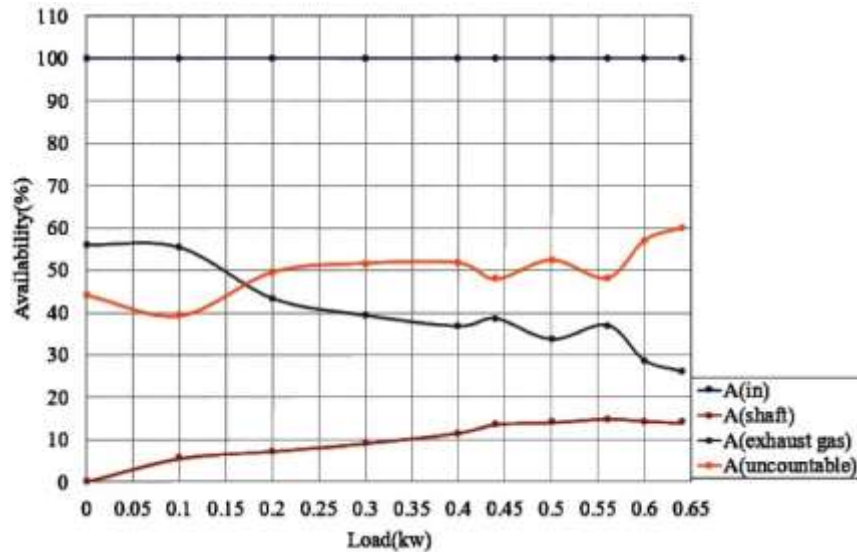


Fig.9: Availability input VS load (E25)

Availability Analysis (E40)

Fig 10 represents the availability of the E40. At low load (0 to 0.2 kW) available energy of shaft is reducing 3% to 5% respectively compare to E0. Exhaust gas availability is almost same to E0. Uncountable available energy increases 2% to 5% compare to E0 respectively. At medium load (0.2 to 0.5 kW) available energy of shaft reduces 3% to 5% respectively compare to E0. Exhaust gas availability also

reduces to 5% to 7% compare to E0 respectively . but uncountable available energy increases 9% to 11% respectively compare to E0. At higher load (0.5 to 0.65 kW) available energy of shaft, exhaust gas availability also reduces to 5% to 10% respectively compare to E0, but uncountable available energy increases 9% to 11% compare to E0 respectively.

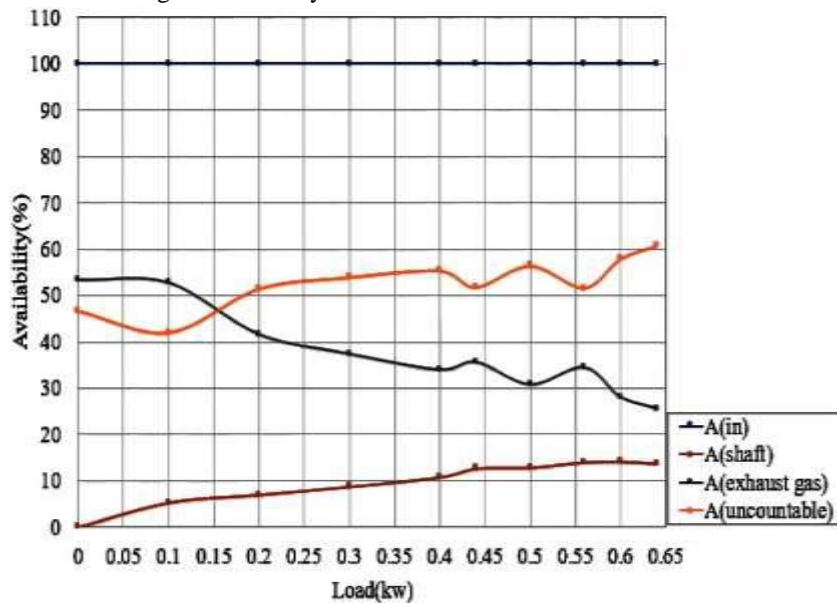


Fig.10: Availability input VS load (E40)

Availability Analysis (E100)

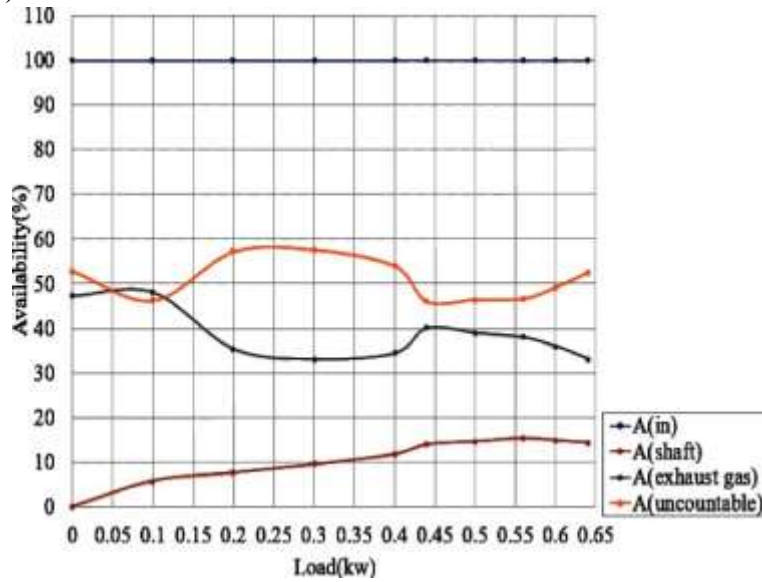


Fig.11: Availability input VS load (E100)

Fig 11 represents the availability of the E100. At low load (0 to 0.2 kW) available energy of shaft is equal to the E0, exhaust gas availability reduces to 30% respectively compare to E0, but uncountable available energy increases 30% compare to E0. At medium load (0.2 to 0.5 kW) available energy of shaft is equal to the E0. Exhaust gas availability reduces to 5% to E0, but uncountable available energy increases 5% to 9% respectively compare to E0. At higher load (0.5 to 0.65 kW) available energy of shaft, exhaust gas

availability and uncountable available energy is same respectively compare to E0.

Destroyed availability

Fig 12 represents destroyed availability distribution at different engine load for operation with petrol and blends of ethanol. To maintain an equal power output as of ethanol mode, dual fuel mode required higher chemical fuel exergy than the ethanol mode due to the poor combustion and low energetic petrol fuel.

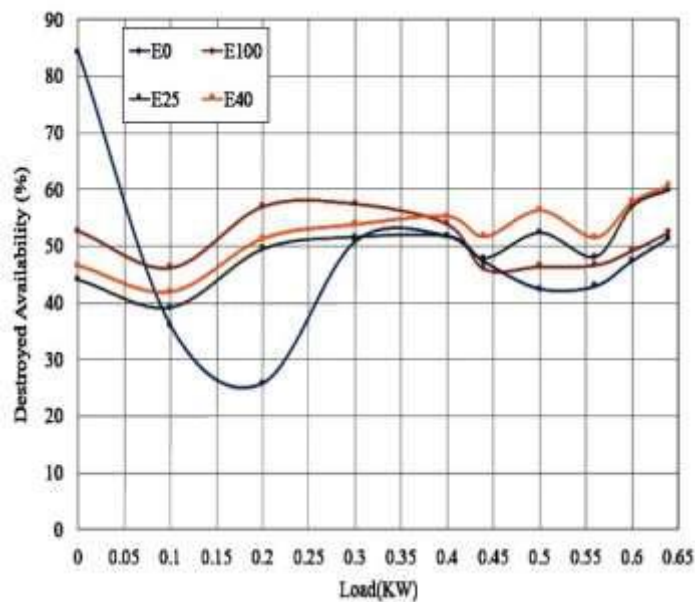


Fig.12: Destroyed availability distribution at different engine load

For lower load (0 to 0.2 kW), destroyed availability increases 11%, 10%, 17% for E25, E40 and E100 respectively compare to E0. At medium load (0.2 to 0.5 kW) destroyed availability reducing 1% for E25 and increases 3% for E40 increases 2% for E100, respectively compare to E0. At higher load (0.5 to 0.65 kW) destroyed availability increases 8%, 10%, 1% for E25, E40 and E100, respectively compare to E0.

Energy efficiency

From the fig 13 it is clear that as the load increases the exergy efficiency increases. This is due to as load increases during engine operation, the rich fuel mixture increased the combustion temperature. Therefore, increased work availability and reduced heat transfer availability losses obtained, as percentages of the fuel chemical availability. For

this, an increase in the exergy efficiency resulted at higher loads for all the tested fuels. In case of Ethanol, at higher loads the exergy efficiency improves significantly than compared to lower loads due to the improved combustion of Ethanol at higher load and decreased ignition delay. Because of the improved combustion of Ethanol at higher loads, the exhaust gas availability was increased. In addition, the shaft availability of the fuels was higher for an increased load.

For lower load (0 to 0.2 kW), exergy efficiency reduces 11%, 10%, 17% for E25, E40 and E100 respectively compare to E0. At medium load (0.2 to 0.5 kW) exergy efficiency increasing 1% for E25 and reducing 3% for E40 reduces 2% for E100, compare to E0 respectively. At higher load (0.5 to 0.65 kW) exergy efficiency is reducing 8%, 10%, 1% for, E25, E40 and E100 respectively compare to E0.

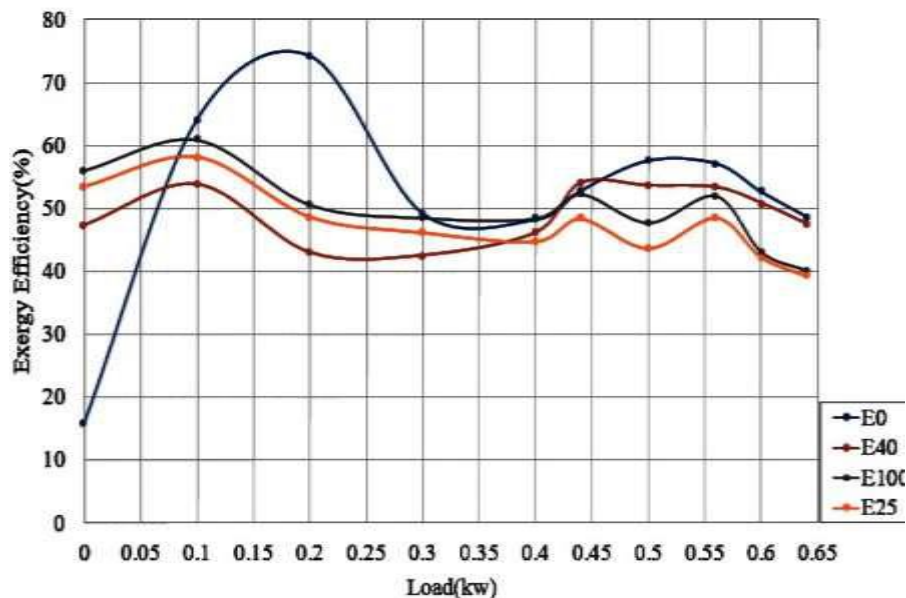


Fig.13: Exergy efficiency versus Load

V. CONCLUSION

From performance analysis of SI engine following concluding remarks obtained-

1. The general performance of E40 found to be better compare to E0. SFC 7-12% lower than E0 at high load condition. SFC was increased 5% to 15% for E40 then E0 low to high load. Ethanol addition reduces the heating value of the petrol-ethanol blends, therefore, more fuel is needed (by mass) to obtain same power when blended fuels are used instead of petrol.
2. The mechanical efficiency reduces by 10-16%, 9-5%, 5-3% for E25 E40 and E100 respectively compare to E0 at varying load condition. When the latent heat of the ethanol is low, as in the case of ethanol, the effect of
3. cooling is not sufficient to overcome the effect of vapor. Which results in reducing thermal efficiency.

3. The heat balance sheet indicates that some amount of heat wasted by fuel. This heat utilized to increase the brake power and some amount of heat is lost in exhaust gas. For lower load to higher load out of total power generated brake power of the engine is same for different fuel blend E25, E40, E100 compare to E0. For exhaust gas energy however it is reducing for lower load to higher load. It reduces 15% to 25% for different blend like E25, E40, and E100 compare to E0 respectively. For Colling water energy, however it increases for lower load to higher load by 10% to 17% for different blend like E25, E40, and E100 compare to E0.

From Exergy analysis of SI engine following concluding remarks obtained-

1. The increase in load resulted in increase of availability for all blend of ethanol and petrol (E0, E25, E40, and E100). For E25, E40, E100 availability increases by 9-13%, 13-19% and 3-5% respectively compare to E0 at varying load condition. For lower to higher load condition, availability increases due to improvement of combustion for different blends of ethanol-petrol (E0, E100, E25, and E40) at high temperature.
2. Due to poor combustion of fuel and lower energy content, it observed that dual fuel (E0, E25, E40, and E100) mode more fuel exergy require to produce same amount of shaft work for E25, E40, E100 respectively then E0. Exergy efficiency increases 5-7% and 9-13% for low and high load respectively for all blend of ethanol-petrol. Exergy efficiency reduces 3-5% for medium load for all blend of ethanol-petrol.
3. Even though destroyed availability decreases as the load increases due to the presence of CO₂ in ethanol blend. Destroyed availability reduces by 7- 9% for lower load and higher load condition for all blend of ethanol-petrol. Destroyed availability increase by 3-5% for medium load condition for all blend of ethanol-petrol

REFERENCES

- [1] Paolo Iodice, Adolfo Senatore, Giuseppe Langella, Amedeo Amoresano, "Effect of ethanol-gasoline blends on CO and HC emissions in last generation SI engines within the cold-start transient: An experimental investigation" *ELSEVIER Applied Energy* 179 (2016) 182-190.
- [2] D.K. Jamuwa, D. Sharma b, S.L. Soni, "Experimental investigation of performance, exhaust emission and combustion parameters of stationary compression ignition engine using ethanol fumigation in dual fuel mode" *ELSEVIER Energy Conversion and Management* 115 (2016) 221-231.
- [3] Hsieh WD, Chen RH, Wu TL, Lin TH, "Engine performance and pollutant emission of an SI engine using ethanol-gasoline blended fuels" *Journal of Atmospheric Environment* 36/3 (2002) 403-410.
- [4] Rakhi maheta, Mousami chakraborty, Parimal A. Parikh, "Comparative study and properties of alcohol-diesel blend", SVNIT, Surat, Jan 2012.
- [5] Modi, A. and Gosai, D., "Experimental Study on Thermal Barrier Coated Diesel Engine Performance with Blends of Diesel and Palm Biodiesel," *SAE Int. J. Fuels Lubr.* 3(2):246-259, 2010, doi: 10.4271/2010-01-1519.
- [6] Modi, A., "Experimental Study of Energy Balance in Thermal Barrier Coated Diesel Engine," *SAE Technical Paper* 2012-01-0389, 2012, doi: 10.4271/2012-01-0389.
- [7] Ashraf Elfasakhany, "Investigations on the effects of ethanol methanol gasoline blends in a spark-ignition engine: Performance and emissions analysis" *ELSEVIER engineering Science and Technology, an International Journal* (2015) 1-7.
- [8] Biplab K. Debnath, Niranjana Sahoo, Ujjwal K. Saha, "Thermodynamic analysis of a variable compression ratio diesel engine running with palm oil methyl ester," *Energy Conversion and Management* 65 (2013) 147-154.
- [9] Agnese Magno, Ezio Mancaruso, Bianca Maria Vaglieco, "Effects of a biodiesel blend on energy distribution and exhaust emissions of a small CI engine," *Energy Conversion and Management* 96 (2015) 72-80.
- [10] Muammer Özkan, Derya Burcu Özkan, Orkun Özener, Hasan Yılmaz, "Experimental study on energy and exergy analyses of a diesel engine performed with multiple injection strategies: Effect of pre-injection timing," *Applied Thermal Engineering* 53 (2013) 21e30, 25th Dec 2012.
- [11] Anubhuti Gupta, Jay Prakash Verma "Sustainable bio-ethanol production from agro-residues" *Institute of Environment and Sustainable Development, Banaras Hindu University, Varanasi 221005, Uttar Pradesh, India, Renewable and Sustainable Energy Reviews* 41 (2015)
- [12] Ahmad Taghizadeh-Alisaraei, "The effect of added ethanol to diesel fuel on performance, vibration, combustion and knocking of a CI engine" *ELSEVIER Fuel* 185 (2016) 718-733.
- [13] Ryojiro Minato, "Advantage of ethanol fuel for gas generator cycle air turbo ramjet engine" *ELSEVIER aerospace Science and Technology Fuel* 185 (2015) 818-833
- [14] Modi A. J., Gosai D.C., "Experimental Analysis of Performance of Thermal Barrier Coated (TBC) Diesel Engine", *International Journal of Advances in Thermal Science and Engineering*, 1(1) June 2010, pp. 17-25, Serials Publication, New Delhi.
- [15] Modi A.J., Gosai D.C., "Biodiesel: The Alternate of Petroleum Diesel", *Proceedings of 3rd International Symposium on Renewable Energy for Rural*

- Development (ISORE - 2010), February 25-27, 2010, S. N. Arts, D. J. Malpani Commerce & B. N. Sarda Science College, Sangamner, Dist. Ahmednagar, Maharastra, India.
- [16] Roy MM, Tomita E, Kawahara N, Harada Y, Sakane A, 2009, "Effect of fuel injection parameters on engine performance and emissions of a supercharged producer gas-diesel dual fuel engine". SAE Technical Paper; SAE, pp. 01-1848.
- [17] Karen, C., Andrés, A., Francisco, C., 2012, "Effects of oxygen enriched air on the operation and performance of a diesel-biogas dual fuel engine". Original Research Article Biomass and Bioenergy, Volume 45, pp. 159-167.
- [18] Biplab, K. D., Niranjana, S., Ujjwal, K. S., 2011, "Thermodynamic analysis of a variable compression ratio diesel engine running with palm oil methyl ester". Original Research Article: Energy Conversion and Management, Volume 65, pp. 147-154.
- [19] Phan, M.D., Kanit, W., 2007, "Study on biogas premixed charge diesel dual fuelled engine". Original Research Article: Energy Conversion and Management, pp. 2286-2308.

Definitions

E0 - Neat petroleum fuel

E25 - Blend of 10% Ethanol with 90% of Conventional petrol

B40 - Blend of 15% Ethanol with 85% of Conventional petrol

B100 - Neat Ethanol fuel

BTE - Brake Thermal Efficiency

BP - Brake Power

HC - Hydrocarbon

CO - Carbon Monoxide

NO_x - Nitrogen oxide

SFC - Specific Fuel Consumption

Seismic Risk Assessment of Existing School Buildings in Egypt

Islam M. Ezz El-Arab

Structural Department of Engineering, Tanat University, Egypt

Abstract— In recent decades, Egypt has had high volume of investments a high density in the existing densely populated school buildings throughout Egypt. It should be noted that the buildings seismic design issued during the construction phase have been inadequate design. Consequently most of the school buildings are facing a seismic risk. In this Paper numerical development of fragility assessment curve for moment resisting frame reinforcement concrete of the existing school buildings in Egypt as the case study is presented herein. The Ambient Vibration Analysis (AVA) has provided a reliable means to evaluate the actual dynamic characteristics of the existing schools buildings, which can be concluded the actual numerical fragility curve of seismic risk mitigation.

The study succeeded to present reliable fragility curves to show the peak ground acceleration for 50% probability of exceeding slight, moderate, and sever damage of ground acceleration approximating from 0.15 to 0.4 g using three real scaled time history of earthquakes Al-Aqaba occurred in 1995, Northridge occurred in 1994, and El-Centro occurred in 1940, respectively, to assess the structural seismic risk performance levels of existing Egyptian schools, for different return period earthquakes, for lives saving, repair costs, and the strengthening works after and/or pre- earthquake excitation.

Keywords— Existing Schools, Seismic risk, Fragility curve, Egypt.

I. INTRODUCTION

In the last decades of Twentieth Century, the damages that have occurred to public buildings due to earthquakes proved to be more serious than that one occurred to the private buildings. In Egypt, school considerable densely populated buildings constitute number of the public buildings. Life's losses of many people and damages levels of public and private buildings so that, evaluating the seismic performance of buildings and proposing some effective methods to rehabilitate them against earthquakes is an essential step toward hazard mitigation and risk assessment. The moderate earthquake that has occurred in October, 1992 near Cairo caused severe damages to hundreds of schools. Many schools have collapsed while others have suffered different degrees of damage [1,2]. Typical projects developed by the Ministry of Educational have been used

throughout all governorates until the year 1992. After 1992, typical projects by the General Authority for Educational Buildings (GAEB) have been implemented. These typical projects are similar architecturally with minor differences regarding the foundation design ranging from one site to another. This is particularly useful in regions of moderate and slightly seismicity, such as Egypt and the Middle East zone, where Egyptian General Authority of Educational Buildings (EGAEB) is currently developing retrofit programs, in addition to setting a pre-earthquake plan.

In order to evaluate the probability of structure is exposure to damages due to various ground motion excitations; the fragility curve can be a good thermometer for pre-earthquake excitation estimation, moreover the planning tools, retrofitting and strengthening of the existing buildings structures; [1]. Developing fragility curves for a specific type of building is a probabilistic method to estimate the probability that the building will exceed a specific state of damage for a definite value of the seismic intensity parameter.

The complex structures the material properties and boundary conditions are often not well known. In addition, inclusion of general damping in finite element analysis is still deemed as a main parameter that has significant effects on the actual dynamic characteristics of these existing schools that has effect on the numerical assessment of fragility curve of schools. Ambient Vibration Analysis is concerned with field testing measurements, which is used to obtain a model for the modal analysis; it can be defined as Experimental Modal Analysis (EMA), which is based on the measured vibration modes of the structure. Hence this generally results in producing a large amount of data, there is a need to compress the amount of data by developing an experimental parametric model of the studied structure that essentially contains the same information as the original vibration data. Generally, the process of establishing a model using the data is called System Identification, [2]. Dynamic system identification will be an important step to obtain the real numerical fragility curve of schools.

Framed Reinforcement Concrete (FRC) structures are commonly found in many countries. FRC represents approximately 75% of the building stock in Egypt; In the recent years, several studies in seismic risk assessment and development of fragility curves for existing RC buildings

are a matter of great concern by the researchers, [3, 4]. Fragility curves of reinforcement existing buildings can be developed empirically as well as analytically. Empirical fragility curves are usually developed based on the damage reports from past earthquakes. When actual reinforcement concrete building damage and ground motion data are not available, analytical fragility curves can be used to assess the performance of building, [5, 6].

The main objective of this study is to find analytical fragility curves for Egyptian typical reinforced concrete school to describe the probability of a structure is exposure a specific damage state due to various levels of ground excitation. This can be used for prioritizing retrofit, pre-earthquake planning, and loss estimation tools based on numerical approach taking into account, the ambient vibration measurements of study's cases reveal results describing the real dynamic behaviour of the structure, the structural parameters and the variation of the input ground motion. Prior to the newly established Egyptian loading seismic regulation code for the building structures and bridges (ECP 201(1993,2003, and 2008))[7,8], the existing schools have been designed using the seismic design coefficient method (scaled Dynamic effect factor (I) to be matching with Egyptian seismic map accelerations values).

II. EGYPTIAN SCHOOLS BUILDINGS CONFIGURATION

In Egypt, the school buildings systems have different certain prototypes prepared by the General Authority for Educational Buildings (GAEB). Provincial directorates have are responsible for construction supervision of these schools. Although these typical projects display minor differences from one province to another, which are architecturally similar.

The (GAEB) has classified the school buildings into seven models. This classification has been done based on two main parameters. The first is numbers of classrooms (capacity of school); while the second is soil profile properties; (bearing capacity, and foundation system) that depends on site condition and soil investigation results.

The structural systems of school buildings designed by (GAEB) are as follows:

1- Reinforcement concrete skeleton system with an ordinary frame action among beam columns connections where no special steel details are available. Bearing wall system has effect partially where all block works are done before casting the horizontal structural system (slabs and beams) in a traditional construction sequence, especially in the urban areas of Egypt.

2- Schools are designed and constructed in accordance with ECP- 201 [7] for the loading and ECP-203 [8] for reinforcement concrete design to resist the vertical loads

and lateral stability of the building. Before 1992 an old school has been designed under the vertical loads only.

The structural system at all existing buildings are Moment Resistance Frame (MRF) to earthquake lateral load stability with filling block works for all perimeters and internal partitions that have significant effect on the dynamic performance of school as it shown at an experimental study conducted by Sobiah, and Ezz El-Arab 2012,[2]. Author, and Sobaih, worked to evaluate and determine the ambient vibration analysis of these types of schools, to determine the actual dynamic characteristics [1,2]; as shown in Fig.1 (a) and (b), respectively. the measurements analysis of experimental results will be used to determine the actual dynamic characteristic of this type of Egyptian existing schools taking into consideration all construction and non-structural parameters, to be verified with the 3D finite element that will be considered as an analysis to assess the seismic risk of existing schools.; as it will present in details in the following sections.

III. NUMERICAL VERIFICATION VERSUS AMBIENT VIBRATION EXPERIMENTAL RESULTS

The dynamic characteristics of the existing schools are considered as one of the important parameters that affecting the numerical analysis, for expecting the fragility curve of these existing school buildings for two reasons; The first reason is the construction sequence in which the slabs and beams are being cast after the building block works for perimeter and internal partition with a heavy density block work, for that the actual system will not be pure Skelton system, but it will be working a partially bearing wall system in addition to the ordinary frame moment resistance. The second reason is the actual behaviour of the block works filled frame of school, which will improve the overall stiffness of school building as a bracing system.

In case of disregarding these two actual parameters, the study will be more conservative moreover, no code formula will be calculating the actual dynamic characteristics of existing school buildings. Hence, the experimental investigation work is the ideal methodology to measure and assess the dynamic characteristics of buildings [9, 10], using the ambient vibration testing techniques. For this purpose, the dynamic response of the chosen school buildings under ambient conditions have been measured using the Kinometrics Altus K2 Strong Motion Accelerograph [11] with an internal triaxial force-

Balance accelerometer in addition to other nine sensors to have a total number of 12 channels, as shown in Fig. 2.



(a): Case 1: Preparatory School with 36 classrooms, (Sehaim School).



(b): Case 2: Secondary School with 8 classrooms, (El-Gaafaria school).

Fig. 1: Photos of Study Cases, Schools

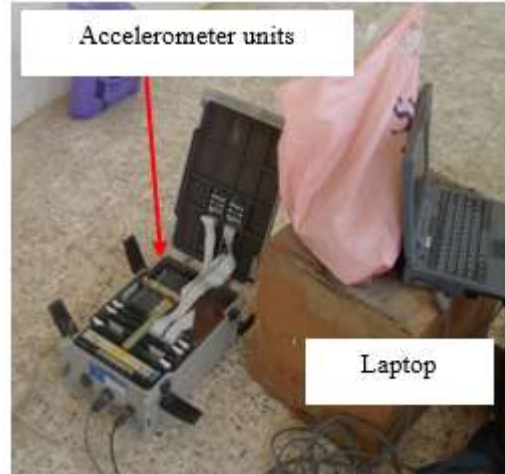


Fig. 2: The Kinemetrics Altus K2 Strong Motion Accelerograph.

These channels are used with cables with different lengths (5, 10, 15, 65, and 120 meters). With ambient vibration measurements, the time history of the forcing function cannot easily be measured. Therefore, the peak amplitude method [12] is used herein to extract the model parameters. In this method, the natural frequencies correspond to peaks of the response in the frequency domain.

Fig. 3 shows the recorded amplitudes versus the angular frequencies for the chosen school buildings, i.e., Sehaim and El-Gaafria schools, respectively (study cases of Delta School located in North of Egypt). The ambient vibrations for each school were measured for 60, 120, and 180 seconds in a trial to verify the accuracy of results. The available recording channels of the accelerograph have been used to perform the modal testing process in the two perpendicular directions, i.e., longitudinal and transversal, for each school building, to estimate the first three time period of each building.

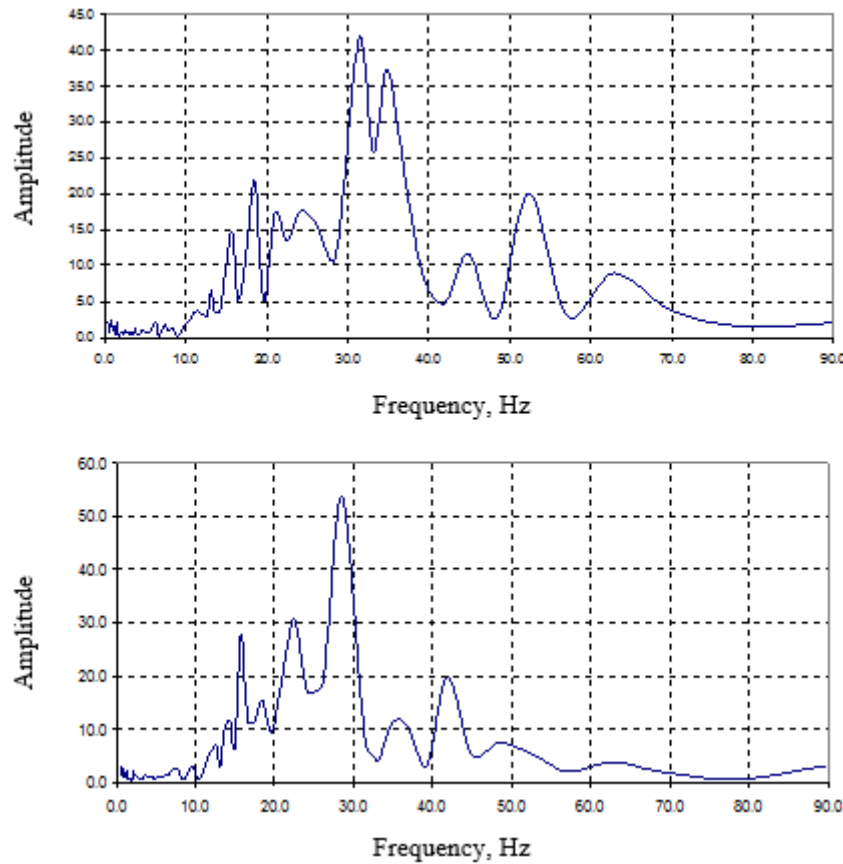


Fig. 3: The Fourier Response in Transversal and Longitudinal Directions of study cases Schools.

In Figs 4 and 5 the ambient vibration measurements results for the two schools buildings with different file durations compared to 3D Finite Element Modelling (FEM) of school taking into consideration the non-structural parameters of block work filling ordinary frame of building as it explained above; concrete strength of reinforcement concrete elements with different concrete strength F_{cu} = 20, 25, and 30 Mpa, and the density of block works that used in wall partitions. It should be noted that the first three measured natural periods agree well for different file durations. Also 3D finite element modelling will be improved and enhanced taking into consideration all other real parameters to get the most compatible dynamic characteristic to be matching with the real ambient vibration experimental results.

The paper succeeded to provide 3D simulation using advanced finite element modelling (Etab Ver.15),[13] taking into consideration all non-structural elements like block works and traditional construction procedure that have significant effect on the overall dynamic characteristics of existing school as it cleared in Figs 4 and 5. Based on that verification the seismic analysis can be done for this actual finite element, so as to start the seismic

risk effects, to estimate fragility curve of Egyptian existing schools.

IV. EARTHQUAKE EXCITATION TIME HISTORY

The earthquake analysis of existing schools will be done under different real time history for three different ground excitations, which are selected to match the seismicity of the school site. One of them is Al-Aqba Earthquake, which shocked Egypt in 1995. The focused point of this earthquake was Al-Aqaba Gulf east of Egypt. The other two earthquakes El-Centro, occurred in 1940, and Northridge, occurred in 1994. The time history of the earthquakes was scaled in consistence with the seismic requirements for the zone of study cases, as shown in Fig. 6. The peak ground acceleration which was used has motion ranges. This range is suitable and compatible to the micro zonation map of seismicity characteristics in Egypt zone. This scaling of earthquake ground acceleration will analyse the results in comparison with the other dynamic and equivalent static load methods in a more rational manner. The response spectrum of the above mentioned earthquakes excitations are presented at Fig. 6.

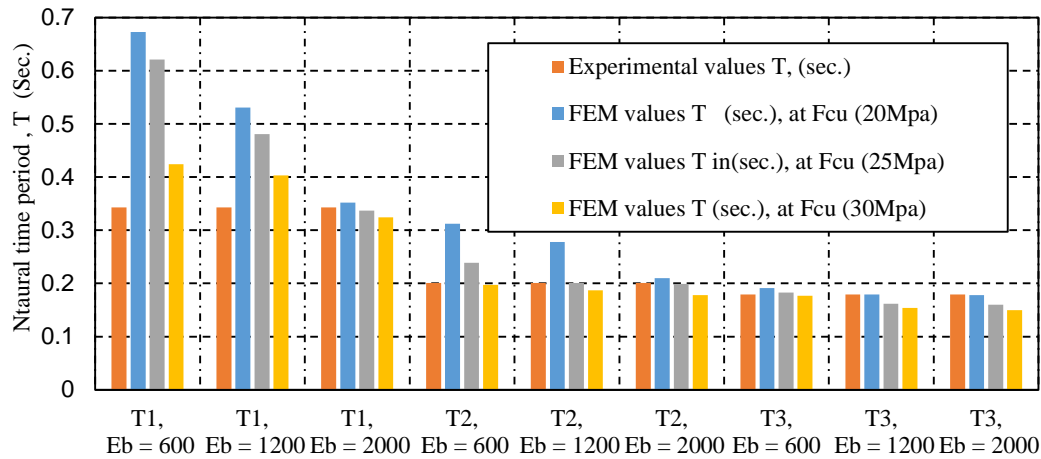


Fig.4: Sehim School Verification of Finite Element Natural Time Period Versus The Experimental Measured Time Period, with Different Block, $E_b= 600, 1200, \text{ and } 2000 \text{ Kg/M}^3$, Respectively. (E_b young's modulus for bricks), (F_{cu} Concrete strength)

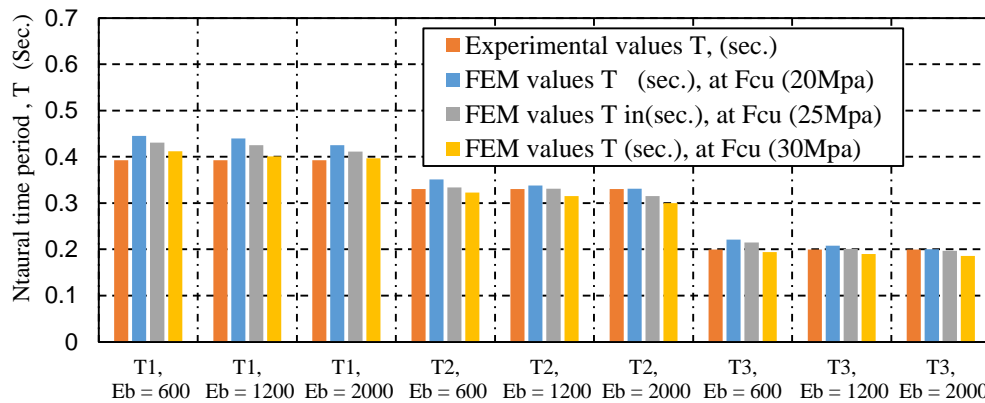


Fig.5: El-Gaafaria School Verification of Finite Element Natural Time Period Versus The Experimental Measured Time Period, with Different, $E_b= 600, 1200, \text{ And } 2000 \text{ Kg/M}^3$, Respectively. (E_b young's modulus for bricks), (F_{cu} Concrete strength).

V. SEISMIC RISK ANALYSIS AND DAMAGE LEVEL OF EXISTING SCHOOLS

The seismic risk performance assessments methodology is briefly reported in this paper. The flowchart methodology is presented at Fig.7.

As shown at Fig.7, the first step in the methodology of seismic risk assessments of existing school buildings in Egypt was the spread and deep investigation in order to understand the peculiarity of seismic performance of the existing school structures. Egyptian existing schools were widely characterized. In this part, a procedure for performance assessment of typical Egyptian school prototypes is established. Egyptian schools are selected prototypes that are designed and constructed based on old EPC, which ignored the seismic lateral stability of the schools.

For the old existing Egyptian schools that was designed and constructed before 2008, they can be classified to two types; the first was designed only under gravity loads as an

intermediate frame system and the second type which can be considered as not fulfilling the structural design requirements where were completely ignored the lateral stability of seismic requirements for super and sub-structural elements.

In order to achieve the main target of this research, the damage levels of existing building are missing in Egyptian Codes EPC, revisions; consider as biggest challenges for any structural design, to estimate the seismic risk of the existing school buildings or any other buildings. Due to the ASCE2007 [10], EMS98 [14]. In ASEC2007 and EMS98, the Damage Level ranges (DL1) for the non-structural damage to severe damage, led to total collapse (DL5). In general, evaluation of the existing buildings the structural engineer and users accept damage level that safe the lives of users and also, give chance for economic repair and rehabilitation works. Then, at each condition of lateral deformation, it should associate a limit state reflecting a section yield level (a specific limit for the Ductility Ratio

of Columns (DRC) and/or beams (DRB)).

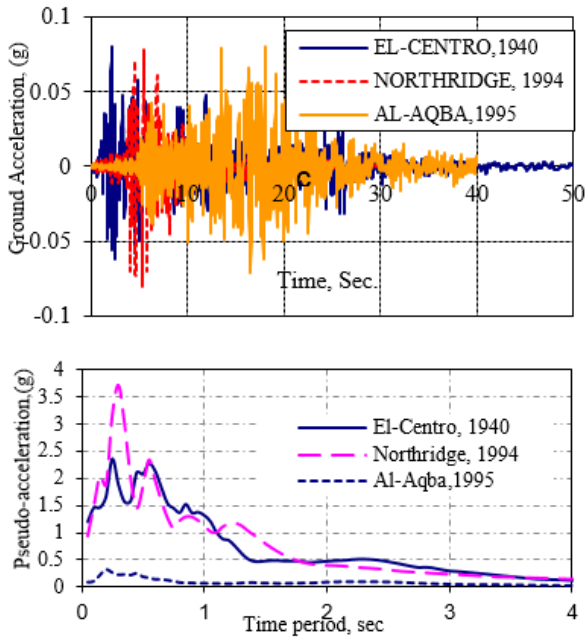


Fig. 6: Scaled Time History Ground Acceleration and Response Spectrum of Earthquakes, Respectively.

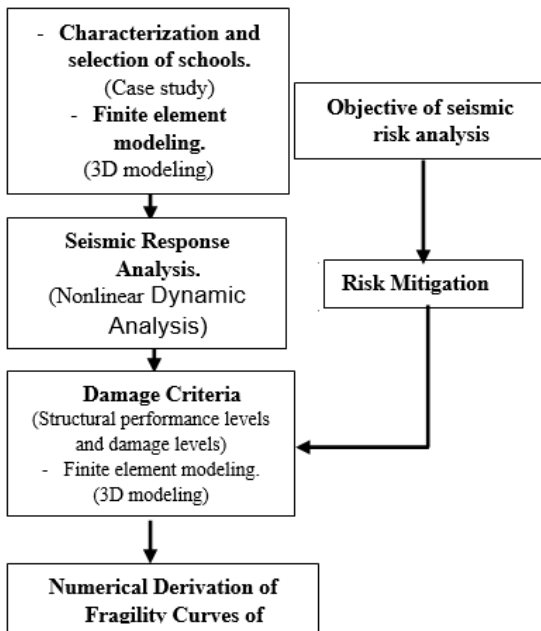


Fig.7: Methodology of Seismic Risk Analysis of Existing Buildings.

Table 1 presents the four damage levels descriptions[10,14], all existing school buildings systems are MRF treated in Egypt, which makes it necessary to build a specific damage levels based on inter storey drift relationship. Relative drift will be determined based on the Ductility Ratio of beams and columns being gotten from the finite element modelling, taking into consideration the fill frame action and actual dynamics characteristics that were measured experimentally at the field.

Egyptian Delta`s schools included at the study cases were analysed in respected three different earthquake ground motions; the first is the earthquake that occurred in Egypt 1995 (Al-Aqaba) and the other two earthquakes that occurred in other parts of the world were scaled the same peak ground acceleration to be adapted with the same one occurred in Egypt as it presented in Fig 6 for the scaled time history and response spectrum, respectively.

Table.1: Damage Criteria to Define Structural Performance (Beam and Columns Considered As Primary Components for Damage Level), [10, 14].

Damage Level	Description	Performance	Ductility Ratio (D.R)
D.L. (4)	Heavy (collapse and near collapse)	For columns and beams considered as primary components the deflection exceed 75% of the ultimate value and at most one structural elements exceed the ultimate value.	$1.00 > DRC_{max}$ $x > 0.75$ $1.00 > DRB_{max}$ $x > 0.75$
D.L. (3)	Significant/Medium Structural	For columns and beams considered as primary components the deflection not exceed 75% of the ultimate value	DRC_{max} (0.25- 0.75) DRB_{max} (0.25- 0.75)
D.L. (2)	Moderate/ Low structural	For columns and beams considered as primary components the deflection not exceed 25% of the ultimate value.	DRC_{max} < 0.25 DRB_{max} < 0.25
D.L. (1)	Weak/ No structural Damage	For columns and beams, the deformation not exceeds elastic limit. Only inter-story drift-sensitive non-structural components are considered.	

VI. SEISMIC RISK AND ANALYTICAL FRAGILITY CURVE OF EGYPTIAN SCHOOLS

There are different methods that can be used for evaluating the seismic risk and estimating the fragility curve of the existing buildings. It can be divided into two main groups by [6, 9] : (1) Obtaining a damage index level by means of

inspection; Estimation of vulnerability based on expert's judgment in case of lack of information about buildings; (2) Evaluation of the damage index level through structural analysis which can be measured analytically based on the ductility ratio of beam and columns in the skeleton building structures. This method that will be presented in the paper, to evaluate the seismic risk and estimate the fragility curve of existing schools in Egypt.

Finite element Models are based on structural analysis provide a greater quantity of results, but reliability depends on their capacity to represent real seismic behavior. Which is based on expert's judgment requires a large number of professionals with in-depth knowledge of the problem having a proven experience, while statistical evaluations which are based on a real damage data can only be applied in zones of moderate or high seismicity where the sufficient data are available.

Therefore, fragility curves have been developed analytically from nonlinear dynamic analyses of typical school prototypes in Egypt. Since damage states are mostly related to structural capacity (C) and the ground motion intensity parameter is related to structural demand (D), the Damage Level (DL) gives the probability that the seismic demand may exceed the structural capacity through determining the ductility ratio of beams and columns.

Under various levels of ground motion excitations selected to be matching with micro-zonation of the ground motion in Egypt; in Fig. 8 the maximum ductility ration of beams, and columns in each floor level of school buildings are presented under different earthquake ground acceleration motions. Fig. 8 a,b,and c show the beam and column ductility ratios under Al-Aqaba,1995, Northridge,1994, and El-Centro,19940, respectively.

As shown in Fig 6 the ground motion acceleration was scaled for two local earthquakes Northridge and El-Centro to be matching and complying with the Egyptian peak Ground Acceleration (PGA) which was presented in Fig.6 for the response spectrum curves for three earthquakes in longitudinal and transversal directions, respectively.

The ductility ratio of columns are higher than the beams by 70% to 80% under all different earthquakes ground acceleration motions, the frame action of the block walls filling among the columns is one of the important parameters that works to improve the overall performance of the super structure of school buildings, where it works as a bracing action at the lower floor levels where the value of base shear and lateral momenta are bigger than the high floor level, The ductility percentage of columns is decreased on top floor levels reaching between 20% to 7% respectively in the third and fourth floor levels, respectively as shown in Fig. 8. The fragility of a structure (or component) is determined with respect to "capacity". Capacity is defined as the limit the seismic load before

failure occurs. Therefore, if Peak Ground Acceleration (PGA) has been chosen to characterize seismic ground motion level, then capacity is also expressed in terms of PGA. In what follows, and in order to simplify the notations, we will consider that PGA as being chosen to characterize the seismic ground motion. The capacity of the structure, is generally supposed to be log-normally distributed [Sobaih et al.2012], [15].

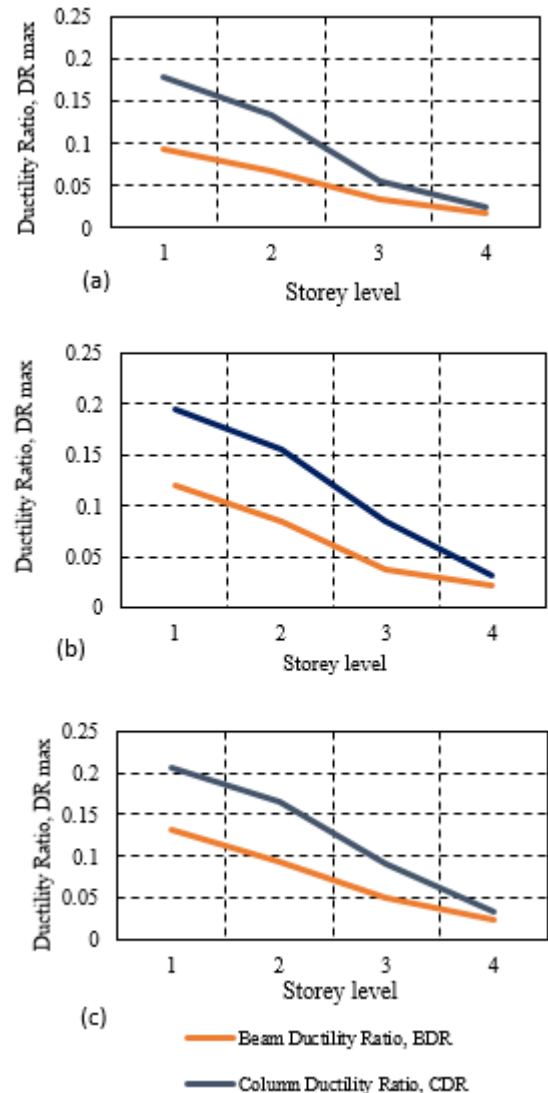


Fig. 8: Maximum Ductility Ratio (DR), of Beam and Column in each Storey levels for Different earthquake ground excitations, (a) Al-Aqaba, 1995, (b) Northridge, 1994, and (c) El-Centro, 1940, respectively.

Beams and columns ductility ratios are the key elements of a seismic probabilistic risk assessment of seismic hazard analysis, seismic fragility evaluation for each component and super structure. These maximum ductility ratios of beams and columns elements allow for the proper risk quantification of the installation, that is the evaluation of failure probability due to all possible earthquake events, which is defined based on the relevant damage level definition that is defined previously in detail at Table 1.

The Seismic Probabilistic Risk Assessment (SPRA) analysis of Egyptian schools (case studies) have been carried out for different PGA value starting from 0.15 up to 0.4g, to be matching with the expected earthquake ground motion accelerations as per EPC-301; in order to assess the seismic safety of existing school buildings or new schools in futures; as shown at Fig.9.

Fig.9 presents the probabilistic seismic hazard analysis that leads to an estimate of the probability of occurrence of different levels of earthquake ground motions at the studied sites. This means that the entire range of possible earthquakes, is considered as potential initiating event and not only design earthquake. A seismic hazard analysis results in the establishment of hazard curves H (a) giving the probability of annual excess of ground motion level a. In general, the output of hazard analysis is a family of curves, each is corresponding to a confidence level and thus accounting for uncertainty in the estimation of seismic hazard. The failure probability is due to the fact that a seismic event is obtained by "convolution" of seismic hazard curve with fragility curve, which is by calculating the total probability by integrating is:

$$P_f = \int_0^{+\infty} P_f(a) \frac{d}{da} (1 - H(a)) = - \int_0^{+\infty} P_{f/a}(x) \frac{dH(a)}{da} da \quad (1)$$

The paper succeeded to present fragility curves associated with peak ground acceleration of 0.15g and 0.2g as being slightly damaged that means the schools RC super structures elements section has a linear behavior for these ground acceleration scales; which can be considered the safety of school structure composed of superstructure. For the peak ground acceleration value being greater than 0.25g to 0.3g, the schools behavior can be considered as moderate damage and the super structures RC elements section will be needing an enhancement procedure, especially for the moderate seismicity zone area in Egypt like North Coast of Egypt, Eastern of Suze Gulf, and Al-Aqba Gulf. For other peak ground acceleration value being greater than 0.35g, the pier will be suffering a severe damage due to such an earthquake excitation and schools super structures RC section will not be safe which is potentially to be subject to a sudden shear failure.

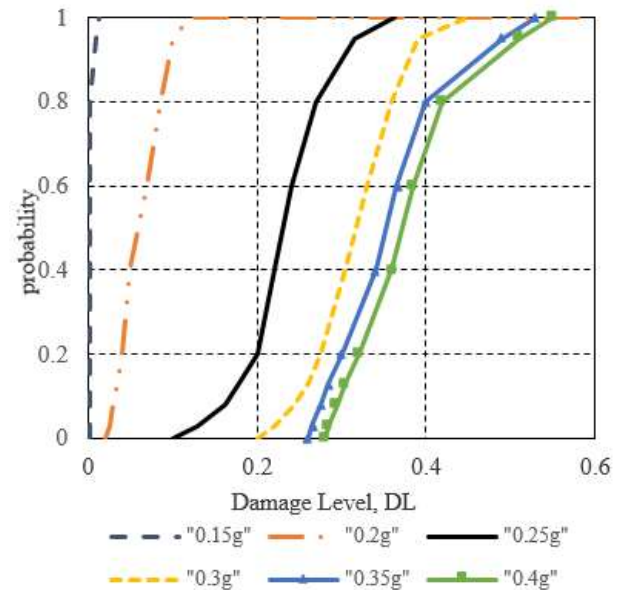


Fig.9: Analytical fragility curve of Egyptian school with different peak ground acceleration.

VII. CONCLUSION

In Egypt, neither schools buildings damages nor their performance have been officially reported after earthquakes which occurred in earlier times. Consequently, this paper proposes a seismic risk and assessment evaluation method based on a structural nonlinear analysis for RC skeleton system of the schools, super structures taking into consideration the real dynamic characteristics that are measured experimentally from field to get into consideration the effect of filling block works that has bracing action on the lateral stability of the buildings. The proposed model is based on the characterization of the maximum ductility ratios of the beams and columns in super structural of school buildings, the damaged level being defined based on the ductility ratios of beams and columns which are under different PGA values.

The paper succeeded to present an easy, accurate, and new analytical propose method to get on the fragility curve of Egyptian schools that are of the most identical statues. The presented fragility curves describe the probability of structure being damaged beyond a specific damage for various levels of ground excitations PGA from 0.15g up to 0.4g. This method will be used for prioritizing the retrofit, pre-earthquake planning, and loss estimation tools. This is particularly useful in certain regions of a moderate seismicity, like Egypt.

The presented reliable fragility curve of the existing schools in Egypt will allow a simple and optimized rules for practical planning, to support the decision makers in Egypt (Egyptian General Authority of Educational Buildings (EGAEB)), as well as consultants simple, applicable, and economic retrofitting strategies can be

defined and integrated in the event of a seismic risk and its mitigation prior to ground motion excitations.

REFERENCES

- [1] Islam M. Ezz El-Arab. Analytical methodology of Seismic Fragility Curve for Reinforcement Concrete Pier Bridges in Egypt. International Journal of Engineering and Advanced Technology (IJEAT) ISSN: 2249 – 8958, Volume-2, Issue-2, December 2010.
- [2] M. Sobaih, I. Ezz El-Arab. A proposed methodology for seismic evaluation of school buildings in Egypt. 14th European Association of Earthquake Engineering Conference EAEE, Makonia, 25-27, August, 2010.
- [3] Vona M, Harabaglia P, and Murgante B. Lesson from Recent Italian Earthquakes. Vienna Congress on Recent Advances in Earthquake Engineering and Structural Dynamics 2013 (VEESD 2013), 28-30 August 2013, Vienna, Austria. Proceedings, In: Adam C. Heuer R. Lenhardt, W. and Schranz C. Eds., ISBN-Nummer, 978-3-902749-04-8.
- [4] Puglia R, Vona M, Klin P, Ladina C, Masi A, Priolo E. and Silvestri F. Analysis of Site Response and Building Damage Distribution Due to the 31 October 2002 Earthquake at San Giuliano di Puglia (Italy). Earthquake Spectra, 29, 497-526. <http://dx.doi.org/10.1193/1.4000134>.
- [5] S A Kurian, S K Deb, and A Dutta. Seismic vulnerability assessment of a railway over bridge using fragility curves. Proceeding of 4th International Conference on Earthquake Engineering, Taipei, Taiwan, 2006.
- [6] Lagomarsino S, and Giovinazzi S. Macroseismic and Mechanical Models for the Vulnerability and Damage Assessment of Current Buildings. Bulletin of Earthquake Engineering, 4, 415-443. <http://dx.doi.org/10.1007/s10518-006-9024-z>.
- [7] ECP-201 Permanent Committee. ECP-201:1993, ECP-201:2003, and ECP-201:2008 - Egyptian Code for calculating loads and forces in structural work and masonry. HBRC, Giza, 1993, 2003, and 2008(Draft), respectively.
- [8] ECP-203 Permanent Committee. ECP-203:2007- Egyptian Code for design and construction of concrete structures. HBRC, Giza, 2007.
- [9] Borzi B, Vona M, Masi A, Pinho R, and Pola D. Seismic Demand Estimation of RC Frame Buildings Based on Simplified and Nonlinear Dynamic Analyses. Earthquakes and Structures, 4, 157-179. <http://dx.doi.org/10.1007/s10518-011-9309-8>.
- [10] Seismic rehabilitation of Existing Buildings (2007) ASCE Standard ASCE/SEI 41-06. American Society of Civil Engineers.
- [11] Altus K2 Strong Motion Accelerograph, Kinematics, Inc. Pasadena, California, USA, <http://www.kinematics.com>.
- [12] Sobaih, M, Abd El-Rahman K, and Mady M. Estimation of Dynamic Characteristics of Existing Common Reinforced Concrete Buildings in Egypt Using Ambient Vibration Tests. Proc., 14th World Conference on Earthquake Engineering, Oct. 12-17, Beijin, China, Paper No. 12-01-0194.
- [13] Computer and Structures CSI. Structural and earthquakes engineering software. ETABS 2015, (<https://www.csiamerica.com/products/etabs>).
- [14] Grünthal G. European Macroseismic Scale 1998 (EMS-98) European Seismological Commission, sub commission on Engineering Seismology Working Group Macroseismic Scales. Conseil de l'Europe, Cahiers du Centre Européen de Géodynamique et de Séismologie, Vol. 15, Luxembourg.
- [15] [Mohamed E Sobaih](#), [Maha A Nazif](#). A proposed methodology for seismic risk evaluation of existing reinforced school buildings. [HBRC Journal](#), [Volume 8](#), [Issue 3](#), PP. 204–211, December 2012. (<http://dx.doi.org/10.1016/j.hbrcej.2012.10.006>).

ITIL Implementation in a Moroccan Stat Organization: The case of incident management process

Mourad EL Baz¹, Malik Motii Armand², Collins Anong³, Belaiassaoui Mustapha⁴

¹Department of Mathematics and Computer Science, University Dakar Bourguiba , Senegal

²Department of Mathematics and Computer Science, University Hassan I, Morocco

³Department of Mathematics and Computer Science, University Dakar Bourguiba , Senegal

⁴Department of Mathematics and Computer Science, University Hassan I, Morocco

Abstract— *IT departments were viewed as a cost center and not as an entity in the service of strategy. But this has changed in recent years because of market competitiveness and also due to the fact that the adoption of a management approach focused on the customer and driven by IT is no longer a luxury but a real necessity. This gave rise to several approaches that recommend best practices for improving IT service quality, including the ITIL framework.*

This paper proposes a method of implementing the ITIL approach with a practical implementation of the Incident Management process in a Moroccan firm.

¹ Information Technology

Keywords— *ITIL, IT services, IT service quality, incident management.*

I. INTRODUCCION

Until recently, IT departments were viewed as a cost center and not as an entity in the service of strategy. But the situation has changed dramatically in recent years. According to Gartner, "... more and more companies are abandoning vision of service-centric IT costs as they become aware of its power to transform business processes [15].

It seems more appropriate to adopt a vision of IT efficiency closer to the concepts of quality of service rendered to the client instead of considering only the standpoint of cost of equipment and resources [1].

This phenomenon owes much to the increased competitiveness of the market and the idea that adopting a management approach focused on the customer and driven by IT is no longer a luxury but a real necessity. The company now expects the IT department to function as a commercial entity and this brings new challenges: improving performance, reducing operating costs, introduction of effective organizational change (addition of new processes and new technologies), all of which will help the IT

department succeed in his new role and demonstrate its impact on business operations.

This type of problem and these recurrent issues have aroused various reactions among computer professionals, but also the quality specialists or organization. To solve problems related to efficiency and response to customer needs what better response than the use of best practices? [1].

ITIL (Information Technology Infrastructure Library) provides a framework of best practice guidance for IT service management and since its creation, ITIL has grown to become the most widely accepted approach to IT service management in the world [2].

Basing IT processes on ITIL guidelines, companies can effectively manage assets, staffing, changes and IT service levels, and thereby transcend the simple asset management and help desk for proactive improvement of IT activities. A good implementation can reduce the occurrence of IT failures, improve service levels and customer satisfaction, and reduce both fixed and variable costs. It allows IT service to gain credibility, improve performance, reduce cost and maximize efficiency in the company by a more productive use of information system.

II. OVERVIEW OF ITIL

ITIL (Information Technology Infrastructure Library) is the result of years of experience and reflection on the problems posed by information technology. ITIL is a framework of best practices for IT service delivery; this framework helps companies achieve their goals of quality and cost control [3]. ITIL was developed in the late 1980s by the CCTA² at the request of the British government, which sought to increase the quality of the provision of its information systems and wanted to have a coherent framework for contracting and evaluation to outsource

operations [4].

The initial version of ITIL consisted of a library of 31 associated books covering all aspects of IT service provision. This initial version was then revised and replaced by seven, more closely connected and consistent books (ITIL V2) consolidated within an overall framework. This second version became universally accepted and is now used in many countries by thousands of organizations as the basis for effective IT service provision. In 2007, ITIL V2 was superseded by an enhanced and consolidated in third version of ITIL, consisting of five core books covering the service lifecycle, together with the Official Introduction [2].

²Central Computer and Telecommunications Agency, now called OGC, Office of Government Commerce

The main new features of version 3 of ITIL are [5]:

- Introduction of the concept lifecycle of the services management, with a focus on service quality IT and services IT "end to end."
- Organization service oriented so that the efforts go towards the customer and the user, rather than towards the technology.
- Awareness by project managers of the importance of ITIL.
- Refocusing very strong around the company's business, source of profit and differentiation.

The five core books cover each stage of the service lifecycle (Figure 1), from the initial definition and analysis of business requirements in service strategy and service design, through migration into the live environment within service transition, to live operation and improvement within service operation and continual service improvement.



Fig.1 : the service lifecycle.

- Service strategy: provides guidance on how to design, develop, and implement service management not only

as an organizational capability but also as a strategic asset. Guidance is provided on the principles underpinning the practice of service management those are useful for developing service management policies, guidelines and processes across the ITIL service lifecycle [6].

- Service design: provides guidance for the design and development of services and service management processes. It covers design principles and methods for converting strategic objectives into portfolios of services and service assets. The scope of service design is not limited to new services. It includes the changes and improvements necessary to increase or maintain value to customers over the lifecycle of services, the continuity of services, achievement of service levels and conformance to standards and regulations. It guides organizations on how to develop design capabilities for service management [7].
- Service transition: provides guidance for the development and improvement of capabilities for transitioning new and changed services into operations. It's a set of guidance on how the requirements of service strategy encoded in service design are effectively realized in service operations while controlling the risks of failure and disruption. It provides guidance on managing the complexity related to changes to services and service management processes, preventing undesired consequences while allowing for innovation [8].
- Service operation: includes guidance on achieving effectiveness and efficiency in the delivery and support of services so as to ensure value for the customer and the service provider. Guidance is provided on how to maintain stability in service operations, allowing for changes in design, scale, scope and service levels. Organizations are provided with detailed process guidelines, methods and tools for use in two major control perspectives: reactive and proactive [9].
- Continual service improvement: provides instrumental guidance in creating and maintaining value for customers through design, better introduction and operation of services. It combines principles, practices and methods from quality management, change management and capability improvement. Organizations learn to realize incremental and large-scale improvements in service quality, operational efficiency and business continuity [10].

III. METHOD PROPOSED FOR THE IMPLEMENTATION OF THE ITIL

Companies are increasingly dependent on IT services to achieve their business goals. This has led them to search for best practices for improving IT services. As part of this work, we propose a method of implementation of the ITIL approach with a practical implementation of the incident Management process in a Moroccan company. This approach is based on a set of previous work aimed at improving the processes (Table 1) and on our experience as a consultant in organization and process in a consulting firm that assists companies in the process of improving the quality of IT service.

Table.1: Process Improvement by the authors

Author	Initialize the project	Assess the current situation	Define the process	Implement tools	Implement process	Assess and evolve
[14]	Business Objective High Level	Analysis of the Processes Gap	- Process Design -Application design		Implementation	
[13]	Workshop on Process	Gap Analysis	Design of project plan	Implementati on and	Implementati on and	Establishmen t of the processes governance
[11]	initializing	initializing	Development	Implementati on	Operation and	
[12]	initializing	Evaluation	Planning	Implementati on	Operation	Review Sustainability

- The first line of table 1 gives the steps of the proposed approach;
- The other lines give the steps by each author.

The proposed method is divided into a series of phases, each phase contains a set of activities to implement and require a number of deliverables. The different steps of the method are:

3.1 Initialize the Project

- Identify areas for improvement and processes to improve: document defining the IT service to improve and the goals to be achieved.
- Define the project: a document giving a description of the project phases (works and resources).
- Obtain direction commitment: presentation the project to the direction and the benefits to be gained for the company.
- Stakeholders awareness: represent the interests of the process and ensure training of stakeholders on the ITIL process.

3.2 Assess the current situation

- Conduct an inventory: a document giving a vision of IT department society (documentation, application, infrastructure, organization, and interfaces with other departments).
- Establish the findings and analysis: a document that outlines the findings and analysis of the current situation.
- Position the current practices of IT department compared to ITIL best practices: a document outlining areas for improvement.

3.3 Define the process

- Design and document the process: define the process activities, procedures, actors and responsibilities.
- Document the new roles and responsibilities: to establish the new organization chart of the new organization.
- Define the action plan for implementation of the process: action plan approved.
- Define the communication plan: a document describing the communication tools to put in place to ensure the implementation process.

3.4 Implement tools

- Implement tools to manage the process: install the platform and tools.
- Set up and prepare documentation process management tools: setup guide,

user's Manual.

- User training on process management tools.

3.5. Implement process

- Implementation of the communication plan: execute communication activities of the process launch.
- Launch the new process into practice: procedures.
- Start reports and reviews.
- Measure progress.

3.6. Assess and Evolve

- Conduct an audit six months after starting.
- Define improvement actions.
- Prepare the next step, to enter a cycle of improvement.

IV. IMPLEMENTATION OF THE ITIL IN A MOROCCAN COMPANY: THE CASE OF INCIDENT MANAGEMENT PROCESS AIM

The company (our case study) is a large company with a workforce of 500 employees organized in the form of a head office and 8 sites in 8 cities.

The aim of this project is the implementation of incident management process based on ITIL and the establishment of a tool for incident management and supervision of the network infrastructure.

4.1 Initialize the Project

The objective of this phase is to define the project boundary. It takes place in the following steps:

- Presentation of the different phases of the project to the IT department;
- Presentation of the approach to the direction of the company and the benefits to be derived for the enterprise;

- Awareness and training the IT department on the ITIL processes.

4.2 Assess the current situation

4.2.1 Inventory

For the company after an initial phase, where the mission of IT department was to implement applications which support business activity, deploy the network and secure it, now she wants to organize the IT team to better meet the expectations of its internal customers and establish a management by the processes.

In this context, the aim of the inventory is to:

- Visit technical facilities, conclude interviews with employees of IT department and 3 staff from other departments;
- Review the applicable documentation;
- Take into account the special constraints of the business, the trades and interfaces with other departments;
- Inventory of applications in production.

Interviews of employees:

This phase consist, firstly to take a tour of technical facilities to get an idea about the organization of facilities adopted by the IT department to manage enterprise infrastructure.

Secondly, to meet the staff of the IT department and 3 employees in other departments. The objective is to analyze the practices of IT department, list the equipment used and have an idea of users satisfaction in other departments.

To accomplish this mission, two questionnaires were based on the type of interlocutor. The first questionnaire's aim is to detect the level of users satisfaction (figure 2).

The second questionnaire used to define the practices of the IT department, it consists of two parts (figure 3 and figure 4).

What is your level of satisfaction on:

	Very satisfied	satisfied	Somewhat satisfied	Not at all satisfied
Information on IT strategy used by your company				
Communication you receive from your IT department				
The information you receive on the software you use				
The quality reception of the help desk				
Listening to and understanding of your request				
Consideration of your emergency				
The information on the status of your request				
The quality of the solution				
Resolution time				
The quality of the intervention				
The adequacy of material in relation to your use				
The adequacy of software in relation to your use				
Speed of access to the internal network of your company				
The quality and functionality of your intranet				

Fig.2: Questionnaire1 (for others departments)

-How many are there of employees in IT department ?

-How many people in the IT department are in charge of IT research and development?

-How many people in the IT department are responsible for incidents treatment?

- Are you able to assess the impact of each incident on the service? Yes No

- If not, how do you prioritize the resolution?

- And if so, is there a way to prioritize the resolution? Yes No

Fig.3: Questionnaire2-part1 (for IT department)

-Solutions to these incidents are recorded to serve? Yes No

-If yes, where and who has access?

-What type of incidents treat you? Equipment Phones Office Network Business applications Others , specify:.....

-How long is the processing of incidents? Urgent:..... Major:..... Minor:.....

-Other departments can they directly involve IT providers? Yes No

-How many incidents you treat an average monthly in the IT department?

-And what percentage of each type? Equipment:..... Phones :..... Office:..... Network:..... Business applications:..... Others :.....

The users have a single point of contact for calls to help desk? Yes No

Fig.4: Questionnaire2-part2 (for IT department)

Documentary analysis

All documents which were the subject of a study and analysis are:

- The organization chart of the company which helps to know the various components of the company and the position of the IT department in the business organization;
- The organization chart of the IT department;
- The change management process;
- The backup management process;
- The form request of change;
- Jobs descriptions of staff IT department.

4.2.2 Findings and Analyses

- Whether a request for assistance, a hardware problem, office automation, messaging, network or application, the technician assesses the impact of the incident,
- diagnoses, treats or redirects the incident to the employee able to handle it. But no solution is noted for being able to capitalize.
- For unresolved incidents, two scenarios are possible: either they are being processed or that the claim is lost and the user receives no feedback.
- No indicators can presently reflect the actual number of incidents treated by the IT department, but the staff
- estimated the daily average is about 10

incidents of application type and 30 of infrastructure type. Which consumes a large portion of the resources of IT department (no indicator of the time allocated to the support function).

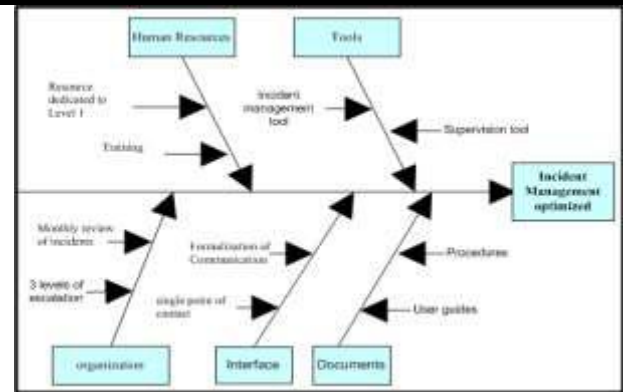
- The lack of traceability has a negative effect on the incident management and causes loss of some queries.
- The lack of capitalization on solutions and a single point of contact are causing a considerable loss of time in the treatment of recurring incidents.
- Limited human resources and the number of incidents, which occupies a large part of resources, impact the success and timing of other projects in the IT department.

4.2.3 Incident Management: Best Practices

The analysis of current practices in IT department of company regarding incident management allows us to position it in relation to ITIL best practices. The areas of analysis are:

- Prerequisites or the necessary minimum level to support process activities;
- Management vision and business objectives;
- Ability to implement the process or the minimum set of activities performed;
- Internal integration to verify whether activities are integrated enough to accomplish the process objective;
- Products or the actual performance of the process;
- Quality or quality control;
- Information Management, or level of information generated from the process, to support management decisions;
- Interface with other processes or external integration;
- Customer focus or customer relationship to ensure satisfaction of customer needs.

Starting from this situation, and in order to establish an effective incident management, the graph 1, summarizes the various areas for improvement, and for which an action plan is defined to accompany the implementation



Graph.1: Areas for improvement

4.3 Define the process

4.3.1 Organization

Based on the current organization chart of IT department and following our discussions of diagnosis, three scenarios for the organization's help desk are proposed. Each proposal has its advantages and disadvantages and the factors of its success.

The choice of the organization's help desk is the starting point for the implementation of incident management process.

4.3.2 Action plan

The following table presents the action plan adopted to implement the process:

Action	Details
Define process	Define process
	Define associated procedures
Implementation of incident management tool	Install the platform
	Designing the incidents as required by category
	Conceive the knowledge base
	Define the reports emerged through the application
Implementation of the network supervision tool	Implement the procedures in the application
	Install the platform
	Integrate servers and peripherals of society in the application
	Test operation of the application tools
	Implement application modules
Training	Installation of modules for remote sites
	Training on incident management tools and network supervision tool
Implement process	-Implementation of communication plan
	-Launch of new process
	-Steering the process

Asses and evolve	- audit after 6 months -define improvement actions. -Prepare the next step, to enter a cycle of improvement.
------------------	--

Breakfast of IT department	Being near to the final user	IT department 2 times a year
Suggestion box	Collect feedback from users, suggestions for improvements:	IT department Permanently

This step consists to implement the various actions outlined in the action plan mentioned above concerning the network supervision tool and incident management tool.

4.4.2 Training

This phase consists of training the staff of the IT department on the incident management process defined and tools incident management and network supervision.

4.5 Implement process

This phase involves the implementation effective of incident management process with the tools of incident management and network supervision.

4.5.1 Implementation of communication plan

This phase involves the implementation of the communication plan below during the launch phase of the process of incident management.

4.5.2 Communication Plan

How	What	Who
Mail	Notify and inform on the incident	Incident Management Tool
Mail	Advise on the establishment of the help desk of the company, communication activity, service levels,	IT department
Stickers, posters, screen savers, mouse pads, t-shirts, memo	Inform the single point of contact (Helpdesk: telephone number and services offered)	IT department
Intranet	Page dedicated to the service desk, services, contacts, statistics, FAQ, ...	IT department
Newsletter IT department (1 to 2 pages, distributed with The payment bulletin)	Presentation of the Help desk, news, ITIL terminology, an image of the Help Desk...	IT department

The communication plan to adopt in order to achieve the objectives of the project is to list the media to put in place at the disposal of the IT department of the company to ensure the implementation of incident management as well as the help desk.

For the IT department:

- scripts for the Help Desk;
- response models;
- forms of diagnosis. For the final users:
- the awareness raising;
- information posters;
- awareness to incident management,
- the communication tools to keep the final user informed.

4.4 Implement tools

4.4.1 Implementation of incident management tool and the network supervision tool

4.5.1 Launch of new process

This phase is to implement the new process which consists of a set of procedures, among which we quote:

- Qualify and save an incident;
- Make the diagnosis and Treatment;
- Closing ;
- Control, monitor and communicate.

This phase is the launch of the help desk work team with incident management process and new practices using the incident management tool.

- Evolution of incidents created by day,
- Evolution of incidents resolved by day,
- Distribution of incidents by level,
- Distribution of incidents resolved by level,
- Distribution of incidents by category,
- Distribution of incidents by status,
- Distribution of incidents per site.

4.5 Assess and evolve

After six months of launching the process, comes the development stage through an audit process to determine what worked well and what worked less well.

This will allow describing the state of practices in relation to original goals and emerging with a set of recommendations to be implemented to improve the quality of the process of incident management.

V. CONCLUSION

The proposed method gave its fruit through an apparent improvement in the company in several aspects, among which we quote:

- Standardization of good practice in the enterprise ;
- Significant improvement of IT service quality ;
- Traceability and visibility of incidents ;
 - Improved visibility of the responsibilities of help desk,
 - Capitalization of knowledge of the help desk.

It should be noted that we were able to implement this method in other companies and it worked, but its success requires a large Commitment of direction (commitment of the management team) as well as the awareness of the staff in order to join in the success of the approach.

REFERENCES

- [1] C. Dumont, ITIL for optimal service, Eyrolles edition, 2007.
- [2] The IT service Management Forum, An Introductory Overview of ITIL V3, It SMF UK, 2007.
- [3] M.Otter, and J.Sidi, and L.Hanaud, IT certification guide, Dunod, 2009.
- [4] Y.Gillette, and M.Bia-Figueiredo, and C.Morley, Business process and information system, Dunod, 2011.
- [5] G.Teneau, J.Ahanda, Guide commented standards and frameworks, organization editions, 2009.
- [6] Office of Government Commerce, ITIL V3 Service strategy, The Stationery Office, 2007.
- [7] Office of Government Commerce, ITIL V3 Service design, The Stationery Office, 2007.
- [8] Office of Government Commerce, ITIL V3 Service transition, The Stationery Office, 2007.
- [9] Office of Government Commerce, ITIL V3 Service operation, The Stationery Office, 2007.
- [10] Office of Government Commerce, ITIL V3 Continual service improvement, The Stationery Office, 2007.
- [11] S.Alter, "Pitfalls in analyzing systems in organizations", Journal of Information Systems Education, Vol. 17(3), 2003, pp.295-302.
- [12] Y.B.Desfossés, and C.Y.Laporte, and A.April, and N.Berhouma, "Method to improve IT services, ITIL-based, in Québec companies", Software Engineering Journal, September 2008, Issue 86, pp. 47-59.
- [13] K.Litten, "Five steps to implementing ITIL", International Network Services, 2005.
- [14] BMC Software, "ITIL for the Small and Mid-sized Business (SMB)", 2005.
- [15] C.Young, "Become and remain the IT provider of choice", Gartner report on IT service management, 2005.

Design and Study of Swirl Injector of Pulse Detonation Engine

Navdeep Banga¹, Kanika²

¹Strategic and Defense Analyst, Research Scholar, Department of Aerospace Engineering, IKG Punjab Technical University, India

²Department of Aerospace Engineering, MRSPTU, India

Abstract— Future Indian Air force and Navy Capabilities indicate the need for a supersonic cruise missile. Therefore, there exists a need for a low cost, light-weight, and efficient means of supersonic propulsion. In this paper my main emphasis on Pulse Detonation Engine, in pulse detonation engine humphey cycle is used ,PDE has thermodynamic efficiency greater than 50% as compared to 35% for present day propulsion technology constant-pressure Brayton cycle currently in use in gas turbines/ramjets/scramjets. Pulse Detonation Engines (PDE's) represent an upcoming new approach to propulsion and with the simplicity of its construction; PDE's produce thrust more efficiently than the current engines and produces a higher specific thrust. Since current rocket engines require heavy and expensive pumps; with mechanical simplicity and thermodynamic efficiency PDE's offer a viable alternative to reduce the cost of launching spacecraft.

Keywords— detonation engines, detonation, PDE, PDE ignition, swirl injector.

I. INTRODUCTION

DRDO is currently developing and working on pulse detonation engine(PDE) as a low-cost, simple, light-weight, and efficient means of supersonic propulsion. The PDE concept has a higher thermodynamic efficiency than the constant-pressure cycles. Detonation is a self-sustaining combustion process that leads to the formation of supersonic combustion products. The wave front produced by the detonation process, is at supersonic speeds, which compresses the unburned fuel and mixture ahead of the wave front. This further compresses the unburned fuel-oxidizer mixture and leads to detonation. Whereas In the process of deflagration the burning of fuels through flames will be moderately simple and gentle and the under the similar condition we observer that main typical that is nothing but the travelling characteristics of this flame will be at subsonic stage. On comparison of deflagration and detonation, detonation is found to be more effective in the terms of pressure and velocity obtained. The PDE concept has a higher thermodynamic efficiency than the constant-pressure cycles currently in

use, such as turbojets, ramjets, and scramjets. A major problem in the development of this type of engine is increasing the propulsive efficiency to acceptable level.

Pulse Detonation Engine

Pulse Detonation Engine typically consists of a sufficiently long tube which is filled with fresh fuel-oxidizer mixtures and ignited by sufficiently strong energy source. Flame initiated by ignition must in relatively short time accelerate to detonation velocity, so the transition from deflagration to detonation must happen in relatively small distance. Detonative combustion produces high pressure which is converted to thrust. After all mixture is consumed by detonation, combustion products have to be evacuated from the tube and fresh mixture must be quickly resupplied, and the cycle is repeated. Typical frequency of such engine operation is usually in range of dozen Hertz.

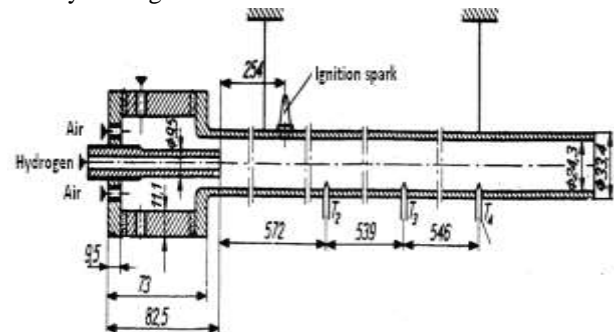
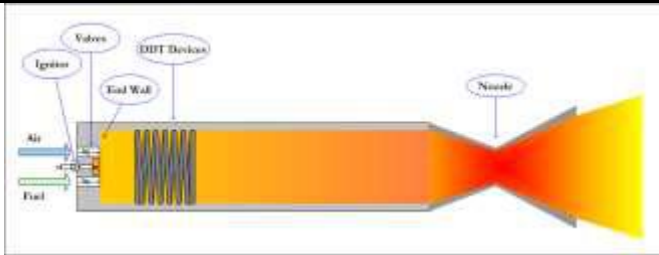


Fig.1: Design of Pulse detonation engine

PDE can operate in wide flight Mach number, ranging from 0 and up to M4+, but the engine operates in a pulsed mode, so the thrust is varying in time and the detonation must be initiated each time. The system is complicated because fast purging and refilling are required. Also the engine is operating in the stoichiometric condition (due to necessity of fast initiation of detonation), and the frequency is relatively low. If the pulsed detonation could be applied for turbojet combustion chambers, it would be necessary to add an extra air to decrease the temperature before the first turbine stage. Also the production of NO_x would be high.

Schematic of the PDE showing the main components

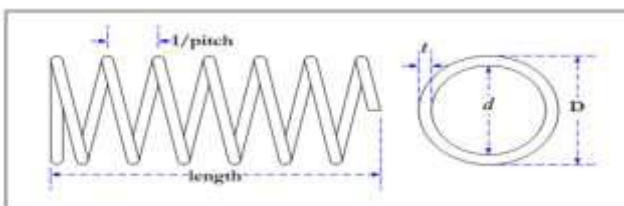


Pre-detonator:-The pre-detonator design was chosen because of its simplicity. At the cost of a small amount of oxygen carried on board, the pre-detonator provides an effortless means of igniting the propane-oxygen mixture quickly with low energy sparks, and makes it possible to transmit an accelerated detonation wave into a less energetic fuel-air mixture.

Shchelkin Spiral:-The pre-detonator has the option of being fitted with a long Shchelkin spiral. The spiral is welded to a flange that enables it to be bolted to the flange of the pre-detonator. The Shchelkin spiral is used to overdrive the detonation wave so that it may be successfully transmitted through the nozzle without decoupling.

II. DDT DEVICES

The deflagration-to-detonation transition (DDT) is a process by which a deflagration flame front is gradually accelerated to form a supersonic detonation wave. As the flame is pushed downstream by the expansion of the burnt gases behind it, the flame front becomes curved and wrinkled by the effects of the boundary layer in front of the flame, flame instabilities and turbulence. As a result, the surface area of the flame grows which increases the rate of reaction of the fuel and oxidizer. Thus, the rate of release of energy is amplified causing the flame front to be accelerated at an even faster rate. Finally, the increased energy release leads to the formation of one or more localized explosions and the transformation of the flame into a detonation wave.



Nozzle:

The nozzle was designed to transmit the detonation wave with minimal loss of velocity. It was found that larger diverging angles or abrupt transition of area cause detonation waves to decouple, due to the excessive curvature of the detonation wave and the cooling of the flow due to the rapid expansion.

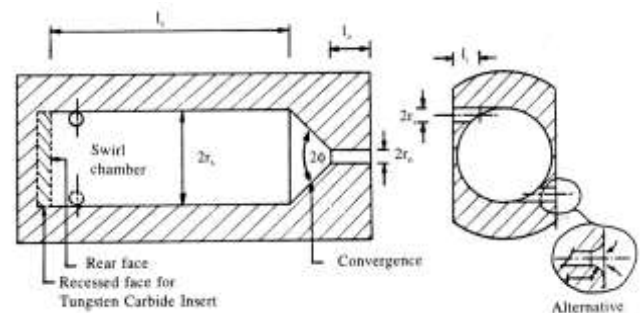
Main Combustion Chamber with Swirl Injector Block:

The carbon steel collars hold pressure and optical transducer ports and contain orifices for water to circulate through them, and also provide additional strength to the

tube. The combustor tube is covered with a layer of sheet metal in between the collars, forming a water cooling jacket. Water is pumped in through four tubes bored into the wall of the main flange on the left and the water exits the cooling cavity through four tubes welded to the last collar on the right hand side of the tube. At the left hand end of the main combustor is the swirl injector block, which has four ports through which a fuel-air mixture is pumped in.

Analysis of swirl injector in pulse detonation engine-

Swirl injectors are used in liquid rocket, gas turbine, and diesel engines to improve atomization and mixing efficiency. The circumferential velocity component is generated as the propellant enters through helical or tangential inlets producing a thin, swirling liquid sheet. A gas-filled hollow core is then formed along the centerline inside the injector due to centrifugal force of the liquid sheet. Because of the presence of the gas core, the discharge coefficient is generally low. In swirl injector, the spray cone angle is controlled by the ratio of the circumferential velocity to the axial velocity and is generally wide compared with non-swirl injectors. The basic internal geometry of the pressure swirl injector consists of a main cylindrical body called the swirl chamber. At, or near, the upstream end of the swirl chamber (the closed end or 'top' face) are attached the inlets. The inlets are one or more cylindrical or rectangular channels positioned tangentially to the swirl chamber. At the opposite end of the swirl chamber, the 'open' end, there is a conical convergence. Toward the apex end of the cone there is a cylindrical outlet, concentric with the swirl chamber.



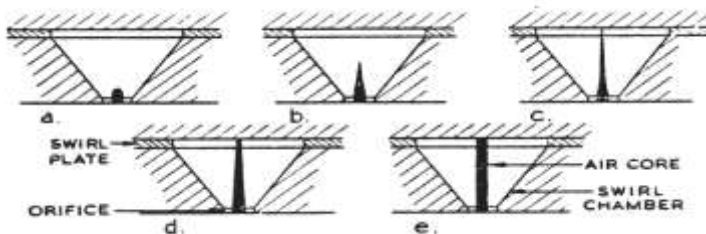
Swirler –

The swirlers used to impart rotation to the airflows were of particular importance. In order to obtain a symmetrical flow, swirlers must be machined to within very tight tolerances. Swirl vanes may be flat, or they may be curved in a variety of ways. No matter what the type of swirler used, however, it is essential to machine the assembly very precisely. The types of machining operations available to produce swirlers are somewhat limited, and, if the swirlers are assembled from separate part, the difficulty of assembling them correctly increases dramatically. For this investigation, twisted-vane swirlers were employed, as

these are compact, can be inserted directly into an air duct, and can be machined from a single piece of stock, without any further assembly steps. In order to machine twisted-vane swirlers, aluminum blanks were first turned down to the precise diameters required. The blanks were initially simple cylinders, with sections cut to two diameters: one that let them fit tightly into sleeve for the next step in the machining process, and one that matched the required final diameter of the swirler. The centers of the blanks were then bored out to the required inner diameter necessary for each swirler. A special rotating assembly, attached to a precision stepper motor, was then attached to a vertical milling machine.

Internal flow of swirler

The air-core is usually seen to initiate from the outlet orifice, where the pressure is already ambient, as one gradually increases the injection pressure. From some observations the air-core is also seen to initiate simultaneously from the upstream face of the swirl chamber. Thus the two ends of the air-core along the axis are not initially joined. The initiation of the air-core at the upstream end of the swirl chamber is likely to be due to one or more of the following mechanisms. Firstly, as the liquid, initially under pressure, enters the swirl chamber, then dissolved gases within the liquid come out of suspension and are buoyed inwards toward the low pressure region on the swirl chamber axis. Secondly, there maybe an intermittent seepage of the ambient gas from the outlet along the axis to the back face, possibly in the form of small bubbles. Figure below is a diagram showing the air-core formation for an atomizer with a short swirl chamber and a negligible length outlet. There is seen to be no air-core formation initiating from the upstream face in this instance. The presence of an air-core ensures that the body of liquid within the nozzle is in the form of an annulus and that the passage of a liquid particle through the nozzle will thus describes helical path.



providing a swirl rotational motion to the fuel inside the injector. The key advantage of hollow cone sprays is the high area to volume ratio, which can lead to the required level of atomization without large penetration lengths. Swirl injectors are used in liquid rocket, gas turbine, and diesel engines to improve atomization and mixing efficiency. The circumferential velocity component is first generated as the propellant enters through helical or

tangential inlets producing a thin, swirling liquid sheet. A gas-filled hollow core is then formed along the centerline inside the injector due to centrifugal force of the liquid sheet. Because of the presence of the gas core, the discharge coefficient is generally low. In swirl injector, the spray cone angle is controlled by the ratio of the circumferential velocity to the axial velocity and is generally wide compared with non-swirl injectors.

Pulsating Flow with Swirl Injectors

The spray and acoustic characteristics of a gas/liquid swirl coaxial injector are studied experimentally. Self-pulsation is defined as a pressure and flow rate oscillations by a time-delayed feedback between liquid and gas phase. Self-pulsation accompanies very intensive scream and this strong scream affects atomization and mixing processes. So, the spray and acoustic characteristics of self-pulsation are different from those of general swirl coaxial spray. The liquid and gas velocity is selected as the variables of injection conditions and recess length is chosen as the variable of geometric conditions. By shadow photography technique, spray patterns are observed in order to investigate the macroscopic spray characteristics and determine the onset of self-pulsation. For acoustic characteristics, a PULSE System was used. Using He-Ne laser and photo detector system frequencies of spray oscillations are measured. And self-pulsation boundary with injection conditions and recess length is obtained. From the experimental results, the increase of recess length leads to the rapid increase of the sound pressure level. And characteristic frequency is mainly dependent on the liquid velocity and linearly proportional to the liquid velocity. The frequency of spray oscillation is the same as that of the acoustic fields by self-pulsation.

III. CONCLUSION

To replace other injectors such as (air blast ,orifice ,etc) used in the pulse detonation engine ,we have studied the concept of swirl injector. The swirl injector will increase the atomisation of the fuel by adding the centrifugal force of the swirler and thus increasing the efficiency of the engine. We have worked in a steady mode with this swirl injector but still the research is to be done on pulsating mode ie. It has to worked on different frequencies such as 8 Hz ,25 Hz and 50 Hz. I have stuided the basic concept of swirl injector and designed it .For testing this swirl injector I have also designed a set up box for it in which various parameters such as spray cone angle ,mass median daimeter (MMD) and mixing is done. Still the results are accurate but more research is to be done on this swirl injector for reaching the exact results.

REFERENCES

- [1] Barrere, M., *La Recherche en Combustion, Pour Quei Faire?, Colloque International Berthelot-Vielle-Mallard-Le Chatelier, Universte de Bordoeaux I – France, 20-24 Juillet, Tom I, pp.XXIII-XLVIII, 1981.*
- [2] Voitsekhovskii, B. V., Mitrofanov, V. V. and Topchiyan, M. E., *Structure of the detonation front in gases, Izdatielstvo SO AN SSSR, Novosibirsk, (in Russian) 1963.*
- [3] Wójcicki, S., *Silniki pulsacyjne, strumieniowe, rakietowe, MON, Warszawa, 1962.*
- [4] *Pulsed and Continuous Detonation*, edited by: Roy G., Frolov S., Sinibaldi J., Torus Press, Moscow, 2006
- [5] *Progress in Pulsed and Continuous Detonations*”, edited by G. D. Roy and S. M. Frolov, Moscow, Torus Press, 2009
- [6] Bykowski, F. A., Mitrofanov, V. V., and Vedernikov, E. F., *Continuous Detonation Combustion of Fuel-Air Mixtures, Combustion, Explosion and Shock Waves, Vol.33, pp.344–353, 1997.*
- [7] Bykovskii, F. A., Zhdan, S. A. and Vedernikov, E. F., *Continuous Spin Detonation of Hydrogen–Oxygen Mixtures. 1. Annular Cylindrical Combustors Combustion, Explosion, and Shock Waves, Vol. 44, No. 2, pp. 150–162, 2008.*
- [8] Bykovskii, F.A. and Vedernikov E. F., *Continuous Detonation of a Subsonic Flow of a Propellant Combustion, Explosion, and Shock Waves, Vol. 39, No. 3, pp. 323-334, 2003.*
- [9] Kindracki J, Fujiwara T. Wolanski P., *An experimental study of small rotating detonation engine, in: Pulsed and continuous detonation. Torus Press, pp.332-338, 2006.*
- [10] Zhdan, S. A., Bykovskii, F. A., and Vedernikov, E. F., *Mathematical Modeling of a Rotating Detonation Wave in a Hydrogen-Oxygen Mixture, Combustion, Explosion and Shock Waves, Vol.43, pp.449–459, 2007.*
- [11] Davidenko, D. M., Gökalp, I., Kudryavtsev, A. N., *Numerical study of the continuous detonation wave rocket engine. 15th AIAA International Space Planes and Hypersonic Systems and Technologies Conference, 2008.*
- [12] Zhdan S., *Mathematical model of continuous detonation in an annular combustor with a supersonic flow velocity, Combustion, Explosion, and Shock Waves. 44, pp. 690-697, 2008.*
- [13] Hishida, M., Fujiwara, T. and Wolanski, P., *Fundamentals of rotating detonation, Shock Waves. 19, 2009.*
- [14] Tae-Hyeong, Yi, Choi, J. Y., Loul, J., Turangan, C. and Wolanski, P., *Propulsive Performance of a Continuously Rotating Detonation-Based Propulsion System, ICDERS, Minsk, 2009.*
- [15] Tobita A., Fujiwara T., and Wolanski P., *Detonation engine and flying object provided therewith, Publication data: 2005-12-29; Japanese Patent, No. 2004-191793 (granted 2009) Patent US 2005_0904A/AND/01983, 2009.*
- [16] Li, J. L., Fan, W., Yan, C. J., Tu, H. Y., Xie, K. C., *Performance Enhancement of a Pulse Detonation Rocket Engine”; Thirty-Third International Symposium on Combustion, Beijing, 1-6 August, 2010.*
- [17] Kasahara, J., Matsuoka, K., Nakamichi, T., Esumi, M., Matsuo, A., Funaki, I., *Study on High Frequency Rotary Valve Pulse Detonation Rocket Engines, Detonation Wave Propulsion Workshop 2011, Bourges France, 11-13 July 2011.*
- [18] Bykovskii, F. A., Zhdan, S. A., *Continuous Spin Detonation of a Hydrogen-Air Mixture in the Air Ejection Mode, Detonation Wave Propulsion Workshop 2011, Bourges France, 11-13 July 2011. 521*
- [19] Kailasanath, K. “Recent Developments in the Research on Pulse Detonation Engines,” AIAA Paper 2002-0470, AIAA 40th Aerospace Sciences Meeting, Reno, NV, 14–17 Jan. 2002.
- [20] Munipalli, R., Shankar V., Wilson, D.R., and Lu F.K., “Preliminary design of a pulse detonation based combined cycle engine,” ISABE Paper 2001–1213, *15th International Symposium on Airbreathing Engines*, Bangalore, India, 2–7 Sep. 2001.
- [21] Stanley, Steven B., “Experimental Investigation of Factors Influencing the Evolution of a Detonation Wave,” Master's Thesis, Department of Mechanical and Aerospace Engineering, The University of Texas at Arlington, Arlington, TX, 1995.
- [22] Borman, G. L. and Ragland, K.W., “Combustion Engineering,” McGraw Hill, 1998.
- [23] Owens, M., Segal, C. and Auslender, A.H., “Effects of Mixing Schemes on Kerosen Combustion in a Supersonic Airstream,” *Journal of Propulsion and Power*, Vol. 13, No. 4, Jul.-Aug. 1997.
- [24] H. Lefebvre, *Atomization and Sprays*, Hemisphere, Washington, D.C., 1989 .
- [25] N . K. Rizk and A. H. Lefebvre, *Internal Flow Characteristics of Simplex Swirl Atomizers, AIAA J. Propulsion*, vol . 1, no. 3, pp. 193-199, 1985 .
- [26] Anderson, D. N., "Effects of Fuel-Injector Design on Ultra-Lean Combustion Performance," NASA-TM-82624, 1981.

Performance Analysis of LEACH, SEP and ZSEP under the Influence of Energy

Sulekha Kumari

Department of ECE, Mody University of Science and Technology, Laxmangarh, Sikar, Rajasthan, India

Abstract— For any wireless sensor network to work effectively and efficiently in any kind of environment, preventing it from any kind of attack internally and externally, it is very important to setup the network keeping in mind the various parameters which must be considered. Some of the most important parameters are energy consumption, throughput, network area and initial energy that we give to the network. Another most important thing is the protocol that we use in the network. In this paper, the wireless sensor network is setup using LEACH (Low Energy Adaptive Clustering Hierarchy), then SEP (Stable Election Protocol) and then ZSEP (Zonal Stable Election Protocol) and then initial energy that we give to the network is varied keeping the network area constant. The effect of change in initial energy is studied on these protocols and their performance is analyzed.

Keywords— Initial Energy, Protocol, LEACH, SEP, ZSEP.

I. INTRODUCTION

In a wireless sensor network, there can be many numbers of nodes which is used to transfer the information from sink to destination. The efficiency of the network depends on various parameters on the basis of requirement. Some of the important parameters which must be taken in consideration are energy consumption, throughput, packet delivery ratio and delay. Also depending on the requirement of the wireless sensor network, the network area is a very important parameter. The network area should be in sync with the initial energy given to the network so that energy consumption in the network can be reduced and throughput is increased. Also the routing protocol which is used in the network is an essential parameter as it is the set of rules which runs the network. Therefore depending upon the requirement, the right protocol must be chosen for the network so that the network runs efficiently [1].

II. PROTOCOL

In a network area which has large number of densely deployed sensor nodes, there is always a limitation of energy. Therefore, it requires a suite of network protocols that can be used to implement various management and

network functions which include network security, proper localization of nodes and synchronization. Therefore the comparative study of various protocols is necessary to analyze the better performance according to the requirements [2].

1. LEACH Protocol

LEACH [3] stands for Low Energy Adaptive Clustering Hierarchy. For reducing power consumption, it is the first proposed energy-efficient hierarchical clustering algorithm for WSNs. The operation of LEACH is divided in to two phases. First one is setup phase where network is organized into clusters, cluster head advertisement is done and transmission schedule is created. Second one is steady state phase where data is aggregated, then compressed and transmitted to the destination. In LEACH single hop routing is used where each node can transmit directly to cluster head or sink.

2. SEP Protocol

SEP [4] stands for Stable Election Protocol where the normal and advanced nodes are deployed randomly. If normal nodes are deployed in majority far away from the base station, the nodes will consume more energy in transmitting data to the base station which will result in less stability period and throughput. Therefore to overcome this, the network area is divided into regions where the far away nodes from base station that is the corners require more energy to transmit the data, so they are given more energy, called advanced nodes, in comparison to the nodes which are near to the base station and they are called normal nodes which directly send data to the base station.

3. ZSEP Protocol

ZSEP [5] stands for Zonal Stable Election Protocol which is an extension of SEP. It is an hybrid protocol in which on the basis of energy level and Y coordinate of the network field, the network area is divided into three zones namely zone 0, zone 1 and zone 2. In zone 0, normal nodes are deployed randomly, in head zone 1, half of the advanced nodes are deployed and in head zone 2, other half of the advanced nodes are deployed. ZSEP uses two techniques to transmit data to base station; one is direct

communication and second is transmission via cluster head. In direct communication, normal nodes in zone 0 sense and gather data of interest and directly send to the base station. In the second case, in head zone 1 and head zone 2, cluster head is selected among nodes in both zones, then cluster head sense and gather data, aggregate it and then send it to base station.

III. RELATED WORK

In WSN [1], the transmission range in sensor nodes are very limited, also as their energy resources are very limited so the performance and storage capabilities. In this paper, the survey for routing protocols for WSNs with the comparison of strengths and limitations is given. In WSNs [2], while designing protocol there is a limitation of node's energy, so energy efficiency is an important parameter to be considered. This paper proposes a new algorithm of LEACH protocol (LEACH-TLCH) which is considered to reduce the energy consumption and increase the network lifetime. In a WSN [3], the node is useful until its battery dies. In this paper, they analyze LEACH protocol, the advantages and disadvantages and various attacks on the protocol. In WSNs [4], the heterogeneity of nodes is introduced in terms of energy and they are hierarchal clustered. Protocols are designed for transmission [5] in WSNs. In this paper, for heterogeneous WSNs, they propose a hybrid routing protocol called ZSEP (Zonal Stable Routing Protocol). In this protocol, some nodes directly send data to base station while some use clustering technique to send data to base station as one in SEP. ZSEP performance is compared with LEACH protocol and SEP protocol. In [6], this paper analyses the energy utilization and lifetime analysis on the basis of LEACH protocol for the cluster based wireless sensor networks. In [7], this paper analyzes the performance of SEP and LEACH in terms of alive nodes and number of rounds for different base stations and terrain area. Network nodes die after more number of rounds if the base station is closer comparing the base station which is far away. In [8], for wireless multihop routing, this paper proposes linear programming model and they are examined over different routing techniques. In [9], the deployment strategy for wireless sensor network is presented for the gain of better strategy, computational power and transmission according to the required scenario.

IV. METHODOLOGY

In this paper, the nodes are deployed in a network field of area 100m X 100m. LEACH, SEP and ZSEP protocols are deployed in the network in heterogeneous environment. Initial energy is E_0 . The network area is kept constant and initial energy E_0 is varied. Here the goal is to study the impact of varying initial energy on the

performance of protocols on the basis of stability period and throughput under the influence of varying initial energy in the network keeping the network area fixed.

For LEACH, there are two phase, setup phase and steady state phase where steady state phase should be longer than setup phase. At the stage of cluster forming in LEACH, a random number is picked randomly between 0 and 1 by nodes. Now this number is compared to the threshold value $T(\alpha)$. If the number is less than this threshold value then that node becomes cluster head for this round otherwise it remains as common node. Threshold $T(\alpha)$ is determined by following;

$$T(\alpha) = \begin{cases} \frac{\mu}{1 - \mu * \left(r \bmod \frac{1}{\mu} \right)} \alpha \in \phi & \\ 0, & \text{otherwise} \end{cases} \quad (1)$$

Where, μ is the probability of each node to become cluster head, r is the number of the round; ϕ is the collections of the nodes that have not yet been head nodes in the first $1/\mu$ rounds.

In SEP, it is based on weighted election probabilities of each node to become cluster head according to the remaining energy in each node. In this, the threshold for normal nodes and advanced nodes are given by following equations;

$$T(\alpha_{nrm}) = \begin{cases} \frac{\mu_{nrm}}{1 - \mu_{nrm} * \left(r \bmod \frac{1}{\mu_{nrm}} \right)} \alpha_{nrm} \in \phi' & \\ 0, & \text{otherwise} \end{cases} \quad (2)$$

Where, $\mu_{nrm} = \frac{\mu_{opt}}{1 + \beta m}$, is the weighted probability for normal nodes, r is the current round and ϕ' is the set of normal nodes that have not become cluster heads the last $1/\mu_{nrm}$ rounds of the epoch. μ_{opt} is the optimal probability. m is the fraction of advanced nodes and β is the additional energy factor between advanced and normal nodes.

$$T(\alpha_{adv}) = \begin{cases} \frac{\mu_{adv}}{1 - \mu_{adv} * \left(r \bmod \frac{1}{\mu_{adv}} \right)} \alpha_{adv} \in \phi'' & \\ 0, & \text{otherwise} \end{cases} \quad (3)$$

Where, $\mu_{adv} = \frac{\mu_{opt}(1 + \beta)}{1 + \beta m}$, is the weighted probability for advanced nodes, r is the current round and ϕ'' is the set

of advance nodes that have not become cluster heads the last $1/\mu_{adv}$ rounds of the epoch.

In ZSEP, every node decides to become cluster head in current round or not by choosing a random number between 0 and 1. This number is then compared with a threshold value, if it is less the node becomes cluster head otherwise remain as normal nodes for this round. Threshold value is given by the following equation;

$$T(\alpha_{adv}) = \frac{\mu_{adv}}{1 - \mu_{adv} * \left(r \bmod \frac{1}{\mu_{adv}} \right)} \alpha \in \phi$$

$$0, \quad \text{otherwise} \quad (4)$$

Where, ϕ is the set of nodes which have not been cluster heads in the last $1/\mu_{adv}$ rounds. Probability for advance nodes to become cluster head which is

$$\mu_{adv} = \frac{\mu_{opt}}{1 + \beta m} \times (1 + \beta) \quad (5)$$

V. SIMULATION AND RESULT

The protocols are implemented in a field of network area $100m^2$ in the presence of heterogeneity. The initial energy is 0.8J in the first simulation and then varied to 0.9J and 1.0J. For the case of $m=0.2$ and $\beta=1$, the simulation is performed in MATLAB. As the initial energy in the network field is varied, the performance of the protocols in respect of alive nodes, dead nodes and packets sent to base station is analyzed. As for $m=0.2$ and $\beta=1$, means that there are 20 advance nodes out of total nodes which are 100. In ZSEP, out of 20 advance nodes, 10 nodes are deployed in head zone 1 and other 10 nodes in head zone 2. The total number of rounds taken is 6000.

1. Simulation Parameters

Simulation scenarios in this article are given as below:

Table.1: Parameter Settings

Parameters	Value
Initial energy of advance nodes	$E_o(1+\beta)$
Energy for data aggregation EDA	5 nJ/bit/signal
Transmitting and receiving energy E_{elec}	5 nJ/bit
Amplification energy for short distance E_{fs}	10 Pj/bit/m ²
Amplification energy for long distance E_{amp}	0.013 pJ/bit/m ⁴
Probability μ_{opt}	0.1

2. Analysis of simulation results

Fig.1 indicates the total number of alive nodes in LEACH, SEP and ZSEP with respect to number of rounds

when initial energy is 0.8 J.

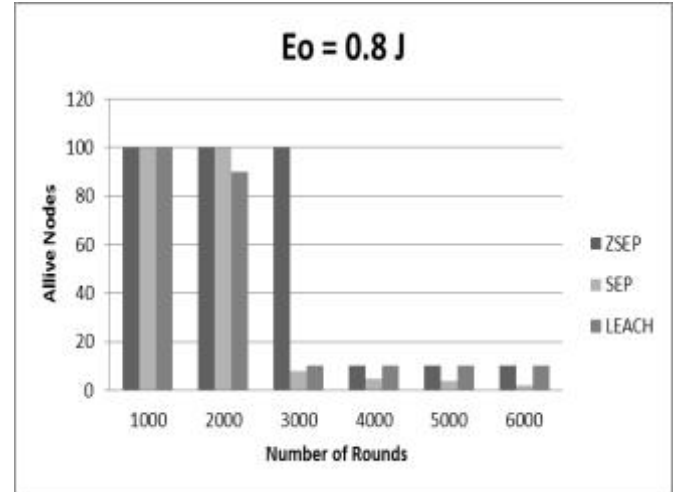


Fig.1: Result for alive nodes for Eo = 0.8 J

Fig.2 shows the scenario for total number of alive nodes in LEACH, SEP and ZSEP with respect to number of rounds when initial energy is 0.9 J.

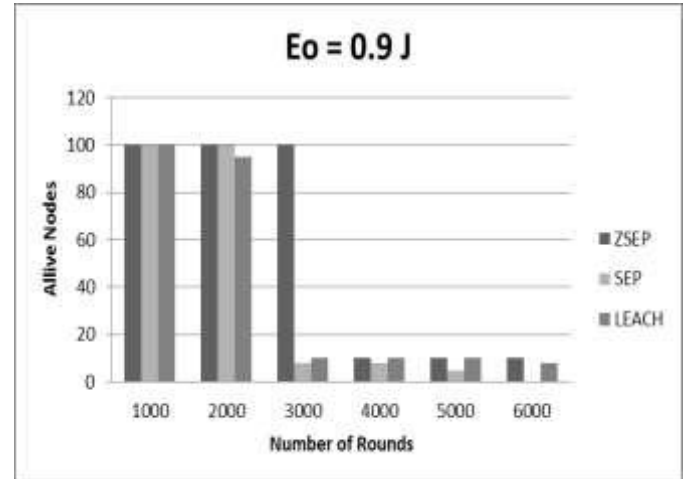


Fig.2: Result for alive nodes for Eo = 0.9 J

Fig.3 shows the scenario for total number of alive nodes in LEACH, SEP and ZSEP with respect to number of rounds when initial energy is 1J.

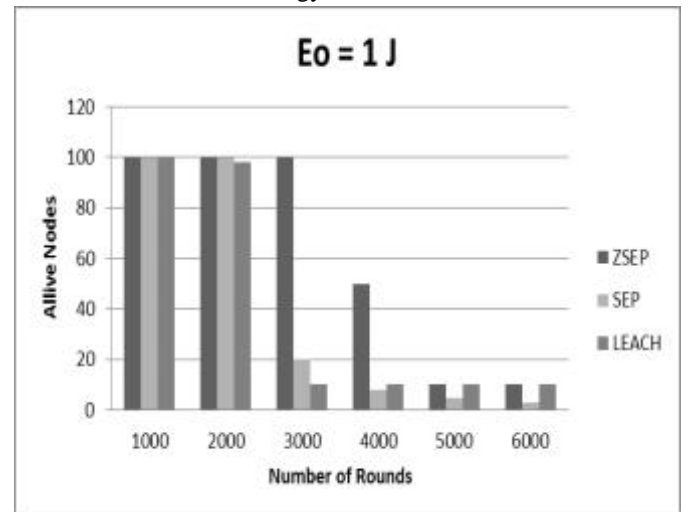


Fig.3: Result for alive nodes for Eo = 1 J

Fig.4 indicates the total number of dead nodes in LEACH, SEP and ZSEP with respect to number of rounds when initial energy is 0.8 J.

As the initial energy varies in the network, the number of alive nodes in the network also varies significantly. From Fig.1, Fig.2 and Fig.3, it can be seen that as the initial energy of the network increases, the stability period of the network in all the three protocols also increases. However ZSEP shows more stability in the network with the change in initial energy. ZSEP is performing better than the other protocols because of its network area divided into three zones. The nodes near to the base station directly communicate to the base station while the faraway nodes communicate to the cluster heads and cluster head sends data to base station. Because of this kind of setup the energy consumption is significantly low, and nodes sustain for longer period. While in SEP, there is shorter network lifetime because of the weighted probability for normal and advanced nodes in the network.

Fig.4 shows the scenario for total number of dead nodes in LEACH, SEP and ZSEP with respect to number of rounds when initial energy is 0.8J.

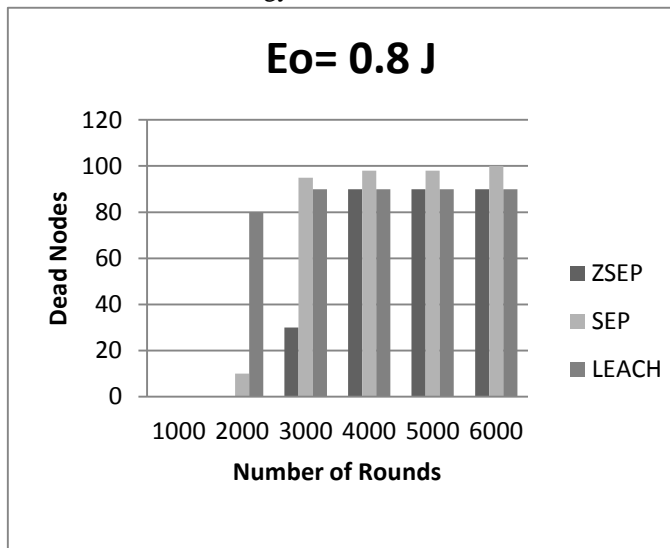


Fig.4: Result for dead nodes for $E_o = 0.8 J$

Fig.5 shows the scenario for total number of dead nodes in LEACH, SEP and ZSEP with respect to number of rounds when initial energy is 0.9J.

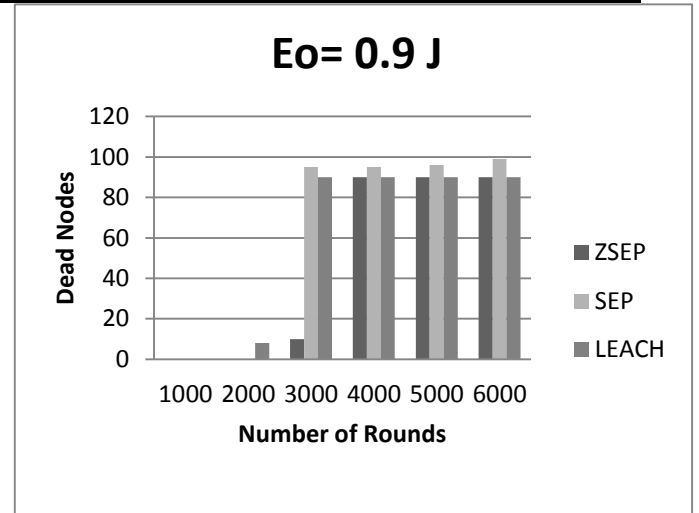


Fig.5: Result for dead nodes for $E_o = 0.9 J$

Fig.6 indicates the total number of dead nodes in LEACH, SEP and ZSEP with respect to number of rounds when initial energy is 1 J.

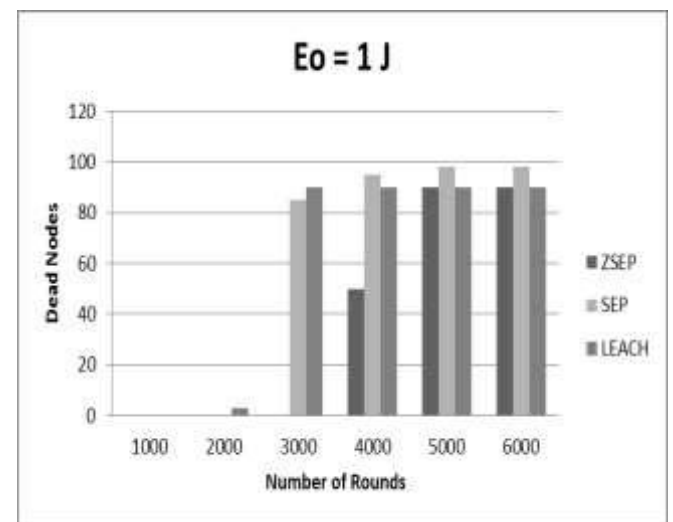


Fig.6: Result for dead nodes for $E_o = 1 J$

From fig.4, fig.5 and fig.6, it can be seen that as the initial energy increases in the network, the stability of each protocol increases for each rounds, in ZSEP, SEP and LEACH comparing the stability of nodes per round for different initial energy that has been taken. However if comparing the performance of protocols with each other, ZSEP still performs much better than others in terms of dead nodes per round. In between LEACH and SEP, LEACH performs better than SEP.

Fig.7 indicates the packets to base station in LEACH, SEP and ZSEP with respect to number of rounds when initial energy is 0.8 J.

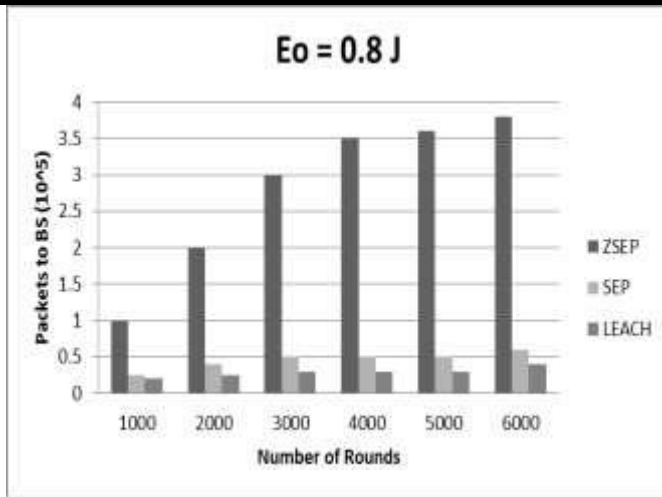


Fig.7: Result for packets to base station for $E_o = 0.8 J$

Fig.8 indicates the packets to base station in LEACH, SEP and ZSEP with respect to number of rounds when initial energy is 0.9 J.

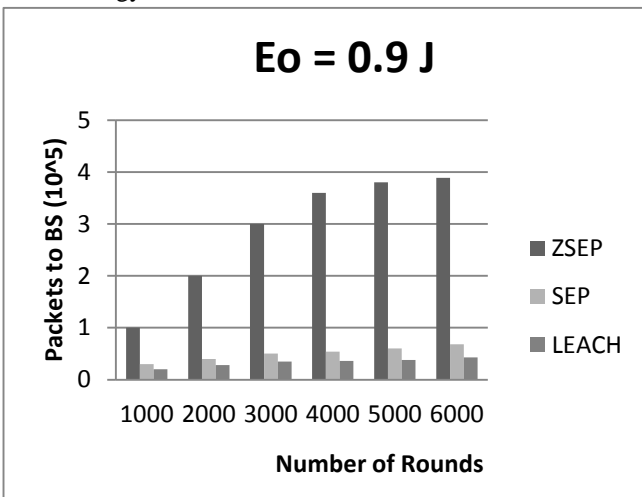


Fig.8: Result for packets to base station for $E_o = 0.9 J$

Fig.9 indicates the packets to base station in LEACH, SEP and ZSEP with respect to number of rounds when initial energy is 1 J.

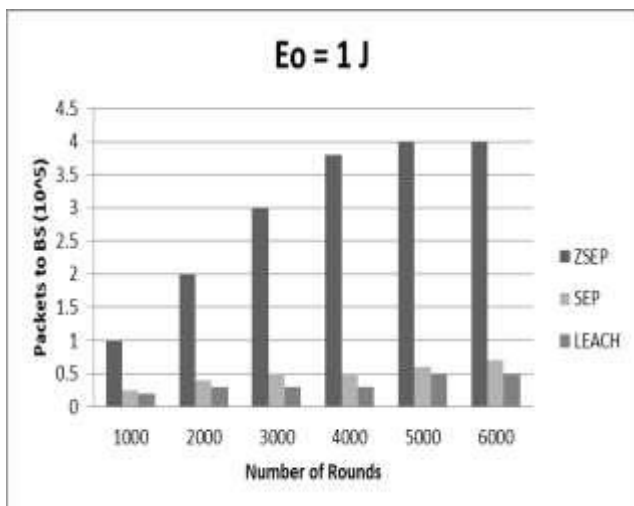


Fig.9: Result for packets to base station for $E_o = 0.9 J$

From Fig.7, Fig.8 and Fig.9, we can analyze the result for number of packets to base station for every round in each protocol. The value increases as the initial energy increases and also the stability for each protocol increases in the network. However, ZSEP is still performing better than other protocols SEP and LEACH. In SEP and LEACH, SEP is performing better than LEACH. As in LEACH there is an equal probability of each node to become cluster head, therefore the advanced nodes become cluster head again after completion of a round, and the normal nodes are not able to perform better in case of data aggregation and transmissions to the base station when they become cluster head. It causes decrease in the number of packets transferred to the base station. While in SEP, there is a system for weighted election probability for advanced and normal nodes.

VI. CONCLUSION

When the initial energy in the network is increased without varying overall network area, there is a significant effect on the performance of protocols implemented in the network. The stability of each protocol increases as the time taken by nodes to sustain increases with increase in number of rounds. Also the number of packets transferred to base station in each round increases. The performance of ZSEP is better than LEACH and SEP, while in terms of number of packets transferred to base station, SEP is performing better than LEACH. It concludes that there should be some trade of or synchronization between the protocols that is being implemented in the network and the initial energy that is being provided. Also, not all the protocols perform similar in the same environment. Therefore it is very necessary to choose a protocol according to the requirement for which the wireless network is being setup in an environment.

REFERENCES

- [1] Shio Kumar Singh, M P Singh, and D K Singh "Routing Protocols in Wireless Sensor Networks –A Survey" In: International Journal of Computer Science & Engineering Survey (IJCSES) Vol.1, No.2, November 2010.
- [2] Chunyao FU, Zhifang JIANG, Wei WEI and Ang WEI "An Energy Balanced Algorithm of LEACH Protocol in WSN" In: IJCSI International Journal of Computer Science Issues, Vol. 10, Issue 1, No 1, January 2013.
- [3] Reenkamal Kaur Gill, Priya Chawla, Monika Sachdeva "Study of LEACH Routing Protocol for Wireless Sensor Networks" 2014 International Conference on Communication, Computing & Systems (ICCCS-2014).

- [4] Georgios Smaragdakis, Ibrahim Matta and Azer Bestavros “SEP: A Stable Election Protocol for clustered heterogeneous wireless sensor networks” In Proceeding of the International Workshop on SANPA, August 2004.
- [5] S. Faisal1, N. Javaid, A. Javaid, M. A. Khan, S. H. Bouk, Z. A. Khan “Z-SEP: Zonal-Stable Election Protocol for Wireless Sensor Networks” In: Journal of Basic and Applied Scientific Research, Vol. 3, No.5, 2013.
- [6] Abdul Sattar Malik and Suhail A. Qureshi “Analyzing the Factors Affecting Network Lifetime for Cluster-based Wireless Sensor Networks” In: Pak. J. Engg. & Appl. Sci. Vol. 6, pp. 9-16, Jan., 2010.
- [7] Upasana Sharma, Sunil Tiwari “Performance Analysis of SEP and LEACH for Heterogeneous Wireless Sensor Networks” In: International Journal of Computer Trends and Technology (IJCTT), Vol. 10 No. 4, Apr 2014.
- [8] N. Javaid, R. D. Khan, M. Ilahi, L. Ali, Z. A. Khan, U. Qasim, ”Wireless Proactive Routing Protocols under Mobility and Scalability Constraints”, J. Basic. Appl. Sci. Res., 3(1)1187-12001, 2013.
- [9] Jasvinder Singh, Er. Vivek Thapar, Er.Amit Kamra “Deployment Strategy of Homogeneous and Heterogeneous Wireless Sensor Network” In: International Journal of Computer Science and Communication Engineering, Volume 1, Issue 2, 2012.

Student's Learning Evaluation Using Learning Analytics

Prof. U. M. Kalshetti, Keyur Kulkarni, Deepenkumar Patel, Sharang Nimbalkar

Department of Information Technology, PVG's COET, Pune, India

Abstract— In the current education system Teachers have to manually access each and every answer sheet of the student. It is very difficult to analyze each and every student and keep track of their progress, what they're good at or are lagging behind. Hence, it's a very time consuming and tedious process. Also there is no system tool for self-evaluation. The proposed system automatically generates Gap-Fill or one line questions from the input text. Provided it has a maintained list of keywords. When the students appear for the test, currently there is no system where automatic questions will be generated according to the test topic selected. This system proposes automatic question generator for a particular topic that would minimize the workload of the teachers by generating number of multiple Fill in the Blank questions for regular class tests. The students are evaluated on the generated questions. System also determines the polarity of the feedback given by the student. System helps teacher analyze student's feedback about a topic and how well they've understood the topic, so that the teachers could resolve their problems and would help students work in particular area in which they're weak.

Keywords—Learning Analytics.

I. INTRODUCTION

To know the behaviour of learners is important. One of the most effective ways to collect this invaluable data is through learning analytics. Learning Analytics is the collection of data that is gathered while learners are engaging in the eLearning experience.

Analytics also consist of the analysis and reporting of this information. Learning Analytics also offer online facilitators and instructors a comprehensive look at how a learner is performing, if the learner may need additional help with a particular lesson or subject, and even if the learner is likely to pass or not an eLearning course. Such data can then be used to make educational analysis and predictions that help to determine which learning materials are appropriate, useful or irrelevant for the learners. This is primarily based upon learner's performance, skill level, and personal interests.

Learning analytics have the power to enhance eLearning experience and create more effective eLearning environments.

Feedback serves to close the gap between the learner's current understanding and the desired understanding. Regular and informative feedback can keep students away from misconceptions and increase confidence and motivation in them.

Currently it is not possible for instructors to provide timely feedback to every individual student and vice versa. In this module we provide students automatic instant feedback after their interactions of online test. However, how students choose to interact with the system and how it has influenced students' learning experience is rarely well understood. The findings provide solutions for improvement in various areas.

In this paper we propose a system which will generate questions automatically, eliminating the extra work of the teachers by minimizing the work load. The questions are generated depending on the sentences in the paragraph. A test is conducted on the generated questions and when students appear for the test, they are evaluated and their process is further analyzed. The student gives feedback about the system and a final report is generated showing the final evaluation of students as well as the system.

II. QUESTION GENERATION

Gap-Fill questions are Fill-in-the-blank questions, where one or more words are removed from a sentence/paragraph and potential answers are listed. These questions, being multiple choice ones, are easy to evaluate. Preparing these questions manually will take a lot of time and effort. This is where automatic Gap-Fill question generation (GFQG) from a given text is useful.

1. INSERT is _____ type of SQL command? (a) Data Definition Language (b) Data Manipulation Language (c) Data Command Language (d) Data Query Language (correct answer: Data Definition Language)

In a gap-fill question (GFQ) such as the one above, we refer to the sentence with the gap as the question sentence(QS) and the sentence in the text that is used to generate the QS as the gap-fill sentence (GFS). The word(s) which is removed from a GFS to form the QS is referred to as the key while the three alternatives in the question are called as distractors, as they are used to distract the students from the correct answer.

In this module the input text will be provided by the

teacher. The input consists of the text document, which contains all the topics in detail taught by the teacher to the students in the class. For current analysis we have considered topic Database Management System. Therefore, teacher after covering any topic from DBMS, when ready to take test, gives input to the system. Along with this text document another input is required which is the list of important keywords which are present in the topic. These Keywords are the important words which a student must minimally know after studying a topic. For the generation of questions these keywords play a vital role, as both the MCQs and the Fill in the Blank questions are dependent on the keywords itself.

Now after taking both the Input text and the keywords list, the input text will be further processed and Gap Fill questions will be generated. Processing of text involves omission of context from the text, i.e., forming context free grammar. It includes replacing all the pronouns with the respective nouns and forming a meaningful question. If the sentence contains unresolved context in it, might cause inappropriate formation of questions. Gap-Fill questions which are the Fill in the Blank questions where one or more words are removed from the sentence or paragraph.

Teacher has the following options of generating questions:

Fill in the blanks question generation:

The Gap-Fill questions are generated in following steps:

1. Finding the keyword from the sentence: The important keywords have to be given by the teacher from the topic been taught. The keywords must cover all the points of the topic. This work has to be done manually.
2. Removing/Replacing the keyword: The Input text document is read sentence by sentence. If the keyword from the keyword file is present in the input text file, The keyword is replaced with blank spaces.
E.g.: SELECT keyword is used for data querying.
2. (where SELECT is the keyword being replaced by the blank spaces.)
3. Generation of question: The blank spaces created in the sentence forms the fill in the blank question. In this way whole document is read and the number of keywords occurring in the text document are replaced and number of questions are formed. Therefore the number of questions generated depends on the occurrence of the keywords in the file.

E.g.: from the above input following question is generated.

_____ keyword is used for data querying.

Multiple Choice Questions Generation:

The Multiple Choice Questions are generated in the following steps:

1. Finding the keyword from the sentence: The important keywords have to be given by the teacher from the topic been taught. The keywords must cover all the points of the topic. This work has to be done manually.
2. Finding Distracters similar to the keyword: The Input text document is read sentence by sentence. The keywords similar to actual answer are selected and given as options.
3. Generation of question: The Distracters created in the sentence forms the MCQs. In this way whole document is read and the number of keywords occurring in the text document are replaced and number of questions are formed. Therefore the number of questions generated depends on the occurrence of the keywords in the file.

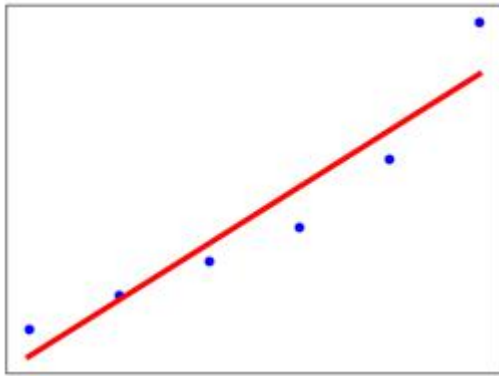
Based on these questions, students will be analyzed and we would come to know that the student has understood the topic or not. System allows Teachers to select the topic of the test and the difficulty level of the questions which need to be generated.

III. EVALUATION

After the successful generation of question the students have to be further evaluated. Now various hypothesis are proposed and results are generated on these hypothesis. The number of questions attempted by the students, total questions answered correctly all play an important role.

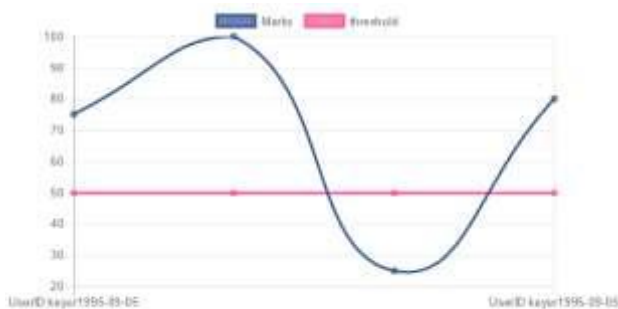
From the students perspective the system provides us with graph based progress to analyze where a particular student stands in the class and the areas in which they are good at or need improvement.

There are Three types of analysis conducted on the students. They are Predictive Analysis :In this analysis we tell what might happen in the future. Predictive analytics is the practice of extracting information from existing data sets in order to determine patterns and predict future outcomes and trends. Linear regression is performed to predict the further values (progress of the student in our case).



Linear Regression depends on one dependent and an independent variable which are the marks and test id respectively for the evaluation of student. Hence the progress of student is next predicted by the current marks scored by the student.

Diagnostic Analysis : The analysis is done in regards to the previous performance of the students on the test. Diagnostic Analysis tells us why did a particular thing happen by looking at the past performance. The result of the analysis is an analytic dashboard. It is used for discovery or to determine why something happened?



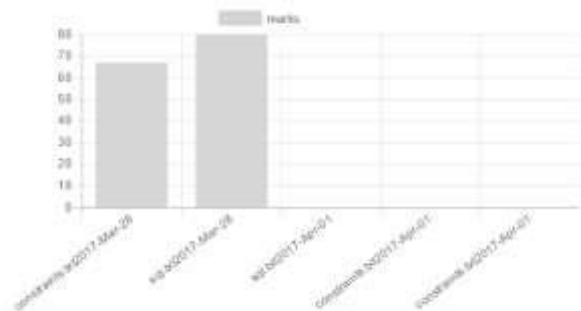
In the proposed system the a student appears of number of tests, the result of each test is calculated. Based on these results students is evaluated and remedies are proposed for further improvement if any required. Students are judged on their attendance and marks obtained in that topic. Hence, the solutions of

- Remedial Teaching: If the marks obtained in the test as well as attendance both are low, the student is advised to attend extra lectures so that he could cover up all the missed topic and come at par of other students in the class.
- Retest: If the attendance of the student is above the threshold value but marks scored are less, the students is suggested to appear for tests again. This would increase the practice of the students and help him score better the upcoming tests.
- Counseling: There are some students who despite having low attendance score better in tests. These students may have better grasping power but are counseled to attend the lectures as

their low attendance can get them in trouble. These students are counseled to know what problems they face while attending lectures? What drives them away from the classroom?

- Consistent Students: These are the students who attend lectures regularly and score good in exams too. But if in any test they lag behind, immediately a notification is sent and the problems they've faced are solved.

Descriptive Analysis : In this analysis statistics are used to describe the basic features of the data in a study. They provide simple summaries about the sample and the measures. Together with simple graphics analysis, they form the basis of virtually every quantitative analysis of data.



When the students appear for the test, The class average of the particular test is calculated and teacher comes to know what actually students have understood from that topic. The results are shown in the form of bar graph.

IV. FEEDBACK

We know that students develop their understanding of a concept based on their prior knowledge and experiences. Feedback plays an important role in closing the gap between current understanding and the desired goal, enhancing student performance and achievement.

Student behaviors in online learning platforms plays an important role. Even if we provide the right level of feedback at the right time, there can still be numerous ways in which students interact with these feedback features online outside of the controlled classroom environment.

The students are asked to give feedback about their learning process. How well they've understood the topics. This is simply done by providing students with the rating feature where students can rate the overall experience as well as about the topic learnt and the shortcomings of the teacher.

Research Questions from feedback

Based on our conceptual framework and existing literature, we ask foundational questions in our study:

- (1) The topic taught was clear or not?

(2) Doubts were been cleared on regular basis or not?

(3) Keywords used by the teacher were relevant or not?

V. CONCLUSION

This paper helps us evaluate the students by answering the questions generated. We look forward to experimenting on larger data by combining the chapters. Evaluation of course coverage by our system and use of semantic features will be part of our future work.

Also the feedback of the students help teachers understand what students actually have understood, and the areas where they need to work more on. We hope that the proposed system will help in the long run to not only test but also to analyze students' in an efficient way. After all, tedious learning must not hinder students understanding about a particular topic.

REFERENCES

- [1] KithsiriJayakodi, MadhushiBandara, and IndikaPerera, "An Automatic Classifier for exam questions in Engineering," IEEE International Conference on Teaching, Assessment and Learning for Engineering 10-12 December 2015, China, Page 195-202.(references)
- [2] Mario Manso-Vazquez, "A monitoring system to ease self-regulated learning processes," IEEE revistaiberoamericana de tecnologias del aprendizaje, vol. 10, no. 2, Page 52-59.
- [3] Ebner M., Kinshuk, Wohlhart D., Taraghi B., & Kumar V. Learning analytics. The journal of universal computer science, 21, 1-6, 2015.
- [4] George Garman, "A Logistic Approach To Predicting Student Success In Online Database Courses", American Journal of Business Education, Vol.3, No.12, 2010.
- [5] Hiroaki Ogata, Songran Liu, KousukeMouri, "Ubiquitous Learning Analytics using Learning Logs".

Smart Waste Management System using IoT

Prof. S.A. Mahajan, Akshay Kokane, Apoorva Shewale, Mrunaya Shinde , Shivani Ingale,

Department of Information Technology, PVG's COET, Pune, India

Abstract— With rapid increase in population, the issues related to sanitation with respect to garbage management are degrading immensely. It creates unhygienic conditions for the citizens in the nearby surrounding, leading to the spread of infectious diseases and illness. To avoid this problem, IoT based “Smart Waste Management” is the best and trending solution. In the proposed system, public dustbins will be provided with embedded device which helps in real time monitoring of level of garbage in garbage bins. The data regarding the garbage levels will be used to provide optimized route for garbage collecting vans, which will reduce cost associated with fuel. The load sensors will increase efficiency of data related to garbage level and moisture sensors will be used to provide data of waste segregation in a dust bin. The analysis of ceaseless data gathered will help municipality and government authorities to improve plans related to smart waste management with the help of various system generated reports.

Keywords— Cloud, ESP8266, Raspberry pi, UV Sensor, Load Cell, Humidity Sensor, Garbage Collecting Vans.

I. INTRODUCTION

Worldwide interest in Smart Cities has aggrandized, fostered by the need to find effective remedies to the major challenges foreseen for the next years. As one of the application of Smart City, Waste Management in a city is a formidable challenge faced by the public administrations. Waste is defined as any material in which something valuable is not being used or is not usable and represents no economic value to its owner, the waste generator. Depending on the physical state of the waste, they are categorized as solid waste and wet waste.

With the proliferation of population, the scenario of cleanliness with respect to waste management has become crucial. Waste management includes planning, collection, transport, treatment, recycle and disposal of waste together with monitoring and regulation. The existing waste management system, where the garbage is collected from the streets, houses and other establishments on quotidian basis, is not able to effectively manage the waste generated.

Giraud village in Raipur district, the capital of Chhattisgarh have deployed garbage bins at every street to collect the garbage, engaged its laborers and vehicles to

clear the trash. The amount of total solid waste generated by the village is 558 kg/day and liquid waste is 108040 lit./day, the garbage is collected daily and dumped into landfills. In case a villager observes illegal dumping of any kind of waste, he/she can complain regarding this to the concerned department. As improper disposal of waste causes serious impact on health, causing the spread of diseases and problems to the surrounding environment, the complete care is taken by the government for collecting and disposal of waste.

In this paper, a model has been proposed for real-time monitoring the garbage level of respective garbage bins and to detect the level when threshold value is reached using combination of Sensors and Raspberry pi. This data will be sent to the control unit and updated timely with the help of WiFi- module, depending on which optimized route have to be found for Garbage Collecting Van (GCV), depriving the fuel consumption, cost, time and labor. The data will be provided whether the waste is segregated completely or not by wet sensor and humidity sensor which will help for recycling, disposal and reuse of waste. Using data mining, qualitative analysis will be carried out to generate reports. The main objective of this system to be implemented is to supersede the tedious existing system which will aid city to become a Smart City.

The rest of the paper is organized as follows. Section II provides a general overview of the system architecture of smart waste management. Section III provides in detail the hardwares deployed in the proposed system. Section IV specifies how the system will be implemented to smartly manage the waste generated.

II. ARCHITECTURE

In the existing system, the sensors being placed at the topmost level in the bin, sense the level of the garbage in that bin. On reaching the threshold a command is generated and sent to the central office through the Zig-Bee technology notifying for the collection of garbage. The authority at the central office conveys this notification to the garbage collecting van through the GSM module. GSM is interfaced with ARM micro-controller through MAX232 chip that checks compatibility between the GSM modem and ARM micro-controller.

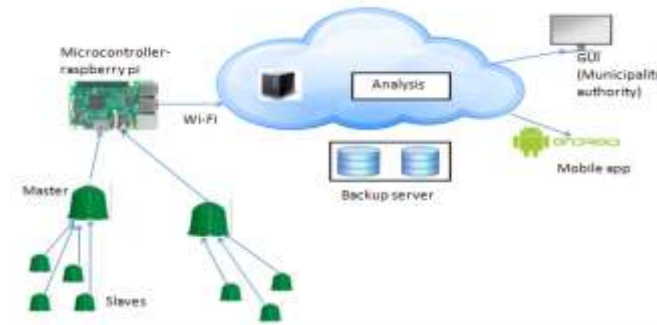


Fig.2: Architecture

The proposed architecture will have a master slave configuration of dustbins. This would overcome the connectivity issues in remote areas. These slave dustbins communicate their information with their corresponding master dustbins. Each master dustbin shall be equipped with a micro-controller. Each of the dustbins has 3 types of sensors:

- 1) Level sensor: The level sensor will provide continuous information of level of dustbin filled. On reaching a threshold, an alert needs to be generated for the collection of garbage.
- 2) Humidity sensor: The humidity sensor will provide information related to the presence of wet waste in the dry waste bin.
- 3) Load cell: The load cell will provide information related to the weight of the garbage in the dustbin.
- 4) On checking for two of the parameters- level sensor and load cell, the error rate of false alarm will greatly reduce. The micro-controller used will be Raspberry-pi 3, which has an inbuilt Wi-Fi module. The information from master bins will be continuously streamed to the cloud using Wi-Fi module.

In the cloud, the real time analysis has to be carried out to generate various reports like- area generating maximum waste, seasonal or function reports on waste, segregation reports etc. which can help the Municipal corporation with better strategies for waste management. The proposed architecture assumes a backup server be provided by the cloud service provider. Along with the real time analysis, the optimized route for collecting the garbage will be found using Google maps. This will provide the advantage of saving fuel costs. Web based applications could be hosted using cloud. The authority at the central office would view all the reports, optimized routes and all the data related to the garbage bins. The person accordingly will direct the collecting vans for the collection of garbage and make efficient plans for the garbage management.

III. HARDWARE DESCRIPTION

3.1 Ultrasonic sensor: Ultrasonic sensor will be used to detect the level of garbage filled in the dustbin. The level of garbage will be depicted in terms of distance between the sensor and garbage in dustbin. This module has 4 pins- VCC (5V), Trig, Echo and GND. Trig have to be used to send out an ultrasonic high level pulse for at least 10 μ s and the Echo pin will then automatically detect the returning pulse. Sensor will calculate the time interval between sending the signal and receiving the echo to determine the distance. Working frequency of ultrasonic sensor is 40Hz. Max range and min range is 4m and 2cm and measuring angle is 15 degree.



Fig. 3.1: HC-SR04 Ultrasonic Sensor

3.2 Humidity sensor: The temperature and humidity sensor have to be used to distinguish between dry and wet waste. For this purpose DHT11 sensor will be used. Depending upon the output temperature, dry and wet waste would be differentiated. The DHT11 is a high-precision digital humidity and temperature sensor. It uses a capacitive humidity sensor and a thermistor to measure the surrounding air, and spits out a digital signal on the data pin. Sensor will only get new data from it once every 2 seconds. It will be good for 0-100% humidity readings with 2-5% accuracy and for -40 to 80°C temperature readings $\pm 0.5^\circ\text{C}$ accuracy.



Fig.3.2: DHT22 Humidity Sensor

3.3 Load Cell: The load cell needs to be used to weigh dustbin. A load cell is a transducer that creates an electrical signal whose magnitude is directly proportional to the force being measured. The load cell ranges from few grams to 200 kg. The electrical signal output will be typically in the order of a few millivolts and will require amplification before it can be used. The HX711 load cell amplifier has to be used to get measurable data out from a load cell.

3.4 Raspberry pi: The information collected by sensor will be processed by micro-controller. For this purpose raspberry pi 3 model B needs to be used. Raspberry-pi 3 is based on Broad-com BCM2837 SoC with a 1.2 GHz 64-bit quad-core ARM Cortex-A53 processor, with 512

KB shared L2 cache. The allocated RAM will be of 1 GB. It will primarily use Raspbian, a Debian-based Linux operating system, but many other operating systems can also run on the Raspberry Pi such as RISC OS Pi, FreeBSD, NetBSD.



Fig.3.4: Raspberry Pi 3

3.5 Serial Wi-Fi wireless transceiver module: ESP8266 is a chip which is wireless network micro-controller module. It will be a system-on-a-chip (SoC) with capabilities for 2.4 GHz Wi-Fi, general-purpose input/output etc.



Fig. 3.5: ESP8266

IV. IMPLEMENTATION METHODOLOGY

In this scenario, garbage bins will be classified as master dustbins and slave dustbins. Master dustbins will be equipped with Raspberry Pi and slaves with IoT module. Every dustbin whether a master or a slave will have to be given a unique id. A database will be maintained containing the information about which dustbin to be placed in which area by their corresponding ids. The dustbin has UV sensor and load sensor for level detection, and humidity sensor for wet and dry garbage detection. Every dustbin, slave or master will have to communicate with Raspberry-pi 3, where Raspberry-pi 3 will act as a broker. The work of Raspberry-pi 3 will be to collect the data from sensors attached to master and slave dustbins, apply noise removal algorithm and send data to server using Wi-Fi. The message has to be sent to server by raspberry-pi 3 about levels of garbage in a bin, wet and dry waste segregation levels along with dustbin id. Server matches ids with database of dustbins, and will find levels of dustbins located in different areas of city. Different IoT protocols can be used for data transmission like MQTT or CoAP.

The collected data in cloud will be analyzed by using analytic tool like Hadoop or Storm, and useful information regarding waste management will be extracted. From the collected the data, user will get to know about real-time garbage level, and the garbage collection van can find optimized route for collection of garbage. Whenever the garbage level crosses threshold level, the alert will be generated for urgent collection of garbage. The data of wet and dry segregation level will help in evaluating the current garbage management plans and also to refine the plans for increasing the efficiency. The simple Web GUI will help the user to use this system efficiently.

V. CONCLUSION

This paper shows how the smart waste management using IoT can be implemented. This proposed system assures the collection of garbage soon when the garbage level reaches its maximum level. The system will thus provide accurate reports, increasing the efficiency of the system. The real-time monitoring of the garbage level with the help of sensors and wireless communication will reduce the total number of trips required of GCV and thus, will reduce the total expenditure associated with the garbage collection. Thus, the dustbins will be cleared as and when filled, giving way to cleaner city, better infrastructure and increased hygiene.

REFERENCES

- [1] S.S.Navghane, M.S.Killedar, Dr.V.M.Rohokale, "IoT based smart garbage and waste collection bin", international journal of advance research in electronics and communication engineering, volume 5, Issue 5, May 2016
- [2] Andrea Zanella, Nicola But, Angelo Castellani, Lorenzo Vangelista, Michele Zorzi, "Internet of Things for Smart Cities", IEEE Internet of Things Journal (Volume: 1, Issue: 1, Feb. 2014)
- [3] Kanchan Mahajan, Prof J.S. Chitode, "Waste bin monitoring system using integrated technology", International Journal of Innovative Research in Science, Engineering and Technology.

On r -Dynamic Chromatic Number of the Coronation of Path and Several Graphs

Arika Indah Kristiana^{1,2}, Dafik^{1,2}, M. Imam Utoyo⁴, Ika Hesti Agustin^{1,3}

¹CGANT University of Jember Indonesia

²Mathematics Edu. Depart. University of Jember, Indonesia

³Mathematics Depart. University of Jember, Indonesia

⁴Mathematics Depart. University of Airlangga, Surabaya, Indonesia

Abstract—This study is a natural extension of k -proper coloring of any simple and connected graph G . By an r -dynamic coloring of a graph G , we mean a proper k -coloring of graph G such that the neighbors of any vertex v receive at least $\min\{r, d(v)\}$ different colors. The r -dynamic chromatic number, written as $\chi_r(G)$, is the minimum k such that graph G has an r -dynamic k -coloring. In this paper we will study the r -dynamic chromatic number of the coronation of path and several graph. We denote the corona product of G and H by $G \odot H$. We will obtain the r -dynamic chromatic number of $\chi_r(P_n \odot P_m)$, $\chi_r(P_n \odot C_m)$ and $\chi_r(P_n \odot W_m)$ for $m, n \geq 3$.

Keyword— r -dynamic chromatic number, path, corona product.

I. INTRODUCTION

An r -dynamic coloring of a graph G is a proper k -coloring of graph G such that the neighbors of any vertex v receive at least $\min\{r, d(v)\}$ different colors. The r -dynamic chromatic number, introduced by Montgomery [4] written as $\chi_r(G)$, is the minimum k such that graph G has an r -dynamic k -coloring. The 1-dynamic chromatic number of a graph G is $\chi_1(G) = \chi(G)$, well-known as the ordinary chromatic number of G . The 2-dynamic chromatic number is simply said to be a dynamic chromatic number, denoted by $\chi_2(G) = \chi_d(G)$, see Montgomery [4]. The r -dynamic chromatic number has been studied by several authors, for instance in [1], [5], [6], [7], [8], [10], [11].

The following observations are useful for our study, proposed by Jahanbekam [11].

Observation 1. [10] Always $\chi(G) = \chi_1(G) \leq \dots \leq \chi_{\Delta(G)}(G)$. If $r \geq \Delta(G)$, then $\chi_r(G) = \chi_{\Delta(G)}(G)$

Observation 2. Let $\Delta(G)$ be the largest degree of graph G . It holds $\chi_r(G) \geq \min\{\Delta(G), r\} + 1$.

Given two simple graphs G and H , the corona product of G and H , denoted by $G \odot H$, is a connected graph obtained by taking a number of vertices $|V(G)|$ copy of H , and making the i^{th} of $V(G)$ adjacent to every vertex of the i^{th} copy of $V(H)$, Furmanczyk [3]. The following example is $P_3 \odot C_3$.

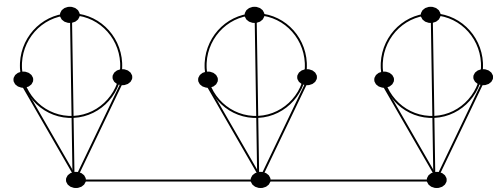


Fig.1: Graph $P_3 \odot C_3$

There have been many results already found, The first one was showed by Akbari et.al [10]. They found that for every two natural number m and n , $m, n \geq 2$, the cartesian product of P_m and P_n is $\chi_2(P_m \square P_n) = 4$ and if $3 \nmid mn$, then $\chi_2(C_m \square C_n) = 3$ and $\chi_2(C_m \square C_n) = 4$. In [2], they then conjectured $\chi_2(G) \leq \chi(G) + 2$ when G is regular, which remains open. Akbari et.al. [9] also proved Montgomery's conjecture for bipartite regular graphs, as well as Lai, et.al. [5] proved that $\chi_2(G) \leq \Delta(G) + 1$ for $\Delta(G) \geq 4$ when no component is the 5-cycle. By a greedy coloring algorithm, Jahanbekam [11] proved that $\chi_r(G) \leq r\Delta(G) + 1$, and equality holds for $\Delta(G) > 2$ if and only if G is r -regular with diameter 2 and girth 5. They improved the bound to $\chi_r(G) \leq \Delta(G) + 2r - 2$ when $\delta(G) > 2r \ln n$ and $\chi_r(G) \leq \Delta(G) + r$ when $\delta(G) > r^2 \ln n$.

II. THE RESULTS

We are ready to show our main theorems. There are three theorems found in this study. Those deal with corona product of graph P_n with P_m , C_m , and W_m .

Theorem 1. Let $G = P_n \odot P_m$ be a corona graph of P_n and P_m . For $n, m \geq 2$, the r -dynamic chromatic number is:

$$\chi_r(G) = \begin{cases} 3 & , r = 1, 2 \\ r + 1 & , 3 \leq r \leq \Delta - 1 \\ m + 3 & , r \geq \Delta \end{cases}$$

$$c_3(y_i) = \begin{cases} 1 & , i = 3t + 1, t \geq 0, 1 \leq i \leq n \\ 2 & , i = 3t + 2, t \geq 0, 1 \leq i \leq n \\ 3 & , i = 3t, t \geq 1, 1 \leq i \leq n \end{cases}$$

Proof. The graph $P_n \odot P_m$ is a connected graph with vertex set $V(P_n \odot P_m) = \{y_i, 1 \leq i \leq n\} \cup \{x_{ij}, 1 \leq i \leq n, 1 \leq j \leq m\}$ and edge set $E(P_n \odot P_m) = \{y_i y_{i+1}; 1 \leq i \leq n - 1\} \cup \{y_i x_{ij}, 1 \leq i \leq n, 1 \leq j \leq m\} \cup \{x_{ij}, x_{i(j+1)}; 1 \leq i \leq n, 1 \leq j \leq m - 1\}$. The order of graph $P_n \odot P_m$ is $|V(P_n \odot P_m)| = n(m + 1)$ and the size of graph $P_n \odot P_m$ is $|E(P_n \odot P_m)| = 2mn - 1$. Thus, $\Delta(P_n \odot P_m) = m + 2$.

By observation 2, $\chi_r(P_n \odot P_m) \geq \min\{r, \Delta(P_n \odot P_m)\} + 1 = \min\{r, m + 2\} + 1$. To find the exact value of r -dynamic chromatic number of $P_n \odot P_m$, we define two cases, namely for $\chi_{r=1,2}(P_n \odot P_m)$ and $\chi_r(P_n \odot P_m)$.

Case 1. For $\chi_{r=1,2}(P_n \odot P_m)$, define $c_1 : V(P_n \odot P_m) \rightarrow \{1, 2, \dots, k\}$ where $n \geq 3, m \geq 3$, by the following:

$$c_1(y_i) = \begin{cases} 1 & , i \text{ odd}, 1 \leq i \leq n \\ 2 & , i \text{ even}, 1 \leq i \leq n \end{cases}$$

$$c_1(x_{ij}) = \begin{cases} 1 & , i \text{ even}, j \text{ odd}, 1 \leq i \leq n, 1 \leq j \leq m \\ 2 & , i \text{ odd}, j \text{ odd}, 1 \leq i \leq n, 1 \leq j \leq m \\ 3 & , j \text{ even}, 1 \leq i \leq n, 1 \leq j \leq m \end{cases}$$

It easy to see that c_1 is map $c_1 : V(P_n \odot P_m) \rightarrow \{1, 2, 3\}$, thus it gives $\chi_{r=1,2}(P_n \odot P_m) = 3$.

Case 2.

Subcase 2.1 For $\chi_r(P_n \odot P_m), 3 \leq r \leq \Delta - 1$, define $c_2 : V(P_n \odot P_m) \rightarrow \{1, 2, \dots, k\}$ where $n \geq 3, m \geq 3$, by the following:

$$c_2(y_i) = \begin{cases} 1 & , i \text{ odd}, 1 \leq i \leq n \\ 2 & , i \text{ even}, 1 \leq i \leq n \end{cases}$$

$$c_2(x_{11}, x_{12}, x_{13}) = 2, 3, 4,$$

for $m = 3, r = 3$

$$c_2(x_{21}, x_{22}, x_{23}) = 1, 3, 4,$$

for $m = 3, r = 3$

$$c_2(x_{11}, x_{12}, x_{13}) = 3, 4, 5,$$

for $m = 3, r = 4$

$$c_2(x_{11}, x_{12}, x_{13}, x_{14}) = 2, 3, 4, 5,$$

for $m = 4, r = 4$

$$c_2(x_{11}, x_{12}, x_{13}, x_{14}) = 3, 4, 5, 6,$$

for $m = 4, r = 5$

It easy to see that c_2 is a map $c_2 : V(P_n \odot P_m) \rightarrow \{1, 2, \dots, r+1\}$, thus it gives $\chi_r(P_n \odot P_m) = r + 1, 3 \leq r \leq \Delta - 1$

Subcase 2.2 The last for $\chi_r(P_n \odot P_m), r \geq \Delta$, define $c_3 : V(P_n \odot P_m) \rightarrow \{1, 2, \dots, k\}$ where $n \geq 3, m \geq 3$, by the following:

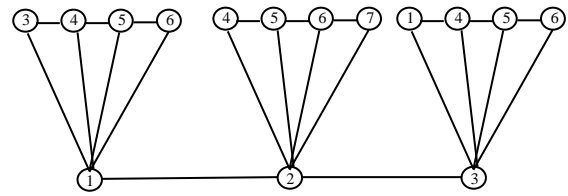


Fig.2: $\chi_6(P_3 \odot P_4) = 7$ with $n = 3, m = 4, r = 6$

$$c_3(x_{11}, x_{12}, x_{13}) = 4, 5, 6, \text{ for } m = 3, r = 5$$

$$c_3(x_{11}, x_{12}, x_{13}, x_{14}) = 3, 4, 5, 6,$$

for $m = 4, r = 6$

$$c_3(x_{21}, x_{22}, x_{23}, x_{24}) = 4, 5, 6, 7$$

for $m = 4, r = 6$

$$c_3(x_{21}, x_{22}, x_{23}, x_{24}, x_{25}) = 4, 5, 6, 7, 8$$

for $m = 5, r = 7$

It easy to see that c_3 is a map $c_3 : V(P_n \odot P_m) \rightarrow \{1, 2, \dots, m+3\}$, so it gives $\chi_r(P_n \odot P_m) = m + 3, r \geq \Delta$. It concludes the proof

Theorem 2. Let $G = P_n \odot C_m$ be a corona graph of P_n and C_m . For $n \geq 3, m \geq 3$, the r -dynamic chromatic number is:

$$\chi_{r=1,2}(G) = \begin{cases} 3 & , m \text{ even or } m = 3k, k \geq 1 \\ 4 & , m \text{ odd or } m = 5 \end{cases}$$

$$\chi_{r=3}(G) = \begin{cases} 4 & , m = 3k, k \geq 1 \\ 6 & , m = 5 \\ 5 & , m \text{ otherwise} \end{cases}$$

$$\chi_r(G) = \begin{cases} r + 1 & , 4 \leq r \leq \Delta - 1 \\ m + 3 & , r \geq \Delta \end{cases}$$

Proof. The graph $P_n \odot C_m$ is connected graph with vertex set $V(P_n \odot C_m) = \{y_i; 1 \leq i \leq n\} \cup \{x_{ij}; 1 \leq i \leq n, 1 \leq j \leq m\}$ and edge set $E(P_n \odot C_m) = \{y_i y_{i+1}; 1 \leq i \leq n - 1\} \cup \{x_{ij} x_{i(j+1)}; 1 \leq i \leq n, 1 \leq j \leq m - 1\} \cup \{x_{i1} x_{im}; 1 \leq i \leq n\} \cup \{y_i x_{ij}; 1 \leq i \leq n, 1 \leq j \leq m\}$. The order of graph $P_n \odot C_m$ is $|V(P_n \odot C_m)| = n(m + 1)$ and the size of graph

$P_n \odot C_m$ is $|E(P_n \odot C_m)| = 2mn + n - 1$, thus $\Delta(P_n \odot C_m) = m + 2$. By Observation 2, we have $\chi_r(P_n \odot C_m) \geq \min\{r, \Delta(P_n \odot C_m)\} + 1 = \min\{r, m + 2\} + 1$. To find the exact value of r -dynamic chromatic

number of $P_n \odot C_m$, we define three case, namely for $\chi_{r=1,2}(P_n \odot C_m)$, $\chi_{r=3}(P_n \odot C_m)$ and $\chi_r(P_n \odot C_m)$.

Case 1.

Subcase 1.1 For $\chi_{r=1,2}(P_n \odot C_m)$, define c_4 : $V(P_n \odot C_m) \rightarrow \{1, 2, \dots, k\}$ where $n \geq 3$, m even or $m = 3k, k \geq 1$, by the following:

$$c_4(y_i) = \begin{cases} 1 & , i \text{ odd}, 1 \leq i \leq n \\ 2 & , i \text{ even}, 1 \leq i \leq n \end{cases}$$

$$c_4(x_{ij}) = \begin{cases} 1 & , i \text{ even}, j \text{ odd}, 1 \leq i \leq n, 1 \leq j \leq m-1 \\ 2 & , i \text{ odd}, j \text{ odd}, 1 \leq i \leq n, 1 \leq j \leq m \\ 3 & , j \text{ even}, 1 \leq i \leq n, 1 \leq j \leq m \\ 4 & , i \text{ even}, 1 \leq i \leq n, j = m \end{cases}$$

It easy to see that c_4 is a map $c_4: V(P_n \odot C_m) \rightarrow \{1, 2, 3\}$, so it gives $\chi_{r=1,2}(P_n \odot C_m) = 3, m$ even or $m = 3k, k \geq 1$

Subcase 1.2 For $\chi_{r=1,2}(P_n \odot C_m)$ define c_5 : $V(P_n \odot C_m) \rightarrow \{1, 2, \dots, k\}$ where $n \geq 3$, m odd or $m = 5$, by the following:

$$c_5(y_i) = \begin{cases} 1 & , i \text{ odd}, 1 \leq i \leq n \\ 2 & , i \text{ even}, 1 \leq i \leq n \end{cases}$$

$$c_5(x_{ij}) = \begin{cases} 1 & , i \text{ even}, j \text{ odd}, 1 \leq i \leq n, 1 \leq j \leq m-1 \\ 2 & , i \text{ odd}, j \text{ odd}, 1 \leq i \leq n, 1 \leq j \leq m-1 \\ 3 & , j \text{ even}, 1 \leq i \leq n, 1 \leq j \leq m-1 \\ 4 & , 1 \leq i \leq n, j = m \end{cases}$$

It easy to see that c_5 is a map $c_5: V(P_n \odot C_m) \rightarrow \{1, 2, 3, 4\}$, so it gives $\chi_{r=1,2}(P_n \odot C_m) = 4, m$ odd or $m = 5$

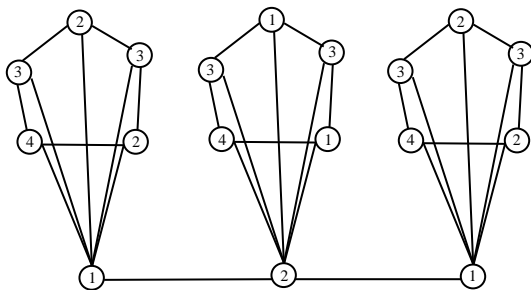


Fig.3: $\chi_2(P_3 \odot C_5) = 4$ with $n = 3, m = 5, r = 2$

Case 2.

Subcase 2.1 For $\chi_{r=3}(P_n \odot C_m)$, define c_6 : $V(P_n \odot C_m) \rightarrow \{1, 2, \dots, k\}$ where $n \geq 3, m = 3k, k \geq 1$, by the following:

$$c_6(y_i) = \begin{cases} 1 & , i \text{ odd}, 1 \leq i \leq n \\ 2 & , i \text{ even}, 1 \leq i \leq n \end{cases}$$

$$c_6(x_{ij}) = \begin{cases} 1 & , i \text{ even}, j = 3t + 1, t \geq 0, 1 \leq i \leq n, 1 \leq j \leq m \\ 2 & , i \text{ odd}, j = 3t + 1, t \geq 0, 1 \leq i \leq n, 1 \leq j \leq m \\ 3 & , j = 3t + 2, t \geq 0, 1 \leq i \leq n, 1 \leq j \leq m \\ 4 & , j = 3t, t \geq 1, 1 \leq i \leq n, 1 \leq j \leq m \end{cases}$$

It easy to see that c_6 is map $c_6: V(P_n \odot C_m) \rightarrow \{1, 2, 3, 4\}$, so it gives $\chi_{r=3}(P_n \odot C_m) = 4, m = 3k, k \geq 1$.

Subcase 2.2 For $\chi_{r=3}(P_n \odot C_m)$, define c_7 : $V(P_n \odot C_m) \rightarrow \{1, 2, \dots, k\}$ where $n \geq 3, m = 5$, by the following:

$$c_7(y_i) = \begin{cases} 1 & , i \text{ odd}, 1 \leq i \leq n \\ 2 & , i \text{ even}, 1 \leq i \leq n \end{cases}$$

$$c_7(x_{11}, x_{12}, x_{13}, x_{14}, x_{15}) = 2, 3, 4, 5, 6$$

$$c_7(x_{21}, x_{22}, x_{23}, x_{24}, x_{25}) = 1, 3, 4, 5, 6$$

It easy to see that c_7 is a map $c_7: V(P_n \odot C_m) \rightarrow \{1, 2, 3, 4, 5, 6\}$. Thus it given $\chi_{r=3}(P_n \odot C_5) = 6$

Subcase 2.3 For $\chi_{r=3}(P_n \odot C_m)$, define c_8 : $V(P_n \odot C_m) \rightarrow \{1, 2, \dots, k\}$ where $n \geq 3, m$ otherwise, by the following:

$$c_8(y_i) = \begin{cases} 1 & , i \text{ odd}, 1 \leq i \leq n \\ 2 & , i \text{ even}, 1 \leq i \leq n \end{cases}$$

$$c_8(x_{ij}) = \begin{cases} 1 & , i \text{ even}, j = 4t + 1, t \geq 0, 1 \leq i \leq n, 1 \leq j \leq m \\ 2 & , i \text{ odd}, j = 4t + 1, t \geq 0, 1 \leq i \leq n, 1 \leq j \leq m \\ 3 & , j = 4t + 2, t \geq 0, 1 \leq i \leq n, 1 \leq j \leq m \\ 4 & , j = 4t + 3, t \geq 1, 1 \leq i \leq n, 1 \leq j \leq m \\ 5 & , j = 4t, t \geq 1, 1 \leq i \leq n, 1 \leq j \leq m \end{cases}$$

It easy to see that c_8 is map $c_8: V(P_n \odot C_m) \rightarrow \{1, 2, 3, 4, 5\}$, so it gives $\chi_{r=3}(P_n \odot C_m) = 5$

Case 3.

Subcase 3.1 For $\chi_r(P_n \odot C_m), 4 \leq r \leq \Delta - 1$, define c_9 : $V(P_n \odot C_m) \rightarrow \{1, 2, \dots, k\}$ where $n \geq 3, m \geq 3$, by the following:

$$c_9(y_i) = \begin{cases} 1 & , i \text{ odd}, 1 \leq i \leq n \\ 2 & , i \text{ even}, 1 \leq i \leq n \end{cases}$$

$$c_9(x_{11}, x_{12}, x_{13}, x_{14}, x_{15}, x_{16}) = 3, 4, 5, 3, 4, 5,$$

for $m = 6, r = 4$

$$c_9(x_{31}, x_{32}, x_{33}, x_{34}, x_{35}, x_{36}) = 3, 4, 5, 3, 4, 5,$$

for $m = 6, r = 4$

$$c_9(x_{11}, x_{12}, x_{13}, x_{14}, x_{15}, x_{16}) = 3, 4, 5, 6, 3, 5,$$

for $m = 6, r = 5$

$$c_9(x_{11}, x_{12}, x_{14}, x_{15}, x_{16}) = 3, 4, 5, 6, 7, 3,$$

for $m = 6, r = 6$

$$c_9(x_{11}, x_{12}, x_{13}, x_{14}, x_{15}, x_{16}) = 3, 4, 5, 6, 7, 8,$$

for $m = 6, r = 7$

It easy to see that c_9 is a map $c_9: V(P_n \odot C_m) \rightarrow \{1, 2, \dots, r+1\}$, so it gives $\chi_r(P_n \odot C_m) = r + 1, 4 \leq r \leq \Delta - 1$

Subcase 3.2 The last for $\chi_r(P_n \odot C_m), r \geq \Delta$, define c_{10} : $V(P_n \odot C_m) \rightarrow \{1, 2, \dots, k\}$ where $n \geq 3, m \geq 3$, by the following:

$$c_{10}(y_i) = \begin{cases} 1 & , i \text{ odd}, 1 \leq i \leq n \\ 2 & , i \text{ even}, 1 \leq i \leq n \end{cases}$$

$$c_{10}(x_{11}, x_{12}, x_{13}, x_{14}, x_{15}, x_{16}) = 4, 5, 6, 7, 8, 9$$

for $m = 6, r = 8$

$$c_{10}(x_{11}, x_{12}, x_{13}, x_{14}, x_{15}, x_{16}, x_{17}) = 4, 5, 6, 7, 8, 9, 10$$

for $m = 7, r = 9$

$$c_{10}(x_{11}, x_{12}, x_{13}, x_{14}, x_{15}, x_{16}, x_{17}, x_{18}) = 4, 5, 6, 7, 8, 9, 10, 11$$

for $m = 8, r = 10$

It easy to see that c_{10} is map $c_{10}: V(P_n \odot C_m) \rightarrow \{1, 2, \dots, m+3\}$, so it given $\chi_r(P_n \odot C_5) = m + 3, r \geq \Delta$. It concludes the proof.

Theorem 3. Let $G = P_n \odot W_m$ be a corona graph of P_n and W_m . For $n \geq 3, m \geq 3$, the r -dynamic chromatic number is:

$$\chi_{r=1,2,3}(G) = \begin{cases} 4, & m \text{ even} \\ 5, & m \text{ odd} \end{cases}$$

$$\chi_{r=4}(G) = \begin{cases} 5, & m = 3k, k \geq 1 \\ 7, & m = 5 \\ 6, & m \text{ otherwise} \end{cases}$$

$$\chi_r(G) = \begin{cases} r + 1, & 5 \leq r \leq \Delta - 1 \\ m + 4, & r \geq \Delta \end{cases}$$

Proof. The graph $P_n \odot W_m$ is a connected graph with vertex set $V(P_n \odot W_m) = \{y_i; 1 \leq i \leq n\} \cup \{x_{ij}; 1 \leq i \leq n, 1 \leq j \leq m\} \cup \{A_i; 1 \leq i \leq n\}$ and edge set $E(P_n \odot W_m) = \{y_i y_{i+1}; 1 \leq i \leq n - 1\} \cup \{x_{ij} x_{i(j+1)}; 1 \leq i \leq n, 1 \leq j \leq m - 1\} \cup \{x_{i1} x_{im}; 1 \leq i \leq n\} \cup \{y_i x_{ij}; 1 \leq i \leq n, 1 \leq j \leq m\} \cup \{A_i x_{ij}; 1 \leq i \leq n, 1 \leq j \leq m\} \cup \{A_i y_i; 1 \leq i \leq n\}$.

The order of graph $P_n \odot W_m$ is $|V(P_n \odot W_m)| = mn + 2n$ and the size of graph $P_n \odot W_m$ is $|E(P_n \odot W_m)| = 3mn + 2n - 1$, thus $\Delta(P_n \odot W_m) = m + 3$.

By observation 2, we have the following

$\chi_r(P_n \odot W_m) \geq \min\{r, \Delta(P_n \odot W_m)\} + 1 = \min\{r, m + 3\} + 1$. To find the exact value of r -dynamic chromatic number of $P_n \odot W_m$, we define three case, namely for $\chi_{r=1,2,3}(P_n \odot W_m), \chi_{r=4}(P_n \odot W_m)$ and $\chi_r(P_n \odot W_m)$.

Case 1

Subcase 1.1 For $\chi_{r=1,2,3}(P_n \odot W_m)$, define $c_{11} : V(P_n \odot W_m) \rightarrow \{1, 2, \dots, k\}$ where $n \geq 3, m$ even by the following:

$$c_{11}(y_i) = \begin{cases} 1, & i \text{ odd}, 1 \leq i \leq n \\ 2, & i \text{ even}, 1 \leq i \leq n \end{cases}$$

$$c_{11}(A_i) = \begin{cases} 1, & i \text{ even}, 1 \leq i \leq n \\ 2, & i \text{ odd}, 1 \leq i \leq n \end{cases}$$

$$c_{11}(x_{ij}) = \begin{cases} 3, & j \text{ odd}, 1 \leq i \leq n, 1 \leq j \leq m \\ 4, & j \text{ even}, 1 \leq i \leq n, 1 \leq j \leq m \end{cases}$$

It easy to see that c_{11} is map $c_{11}: V(P_n \odot W_m) \rightarrow \{1, 2, 3, 4\}$, so it gives $\chi_{r=1,2,3}(P_n \odot W_m) = 4, m$ even .

Subcase 1.2 For $\chi_{r=1,2,3}(P_n \odot W_m)$, define $c_{12} : V(P_n \odot W_m) \rightarrow \{1, 2, \dots, k\}$ where $n \geq 3, m$ odd by the following:

$$c_{12}(y_i) = \begin{cases} 1, & i \text{ odd}, 1 \leq i \leq n \\ 2, & i \text{ even}, 1 \leq i \leq n \end{cases}$$

$$c_{12}(A_i) = \begin{cases} 1, & i \text{ even}, 1 \leq i \leq n \\ 2, & i \text{ odd}, 1 \leq i \leq n \end{cases}$$

$$c_{12}(x_{ij}) = \begin{cases} 3, & j \text{ odd}, 1 \leq i \leq n, 1 \leq j \leq m - 1 \\ 4, & j \text{ even}, 1 \leq i \leq n, 1 \leq j \leq m - 1 \\ 5, & j = m, 1 \leq i \leq n \end{cases}$$

It easy to see that c_{12} is a map $c_{12}: V(P_n \odot W_m) \rightarrow \{1, 2, 3, 4, 5\}$, so it gives $\chi_{r=1,2,3}(P_n \odot W_m) = 5, m$ even.

Case 2

Subcase 2.1 For $\chi_{r=4}(P_n \odot W_m)$, define $c_{13} : V(P_n \odot W_m) \rightarrow \{1, 2, \dots, k\}$ where $n \geq 3, m = 3k, k \geq 1$ by the following:

$$c_{13}(y_i) = \begin{cases} 1, & i \text{ odd}, 1 \leq i \leq n \\ 2, & i \text{ even}, 1 \leq i \leq n \end{cases}$$

$$c_{13}(A_i) = \begin{cases} 1, & i \text{ even}, 1 \leq i \leq n \\ 2, & i \text{ odd}, 1 \leq i \leq n \end{cases}$$

$$c_{13}(x_{ij}) = \begin{cases} 3, & j = 3t + 1, t \geq 0, 1 \leq i \leq n, 1 \leq j \leq m \\ 4, & j = 3t + 2, t \geq 0, 1 \leq i \leq n, 1 \leq j \leq m \\ 5, & j = 3t, t \geq 1, 1 \leq i \leq n, 1 \leq j \leq m \end{cases}$$

It easy to see that c_{13} is a map $c_{13}: V(P_n \odot W_m) \rightarrow \{1, 2, 3, 4, 5\}$, so it given $\chi_{r=4}(P_n \odot W_m) = 5, m = 3k, k \geq 1$.

Subcase 2.2 For $\chi_{r=4}(P_n \odot W_m)$, define $c_{14} : V(P_n \odot W_m) \rightarrow \{1, 2, \dots, k\}$ where $n \geq 3, m = 5$ by the following:

$$c_{14}(y_i) = \begin{cases} 1, & i \text{ odd}, 1 \leq i \leq n \\ 2, & i \text{ even}, 1 \leq i \leq n \end{cases}$$

$$c_{14}(A_i) = \begin{cases} 1, & i \text{ even}, 1 \leq i \leq n \\ 2, & i \text{ odd}, 1 \leq i \leq n \end{cases}$$

$$c_{14}(x_{11}, x_{12}, x_{13}, x_{14}, x_{15}) = 3, 4, 5, 6, 7$$

It easy to see that c_{14} is a map $c_{14}: V(P_n \odot W_m) \rightarrow \{1, 2, 3, 4, 5, 6, 7\}$, so it gives $\chi_{r=4}(P_n \odot W_m) = 7, m = 5$.

Subcase 2.3 For $\chi_{r=4}(P_n \odot W_m)$, define $c_{15} : V(P_n \odot W_m) \rightarrow \{1, 2, \dots, k\}$ where $n \geq 3, m$ otherwise by the following:

$$c_{15}(y_i) = \begin{cases} 1, & i \text{ odd}, 1 \leq i \leq n \\ 2, & i \text{ even}, 1 \leq i \leq n \end{cases}$$

$$c_{15}(A_i) = \begin{cases} 1, & i \text{ even}, 1 \leq i \leq n \\ 2, & i \text{ odd}, 1 \leq i \leq n \end{cases}$$

$$c_{15}(x_{ij}) = \begin{cases} 3, & j = 3t + 1, t \geq 0, 1 \leq i \leq n, 1 \leq j \leq m - 1 \\ 4, & j = 3t + 2, t \geq 0, 1 \leq i \leq n, 1 \leq j \leq m - 1 \\ 5, & j = 3t, t \geq 1, 1 \leq i \leq n, 1 \leq j \leq m - 1 \\ 6, & j = m, 1 \leq i \leq n \end{cases}$$

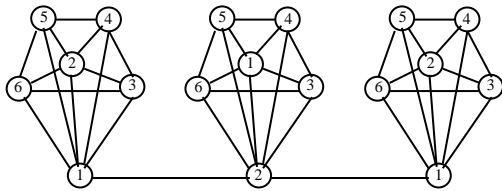


Fig.4.: $\chi_4(P_3 \odot W_4) = 6$ with $n = 3, m = 4, r = 6$

It easy to see that c_{15} is map $c_{15}: V(P_n \odot W_m) \rightarrow \{1, 2, 3, 4, 5, 6\}$, so it gives $\chi_{r=4}(P_n \odot W_m) = 6, m$ otherwise.

Case 3.

Subcase 3.1 For $\chi_r(P_n \odot W_m) 5 \leq r \leq \Delta - 1$, define $c_{16}: V(P_n \odot W_m) \rightarrow \{1, 2, \dots, k\}$ where $n \geq 3, m \geq 3$ by the following:

$$c_{16}(y_i) = \begin{cases} 1 & , i \text{ odd}, 1 \leq i \leq n \\ 2 & , i \text{ even}, 1 \leq i \leq n \end{cases}$$

$$c_{16}(A_i) = \begin{cases} 1 & , i \text{ even}, 1 \leq i \leq n \\ 2 & , i \text{ odd}, 1 \leq i \leq n \end{cases}$$

$$c_{16}(x_{11}, x_{12}, x_{13}, x_{14}, x_{15}, x_{16}, x_{17}) = 3, 4, 5, 3, 4, 5, 6, \text{ for } m = 7, r = 5$$

$$c_{16}(x_{11}, x_{12}, x_{13}, x_{14}, x_{15}, x_{16}, x_{17}) = 3, 4, 5, 6, 7, 4, 5, \text{ for } m = 7, r = 6$$

$$c_{16}(x_{11}, x_{12}, x_{13}, x_{14}, x_{15}, x_{16}, x_{17}) = 3, 4, 5, 6, 7, 8, 5, \text{ for } m = 7, r = 7$$

$$c_{16}(x_{11}, x_{12}, x_{13}, x_{14}, x_{15}, x_{16}, x_{17}) = 3, 4, 5, 6, 7, 8, 9, \text{ for } m = 7, r = 8$$

It easy to see that c_{16} is a map $c_{16}: V(P_n \odot W_m) \rightarrow \{1, 2, \dots, r+1\}$, so it gives $\chi_r(P_n \odot W_m) = r + 1, 5 \leq r \leq \Delta - 1$.

Subcase 3.2 For $\chi_r(P_n \odot W_m), r \geq \Delta$, define $c_{17}: V(P_n \odot W_m) \rightarrow \{1, 2, \dots, k\}$ where $n \geq 3, m \geq 3$ by the following:

$$c_{17}(y_i) = \begin{cases} 1 & , i = 3t + 1, t \geq 0, 1 \leq i \leq n \\ 2 & , i = 3t + 2, t \geq 0, 1 \leq i \leq n \\ 3 & , i = 3t, t \geq 1, 1 \leq i \leq n \end{cases}$$

$$c_{17}(A_i) = \begin{cases} 1 & , i = 4t + 3, t \geq 0, 1 \leq i \leq n \\ 2 & , i = 4t, t \geq 1, 1 \leq i \leq n \\ 3 & , i = 4t + 1, t \geq 0, 1 \leq i \leq n \\ 4 & , i = 4t + 2, t \geq 0, 1 \leq i \leq n \end{cases}$$

$$c_{17}(x_{11}, x_{12}, x_{13}, x_{14}, x_{15}, x_{16}) = 4, 5, 6, 7, 8, 9, \text{ for } m = 6, r = 9$$

$$c_{17}(x_{21}, x_{22}, x_{23}, x_{24}, x_{25}, x_{26}) = 5, 6, 7, 8, 9, 10, \text{ for } m = 6, r = 9$$

$$c_{17}(x_{11}, x_{12}, x_{13}, x_{14}, x_{15}) = 4, 5, 6, 7, 8, \text{ for } m = 5, r = 8$$

$$c_{17}(x_{21}, x_{22}, x_{23}, x_{24}, x_{25}) = 5, 6, 7, 8, 9, \text{ for } m = 5, r = 8$$

$$c_{17}(x_{11}, x_{12}, x_{13}, x_{14}) = 4, 5, 6, 7, \text{ for } m = 4, r = 7$$

$$c_{17}(x_{21}, x_{22}, x_{23}, x_{24}) = 5, 6, 7, 8, \text{ for } m = 4, r = 7$$

It easy to see that c_{17} is map $c_{17}: V(P_n \odot W_m) \rightarrow \{1, 2, \dots, m+4\}$, so it gives $\chi_r(P_n \odot W_m) = m + 4, r \geq \Delta$.

It concludes the proof.

III. CONCLUSION

We have found some r -dynamic chromatic number of corona product of graphs, namely $\chi_r(P_n \odot P_m) = \chi_r(P_n \odot C_m) = \chi_r(P_n \odot W_m) = r + 1$, for $4 \leq r \leq \Delta - 1$. and $\chi_r(P_n \odot P_m) = \chi_r(P_n \odot C_m) = m + 3$, for $r \geq \Delta$. All numbers attaina best lower bound. For the characterization of the lower bound of $\chi_r(G \odot H)$ for any connected graphs G and H , we have not found any result yet, thus we propose the following open problem.

Open Problem 1. Given that any connected graphs G and H . Determine the sharp lower bound of $\chi_r(G \odot H)$.

ACKNOWLEDGEMENT

We gratefully acknowledge to the support from CGANT – University of Jember of year 2017.

REFERENCES

- [1] Ali Taherkhani. On r -Dynamic Chromatic Number of Graphs. Discrete Applied Mathematics 201 (2016) 222 – 227
- [2] B. Montgomery, Dynamic Coloring of Graphs (Ph.D Dissertation), West Virginia University, 2001
- [3] Hanna Furmanczyk, Marek Kubale. Equitable Coloring of Corona Products of Cubic Graphs is Harder Than Ordinary Coloring. Ars Mathematica Contemporanea 10 (2016) 333 – 347
- [4] H.J. Lai, B. Montgomery. Dynamic Coloring of Graph. Department of Mathematics, West Virginia University, Morgantown WV 26506-6310. 2002
- [5] H.J. Lai, B. Montgomery, H. Poon. Upper Bounds of Dynamic Chromatic Number. ArsCombinatoria. 68 (2003) 193 – 201
- [6] M. Alishahi, On the dynamic coloring of graphs, Discrete Appl. Math. 159 (2011) 152–156.
- [7] M. Alishahi, Dynamic chromatic number of regular graphs, Discrete Appl. Math. 160 (2012) 2098–2103.
- [8] Ross Kang, Tobias Muller, Douglas B. West. On r -Dynamic Coloring of Grids. Discrete Applied Mathematics 186 (2015) 286 – 290
- [9] S. Akbari, M. Ghanbari, S. Jahanbekam. On The Dynamic Chromatic Number of Graphs, Combinatorics and Graph, in: Contemporary

Mathematics – American Mathematical Society 513
(2010) 11 – 18

[10] S. Akbari, M. Ghanbari, S. Jahanbekam. On The
Dynamic Coloring of Cartesian Product Graphs,
ArsCombinatoria 114 (2014) 161 – 167

[11] Sogol Jahanbekam, Jaehoon Kim, Suil O, Douglas B.
West. On r -Dynamic Coloring of Graph. Discrete
Applied Mathematics 206 (2016) 65 – 72

Determinants of Stock Prices of Joint - Stock Companies in Industrial Sector Listed On Hcm City Stock Exchange

Vuong Quoc Duy¹, Le Long Hau², Nguyen Huu Dang³

¹Associate Professor and Doctor in Economics, College of Economics, Can Tho University, Vietnam

²Doctor in Applied Economics, College of Economics, Can Tho University, Vietnam

³Doctor in Agricultural Economics, College of Economics, Can Tho University, Vietnam

Abstract—This paper investigates the factors that affect the price of the shares of industrial companies listed on the Stock Exchange in Ho Chi Minh City (HOSE). The data used in this study are collected according to the date of publication unified consumer price index of the Central Statistical Office (on the 24th of the last month of the quarter) from 2012 to 2015. Using regression analysis showed that EPS and exchange rate (USD / VND) and interest rate correlated to the profitability ratio of the shares the price of gold and the rate of inflation measured by the consumer price index (CPI) has negative correlation to rate profitability of the shares.

Keywords— Industrial sectors, price, stocks returns, HOSE.

I. INTRODUCTION

Vietnam's stock market since its inception has been through the ups and down in its development stages in line with the volatility of the domestic economy. However, it also fully embodies the essence of a true market, where business owners can raise capital in the fastest and most effective way to meet their business needs in time, through the issuance of securities. Particularly, businesses in industrial sectors are considered to be highly attractive. The sector plays an important role in the development of the national economy in order to ensure domestic demand and exports and facilitate international trade and bring the country more revenue with an average growth rate of 9.8% in 2015, compared to this of 2014. Therefore, investments in this field promise more profitable prospects. This research is aimed to find out the factors that affect stock price fluctuations of companies in the industrial sector. Then judgments and recommendations on the supply and demand of shares of companies in the industrial sector made in order to contribute to the development of stock

markets in general and the stock market of the companies in industrial sector are particularly necessary and urgent in today's international economic integration.

This paper analyzes factors affecting the stock prices of companies in the industrial sector listed on HOSE. Then solutions are proposed to help investors overcome the negative impacts and take advantage of business opportunities.

II. THEORIES & PREVIOUS STUDIES

2.1. Stock market

Stock market, in terms of the modern economy, is defined as a place to trade securities in medium and long-term. The trade is carried out in the primary market when buyers first buy securities from the issuers and in the secondary market when the buyer resells the securities in market primary market.

Naturally, the stock market reflects the exchange relations, the purchase of ownership of means of production and capital, i.e. the purchase of capital ownership. In the market economy, capital has been circulated as a commodity that has value and use value. The stock market is a highly developed form of commodity production.

In terms of characteristics, the stock market is a part of the financial market and specializes in buying and selling medium and long-term securities. The inception of stock market is an objective necessity.

The role of stock market is a mean of raising investment capital for production in businesses and economic development. In addition, it is a tool to encourage people to save and use these savings to invest, thereby promote socialization of investment. Furthermore, it also helps businesses use capital efficiently and contributes capital among sectors in the economy and creates a fast and uniform development of the economy. Lastly, the stock

market is a tool to attract and control foreign investments.

The stock market can be classified in following issues. If based on the legal forms, it can be divided into official market and the unofficial market. Regarding to the nature of the issuance or circulation of securities, there are primary market and secondary market. If the trading methods considered, there are spot market and the future market. Lastly, based on the characteristics of the commodities circulated, there are stock market, bond market and instruments and securities-origin market.

2.2. Stock Price

A stock is evidence confirming the lawful rights and interests of the owners of assets or capital of the issuer. Securities are in the form of certificates, book-entry or electronic data including stocks, bonds, fund certificates, stock options, warrants, call-options, put-options, futures contracts or securities indices. Characteristically, A stock is a long-term financing instrument. The stock is a very effective tool in the market economy to create a huge amount of capital to finance the expanding of production or the state's and individuals' investments. Securities are commercial papers with economic value or, in other words, financial instruments that have the corresponding value and can be sold or transferred. Securities are a very typical kind of goods in the mechanism.

2.3. Factors affecting the price of stock

The stock price can be influenced by the political, social and legal environment. Firstly, the political environment has a strong influence on the stock market. The society always has certain impacts on the operation of the stock market. Political factors include changes in government and politics. Because Vietnam is relatively politically stable, this factor can be ignored. In addition, the policy system has a huge impact on the stock market itself as well as the operation of businesses. Every policy change may entail impacts as stock prices would increase or decrease, especially during sensitive times.

Besides, the stock price also is affected by the macro-economic factors. Firstly, the exchange rate has an influence on the stock market on two sides: financial environment and activities of enterprises, particularly those businesses importing raw materials. Rising exchange rate has a strong impact on the stock market. Foreign capital is invested heavily in the stock market but the rise in the exchange is a strong reason for foreign investors to withdraw from the market. A large amount of capital is quickly withdrawn from the market and stock prices will decrease and this in turn will cause the

interest rate to go up. If interest rates rise, they will become a burden for the economy, and vice versa. Moreover, the inflation is the depreciation of the currency. It changes consumer behaviors and individuals' and businesses' savings behaviors. Unreasonable increase in inflation rate would cause difficulties for production and business activities and prevent the business from growth and innovation. Inflation is often a signal of sluggish growth of the economy and interest rates will rise. Then the businesses' profitability drops and the share prices fall. The lower inflation rate, the more capable the stock price will rise and vice versa. Normally, stock prices tend to rise when the economy is well-developed and tend to fall as the economy deteriorates. Thus, if the development trends of the economy are predicted, the general development trend of the stock market can be predicted. Therefore, predicting the economic situation to consider its impacts on the stock price is also very important to investors. Lastly, changes in interest rates of government bonds will affect the value of securities. The increase in benchmark interest rate makes the prices of other securities decrease and vice versa.

2.4. The experimental studies

Factors affecting the prices of the stock (rate of return) are a concern of many research economists in recent years. The resulting lessons from these empirical studies include two groups of factors: macro factors and internal factors related to the financial situation and performance of the company. Here, the authors would like to list some typical research as the basis for this article.

2.4.1. Earnings per share (EPS)

EPS is considered as an important variable when calculating share prices. The higher EPS, the stronger the company's capability is and the higher the ability is to pay dividends and more likely the stock prices is to rise. Therefore, EPS can be seen as a combined indicator reflecting the results of a business' operations. It helps individual and organizational investors and analysts easily understand and compare different shares. Studies by Al-Qenae et al (2002), Al-Tamimi et al (2007), Mehr-un-Nisa and Nishat (2012), Uddin et al (2013) and Truong Dong Loc (2014) conclude that EPS is positively correlated with the stock price.

2.4.2. Exchange rate (USD / VND)

The exchange rate is a very important variable affecting the equilibrium of the balance of trade and balance of payments; thus, it affects production, employment and the balance of the economy. The volatility of the

exchange rate has a strong impact on businesses in general and most seriously on import - export businesses in particular. Affecting the prices of imported goods, exchange rate changes lead to the changes in the prices of exports and imports, thereby affect the business activities then the stock prices.

Similar to EPS, regression analysis results indicate that the USD / VND exchange rate are positively correlated with profitability ratios of the stock. This result is consistent with studies by Eita (2012), Aurangzeb (2012), Phan Thi Bich Nguyet and Pham Duong Phuong Thao (2013), Truong Dong Loc (2014). Meanwhile, research by Liu and Shrestha (2008) is against the conclusion that exchange rates have an inverse relationship with the company's stock price.

2.4.3. Interest rate

Government bonds interest rates are considered as the benchmark rate. Changes in these rates will affect the stock prices. The benchmark interest rate increase makes the prices of other securities fall. On the contrary, decline in these rates causes the prices of securities to increase. Relationship between market interest rates and securities interest rate is an indirect relationship that impacts the stock price. If market interest rates are higher than the interest rate of securities, securities prices will fall, which makes activities on the stock market decline because people like to save rather than invest in the stock market. Some experimental studies by Al-Qenae et al (2002), Liu and Shrestha (2008), Hussainey and Ngoc (2009), Mehr-un-Nisa and Nishat (2012), Eita (2012), Aurangzeb (2012) also share the same view that interest rates have a negative correlation with the stock price.

2.4.4. Gold price

In Vietnam, the stock market and real estate market are already applicable to state channel management measures, while the gold market is not, so cash flows into the gold market is inevitable and gold is also seen as an investment channel for many people. The changes in the price of gold in the country are expected to have certain effects on the prices of listed shares. The reason is that when gold prices rise, gold is an attractive investment channel for investors. Meanwhile, cash flow shifts from stock markets to gold market make the stock price fall and vice versa. In other words, the relationship between the stock price and the gold price is an inverse relationship. Study by Truong Dong Loc (2014) about the factors affecting share prices of companies listed on the Ho Chi Minh Stock Exchange also gave similar conclusion.

2.4.5. Inflation

Inflation is defined as the devaluation of the currency, it changes consumer behavior and people's and businesses' savings. The unreasonable inflation rate will cause some problems to production and business activities. It slows down the business' growth and innovation. Increase in inflation rate is often a signal of an unstable economy, interest rates will increase, the profitability of the business will be lower and then the stock prices will fall. The lower inflation, the more capable the stock price will rise and vice versa. This is consistent with the studies by Al-Qenae et al (2002), Al-Tamimi et al (2007), Liu and Shrestha (2008), Mehr-un-Nisa and Nishat (2012), Aurangzeb (2012), Phan Thi Bich Nguyet and Pham Duong Phuong Thao (2013) and Zhang Dong Loc (2014).

Usually, stock prices tend to rise when the economy grows well and tend to fall as the economy deteriorates. Thus, if the development trends of the economy are predicted, the general development trend of the stock market can be predicted. Therefore, predicting the economic situation to consider its impacts on the stock price is also very important to investors.

2.4 Research Methodology

2.4.1. Data collection

This study analyzes data from audited balance sheets and income statements of the companies listed on HOSE, Vietnam from 2012 to 2015. The selection of the listed companies and the audited reports ensures levels of accuracy because the figures have been checked for transparency and fairness. In unlisted companies, the audit of financial statements is not officially required so that the figures may not accurately reflect the situation of the company. Therefore, using data from these companies will not accurately reflect the research results. The data on lending rates, USD / VND exchange rate, gold price and consumer price index are collected from official sources of the State Bank of Vietnam (www.sbv.gov.vn), General statistics Office of Vietnam (www.gso.gov.vn) Saigon Jewelry Company- SJC (www.sjc.com.vn). The data are collected on the same date of the publication of consumer price index by the general Statistics Office (the 24th of the last month of the quarter).

The figures in the financial reports after collected will be calculated on Excel to be indicators used in this research.

2.4.2. Research Methodology

Descriptive Statistics is related to the collection of data, summarizing, presenting, calculating and describing the

different characteristics to reflect a general object of study. In the study the dependent variable and independent variables from 2012 to 2015 are described through mean, median, maximum value, minimum value and standard deviation of the variables. Through analysis of these values, the typical level of the variables will be seen. Sometimes in some special cases (data with big changes or unusual differences), the average value does not represent the overall nature for too small or too large big value will distort the results of the average. While the median is an average value which better represents the average. Maximum and minimum values and standard deviation are used to evaluate the degree of representing of the average value for the overall study. If the value of the standard deviation is larger, the variance of variables is larger; thus, representative of the average figures is lower and vice versa.

Correlation regression analysis is used to determine the relationship between changes in stock prices and the variables: EPS, interest rates, exchange rates, gold prices, rate of inflation. Research model is as follow:

$$Y_t = \beta_0 + \beta_1 X_{1t} + \beta_2 X_{2t} + \beta_3 X_{3t} + \beta_4 X_{4t} + \beta_5 X_{5t} + u_t$$

In which: Y_t (the dependent variable) is the change in price (profitability ratios) of the stocks in the portfolio and is calculated as follows:

$$Y_t = R_t = \log(p_t) - \log(p_{t-1}) = \log(p_t / p_{t-1})$$

P_t : price index in the second quarter t ;

P_{t-1} : Price Index in quarter $t-1$.

X_1, X_2, X_3, X_4, X_5 are the independent variables and are explained in details.

Table.1: The independent variables used in the regression model

Variables	Explanation	Expectation
EPS (X_1)	EPS of the portfolio	+
USD/VND Exchange rate (X_2)	Log of the exchange rate (USD / VND)	+
Interest rate (X_3)	short-term lending interest rate (% /year)	-
Gold rate (X_4)	Log of gold price (SJC) in domestic market	-
Inflation rate (X_5)	Consumer Price Index (%) by the General Bureau of Statistics	-

III. FINDINGS AND DISCUSSION

Table.2: Results of regression analysis

Variables	Correlation coefficient	T-statistic Value
Constant	0.9012	0.63
EPS (X_1)	0.0026	0.72
USD/VND Exchange rate (X_2)	0,0005	1,2
Interest rate (X_3)	0,0059	1,36
Gold price (X_4)	-0,0075	-2,01
Inflation rate (X_5)	-0,002	-0,14
Observations	464	
Adjusted R2	32,47	
F- statistic value	1,74	

EPS (X_1) - (Earning Per Share/ profit per share)

This is the portion of profit which the company attributes to each ordinary outstanding share. EPS is considered as the single most important variable in calculating the share price. In addition, to investors EPS is an indication of profitability on each share. Comparison of EPS over time will help investors know the growth of the company. Firms with higher EPS mean higher profitability. This means more value for investors and vice versa.

According to the regression results, the EPS and the profitability ratio of the stock is positively correlated. This is consistent with the theory and with results of previous studies (Al- Qenae et al., 2002; al-Tamimi et al., 2007; Uddin et al., 2013) etc, on the Taiwan and China stock markets.

Particularly, when the EPS increases by 1%, the price of the equity portfolio rises 0.0026 respectively. This relationship is statistically significant at 1%. This is the explanation for the positive correlation between EPS and profitability ratios of the stocks.

Exchange rate USD / VND (X_2)

Similar to EPS, regression analysis results indicate that the exchange rate is positively correlated with the profitability ratio of the stocks at a statistically significant level of 5%. This result is consistent with studies by Eita (2012), Aurangzeb (2012), Phan Thi Bich Nguyet and Pham Duong Phuong Thao (2013) in Vietnam stock market as well as overseas stock markets. However, the levels of impacts are different in each market. Specifically, when the USD / VND exchange rate rises 1%, the profitability ratio of the stock rises 0.05%.

This effect can be explained as follows: when the rate increases, the dollar rises, which is synonymous with

devaluation the VND. At that time, \$ 1 will exchange for over more VND, and so there will be an excess from the increase in this rate. Therefore, the dollar appreciation gives investors more business opportunities. This encourages more indirect investment flow into Vietnam. This means that the demand for shares in the market should increase and the stock price will rise.

Interest rates (X3)

Regression results from the study show that the relationship between interest rates and the profitability ratio of the stocks is positively correlated. This is inconsistent with the expected hypothesis. Specifically, as interest rates increase or decrease by 1%, the profitability ratio of the stock will increase or decrease of 0.0059%.

This result is inconsistent with the findings demonstrated by Al Qenae et al., 2002; Al-Tamimi et al., 2007, Phan Thi Bich Nguyet and Pham Duong Phuong Thao (2013). When analyzing an economy in general to invest in the stock market, it is necessary to take interest rates and fundamentals of investment decision into account. Many previous studies have explained that increase in market interest rates means a fall in bond prices. As a result, investors will shift from stocks to bonds. This causes the stock price to fall. However, in the authors' opinion, the differences are in part because of the ineffectiveness of the government's monetary policy in recent years. Therefore, the change in interest rates is not well-absorbed by the stock market.

Gold prices (X4)

In Vietnam, gold is also seen as an investment channel for many people. Therefore, the domestic gold price changes are expected to have certain effects on the price of the shares listed on the market.

The results of the study show that the volatility of the gold price is negatively correlated with profitability ratio of the stock. Quantitatively, while gold prices increase or decrease by 1%, the profitability ratio of the stock will go down or up by 0.75%. In terms of statistics, the negative correlation between the gold price movements and the profitability ratio of the stock is significant at the 5% level. This is consistent with findings by John Leyers (2007) and Twite (2002) on the Australian stock market. However, the finding is contradicted with Truong Dong Loc and Vo Thi Hong Doan (2009) who stated that the gold price and profitability ratio of the stock are positively correlated. Explanation for this relationship is based on the theory stating that capital flows will shift from investment channels with lower profitability ratios to a channel with a higher profitability rate. Therefore, when gold prices rise, investment in gold is an attractive

channel, and investors can "avoid" inflation. Meanwhile, cash flow shifts from stock markets to gold markets should make the market stock price fall, and vice versa.

Inflation rate (X5)

In this study, the rate of inflation is measured by consumer price index (CPI) announced by the general statistics office. It is consistent with results from previous studies (Al-Qenae et al., 2002; Al-Tamimi et al., 2007; Liu and Shrestha, 2008, Mehr-un-Nisa and Nishat, 2012). Regression analysis results obtained from this study show that the profitability ratio of stocks are negatively correlated with the rate of inflation. Specifically, when the rate of inflation rise by 1%, the profit rate of stocks will decrease .002% and vice versa. The inversely proportional relationship is statistically significant at 1%. This result is completely in line with what have been happening in Vietnam stock markets recently. For investors, inflation is an important indicator of the "health" of the economy, and so it has a direct impact on the price of the stocks on the market. Rising inflation means higher cost of inputs for production and business activities of enterprises. Meanwhile the prices of products and services will also increase accordingly to ensure business operations profit. However, the consumption of products and services will decline due to higher selling prices, particularly in the short-term and when consumers look for alternative products. This makes the targeted profitability is now difficult to achieve or even decline, affecting the profit expectations of the business in the future. As a result, the share prices decline. Therefore, inflation is an expression of the uncertainty of the economy and the psychology of investors in the stock market will be affected severely. For safety, many investors will withdraw from the market and invest in other safer channels. Consequently, the share price will fall as inflation rate goes up.

Based on the results of the regression model, the F-statistic value of 1.74 indicates that the model used is highly reliable at statistical significance at 1%. Besides, the value of R^2 is 32.43%, which means that the independent variables in the model can explain 32.43% of the changes of the dependent variable.

IV. CONCLUSIONS AND SUGGESTIONS

4.1. Conclusions

The main objective of the study is to find out the internal and macroeconomic factors having impacts on the stock prices of the companies in industrial sector listed on HOSE. By means of regression analysis of data on stock prices and EPS of 29 companies in the industrial sector and macro indicators such as exchange rates, gold prices,

interest rates and inflation in the period of 2012-2015. The research concludes that EPS and USD / VND exchange rate are positively correlated with stock price fluctuations; on the other hand, gold price and inflation are inversely correlated with stock prices. However, due to data is secondary and may be distorted so the results may not reflect the most accurate market movements; little time and limited knowledge cause unavoidable shortcomings and errors in the research.

4.2 Suggestions

The study results show that the share price of companies in industrial sector listed on HOSE are influenced by internal factors (earnings per share - EPS) and macroeconomic factors (exchange rates, gold prices and inflation rate).

However, these effects have different impacts on each stock price index. On that basis, the study makes a number of recommendations for policy - making with the aim of increasing the positive impacts and minimizing the negative impacts of these factors on the stock prices of the companies in industrial sector in Vietnam.

4.2.1 Fair allocation of earnings per share

EPS is used as an indicator of the profitability of enterprises, often regarded as the single most important variable in calculating the share prices. This is also the principal components of P / E (price-earnings ratio). This coefficient (P / E) is one of the important indicators in analyzing securities investment. Income from shares will have a decisive effect on the market price of shares. Therefore, the joint-stock companies should focus on reasonable dividend to meet the goal of attracting investment from outside sources and maintaining the company's net income to meet business operations and reinvestment in the future at the same time.

4.2.2 Inflation control

There should be coordination, flexibility between monetary policy and fiscal policy in order to avoid the adverse effects on effective implementation of each policy. Inflation is affected by many factors such as economic structure, import and export situations, the credit policy of commercial banks or the fiscal policy of the State. However, inflation is possible mainly from the money supply to the economy. Therefore, inflation control requires measures on the money supply such as tight monetary policy, control of interest rates in line with different situations of the market, directing credit policy to key economic activities. The application of this solution requires the supervision and management of the State Bank as well as the coordinated implementation of

credit institutions to ensure the objectives and maintain effective operational stability of the banking system to keep inflation rate at a reasonable level.

Besides, there should be a focus on collecting information, processing data quickly and promptly and accurately on inflation in order to provide sufficient information to meet the assessment of the state of the economy in general and business activities of manufacturing companies in particular. From that there are solutions to respond promptly to bad situations to minimize the risks to the economy.

4.2.3 Stable exchange rates

The exchange rate plays an important role in the commercial activities of the economy. Specifically, in the current period, while Vietnam is implementing open policies to attract foreign investment, especially indirect investment through the draft content allowing foreign investors to buy shares, own 51% of the charter capital of the active securities firms, establish foreign-own securities businesses, buy and own 100% of foreign securities organizations operating in Vietnam. The stable exchange rate would help the policy of attracting foreign capital be more efficient; help to build confidence among investors about a stable business environment to have many preferential policies; to create steps forward in attracting more capital from abroad to invest and develop the securities market in the future.

To achieve stable exchange rates, it is necessary to increase economic activities to generate foreign currency revenues such as improving the balance of international payments, foreign currency reserves increase, and the State Bank can use these funds to regulate and maintain the exchange rate at a stable level. Besides, the relevant departments should perform well their functions in macro management to make timely regulatory and suitable policies when there are fluctuations in the economy and the impact on the exchange rate. When being carried out, the above solutions will boost the economic potentials and there are enough tools to maintain stability of the foreign exchange market against external shocks to help macroeconomic stability, limit extraordinary impact of macroeconomic factors on the stock price index.

4.2.4 Executive flexible monetary policy

The management of monetary policy plays an important role in the economy. It helps the economy achieve the macroeconomic objectives such as inflation and exchange rate stability and further economic growth. Monetary policy uses changes in the money supply to

affect the entities in the economy. Monetary policy affects the money supply and then the investment decisions in the securities market. Implementing monetary policies to expand the money supply will cause the general level of interest rates to fall, encouraging people to save more and investors can borrow at lower cost than before. This helps investors seek a more attractive investment channel and one of which is in securities markets. Hence, the stock rising demand leads to share price increases.

Performing active and more flexible monetary policy in order to fit the actual situation helps control inflation, macroeconomic stability and economic growth. Besides, this helps to limit the negative impacts on the stock price index when there are effects from the economy and stimulate confidence in investors to enter the market.

In addition, the state should strengthen their supervision in the currency markets, quality control activities and treatment of bad debts at credit institutions to find out and deal with errors promptly to ensure full operation security of the institutions; to help minimize the negative impacts on the share price index and stock market in general and the stock prices of companies in the industrial sector listed on HOSE in particular.

macroeconomic variables and the Chinese stock market using heteroscedastic cointegration, *Managerial Finance*, 34, p.744-755.

- [8] Mehr-un-Nisa and Mohammad Nishat, 2012. The determinants of stock prices in Pakistan, *Asian Economic and Financial Review*, 1(4), p. 276-291.
- [9] Phan Thi Bich Nguyet and Pham Duong Phuong Thao, 2013. Analyze the impact of macroeconomic factors to Vietnam stock market, *Journal of Development and Intergration*, 8 (18), p. 34-41.
- [10] Uddin, Reaz, Zahidur Rahman và Rajib Hossain, 2013. Determinants of stock prices in financial sector companies in Bangladesh: A study on Dhaka Stock Exchange (DSE), *Interdisciplinary Journal of Contemporary Research in Business*, 5(3), p. 471-480.
- [11] Truong Dong Loc, 2014. Determinants of stock returns: Evidence from the Ho Chi Minh Stock Exchange, *Can Tho University Journal of Science*, 33, p. 72-78.

REFERENCES

- [1] Al- Qenae, Rashid, Carmen Li và Bob Wearing, 2002. The information content of earnings on stock price: The Kuwait Stock Exchange, *Multinational Finance Journal*, 6(3), p. 197-221.
- [2] Al-Tamimi, Hussein, 2007. Factors affecting stock price in the UAE financial markets, *The Business Review*, 5(2), p. 225-223.
- [3] Aurangzeb, 2012. Factors affecting performance of stock market: Evidence from South Asian countries, *International Journal of Academic Research in Business and Social Sciences*, 2(9), p. 1-15.
- [4] Eita, Joel Hinaunye, 2012. Modelling macroeconomic determinants of stock market prices: Evidence from Namibia, *The Journal of Applied Business Research*, 28(5), p. 871-884.
- [5] Fama, Eugene F., 1970. Efficient capital markets: A review of theory and empirical work, *Journal of Finance*, 25, p. 383-417.
- [6] Hussainey, Khaled and Le Khanh Ngoc, 2009. The impact of macroeconomic indicators on Vietnamese stock prices, *Journal of Risk Finance*, 10(4), p. 321-332.
- [7] Liu, Ming-Hua and Keshab Shrestha, 2008. Analysis of the long-term relationship between

Efficiency and Performance analysis of routing protocols in WSN

Kaysar Ahmed Bhuiyan¹, Md Whaiduzzaman², Mostofa Kamal Nasir³

^{1,2}Institute of Information Technology, Jahangirnagar University, Bangladesh

³CSE, Mawlana Bhashani Science and Technology University, Bangladesh

Abstract— Routing is very important in data communication, especially in Wireless Sensor Network (WSN). In WSN, every node acts as a router, forwarding data packets to other nodes. There are various kinds of routing protocol and they act different in different scenario by their specialty. Routing protocols performance can be vary with various parameters such as speed time, seed time, pause time, number of node and network topology. In this paper, we discuss several routing protocols such as Ad Hoc On Demand Distance Vector (AODV), Ad hoc On-demand Multipath Distance Vector (AOMDV), Dynamic Source Routing (DSR), Destination-Sequenced Distance-Vector Routing (DSDV) and different connection types such as TCP, Constant Bit Rate (CBR) for WSN. In this research, we analyzed performance of routing protocols by considering different scenarios and metrics. We compare protocols performance by using several metrics such as Packet Delivery Ratio (PDR), Loss Packet Ratio (LPR) and Average End to End Delay (E2E) with varying pause time and speed time. We use network simulator NS2.35 for compare and analyze WSN protocol performance.

Keywords---Routing protocols, Proactive and Reactive routing, Performance analysis, Wireless sensor network.

I. INTRODUCTION

WSN is very popular network topology nowadays. It does establish network autonomously without human interaction [1]. In wireless network every distributed autonomous device using sensors to monitor physical or environmental conditions [2]. Routing protocol establishes a link to send data from source to destination node. In WSN it is not possible to establish fixed path or route infrastructure between two nodes because nodes could be moveable [3]. Routing protocol is very important because it provides all the information about the network and routers and store information into the routing table. According to this routing table information routing algorithm compute its routing decisions to calculate the best path from source to destination. Routing protocol is basically designed for the

dynamic network environment. In routing every node makes its own routing decision by using a routing protocol to find out the next node. This process is repeated until the packet is reached to the destination. Every routing information is stored in the routing table and according to routing algorithm its find out the shortest path. Routing table can synchronize by two ways one is static and other is dynamic routing. In static routing every router is configured by manually and set the list of destination and next hop/node. It is possible in static network, however, difficult in dynamic routing. Dynamic network may change or update frequently. Therefore, it is complicated to establish fixed/static routing path. For this reason dynamic routing uses a routing protocol that update routing table frequently and determine the best path to send data packet from source to destination.

The remainder of the paper is organized as follows: Section 2 shortly describes about related work related to performance evaluation of protocols. Section 3 discusses about routing protocol of AODV, AOMDV, DSR and DSDV. Section 4 presents two connection types. Section 5 describes the performance metrics and network parameter simulations. Section 6 describes implementation and simulation results. Section 7 discuss performance analysis and Section 8 concludes the paper with conclusion.

II. RELATED WORK

In literature, several papers discussed related to WSN performance evaluation of AODV, AOMDV, DSR and DSDV protocols.

In paper [1] authors discuss about performance evaluation of quality of service in DS-AODV in MANET. Also they focused on using a reactive routing approach, AODV, to discover the delay-aware routes during its route discovery phase.

In paper [3] two protocol AODV and DSDV have been simulated using NS-2 package and compared in terms of packet delivery fraction, end to end delay and throughput in different environment; varying period of pause time and

number of expired nodes. In paper [5] authors focused on routing, protocols, their challenges and issues. The purpose of this paper is to explore different challenges and issues of routing algorithms in a classified way for IP network and ad hoc network.

In paper [9], performance is analyzed of WSN according to End-to-End delay, Number of packet received, Loss Packet ratio and Average end to end delay. Authors analyzed performance of 50,100,150 nodes using simulation area 1200m*1200m and size of packets is 512 bytes. In paper [19] authors consider analysis performance of WSN according to End-to-End delay, Number of packet received, Packet drop ratio and Energy consumption of the Network. They analyzed performance of 50 nodes, using simulation area 100m*100m and size of packets is 100 bytes. In [20,21] authors discussed intelligent transportation protocol systems.

III. ROUTING PROTOCOL

Internet Engineering Task Force (IETF) has been proposed various protocols into two categories of routing used in ad hoc network are proactive routing and reactive routing. In reactive routing protocols route are established only when source and destination want to communicate each other. But in proactive routing protocol every node maintains one or more routing tables the entire topology of the network to communicate with another node [4].

Destination Sequenced Distance Vector (DSDV) is one of the proactive routing algorithm and Ad hoc On Demand distance Vector (AODV), Ad hoc On demand Multipath Distance Vector (AOMDV), Dynamic Source Routing (DSR) are the reactive routing algorithm [5].

3.1 AODV

AODV [6] is an Ad Hoc on Demand Distance Vector routing protocol is a best example of reactive routing protocol. Only when source node wants to send packet to destination node then AODV establish a route. AODV contain routing table to check route for sending message. It's also has ability to unicast and multicast routing. AODV is different from other on demand routing protocols because it used destination sequence number (DestSeqNum). For route discovery AODV used route Request (RREQ) and Route Reply (RREP) messages also used HELLO message for maintenance route.

3.2 AOMDV

AOMDV [7] that means Ad hoc On-demand Multipath Distance Vector Routing is one of the best examples of multipath routing protocol. AOMDV create multipath for backup route purpose. For data sending purpose it's

discover several paths from source to destination. If existing path become down its used backup path to stable network. By sending temporary message backup path are kept stable. Destination node also replies multiple RREQs to the source for acknowledgment.

3.3 Dynamic Source Routing (DSR)

DSR is a reactive routing protocol [8]. Link state algorithm is used into DSR protocol. That means best route from source to destination are saved into every node. For any kind of change into network topology, the whole network will get the information by flooding. Node generates an error message when any failure occurred into link. DSR stored all intermediate nodes ID in the packet header and stores all routing information of multiple paths, if there has multiple paths to go to the destination [9].

3.4 Destination-Sequenced Distance-Vector Routing (DSDV)

DSDV [10] is a Proactive routing protocol. It used on Bellman-Ford routing algorithm for exchanges the messages within the neighbor nodes. Every node maintains a routing table of the entire possible destination and keeps the record of all number of hops in the network. If any kinds of update occurred into network, then every neighbor nodes exchange routing table and routing data are updated with new data. Loop free paths and low latency for real time application is one of the best advantages of DSDV routing protocol. DSDV doesn't support Multi path routing that's why unused paths occupy a significant part of the available bandwidth.

IV. CONNECTION TYPE

For our experimental purpose we used two types of traffic: Transmission Control Protocol (TCP) Traffic and constant-bit-rate traffic (CBR).

4.1 Transmission Control Protocol (TCP) Traffic

Transmission Control Protocol (TCP) is one of the valuable protocols of the internet protocol suite. It's complemented the Internet Protocol (IP) by implementation originated in the initial network [11]. That means connection of TCP is an oriented, reliable, flow control, avoid overloading and conforming transport protocol [12]. TCP uses acknowledgement, time outs and retransmission process. In TCP, destination node gives feedback or positive acknowledgments. That means successful transmission of packets from source to destination. Timeouts system required that data to be successfully delivered between the source to the destination. If any acknowledgement is not received during a certain period of time then the system become time out and then TCP send the data again.

4.2 Constant Bit Rate (CBR) Traffic

Constant bit rate means the data are sent at a fixed bit rate [13]. In the network fixed bit rate are supplied. Between two nodes establishment phase of connection is not required, also the receiving or destination node don't send any acknowledgment or "hello" message. Traffic is flowing only from source to destination without giving any feedback or acknowledgment from the destination.

V. PERFORMANCE METRICS & NETWORK PARAMETERS SIMULATIONS

There have been many performance metrics are available for measure network performance. According to this metrics we can evaluate the performance of network. For example we can say: Quality of Service (QoS), Packet Delivery Ratio (PDR), Average end-to-end delay, Loss Packet Ratio (LPR). For our experiment purpose we use three performance metrics. These are Packet Delivery Ratio (PDR), Average end-to-end delay, Loss Packet Ratio (LPR).

5.1 Packet Delivery Ratio (PDR)

Packet delivery ratio is the ratio of delivery packets which is send by the source node and received by the destination node. When packet delivery ratio is high then we can say that performance is better.

5.2 Average end-to-end delay (E2E)

Average time delay (how much time needed?) For send data packet from the source node & received by the destination node. Total time difference over the total number of packet received is dividing with single packet send and received time (which was stored before) give the average end-to-end delay for the received packets. When average end-to-end delay is less than the performance is better.

5.3 Loss Packet Ratio (LPR)

Loss Packet means, Packet can't reached the destination from the source. Loss Packet Ratio means, number of packets that can't receive by destination or that never reached the destination which is send by the source. Normally when Loss Packet Ratio (LPR) is lower than the performance is better.

VI. IMPLEMENTATION & SIMULATIONS RESULTS

We use g Network simulator (NS) version 2.35 under Linux (Ubuntu) platform for our all simulation work [14, 15]. NS2

software is open source simulator software and main goal of NS2 simulator is to provide educational support for research in networking. NS2 provide two language: object oriented language C++ & Object oriented variant of Tool Command Language (OTCL) [16, 17, 18]

We use wireless node random waypoint mobility model for our simulation purpose by Network Simulator NS-2. 35 [9-13]. We employ same scenario and same metrics for every protocol (AODV, AOMDV, DSR and DSDV) to measure the performance.

6.1 Parameters of Simulations

For our experiment purpose, we used 1200 x 1200 size environment. Number of node is 100 with constant Seed time 1.0 and variable Speed time 10s, 20s, 30s and variable Pause time is 10s, 20s, and 30s. We did the simulation for simulation time 200s. The network parameters which we used for our simulation purpose shown in the table 1.

Table.1: Simulation Parameters

Parameter	Value
Protocols	AODV, AOMDV, DSR, DSDV
Simulation Area	1200*1200
Packet Size	512
Simulation Time	200s
Pause Time	10s,20s,30s
Speed Time	10s,20s,30s
Seed Time	1.0
Number of Nodes	100
Traffic generation	TCP, CBR
Mobility Model	Random Waypoint
Network Simulator	NS 2.35

6.2 Simulation Results

Connection types TCP & CBR are used in our simulation purpose. Performance of routing protocols AODV, AOMDV, DSR & DSDV has been compared with varying Pause time 10s, 20s, 30s and variable Speed time 10s, 20s, 30s according to constant number of nodes 100. Mobility Model is Random Waypoint and seed time is 1.0 (fixed). We do compare AODV, AOMDV, DSR & DSDV protocols according to packet delivery ratio (PDR), average end-to-end delay, Loss packet ratio (LPR). By using Table and Graphs we show all the simulation output.

Table.2: Variations of PDR, LPR AND E2E with Speed Time & Pause Time for AODV

AODV								
Number of Node	Speed Time	Pause Time	Pkt Types	Pkt Sent	Pkt Receive	LPR	PDR	E2E
100	10	10	TCP	27836	26652	4.251688461	95.74831154	101.44795
			CBR	4828	4591	4.918711815	95.08128818	75.1822
		20	TCP	21381	20540	3.93340	96.06660	112.454
			CBR	4817	4561	5.31451	94.68549	102.81
		30	TCP	30102	28997	3.672452454	96.32754755	98.3092
			CBR	4811	4604	4.302192663	95.69780734	85.32735
	20	10	TCP	34291	32765	4.45015	95.54985	90.4419
			CBR	4840	4621	4.52479	95.47521	47.5544
		20	TCP	32958	31792	3.53784	96.46216	99.765
			CBR	4818	4590	4.7325	95.26775	85.1383
		30	TCP	38824	37454	3.52875	96.47125	84.1644
			CBR	4806	4648	3.28756	96.71244	67.8447
	30	10	TCP	27476	26009	5.340927702	94.6590723	105.02145
			CBR	4825	4503	6.672883639	93.32711636	77.7462
		20	TCP	20662	19253	6.81928	93.18072	119.601
			CBR	4811	4386	8.83392	91.16608	107.938
		30	TCP	29743	28353	4.671687456	95.32831254	101.8827
			CBR	4808	4517	6.062181553	93.93781845	87.89135

Table3: Variations of PDR, LPR AND E2E with Speed Time & Pause Time for AOMDV

AOMDV								
Number of Node	Speed Time	Pause Time	Pkt Types	Pkt Sent	Pkt Receive	LPR	PDR	E2E
100	10	10	TCP	22682	21448	5.440317425	94.55968257	109.0034
			CBR	4807	3237	32.65730629	67.34269371	41.83105
		20	TCP	31163	29589	5.05086	94.94914	88.8379
			CBR	4830	3701	23.37474	76.62526	26.6085
		30	TCP	32879	31316	4.755242628	95.24475737	77.39245
			CBR	4827	3541	26.63904713	73.36095287	31.13315
	20	10	TCP	14202	13308	6.29489	93.70511	129.169
			CBR	4785	2774	42.02717	57.97283	57.0536
		20	TCP	32709	31257	4.43915	95.56085	72.5143
			CBR	4825	2894	40.02073	59.97927	37.0094
		30	TCP	34596	33043	4.48896	95.51104	65.947
			CBR	4825	3382	29.90674	70.09326	35.6578
	30	10	TCP	26197	25143	4.023361454	95.97663855	97.51785
			CBR	4805	2690	44.01664932	55.98335068	48.08455
		20	TCP	38192	36978	3.17868	96.82132	65.8667
			CBR	4825	2606	45.98964	54.01036	39.1155
		30	TCP	36394	35010	3.801450789	96.19854921	65.90685
			CBR	4825	2994	37.94818653	62.05181347	37.38665

Table.4: Variations of PDR, LPR AND E2E with speed time & pause time for DSR

DSR								
Number of Node	Speed Time	Pause Time	Pkt Types	Pkt Sent	Pkt Receive	LPR	PDR	E2E
100	10	10	TCP	33526	33301	0.67260227	99.32739773	286.0805
			CBR	4797	4304	10.28660761	89.71339239	201.6955
		20	TCP	51437	51176	0.50742	99.49258	275.701
			CBR	4786	4619	3.48934	96.51066	48.853
		30	TCP	42229	41964	0.627523414	99.37247659	316.9975
			CBR	4808	4603.5	4.253327787	95.74667221	107.776
	20	10	TCP	15616	15426	1.21670	98.78	296.46
			CBR	4809	3989	17.05136	82.94864	354.538
		20	TCP	11388	11167	1.94064	98.05936	665.343
			CBR	4814	3756	21.97757	78.02243	1464.92
		30	TCP	33022	32753	0.81461	99.18539	358.294
			CBR	4830	4588	5.01035	94.98965	166.699
	30	10	TCP	22196	21795	1.808843737	98.19115626	291.3705
			CBR	4808	3566	25.83194676	74.16805324	589.5535
		20	TCP	28777	28164	2.13017	97.86983	286.281
			CBR	4807	3143	34.61618	65.38382	824.569
		30	TCP	30899	30458	1.42720756	98.57279244	322.2875
			CBR	4818	3865	19.77793919	80.22206081	495.634

Table.5: Variations of PDR, LPR and E2E with speed time & pause time for DSDV

DSDV								
Number of Node	Speed Time	Pause Time	Pkt Types	Pkt Sent	Pkt Receive	LPR	PDR	E2E
100	10	10	TCP	22711	22020	3.042511503	96.9574885	65.0067
			CBR	4793	1892	60.52576674	39.47423326	28.18215
		20	TCP	12315	11842	3.84084	96.15916	81.0275
			CBR	4784	2191	54.20151	45.79849	30.2092
		30	TCP	17498	16952	3.120267451	96.87973255	78.0724
			CBR	4784	2108	55.93060926	44.06939074	44.3043
	20	10	TCP	33108	32199	2.74556	97.25444	48.9859
			CBR	4802	1593	66.82632	33.17368	26.1551
		20	TCP	35900	34983	2.55432	97.44568	50.0487
			CBR	4822	2409	50.04148	49.95852	78.02243
		30	TCP	22682	22063	2.72904	97.27096	75.1173
			CBR	4785	2026	57.65935	42.34065	58.3994
	30	10	TCP	24750	23955	3.212121212	96.78787879	53.86835
			CBR	4822	1573	67.3683119	32.6316881	40.91105
		20	TCP	16392	15711	4.15447	95.84553	58.7508
			CBR	4842	1554	67.90582	32.09418	55.667
		30	TCP	19537	18887	3.327020525	96.67297947	66.93405
			CBR	4813	1790	62.81292199	37.18707801	57.0332

6.3 Performance Graphs

We generated the graph based on our simulation result Data in network simulator NS-2.35. This shows the differences of performance between AODV, AOMDV, DSR and DSDV. The graph is given below.

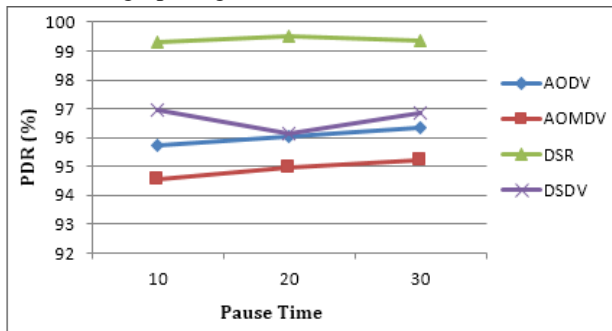


Fig.1: PDR of Speed time 10 using TCP

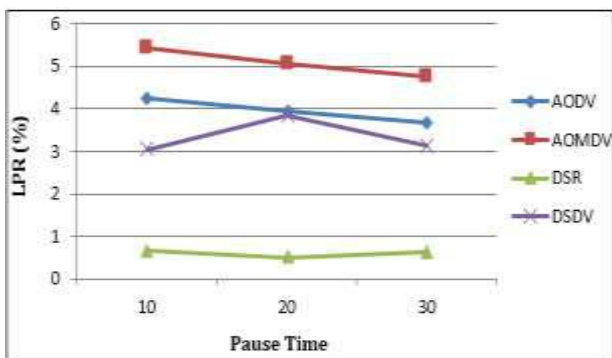


Fig.2: LPR of Speed time 10 using TCP

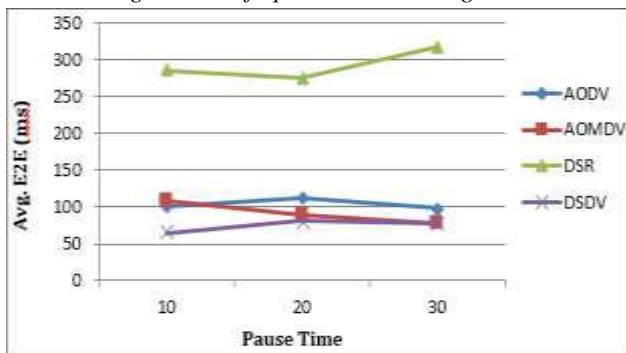


Fig.3: E2E delay of Speed time 10 using TCP

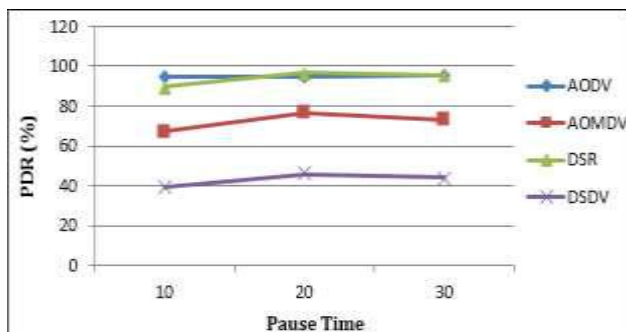


Fig.4: PDR of Speed time 10 using CBR

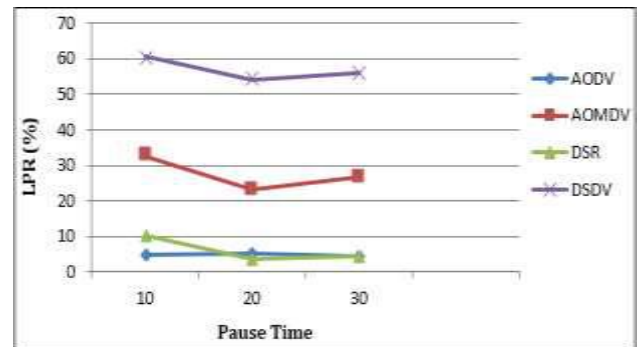


Fig.5: LPR of Speed time 10 using CBR

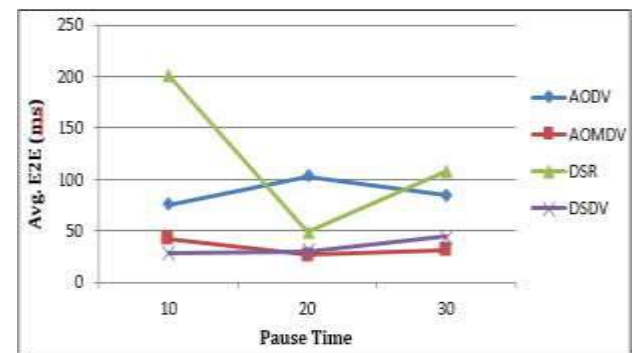


Fig.6: E2E delay of Speed time 10 using CBR

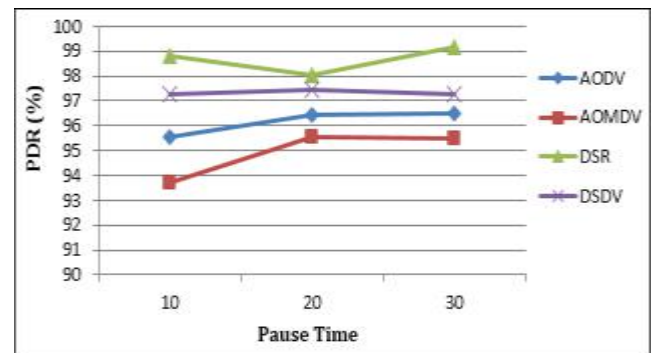


Fig.7: PDR of Speed time 20 using TCP

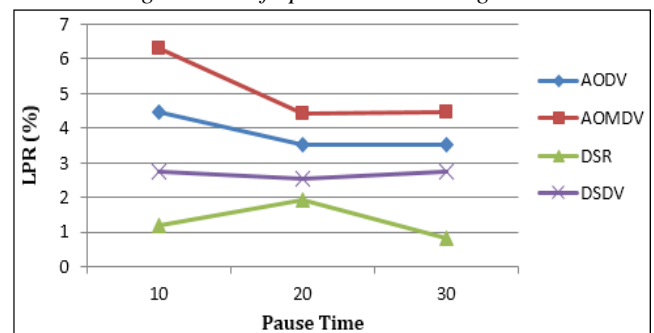


Fig.8: LPR of Speed time 20 using TCP

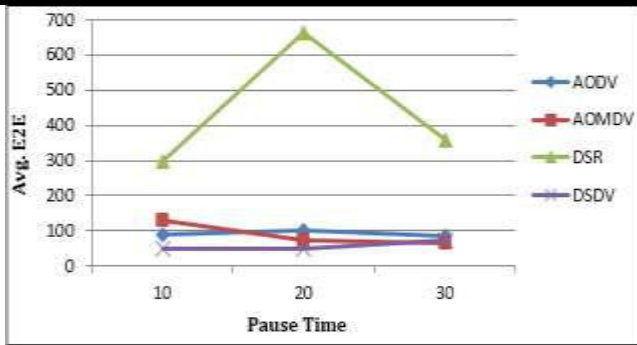


Fig.9: E2E delay of Speed time 20 using TCP

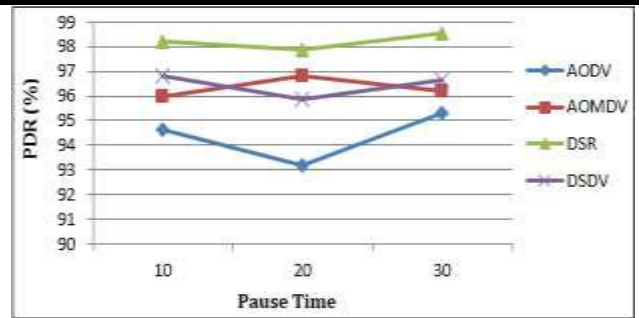


Fig.13: PDR of Speed time 30 using TCP

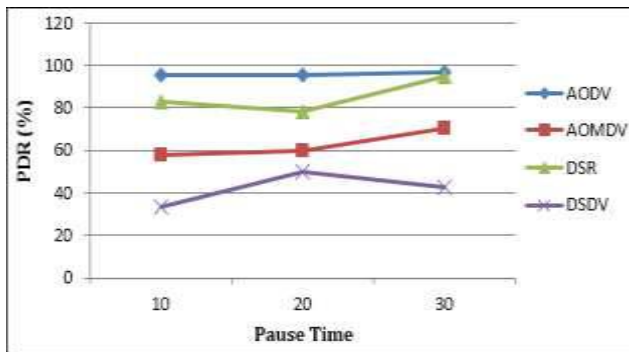


Fig.10: PDR of Speed time 20 using CBR

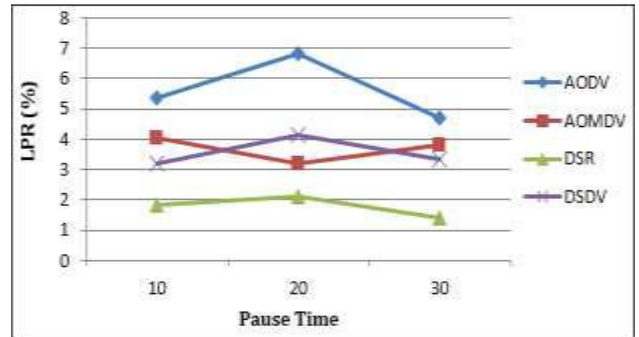


Fig.14: LPR of Speed time 30 using TCP

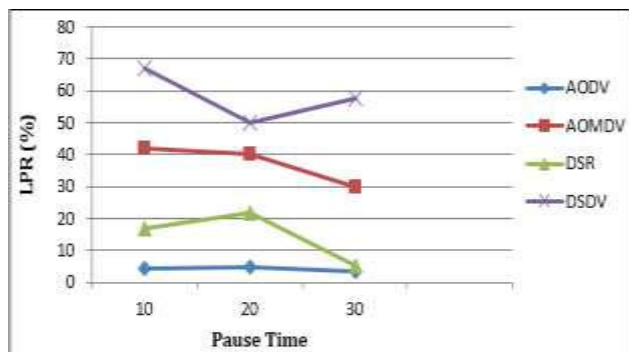


Fig.11: LPR of Speed time 20 using CBR

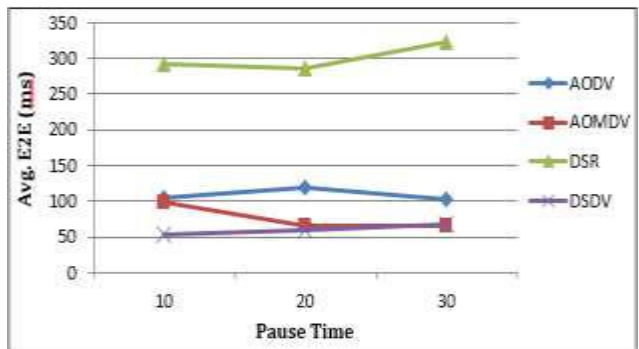


Fig.15: E2E delay of Speed time 30 using TCP

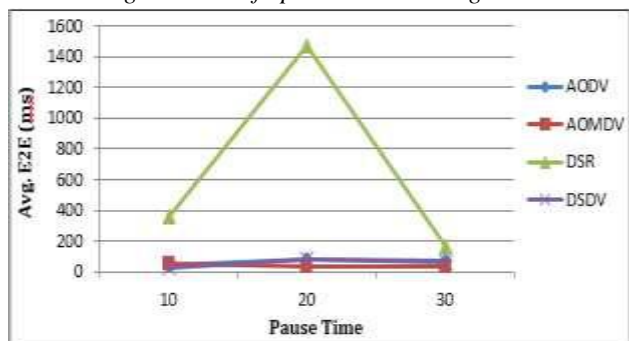


Fig.12: E2E delay of Speed time 20 using CBR

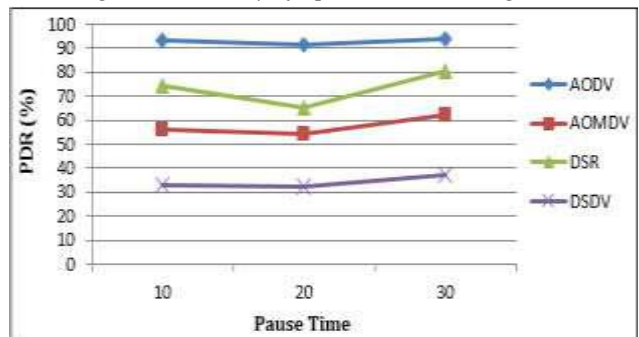


Fig.16: PDR of Speed time 30 using CBR

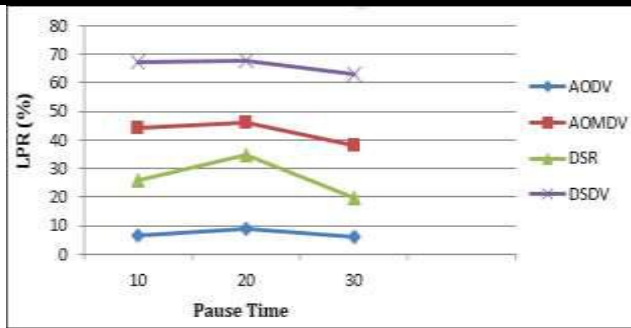


Fig.17: LPR of Speed time 30 using CBR

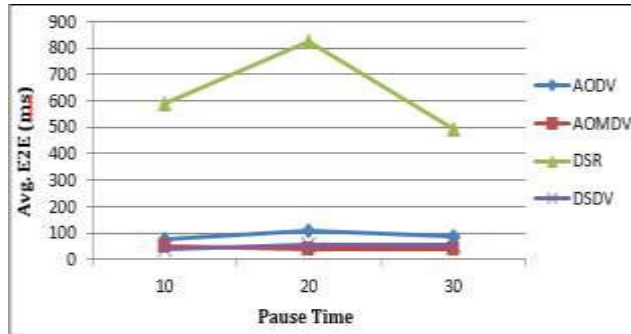


Fig.18: E2E delay of Speed time 30 using CBR

VII. PERFORMANCE ANALYSIS

The analysis performance of AODV, AOMDV, DSR and DSDV results have been shown in several tables. We consider 10 is the low speed, 20 is the average speed and 30 is the high speed. As the same time 10 is the low pause time 20 is the average pause time and 30 is the high pause time. The standard for PDR values (approx.) defines below:

High: >95%

Average: =90% to 95%

Low: <90 %

The standard for E-to-E values (approx.) defines below:

High: >150ms

Average: = 50ms to 150ms

Low: <50ms

The standard for LPR values (approx.) define below:

High: > 4% , Average: = 2.5% to 4% , Low: < 2.5%

By using this approximate parameter we summarize the performances between AODV, AOMDV, DSR and DSDV. After performance analysis of AODV, AOMDV, DSR & DSDV by using Performance analysis table we shown our decision below.

Table.6: Packet Delivery Ratio (PDR) with respect to speed time & pause time for TCP & CBR connections

Packet Delivery Ratio (PDR)									
Speed Time	Pause Time	AODV		AOMDV		DSR		DSDV	
		TCP	CBR	TCP	CBR	TCP	CBR	TCP	CBR
10	10	High	High	Avg	Low	High	Low	High	Low
	20	High	Avg	Avg	Low	High	High	High	Low
	30	High	High	High	Low	High	High	High	Low
20	10	High	High	Avg	Low	High	Low	High	Low
	20	High	High	High	Low	High	Low	High	Low
	30	High	High	High	Low	High	Low	High	Low
30	10	Avg	Avg	High	Low	High	Low	High	Low
	20	Avg	Avg	High	Low	High	Low	High	Low
	30	High	Avg	High	Low	High	Low	High	Low

Table.7: Loss Packet Ratio Respect to Speed Time & Pause Time for TCP & CBR

Loss Packet Ratio (LPR)									
Speed Time	Pause Time	AODV		AOMDV		DSR		DSDV	
		TCP	CBR	TCP	CBR	TCP	CBR	TCP	CBR
10	10	High	High	High	High	Low	High	Avg	High
	20	Avg	High	High	High	Low	Avg	Avg	High
	30	Avg	High	High	High	Low	High	Avg	High
20	10	High	High	High	High	Low	High	Avg	High

	20	Avg	High	High	High	Low	High	Avg	High
	30	Avg	Avg	High	High	Low	High	Avg	High
30	10	High	High	High	High	Low	High	Avg	High
	20	High	High	Avg	High	Low	High	High	High
	30	High	High	Avg	High	Low	High	Avg	High

Table.8: Average End-To-End Delay (E2E) With Respect To Speed Time & Pause Time for TCP & CBR Connections

Average end-to-end Delay (E2E)									
Speed Time	Pause Time	AODV		AOMDV		DSR		DSDV	
		TCP	CBR	TCP	CBR	TCP	CBR	TCP	CBR
10	10	Avg	Avg	Avg	Low	High	High	Avg	Low
	20	Avg	Avg	Avg	Low	High	Low	Avg	Low
	30	Avg	Avg	Avg	Low	High	Avg	Avg	Low
20	10	Avg	Low	Avg	Avg	High	High	Low	Low
	20	Avg	Avg	Avg	Low	High	High	Avg	Avg
	30	Avg	Avg	Avg	Low	High	High	Avg	Avg
30	10	Avg	Avg	Avg	Low	High	High	Avg	Low
	20	Avg	Avg	Avg	Low	High	High	Avg	Avg
	30	Avg	Avg	Avg	Low	High	High	Avg	Avg

VIII. CONCLUSION

In this article, four protocols AODV, AOMDV, DSR and DSDV are compared based on connection type TCP and CBR according to PDR, LPR and average end-to-end delay. According to the all simulation and graphical results, which are simulated by using NS2 simulator, we observed packet delivery ratio of DSR is high at TCP platform on the other hand packet delivery ratio of AODV is high at CBR platform. Loss packet ratio of DSR is very low at TCP platform also CBR platform DSR and AODV are same. But average end-to-end delay is low of AOMDV for both TCP and CBR platform. In addition, we can say that DSR is the best solution at TCP platform and CBR platform AODV is better from others protocol. This result will help the designers and engineers for implement in real life of wireless sensor network and also further research and development of these protocols.

REFERENCES

- [1] J. A. Hamilton et al "Global Journal of Computer Science and Technology: E Network, Web & Security", Volume 14 Issue 6 Version 1.0 , 2014
- [2] <http://www.ni.com/white-paper/7142/en/>
- [3] Adel.S.El ashheb. "Performance Evaluation of AODV and DSDV Routing Protocol in wireless sensor network Environment", International Conference on Computer Networks and Communication Systems vol.35, 2012, Singapore.
- [4] <https://folk.uio.no/kenneho/studies/essay/node12.html>
- [5] Charles E. Perkins, "Ad hoc Networking", Pearson, ISBN 978-81-317-2096-7, First Impression, 2008
- [6] Perkins, C.; Belding-Royer, E.; Das, S. "Ad hoc On-Demand Distance Vector (AODV) Routing". July, 2013
- [7] M.K.Marina and S.R.Das, "On-Demand multipath distance vector routing in ad hoc networks" in: Proceedings of the 9th IEEE International Conference on Network Protocols (ICNP), 2001.
- [8] Johnson, D. B. and Maltz, D. A. , "Dynamic Source Routing in Ad Hoc Wireless Network," Mobile Computing, T. Imielinski and H. Korth, Eds., Ch. 5, Kluwer, 1996, pp. 153-81.
- [9] Bijan Paul, Kaysar Ahmed Bhuiyan, Kaniz Fatema, Partha Pratim Das; Analysis of AOMDV, AODV, DSR and DSDV ROUTING PROTOCOLS for Wireless Sensor Network using Network simulator (Ns-2.35). Computational Intelligence and Communication Networks (CICN), IEEE International Conference, 2014
- [10] Charles E. Perkins, Pravin Bhagwat, "Highly dynamic Destination-Sequenced Distance-Vector routing (DSDV) for mobile computers", SIGCOMM , the

- conference on Communications architectures, protocols and applications, 2014, Pages 234-244.
- [11] https://en.wikipedia.org/wiki/Transmission_Control_Protocol
- [12] Raheleh Hashemzahi, Reza Noormandipour , “Comparison of Technical Features of Transport Protocols for Wireless Sensor Networks” Greener Journal of Internet, Information and Communication Systems , Vol. 1 (1), 2013, pp. 033-039.
- [13] Suresh Kumar, Jogendra Kumar,” Comparative Performance Study of Zone Routing Protocol over AODV and DSR Routing Protocols on Constant Bit Rate (CBR)” International Journal of Computer Applications , 2012, Volume 45– No.4, .
- [14] <http://www.isi.edu/nsnam/ns>
- [15] <http://www.isi.edu/nsnam/ns/tutorial/>
- [16] <http://itantenna.blogspot.com/2012/01/install-ns234-on-ubuntu-1004.html>
- [17] The Network Simulator - ns-2 available at: <http://www.isi.edu/nsnam/ns/>
- [18] Ns (simulator) - Wikipedia, the free encyclopedia en.wikipedia.org/wiki/Ns
- [19] D.D.Chaudhary, Pranav Pawar, Dr. L.M. Waghmare, “Comparison and Performance Evaluation of Wireless Sensor Network with different Routing Protocols”, International Conference on Information and Electronics Engineering, 2011
- [20] MK Nasir, M Whaiduzzaman, “Use of Cell Phone Density for Intelligent Transportation System (ITS) in Bangladesh” Jahangirnagar University Journal of Information Technology, Volume 1, 2012
- [21] M Whaiduzzaman, M Sookhak, A Gani, R Buyya, “A survey on vehicular cloud computing.”, Journal of Network and Computer Applications, 2014, pp 325-344.

Study of Electron Transport in Fullerene (C₆₀) Quantum Confined Channel Layer Based Field Effect Transistor

Cyril Robinson Azariah John Chelliah^{1§}, Barbara Szymanik², Rajesh Swaminathan^{1#*}

[§]PhD scholar, [#]Professor and Programme Coordinator

¹Department of Nanosciences and Technology, Karunya University, Coimbatore, India – 641114.

²Professor, Department of Electrical and Computer Science Engineering,
West Pomeranian University of Technology, Szczecin, Poland – 70 313.

*Corresponding Author: drsrajesh@karunya.edu

Abstract— In this work, we modelled a simple n-channel Si Metal-Quantum confined layer-Semiconductor Field Effect Transistor (MQSFET), which resembles exactly as the conventional Si Metal-Oxide-Semiconductor Field Effect Transistor (MOSFET) where SiO₂ dielectric layer is replaced with a wide band gap C₆₀ quantum confined layer of thickness 3nm and gold ($\Psi=5.1eV$) as metal contact. The capacitance and voltage characteristics at different temperatures from 100 K to 500 K and energy band gap are studied using Multi-dielectric Energy Band Diagram Program (MEBDP) simulation software, performed current-voltage transistor characteristics and analyzed the mobility of the charge carrier in the MQS sandwiched device structure using the Caughey-Thomas high saturation mobility model and the Lombardi surface mobility model. In these studies, we inferred a very low threshold voltage, when the donor concentration in the p-Si substrate is tuned between 1E16 to 1E17 cm⁻³ and a saturated flow of nanoamperes range of charge carrier at a low gate potential is even possible.

Keywords— C₆₀, quantum confined layer, Metal-Quantum Confined Layer-Semiconductor Field Effect Transistor (MQSFET), Multi-dielectric Energy Band Diagram Program (MEBDP), Capacitance-Voltage characteristics, Current-Voltage characteristics, Mobility modelling.

I. INTRODUCTION

Gordon Moore prophesied that transistor built on a single die of the Si chip doubles every eighteen months [1, 2]. With respect to the Moore's law, the gate length of the MOSFET will eventually shrink to 5 nm by 2020 [3]. As the transistor feature size keeps decreasing, the enhancement in the VLSI MOSFET device models is essential so that the exact behavior of deep sub-micron and nanometer scaled MOSFETs can be defined with accuracy. When we keep miniaturizing the MOSFET,

there is a reduction in charge transport (also known as carrier mobility) [4, 5]. The reduction in charge transport is the prime cause of drain current degradation. This reduces the switching speed of the device [6]. Hence, carrier mobility on the surface inversion has been of great interest in MOSFET can be studied using various mathematical modeling [7, 8]. In this work, we use Caughey-Thomas mobility (CTM) model and Lombardi surface mobility (LSM) model to study the charge mobility performance of the proposed C₆₀ quantum confined layer, a thin film of 3 nm thickness as gate dielectric layer.

CTM model helps to demonstrate a high field velocity scattering to an existing mobility models such as constant input mobility [9]. Above the ambient thermal energy, the charge carriers can gain energy, with an added input of the applied field. Thus, this gained energy can be able to transfer from the applied field to the lattice. This is due to the optical phonon emission. Field dependent mobility makes a problem which is already highly non-linear. It is hence important to use the continuation study extension to obtain convergence in the high field limit [10].

This model helps us to determine the electron ($\mu_{n,ct}$) and hole ($\mu_{p,ct}$) mobility by the following equations:

$$\mu_{n,ct} = \frac{\mu_{in,n}}{\left(1 + \left(\frac{\mu_{in,n} F_n}{v_{sat,n}}\right)^{\alpha_n}\right)^{1/\alpha_n}} \quad (1)$$

$$\alpha_n = \alpha_{0,n} \left(\frac{T}{T_{ref}}\right)^{\beta_{1,n}} \quad (2)$$

$$v_{sat,n} = v_{0,n} \left(\frac{T}{T_{ref}}\right)^{\beta_{2,n}} \quad (3)$$

$$\mu_{p,ct} = \frac{\mu_{in,p}}{\left(1 + \left(\frac{\mu_{in,p} F_p}{v_{sat,p}}\right)^{\alpha_p}\right)^{1/\alpha_p}} \quad (4)$$

$$\alpha_p = \alpha_{0,p} \left(\frac{T}{T_{ref}}\right)^{\beta_{1,p}} \quad (5)$$

$$v_{sat,p} = v_{0,p} \left(\frac{T}{T_{ref}} \right)^{\beta_{2,p}} \quad (6)$$

where T: the lattice temperature (K),
 F_n and F_p : the driving forces for electrons & holes
 $F_n = E_{||,n}$: component of the electric field parallel to the electron current
 $F_p = E_{||,p}$: component of the electric field parallel to the hole current
 $\mu_{in,n}$ and $\mu_{in,p}$: the electron and hole input mobility.
 $v_{0,n}$ and $v_{0,p}$: the saturation velocities for electrons and holes (m/s)

All the other parameters used in the model are the material properties of Si [11-14, 30-31] (Refer Appendix).

The Lombardi surface mobility model is used for understanding the electron mobility in a simplified MOSFET (Metal Oxide Semiconductor Field Effect Transistor) [15]. We can compare the current density profile and total current flowing into the terminal with the constant mobility model. Especially in the thin inversion layer under the gate in MOSFETs, two factors have an important effect on the carrier mobility. They are the surface roughness and the surface acoustic phonons. This model adds interesting resultant effects with the surface scattering to the already existing Matthiessen's rule-based modeling [16]. The electron mobility ($\mu_{n,lo}$) and hole mobility ($\mu_{p,lo}$) are calculated by the following equations:

$$\frac{1}{\mu_{n,lo}} = \frac{1}{\mu_{in,n}} + \frac{1}{\mu_{ac,n}} + \frac{1}{\mu_{sr,n}} \quad (7)$$

$$\mu_{ac,n} = \frac{\mu_{1,n}}{\left(\frac{E_{\perp,n}}{E_{ref}} \right)} + \frac{\mu_{2,n} \left(\frac{N}{N_{ref}} \right)^{\beta_n}}{\left(\frac{E_{\perp,n}}{E_{ref}} \right)^{1/3} \left(\frac{T}{T_{ref}} \right)} \quad (8)$$

$$\mu_{sr,n} = \frac{\delta_n}{E_{\perp,n}^2} \quad (9)$$

$$\frac{1}{\mu_{p,lo}} = \frac{1}{\mu_{in,p}} + \frac{1}{\mu_{ac,p}} + \frac{1}{\mu_{sr,p}} \quad (10)$$

$$\mu_{ac,p} = \frac{\mu_{1,p}}{\left(\frac{E_{\perp,p}}{E_{ref}} \right)} + \frac{\mu_{2,p} \left(\frac{N}{N_{ref}} \right)^{\beta_p}}{\left(\frac{E_{\perp,p}}{E_{ref}} \right)^{1/3} \left(\frac{T}{T_{ref}} \right)} \quad (11)$$

$$\mu_{sr,p} = \frac{\delta_p}{E_{\perp,p}^2} \quad (12)$$

$$N = N_a^- + N_d^+ \quad (13)$$

where T: the lattice temperature (K),
 N_a^- and N_d^+ : the ionized acceptor and donor concentration,
 $E_{\perp,n}$ & $E_{\perp,p}$: the component of the electric field perpendicular to the electron and hole current,
 $\mu_{in,n}$ and $\mu_{in,p}$: the electron and hole input mobility,
 δ_n and δ_p : the delta coefficients for electrons and holes (V/s).

All other parameters in the model are the material properties of silicon. (Refer Appendix).

We choose buckminsterfullerene (C_{60}), because of its excellent properties. It includes: wide bandgap, high dielectric properties, withstand high temperatures, possess great current density, fast switching speed and less on-resistance. It is also an active element in n-channel field effect transistor, because of its very high electron mobility. [18, 19].

II. DEVICE THEORY AND MODELLING

As portrayed in figure 1, C_{60} Quantum structure embedded thin film layer of thickness 3nm is deposited on the p-Si substrate [20-23]. The source and drain are the n-type Si. Au is used as gate metal. We characterized this MQS structure as a capacitor and a FET structure. Hence we analyzed the capacitance-voltage (CV) characteristics, current-voltage (IV) characteristics and charge transport behavior in different mobility models.

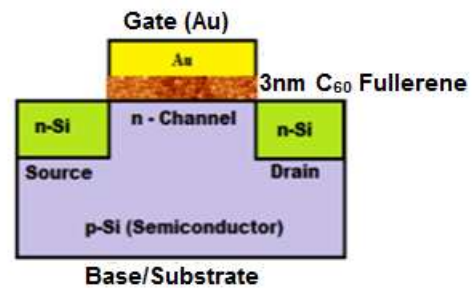


Fig.1: Proposed structure of MQSFET using 3nm C_{60} quantum confined layer

A. Caughey-Thomas Mobility Model

In this model, we swept the drain to source voltage from 0 to 1 V, at no applied field ($V_{gs}=0V$). Sweeping the drain voltage creates an important electric field at the left side of the gate at the junction between the n-doped and p-doped regions. In order to ensure convergence of the linear model, a solver continuation parameter is used to rise up the electron and the hole driving forces (F_n and F_p) as the drain voltage is swept. Table 1 shows the CTM model parameters for Si [26,27].

Table.1: CTM model parameters for Si

Description	Value
Electron alpha coefficient	1.11
Hole alpha coefficient	1.21
Electron saturation velocity	1E7[cm/s]
Hole saturation velocity	8.37E6[cm/s]
Electron alpha exponent	0.66

Hole alpha exponent	0.17
Electron velocity saturation exponent	-0.87
Hole velocity saturation exponent	-0.52
Reference temperature	300[K]

fullerene C₆₀ acts as a gate channel, an active element in this MQSFET. C₆₀ possess a band gap of 1.9eV and a dielectric constant (κ) of 4.5.

Table.4: Energy-gap (Eg) and dielectric constant (κ) of various materials

	Si	SiO ₂	C ₆₀
Band gap 'Eg' (eV)	1.12	9	1.9
Dielectric constant ' κ '	11.8	3.9	4.5

B. Lombardi Surface Mobility Model

In this model, when the gate voltage of 1V is applied, the drain voltage is swept from 0V to 1V. We can observe an important perpendicular electric field to the flow of charges underneath the gate contact. In order to ensure convergence of the nonlinear model, a solver continuation parameter is used to rise up the electron and hole perpendicular to the field ($E_{\perp, n}$ and $E_{\perp, p}$), as the drain voltage is swept [24, 25]. Table 2 shows the LSM model parameters for Si [26-29].

Table.2: LSM model parameters for Si

Description	Value
Electron delta coefficient	5.82E14[V/s]
Hole delta coefficient	2.05E14[V/s]
Electron mobility reference	4.75E7[cm ² /(V*s)]
Hole mobility reference	9.93E7[cm ² /(V*s)]
Electron mobility reference	1.74E5[cm ² /(V*s)]
Hole mobility reference	8.84E5[cm ² /(V*s)]
Electron alpha coefficient	0.125
Hole alpha coefficient	0.0317
Reference temperature	1[K]
Electric field reference	1[V/cm]
Doping concentration reference	1[1/cm ³]

C. Other Parameters Used

The CTM model and the LSM model has the following parameters for the quantum confined layer C₆₀, as listed in Table 3.

Table.3: Description of C₆₀ confined layer

Description	Value
Terminal name	3
Terminal type	Voltage
Voltage	Vgs
C ₆₀ relative permittivity	4.5
C ₆₀ layer thickness	tq = 3 [nm]
Au Metal work function	5.1 [V]

Table 4 shows the materials energy gap and dielectric constant values which are used in the modelling. The

III. RESULTS AND DISCUSSIONS

Initially, we performed simulation for the Au/C₆₀/p-Si MQS structure using Multi-dielectric Energy Band Diagram Program (MEBDP) to study the energy band diagram of the proposed device, capacitance-voltage characteristics and CV at various temperatures. The flat band condition of the Au/C₆₀/p-Si MQS structure obtained at V_{fb} = -0.28V.

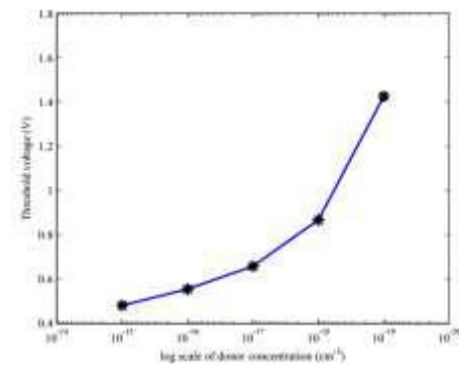


Fig.2: Threshold voltages at various log scale of donor concentrations.

Using MEBDP simulation software, we simulated the model. We inferred that the threshold voltage of this device can be tuned to our desirable value, as we keep decreasing the donor concentration of the p-Si substrate. As shown in figure 2, as the donor concentration of the p-Si substrate keeps increases, the threshold voltage of the device also increases.

The stack capacitance is calculated by sweeping the voltage from -5 to +5 V, at various temperatures 100 K to 500 K. The CV characteristics at various temperatures are shown in figure 3. From the CV characteristics, we study the accumulation, depletion and inversion occurrence in the device. As there is increase in temperature, the stack capacitance in the accumulation mode keeps increases. In the depletion region, there is a decrease in stack capacitance as the temperature increase and in the saturation region, there is a gradual increase in stack capacitance but lesser than the device capacitance, as the

temperature increases. The device can work efficiently even at higher temperatures around 500K.

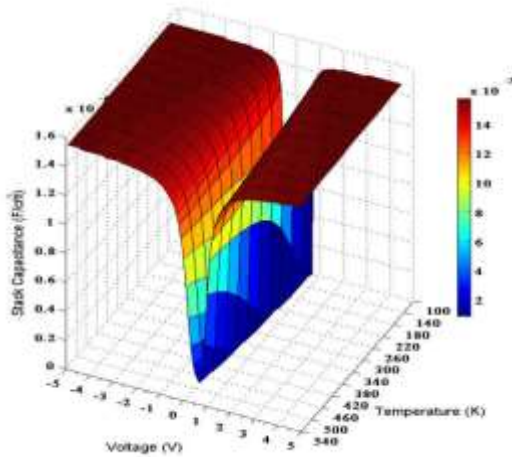


Fig.3: Stack capacitance Vs Voltage (CV) characteristics of the Au/C₆₀/p-Si MQS Capacitor at various temperatures.

Figure 4 shows the drain current versus gate voltage, for a fixed drain voltage of 10mV simulated for the C₆₀ quantum confined nanolayer based MQSFET. From this plot, we found out that the threshold voltage (V_{th}) is approximately 0.8V. For a minimum drain voltage, the threshold voltage is little higher. For higher drain voltages, the threshold voltage will reduce below 0.8V. The switching of the device will be faster for higher drain voltages.

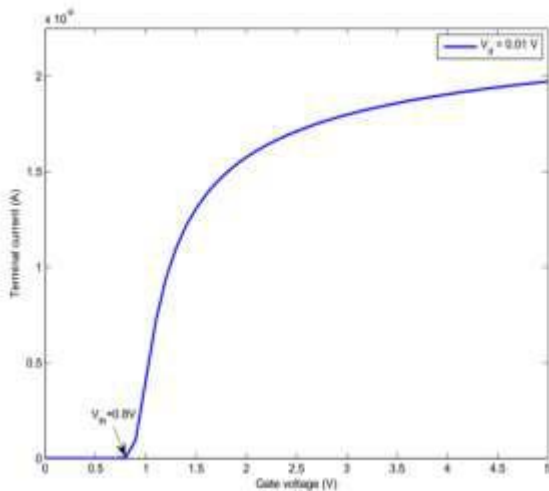


Fig.4: Drain current versus gate voltage at $V_d = 0.01V$ of Au/C₆₀/p-Si MQSFET device.

Also for the quantum confined C₆₀ nanolayer MQSFET, the drain current and drain voltage characteristics simulated and the characteristics plot for various gate voltages at V_g ranges from 1 to 4V shown in figure 5. It is very clear from the plot that, a linear region is seen at the low voltages, a nonlinear region at the intermediate

voltages and saturation region at higher voltages. It is observed that a small current flow, when the gate voltage is very small and a maximum current flow saturated at the positive and greater gate voltages.

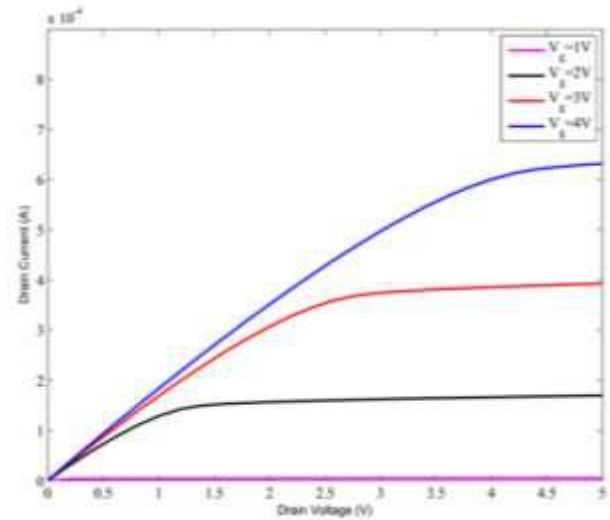


Fig.5: Drain current (I_d) vs drain voltage (V_d) characteristics of the Au/C₆₀/p-Si MQSFET device.

A. Caughey-Thomas mobility model:

Figure 6 shows the comparison of the terminal current for the constant mobility and Caughey-Thomas mobility of Au/C₆₀/p-Si MQSFET device. The effect of the CTM on the solution is well seen. The comparison of the constant mobility (the driving forces are multiplied by 1E-6) and the CTM (F_n and F_p multiplied by 1) models shows a more pronounced saturation effect for this model. The current is lower and level off more rapidly due to the fact that the mobility decreases when the electric field is high.

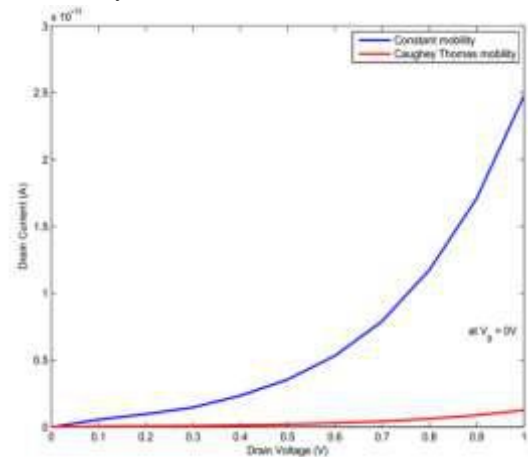


Fig.6: Comparison of the terminal current for the constant mobility and Caughey-Thomas mobility of Au/C₆₀/p-Si MQSFET device.

B. Lombardi surface mobility model:

The effect of the Lombardi surface mobility model of the Au/C₆₀/p-Si MQSFET device is shown in figure 7, which

explains the comparison of the constant mobility (the perpendicular fields are multiplied by 1E-6) and the Lombardi surface mobility (E_{L,n} and E_{L,p} multiplied by 1) models shows a more pronounced saturation effect for the Lombardi surface mobility model than for the constant mobility model (without field dependent parameters).

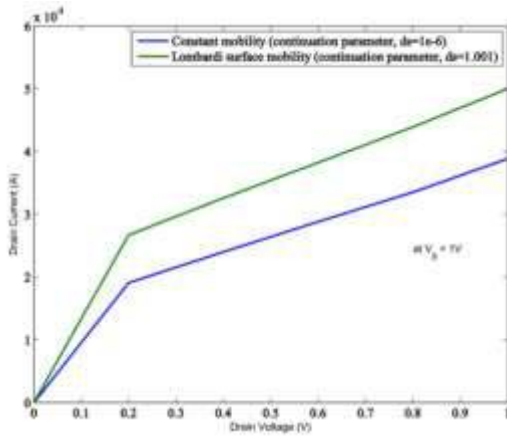


Fig.7: Plot of terminal current for the constant mobility and surface mobility cases of Au/C₆₀/p-Si MQSFET device. The current is inhibited when the surface mobility is active.

IV. CONCLUSIONS

Through the Caughey-Thomas mobility model, we studied that in C₆₀ MQSFET, the current is lower and level off more rapidly due to the fact that the mobility decreases when the electric field is high. And the study from the Lombardi surface mobility model of C₆₀ MQSFET explains that as a consequence of the inversion layer

generated by the applied potential on the gate contact and due to the presence of C₆₀ quantum layer bonded with the surface of the semiconductor Si, the electron mobility is slightly smaller in the vicinity of the C₆₀ gate junction. Hence, C₆₀ quantum confined layer can be able to work well as a gate dielectric channel and behave well as a better replacement for Si channel, for a low power and can withstand a high temperature upto 500K in future device applications.

ACKNOWLEDGMENT

We extend our sincere thanks for laboratory facility and guidance in COMSOL Multiphysics at the Faculty of Electrical Engineering, West Pomeranian University of Technology, Szczecin, Poland and for research support at the Department of Nanosciences and Technology, Karunya University, Coimbatore, India.

CONFLICT OF INTERESTS

The authors declare no conflict of interest.

AUTHOR CONTRIBUTIONS

Cyril R. A. John Chelliah - performed the simulation experiments, analyzed the data and wrote the article; Barbara Szymanik – contribution in teaching simulation using COMSOL; Rajesh Swaminathan - leading the research project, contributed ideas and suggestions.

SUPPLEMENTARY MATERIALS

Nanohub, Multidielectric Energy Band Diagram Program, COMSOL multiphysics.

APPENDIX

Material properties of Silicon	Value	Unit
Relative permittivity	11.7	1
Electron lifetime, SRH	10[us]	S
Hole lifetime, SRH	10[us]	S
Band gap	1.12[V]	V
Electron affinity	4.05[V]	V
Effective density of states, valence band	(T/300[K]) ^{3/2} *1.04E19[1/cm ³]	1/m ³
Effective density of states, conduction band	(T/300[K]) ^{3/2} *2.8E19[1/cm ³]	1/m ³
Hole mobility	500[cm ² /(V*s)]	m ² /(V*s)
Electron delta coefficient	5.82E14[V/s]	V/s
Hole delta coefficient	2.05E14[V/s]	V/s
Electron mobility reference	4.75E7[cm ² /(V*s)]	m ² /(V*s)
Hole mobility reference	9.93E7[cm ² /(V*s)]	m ² /(V*s)
Electron mobility reference	1.74E5[cm ² /(V*s)]	m ² /(V*s)
Hole mobility reference	8.84E5[cm ² /(V*s)]	m ² /(V*s)
Electron alpha coefficient	0.125	1
Hole alpha coefficient	0.0317	1
Reference temperature	1[K]	K

Electric field reference	1[V/cm]	V/m
Doping concentration reference	1[1/cm ³]	1/m ³

REFERENCES

- [1] Moore, Gordon E. "Cramming More Components onto Integrated Circuits, Reprinted from Electronics, Volume 38, Number 8, April 19, 1965, pp.114 Ff." *IEEE Solid-State Circuits Newsletter* 20.3 (2006): 33–35.
- [2] Forever, Law. "Moore's Law Forever?" *Science* 773.2002 (2003): 3–4.
- [3] Iwai, H. "Roadmap for 22 Nm and beyond (Invited Paper)." *Microelectronic Engineering* 86.7-9 (2009): 1520–1528.
- [4] M. J. Sharifi and A. Adibi. "Semiconductor device simulation by a new method of solving Poisson, Laplace and Schrodinger equations", *International Journal of Engineering (IJE)*, Vol. 13, No. 1, (2000) 89.
- [5] Klaassen, D. B M. "A Unified Mobility Model for Device Simulation-II. Temperature Dependence of Carrier Mobility and Lifetime." *Solid State Electronics* 35.7 (1992): 961–967.
- [6] Pao, H.C., and C.T. Sah. "Effects of Diffusion Current on Characteristics of Metal-Oxide (insulator)-Semiconductor Transistors." *Solid-State Electronics* 9.10 (1966): 927–937.
- [7] Sallese, Jean Michel et al. "Inversion Charge Linearization in MOSFET Modeling and Rigorous Derivation of the EKV Compact Model." *Solid-State Electronics* 47.4 (2003): 677–683.
- [8] Wacker, Nicoleta et al. "Compact Modeling of CMOS Transistors under Variable Uniaxial Stress." *Solid-State Electronics* 57.1 (2011): 52–60.
- [9] Klaassen, D. B M. "A Unified Mobility Model for Device Simulation-I. Model Equations and Concentration Dependence." *Solid State Electronics* 35.7 (1992): 953–959.
- [10] Turin, Valentin O. "A Modified Transferred-Electron High-Field Mobility Model for C60 Devices Simulation." *Solid-State Electronics* 49.10 (2005): 1678–1682.
- [11] Chaudhry, Amit, and Sonu Sangwan. "Modeling of the Effect of Uniaxial Mechanical Strain on Drain Current and Threshold Voltage of an N-Type MOSFET." *Solid-State Electronics* 79 (2013): 133–137.
- [12] Sun, Wookyung, and Hyungsoon Shin. "Optimization of Uniaxial Stress for High Electron Mobility on Biaxially-Strained N-MOSFETs." *Solid-State Electronics* 94 (2014): 23–27.
- [13] Tienda-Luna, I. M. et al. "An Analytical Mobility Model for Square Gate-All-Around MOSFETs." *Solid-State Electronics* 90 (2013): 18–22.
- [14] Canali, C. et al. "Electron and Hole Drift Velocity Measurements in Silicon and Their Empirical Relation to Electric Field and Temperature." *IEEE Transactions on Electron Devices* 22.11 (1975): 1045–1047.
- [15] Lombardi, C. et al. "A Physically Based Mobility Model for Numerical Simulation of Nonplanar Devices." *IEEE Transactions on Computer-Aided Design of Integrated Circuits and Systems* 7.11 (1988): 1164–1171.
- [16] Mannan, M. A., M. S. Anjan, and M. Z. Kabir. "Modeling of Current-Voltage Characteristics of Thin Film Solar Cells." *Solid-State Electronics* 63.1 (2011): 49–54.
- [17] Yu, Lam H., and Douglas Natelson. "The Kondo effect in C60 single-molecule transistors." *Nano Letters* 4, no. 1 (2004): 79-83.
- [18] Anthopoulos, Thomas D., Birendra Singh, Nenad Marjanovic, Niyazi S. Sariciftci, Alberto Moutaigne Ramil, Helmut Sitter, Michael Cölle, and Dago M. de Leeuw. "High performance n-channel organic field-effect transistors and ring oscillators based on C 60 fullerene films." *Applied Physics Letters* 89, no. 21 (2006): 213504.
- [19] Chang, Hsuan-Chun, Chien Lu, Cheng-Liang Liu, and Wen-Chang Chen. "Single-Crystal C60 Needle/CuPc Nanoparticle Double Floating-Gate for Low-Voltage Organic Transistors Based Non-Volatile Memory Devices." *Advanced Materials* 27, no. 1 (2015): 27-33.
- [20] Fishchuk, I. I., Andriy Kadashchuk, S. V. Novikov, Mujeeb Ullah, Jan Genoe, N. S. Sariciftci, Helmut Sitter, and H. Bässler. "Origin of electric field dependence of the charge mobility and spatial energy correlations in C60-based field effect transistors." *Molecular Crystals and Liquid Crystals* 589, no. 1 (2014): 18-28.
- [21] Boubaker, A., B. Hafsi, K. Lmimouni, and A. Kalboussi. "A comparative TCAD simulations of a P-and N-type organic field effect transistors: field-dependent mobility, bulk and interface traps models." *Journal of Materials Science: Materials in Electronics* (2017): 1-10.
- [22] Lörtscher, Emanuel, Victor Geskin, Bernd Gotsmann, Jeppe Fock, Jakob Kryger Sørensen, Thomas Bjørnholm, Jérôme Cornil, Herre SJ van der Zant, and Heike Riel. "Molecular Electronics:

- Bonding and Electronic Transport Properties of Fullerene and Fullerene Derivatives in Break-Junction Geometries (Small 2/2013)." *Small* 9, no. 2 (2013): 332-332.
- [23] Cooling, N. A., E. F. Barnes, F. Almyahi, K. Feron, M. F. Al-Mudhaffer, A. Al-Ahmad, B. Vaughan et al. "A low-cost mixed fullerene acceptor blend for printed electronics." *Journal of Materials Chemistry A* 4, no. 26 (2016): 10274-10281.
- [24] Iñiguez, Benjamin et al. "Universal Compact Model for Long- and Short-Channel Thin-Film Transistors." *Solid-State Electronics* 52.3 (2008): 400-405.
- [25] Wacker, Nicoleta et al. "Compact Modeling of CMOS Transistors under Variable Uniaxial Stress." *Solid-State Electronics* 57.1 (2011): 52-60.
- [26] Ávila-Herrera, F. et al. "Compact Model for Short-Channel Symmetric Double-Gate Junctionless Transistors." *Solid-State Electronics* 111 (2015): 196-203.
- [27] Fell, Andreas et al. "Input Parameters for the Simulation of Silicon Solar Cells in 2014." *IEEE Journal of Photovoltaics* 5.4 (2015): 1250-1263.
- [28] Radziemska, E., and E. Klugmann. "Thermally Affected Parameters of the Current-Voltage Characteristics of Silicon Photocell." *Energy Conversion and Management* 43.14 (2002): 1889-1900.
- [29] Lovelace, D., J. Costa, and N. Camilleri. "Extracting Small-Signal Model Parameters of Silicon MOSFETs." *1994 IEEE MTT-S International Microwave Symposium Digest (Cat. No.94CH3389-4)* (1994): 865-868.
- [30] Vandooren, A. et al. "Impact of Process and Geometrical Parameters on the Electrical Characteristics of Vertical Nanowire Silicon N-TFETs." *Solid-State Electronics* 72 (2012): 82-87.
- [31] Southwick, Richard G., and William B. Knowlton. "Stacked Dual-Oxide MOS Energy Band Diagram Visual Representation Program (IRW Student Paper)." *IEEE Transactions on Device and Materials Reliability*. Vol. 6. N.p., (2006): 136-145.

Low Power and Low Voltage Double Tail Dynamic Latch Comparator using 180nm Technology

Balayan Sapna, Gupta Anshu

Mody University of Science and Technology, Lakshmanagarh, India

Abstract—The requirement for highly integrated and programmable analog-to-digital converters (ADCs), area efficiency, and ultra-low-power and high speed analog-to-digital converters is pushing toward the use of dynamic regenerative comparators to amplify speed and power efficiency. In this paper, analytical expressions are derived and an analysis on the delay of the dynamic comparators will be presented. From the analytical expressions, designers can obtain an instinct about the main contributors to the comparator delay and fully explore the tradeoffs in dynamic comparator design. Based on the analysis made, a new dynamic comparator is proposed, where the circuit of a conventional double tail comparator is modified for fast operation and low-power even in small supply voltages. By adding few transistors, the positive feedback during the regeneration is strengthened, which results in remarkably reduced delay time. Post-layout simulation results in an 180nm CMOS technology confirm the analysis results.

Keywords— *Double-tail comparator, dynamic clocked comparator, high-speed analog-to-digital converters (ADCs), low-power analog design.*

I. INTRODUCTION

ANALOG-TO-DIGITAL converters (ADCs) are being continuously driving towards their performance limits as technology scales down and system specifications become more challenging. Comparator is one of the basic fundamental building blocks in most analog-to-digital converters (ADCs). Many high speed ADCs, such as flash ADCs, require low power, maximum-speed comparators with compact chip area. High-speed comparators in ultra-deep sub-micrometer (UDSM) CMOS technologies tolerate low supply voltages especially when considering that the threshold voltages of the devices have not mount at the same rate as the supply voltages of the modern CMOS operation [1]. Hence, design of high-speed comparators is more challenging when the provided supply voltage is

smaller. In other words, in a given technology, to achieve high speed, large numbers of transistors are required to compensate the reduction of supply voltage, which also means that more chip area and power is needed. Besides, low-supply-voltage operation results in limited common-mode input range, which is important for many high-speed ADC architectures, such as flash ADCs. Many techniques, such as techniques employing body-driven transistors [2], [3], current-mode design [4], supply boosting methods [5],[6] and those using dual-oxide processes, which can handle higher supply voltages have been developed to undergo the low-voltage design challenges. Bootstrapping and boosting are two techniques based on raising the supply, reference, or clock voltage to mark input-range and switching problems. These techniques are effective, but they introduce reliability barriers especially in UDSM CMOS technologies. Despite the advantages, the body-driven transistor tolerate smaller trans-conductance (equal to g_{mb} of the transistor) compared to its gate-driven equivalent while particular fabrication process, such as deep n-well is needed to have both nMOS and pMOS transistors operate in the body-driven layout. Apart from technological modifications, developing new circuit structures which avoid stacking too many transistors between the supply voltages is preferable for low-voltage operation, especially if they do not expand the circuit complication. Body-driven technique embrace by Blalock [2], removes the threshold voltage necessity such that body-driven MOSFET operates as a depletion-type device. Based on this approach, in [3], a 1-bit quantizer for sub-1V $\Sigma\Delta$ modulator is proposed. In [7]–[9], additional circuit is added to the conventional dynamic comparator to enhance the speed of a comparator when provided with low supply voltages. The proposed comparator of [7] works down with a provided supply voltage of 0.5 V with a maximum provided clock frequency of 600 MHz and consumes 18 μ W. Despite the advantages of this approach, the effect of component mismatch in the additional circuit on the performance of the comparator

should be examined. The structure of double-tail dynamic comparator first proposed in [10] is based on designing a separate input and cross-coupled stage. This separation allows fast operation over a wide common-mode and supply voltage range [10]. In this paper, an inclusive analysis about the delay of dynamic comparators has been made for various architectures. Furthermore, based on the double-tail circuitry proposed in [10], a new dynamic comparator is presented, which does not need boosted voltage or stacking of too many transistors. Simply by adding a few minimum-size transistors to the conventional double-tail dynamic comparator, latch delay time is profoundly minimized. This moderation also results in significant power savings when compared to the conventional dynamic comparator and double-tail comparator. The rest of this paper is categorized as follows. Section II explores the operation of the conventional clocked regenerative comparators and the pros and cons of each structure are discussed. Delay review is also presented and the analytical expressions for the delay of the comparators are obtained. The proposed comparator is presented in Section III. Section IV discusses the design issues. Simulation results are shown in Section V, followed by conclusions in Section VI.

II. CLOCKED REGENERATIVE COMPARATORS

The Clocked regenerative comparators have found vast applications in many high-speed ADCs since they can frame quick decisions due to the extreme positive feedback in the regenerative latch. Latterly, many comprehensive analyses have been presented, which explore the performance of these comparators from different aspects, such as offset [12], [13], and [14], noise [11], kick-back noise [16] and random decision errors [15]. In this section, a complete delay analysis is presented, the delay time of two common structures, i.e. Conventional dynamic double-tail comparator and conventional dynamic comparator are examined, based on which the proposed comparator will be presented.

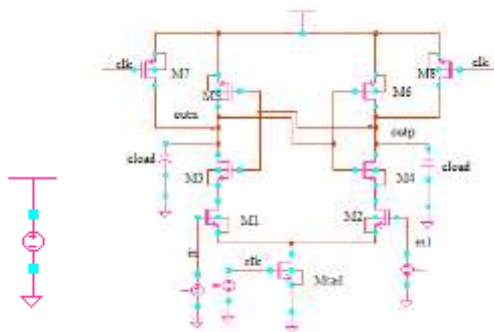


Fig.1: Schematic diagram of the conventional dynamic comparator

A. Conventional Dynamic Comparator

The schematic diagram of the conventional dynamic comparator generally used in A/D converters, with high input impedance, no static power consumption and rail-to-rail output swing, is shown in Fig.1 [1], [17]. A differential amplifier is consisting of pMOS and nMOS transistor (*M3, M4, M5, M6*) with combination of current mirror consisting of nMOS transistor (*M1, M2*), transistor *M7* and *M8* are used in the circuitry parallel to the differential amplifier. Two input voltages are used *INN, INP* provided to transistors *M1* and *M2* respectively. The operation of the comparator is as follows:-

During the reset phase i.e. when $CLK = 0$ then the nMOS transistor *Mtail* is *OFF*, because when provided input logic level is low it turns off the nMOS, which reset pMOS transistors (*M7–M8*) pull both output nodes *Outn* and *Outp* to *VDD* to define a start state and to have a valid logical level during reset. In the comparison phase i.e. when $CLK = VDD$, pMOS transistors *M7* and *M8* are *OFF*, and *Mtail* is *ON*, because when provided input logic level is high it turns on the nMOS. Output voltages (*Outp, Outn*), which had been pre-charged to *VDD*, start to discharge with different discharging rates based on the corresponding input voltage (*INN/INP*). Assuming the case where $VINP > VINN$, *Outp* discharges faster than compare to *Outn*, hence when *Outp* (discharged by the nMOS transistor *M2* drain current), falls down to $VDD - |V_{thp}|$ before the node *Outn* (discharged by transistor *M1* drain current), the corresponding pMOS transistor (*M5*) will turn *ON* actuate the latch regeneration caused by back-to-back inverters (*M3, M5* and *M4, M6*). Thus, *Outn* is pulled upto *VDD* and *Outp* discharges to ground. Case, if $VINP < VINN$, then the circuits works vice versa.

The delay of this comparator is comprised of two time delays, i.e. t_0 and t_{latch} . Where, the delay t_0 of the comparator represents the capacitive discharge of the load capacitance C_{load} till the first p-channel transistor i.e. either *M5* or *M6* turns *ON*. In case, the voltage at the node *INP* is greater than the voltage at node *INN* (i.e., $VINP > VINN$), the drain current of the nMOS transistor *M2* (I_2) causes faster discharge of *Outp* node as compared to the *Outn* node, which is driven by transistor *M1* with smaller current. Hence, the discharge delay (t_0) is given by

$$t_0 = C_{load} \frac{|V_{thp}|}{I_2} \cong 2C_{load} \frac{|V_{thp}|}{I_{tail}} \tag{1}$$

In (1), since $I_2 = \frac{I_{tail}}{2} + \Delta I_{in} = \frac{I_{tail}}{2} + g_{m1,2} \Delta V_{in}$, for a small differential input (V_{in}), I_2 can be approx. to be persistent and is equal to the half of the tail current. Whereas, t_{latch} , is the latching delay of two cross-coupled inverters, it is assumed that a voltage swing of $\Delta V_{out} = \frac{V_{DD}}{2}$ has to be obtained from an initial output voltage difference V_0 at the falling output. Half of the supply voltage is considered to be the threshold voltage of the comparator following inverter or the SR latch. Hence, the latch delay time is given by,

$$t_{latch} = \frac{C_{load}}{g_{m,eff}} \ln\left(\frac{\Delta V_{out}}{\Delta V_0}\right) = \frac{C_{load}}{g_{m,eff}} \ln\left(\frac{V_{DD}/2}{\Delta V_0}\right) \quad (2)$$

Whereas, $g_{m,eff}$ is the effective trans-conductance of the back-to-back inverters. In fact, this delay determined, in a logarithmic way, at the beginning of the regeneration on the initial output voltage difference (i.e., when $t=t_0$). Based on (1), V_0 can be calculated from (3)

$$\begin{aligned} \Delta V_0 &= |V_{outp}(t=t_0) - V_{outm}(t=t_0)| \\ &= |V_{thp} - \frac{I_2 t_0}{C_{load}}| = |V_{thp} - \left(1 - \frac{I_2}{I_1}\right)| \end{aligned} \quad (3)$$

The current difference, $\Delta I_{in} = |I_1 - I_2|$ between the branches is much smaller than the current I_1 and I_2 . Thus, I_1 can be approximated by $\frac{I_{tail}}{2}$ and (3) can be rewritten as

$$\begin{aligned} \Delta V_0 &= |V_{thp} - \frac{\Delta I_{in}}{I_1}| \approx 2 |V_{thp} - \frac{\Delta I_{in}}{I_{tail}}| \\ &= 2 |V_{thp} - \frac{\sqrt{\beta_{1,2}} I_{tail}}{I_{tail}} \Delta V_{in}| \\ &= 2 |V_{thp} - \frac{\sqrt{\beta_{1,2}}}{I_{tail}} \Delta V_{in}| \end{aligned} \quad (4)$$

In the above equation, $\beta_{1,2}$ is the input transistor's current factor and I_{tail} is the function of input common-mode voltage (V_{cm}) and V_{DD} . Substituting V_0 in latch delay expression and considering t_0 , the equation for the delay of the conventional dynamic comparator is obtained as

$$\begin{aligned} t_{delay} &= t_0 + t_{latch} \\ &= C_{load} \frac{|V_{thp}|}{I_2} + \frac{C_{load}}{g_{m,eff}} \cdot \ln\left(\frac{\Delta V_{out}}{\Delta V_0}\right) \\ &= 2C_{load} \frac{|V_{thp}|}{I_2} + \frac{C_{load}}{g_{m,eff}} \cdot \ln\left(\frac{\Delta V_{DD}/2}{\Delta V_0}\right) \\ &= 2C_{load} \frac{|V_{thp}|}{I_{tail}} + \frac{C_{load}}{g_{m,eff}} \cdot \ln\left(\frac{V_{DD}}{4|V_{thp}| \Delta V_{in}} \sqrt{\frac{I_{tail}}{\beta_{1,2}}}\right) \end{aligned} \quad (5)$$

Equation (5) elaborates the impact of various parameters. The overall delay is inversely proportional to the input difference voltage (V_{in}) and directly proportional to the comparator load capacitance C_{load} . Besides, the delay depends in-directly on the input common-mode voltage (V_{cm}). By reducing V_{cm} , the delay t_0 of the first phase

increases because lower V_{cm} causes smaller bias current i.e. (I_{tail}). Whereas, (4) shows that a delayed discharge with smaller I_{tail} results in an increased initial voltage difference (V_0), reducing t_{latch} . Simulation output show that the effect of minimizing the V_{cm} on increasing of t_0 and reducing of t_{latch} will finally lead to an increase in the overall delay. In it has been shown that the input common-mode voltage is 70% of the supply voltage is optimal regarding speed and yield.

In principle, this design has the advantage of high no static power consumption, input impedance, rail-to-rail output swing, and good strength against noise and mismatch. Due to the factor that parasitic capacitances of input transistors do not instantly affect the switching speed of the nodes at the output, it is possible to design large input transistors to minimize the offset. Whereas, the disadvantage is the fact that due to several stacked transistors, a tolerably high supply voltage is needed for a proper delay time. The reason is that, at the beginning of the conclusion, only transistors $M3$ and $M4$ of the latch contribute to the positive feedback until the voltage level of one output node has fall below a level small enough to turn "ON" transistors $M5$ or $M6$ to initiate complete regeneration. At a low supply voltage, this voltage drop only give a small gate-source voltage for transistors $M3$ and $M4$, where the gate to source voltage of $M5$ and $M6$ is also very small, thus, the delay time of the latch becomes large due to lower trans-conductance. Another important drawback of this design is that there is only one current way, via tail transistor $Mtail$, which defines the current for the latch (the cross-coupled inverters) and for both the differential amplifier. While a small tail current is required to keep the differential pair in weak inversion interval and a better g_m/I ratio, a large tail current would be needed to enable fast regeneration in the latch. Besides, as far as $Mtail$ conduct mostly in triode region, the tail current depends on the input common-mode voltage, which is not advantageous for regeneration.

B. Conventional Double-Tail Dynamic Comparator

A conventional double-tail comparator is shown in the below figure. This topography has less stacking and therefore it can operate at low supply voltages compared to the conventional dynamic comparator. The double tail allow both a large current in the latching stage and wider $Mtail2$, for fast latching unconventional of the input common-mode voltage (V_{cm}), and a small current in the input level (small $Mtail1$), for low offset. The operation of this comparator is as follows. During reset phase clock ($CLK = 0$, so transistor $Mtail1$, and $Mtail2$ are OFF), transistors $M3$ - $M4$ pre-charge

the fn and fp nodes to VDD , which in turn causes transistors MR_1 and MR_2 to discharge the output nodes to ground. During decision-making phase i.e. when ($CLK = VDD$, then transistors $Mtail1$ and $Mtail2$ turn ON), transistors $M3$ - $M4$ turn OFF and voltages at nodes fn and fp start to drop with the rate defined by $IM_{tail1} / C_{fn(p)}$ and on top of this, an input-dependent differential voltage $V_{fn(p)}$ will build up.

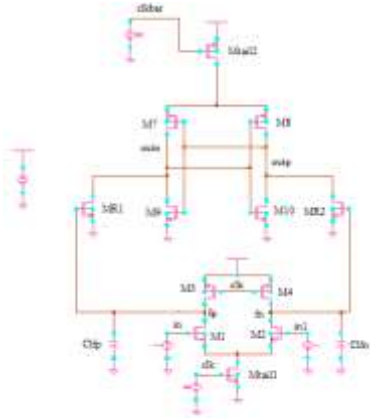


Fig.2: Schematic diagram of the conventional double-tail dynamic latch comparator

Same to the conventional dynamic comparator, the delay of this comparator comprises two main parts, t_0 and t_{latch} . The delay t_0 represents the capacitive charging of the load capacitance $C_{loadout}$ (at the latch stage output nodes, $Outn$ and $Outp$) until the first n-channel transistor ($M9/M10$) turns ON , after which the latch regeneration starts, thus t_0 is obtained from

$$t_0 = \frac{V_{THN} C_{Loadout}}{I_{B1}} \approx 2 \frac{V_{THN} C_{Loadout}}{I_{tail2}} \quad (6)$$

Where I_{B1} is the drain current of the transistor $M9$ (assuming $V_{INP} > V_{INN}$) and is equal to approx. of the half of the tail current (I_{tail2}). After the first n-channel transistor of the latch turns on (for the instance, M_9), the corresponding output (e.g., $Outn$) will be discharged to the ground, leading front p-channel transistor to turn on, charging another output ($Outp$) to the supply voltage (VDD). The regeneration time (t_{latch}) is reached according to equation (2). For the initial output voltage difference at time t_0 , V_0 we have

$$\begin{aligned} \Delta V_0 &= |V_{outp}(t=t_0) - V_{outn}(t=t_0)| = V_{THN} - \frac{I_{B2} t_0}{C_{loadout}} \\ &= V_{THN} \left(1 - \frac{I_{B2}}{I_{B1}}\right) \quad (7) \end{aligned}$$

Where I_{B2} and I_{B1} are the currents of the left latch and right side branches of the second stage, respectively

Considering $I_{latch} = |IB1 - IB2| = gm R1, 2V_{fn}/fp$, (7) can be rewritten as

$$\Delta V_0 = V_{THN} \frac{I_{latch}}{I_{B1}} \approx 2V_{THN} \frac{I_{latch}}{I_{tail2}} = 2V_{THN} \frac{g_{mR_{1,2}}}{I_{tail2}} \Delta V_{fn} / f_p \quad (8)$$

Where $gmR_{1,2}$ is the trans-conductance of the intermediate stage transistors (MR_1 and MR_2) and V_{fn}/fp is the difference in voltage at the first stage outputs (fn and fp) at time t_0 . Thus, it can be observed that two main parameters which influence the initial output differential voltage (V_0) and therefore the latch regeneration time is the trans-conductance of the intermediate stage transistors ($gmR_{1,2}$) and the voltage difference of the first stage outputs (fn and fp) at time t_0 . In fact, intermediate stage transistors amplify the voltage difference of V_{fn}/fp causing the latch to be disparity. The differential voltage at nodes fn/fp (V_{fn}/fp) at time t_0 can be achieved from

$$\begin{aligned} \Delta V_{fn/fp} &= |V_{fn}(t=t_0) - V_{fp}(t=t_0)| \\ &= t_0 \cdot \frac{I_{N1} - I_{N2}}{C_{Load,fn(p)}} \\ &= t_0 \cdot \frac{g_{m1,2} \Delta V_{in}}{C_{Load,fn(p)}} \quad (9) \end{aligned}$$

In the above equation, I_{N1} and I_{N2} refer to the discharging currents of input transistors ($M1$ and $M2$), which are dependent on the input difference voltage (i.e., $IN = gmI, 2Vin$). Substituting (9) in (8), V_0 will be

$$\begin{aligned} \Delta V_0 &= 2V_{Thn} \frac{g_{mR_{1,2}}}{I_{tail2}} \Delta V_{fn/fp} \\ &= \left(\frac{2V_{THN}}{I_{tail2}}\right)^2 \left[\frac{C_{loadout}}{C_{load,fn(p)}}\right] g_{mR_{1,2}} g_{m1,2} \Delta V_{in} \quad (10) \end{aligned}$$

This equation shows that V_0 depends strongly on the trans-conductance of input and intermediate stage transistors, input voltage difference (V_{in}), the capacitive ratio of $C_{Loadout}$ to $C_{Load,fn(p)}$ and latch tail current.

Some important notes can be concluded.

- 1) The difference in voltage at the first stage outputs (V_{fn}/fp) at time t_0 has a great effect on latch initial differential output voltage (V_0) and consequently on the latch delay. Therefore, increasing it would greatly reduce the delay of the comparator.
- 2) In this comparator, both intermediate stage and transistors will be finally cut-off, (since fn and fp nodes both discharge to the ground), hence they do not play any important role in improving the effective trans-conductance of the latch. Besides, during reset phase, these nodes have to be charged from ground to VDD , which means power utilized.

III. PROPOSED DOUBLE-TAIL DYNAMIC COMPARATOR

Fig.3 indicates the schematic diagram of the proposed dynamic double-tail comparator. Because of the better performance of double-tail architecture in low-voltage applications, the proposed comparator design is based on the double-tail structure. The main objective of the proposed comparator is to increase $V_{fn/fp}$ in order to increase the latch regeneration speed. For this the, two control transistors (M_{c1} and M_{c2}) have been added to the first stage of proposed idea in parallel to $M3/M4$ transistors but in a cross-coupled manner.

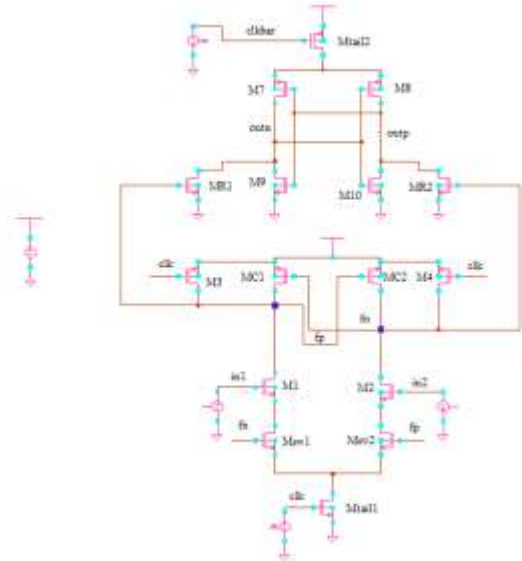


Fig.3: Schematic diagram of the proposed dynamic comparator

A. Operation of the Proposed Comparator

The operation of proposed comparator is as follows. During reset phase i.e., when ($CLK = 0$) transistor M_{tail1} and M_{tail2} are OFF (avoiding static power), transistor $M3$ and $M4$ pulls both nodes fn and fp to VDD , hence transistor M_{c1} and M_{c2} are in cut off region. Intermediate stage transistors i.e., M_{R1} and M_{R2} , reset both latch outputs to ground. During decision-making phase i.e., when ($CLK = VDD$) transistor M_{tail1} , and M_{tail2} are ON, transistors $M3$ and $M4$ turn OFF. Further, at the beginning of this phase, the control transistors are OFF (and transistor fn and fp are charged to VDD). Thus, transistor fn and fp start to drop with different rates according to the provided input voltages. Suppose $V_{INP} > V_{INN}$, then fn drops faster than fp , (because $M2$ provides more current than $M1$). Since fn continues to fall, the corresponding pMOS control transistor (M_{c1} in this case) starts to turn ON, pulling other node fp back to the VDD ; so another control transistor (M_{c2}) remains OFF, allowing fn to be discharged completely.

Whereas, unlike conventional double-tail dynamic comparator, in which $V_{fn/fp}$ is just a function of input voltage difference and input transistor trans-conductance, in the proposed architecture as soon as the comparator detects that for instance fn node discharges faster, a pMOS transistor (M_{c1}) turns on, pulling the node fp back to the VDD . Hence, by the time passing, the difference between fn and fp ($V_{fn/fp}$) increases in an exponential manner, leading to the reduction of latch regeneration time. In spite the effectiveness of the proposed architecture, one of the points which should be considered is that in this circuit, when one control transistor (e.g., M_{c1}) turns ON, input and tail transistor (e.g., M_{c1} , $M1$, and M_{tail1}) draw current from VDD to the ground, resulting in static power consumption. To overcome the issue of static power consumption, two nMOS switches [M_{sw1} and M_{sw2}] are used below the input transistors.

At the beginning of the decision making phase, due to the fact that both nodes fn and fp have been pre-charged to VDD (during the reset phase), both switches i.e., M_{sw1} and M_{sw2} are closed and fn and fp start to drop with different discharging rates. As soon as the comparator finds that one of the node fn/fp is discharging faster, control transistors will act to increase their voltage difference. Suppose that node fp is pulling up to the VDD and node fn should be discharged completely, hence the switch in the charging path of fp will be opened (in order to prevent any current drawn from VDD) but the other switch connected to node fn will be closed to allow the complete discharge of fn node. That is the operation of the control transistors with the switches follows the operation of the latch.

B. Delay Analysis

In order to theoretically signify how the delay is reduced, delay equations are derived for this structure the proposed dynamic comparator maximizes the speed of the double-tail comparator by affecting two important factors., first, it rise the initial output voltage difference ($V0$) at the beginning of the regeneration ($t = t0$); and second, it enhances the effective trans-conductance (g_{meff}) of the latch.

- 1) *Effect of Enhancing $V0$* : Time after which latch regeneration starts is $t0$, we can say $t0$ is considered to be the time it takes (while both latch outputs are rising with different rates) until the first nMOS transistor of the cascaded inverters turns on, so that it will pull down one of the outputs and regeneration will commence.

$$\begin{aligned} \Delta V_0 &= V_{Thn} \frac{\Delta I_{latch}}{I_{B1}} \\ &\approx 2V_{Thn} \frac{\Delta I_{latch}}{I_{tail2}} \\ &= 2V_{Thn} \frac{g_{mR1,2}}{I_{tail2}} \Delta V_{fn/fp} \end{aligned} \quad (11)$$

To find $V_{fn/fp}$ at $t = t_0$, it is important to notice that the combination of the control transistors ($Mc1$ and $Mc2$) with two serial switches ($Msw1$, $Msw2$) follow the operation of a cascaded inverter pair; $V_{fn/fp}$ is calculated by

$$V_{fn/fp} = V_{fn(p)0} \exp((A_v - 1) t/\tau) \quad (12)$$

Where in the equation, $\tau \equiv \frac{C_{L,fn(p)}}{A_v - 1} \frac{1}{g_{m,eff}}$ and $\Delta V_{fn(p)0}$ is the initial fn/fp difference node voltage corresponding pMOS control transistor in turned ON. Hence, $\Delta V_{fn(p)0}$ can be obtained from-

$$\Delta V_{fn(p)0} = 2 \left| V_{Thp} \right| \frac{g_{m1,2} \Delta V_{in}}{I_{tail1}} \quad (13)$$

Substituting (12) in (13), V_0 will be

$$\begin{aligned} \Delta V &= 2V_{Thn} \frac{g_{m1,2}}{I_{tail2}} \Delta V_{fn/fp} \\ &= 4V_{Thn} \left| V_{Thp} \right| \frac{g_{mR1,2}}{I_{tail2}} \frac{g_{m1,2} \Delta V_{in}}{I_{tail1}} \exp\left(\frac{G_{m,eff} t_0}{C_{L,fn(p)}}\right) \end{aligned} \quad (14)$$

Comparing (14) with (10), it is observed that V_0 has been increased remarkably (in an exponential manner) in compare with the conventional dynamic comparator.

2) Effect of Enhancing Latch Effective Trans-conductance:

In conventional double-tail comparator, both the nodes fn and fp finally discharge's completely. In the proposed comparator, one of the first stage output (fn/fp) nodes will charge up to the VDD at the beginning of the decision making phase, and will turn ON one of the intermediate stage transistors, thus the effective trans-conductance of the latch is maximized. That is positive feedback is strengthened. Hence, t_{latch} will be

$$\begin{aligned} t_{latch} &= \frac{C_{Lout}}{g_{m,eff} + g_{mR1,2}} \cdot \ln\left(\frac{\Delta V_{out}}{\Delta V_0}\right) \\ &= \frac{C_{Lout}}{g_{m,eff} + g_{mR1,2}} \cdot \ln\left(\frac{VDD/2}{\Delta V_0}\right) \end{aligned} \quad (15)$$

Finally, including both the effects-

$$\begin{aligned} t_{delay} &= t_0 + t_{latch} \\ &= 2 \frac{V_{Thn} C_{Lout}}{I_{tail2}} + \frac{C_{Lout}}{g_{m,eff} + g_{mR1,2}} \cdot \ln\left(\frac{VDD/2}{\Delta V_0}\right) \\ &= 2 \frac{V_{Thn} C_{Lout}}{I_{tail2}} + \frac{C_{Lout}}{g_{m,eff} + g_{mR1,2}} \cdot \ln\left(\frac{VDD/2}{4V_{Thn} \left| V_{Thp} \right| \frac{g_{mR1,2}}{I_{tail2}} \frac{g_{m1,2} \Delta V_{in}}{I_{tail1}} \exp\left(\frac{G_{m,eff} t_0}{C_{L,fn(p)}}\right)}\right) \end{aligned} \quad (16)$$

By comparing the expressions it can be seen that the proposed comparator takes gain of an inner positive feedback in double-tail operation, which strengthen the latch regeneration. This speed improvement is even clearer in lower supply voltages. This is due to the fact that for larger values of V_{Th}/VDD , the trans-conductance of the transistors minimizes, thus the existence of an inner positive feedback in the structure of the first stage will lead to the comparator's improved performance.

3) Reducing the Energy per Comparison: In the modified proposed comparator, the energy per conversion is reduced as well delay parameter is also improved. As discussed earlier, in conventional double-tail topology, both nodes fn and fp discharge to the ground during the period of decision making and each time during the reset phase they should be pulled up back to the VDD . However, in proposed comparator, only one of the nodes (fn/fp) has to be charged during the reset phase. This is because during the previous decision making phase, based on the status of control transistors, one of the nodes had not been discharged and thus less power is required.

IV. DESIGN CONSIDERATIONS

While determining the size of tail transistors i.e., ($Mtail1$ and $Mtail2$), it is necessary to ensure that the time it takes that one of the control transistors turns on must be smaller than t_0 . This condition can be achieved by properly designing the first and second stage tail currents.

$$\begin{aligned} t_{on,Mc1(2)} &< t_0 < \frac{\left| V_{Thp} \right| \cdot C_{L,fn(p)}}{I_{n1,2}} < \frac{V_{Thn} C_{Lout}}{I_{B1}} \\ &< \frac{\left| V_{Thp} \right| \cdot C_{L,fn(p)}}{I_{tail1}} < \frac{V_{Thn} C_{Lout}}{I_{tail2}} \end{aligned} \quad (17)$$

In designing the nMOS switches, the drain-source voltage of these switches must be considered since it might limit the voltage headroom, restricting the advantage of being used in low-voltage applications. In order to reduce this effect, low-on-resistance nMOS switches are required. In other words, large transistors can be used. Since the parasitic capacitances of these switches do not affect the parasitic capacitances of the nodes *fn*/*fp*, it is possible to select the size of the nMOS switch transistors in a way that both low-voltage and low-power operations are maintained.

A. Mismatch Analysis

In principle, the situation where input differential voltage (*V_{in}*) is very small where *fn* and *fp* have approximately similar discharging rates except this, the effect of current factor mismatch and threshold voltage mismatch of controlling transistors is almost negligible in most cases. The differential input signal is already amplified to large amplitude compared to the mismatches by the time that the controlling transistor (*Mc1* or *MC2*) turns ON. In other words, offset due to the controlling transistor mismatches is divided by the gain from the input to the output. However, in case of small *V_{in}*, when nodes *fn* and *fp* follow each other tightly, the mismatch of the controlling transistors might influence the result of the comparison. Hence, the following brief analyzes the effect of current and threshold factor mismatches of controlling transistors on the total input-referred offset voltage.

1) *Effect of Threshold Voltage Mismatch of transistor MC1, MC2, i.e., V_{ThC1, 2}*: Due to the threshold voltage mismatch the differential current can be obtained from

$$i_{diff} = g_{mc1,2} \Delta V_{Thc1,2} \tag{18}$$

Where, *g_{mc1, 2}* is the trans-conductance of the controlling transistors. So, the input-referred offset voltage due to the *Mc1, 2* threshold voltage mismatch is obtained as follows:

$$\Delta V_{eq, due \Delta V_{Thc1,2}} = \frac{g_{mc1,2} \Delta V_{Thc1,2}}{g_{m1,2}}$$

$$= \frac{\mu_p W_{C1,2} V_{ODC1,2}}{\mu_n W_{1,2} V_{OD1,2}} \Delta V_{Thc1,2} \tag{19}$$

2) *Effect of Current-Factor Mismatch MC1, MC2, i.e. ΔβC1,2*: In order to find the input-referred offset due to the

current factor mismatch of *MC1,2*, *ΔβC1,2* is modeled as a channel width mismatch *ΔW*, i.e., *Δβ/β = ΔW/W*.

$$i_{diff} = \frac{1}{2} \mu_p C_{ox} \frac{\Delta W}{L} (V_{gsc1,2} - V_{thc1,2})^2 \tag{20}$$

B. Kickback Noise

Principally in latched comparators, on the regeneration nodes the large voltage variations are coupled, through the parasitic capacitances of the transistors, to the input of the comparator. Since the circuit introduce it does not have zero output impedance, the input voltage is disturbed, due to which there may be degradation in accuracy of the converter. This disturbance is usually called “kickback noise.” However it improves the double-tail topology in terms of energy per comparison and thus operation speed, the kickback noise is increased in comparison to conventional double-tail structure.

V. SIMULATION RESULTS

To compare the proposed comparator with the conventional and double-tail dynamic comparators, all three circuits have been simulated in a 0.18-μm CMOS technology with power supply *VDD = 1.2 V*. The comparators were optimized and the transistor dimensions were scaled.

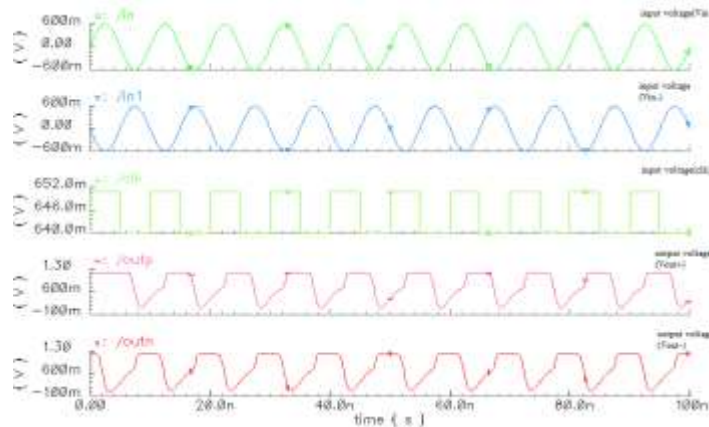


Fig.4: Transient analysis of Conventional Dynamic Latch Comparator

Table.I: result of conventional dynamic latch comparator

Design parameters	Comparator Value
Technology	180nm
Supply voltage	1.2 V
Slew rate+	265.498 M V/ns
Slew rate-	706.615M V/ns
Rise time	4ns
Fall time	2ns
Hold time	3ns
Delay	5ns
Power dissipation	93.49μw

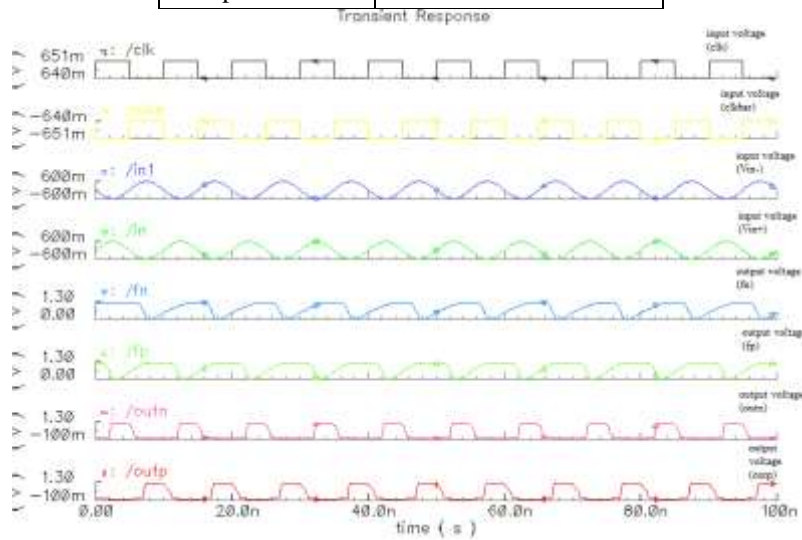


Fig.5 Transient analysis of Conventional Double Tail Dynamic Latch Comparator

Table.II: result of conventional double tail dynamic latch comparator

Design parameters	Comparator Value
Technology	180nm
Supply voltage	1.2 V
Slew rate+	2.84G/ns
Slew rate-	1G/ns
Rise time	1.6ns
Fall time	2ns
Hold time	4ns
Delay	4ns
Power dissipation	25.25uw

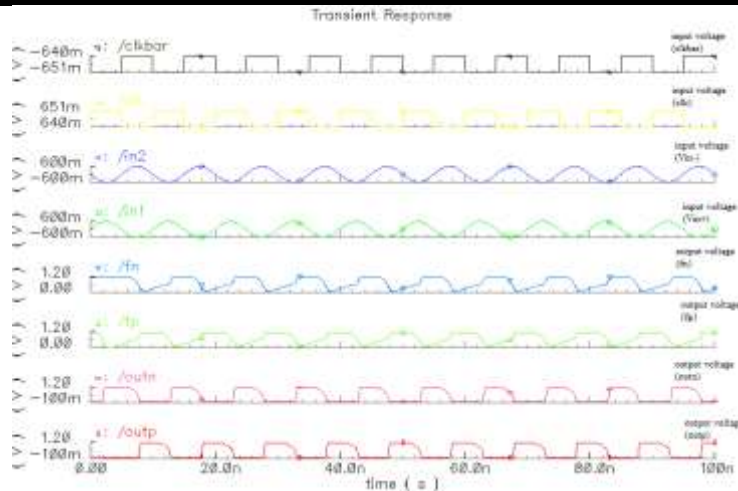


Fig.6: Transient analysis of proposed Comparator

Table.III.:Result of proposed comparator

Design parameters	Comparator Value
Technology	180nm
Supply voltage	1.2 V
Slew rate+	3.02006G
Slew rate-	577.531M
Rise time	0.5ns
Fall time	1ns
Hold time	3ns
Delay	2ns
Power dissipation	22.4456μw

VI. CONCLUSION

In this paper, a comprehensive delay analysis for clocked dynamic comparators is presented and expressions were derived. Two common structures conventional double-tail dynamic comparator and of conventional dynamic comparators were analyzed. Also, based on theoretical analyses, a new dynamic comparator with low-voltage low-power capability was proposed in order to improve the performance of the comparator. Post-layout simulation of the circuit results in 0.18-μm CMOS technology confirmed that the energy per conversion and delay of the proposed comparator is reduced to a great extent in comparison with the double-tail comparator and conventional dynamic comparator.

REFERENCES

[1] B. Goll and H. Zimmermann, "A comparator with reduced delay time in 65-nm CMOS for supply

voltages down to 0.65," *IEEE Trans. Circuits Syst. II, Exp. Briefs*, vol. 56, no. 11, pp. 810–814, Nov. 2009.

[2] B. J. Blalock, "Body-driving as a Low-Voltage Analog Design Technique for CMOS technology," in *Proc. IEEE Southwest Symp. Mixed-Signal Design*, Feb. 2000, pp. 113–118.

[3] M. Maymandi-Nejad and M. Sachdev, "1-bit quantiser with rail to rail input range for sub-1V modulators," *IEEE Electron. Lett.*, vol. 39, no. 12, pp. 894–895, Jan. 2003.

[4] Y. Okaniwa, H. Tamura, M. Kibune, D. Yamazaki, T.-S. Cheung, J. Ogawa, N. Tzartzanis, W. W. Walker, and T. Kuroda, "A 40Gb/s CMOS clocked comparator with bandwidth modulation technique," *IEEE J. Solid-State Circuits*, vol. 40, no. 8, pp. 1680–1687, Aug. 2005.

[5] S. U. Ay, "A sub-1 volt 10-bit supply boosted SAR ADC design in standard CMOS," *Int. J. Analog Integr. Circuits Signal Process.*, vol. 66, no. 2, pp. 213–221, Feb. 2011.

[6] A. Mesgarani, M. N. Alam, F. Z. Nelson, and S. U. Ay, "Supply boosting technique for designing very low-voltage mixed-signal circuits in standard CMOS," in *Proc. IEEE Int. Midwest Symp. Circuits Syst. Dig. Tech. Papers*, Aug. 2010, pp. 893–896.

[7] B. Goll and H. Zimmermann, "A 0.12 μm CMOS comparator requiring 0.5V at 600MHz and 1.5V at 6 GHz," in *Proc. IEEE Int. Solid-State Circuits Conf., Dig. Tech. Papers*, Feb. 2007, pp. 316–317.

[8] B. Goll and H. Zimmermann, "A 65nm CMOS comparator with modified latch to achieve 7GHz/1.3mW at 1.2V and 700MHz/47μW at 0.6V," in *Proc. IEEE Int. Solid-State Circuits Conf. Dig. Tech. Papers*, Feb. 2009, pp. 328–329.

- [9] B. Goll and H. Zimmermann, "Low-power 600MHz comparator for 0.5 V supply voltage in 0.12 μm CMOS," *IEEE Electron Lett*, vol. 43, no. 7, pp. 388–390, Mar. 2007.
- [10] D. Shinkel, E. Mensink, E. Klumperink, E. van Tuijl, and B. Nauta, "A double-tail latch-type voltage sense amplifier with 18ps Setup+Hold time," in *Proc. IEEE Int. Solid-State Circuits Conf., Dig. Tech. Papers*, Feb. 2007, pp. 314–315.
- [11] A. Nikoozadeh and B. Murmann, "An analysis of latched comparator offset due to load capacitor mismatch," *IEEE Trans. Circuits Syst. II, Exp. Briefs*, vol. 53, no. 12, pp. 1398–1402, Dec. 2006.
- [12] S. Babayan-Mashhadi and R. Lotfi, "An offset cancellation technique for comparators using body-voltage trimming," *Int. J. Analog Integr. Circuits Signal Process*, vol. 73, no. 3, pp. 673–682, Dec. 2012.
- [13] J. He, S. Zhan, D. Chen, and R. J. Geiger, "Analyses of static and dynamic random offset voltages in dynamic comparators," *IEEE Trans. Circuits Syst. I, Reg. Papers*, vol. 56, no. 5, pp. 911–919, May 2009.
- [14] P. Nuzzo, F. D. Bernardinis, P. Terreni, and G. Van der Plas, "Noise analysis of regenerative comparators for reconfigurable ADC architectures," *IEEE Trans. Circuits Syst. I, Reg. Papers*, vol. 55, no. 6, pp. 1441–1454, Jul. 2008.
- [15] P. M. Figueiredo and J. C. Vital, "Kickback noise reduction technique for CMOS latched comparators," *IEEE Trans. Circuits Syst. II, Exp. Briefs*, vol. 53, no. 7, pp. 541–545, Jul. 2006.
- [16] J. Kim, B. S. Leibowitz, J. Ren, and C. J. Madden, "Simulation and analysis of random decision errors in clocked comparators," *IEEE Trans. Circuits Syst. I, Reg. Papers*, vol. 56, no. 8, pp. 1844–1857, Aug. 2009.
- [17] B. Wicht, T. Nirschl, and D. Schmitt-Landsiedel, "Yield and speed optimization of a latch-type voltage sense amplifier," *IEEE J. Solid-State Circuits*, vol. 39, no. 7, pp. 1148–1158, Jul. 2004.

Enhancement of Analytical OBR (Out of Band Radiation) and BER Calculation for Digital Audio-Video Broadcasting in Companded OFDM System using Non-Symmetric QAM/QPSK Techniques

Santosh, Prof. Piyush Vyas, Prof. K. K. Arora

M. Tech. Scholar, Dept. of ECE Engg., J.I.E.T., Jodhpur, Rajasthan, India

Associate Professor, Dept. of ECE Engg., J.I.E.T., Jodhpur, Rajasthan, India

Associate Professor, HOD M.Tech. (DC), Dept. of ECE Engg., J.I.E.T., Jodhpur, Rajasthan, India

Abstract— Companding transforms useful under assumption of infinite bandwidth. Under band limited conditions OBR parameter filters out. So bandwidth is a factor that decides the filtering out OBR on the performance of companded OFDM systems. As a result filtering becomes essential under band limited conditions in turn this does deteriorate the system performance significantly. In this paper method proposed to overcome the performance degradation. Method called non symmetric scheme based on the use of curve fitting method to find out a suitable polynomial to be used for decompanding at the receiver. This method indeed improves the performance in comparison to existing symmetric methods when filtering is necessary for band limited conditions.

Keywords— Companding, OFDMA, CDMA, TDMA, FDMA, Digital Techniques and their performance.

I. INTRODUCTION

Orthogonal Frequency Division Multiplexing (OFDM) is a digital modulation technique who consists of transmitting a data stream using a large number of parallel narrow-band sub carriers instead of a single wide-band carrier i.e. in OFDM multiplexing is applied to independent signals but these independent signals are a subset of one main signal. Therefore OFDM is a combination of modulation and multiplexing with better immunity to impulse noise and intersymbol interference (ISI), low complexity and high spectral efficiency. Implementation of OFDM modulation is illustrated by the OFDM system as shown in figure 1.1 .

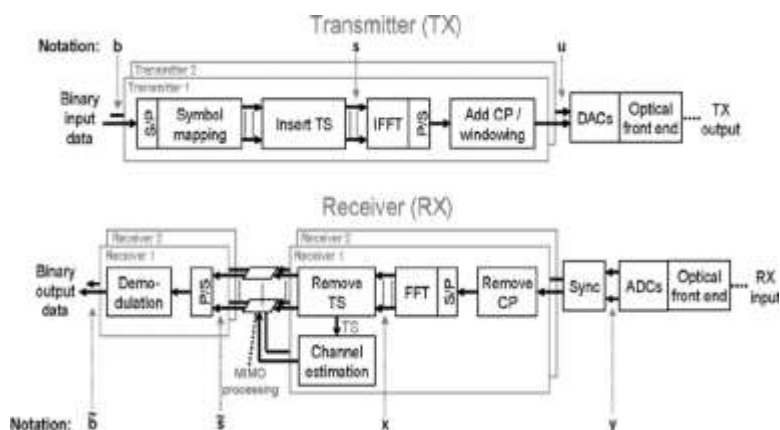


Fig. 1.1: OFDM System

II. SYSTEM FUNCTIONING

OFDM Transmitter: Data coming from the input are arranged into vectors with number of components equal to the N number of carriers. Each component is composed by a number of bits depending on the alphabet of the modulation scheme used on the next stage. Each component (group of bits) is mapped into a complex symbol depending on the alphabet of the modulation scheme used[3]. The Inverse Fast Fourier Transform algorithm (IFFT) is applied to the vector giving a real samples vector. The guard interval is added at the beginning of the vector by repeating the components of the end. Vectors are concatenated to form a time signal (parallel/serial conversion). Windowing the signal is necessary to limit the bandwidth. Most used window is the raised cosine.

Channel : The signal is then passed through the channel. Channel is modeled by a linear system with frequency res-

ponse $c(t)$ together with a source of additive Gaussian noise[4].

OFDM Receiver: At the reception, signal is rearranged again into vectors (serial/parallel conversion) and guard interval is dropped. Fast Fourier Transform (FFT) is computed in order to get back the complex vector of symbols.

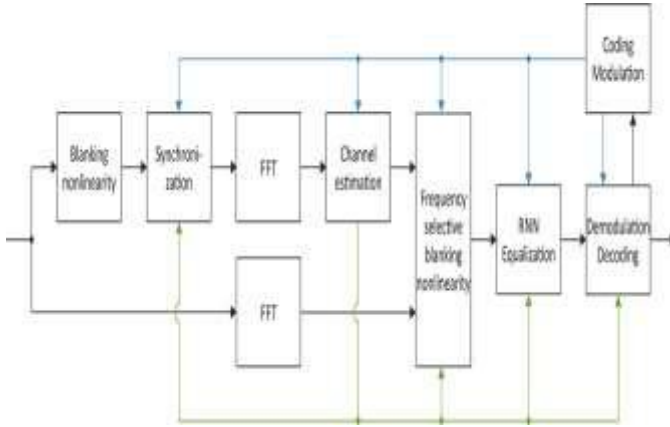


Fig.1.2: OFDM Receiver System

III. COMPANDED OFDM SYSTEM

OFDM system has been used for the high-speed digital communications such as DAB (digital audio broadcasting), DVB (digital video broadcasting), digital high definition television (HDTV) and asymmetric digital subscriber line (ADSDL) due to robustness to the narrowband interference and severe multi-path fading. One major difficulty, however, is its large peak-to-average power ratio (PAPR) which reduces the resolution of the digital-to-analog (D/A) and analog-to-digital (A/D) converters in the transmitter and receiver[2]. A simple as well as an effective companding technique to reduce the peak-to-average power ratio of OFDM signal. The idea is to make use of companding in speech processing. Since OFDM signal is similar to speech signal in the sense that large signals only occur very infrequently, the same companding technique can be used to improve OFDM transmission performance. The block diagram of OFDM system with commanding technique is shown in fig 1.2 as follows.

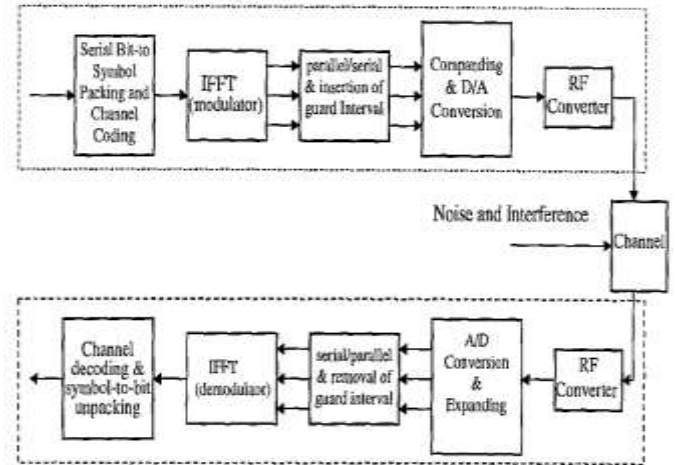


Fig.1.3: Proposed Companded OFDM System

IV. LIMITATIONS IN COMPANDED OFDM SYSTEM

In companded OFDM system the PAPR of OFDM signals is reduced by increasing the average power of signals while keeping the peak unchanged, but this reduction in PAPR may be very limited under certain BER performance constraint. i.e. Out of band radiation (OBR), filtering in system and even the bandwidth plays a key role on the performance of companded OFDM systems [1].

Problem Statement

- Companding transforms mitigate the effects of OFDM only under sufficient bandwidth.
- Band limited case; the OBR value is not satisfied. Thus we filter the OBR parameter.
- To avoid PAPR regrowth companding parameters are tighten to compress large amplitude and enhance small amplitude. In spite of these remedies, the overall system performance degrades with BER performance degradation.

V. PAPER WORK AND OBJECTIVE

- Analysis & study of the effects of filtering on the performance of various companding transforms.
- To overcome this and improve system performance, a simple effective method of Non symmetric companding and decompanding is used.
- To improve the performance degradation, Non symmetric companding and decompanding method is used based on the use of curve fitting method to find out a suitable polynomial, used for decompanding at the receiver. The main objective of this paper is to develop a method based on companding transform that provides a simple but effective tradeoff between reduction in

PAPR and bit error rate (BER) performance which is required in modern wireless transmission systems.

ber of sub carriers chosen is $N=256$, oversampling factor of 4.

Clipping: The clipping operation is done on the over sampled OFDM signal after the base band OFDM is digitally modulated into band pass signal [7]. The over sampled OFDM signal after IFFT is

$$X_k' = \begin{cases} X_{k+N/2}, & 0 \leq k \leq N/2 - 1 \\ 0, & N/2 \leq k \leq mN - N/2 - 1 \\ X_{k-(mN-N/2)}, & mN - N/2 \leq k \leq mN - 1 \end{cases} \quad (6.1)$$

To generate the bandpass signal digitally, let the bandpass carrier frequency f_c be $1/4$ of the sampling frequency f_s then, the real bandpass samples can be written as

$$\begin{aligned} y_n &= x_n \cos(2\pi \frac{f_c}{f_s} n) - x_n \sin(2\pi \frac{f_c}{f_s} n) \\ &= x_n \cos(\frac{n\pi}{2}) - x_n \sin(\frac{n\pi}{2}). \end{aligned} \quad (6.2)$$

The output power of the clipped OFDM signals after the BPF is given by

$$\hat{P}_{av} \triangleq \frac{1}{N} \sum_{k=0}^{N-1} E \left[|\tilde{A}_k|^2 \right] \quad (6.3)$$

Where A_k is the distorted version of the original data A_k . So the out band power to in band power is equivalent to average output power after clipping to the output power before clipping is less than or equal to 1 as shown by equation below and over sampling factor ($J=1$)

$$\frac{\hat{P}_{av}}{P_{out}} = \frac{\sum_{k=0}^{N-1} E \left[|\tilde{A}_k|^2 \right]}{\sum_{k=0}^{JN-1} E \left[|\tilde{A}_k|^2 \right]} \leq 1 \quad (6.4)$$

So the constant value of OBR/IBR is -15 under band limited case.

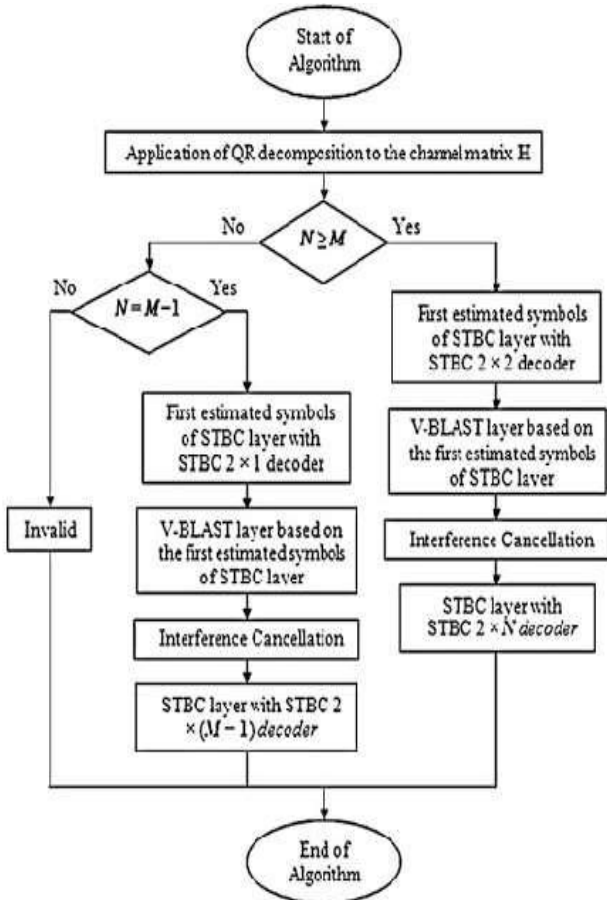


Fig.1.4: Proposed STBC Companded OFDM System based on FFT- IFFT functioning flow chart

VI. ALGORITHM FOR SOLUTION APPROACH
Calculation of OBR to IBR Ratio

Unwanted emissions [15] are composed by out of band and spurious emission. Spurious emission according to ITU_R recommendation defines that any unwanted emission which falls at frequencies separated from the centre frequency of the emission by 250% or more of the relevant channel separation, where the system is intended to be used, will generally be considered spurious emission. Out of band emissions, defined based on their source, occur in the out of band domain and, to a lesser extent in the spurious domain. Spurious emissions likewise may occur in the out of band domain as well as in the spurious domain. We also analyzed theoretically the average value of OBR to IBR ratio for clipping and different companding schemes that achieve a reasonable level of PAPR. The parameter constraints considered are target PAPR of 6.5 dB, CCDF of atleast 10^{-5} at this value of PAPR. The modulation scheme used is QPSK and the num-

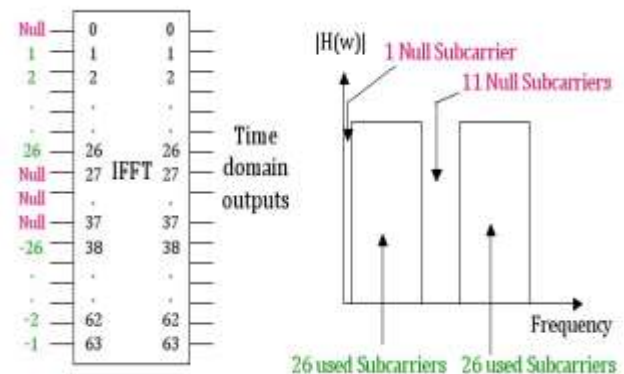


Fig 1.5: Distributive Subcarrier OFDM System

Exponential Companding: The outputs of the N-point Inverse Fast Fourier transform (IFFT) of S_k are the OFDM signal samples over one symbol interval [13], or mathematically

$$s_n = \frac{1}{\sqrt{N}} \sum_{k=0}^{N-1} S_k \exp\left(\frac{j \cdot 2\pi kn}{N}\right) \tag{6.5}$$

The amplitude, or modulus, of OFDM signal s_n is given by

$$|s_n| = \sqrt{Re^2\{s_n\} + Im^2\{s_n\}} \tag{6.6}$$

Considering the phase of input signals, the companding function $h(x)$ is given by

$$h(x) = \text{sgn}(x) F_{\tau_n}^{-1} (F_{|s_n|}(x)) = \text{sgn}(x) \sqrt{\alpha \left[1 - \exp\left(-\frac{x^2}{\sigma^2}\right) \right]} \tag{6.7}$$

The positive constant α determines the average power of output signals given by

$$\alpha = \left(\frac{E[|s_n|^2]}{E\left[\sqrt{1 - \exp\left(-\frac{|s_n|^2}{\sigma^2}\right)}\right]^2} \right)^{\frac{1}{2}} \tag{6.8}$$

Where $\sigma^2 = E[|S_k|^2]/2$ is the common variance. So this constant determines the power OBR/IBR whose constant value is -12 under the case of limited bandwidth.

A-Law Companding: The OFDM signal samples in real form after inverse fast Fourier transform (IFFT) [10] can be formulated as

$$s(n) = \frac{2}{\sqrt{N}} \sum_{k=1}^{\left(\frac{N}{2}\right)-1} \left\{ a_k \cos\left(\frac{2\pi kn}{N}\right) + b_k \sin\left(\frac{2\pi kn}{N}\right) \right\} \tag{6.9}$$

$a_k - j b_k$ is the transmitted data for the k^{th} sub carrier and N is the IFFT size.

From the central limit theorem, the variance of the Gaussian distributed MCM signal can be easily determined as

$$\sigma_s^2 = \frac{2(N-2)}{N} P_s \tag{6.10}$$

Where $P_s = E\{1/2(a_k^2 + b_k^2)\}$ is the signal power for each sub carrier.

The maximum peak value of OFDM signal is found as

$$A = (N-2) \sqrt{\frac{2P_s}{N}} \tag{6.11}$$

The A-law compressed OFDM signal in our proposed PAPR reduction technique is described by

$$s_c(n) = \begin{cases} \frac{\mu s(n)}{1 + \ln \mu} & 0 \leq s(n) \leq \frac{A}{\mu} \\ \frac{A + A \ln\left(\frac{\mu s(n)}{A}\right)}{1 + \ln \mu} & \frac{A}{\mu} \leq s(n) \leq A \end{cases} \tag{6.12}$$

Where μ is the companding coefficient. So the maximum peak value determines the OBR/IBR ratio under band limited case whose value is -10.

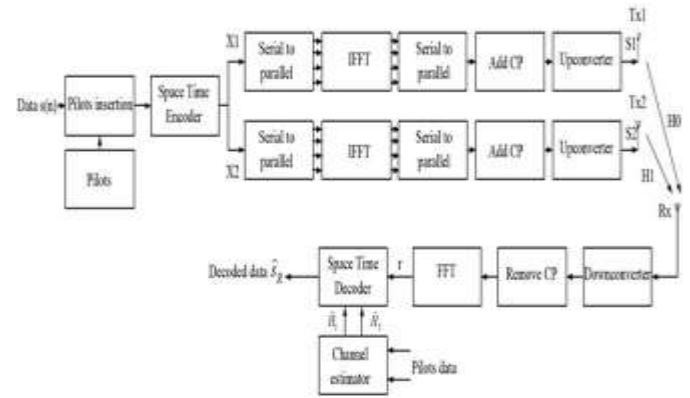


Fig 1.6 STBC functioning based transmitter receiver data communication OFDM System

Linear Symmetric Transform (LST): With linear symmetrical transform [10], the transmitted signals may be expressed by

$$S'_{k,m} = u \cdot S_{k,m} + \text{Sgn}(S_{k,m}) \cdot v \tag{6.13}$$

where $0 < u \leq 1$ and $0 < v \leq A$ are the transform parameters. Further, the received signal is

$$R'_{k,m} = S'_{k,m} + n_{k,m} + q_{k,m} \tag{6.14}$$

Where $n_{k,m}$ denotes the AWGN term with zero mean and variance $\sigma_0^2 = N_0/2$

Therefore the OBR to IBR ratio determined at the receiver using above equation and the constant value is -9 under band limited case.

Non Linear Symmetric Transform (NLST)

With NLST [10], the transmitted signals can be expressed by,

$$S'_{k,m} = \begin{cases} \text{Sgn}(S_{k,m}) \frac{M}{|S_{k,m}|} \ln\left[1 + \frac{u}{M} |S_{k,m}|\right], & |S_{k,m}| \leq M \\ \text{Sgn}(S_{k,m}) \frac{M}{v} \left\{ \exp\left[\frac{\ln(1+u)}{v} |S_{k,m}| - \text{Sgn}(S_{k,m}) M\right] - 1 \right\} + \text{Sgn}(S_{k,m}) M, & |S_{k,m}| > M \end{cases} \tag{6.15}$$

Where $u > 0$ and $0 < v \leq A - M$

By the inverse transform of the above equation, we get the received signal through which OBR to IBR ratio constant value is -14 under the band limited case.

Non Linear Non Symmetric Transform (NLNST):

The assumption of any type of companding is for NLNST. The transformed signals is expressed as

$$S'_{k,m} = Sgn(S_{k,m}) \frac{v}{\ln(1+u)} \ln \left(1 + \frac{u}{v} |S_{k,m}| \right)$$

(6.16)

Where $u > 0$ and $0 < v \leq A$

For the case of large signal-to-noise ratio (SNR), the received signals through the inverse transform can be approximated as

$$R_{k,m} = Sgn(R'_{k,m}) \frac{v}{u} \left\{ \exp \left[|R'_{k,m}| \frac{\ln(1+u)}{v} \right] - 1 \right\} \\ \approx S_{k,m} + \ln(1+u) \left[\frac{1}{u} + \frac{|S_{k,m}|}{v} \right] (n_{k,m} + q_{k,m}).$$

(6.17)

The relevant OBR to IBR ratio under band limited case with receive and transmitted average power known the constant value is -13. By the above analysis we found that all the schemes are not able to meet the stringent requirement of OBR in order to prevent interference with adjacent channels and generally less than 1 [7].

Simulation Results:

Simulation was performed to measure the BER Vs SNR for various companding schemes with filtering and without filtering using symmetric method and verified PAPR calculation. The results were analyzed by taking following constraints $N=256$ (no of subcarriers), target PAPR=6.5DB, modulation scheme used QPSK. BER Vs SNR analysis also done for the proposed technique non symmetric method for modulation schemes QPSK and 16-PSK. comparison done between symmetric and non symmetric methods and PAPR calculated for all schemes.

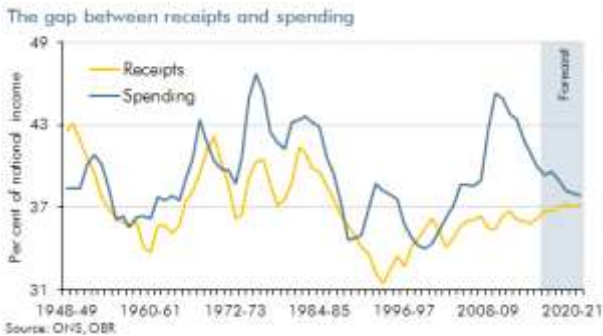


Fig.6.1: Performance Analysis of the Filtered and Non Filtered case for spending and receiving packets

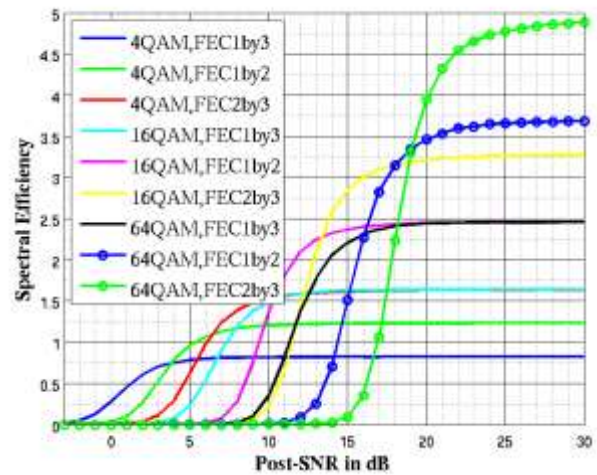


Fig.6.2 : Performance Analysis of spectral efficiency method with 4, 16 and 64 QAM w. r. t. FEC by 3

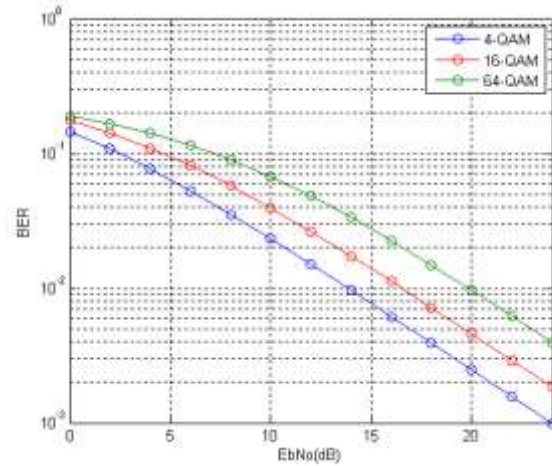


Fig.6.3 : Performance Analysis of BER with 4, 16 and 64 QAM w. r. t. $E_b N_0$ (dB)

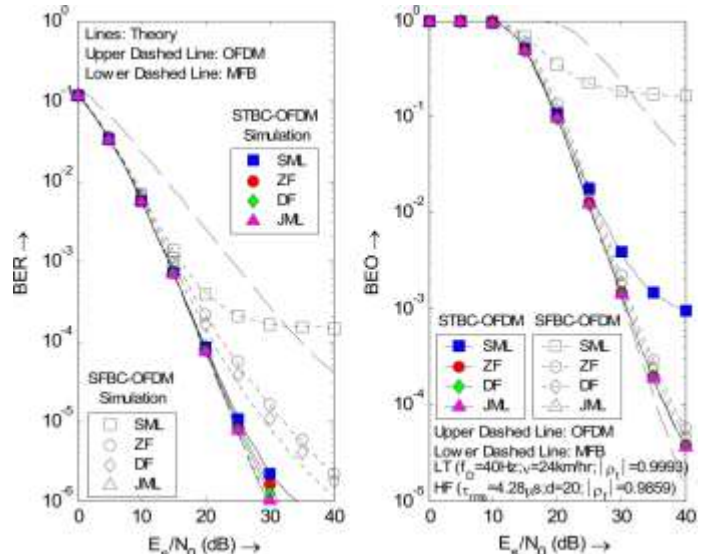


Fig.6.4 : STBC –OFDM Simulation for BER Performance

VII. CONCLUSION

The poor performance of companding schemes under band limited conditions is portrayed. The impact of filtering and without filtering on various companding schemes and respective PAPR analysis infers that the required objective is met. A nonsymmetric companding method is used to improve the performance of this BER degradation in symmetric methods. Extensive simulation results and qualitative discussions have shown that the method used does perform better than previous symmetric method [16]. Main aspects of this research paper is to implement design a algorithm for following features like with comparisons of clipping and companding techniques, all the above simulation results show one common feature, with previous symmetric methods, achieved a better performance closely to clipping under band limited conditions, with proposed scheme. The future scope of the project is likely to be that we can put forth the proposed technique using some other advanced mathematical method or method from any respective domain like networking, optical to have further more reduction in target PAPR

REFERENCES

- [1] "Non Symmetric Decomparing for Improved Performance of Companded OFDM System" IEEE Transactions on wireless communications VOL.6. NO.8. August 2007.
- [2] Y. S. Cho, J. Kim, W. Y. Yang and C. G. Kang, "MIMOOFDM Wireless Communications with MATLAB," Wiley, 2010, 263 Pages.
- [3] F. Meucci, "Multiple Input Multiple Output: From Signal Processing to Protocol Gain," Ph.D. Thesis, University of Florence, Florence, 2009.
- [4] S. M. Alamouti, "A Simple Transmit Diversity Technique for Wireless Communications," IEEE Journal on Select Areas in Communications, Vol. 16, No. 8, 1998, pp. 1451-1458.
- [5] Z. S. Wu, "MIMO-OFDM Communication Systems: Channel Estimation and Wireless Location," Louisiana State University, Ph.D. Thesis, Louisiana State University, Baton Rouge, 2006.
- [6] S. Kaiser, "Space Frequency Block Codes and Code Division Multiplexing in OFDM Systems," Global Telecommunications Conference, San Francisco, 1-5 December 2003.
- [7] K. Lee, Y. Kim and J. Kang, "Adaptive Switching between Space-Time and Space-Frequency Block Coded OFDM Systems," Military Communications Conference, Milcom, 2008, pp. 1-5.
- [8] L. Hanzo, J. Akhtman, M. Jiang and L. Wang, "MIMOOFDM for LTE, WIFI and WIMAX," Wiley IEEE Press, 2010, 591 Pages.
- [9] B. Sklar, "Rayleigh Fading Channels in Mobile Digital Communication Systems Part I: Characterization," IEEE Communications Magazine, Vol. 35, No. 9, 1997, pp. 90- 100.
- [10] D. Tse and P. Viswanath, "Fundamentals of Wireless Communication," Cambridge University Press, Cambridge, 2005. [doi:10.1017/CBO9780511807213](https://doi.org/10.1017/CBO9780511807213).
- [11] D. B. Lin, P. H. Chiang and H. J. Li, "Performance Analysis of Two-Branch Transmit Diversity Block Coded OFDM Systems in Time-Varying Multipath Rayleigh Fading Channels," IEEE Transactions on Vehicular Technology, Vol. 54, No. 1, 2005, pp. 136-148. [doi:10.1109/TVT.2004.838826](https://doi.org/10.1109/TVT.2004.838826).

Review of Dehumidifier with Association to Solar Circular Collector for Close Water Open Air System (CWOA) Humidification & Dehumidification Process

Anilkumar Motiram Patel

¹Department of Mechanical engineering, Faculty of Tech.& Engg., The MS University of Baroda, Gujarat

Abstract— Coastal area where clean drinking water availability is measured problem, which insist to innovate cheap, decentralized small-scale water production. The geographical conditions of vadodara (22.00N, 72.10E), and kachh, Gujarat are best suitable for humidification-dehumidification (HDH) technique based on closed-water, open-air cycle where air heated system is used. There are different types of heat exchangers available as dehumidifiers for HDH applications vary but they have required strength to withstand corrosive nature of seawater, there for frames, collecting plates, fins are made of aluminum. In addition, special attention was exercised to avoid leakage of distillate water. Dehumidifiers is heat exchanger in which heat exchange is takes places between two fluids i.e. hot and cold that are at different temperatures. The heat exchange in the heat exchanger may be in the form of latent heat or sensible heat or combination of both. The HDH concept are also reviewed and compared. Further, novel proposals for improvement of the HDH cycle are outlined. It is notice that HDH technology has great promise to produced fresh water using circular solar collector, although additional research and development is needed for improving system efficiency and reducing capital cost.

Keywords— Humidification, Dehumidification, Desalination, Decentralized Water Production, Solar power, Small-Scale Water Production.

I. INTRODUCTION

Many process are used to bringing down total dissolved solids of 35000ppm to an acceptable level of 500ppm. More power required to run such plants can be obtained from renewable sources or non-renewable sources of energy Desalination plants driven by renewable energy sources are generally economically competitive compared to the classical processes powered by fossil energy. Therefore distillation with solar energy remains one of the most favorable processes. For small-capacity water desalting for remote regions, where there is substantial

solar radiation, lack of skilled personnel or erection and maintenance facilities. Combining the principle of humidification–dehumidification (HD) with solar desalination results in an increase in the overall efficiency of the desalination plant and therefore appears to be the best method of water desalination with solar energy. Al-Hallaj and Selman have concluded that a better understanding of this method of desalination is highly desirable. performance of a unit can be optimize by Simulation verification and design of varying the three major components (humidifier, condenser and collector area) of the unit is perhaps such first optimization till date that could be the critical step in the commercialization of solar desalination based on humidification–dehumidification principle. The main important attraction of the air humidification–dehumidification technique is its conceptual less complex with respect to other desalination processes. This can be described by bringing warm unsaturated air into contact with warm water under specified conditions in order to reach certain desired air humidity. This step, is then, followed by stripping out the water vapor in the humidified air by passing it through a dehumidifier . The vapor carrying capability of air increases with temperature; 1 kg of dry air can carry 0.5 kg of water vapor and about 2803 kJ when its temperature increases from 30 to 80°C. The HD process should essentially include a heating device for both air and water and a humidifying apparatus in order to bring them into contact. The dehumidification technique could be either a direct spray of fresh water on humidified air or condensation of the water content in the humidified air by a heat exchanger.

II. HISTORICAL BACKGROUND OF HD TECHNIQUE

The literature review in this work was based mostly on works of Al-Hallaj and Selman, which represent, to our knowledge, the most comprehensive state-of-the-art project-study helpful for further development of HD

techniques. The solar HD technique has attracted many researchers since early periods. In 1967, Garg reported a study with the aim of developing the HD technique for water desalination in arid zones of India. A 3.4-L/d capacity experimental unit was fabricated having a packed tower with packing height of 30 cm with Raschig rings as packing material. The humidification unit was coupled with a surface condenser (dehumidifier). In 1972, Mehta improved this technique by using an air-recycling system driving the air from the outlet-dehumidifier to the humidifier-inlet. The main advantages of this air-recycling system are a 20% reduction or more of the volume of the packed-column humidifier and higher stability in the operation mode of the plant. In 1970, Grune introduced the multiple effect- humidity (MEH) process, which he had been investigating since early 1960s. In reality, the term “multiple effect” used there did not refer to the number of constructed stages, but to the ratio of heat input to heat utilized for distillate production ($GOR > 1$). The University of Arizona, based on a pilot plant work performed from 1956 to 1963, initiated construction of an experimental pilot plant working on the principle of solar energy MEH. Further work was initiated in 1964 by the University of Arizona in cooperation with the University of Sonora (Mexico) whereby a larger pilot-scale solar desalting plant at Puerto Penasco, Sonora, Mexico, were constructed. Kheder performed a techno-economic investigation of an air HD desalination process. The results showed that 76% of the energy consumed in the humidifier was recovered by condensation. Their cost calculation showed that HD process has a significant potential as an alternative for small capacity desalination plants below 10 m³/d. During the period 1990 to 1996, Farid and coworkers had built three MEH desalination units in Iraq (Basra), Jordan and Malaysia. The unit constructed in Iraq was operated with forced air circulation and produced 12 L/m²d; while the unit constructed in Jordan was operated with both forced and natural draft air circulation. Based on the experience of operating these units, a third unit operated with natural draft air circulation was constructed in Malaysia. These units were built in order to develop a computer simulation program, which could be used to predict the performance of the HD units operating on natural or forced draft air circulation. The University of Munich and the Bavarian Center of Applied Energy Research installed and tested a MEH natural-convection unit in the Canary Islands in Spain during the period 1992–1997. The performance of the unit was improved over the years and an average daily production of 100 L out of 8.5m of collector area (11.8 L/m²d) was obtained by the system without thermal storage. 2Müller-Holst studied and installed a MEH unit without thermal storage in the island of Fuerteventura with a GOR ranging between 3 and 4.5.

But this unit did not reach a GOR of 8 obtained in the laboratory at ZAE Bayern at steady-state conditions. In a related study, Ulber investigated and installed in 1997 in Sfax (Tunisia) a unit with a conventional heat storage tank (2 m³) and heat exchange between the collector circuit (38 m²) and the distillation circuit. This enabled continuous (24 h/d) distillate production. In 1991, Graef studied a desalination process based on a solar multiple condensation– evaporation cycle (SME). Two types of desalination units SME 3.6 (50 L/d) and SME 200 had been in operation in Sfax (Tunisia) since 1991. Experimental study on these units performed by Ben Bacha had deliberated a condensate production of 4 L/m²d with a collector efficiency of 46% (theoretical production: 14.3 L). Delyannis and Belessiotis built at Kuwait University a unit based on open-air/closed-water cycle of 9.8-m³/d capacities. A salt gradient solar pond of 1700 m² (5.8 L/m²) provided the unit with thermal energy. Khalil noted that this method of desalination might be economical only if the produced fresh water was considered as an air-conditioning by-product. Dai and Zhang also built an MEH unit operated in an open-air/ closed-water cycle of 100 L/h fresh water with maximum production capacity (6.2 L/m²d). Another MEH unit based on open-air/closed-water cycle and referred to as “Dew vapouration” was built at Arizona State University, for the production of 45.4 kg/d of condensate, with GOR values in excess of 7.5.

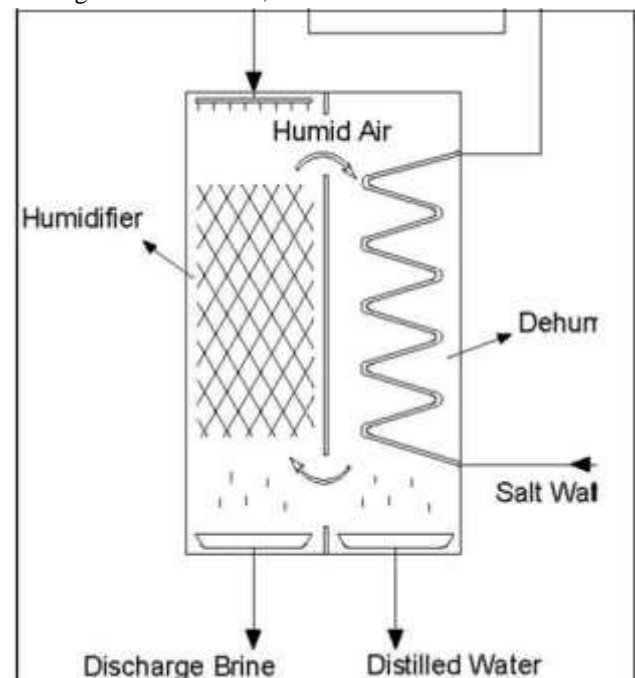


Fig.1: Schematic Diagram of Dehumidifier

III. HEAT EXCHANGERS USED AS DEHUMIDIFIERS

For example, flat-plate heat exchangers were used by Müller-Holst et al. [17]. Others used finned tube heat exchangers ([16], [18] & [50]). A long tube with

longitudinal fins was used in one study [59], while a stack of plates with copper tubes mounted on them in another study ([60] & [61]) used a horizontal falling film-type condenser. Direct contact heat exchangers were also used as a condenser in some other studies [62] in combination with a shell- and-tube heat exchanger to provide enhanced condensation and improved heat recovery for the cycle. A flat plate heat exchanger made of double webbed slabs of propylene was used by Muller-Holst [17] in his HDH system. The distillate runs down the plates trickling into the collecting basin. Heat recovery is achieved by transferring heat to the cold sea water flowing inside the flat plate heat exchanger. The temperature of sea water in the condenser increases from 40°C to 75°C. In a similar study, Chafik ([16] & [18]) used seawater as a coolant wherein the water is heated by the humid air before it is pumped to the humidifiers. Three heat exchangers were used in three different condensation stages. An additional heat exchanger is added at the intake of sea water (low temperature level) for further dehumidification of air. The heat exchangers (or dehumidifiers) are finned tube type air coolers. They developed a theoretical model by using TRNSYS to calculate heat transfer coefficients from both the hot- and cold-sides of the heat exchanger from which the system operating conditions were set. It is important to note that to withstand corrosive nature of seawater; stainless steel is used for frames, collecting plates, while the fins are made of aluminum. In addition, special attention was exercised to avoid leakage of distillate water. Different designs of condensers in a HDH cycle were used by Farid et al. ([59] & [63]). In a pilot plant built in Malaysia, the dehumidifier was made of a long copper galvanized steel tube (3 m length, 170 mm diameter) with 10 longitudinal fins of 50 mm height on the outer tube surface and 9 fins on the inner side. In another location, they used a simplified stack of flat condenser made of 2 x 1 m² galvanized steel plates with long copper tubes mounted on each side of the plate to provide a large surface area. The condenser size was made large, particularly to overcome the small heat transfer coefficients both on the air- and water-sides due to relatively low air velocity, as well as low water flow rates. In another design, the dehumidifier was made of 27 m long copper pipe having a 10 mm OD, mechanically bent to form a 4 m long helical coil fixed in the PVC pipe. The preheated feed water was further heated in a flat plate collector. The hot water leaving the collector was uniformly distributed over a wooden shaving packing in a 2 m long humidifier. It is important to note that the condenser or dehumidifier was made of hard PVC pipes connected to form a loop with the blower fixed at the bottom. The condenser was made of a copper pipe mechanically bent to form a helical coil fixed in the PVC

pipe. Two types of condensers were reported in another study by [60]. These were constructed from galvanized steel plates for both the bench and pilot units. In the pilot unit, a copper tube having 11 mm OD and 18 m long was welded to the galvanized plate in a helical shape. The tube outside diameter and length in the bench unit were 8 mm and 3 m, respectively. Either one or two condensers, connected in series, were fixed vertically in one of the ducts for both the units. In one unit, the condenser was simply a 3 m long cylinder having a diameter of 170 mm and made of galvanized steel plates. Ten longitudinal fins were soldered to the outer surface of the cylinder and nine similar were soldered to the inner surface. The height of inside and outside fins was 50 mm. The thickness of the plate that was used to make the cylinder and the fins was 1.0 mm. A copper tube having 9.5 mm inside diameter was soldered to the surface of the cylinder. The condenser was fixed vertically in the 316 mm diameter PVC pipe which is connected to the humidifier section by two short horizontal pipes. Bourouni et al. [61] used a condenser made of polypropylene which was designed to work at low temperatures (70-90°C) for a HDH system. It is similar to a horizontal falling film-type condenser. At the top of the dehumidifier, the hot humid air is forced down where the distilled water is recovered. It is important to note that heat recovery in an HDH system requires a larger heat transfer area for improving the overall system performance. For this reason, 2000 m of tubes are used in the evaporator, while 3000 m of tubes in the condenser. The system Orfi et al. [52] used had two solar heaters, one for heating water and the other for heating air. The condenser, that uses seawater for cooling, consists of a chamber with a rectangular cross section. It contains two rows of long cylinders made of copper in which the feed water flows. Longitudinal fins were soldered to the outer surface of the cylinders. The condenser is characterized by heat-transfer surface area of 1.5 m² having 28 m as a total length of the coil. Packed bed direct contact heat exchangers were used in a few researchers ([52], [64] & [65]), because the film condensation heat transfer is tremendously degraded in the presence of non-condensable gas. An additional shell and tube heat exchanger is used to cool the desalinated water from which a portion is re-circulated and sprayed in the condenser. Threlkeld [66] explains the governing equations for the dehumidifier in differential form. Also, design correlations for both friction factor and heat transfer coefficients that can be used for dehumidifiers are summarized by Pacheco-Vega et al. [67]. The standard method as developed by McQuiston ([68] & [69]) considers finned-tube multi row multi-column compact heat exchangers and predicts heat and mass transfer rates using Colburn j-factors along with flow rate, dry and wet bulb temperatures, fin spacing and other dimensions. The

air side heat transfer coefficient is based on log-mean temperature difference for the dry surface whereas under the condensing conditions, the moist air enthalpy difference is used as a driving potential. Pacheco-Vega et al. [67] used neural network techniques and the experimental data collated by McQuiston, to create a trained network that predicted the exchanger's heat rate directly. Remarkably accurate results were obtained as compared with the method of using correlations of heat and mass transfer coefficient and Colburn j factors. They focused on the exchanger heat rate since it is the value ultimately desired by users. A significant improvement in the accuracy of predictions compared to the conventional jfactor approach was demonstrated, e.g., 56.9% less error for drop wise condensation and 58.6 % less error for film wise condensation have been reported

IV. CLASSIFICATION OF DEHUMIDIFIER

Dehumidifiers is heat exchanger in which heat exchange takes places between two fluids i.e. hot and cold that are at different temperatures. The heat exchange in the heat exchanger may be in the form of latent heat or sensible heat or combination of both. Solid wall may or may not separate two fluids.

Dehumidifier Classified On The Basis Of The Following.

4.1 Nature of heat exchange process:

Direct contact (open): Heat exchange takes place through direct mixing of hot and cold fluids. Examples are cooling towers, jet condensers and direct contact feed heaters.

Indirect contact (surface): Regenerators- In this hot and cold fluids are flow alternately through same space alternately with no or little mixing between the streams. Examples are the regenerators are used in most of the gas to gas heat exchangers such as internal combustion engine and gas turbines. Other applications include open hearth and glass melting furnaces and air heaters of blast furnaces.

Recuperates- This is the most common type of heat exchanger in which two fluids are separated by surface between them. Examples are oil coolers, intercoolers, economizer super heaters, condensers, radiators and evaporator.

4.2 Relative Directions of Fluid Motions:

Parallel flow-In this hot and cold fluids flow in the same directions. Examples are water heaters, oil coolers etc.

Counter flow- This is the most favorable device in which hot and cold fluid flows in opposite directions. Cross flow- Two fluids are flow in normal to each other for example automobile radiators

4.3 Design and Construction Features:

It includes concentric tube, shell and tubes; multiple shells and tube passes and compact heat exchanger.

4.4 Physical State of the Fluids:

In this category Condensers and Evaporators are present according to state of fluid.

V. TYPES OF DEHUMIDIFIER

There are following type of Dehumidifier(a).Air cooled (b)Water cooled (c).Evaporative type dehumidifier

5.1.1 AIR COOLED: - In this type of dehumidifier heat is removed by air using either natural or forced circulation. The dehumidifier is made up of steel, copper or aluminum tubing provided with fins to improve airside heat transfer. The refrigerant flows inside the tubes and the air outside.

They are used for small capacity machines, such as refrigerators and small water and small water coolers, which use vertical wire and tube or plate and tube construction with natural circulation. These are seldom made in sizes over 5TR because of high head pressure, excessive power consumption and objectionable fan noise.

5.1.2 Water-cooled: - In this type, the arrangement can either be namely, shell and tube, shell and coil or double tube.

52.1 Shell and tube: - in this the water flowing through passes inside the tube and the refrigerant condensing in the shell is most commonly used condenser. This type of dehumidifier also serves the purpose of a receiver, specially for pumping down the refrigerant, because there is enough in the shell and the bottom part serves the purpose of a sub-cooler as the condensed as the condensing liquid comes in contact with the entering water at a lower temperature.

5.2.2 Shell and coil: - it consists of an electrically welded closed shell containing a water coil sometimes of finned tubing.

5.2.3 Double tube: - the refrigerant condenses in the outer tube and the water flows through the inner tube in opposite direction.

Water cooled condensers are invariably used in conjunction with cooling towers, spray ponds etc. heated water from the condenser is led to the cooling tower where it is cooled by self-evaporation into the stream of air. After cooling, the water is pumped back to the condenser.

5.3 Evaporative dehumidifier The refrigerant first rejects its heat to the water and then water rejects its heat to the air, mainly in the form of evaporated water. Air leaves with high humidity as in a cooling tower. Thus an evaporative condenser combines the function of a condenser and cooling tower. Evaporative condensers are generally used on large ammonia plants as they are found to be cheaper. Such condensers require a larger amount of

refrigerant charge due to longer length of the refrigerant piping. But in case of ammonia systems this is immaterial since the refrigerant is quite cheap.

The following heat balance is confirmed for the C.V.2 (water side).

$$C.C.V.2 \quad \frac{dT_{wc}}{dz} = \frac{h_{wc}\alpha_{Hc}(T_{wi}-T_{wc})}{m_{wc}c_{wc}}$$

For C.V.3 (air side) two equations can be written. The first is a mass balance and the second is a heat balance

$$C.C.V.3 \quad \frac{d\omega_c}{dz} = \frac{k_{ac}\alpha_{Mc}(\omega_c-\omega_{ic})}{m_{ac}}$$

$$\frac{dT_{ac}}{dz} = \frac{h_{ac}\alpha_{Hc}(T_{ac}-T_{ic})}{m_{ac}(C_{ac} + \omega_c C_{vc})}$$

Finally heat balance for interface is as follows:

$$h_{wc}\alpha_{Hc}(T_{wi}-T_{wc}) = h_{ac}\alpha_{Hc}(T_{ac}-T_{ic}) + L_{ve}k_{ac}\alpha_{Mc}(\omega_c-\omega_{ic})$$

The interface is assumed to be a film of saturated air. Therefore T_{ie} and ω_{ie} are dependent variables. Stocker and Jones [10] introduced an experimental relation for evaluation of absolute humidity according to temperature which has a suitable accuracy:

$$\omega_{ie} = f_{exp}(T_{ie}) = 2.19 \times 10^{-6}T_{ie}^3 - 1.85 \times 10^{-2}T_{ie}^2 - 7.06 \times 10^{-3}T_{ie}^0 - 0.077$$

VI. ENERGY AND MASS BALANCES EQUATIONS

Energy and mass balances are applied to a segment of height Δy as shown in Fig

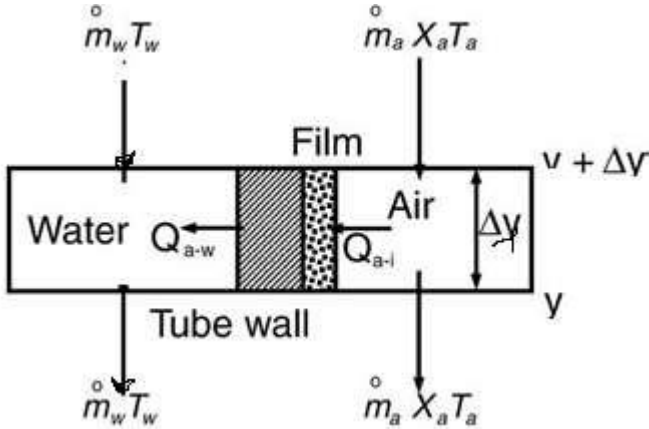


Fig.2: An element of the dehumidifier

$$M_{cw}Cp_{cw}(T_{cwo} - T_{cwi}) = M_a(H_o - H_c) \quad (1)$$

$$M_{cw}Cp_{cw}(T_{cwo} - T_{cwi}) = U_c A_c LMTD_c \quad (2)$$

The logarithmic mean

$$LMTD_c = \frac{(T_{ac} - T_{cwo})(T_{ac} - T_{cwi})}{\ln\left(\frac{T_{ao} - T_{cwo}}{T_{ac} - T_{cwi}}\right)}$$

The production of distilled water is given by the following balance equation

$$M_d = M_a(W_o - W_c)$$

Dehumidifier effectiveness η

$$\eta = \frac{T_3 - T_4}{T_3 - T_{amb}}$$

VII. THE GOVERNING EQUATIONS OF THE DEHUMIDIFICATION PROCESS

The following equations were derived to describe the heat and mass balances in the dehumidifier

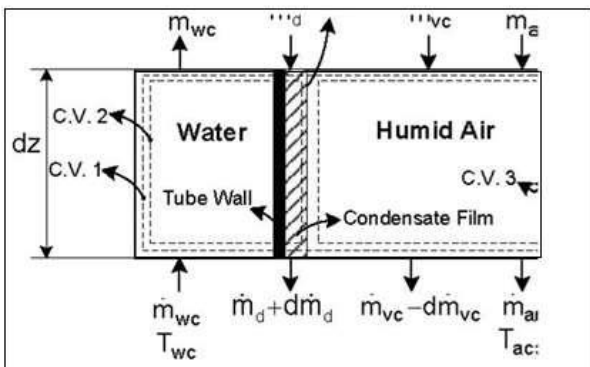


Fig. 3: Element of dehumidifier

As shown in Fig. 3 it can be written for control volume 1

$$C.V.1: \quad d\dot{m}_d = d\dot{m}_{vc} = \dot{m}_{ac}d\omega_c$$

VIII. CONCLUSION

It is important to note that to withstand corrosive nature of seawater; stainless steel is used for frames, collecting plates, while the fins are made of aluminum. In addition, special attention was exercised to avoid leakage of distillate water. The condenser size was made large, particularly to overcome the small heat transfer coefficients both on the air- and water-sides due to relatively low air velocity, as well as low water flow rates.

REFERENCES

- [1] United Nations, 2008. The Millenium Development Goals Report. United Nations, New York.
- [2] El-Dessouky, H.T. and Ettouney, H.M., 2002. Fundamentals of salt water desalination. Elsevier.
- [3] Wilf, 2007. The guidebook to membrane desalination technology. Balaban Desalination Publications, L'Aquila, Italy.33
- [4] Strathmann, H., 2004. Ion-Exchange Membrane Separation Processes. Elsevier, New York.
- [5] Alshareff, F.F., 2008. Investment opportunities in the desalination sector of the Kingdom of Saudi Arabia resulting from privatization and restructuring. Saudi Water and Power Forum, Jeddah, 1-4 November.
- [6] Sauvet-Goichon, B., 2007. Ashkelon Desalination Plant - A Successful Challenge. Desalination 203, 75-81
- [7] Cath, T.Y., Childress, A.E., Elimelech, M., 2006. Forward osmosis: Principles, applications, and recent developments. Journal of Membrane Science 281, 70-87.

- [8] Qiblawey, H.M., Banat, F., 2008. Solar thermal desalination technologies. *Desalination* 220, 633–644.
- [9] Trieb, F., et al., 2007. Concentrating solar power for seawater desalination. Final Report, German Aerospace Center (DLR), Stuttgart.
- [10] Peter-Varbanets, M., Zurbru, C., Swartz, C., Pronk, W., 2009. Decentralized systems for potable water and the potential of membrane technology. *Water Research* 43,245–265.
- [11] Müller-Holst, H., 2007. Solar Thermal Desalination using the Multiple Effect Humidification (MEH) method, Book Chapter, *Solar Desalination for the 21st Century*, 215–225.
- [12] Tiwari, G.N., Singh, H.N., Tripathi, R., 2003. Present status of solar distillation. *Solar Energy* 75(5), 367–373.
- [13] Fath, H. E. S., 1998. Solar distillation: a promising alternative for water provision with free energy, simple technology and a clean environment. *Desalination*, 116,45-56.
- [14] Lawand, T.A., 1975. Systems for solar distillation. Brace Research Institute, Report No. R 115.
- [15] Houcine, I., Amara, M. B., Guizani, A., Maalej, M., 2006. Pilot plant testing of anew solar desalination process by a multiple-effect-humidification technique. *Desalination* 196 105–124.
- [16] Chafik, E., 2004. Design of plants for solar desalination using the multi-stage heating/humidifying technique. *Desalination* 168, 55-71.34
- [17] Müller-Holst, H., Engelhardt, M., Herve, M., Scholkopf, W., 1998. Solar thermal seawater desalination systems for decentralized use. *Renewable Energy* 14(1-4), 311-318.
- [18] Chafik, E., 2003. A new type of seawater desalination plants using solar energy. *Desalination* 156, 333–348.
- [19] Klausner, J.F., Mei, R., Li, Y., 2003. Innovative Fresh Water Production Process for Fossil Fuel Plants, U.S. DOE - Energy Information Administration annual report.
- [20] Hamieh, B.M., Beckmann, J. R., 2006. Seawater desalination using Dew-vaporation technique: theoretical development and design evolution. *Desalination* 195, 1–13.
- [21] Ben-Bacha, H., Damak, T., Bouzguenda, M., 2003. Experimental validation of the distillation module of a desalination station using the SMCEC principle. *Renewable Energy* 28, 2335–2354.
- [22] Garg, H.P, 1975. Year round performance studies on a built-in storage type solar water heater at Jodhpur, India. *Solar Energy* 17, 167-172.
- [23] Garg, H.P, 1985. *Solar Water Heating Systems*. Proceedings of the Workshop on Solar Water Heating Systems, New Delhi, India.
- [24] Eggers-Lura, A., 1978. *Solar Energy for Domestic Heating and Cooling: A Bibliography with Abstracts, and a Survey of Literature and Information Sources*. Pergamon Press.
- [25] Rojas, D., Beermann, J., Klein, S.A., Reindl, D.T., 2008. Thermal performance testing of flat-plate collectors, *Solar Energy*, Volume 82, Issue 8, Pages 746-757.
- [26] Ho, C.D., Yeh, H.M., Wang, R.C., 2005. Heat-transfer enhancement in double-pass flat-plate solar air heaters with recycle. *Energy* 30 (15), 2796-2817.
- [27] Lof, G.O.G., El-Wakil, M.M., Chiou, J.P., 1963. Residential heating with solarheated air - Colorado solar house, *ASHRAE Journal* 5 (10), 77-86.
- [28] Gupta, C. L., Garg, H. P., 1967. Performance studies on solar air heaters. *Solar Energy*, 11(1), 25-31.
- [29] Whillier, A. 1963. Plastic covers for solar collectors. *Solar Energy* 7 (3), 148-151.
- [30] Bansal, N.K., 1987. Thermal performance of plastic film solar air and water heaters. *International Journal of Energy Research* 11 (1), 35-43.
- [31] McCullough, R. W., 1977. Solar Air Heater. US Patent 4262657.
- [32] Satcunanathan, S., Deonaraine, S., 1973. A two-pass solar air heater. *Solar Energy* 15(1), 41-49.
- [33] Severson, A. M., 1978. Solar Air Heater. US Patent 4085730.
- [34] Schmidt, R.N., 1976. Solar Air Heater. US Patent 4085729.
- [35] Vincent, O.W., 1977. Dome Solar Air Heater. US Patent 4236507.
- [36] Choudhury, C., Garg, H. P., 1993. Performance of air-heating collectors with packed airflow passage. *Solar Energy* 50 (3), 205-221.
- [37] Sharma, V. K., Sharma, S., Mahajan, R. B., Garg, H. P., 1990. Evaluation of a matrix solar air heater. *Energy Conversion and Management* 30(1), 1-8.
- [38] Mittal, M.K., Varshney, L., 2006. Optimal thermo hydraulic performance of a wire mesh packed solar air heater. *Solar Energy* 80 (9), 1112-1120.
- [39] Mohamad, A. A., 1997. High efficiency solar air heater. *Solar Energy* 60 (2), 71-76.
- [40] Esen, H., 2008. Experimental energy and exergy analysis of a double-flow solar air heater having different obstacles on absorber plates. *Building and Environment* 43(6), 1046-1054.
- [41] Romdhane, B.S., 2007. The air solar collectors: Comparative study, introduction of baffles to favor the heat transfer. *Solar Energy*, 81 (1), 139-149.

- [42] Ramadan, M.R.I., El-Sebaei, Aboul-Enein, S., El-Bialy, E., 2007. Thermal performance of a packed bed double-pass solar air heater. *Energy* 32(8), 1524
- [43] Koyuncu, T., 2006. Performance of various designs of solar air heaters for crop drying applications. *Renewable Energy* 31(7), 1073-1088.
- [44] Matrawy, K. K., 1998. Theoretical analysis for an air heater with a box-type absorber. *Solar Energy* 63(3), 191-198.
- [45] Duffie, J.A., Beckmann, W.A., 1974. *Solar energy thermal processes*. Wiley, NY.
- [46] Treybal R. E., 1980. *Mass Transfer Operations*. 3rd edition, McGraw-Hill, NY.
- [46] Kreith F. and Bohem R. F., 1988. *Direct-contact heat transfer*, Hemisphere Pub. Corp., Washington.
- [47] Younis, M.A., Darwish, M.A., Juwayhel, F., 1993. Experimental and theoretical study of a humidification-dehumidification desalting system. *Desalination* 94, 11-24.
- [48] Ben-Amara, M., Houcine, I., Guizani, A., Maalej, M., 2004. Experimental study of a multiple-effect humidification solar desalination technique. *Desalination* 170, 209-221.
- [49] El-Agouz, S.A. and Abugderah M., 2008. Experimental analysis of humidification process by air passing through seawater, *Energy Conversion and Management*, Vol. 49 (12), 3698 – 3703.
- [50] Lydersen A. L., 1983. *Mass Transfer in Engineering Practice*, John Wiley & Sons, NY.
- [51] Orfi, J., Laplante, M., Marmouch, H., Galanis, N., Benhamou, B., Nasrallah S. B., Nguyen, C.T., 2004. Experimental and theoretical study of a humidification dehumidification water desalination system using solar energy. *Desalination* 168,151.
- [52] Wallis, J.S. and Aull, R.J., 1999. Improving Cooling Tower Performance, *Hydrocarbon Engineering*, pp. 92-95, May.
- [53] Mirsky, G.R. and Bauthier, J., 1993. Evolution of Cooling Tower Fill, *CTI Journal*, Vol. 14, No. 1, pp. 12-19.
- [54] Aull, R.J., and Krell, T., 2000. Design Features of Cross-Fluted Film Fill and Their Effect on Thermal Performance, *CTI Journal*, Vol. 21, No. 2, pp. 12-33.
- [55] Kloppers, J.C., 2003. A critical evaluation and refinement of the performance prediction of wet-cooling towers. PhD dissertation. University of Stellenbosch.
- [56] Kroger D. G., 2004. Air-cooled heat exchangers and cooling towers thermal-flow performance evaluation and design, Tulsa, Okla. Penwell Corp. Vol I and II.
- [57] ASHRAE Handbook: Fundamentals, 2005. Society of Heating, American, Refrigerating, Air-Conditioning Engineers, and Inc., ASHRAE.
- [58] Farid M.M., Parekh S., Selman J.R., Al-Hallaj S., 2002. Solar desalination with humidification dehumidification cycle: mathematical modeling of the unit, *Desalination* 151, 153-164.
- [59] Nawayseh, N.K., Farid, M.M., Al-Hallaj, S., Tamimi, A.R., 1999. Solar desalination based on humidification process-Part I. Evaluating the heat and mass transfer coefficients. *Energy Conversion Management*, 40, 1423-1439.
- [60] Bourouni K, Chaibi M, Martin R and Tadriss L, 1999. *Appl. Energy*, 64, 129.
- [61] Klausner JF, Li Y, Darwish M and Mei R., 2004. Innovative Diffusion Driven Desalination Process. *ASME J Energy Resources Technology*, 126, 219-225.
- [62] Farid, M.M. and Al-Hajaj, A.W., 1996. Solar desalination with humidification dehumidification cycle. *Desalination* 106, 427-429.
- [63] Li Y, Klausner JF, Mei R and Knight J, 2006a. Direct contact condensation in packed beds, *International Journal of Heat and Mass Transfer* 49, 4751–4761.
- [64] Li Y, Klausner JF, Mei R, 2006b. Performance characteristics of the diffusion driven Desalination process, *Desalination* 196, 188–209
- [65] Threlkeld, J.L., 1970. *Thermal environmental engineering*. Prentice-Hall Inc. Edition 2, 254-265.
- [66] Pacheco-Vega, A., Diaz, G., Sen, M., Yang, K.T. and McClain R.L., 2001. Heat Rate Prediction in Humid Air-Water Heat Exchangers Using Correlations and Neural Networks. *ASME J Heat Transfer*, 123, 348-354.
- [67] McQuiston F.C., 1978. Heat, mass and momentum transfer data for five plate-fin tube heat transfer surfaces, *ASHRAE Trans.*, 84 Part 1, 266-293.
- [68] McQuiston F.C., 1978. Correlation for heat, mass and momentum transport coefficients for plate-fin tube heat transfer surfaces with staggered tubes, *ASHRAE Trans.*, 84 Part 1, 294-309.
- [69] Beckmann, J. R., 2005. Method and apparatus for simultaneous heat and mass transfer utilizing a carrier gas. US Patent No. 6,911,121.
- [70] Beckmann, J. R., 2008. Dew-vaporation Desalination 5,000-Gallon-Per-Day Pilot Plant. *Desalination and Water Purification Research and Development Program Report No. 120*.
- [71] Klausner, J.F., Mei, R., 2005. Diffusion driven desalination apparatus and process. US Patent No. 6,919,000.
- [72] Khedr, M., 1993. Techno-Economic Investigation of an Air Humidification-Dehumidification Desalination Process, *Chemical Engineering Technology* 16, 270-274.

- [73] Wahlgren, R.V., 2001. Atmospheric water vapor processor designs for potable water production: a review. *Water Research* 35, 1-22.
- [74] Narayan, G. P., Elsharqawy, M.H., Lienhard J.H., Zubair, S.M., 2009. Humidification dehumidification desalination cycles. Manuscript under preparation.
- [75] Al-Hallaj, S., Farid, M.M., Tamimi, A.R., 1998. Solar desalination with humidification-dehumidification cycle: performance of the unit. *Desalination* 120,273-280.
- [76] Garg, H.P., Adhikari, R.S., Kumar, R., 2002. Experimental design and computer simulation of multi-effect humidification (MEH)-dehumidification solar distillation. *Desalination* 153, 81-86.
- [77] Nafey, A.S., Fath, H.E.S., El-Helaby, S.O., Soliman, A.M., 2004. Solar desalination using humidification-dehumidification processes- Part II. An experimental investigation. *Energy Conversion Management* 45(7-8), 1263-1277.
- [78] Al-Enezi, G., Ettouney, H.M., Fawzi, N., 2006. Low temperature humidification dehumidification desalination process. *Energy Conversion and Management* 47, 470-484.
- [79] Dai, Y.J., Zhang, H.F., 2000. Experimental investigation of a solar desalination unit with humidification and dehumidification. *Desalination* 130, 169-175.
- [80] Dai Y.J., Wang R.Z., and Zhang HF, 2002. Parametric analysis to improve the performance of a solar desalination unit with humidification and dehumidification, *Desalination* 142 107-118.
- [81] Yamali, C., Solmus, I., 2008. A solar desalination system using humidification-dehumidification process: experimental study and comparison with the theoretical results. *Desalination* 220, 538-551.
- [82] Guofeng Yuan, Zhifeng Wang, Hongyong Li, Xing Li, —Experimental study of a solar desalination system based on humidification –dehumidification process, *Desalination* 277 (2011) 92-98.
- [83] Cemil Yamale, Ismail Solmus—A solar desalination system using humidification-dehumidification process: experimental study and comparison with the theoretical results *Desalination* 220 (2008) 538-551, Received 14 December 2006; accepted 3 January 2007.
- [84] Bourounia, M.T. Chaibib, L. Tadrist, —Water desalination by humidification and dehumidification of air: state of the art, *Desalination* 137 (2001) 167-176, Received 3 November 2000; accepted 17 November 2000.
- [85] EfatChafik, A new seawater desalination process using solar energy *Desalination* 153 (2002) 25 -37, Received 15 April 2002; accepted 30 April 2002.
- [86] G. Prakash Narayan, Mostafa H. Sharqawy, Edward K. Summers, John H. Lienhard, Syed M. Zubair, M.A. Antar,—The potential of solar-driven humidification-dehumidification desalination for small-scale decentralized water production *Renewable and Sustainable Energy Reviews* 14 (2010) 1187-1201.

An Empirical Estimation of CSS Cognitive Radio Network Performance under Spectrum Sensing Data Falsification Attack

Rajesh D. Kadu¹, Dr. Pravin P. Karde², Dr. V. M. Thakare³

¹ Research Scholar, SGB Amravati University, Amravati, India

²Department of Information Technology, Government Polytechnic, Amravati, India

³Department of Computer Science, SGB Amravati University, Amravati, India

Abstract—Cooperative spectrum sensing (CSS) significantly improves the performance of spectrum sensing process in cognitive radio networks (CRNs). Individual spectrum sensing by a cognitive radio (CR) is often inaccurate as the channel often experiences fading and shadowing effects. CSS has been shown to have many advantages in terms of spectrum use and robustness. Despite these facts, a CSS scheme also vulnerable to many security attacks from malicious users (MUs). In order to get unfair usage of spectrum band, MUs can generate false spectrum sensing reports to disturb the good secondary users (SUs) decision about presence of primary user (PU). In this paper, we consider the spectrum sensing data falsification attack (SSDF) in CSS and propose the protocol to identify and eliminate the attacker or malicious user (MU) to improve the network performance. In SSDF attack, MUs send the false spectrum sensing results to fusion center (FC) with the intension that it should make wrong decision about spectrum sensing. In this scenario, FC acts as a data collector to fuse the reports sent by SUs.
Keywords— CR, CRNs, CSS, FC, SSDF.

I. INTRODUCTION

The fast growing smart phone users and mobile internet based applications demands for optimum utilization of spectrum. CRNs improves the efficiency of spectrum utilization under the current static spectrum allocation policy. In conventional spectrum regulation models, majority of the spectrum is allocated to PUs or licensed users for exclusive use. CRNs allows SUs or unlicensed users to use idle spectrum without causing interference with PUs.

Cognitive radio (CR) technology allows the SUs to access the spectrum in opportunistic manner when PUs are not using it. The SUs continuously carry out the sensing process to detect the white spaces available in spectrum band. The white spaces are the frequency bands which are not used by PUs. The SUs should sense the idle spectrum in order to avoid the interference with PUs. Moreover, in

order to avoid the disturbance to PUs, SUs should vacate the spectrum timely if PUs appears to be using it [1].

Individual spectrum sensing by a cognitive radio (CR) is often inaccurate as the channel often experiences fading and shadowing effects. CSS significantly improves the accuracy in detection of PUs presence and helps to increase channel sensing accuracy in CRNs [2]. Moreover CSS is more accurate and have more advantages as it exploits the cooperation among many CRs or SUs.

For detection of PU in a spectrum band, good SUs mainly uses three methods. These are matched filter detection, cyclostationary feature detection, and energy detection. [3] [4]. Energy detection method of spectrum sensing has low computational and implementation complexities. Hence, it is more preferred method for spectrum sensing. Energy based detection can be carried out in both the time and frequency domains.

II. RELATED WORK

Saud Althunibat et al. [5] have proposed protocol for secured CSS. This protocol improves the improves the energy efficiency in presence of malicious users (MUs). In this approach, a Message Authentication Code (MAC) is produced by using a low-overhead symmetric cryptographic mechanism. This code is used to authenticate spectrum sensing data reports under a trade-off between energy and security. With increase in number of MUs, achievable energy efficiency decreases without using security algorithm. The proposed secure CSS greatly improves the energy efficiency compared to the conventional insecure CSS.

Chowdhury Sayeed Hyder et al. [6] proposed adaptive reputation based clustering algorithm as a countermeasure against SSDF attack. The algorithm does not consider the past information of attacker distribution or full identification of MU. The performance evaluation of the proposed algorithm is carried out with respect to independent and collaborative SSDF attacks. The proposed algorithm considerably reduces error rate with compare to

existing collaborative sensing schemes and improves the spectrum utilization.

The defense scheme proposed by Hong Du, Shuang Fu and Hongna Chu [7] use the credit value with each CR user and this value is updated if sensing result is consistency with final decision. In this approach, if reputation value is greater than minimum credit threshold then CR user can take part in next round of sensing. Otherwise, it is identified as MU. The proposed schemes based on credibility weighting and excluded MUs results in higher probability of collaborative detection. Furthermore, sensing performance of the proposed scheme has been further improved. Probability of false alarm remains constant with increase in number of malicious users.

The Majority-based Assessment approach identifies and eliminates the attackers. The Delivery-based Assessment approach evaluates the local decisions on the basis of delivery of the transmitted data by scheduled cognitive user (CU). For the identified unused spectrum, CU gets scheduled for transmission of data. As a result, based on the success of delivering the transmitted data, the real spectrum status can be appropriately defined at the BS, and then used to evaluate the local decisions. Due to removal of attackers detection, probability improves and probability of false alarm reduces. In presence of the proposed punishment policy, individual energy efficiency of the honest CU improves and of attacker reduces with increase in attack-removal threshold [8].

Insistent Spectrum Sensing Data Falsification (ISSDF) attack is addressed by Aida Vosoughi et al. [9]. This attack is different from traditional SSDF attack. In this attack, MU falsifies its sensing data and sends the same falsified value in every iteration of consensus to all the nodes. In this approach, each CR node is associated with some trust value. If trust management not executed, then error rates increase quickly with more consensus iterations. The trust-aware schemes converge to much lower error rates compared to oblivious schemes within only a small number of consensus iterations. The misdetection probability and false alarm probability improves with more number of consensus iterations in presence of ISSDF nodes in network.

Linyuan Zhang et al. [10] proposed a defense reference scheme which in cooperation makes use of the cognitive spectrum sensing process and spectrum access in closed loop manner. This approach gives feedback to SUs about extended sensing result because of PU presence or transmission success or failure outcome to reassess the sensors local sensing performance. The proposed reference scheme improves the global sensing performance with increase in attack population with compare to other approaches such as no defense, ideal abandoning, optimal fusion, global filtering, soft fusion and trusted node. The

global performance is deteriorated with increase in attack probability. If attack probability varies then performance changes in this approach.

Ji Wang et al. [11] proposed a trust-based data fusion rules which decouple erroneous reports as a result of low sensing abilities from false reports because of attacks in distributed CNNs. An individual, majority voting, and capability-weighted majority voting approaches are used to compare with the proposed approach. The parameters used for this comparison are individual success rate, or the probability of successfully detecting the actual status of the channel. The proposed trust-based data fusion scheme outperforms traditional data fusion rules and can distinguish MUs carrying out data falsification attacks through their low trust scores in the long run.

CAO Long et al. [12] proposed the symmetric cryptographic approach which use message authentication code to authenticate the sensing results of SUs as a solution over SSDF attack. The proposed approach maximize the energy efficiency of the SUs. Sasa Maric et al. [13] proposed modified belief propagation algorithm which use reputation as weighted scalar in distributed spectrum sensing scheme. In this approach, honest users are rewarded with increase in reputation while untruthful users are penalized with decrease in their reputation. The honest users with high reputation have high impact on final decision about channel is vacant or occupied.

Abbas Ali Sharifi and Mir Javad Musevi Niya [14] proposed attack proof CSS scheme which estimates attack strength. The attack strength is considered as the probability that a given user is MU. In this approach, attack strength is used in k out of N rule to find the best value of k that reduces the Bays risk. Saud Althunibat et al. [15] considered the infrastructure based CRN in which policy is proposed to identify the attackers. Once the attackers are identified, their sensing result reports are ignored. The other proposed policy punish the attacker by redistributing the transmission opportunities among users based on their local performance.

The remaining paper is organized as follows. Section III presents overview of SSDF attack in CSS. Section IV gives proposed protocol. In section V, simulation environment and result analysis is given. Section VI concludes the paper.

III. SSDF ATTACK IN CSS

The performance of spectrum sensing process can be improved by exploiting spatial diversity called as CSS. CSS can be carried out in both centralized and distributed CRNs. In a centralized CRN, there is a data collector called as fusion center (FC) to which all the SUs reports the spectrum sensing results.. Also FC gives instructions to SUs and takes decision about presence or absence of PU

based on received results. In a distributed CRN, there is no FC and CRs exchange the spectrum sensing results with other CRs. Hence, Each CR receiving the spectrum sensing results from other CRs plays role of FC. Although CSS scheme is more accurate and reliable, it is more vulnerable to many security threats and attacks such as jamming attack, primary user emulation attack (PUEA) and spectrum sensing data falsification attack (SSDF). In SSDF attack, MUs intentionally send fake spectrum sensing results to mislead decision making of FC.

The local spectrum sensing results of each SUs are sent to FC which makes a final decision according to fusion rule. FC then sends this decision to all the SUs. The fusion schemes used by FC are soft decision fusion and hard decision fusion. In soft decision fusion, all the SUs sends the complete local spectrum sensing results to FC. In hard decision fusion SUs send one bit information to FC regarding presence or absence of PU. Fig. 1 shows scenario in which good SU sends the honest local spectrum sensing reports to FC while attackers sends the false reports.

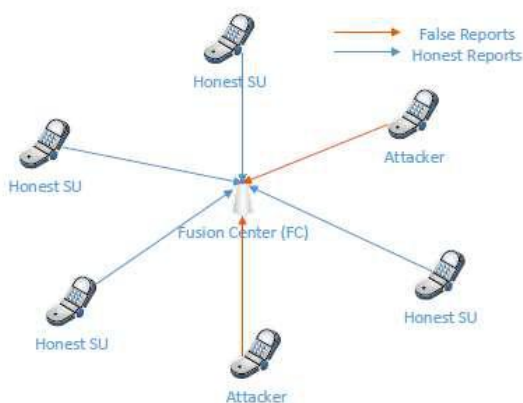


Fig. 1: SSDF attack in CSS

IV. PROPOSED PROTOCOL APPROACH

In proposed model of SSDF attack one PU, several SU's and FC is considered. PU transmits on communication channel and in order to detect the presence of PU, SUs sense the PU signals periodically. The SUs then sends spectrum sensing results to FC at the end of the sensing period. FC then makes the final decision about PU exist or not based on the information sent by SUs in the network. The attackers or dishonest SUs sends the false spectrum sensing results order to mislead the decision making of FC. The attacker node randomly select the available channel list and remove it from the sensed list.

After collecting the reports from all cognitive nodes in the region, FC compares the report of each device and compute its relativity between the reports. FC identifies missed active reports from all the sensed reports. False count for the corresponding node is incremented and

compared with the threshold limit of the missed report. If the missed report count is greater than the threshold then corresponding device is classified as data falsification misbehavior node and eliminated from the network.

4.1 Performance of Proposed Approach

The performance of the proposed protocol is measured with various network parameters. These are packet delivery ratio (PDR), delay, control overhead, dropping ratio, average energy consumption, average residual energy, jitter and throughput. The packet delivery ratio is number of received packets by node divided by number of sent packets multiplied by 100. Delay is changes in data transmission time from source node to destination node. The total number of control packets needed to discover correct path to reach final destination is control overhead. Dropping ratio is ((number of sent packets - number of received packets)/sent)*100. Energy consumed by all nodes is total energy consumed. Total energy consumed divided by number of nodes is average energy consumption. Average residual energy is total residual energy divided by number of nodes. Throughput is number of bits delivered per second. We used traffic to measure the network performance when SSDF attacker is present with all above mentioned parameters. Traffic increases as number of senders increases.

V. SIMULATION ENVIRONMENT AND RESULT ANALYSIS

NS-2 environment is used to test the proposed protocol. The proposed protocol detects SSDF attacker and eliminates it from the network. Each node estimate its energy level to extend the network lifetime. Energy threshold is maintained and total number of nodes considered in network are 50. The total simulation time is set as 200 seconds. the data packet size considered for the simulation is 512 byte. Initial energy is 100 Jules. By considering the all optimum parameters, following results are obtained after simulation. Fig.2 shows PDR and dropping ratio results for varying traffic. The PDR does not affected much more and hence dropping ratio with increase in traffic. PDR improves due to minimum drop of packets. Protocol reduces flooding and hence collisions not occurred.

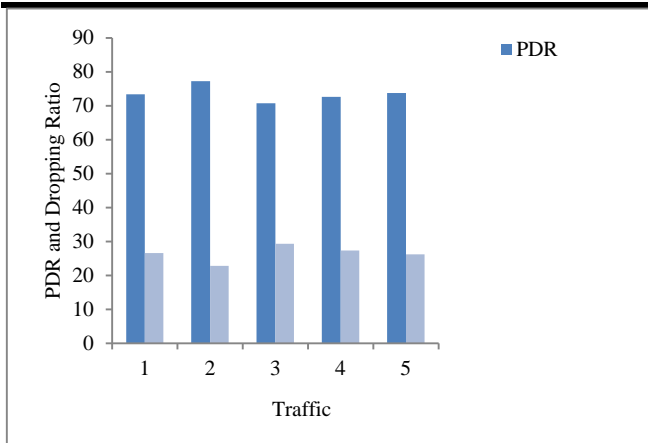


Fig. 2: Traffic vs. PDR and Dropping ratio

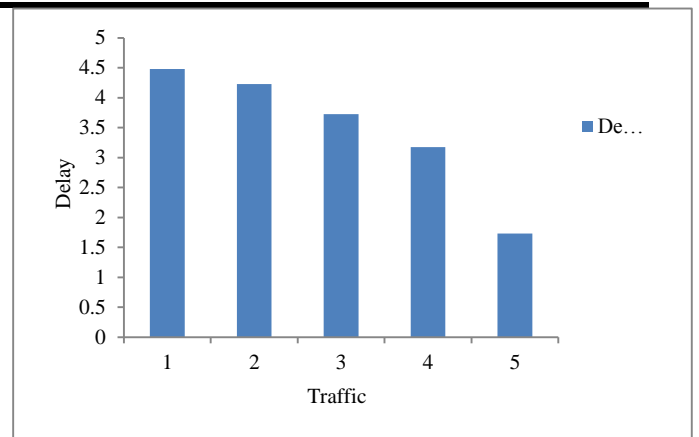


Fig. 4: Traffic vs. Delay

Fig.3 shows the number of control packets that are used to find correct path to reach final destination for increasing traffic in network. With increase in traffic, less number of control packets are required. It shows good performance of the network due to identification and elimination of SSDF attacker.

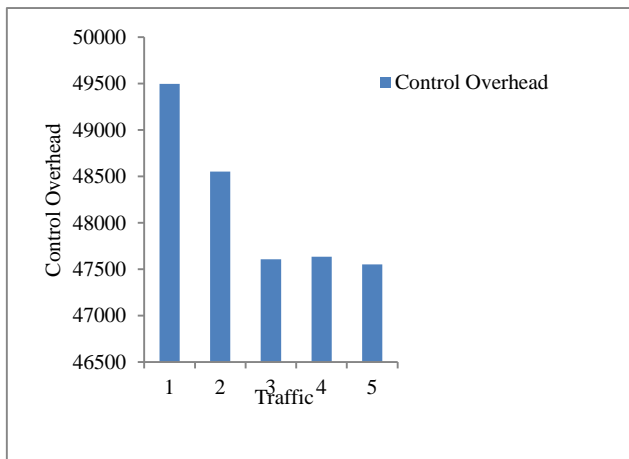


Fig. 3: Traffic vs. Control Overhead

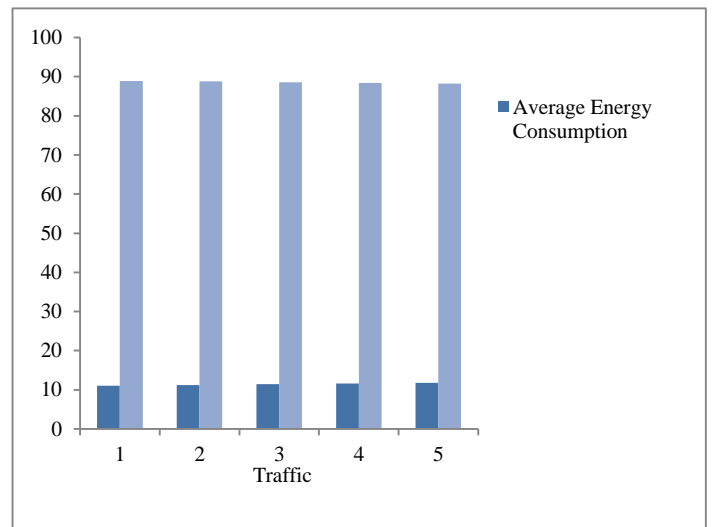


Fig. 5: Traffic vs. Average Energy consumption and Average Residual energy

In Fig. 4 delay is shown which is changes in data transmission time from source to destination. In Fig. 5 Average energy consumption is shown with increase in traffic. It is not affected much more and hence average residual energy is showing better results. As shown in Fig.6, jitter is improved with increase in traffic and Fig. 7 shows better improvement in throughput with increased in traffic. The proposed protocol is scalable with respect to traffic. It identifies SSDF attacker and eliminates it from network thereby improving network performance.

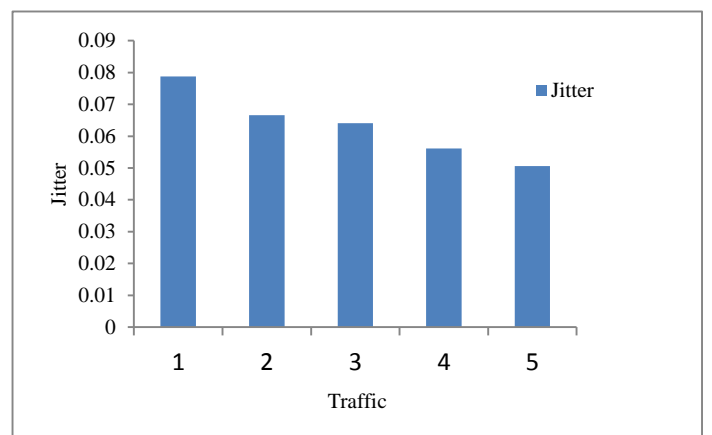


Fig. 6: Traffic vs. Jitter

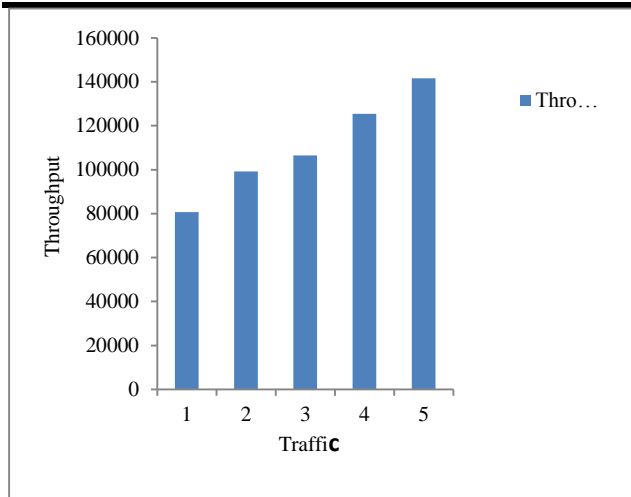


Fig. 7: Traffic vs. Throughput

VI. CONCLUSION

In this paper, we have proposed protocol which implements SSDF attack. The proposed protocol accurately detects the SSDF attacker and isolate it from the network. The proposed protocol shows better performance under the parameters considered with increase in traffic. As protocol identifies the SSDF attacker and eliminates it, network performance is not very much affected with increase in traffic.

REFERENCES

- [1] J. Mitola and G. Maguire.: ‘Cognitive radio: making software radios more personal’ ,IEEE Personal Communications, Aug 1999,Mag., vol. 6, no. 4, pp. 13-18
- [2] L. Li, F.W. Li, and J. Zhu. "A method to defense against cooperative SSDF attacks in Cognitive Radio Networks." IEEE International Conference on Signal Processing, Communication and Computing, pp. 1-6, 2013
- [3] I. F. Akyildiz, W. Lee, M. C. Vuran, and S. Mohanty, “NeXt generation/dynamic spectrum access/cognitive radio wireless networks: A survey,” Computer Networks, vol. 50, 2006, pp. 2127-2159.
- [4] T. Yucek and H. Arslan, “A survey of spectrum sensing algorithms for cognitive radio applications,” IEEE Communications Surveys & Tutorials, vol. 11, no. 1, 2009
- [5] Saud Althunibat, Victor Sucasas, Hugo Marques, Jonathan Rodriguez, Rahim Tafazolli, and Fabrizio Granelli" On the Trade-Off Between Security and Energy Efficiency in Cooperative Spectrum Sensing for Cognitive Radio" IEEE communications letters, vol. 17, no. 8, August 2013.
- [6] Chowdhury Sayeed Hyder, Brendan Grebur, and Li Xiao “Defense against Spectrum Sensing Data Falsification attacks in CR networks.” Springerlink, Journal of security and privacy in computer networks. Volume 76, 2012, p.p. 154-171.
- [7]] Hong Du, Shuang Fu ,Hongna Chu "A Credibility-based Defense SSDF Attacks Scheme for the Expulsion of Malicious Users in Cognitive Radio" International Journal of Hybrid Information Technology Vol.8, No.9 (2015), pp.269-280.
- [8] Saud Althunibat, Birabwa J. Denise and Fabrizio Granelli "A Punishment Policy for Spectrum Sensing Data Falsification Attackers in Cognitive Radio Networks’ IEEE 80th Vehicular Technology Conference (VTC Fall) ,14-17 Sept. 2014.
- [9] Aida Vosoughi, Joseph R. Cavallaro, Alan Marshall “Robust Consensus-based Cooperative Spectrum Sensing under Insistent Spectrum Sensing Data Falsification Attacks" IEEE Global Communications Conference (GLOBECOM) , 6-10 Dec. 2015.
- [10] Linyuan Zhang, Guoru Ding, Fei Song, Qiao Su “Defending Against Byzantine Attack in Cooperative Spectrum Sensing Relying on a reliable Reference” IEEE/CIC International Conference on Communications in China (ICCC), 27-29 July 2016.
- [11] Ji Wang, Ing-Ray Chen, Jeffrey J.P. Tsai, Ding-Chau Wang “Trust-based Cooperative Spectrum Sensing Against SSDF Attacks in Distributed Cognitive Radio Networks” IEEE International Workshop Technical Committee on Communications Quality and Reliability (CQR 2016), 10-12 May 2016.
- [12] CAO Long, ZHAO Hangsheng, ZHANG Jianzhao, LIU Yongxiang2 "Secure cooperative spectrum sensing based on energy efficiency under SSDF attack" IEEE International Wireless Symposium (IWS 2015), 30 march-1 April 2015.
- [13] Sasa Maric, Sam Reisenfeld, Leonardo Goratti " A Simple and Highly Effective SSDF attacks Mitigation Method" IEEE 10th International Conference on Signal Processing and Communication Systems (ICSPCS), 19-21 December 2016.
- [14] Abbas Ali Sharifi, Mir Javad Musevi Niya "Defense Against SSDF Attack in Cognitive Radio Networks: Attack-Aware Collaborative Spectrum Sensing Approach", IEEE Communications Letters, VolL. 20, NO. 1, January 2016.
- [15] Saud Althunibat, Birabwa Joanitah Denise, Fabrizio Granelli " Identification and Punishment Policies for Spectrum Sensing Data Falsification Attackers Using Delivery-Based Assessment" IEEE Transactions On Vehicular Technology, Vol. 65, No. 9, September 2016.

High quality techniques for Multiple Sequences Alignment

Shalini Mehra

Department of CSE, MITRC, Alwar, Rajasthan

Abstract—This paper describe different techniques we can use for multiple sequence alignment. we have analyze different techniques we can use and find which one is better .We have taken several example as parameter. There is different approach that we can apply in various conditions. This paper is concerned with the efficient execution Multiple sequence alignment methods in multiple client environments Multiple order alignment (MSA) is in a computational form Expensive method, which is commonly used in Large databases of computational and molecular biology Protein and gene sequences are available for scientists Community frequent, these databases are accessed to execute multiple user MSA queries Data is in server.

Keywords— multiple sequence alignment, optimization, protein and DNA, Dynamic programming, Progressive alignment construction, Genetic algorithms and simulated annealing.

I. INTRODUCTION

A multiple sequence alignment (MSA) of three or more biological sequences, generally protein, DNA, RNA, or a view of the alignment. In many cases, the input set of query sequences is evolutionary relationships by which they share a lineage and are descended from a common ancestor are assumed. From the resulting MSA, sequence homology can be inferred and phylogenetic analysis sequences shared evolutionary origins can be conducted to assess. Correct alignment as image depicting scenes of mutation events such as point mutations (single amino acid or nucleotide changes) that appear as different characters in a single alignment column, and insertion or deletion mutations illustrate (indels or gaps) that appear as hyphens in one or more of the sequences in the alignment. Multiple sequence alignment often protein domains, tertiary and secondary structures, and even individual amino acids or nucleotides in the sequence is used to access protection.

Multiple sequence alignment process of aligning such a sequence set shows. MSAs require more sophisticated way than pairwise alignment because they are more

computationally complex. Most multiple sequence alignment programs, more than a few shots of medium length because identifying the optimal alignment heuristic methods rather than global optimization is extremely computationally expensive.

Dynamic programming and computational complexity

A direct method for producing an MSA uses dynamic programming technique to identify the globally optimal alignment solution. A gap penalty and a substitution matrix of amino acids' chemical properties and the evolutionary probability based on the similarity of the amino acid or the possibility of assigning a score to each possible alignment couple: For protein, this method usually involves two sets of parameters change. For nucleotide sequences a similar gap penalty is used, but a very simple substitution matrix, which corresponds only and is incompatible, is typical. Substitution matrix score in either all positive or a mixture of positive and negative in the case of a global alignment is, however, should be both positive and negative in the case of a local alignment. Commonly used to measure computational complexity with big O notation expresses a naïve MSA $O(\text{Length}N_{\text{seqs}})$ takes time to produce. N sequences for global optimal way is shown to be an NP-complete problem are to find. In 1989, Carrillo- based on Lipman algorithm, Altschul is a practical method that uses pairwise alignments to constrain the n-dimensional search space presented. In this approach pair wise dynamic programming alignments are performed on each pair of sequences in the query set, and only the alignment of the N-dimensional space near the intersection en route alignment is searched for. The MSA program in alignment each position (the so-called sum pair score) the sum of all of the pairs of characters and multiple sequence alignment, optimize building has been implemented in a software program emented in a software program for constructing multiple sequence alignments.

II. ITERATIVE METHODS

A set of methods to produce MSAs while reducing the errors inherent in progressive methods as "walk" are

classified because they work similarly to progressive methods but repeatedly the initial scenes as well as to organize new scenes add to the growing MSA. is not considered further. This approximation improves efficiency at the expense of accuracy. Easily applied to a variety of different ways to walk and is made available in software packages; Review and comparison is useful, but typically a "best" technique should avoid choosing. Software package PRRN / PRRP its MSA alignment score to optimize the use of a hill climbing algorithm and iteratively both alignment weights and locally different or "incomplete" the growing areas of MSA. When refining an alignment previously constructed by a faster method performs best PRRP.

Another running program, DIALIGN, without introducing a gap penalty Berry sub-segments or sequence to focus narrowly on the local alignment takes an unusual approach. The alignment of individual motifs, a dot matrix plot in a pairwise alignment similar to that achieved with a matrix representation. An alternative way to fast local alignments as anchor points or for a slower global alignment process "seed" that uses the chaos / DIALIGN suite is implemented. A third popular iteration method based muscle (Log expectation multiple sequence alignment), a more accurate distance measure to assess the association of two scenes with the progressive improvement of the methods cited. The distance measure is updated between iteration stages (although, in its original form, depending on the muscle that was able refinement contained only 2-3 iterations).

Consensus methods

The consensus sequences of the same set of methods have many different alignments try to find the optimal multiple sequence alignment. There are two commonly used methods of consensus, M-Coffee and MergeAlign. M-coffee from seven different ways to generate multiple sequence alignment alignment consensus uses. MergeAlign sequence development or various models of multiple sequence alignments generated using different methods of input from any number of alignment alignment consensus is capable of generating. MergeAlign default options for developing the protein sequence alignment generated using 91 different models using an alignment consensus estimates.

Hidden Markov models

Hidden Markov models are probabilistic models that gap, can assign likelihoods to all possible combinations of matches and mismatches to determine the most likely MSA or set of possible MSAs are. HMMs can produce both global and local alignment. Although HMM-based methods have been developed relatively recently, they specifically

for sequences that contain overlapping areas offer significant improvements in computational speed typical HMM-based methods directed acyclic MSA possible entries in the columns of an MSA, which consists of a series of nodes representing a partial order graph, known as the graph representing it as a form of work. in the next column possible characters alignment. In terms of a typical hidden Markov model, the observed state individual alignment columns and the "hidden" states represent the presumed ancestral sequence from which the sequences in the query set are hypothesized to have landed. An efficient search variant of the dynamic programming method, Viterbi algorithm is known as, generally subsequent query set to produce a new MSA to the next scene in the growing line is used for MSA .Because the alignment of prior sequences is updated at each new addition to the scene is different from progressive alignment methods. However, like progressive methods, this technology sets the order in which the query sequences are integrated into alignment, especially when the sequences are distantly related can be affected.

Genetic algorithms and simulated annealing

Standard optimization techniques in computer science - both of which were inspired by, but directly not reproduce the physical processes - even more efficiently produce quality MSAs have been used in an attempt to. One such technique, genetic algorithms, an attempt is roughly estimated that the evolutionary process has lead to divergence in the query set to emulate the MSA has been used for production. Method possible MSAs into fragments and repeatedly breaking a series of different positions by rearranging those fragments with the introduction of interval functions. A general objective function is optimized during the simulation, most generally, "added amount" maximum function introduced in dynamic programming-based MSA methods. A technique for protein sequences software Saga (by genetic sequence alignment algorithm) and has been applied to its counterpart in the RNA is called passion.

ATATATAT -

||| ||| |

- TATATATA

Alignment of ATATATAT against TATATATA.

The technique of simulated annealing is another method by which an existing MSA produced by an input alignment already occupies space better than the alignment designed to find areas is refined by a series of rearrangements. Like the genetic algorithm method, simulated annealing sum-Of-pairs function maximizes an objective function. A simulated annealing symbolic "C" factor that the rate at

which rearrangements proceed and determine the likelihood of each rearrangement uses; to find out. This approach program MSASA (simulated annealing multiple sequence alignment) has been implemented in.

Non-Coding Multiple Sequence Alignment

Non-coding DNA regions, especially TFBSs, but not necessarily more protected and are evolutionarily related, and may be associated with a non-common ancestor. Thus, the protein-coding regions of DNA sequences and the assumptions used in line with those that hold for TFBS sequences are inherently different have little meaning for the TFBS sequences. This is especially important when the same TFBS monitoring model to predict the unknown places known to be trying to align the sequences TFBS. Therefore, multiple sequence alignment methods and working hypothesis underlying evolutionary basis neighbor thermodynamic information binding site, Edna's lowest thermodynamic binding sites for the alignment of the line for the protection of exclusivity to include use as operators adjust published need to.

Alignment visualization and quality control

Necessary use of heuristics for multiple alignment means an arbitrary set of proteins, there is always a good chance that an alignment will contain errors is. For example, evaluation of programs using key benchmark alignment BALiBase coalition found that at least 24% of all pairs of amino acids were aligned incorrectly. As the number of sequence divergence increases and many more errors because of the nature simply will MSA heuristic algorithms. Multiple sequence alignment audience visually, often two or more views to be reviewed and annotated functional sites inspected by the quality of the alignment enable alignment. Many also be edited in order to enable an optimal alignment 'curated' alignment suitable for use in phylogenetic analysis or comparative modeling to achieve these (usually minor) to correct errors.

Use in phylogenetics

Multiple sequence alignments can be used to create a phylogenetic tree. This is made possible by two factors. The first is known as the functional domain that annotated sequences in non-annotated sequences can be used for alignment. The other is known to be functionally important protected areas can be found. This makes it possible to analyze multiple sequence alignment and symmetry through the evolutionary relationships between the sequences to be used to find. Point mutations and insertion or deletion events (called indels) can be detected.

Multiple sequence alignment such binding sites, active sites, or sites similar to other important tasks, such as by applying protected domain to identify functionally important sites can be used. When multiple sequence alignment, looking at different aspects of the scenery when the scenery than useful. Identifying these aspects, equality, and compliance are included. Means of identification of the remains that have similar views on their respective positions. On the other hand, the similarity with the sequences being compared quantitatively similar to what remains. For example, in the case of nucleotide sequences, pyrimidines are considered similar to each other, as are purines. Eventually equality, in conformity leads to scenes that are more similar, they are close to being homologous. This similarity in views can go to for help finding the common ancestry.

III. CONCLUSION

Multiple Sequence Alignment is an extension of Junk alignment to include more than two scenes at one time. Many of our alignment methods try to align all the sequences in a given query set. Efficient fitness value function, crossover and mutation strategy is the result of work. After all, it is trying that our methods will be greatly contributed to the efficient solution of many sequence alignment problems.

REFERENCES

- [1] S. Altschul, W. Gish, W. Miller, E. Myers, and D. Lipman. Basic local alignment search tool. *J. Mol. Biol.*, 215(3):403–410, Oct 1990.
- [2] H. Andrade, T. Kurc, A. Sussman, and J. Saltz. Efficient execution of multiple workloads in data analysis applications. In *Proceedings of the 2001 ACM/IEEE SC'01 Conference*, Denver, CO, Nov. 2001.
- [3] H. Andrade, T. Kurc, A. Sussman, and J. Saltz. Scheduling multiple data visualization query workloads on a shared memory machine. Technical Report CS-TR-4290 and UMIACS-TR-2001-68, University of Maryland, Department of Computer Science and UMIACS, Oct. 2001. Submitted to IPDPS 2002.
- [4] M. D. Beynon, T. Kurc, U. Catalyurek, C. Chang, A. Sussman, and J. Saltz. Distributed processing of very large datasets with DataCutter. *Parallel Computing*, 27(11):1457–1478, Oct. 2001.
- [5] U. S. Chakravarthy and J. Minker. Multiple query processing in deductive databases using query graphs. In *Proceedings of the 12th VLDB Conference*, pages 384–391, 1986.

- [6] Kuipers RK, Joosten HJ, van Berkel WJ, et al. 3DM: systematic analysis of heterogeneous superfamily data to discover proteinfunctionalities. *Proteins*. 2010,78:2101–2113.
- [7] Kim J, Ma J. PSAR: measuring multiple sequence alignment reliability by probabilistic sampling. *Nucl Acids Res*. 2011,39(15):6359–6368.

Design of High Performance and Energy Efficient Explicit Pulsed Sense Amplifier Based Flip-Flop

Priyanka Sharma

Assistant Professor, Department of Electronics and Communication, Swami Keshvanand Institute of Technology Management & Gramothan, Jaipur, India

Abstract— In this paper, we have presented a new design of explicit pulsed sense amplifier based flip-flop (SAFF) which gives high performance parameters. The most important factors need to be considered while designing efficient circuits are low power with less delay. Our proposed design attracted these performance parameters due to its design using GDI technique. Different topologies along with their layout simulations have been compared with respect to power consumption, delay and temperature sustainability in order to prove the superiority of proposed design. The simulation has been carried out on Tanner EDA tool on BSIM3v3 45nm technology.

Keywords— Explicit pulsed SAFF, GDI Technique, latch topology, low power, delay, Power consumption, Dual edge triggered flip flops, sense-amplifier, Tanner EDA.

I. INTRODUCTION

With the increasing demand for high-performance and energy efficient memory devices, there is a lot of attraction in the design work towards meeting the above requirements. An explicit-pulsed flip-flop is used for critical paths due to its energy efficient feature. All simulations have been carried out on Tanner EDA Tool on BSIM3v3 45 nm technology. Using GDI technique, SAFF-GDI latch is simulated first, there after we have modified it by adding explicit pulse to trigger it which is shown as explicit pulsed SAFF-GDI latch.

II. SAFF USING GDI TECHNIQUE

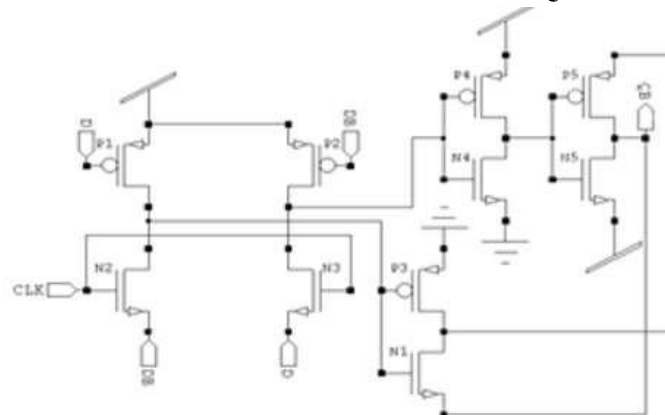


Fig.1: Schematic of SAFF-GDI latch

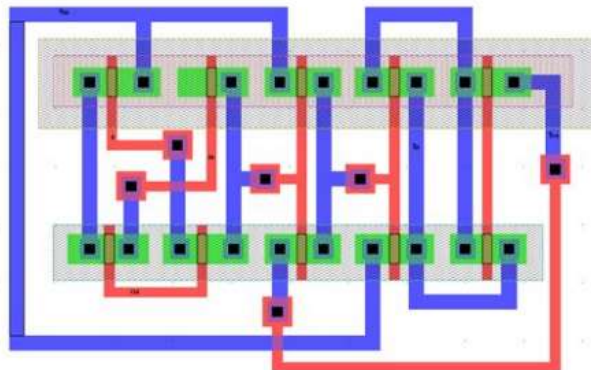


Fig.2: SAFF-GDI latch layout

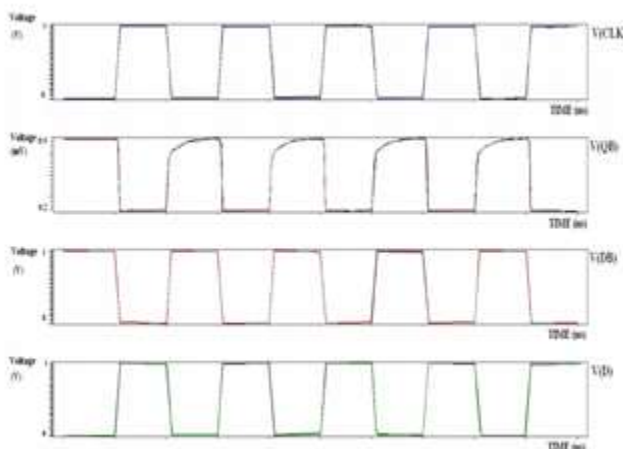


Fig.3: Waveforms of SAFF-GDI latch

Explicit pulsed proposed SAFF

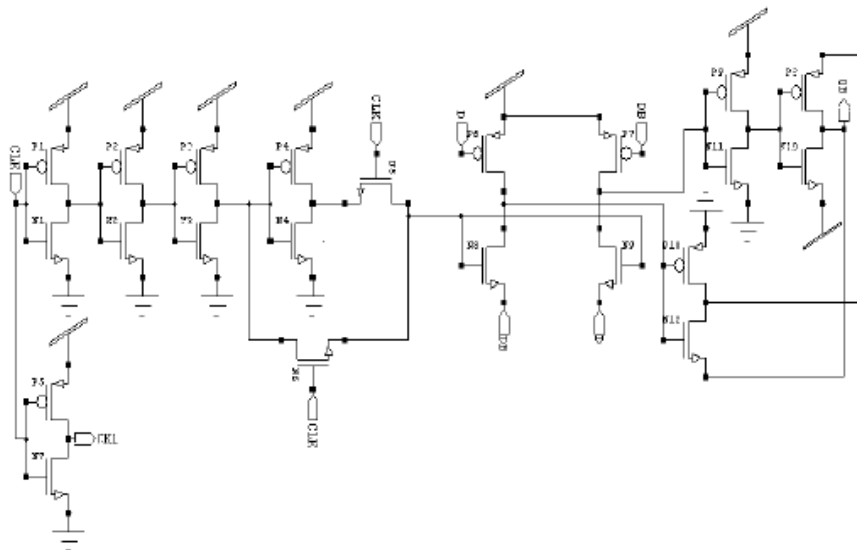


Fig.4: Schematic of Explicit pulsed proposed SAFF

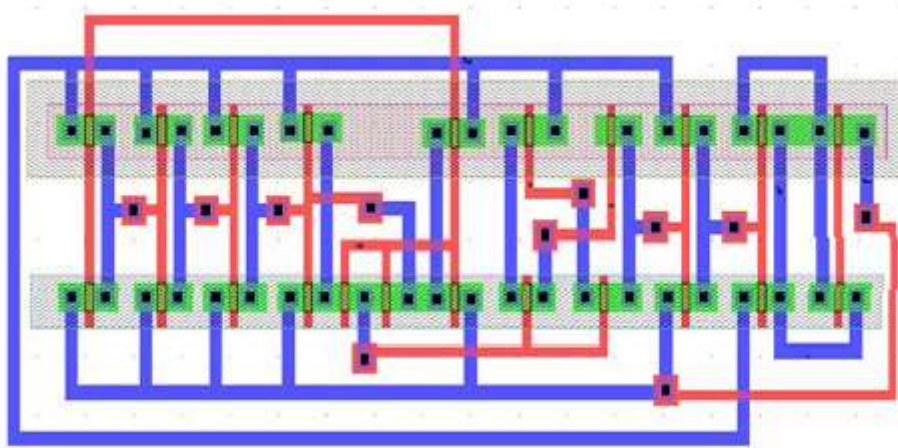


Fig.5: Explicit pulsed proposed SAFF layout

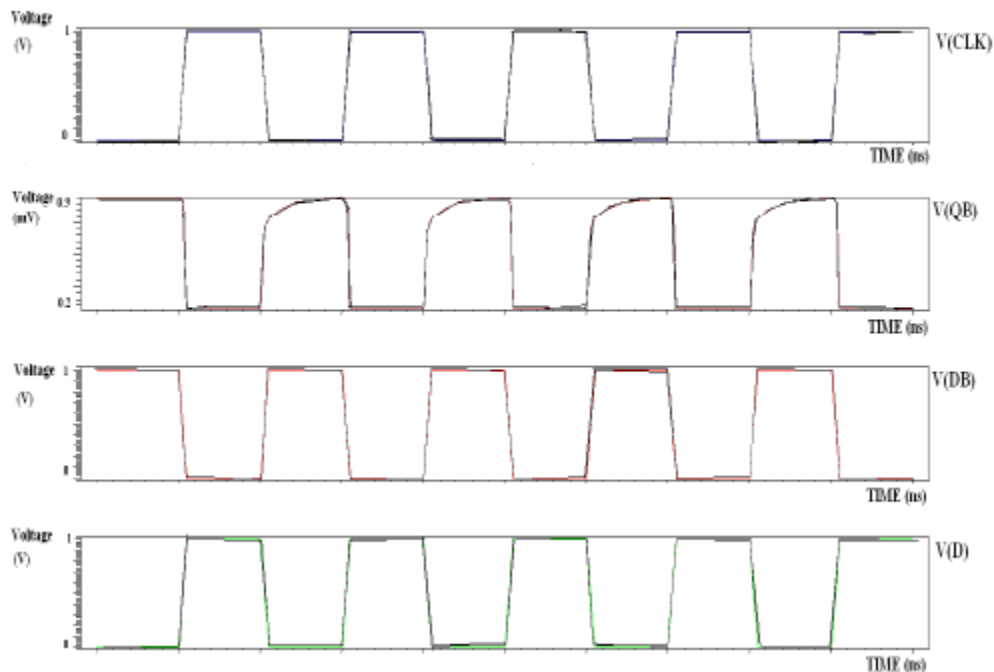


Fig.6: Waveforms of Explicit pulsed proposed SAFF

Explicit pulsed design of proposed SAFF is beneficial in that case when there are numerous neighboring SAFF's. Only one pulse generator, embedded on single chip, is sufficient to give power supply to entire chip.

III. SIMULATION AND COMPARISON

Simulation Environment:

All the circuits have been simulated using BSIM3v3 45 nm technology on Tanner EDA tool. To make the impartial testing environment, all the circuits have been simulated on the same input patterns. All experimental results for

temperature, frequencies and supply voltages are carried out at $V_{DD}=1.25$ V.

Pre-Layout Simulation of Explicit pulsed proposed SAFF (EP SAFF):

Pre-layout simulation graphs for explicit pulsed proposed SAFF are given below. Fig. 7 shows power consumption variation versus temperature. Fig.8-12 show delay variation, power consumption variation versus supply voltage, delay variation versus frequency, power consumption and delay variation versus output load capacitance respectively.

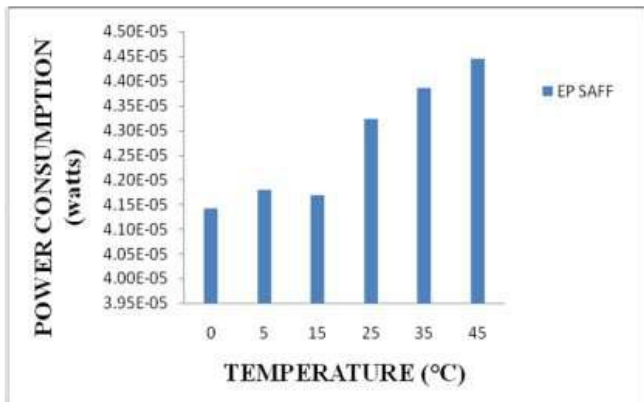


Fig.7: Power consumption variation over different operating ranges of temperature

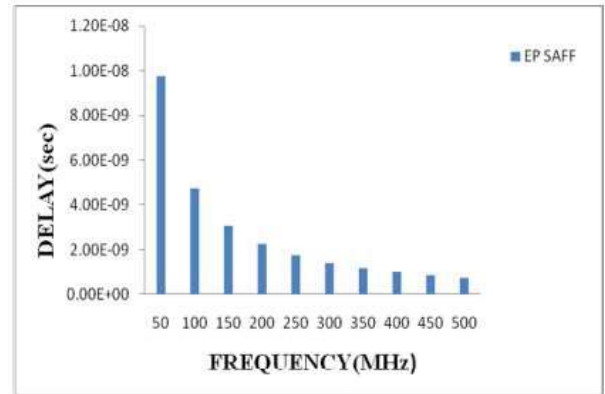


Fig.10: Delay variation over different operating ranges of frequency

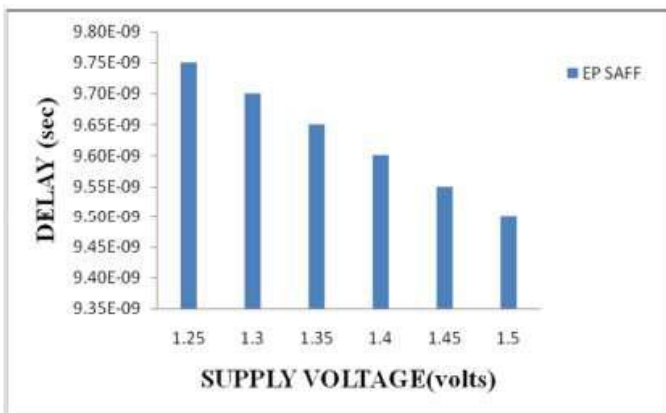


Fig.8: Delay variation over different operating ranges of supply voltage

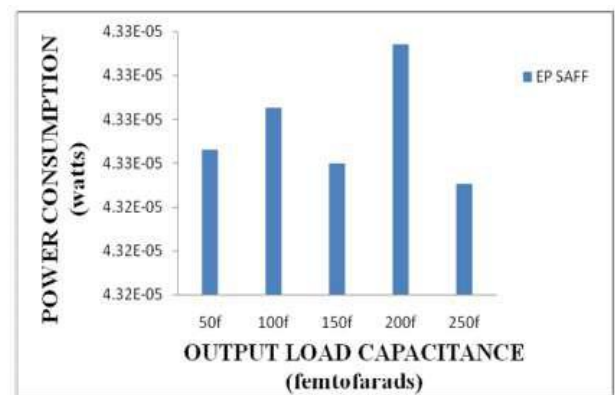


Fig.11: Power consumption variation over different values of output load capacitance

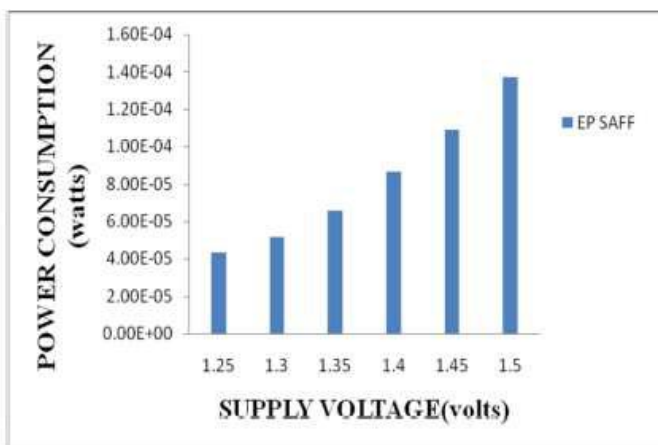


Fig.9: Power consumption variation over different operating ranges of supply voltage

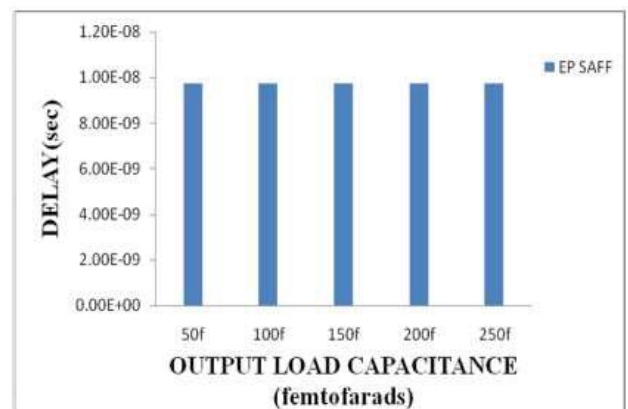


Fig.12: Delay variation over different values of output load capacitance

Post Layout Simulation of Explicit pulsed proposed SAFF:

Post-layout simulation results are shown with the help of following graphs. Fig.13 shows power consumption variation over different operating ranges of temperature.

Power consumption is almost constant with temperature because of same order. Fig.14-15 shows power consumption and delay variation with supply voltage respectively. Fig.16 shows power consumption variation with frequency. Power consumption is continuously increasing with increase in frequency. Fig. 17 shows delay variation with respect to frequency.

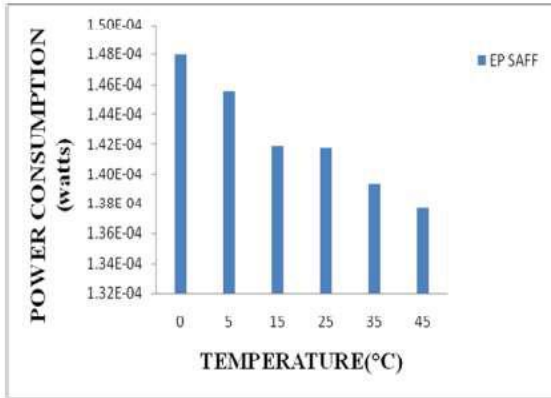


Fig.13: Power consumption variation over different operating ranges of temperature

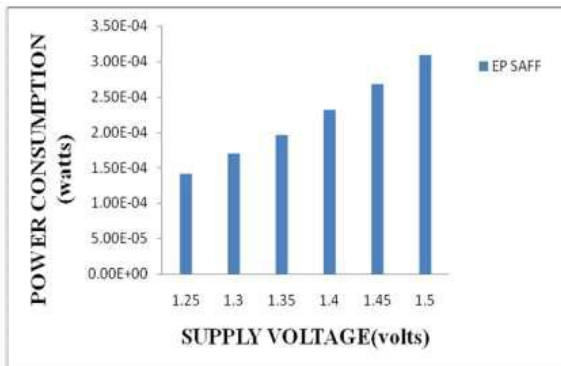


Fig.14: Power consumption variation over different operating ranges of supply voltage

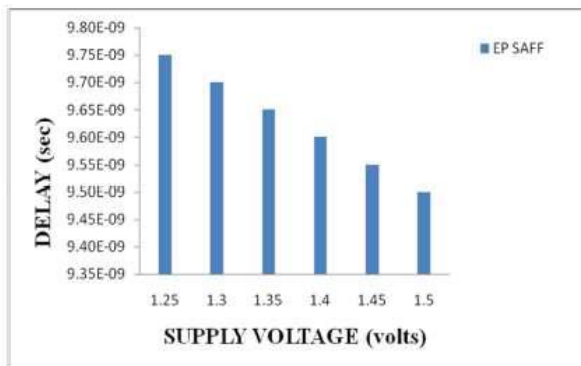


Fig.15: Delay variation over different operating ranges of supply voltage

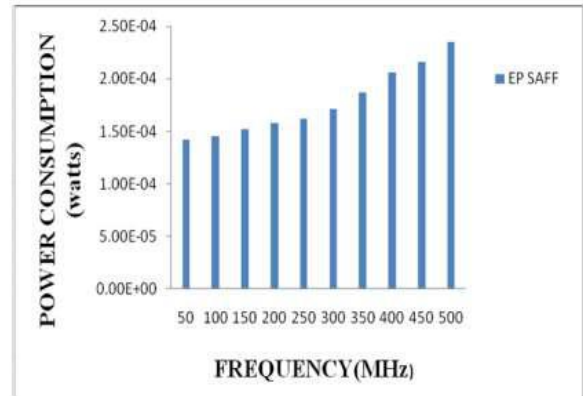


Fig.16: Power consumption variation over different operating ranges of frequency

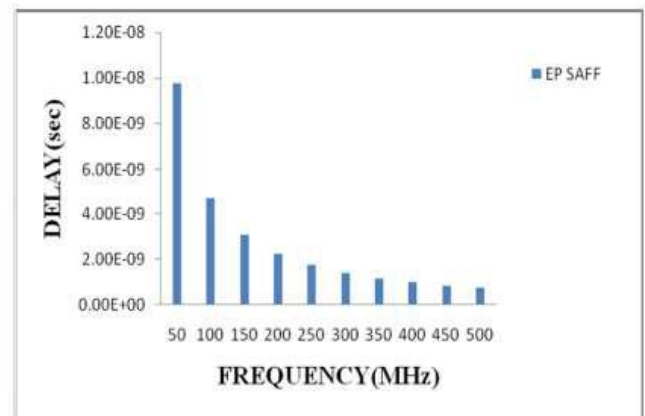


Fig.17: Delay variation over different operating ranges of frequency

At last, we designed explicit pulsed proposed SAFF and analyzed its simulation results.

IV. CONCLUSION

In this paper, we have proposed an explicit pulsed SAFF-GDI latch and compared it with implicit pulsed SAFF-GDI latch on the basis of its performance parameters i.e power consumption and delay over a wide range of temperature, supply voltages and frequencies. With the help of simulation results, it is proved that our proposed design of explicit pulsed SAFF is high performance and energy efficient over that of implicit pulsed SAFF-GDI latch.

ACKNOWLEDGMENT

The authors would like to thank Mody Institute of Technology & Science, Laxmangarh for supporting in carrying out this work.

REFERENCES

- [1] A. Chandrakasan and R. Brodersen, Low-Power CMOS Design, IEEE Press, 1998, pp. 233-238.
- [2] N. H. Weste and K. Eshragian, Principles of CMOS VLSI Design: A Systems Perspective, 2nd ed. Reading, MA: Addison-Wesley, 1994.
- [3] M. Pedram, Q. Wu, and X. Wu, "A new design of double edge triggered flip-flops," in Design Automation Conference, Asia and South Pacific, pp. 417-421, 1998.
- [4] B. Nikolic', V. G. Oklobd'zija, V. Stojanovic', W. Jia, J. Chiu, and M. Leung, "Sense amplifier-based flip-flop," in IEEE Int. Solid-State Circuits Conf. Dig. Tech. Papers, Feb. 1999, pp. 282-283.
- [5] J. Tschanz, S. Narendra, Z. P. Chen, S. Borkar, M. Sachdev, and V. De, "Comparative delay and energy of single edge-triggered & dual edge triggered pulsed flip-flops for high performance microprocessors," in IEEE. Int. Symp. Low Power Electronics and Design, ISLPED Huntington Beach, pp. 147-152, 2001.
- [6] Priyanka Sharma, Neha Arora, Prof. B. P .Singh "Design of Efficient Sense Amplifier based Flip-flop using GDI Technique", International Journal of Scientific and Engineering Research, Volume 3, Issue 5, May 2012 Edition, (ISSN 2229-5518)
- [7] Priyanka Sharma, Neha Arora, Prof. B. P .Singh "Low Power Different Sense Amplifier Based Flip-flop Configurations implemented using GDI Technique", International Journal of Scientific and Research Publications, Volume 2, Issue 4, April 2012, (ISSN 2250-3153) flops for low-power systems," in Proc. Int. Symp. Low-Power Electronics and Design, Monterey, CA, Aug. 10-12, 1998, pp. 227-232.
- [8] H. Partovi et al., "Flow-through latch and edge-triggered flip-flop hybrid elements," ISSCC Dig. Tech. Papers, pp. 138-139, Feb. 1996.
- [9] C. Svensson and J. Yuan, "Latches and flip-flops for low power systems," in Low Power CMOS Design, A. Chandrakasan and R. Brodersen, Eds. Piscataway, NJ: IEEE Press, 1998, pp. 233-238.
- [10] M. Pedram, Q. Wu, and X. Wu, "A new design of double edge triggered flip-flops," in Design Automation Conference, Asia and South Pacific, pp. 417-421, 1998.

Effects of Refinery Processes on the Quality of Various Water Samples from Kaduna Refinery and Petrochemical Company (KRPC) Limited

C.T.Onyema*, J.J. Ilebaye

Pure and Industrial Chemistry Department, Nnamdi Azikiwe University, Awka, Anambra State, Nigeria
ct.onyema@unizik.edu.ng* and josephilebaye25@gmail.com

Abstract— *Effects of refinery processes on the quality of various water samples from Kaduna Refinery and Petrochemical Company (KRPC) Limited was investigated. Water quality assessment was carried out on samples collected at different water treatment sampling points in the refinery. The physicochemical parameters and other forms of analytical processes used in the work were of the standards of American Standards of Testing Materials (ASTM) and American Public Health Association (APHA) using spectrophotometric and volumetric methods. Results obtained showed that the quality of water samples subjected to treatment at each water treatment section in KRPC during the course of study was acceptable from physicochemical parameters assessed and may not be injurious to the boiler and its other end uses. Also, result of the pre and post refinery operations on cooling water sample assessed showed the significant effect the refinery operation had on the cooling water.*

Keywords— *Refinery, water quality, Water treatment, Heavy metals, Kaduna refinery, ASTM and APHA.*

I. INTRODUCTION

Water is a liquid without colour, smell or taste that falls as rain, in lakes, rivers and seas and is used for drinking, washing and a host of other industrial processes (Hornby, 1987). Water has a freezing point of 0°C, boiling point of 100°C, maximum density of 1g/cm³ at 4 °C and it's neutral to litmus paper (Jones and Atkins, 2002). It is chemically composed of hydrogen and oxygen in the ratio of 2:1. An essential and indispensable element/resource in nearly all industrial processes (Lorch, 1987). In industrial sectors such as petroleum refinery, food and beverage or pharmaceutical production, water is either used as a primary product or in the area of cooling, steam generation or boiler feed systems. Using water in the industrial environment requires consistently high water quality with adequate physicochemical parameters which is achieved by treatment

at each stage of its usage (Dara, 1995). Water treatment is the process of converting raw water from surface or sub-surface source into a portable form that is suitable for drinking, domestic and industrial uses (Ojo *et al.*, 2012). The water for the production processes and for vital services must be of high quality, equivalent to the drinking water. For the boilers and some production processes, the water must be additionally demineralized (Aderogba, 2011).

Kaduna Refinery and Petrochemical Company (KRPC) was established for the purpose of refining crude oil into Premium Motor Spirit (PMS) and other petrochemical products with the view of providing fuels for automobile engines and other outputs, without threatening environmental safety (Ahmad, 2014). The process of refining crude oil consumes large amounts of water. It is used in varying quantities and ways in all stages/processes of production in the refinery as its operation is highly dependent on adequate supply of water. Refinery water needs to be treated before being used in different processes and the type of treatment depends on the quality of the source water and its ultimate use in the refinery. Turbidity, sediments and hardness are examples of source water constituents that may require treatment. The raw water comes from River Kaduna but undergoes various purification stages such as coagulation and filtration before usage. Subsequent treatment will depend on the ultimate use for each water system (Aderogba, 2011).

This study therefore seeks to comparatively ascertain the physicochemical and heavy metals characteristics of the various treated refinery water samples, pre and post refinery operations on cooling water.

II. MATERIALS AND METHODS

2.1 Description of study area

The study area is KRPC which is located at Chukun Local Government Area of Kaduna State, Nigeria. It lies between latitudes 10° to 11° North and longitudes 7° to 8° east.

KRPC facility lies between latitudes 10° 24' 36.18"N and longitudes 7° 29'17.37"E. The facility occupies approximately 1.8 square Kilometers; about 7% of the total area of the region.

The study area was initially characterized by over 80% agricultural land uses. River Romi is one of the tributaries of River Rigasa, it is the largest river in the study area which adds to drain the region into the Kaduna River system. The provision of disposing refinery liquid waste into River Romi was one of the reasons why the refinery was located in the Rido region.

2.2 Samples collection

Water samples from different treatment/sampling units in KRPC stipulated as follows: raw, filtered, demineralized, boiler and cooling were collected with a 2 litre plastic water sampler and transferred to a clean 2 litre polyethylene containers, properly labelled and taken to the refinery quality control laboratory for analysis. The raw, filtered, demineralized and boiler feed water samples were collected for physico-chemical examination while the cooling and water samples were collected for analysis/comparison of pre

and post refining operation. All other quality control procedures relevant to samples collection, preservation and analyses were strictly adhered to for the determination of physicochemical parameters and heavy metals content.

2.3 Physico-chemical examination

The physico-chemical parameters were determined according to procedures outlined in the Standard Method for the Examination of Water and Waste Water (APHA, 1998 and 1992) and American Society for Testing Material (1990). The parameters analyzed are those believed to have effects on water quality and referred to by WHO (2008) and FMEnv. (2007). These parameters are Conductivity measured using Conductivity meter (HI 2300), pH and Temperature were measured using HACH pH meter, Turbidity was measured using Turbidimeter (HI 88713-ISO), Silica content and Phosphate were analysed using Spectrophotometer (Hach DR/2010 and Hach DR 2800), Total alkalinity by titration with HCl and Hardness by complexometric titration. A Perkin Elmer model 2380 Atomic Absorption Spectrophotometer was used for the determination of some heavy metals.

III. RESULTS AND DISCUSSION

Table.1: Results of the physico-chemical parameters of treated water samples in Kaduna Refinery and Petrochemical Company

Parameters	Raw	Filtered	Demineralized	Boiler
pH	7.69±0.01	6.61±0.01	8.02±0.006	10.25±0.03
Temp. (°C)	25.33±0.58	26.5±0.36	27.3±0.10	26.07±0.15
Turb. (ntu)	82.27±0.23	0.44±0.03	0.02±0.006	
Cond. (us/cm)	52.43±0.12	59.07±0.32	0.57±0.06	12.13±0.23
Silica (ppm)	8.13±0.12	4.73±0.06	0.07±0.01	1.15±0.13
Alkalinity (ppm)	62.33±0.58	74.0±1.00	24.00±1.00	19.01±0.02
Tot. Hardness (ppm)	46.90±1.01	32.93±1.007	19.53±2.16	27.8±0.20
Ca. Hardness (ppm)	45.07±0.90	25.67±0.58	16.33±0.58	13.37±2.28
Mg. Hardness (ppm)	18.33±1.53	7.27±0.64	3.20±1.59	14.43±2.11
PO ₄ ³⁻ (ppm)	ND	ND	3.76±0.02	2.77±0.12
ND = Not done.				

The physico-chemical parameters of the water samples treated at each water treatment section in Kaduna Refinery and Petrochemical Company were investigated and the level of treatment estimated. The result of the analysis as shown in Table 1 shows that the average pH of the raw water sample is slightly alkaline (7.69). This is in line with the neutral (pH 7) or slightly alkaline (pH 8) permissible levels for pH value for stream water or natural water as set by World Health Organization (WHO). The pH of the filtered

water sample was observed to be acidic (6.61). These significant change in pH maybe attributed to the preliminary treatment of the raw water by addition of poly-aluminiumchloride, a coagulant whose dosage is pH dependent (Jowa and Liberty, 2015). The average pH of the assessed demineralized and boiler water were found to be 8.02 and 10.25 respectively. The subsequent increase in pH of the demineralized water to the basic medium is due to the addition of tri-sodium phosphate (a buffer) which help to

regulate the pH to meet the requirements of the boiler. The irregular trend and required degree of water pH control depends on the particular use as the pH which measures the acidity or alkalinity (basicity) of any water is one of the most important determination in water chemistry because many of the processes involved in water treatment are pH dependent (Lateef, 2004).

The study also revealed that the average turbidity of the raw water is 82.27 ntu. The high turbidity value obtained might be as a result of dissolution of organic wastes such as faeces and other nitrogenous wastes being discharged by some villagers inhabiting the area of the source water. Another natural primary cause of the turbidity of source water is silt, which consists of suspended minerals particles resulting from land erosion and other dissolved solids. The turbidity of the filtered water is 0.44 ntu. These significant decrease in turbidity from raw to filtered water along the treatment line is due to the addition of poly aluminium chloride (PAC), a coagulant which accounts for 99% turbidity removal (Jowa and Liberty, 2015). Also, the turbidity of the demineralized water is 0.02 ntu. These significant variation in turbidity as compared to the filtered water is attributed to its treatment by Ion exchange which is a reversible chemical reaction where positively or negatively charged ions present in the water are replaced by similarly charged ions present within the resin, thus removes both suspended and dissolved solids. Turbidity level is an important water quality criteria as it makes water cloudy and deposits in water lines and process equipment such as boilers in the refinery. Its complete elimination at the boiler as observed in Table 1 is due to water preliminary treatment by filtration and ion exchange to meet the requirement of the boiler as its presence may be injurious to the boiler (Odigure *et al.*, 2005). The average conductivity value of the raw water is 52.43 us/cm. These value increased slightly to 59.07 us/cm following filtration. Subsequent treatment by demineralization led to a significant decrease in conductivity value to 0.57 us/cm. This is possible as processes such as ion exchange which decreases dissolved solids content will decrease conductivity to a large extent. Conductivity is the measurement of the ability of a solution to carry electric current. Since this ability depends on ions or ionizable solids in solution, a conductivity measurement is an excellent indicator of the total dissolved solids in water (Jernand Wun, 2006). Hence, high conductivity can increase the corrosive characteristics of water in the refinery.

The study also showed that the average silica content of the raw water is 8.13 ppm which reveals the level of suspended solids in the raw water sample. Its presence in the source water maybe attributed to minerals such as sodium feldsparalbite ($\text{NaAlSi}_3\text{O}_8$) present due to erosion of rocks, atmospheric precipitation and industrial sewage and these maybe harmful to the refining plant. Subsequent treatment by filtration decreased the silica content to 4.73 ppm. This is attributed to the dual media filters which comprised of a layer of anthracite over sand where the larger solid particles are trapped by the anthracite and the finer solids are held up in the sand. Also, the silica content of the demineralized water is 0.07 ppm. These significant decrease is due to treatment by ion exchange following filtration. Silica which if allowed to pass with the water as boiler feed will deposit on boiler tubes which form resistance to efficient heat transfer, scaling on heating, cooling equipment and pipelines (Aderogba, 2011). Hence, silica content assessment is an important water treatment quality criteria.

The alkalinity of the raw water is 62.33 ppm. These value which determine a stream's buffering capacity is within the WHO permissible limit of 32-118 mg/l. Also, a slight increase (74.0 ppm) was recorded upon filtration which fluctuate to 24.00 ppm following demineralization by ion exchange. These irregular trend / fluctuation in alkalinity of water samples along the treatment line maybe due to the chemicals used in water treatment such as poly-aluminium chloride, tri-sodium phosphate and others which causes changes in alkalinity. Determining alkalinity is required when calculating chemical dosages for coagulation (Jowa and Liberty, 2015). It's also an important parameter in water treatment in refinery as it causes foaming in steam systems and attacks boiler steel.

The study also revealed that the average total hardness of the raw water is 46.90 ppm. This is due to the source water coming in contact with limestone (CaCO_3) or dolomite ($\text{CaCO}_3 \cdot \text{MgCO}_3$), as such picks up calcium ions and magnesium ions which makes it too hard for refinery use. Following subsequent treatment by ion exchange, total hardness of the demineralized water was observed to be 19.53 ppm. These subsequent variation was due to treatment by ion exchange where the mobile hydrated ions of solid are exchanged equivalently with ions of same charge in the water (Walter, 1981). Sodium and Hydrogen cation exchange process are the methods employed in KRPC as hardness is the primary source of scale formation in heat exchangers and pipelines.

Table.2: Heavy metals result of treated water samples in Kaduna Refinery and Petrochemical Company

Parameters	Raw	Filtered	Demineralized	Boiler
------------	-----	----------	---------------	--------

(ppm)				
V	0.00±0.00	0.00±0.00	0.00±0.00	0.00±0.00
Pb	0.05±8.49	0.04±0.00	0.01±0.006	0.01±0.00
Zn	0.18±0.01	0.10±0.006	0.01±0.00	0.00±0.00
Fe	0.74±0.01	0.63±0.02	0.23±0.01	0.44±0.02
Cd	0.00±0.00	0.02±0.01	0.01±0.006	0.05±0.02
Cu	0.03±0.006	0.00±0.00	0.00±0.00	0.00±0.00
Ni	0.00±0.00	0.00±0.00	0.00±0.00	0.00±0.00
Cr	0.00±0.00	0.00±0.00	0.00±0.00	0.00±0.00

Table 2 shows that Vanadium, Nickel and chromium were not detected in the source water sample (raw water) and water samples along the water treatment line (Filtered, demineralized and boiler water). The average concentration of K, Fe and Zn in the source water sample were 9.64 ppm, 0.74 ppm and 0.18 ppm respectively. The reason for the high concentration of these metals in the source water maybe attributed to the erosion of minerals from rocks and soil, forest fire runoff, industrial and agricultural sewage (Cohen, 1960). The low concentration of Pb in the source water as shown in table 2 is a plus as the Kaduna River is expected to be polluted with less Pb concentrations and devoid of its associated problems. There was a significant decrease in the concentration of these heavy metal in the source water following filtration and demineralization

processes as given in table 2. This is attributed to the use of dual filter media and ion exchange in these treatment processes which effectively removes heavy metals (Marcovecchio,2007).The appearance of Cd in the filtered water which was originally absent in the raw water sample could be as a result of the leaching out of Cd from the sand bed into the water. In summary, there was a significant decrease in the level of the metals originally present in the source water sample and the level at each water treatment section in the plant. These could be attributed to the treatment processes they undergo except for cadmium which was spotted along the water treatment process line and the random trend in Fe and K that both increased at the boiler after initial continual decreasing trend.

Table.3: Results of physico-chemical parameters of the pre and post refinery water sample from KRPC

Parameters	CBR	CAR
pH	8.41±0.01	7.74±0.005
Temp. (0°)	21.53±0.31	29.10±0.30
Turb. (ntu)	9.52±0.03	33.67±1.15
Cond. (us/cm)	295.67±0.58	293.67±2.31
Silica (ppm)	7.10±0.10	54.67±1.15
Alkalinity (ppm)	62.13±0.23	203.0±4.36
Tot. Hardness (ppm)	71.10±0.006	134.83±1.04
Ca. Hardness (ppm)	65.72±0.03	95.33±0.58
Mg. Hardness (ppm)	5.39±0.02	39.5±0.50
PO ₄ ³⁻ (ppm)	4.57±0.12	4.57±0.06

CBR= Cooling water before refining. CAR= Cooling water after refining / Cooling effluent. ND= Not done.

In this study, it was also observed from Table 3 that after refining operation, there was a significant increase in temperature (29.10 °C), turbidity (33.67 ntu), silica content (54.67 ppm), alkalinity (203.0 ppm) and total hardness (134.83 ppm) of the cooling effluent as compared to the temp. (21.53 °C), turbidity (9.52 ntu), silica content (7.10 ppm), alkalinity (62.13 ppm) and total hardness (71.10

ppm) of the cooling water sample before refining. The sharp increase in the temperature may be as a result of heat from cooling since the water is being used in exchanger units to reduce heat to between 80-90 °C. Otherwise, the exchanger gets defective during the refining operations. The increase in turbidity could be attributed to the exchange of turbid content alongside heat from petroleum products after its

usage. Also, the increase in alkalinity, total hardness, silica content could be attributed to the chemicals such as orthophosphate, silicate, bicarbonate and calcium carbonate which act as inhibitors dosed to the cooling water samples

before refining operations/usage. These chemicals are essential for effective scaling, corrosion and fouling control which can hamper the operation of plant equipment or contribute to its deterioration after usage.

Table.4: Results of heavy metal content of the pre and post refinery operations cooling water sample from KRPC

Parameters (ppm)	CBR	CAR
V	0.00±0.00	0.00±0.00
Pb	0.03±0.01	0.12±0.02
Zn	0.19±0.02	0.37±0.01
Fe	0.31±0.20	0.61±0.01
Cd	0.00±0.00	0.00±0.00
Cu	0.01±0.006	0.05±8.50
Ni	0.14±0.006	0.20±0.006
Cr	0.00±0.00	0.01±0.005
K	14.43±0.0	9.62±0.02

CBR = Cooling water before refining. CAR = Cooling water after refining / Cooling effluent. ND = Not done.

From Table 4, the levels of heavy metals in the cooling effluent were in the order of K > Fe > Zn > Ni >Pd> Cu > Cr with V and Cd being absent. These were higher when compared to that of the cooling water samples before refining operation with a trend of K > Fe > Zn > Ni >Pd> Cu with Cr, V and Cd absent. The only exception was the concentration of K which was higher in cooling water sample before refining than the cooling effluent sample. Also, Chromium was originally absent in the cooling water sample before refining but was spotted in the cooling effluent (0.01 ppm). These may be due to chromium dissociation from electroplated materials used in petroleum refining process (Abui,2012). The high level of Pb in the cooling effluent (0.12 ppm) can be attributed to its usage as coolant for lubricating oil fraction and parts of the equipment or machinery used at different stages of crude oil refining. Also, the increase in the concentration of Ni (0.20 ppm), Cu (0.05 ppm), Fe (0.61 ppm) and Zn (0.37 ppm) of the cooling effluent as compared to the cooling water before refining operation maybe attributed to corrosion of pipelines and parts of heat exchangers which the water passes through.

IV. CONCLUSION AND RECOMMENDATION

In conclusion, the result of the study revealed that the refining processes have individual and peculiar influences on the level of physico-chemical parameters of the water leaving each treatment section. The quality of water samples subjected to treatment at each water treatment section in KRPC during the course of study was acceptable

from physico-chemical parameters assessed and may not be injurious to the boiler and its other end uses. Also, results of the pre and post refinery operation cooling water sample assessed showed the significant effect the refinery operation had on the cooling water.

Based on the results obtained above, the water treatment before usage in KRPC should be encouraged and continued as poorly treated water used in the boiler for steam production could be manifested through scaling and eventual failure of the boiler.

REFERENCES

- [1] Abui, Y.M., (2012). Environmental effect of Kaduna Refinery and Petrochemical Company effluents discharge in the Romi area of Kaduna State, Unpublished PhD Dissertation submitted to the department of Geography and Planning, University of Jos, Nigeria, P. 394.
- [2] Ahmad, H.A., (2014). Determination of Effectiveness of Waste Water (Effluent) Treatment process of Kaduna Refinery and Petrochemical Company (KRPC), *American Journal of Environmental Engineering and Science*, 1(1): 6-12.
- [3] Aderogba, K.A., (2011). Significance of Kaduna River to Kaduna Refining and Petrochemicals Complex, *International Multidisciplinary Journal*, 5(22): 6-9.
- [4] APHA.,(1992). Standard Methods for the Examination of Water and Wastewater, 18th Ed., American Public Health Association (APHA), inc., Washington D.C., pp. 3-18.

- [5] APHA.,(1998). Standard Methods for the Examination of Water and Wastewater, 20th Ed., American Public Health Association (APHA), Washington D.C., pp. 12-27.
- [6] ASTM International, (1990). Annual Book of ASTM Standards, Water and Environmental Technology, West Conshohocken, Pennsylvania, P. 285.
- [7] Cohen, J.M., (1960). Taste Threshold Concentration of Heavy Metals in Drinking Water, *Journal of American Water Works Association*, 52(5): 660-663.
- [8] Dara, S.S., (1995). A Textbook of Environmental Chemistry and Pollution Control, Chand, S. and Company Limited, P. 65.
- [9] Hornby, A.S., (1995). Oxford Advanced Learners Dictionary of Current English, 5th Ed., Oxford University Press, P. 1344.
- [10] Jern, N.G. and Wun, J., (2006). Industrial Wastewater Treatment, Imperial College Press, London, pp. 6-8.
- [11] Jones, L. and Atkins, P. (2002). Chemistry: molecules, matter and change, 4th Ed., New York, Freeman and company. pp. 421-422.
- [12] Jowa, T. and Liberty, L.M., (2015). Treatment of Low Turbidity Water Using Poly-Aluminium Chloride (PAC) and Recycled Sludge, *Zimbabwe Journal of Science & Technology*, 10: 1-8.
- [13] Lateef, A., (2004). The Microbiology of Pharmaceutical effluent and its public health implications, *World J. Microbiol. Biotechnol*, 20: 167-171.
- [14] Lorch, W., (1987). Handbook of Water Pollution, 2nd Ed., Ellis Harwood Ltd, London Press Publication, pp. 84-93.
- [15] Marcovecchio, J.E., Botte, S.E. and Freije, R.H., (2007). Heavy Metals, Handbook of Water Analysis, Nollet, L.M., 2nd Ed., London: CRC Press, p. 275.
- [16] Odigure, J.O., Abdulkareem, A.S. and Asuquo, E.T., (2005). Effect of Water Quality on the Performance of Boiler in Nigerian Petroleum Industry, *Leonardo Electronic Journal of Practices and Technologies*, 7: 41-48.
- [17] Ojo, I., Fred, A.O. and Ochieng, G.M., (2012). Groundwater Characteristics, qualities, pollutions and treatments, *International Journal of Water Resources and Environmental Engineering*, 4(6): 162-170.
- [18] Pearson, H. W., Mara, D. D., Konig, A., De Oliveira, R., Mills, S. W., Smallman, D. J. and Silva, S.A.,(1987). Water Column Sampling as a Rapid and Efficient Method of Determining Effluent Quality and the Performance of Waste Stabilization Ponds, *Water Science & Technology*, 19(12): 109–113.
- [19] Walter, L., (1987). Handbook of water purification, Ellis Horwood, New York, pp. 85-90.

Implementation & Comparative Analysis of CMOS vs GDI for 8T SRAM Functionality under Power, Delay over Performance

T. Vasudeva Reddy¹, Dr B. K. Madhavi²

¹Department of ECE, Research Scholar, Rayalaseema University, Andhra Pradesh, India

²Professor, Dept of ECE, Sridevi Womens Engg College, Hyderabad, Telangana, India

Abstract— *The Technology behind every electronic gadgets or device has a rapid growth in the market and also in the industry. As all the complex electronic devices are operating at higher frequency and operating in sub threshold region, which leads to delivering higher leakage power at lower operating voltages, and especially when the technology is gradually increasing, mostly in cmos design. So there ought to be a reliable mode of circuit or structure which can be a tradeoff between speed, power and area. So the broad side of this work designates the analysis of Gate diffused input method (GDI) which can be an alternative logic for the implementation of SRAM bit cell instead of CMOS, and relative, comparative analysis of delay & power of CMOS with GDI at 0.4v at 32nm Synopsys tools by obtaining the proper characteristics of ac and dc analysis.*

Keywords— *cmos, GDI, Subthreshold operation, Static, Dynamic power.*

I. INTRODUCTION

The demand for portable electronic devices increasing day by day, as the Technology has a rapid growth in the industry. As Most of the electronics gadgets are battery operated and increasing the demand for portable and popularity of electronic products, the researchers have driven strive to achieve higher speed and longer battery life.

There were number of techniques proposed in past decades, to reduce the power and leakage, by operating the device under sub threshold region. But generously there are drastic changes in higher leakage power & current. More predominantly this leakage power is dominating the dynamic and static power.

But the problem in the Cmos design is leakage power when the technology is moving on to higher levels. According to the survey given by Intel, leakage power is dominating when the technology is upgrading, as technology has a rapid growth, the amount of complexity of electronic circuits is also increasing according to the customer needs and the relationship is as showed below Fig 1. So there

fore, there must be alternating circuit model to reduce the amount of leakage power when the technology has a rapid growth[4].

Cmos circuits plays a vital role in the designing of memory circuit modeling, as it deals with higher switching speed, a basic circuit to implement all the kind of design. an implementation of SRAM is done with 8T model. RAM is one of the main functional unit and takes maximum power especially when it is under dynamic mode of operation The amount of static power is maximum when the circuit is in cutoff state.

This leakage power is dominating the dynamic power when the technology is rapidly growing. SRAM is one of the hearts of the processing element and processing read and writes operations simultaneously. For achieving high performance and more reliable operation, there by changing the different parameters. Therefore the energy consumption per bit is drastically reduced, which will leads to more efficient design. In order to reduce the power consumption of SRAM ,there is relay on different types of process variations like sensing unit, supply voltage, size reduction.

This paper characterizes SRM is design model starting of inverter, 8T SRAM In cmos & GDI of different parameters static and dynamic power, rise and fall time delay & its characteristics by considering the advantages[3][4]

This Paper designated as follows section I clarify operation of cmos inverter, and its characteristics. Section II enlightens the operation GDI inverter. Performance & Implementation of Gate diffused input (GDI) sram in section III. In section IV explains the power analysis of 8T CMOS SRAM. power analysis of GDI 8T SRAM describes in section V. delay estimation of sram cmos is done in section VI.in section VII GDI delay estimation ids done.[1]

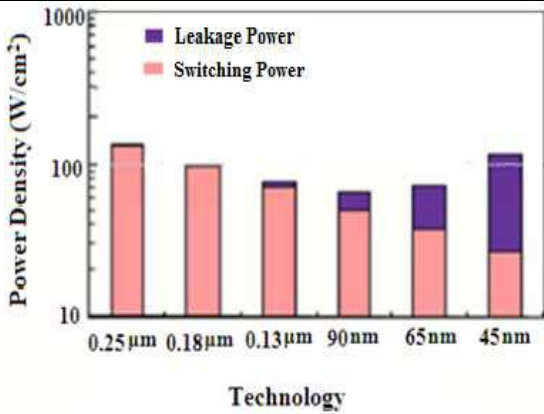


Fig.1: Technology Vs power relationship

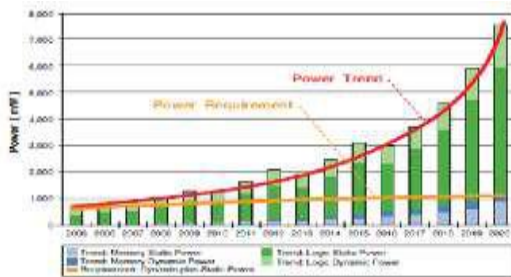


Fig.2: power Vs year correlation

II. OPERATION OF CMOS INVERTER

A basic component for the operating of kind logic of sop or pos. The challenges of sub threshold memory design are compromised with inverter operation and shows the circuit diagram of static CMOS inverter circuit. Its operation is readily understood with the simple switch model of the MOS transistor, introducing in the transistor is nothing more than a switch with an infinite off mode resistance for $|VGS| < |VT|$, and a finite on-resistance for $|VGS| > |VT|$.

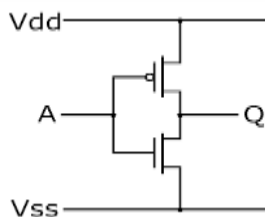


Fig.3: cmos inverter inverter

Performance of the following operation. When input V_{in} is high and equal to V_{DD} , the NMOS transistor is on state, while the PMOS is off condition. The equivalent circuit of exists between V_{out} and the ground node, resulting in a steady-state value of 0 V. On the other hand, when the input voltage is low (0 V), NMOS and PMOS transistors are off and on, respectively. And as showed in fig 2.

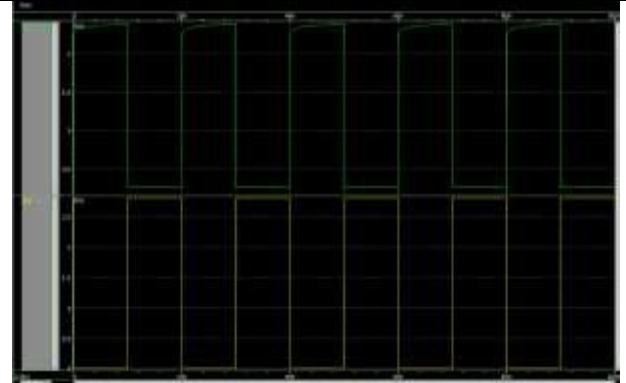


Fig.4 : characteristics of cmos inverter

As the transistor is Low power means operating the design at less than the threshold voltage or sub threshold without degrading the performance. Sub-threshold is one of the methods to achieve low power design. There are basically three Inversion regions: a) Strong inversion region ($V_{gs} > V_t$), b) Moderate inversion region ($V_{gs} = V_t$), c) Weak inversion region ($0 < V_{gs} < V_t$) operation. [2]

The amount of leakage power and delay need to minimize, as the complexity of the circuit is increasing with respect to the technology. and also delay and power is minimized by considering V_{DD} and V_{SS} are also another inputs along with the input.

III. OPERATIONAL ANALYSIS OF GDI CIRCUITS

Gate Diffused Input (GDI) is one of the method and a new technique of digital low power circuit design is operation explained. It allows to reduction of power consumption, delay and area of digital logic circuits, by maintaining lower complexity of logic model design. Performance comparison of traditional CMOS and GDI were presented [3], to reduce layout area, number of logic cells or devices and also to estimate the delay and power, performance is as showed below. where the gdi has the low swing operation.

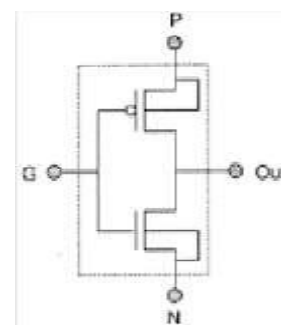


Fig.5: GDI Inverter

The schematic diagram of GDI cell is showed below and the input is applied as a train of pulse with the logic levels are 1 and 0. and another two inputs of v_{dd} and v_{ss} are applied as DC signal.

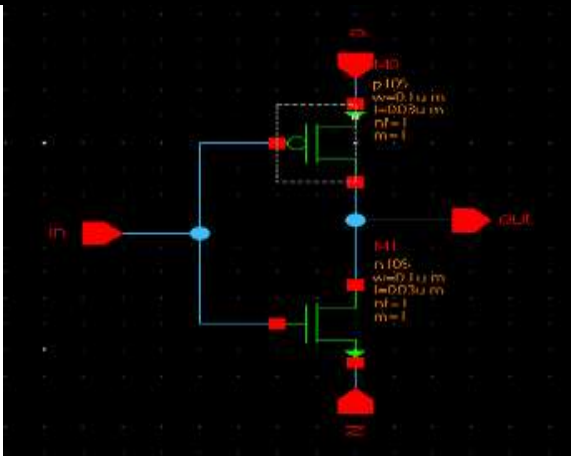


Fig.6: schematic diagram of GDI Inverter

The characteristics of the GDI inverter is as mentioned below. Most of functions are complex in CMOS, as well as in standard logic PTL implementations, but simple as only 2 transistors / function) in GDI design method.[1]

A	B	Functionality	FI
0	0	pMOS Trans Gate	V_{Tp}
0	V_{DD}	CMOS Inverter	V_{DD}
V_{DD}	0	nMOS Trans Gate	0
V_{DD}	V_{DD}	CMOS Inverter	0

Fig.7: Functional characteristics of GDI pass transistor logic

As GDI cell structure is different from existing Pass Transistor Logic techniques, it has some important features, allows to Improvements in design complexity, count of transistor, static power dissipation and low logic level swing.

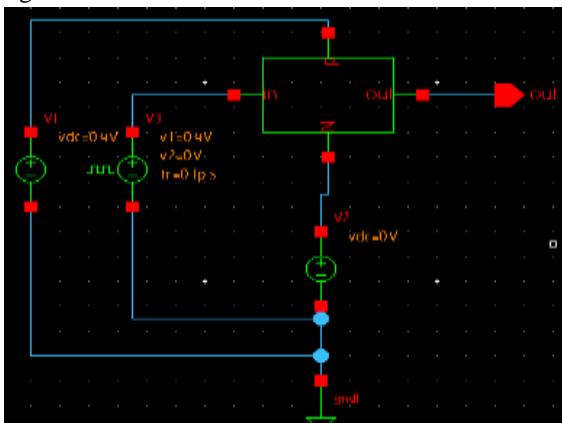


Fig.8: a cell view of representation is done 1 bit

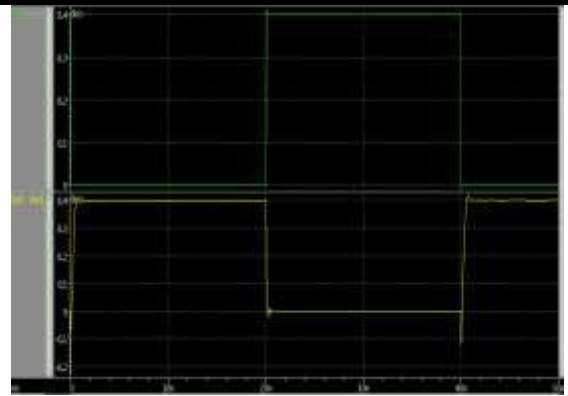


Fig.9: Functional characteristics of GDI inverter logic

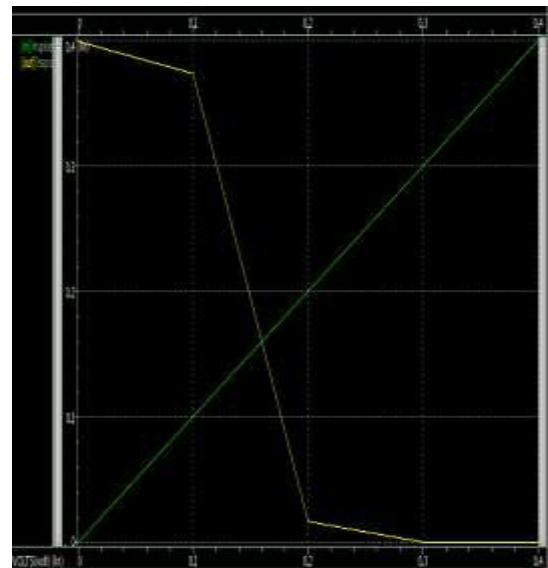


Fig.10: Dc Analysis

An cell view representation is showed in the figure 8 and the dc voltage of 1.5v is applied as input to vdd and vss, and a dc voltage of 0.4v is applied as input to the inverter logic circuit.

IV. GDI BASED 8T SRAM



Fig.11: schematic representation of 8T SRAM

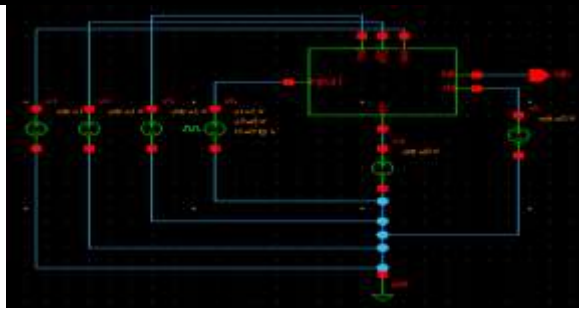


Fig.12: Symbolic view of 8T SRAM

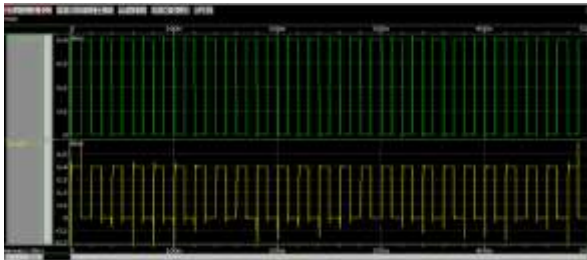


Fig.13: characteristic of 8T GDI SRAM

Power analysis of 8T CMOS SRAM
 Static power dissipation



Fig.14: static power Analysis
 Static power dissipation= 1.2621 uw

Dynamic power dissipation



Fig.15.Total power dissipation= 7.2593uw
 Dynamic Power=Total –Static Power=5.9962 uw

V. POWER ANALYSIS OF 8T GDI SRAM
 Static power dissipation

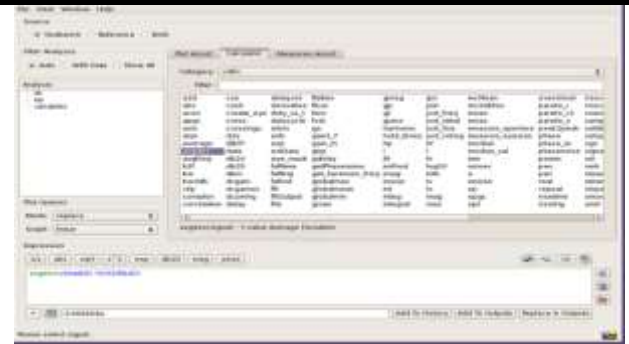


Fig.16: Static power dissipation= 0.668uw



Fig.17: Total power dissipation= 4.073uw
 Dynamic Power=Total –Static Power=4.073uw

VI. DELAY ESTIMATION OF 8T SRAM CMOS

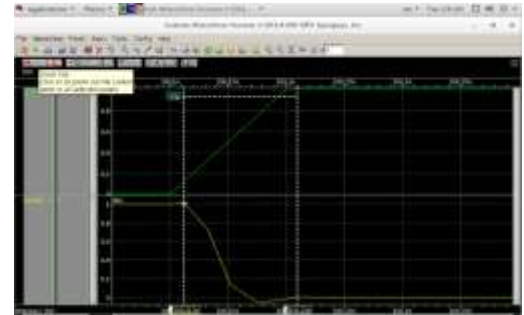


Fig.18: Rise Time Time Delay

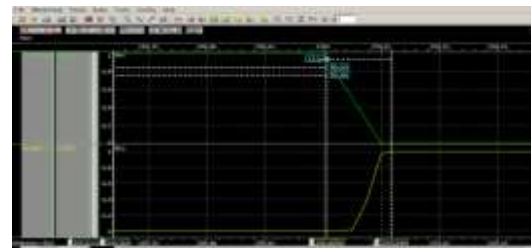


Fig.19 : Fall Time Delay

VII. DELAY ESTIMATION OF 8T SRAM GDI MODEL



Fig.20: Rise & Fall Time Delay

Comparative Analysis

The following representation indicates the analysis about the power and delay of 8T SRAM implemented in CMOS and GDI.

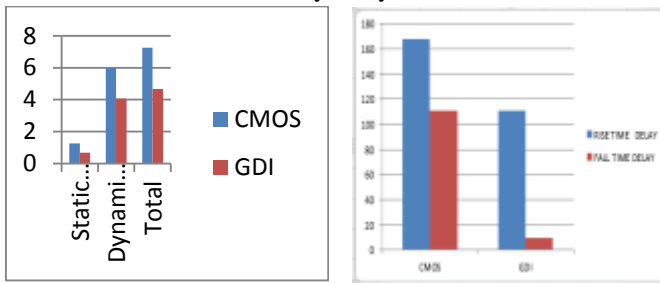
Power analysis micro watts

	CMOS	GDI
Static Power	1.2621	0.668
Dynamic Power	5.9962	4.073
Total	7.2583	4.6672

Delay analysis in Pico seconds

Delay in Ps	CMOS	GDI
Rise Time	168	111
Fall Time	111	9.6
Total Delay	279	121

Delay analysis



VIII. CONCLUSION

Static Power is reduced by a factor 63 % dynamic Power is reduced by a factor of 46% and Approximately 55 % on total power but In GDI The Rise Time Is Reduced By 1.5 % And Fall Time Is Decreased By 11% Approximately 6 % on total delay by maintaining the performance. Tools used were Synopsys Designer -implementation & modelling ,Custom Ic Designer performance and Custom Compiler power and delay.

REFERENCES

[1] GDI based full adders for energy efficient arithmetic applications by Mohan Shoba & Rangaswamy Nakkeeran, <http://dx.doi.org/10.1016/j.jestch.2015.09.006>, 2215-0986/Copyright © 2015.
 [2] Ref:digital subthreshold logic design – motivation and challenges by Sagi Fisher, The VLSI Systems Center, Ben-Gurion University, Beer-Sheva, Israel 1-4244-2482-5/08/\$20.00 ©2008 IEEE 702 IEEEI 2008
 [3] Energy-Efficient Subthreshold Processor DesignBo Zhai, Sanjay Pant, by iee transactions on very large scale integration (vlsi) systems, vol. 17, no. 8, august 2009.

[4] Subthres hold Region for Ultralow-Power Applications Ramesh Vaddi, S. Dasgupta, and R. P. Agarwal semiconductor Devices and VLSI Technology (SDVT) Group, Department of Electronics & Computer Engineering (E & CE), Indian Institute of Technology (IIT), Roorkee, Roorkee-247667, Uttarakhand, India, Hindawi Publishing Corporation VLSI Design.

Comparison of Measured and Predicted Performance and the Emission Characteristics of Single Cylinder CI Engine using Pongamia Pinnata based Bio-Diesel

A. Yazharsu, T. Rajagopal, U. Karthick, V.P. Srinivasan

¹Department of Mechanical Engineering, Bannari Amman Institute of Technology, Erode – 638 401, India

²Department of Mechanical Engineering, Kongu Engineering College, Erode – 638 060, India

³Department of Mechanical Engineering, SNS Group of Institutions, Coimbatore – 641 107, India

⁴Department of Mechanical Engineering, Sri Krishna Institutions, Coimbatore – 641 008, India

Abstract— Diesel being the main transport fuel, developing countries like India spends a lot of money to import petroleum and the use of petroleum based fuels increased in the recent years is the main contributor to the urban air pollution. Finding a suitable alternative to diesel is an urgent need. Biofuels are renewable, can supplement petroleum based fuels. Due to pressure on edible oils, non-edible oils of Pongamia Pinnata (karanja) and Jatropha Curcas are evaluated as diesel fuel extender. Pongamia pinnata based bio-diesel (PBD) is receiving increasing attention in India because of its potential to increase the rural employment and relatively low impact on environment. Diesel engines running on PBD are found to emit higher oxides of nitrogen. In this work a single cylinder constant speed water cooled four stroke direct injection diesel engine is selected for the experimental investigations to model the performance and emission characteristics fueled with plain Diesel and Pongamia Bio-diesel blends PBD10 (10% Pongamia Bio-diesel and 90% Diesel) and PBD20 (20% Pongamia Bio-diesel and 80% Diesel) with different cooled EGR rates (0%, 5%, 10%, 15% and 20%). The performance parameters are analyzed include specific fuel consumption and brake thermal efficiency whereas exhaust emissions include nitric oxide (NO), carbon monoxide (CO) and smoke opacity. The results of the experiments in each case were used to model the performance and emission parameters. Multivariate non linear regression analysis is carried out in Minitab software to model the performance and emission parameters. The predicted values were compared with experimental data.

Keywords— Bio-diesel, EGR, Pongamia Pinnata, Engine modeling, Multiple nonlinear Regression.

I. INTRODUCTION

Share of diesel engine is consistently rising in vehicle market worldwide. New technologies and improvements

made the diesel engine more fuel efficient. The main advantage of the diesel engine compared to spark ignition engine is its fuel economy. Extensive usage of automobiles has some demerits and one of them is its negative effect on environment.

Diesel exhaust is produced when an engine burns diesel fuel. It is a complex mixture of many of gases including carbon dioxide (CO₂), carbon monoxide (CO), oxides of nitrogen (NO_x), hydrocarbons (HC), sulphur dioxide (SO₂), soot particles, etc., Hence, stringent emission norms are continuously being imposed on diesel engines. To meet the future emission norms suitable measures need to be taken [1-3]. Bio-fuels have the potential to meet the rapidly growing energy demand in sustainable way. Bio diesels have almost similar energy density, cetane number, heat of vaporization and stoichiometric air fuel ratio compared to plain diesel [4-5]. Using bio-diesel in diesel engine has reduced emissions of CO₂, CO and HC. Most bio-diesels in diesel engine will increase the NO_x emission. But pongamia pinnata based bio-diesel has also reduced NO_x emission. NO_x emission can be further reduced by various techniques like EGR, SCR, etc.

Pongamia pinnata is a non-edible species capable of growing in almost all types of land. The annual production potential is about 9,000 kg per hectare. In India the estimated oil from seeds is about 50,000 tones. The yield from a single tree would be around 25 to 90 kg of seed containing around 27 to 50% of oil. The characteristics of these oils fall within a fairly narrow band and are quite close to those of diesel [4-5].

Raw pongamia oil has less calorific value compared to diesel. This is due to the oxygen content in their molecules. Previous research works show that using straight vegetable oil (SVO) in diesel engines leading to problems in pumping, atomization and gumming, injector fouling, piston and ring sticking and contamination of lubricating oils in the long

run operation due to its high viscosity, density, iodine value and poor non volatility [5]. Hence it is essential to reduce the viscosity of the pongamia by methods like preheating, thermal cracking and transesterification etc. Transesterification is the best way to convert the vegetable oils to suit for the use in diesel engines. So pongamia oil (SVO) is converted into bio-diesel through a transesterification process [6]. The obtained Pongamia bio-diesel has properties close to diesel fuel and is found that it can be in engine without any modification. Pongamia bio-diesel was mixed with diesel in varying proportions 10% and 20% by volume (PBD10 and PBD20) with the help of a stirrer. The blends were stirred continuously to achieve stable property values. Properties of diesel, PBD10 and PBD20 are shown in Table 1.

Table.1: Properties of Fuel

Properties	Diesel	PBD10	PBD20
Density at 30 °C	0.832	0.836	0.841
Calorific Value (kJ/kg)	44000	42600	41500
Viscosity (cSt at 30 °C)	3.02	3.5	4.3
Flash Point (°C)	60	68	75

Diesel engines are more efficient than petrol engines. However, when compared to petrol engine, diesel engines have higher emissions of NO_x and much higher emissions of particulate matter. The recycling of some of the exhaust back into the engine intake system, commonly known as exhaust gas recirculation (EGR) has become almost essential for achieving significant NO_x reductions to meet the current and future diesel emission regulations [E,F,G]. Exhaust Gas Recirculation (EGR) is a simple and most effective way of reducing NO_x emissions from diesel engines [E]. EGR changes the diesel combustion process of engine because of three broadly defined effects [7-9, 11].

Thermal Effect: The recycled inert gases, predominantly carbon dioxide (CO₂) and water vapor (H₂O) increase the specific heat capacity of the intake charge, thereby lowering the temperatures during the compression and combustion processes.

Dilution Effect: The replacement of intake oxygen with the inert gases dilutes the intake charge, results in a reduced excess-air ratio (k), increases the ignition delay and slows down the fuel burning rate due to the deceleration of the mixing between oxygen (O₂) and fuel. Furthermore, the dilution effect contributes to the reduction of the oxygen partial pressure and thus affects the kinetics of the elementary NO formation reactions.

Chemical Effect: The recycled gases also introduce free radicals such as O, H and OH in the cylinder charge, formed by the dissociation of CO₂ and H₂O that are believed to

affect the combustion process and NO_x formation. In particular, a reduction in the flame temperature is caused by the endothermic dissociation of H₂O.

The EGR (%) is defined as the mass percent of the re-circulated exhaust (M_{EGR}) in the total intake mixture (M_i).

$$\% \text{ EGR} = (M_{\text{EGR}} / M_i) * 100$$

However, application of EGR also leads to penalties. In case of diesel engines, these penalties include higher specific fuel consumption and particulate matter emissions. Effectively, a tradeoff between NO_x and soot is observed with the use of EGR [12-15]. The reduction in flame temperature reduces the rate of soot oxidation/re-burning. As a result, in EGR system, more soot is formed during combustion and it remains un-oxidized and eventually appears in the exhaust. The rise in smoke (soot) level of engine exhaust due to EGR affects the engine performance in various ways. Increased soot level causes considerable increase in the carbon deposits and wear of the various vital engine parts such as cylinder liner, piston rings, valve train and bearings.

Regression analysis is a statistical method for estimating the relationships among variables. It includes many techniques for modeling and analyzing several variables, when the focus is on the relationship between a dependent variable and one or more independent variables. Regression analysis is used for prediction and forecasting [16]. Simple linear regression and multiple linear regression are related statistical methods for modeling the relationship between two or more variables using a linear equation. Simple linear regression refers to a regression on two variables while multiple regression refers to a regression on more than two variables. Linear regression assumes the best estimate of the response is a linear function of some parameters. Sometimes the true relationship is curved, rather than flat. To fit this type of curves, non-linear regression is used.

In this work multivariable non linear regression is carried out using Minitab 16 to predict the engine performance and emission parameter. Gauss-Newton algorithm is used to solve the equations. In this work exponential and power model equations are selected for regression modeling. These non-linear equations can be put into a linear form by appropriate transformations of the either the dependent variable Y or some (or all) of the independent variables X₁, X₂, ..., X_n. This leads to the wide utility of the linear model. Exponential model and power model equations and their linear form are given in equation (1) and equation (2).

Exponential model equation,

$$y = e^{\beta_0 + \beta_1 x_1 + \beta_2 x_2 + \beta_3 x_3 + \dots} \quad (1)$$

Linear form $Y = \beta_0 + \beta_1 X_1 + \beta_2 X_2 + \beta_3 X_3 + \dots$

Here, $Y = \ln y$, $X_1 = x_1$, $X_2 = x_2$, $X_3 = x_3$

Power model equation,

$$y = ax^b \quad (2)$$

Linear form: $\ln y = \ln a + b \ln x$ or $Y = \beta_0 + \beta_1 X$

Here, $Y = \ln y$, $X = \ln x$, $\beta_0 = \ln a$, $\beta_1 = b$.

Here a, b and $\beta_0, \beta_1, \beta_2, \dots$ are coefficients, x, X_1, X_2, \dots are variables.

II. EXPERIMENTAL WORK

The test rig used in this study is kirloskar single cylinder variable compression direct injection four stroke diesel engine. The specifications of the engine are listed in Table 2. The EGR system consists of a piping system taken from the engine exhaust pipe, a heat exchanger to cool the exhaust gases, two control valves (CV1 and CV2) to change the quantity of gases being recycled. The schematic representation of the EGR system shown in Fig.1.

The engine is loaded by an eddy current dynamometer. A computerized data acquisition system is used to collect all engine data and store it in a computer for off line analysis. The data acquisition system collects the following parameters: engine speed, torque, fuel flow rate, air flow rate, and coolant flow rate, temperature of air/coolant/exhaust gas before EGR cooler/exhaust gas after EGR cooler, cylinder pressure data and crank angle degrees. A computer software Engine Test Express V20.25 is used to collect the data and manage the system. The engine was run by using plain diesel and pongamia bio-diesel blends (PBD10 and PBD20) with different EGR rates. For all three fuels readings are taken in 0%, 25%, 50%, 75% and 100% load. The emissions like CO, NO and smoke opacity are measured using Endee portable gas analyzer.

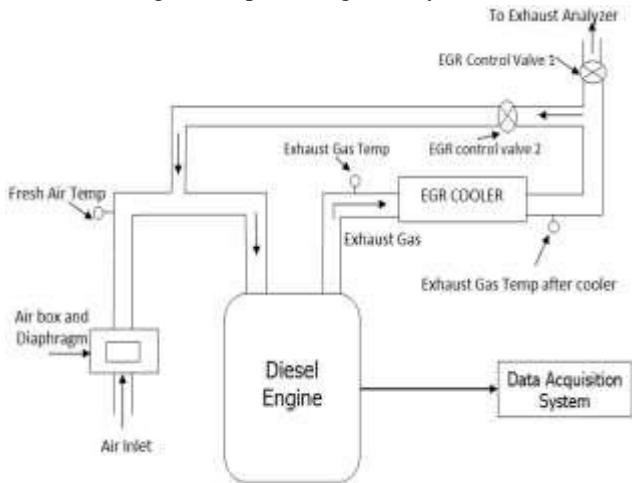


Fig.1: Experimental Setup

Table.II: Specifications of The Engine

Make	Legion brothers, Bangalore.
Type	Kirloskar, single cylinder.
No. of strokes	Four
Bore/stroke	80 mm/110mm
Rated rpm	1500
Injection timing	23 deg bt/dc
Type of ignition	Compression ignition
Method of loading	Eddy current dynamometer
Method of starting	Manual crank shaft
Method of cooling	Water
Injection pressure	200 bar

III. RESULTS AND DISCUSSION

A. Brake Thermal Efficiency

Fig. 2 shows the comparison of brake thermal efficiency (BTE) for PBD10, PBD20 and diesel (DI) without EGR. BTE is almost comparable for bio-diesel blends and diesel. BTE is slightly increased with EGR at lower engine loads. This is presumably due to the re-burning of hydrocarbons that enter into the combustion chamber with the re-circulated exhaust gas [10, 15]. At higher engine loads, the BTE slightly decreased by EGR. At full load condition % reduction in BTE over an EGR range of 0–20% is 3.8, 3.12 and 3.5 for diesel, PBD10 and PBD20 respectively. The drop in BTE at 20% EGR level is possibly due to predominant dilution effect of EGR leaving more exhaust gases in combustion chamber. The non linear regression equation to predict the BTE in terms of load (W), EGR %, fuel density (FD) and heating value (CV) of fuel is given in equation (3).

$$\ln(\text{BTE}) = -1.4 + 0.507 \ln(W) + 0.00065 \ln(\text{EGR}) + 0.36 \ln(\text{CV}) - 0.13 \ln(\text{FD}) \quad (3)$$

BTE of an engine depends on the speed, load, heating value of the fuel and EGR rate. The regression coefficient (R^2), adjusted regression coefficient (R^2 adj.) and standard error of estimate (SEE) for predicting equations are given in Table 3. In the above equation the load and heating value of fuel having larger influence on predicted BTE of the engine. EGR rate have very less influence on BTE. Fig. 2 and Fig. 3 indicates the measured and predicted BTE of diesel (DI M-Diesel Measured and DI P-Diesel Predicted), PBD10 (PBD10 M-PBD10 measured and PBD10 P-PBD10 predicted) and PBD20 (PBD20 M-PBD20 measured and PBD20 P-PBD20 predicted) with 15% EGR. At lower loads predicted and measured BTE are comparable. At full load condition predicted BTE shows 10.5 % of average deviation from the measured BTE.

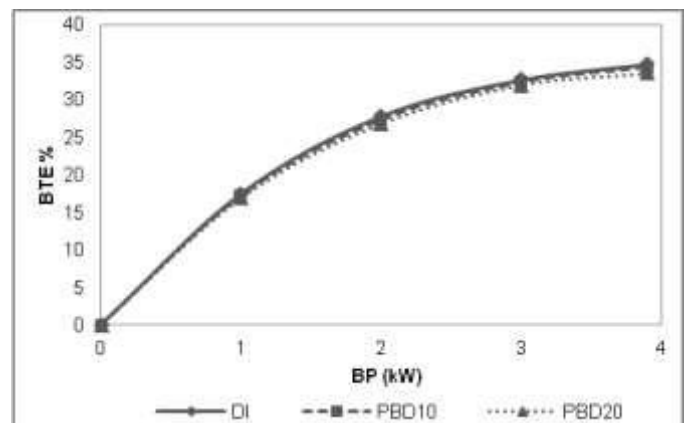


Fig. 2: Comparison of brake thermal efficiency (0% EGR)

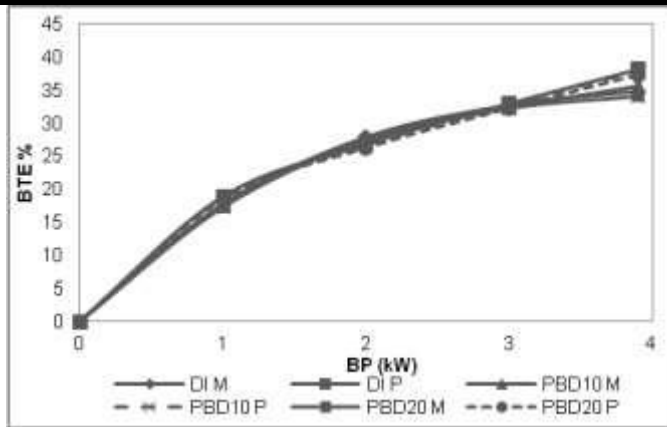


Fig.3: Comparison of Measured and Predicted BTE with 15% EGR

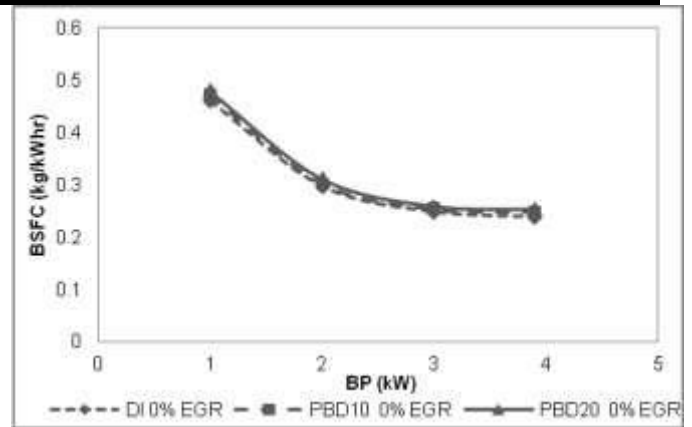


Fig. 4: Comparison of BSFC (0% EGR)

Table.III: Statistical Results of Predicting Equations

Parameter	R ²	R ² Adj.	SEE
BTE	95.3	94.9	0.06139
BSFC	93.9	93.4	0.06672
NO	96.8	96.6	0.10579
CO	89.3	88.7	0.13199
Smoke	95	94.7	0.15431

B. Brake Specific Fuel Consumption

Fig. 4 demonstrates the variation of brake specific fuel consumption (BSFC) with brake power for diesel, PBD10 and PBD20. BSFC is found to be decreased with increase in brake power. This is due to higher percentage increase in brake power with load as compared to increase in the fuel consumption. BSFC of bio-diesel blends are slightly higher for all experimental range of EGR compared to corresponding BSFC of diesel fuel [10, 15]. This is presumably due to lower calorific value, higher boiling point and viscosity. PBD20 when used with the 20% EGR shows an average increase of 3.8% in BSFC compared to without EGR and 5.3% compared to neat diesel fuel. This may be due to the penalty of exhaust gases containing CO₂ made the combustion difficult. The non linear regression equation to predict the BSFC in terms of load (W), EGR %, fuel density (FD) and heating value (CV) of fuel is given in equation (4).

$$\ln(\text{BSFC}) = -18.9 - 0.481 \ln(W) + 0.00164 \ln(\text{EGR}) + 1.85 \ln(\text{CV}) + 6.68 \ln(\text{FD}) \quad (4)$$

BSFC of an engine depends on the speed, load, heating value of the fuel and EGR rate. Load applied is having more influence on specific fuel consumption. The comparison of measured and predicted BSFC for diesel, PBD10 and PBD20 with 5% and 15% EGR level are shown in Fig. 5 and Fig. 6. At 15% EGR rate predicted BSFC of diesel, PBD10 and PBD20 shows average of 7%, 6.2% and 5.9% variation from the measured BSFC respectively.

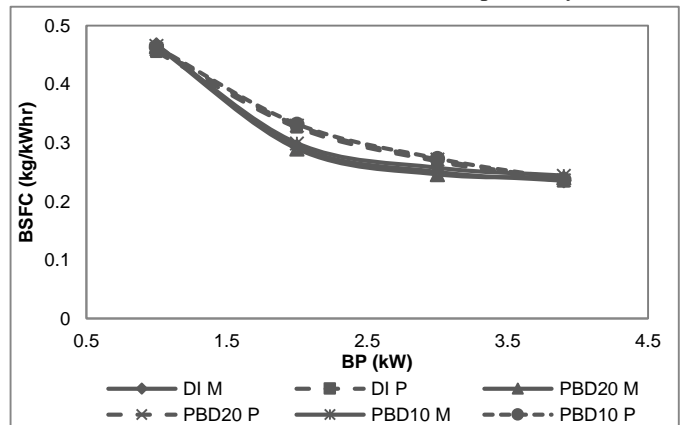


Fig. 5: Measured and Predicted BSFC of Diesel and PBD20 with 5% EGR

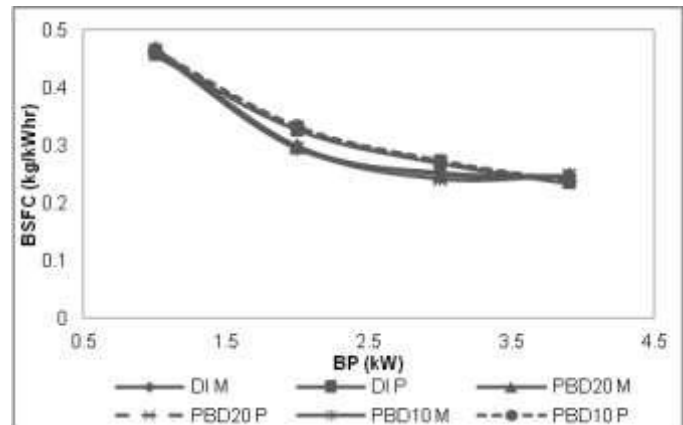


Fig. 6: Measured and Predicted BSFC of Diesel and PBD20 with 15% EGR

C. Nitric Oxide (NO)

Fig. 7 indicates the variation of NO emission with EGR % for diesel, PBD10 and PBD20. NO emission for all fuels

increases with the increase in brake power. The reason could be the higher average gas temperature, residence time at higher brake power. A greater reduction in the NO emission for both the bio-diesel blends as compared to diesel is noted. NO emission from bio-diesel at all loads, for all EGR rate, is lower compared to diesel under no EGR condition. At full load and 0% EGR condition NO emission level are 66 ppm for diesel, 59 ppm for PBD10 and 42 ppm for PBD20. This is due to the lower heating value of the bio-diesel blends. As EGR level increases NO emission decreases for all three fuels for all the operation range of engine brake power [10, 15, 17, 18]. The reason for the greater reduction in NO with EGR is the reduction of combustion temperature as a result of the addition of exhaust gases to the intake air which increases the amount of combustion accompanying gases mainly CO₂ which reduces the combustion temperature. Even though 20% EGR is able to reduce NO by a large amount, reduction in BTE and large increase in smoke and CO emissions are observed. The NO emission of an engine is determined by peak combustion temperature, pressure and oxygen concentration. The non linear regression equation to predict the NO in terms of load (W), EGR %, fuel density (FD) and heating value (CV) of fuel is given in equation (5).

$$\ln(\text{NO}) = -16.1 + (0.126 W) - (0.0398 \text{ EGR}) + (0.000241 \text{ CV}) + (10.3 \text{ FD}) \quad (5)$$

The comparison of measured and predicted NO emission for diesel, PBD10 and PB20 blends with 0% and 15% are shown in Fig. 8 and Fig. 9.

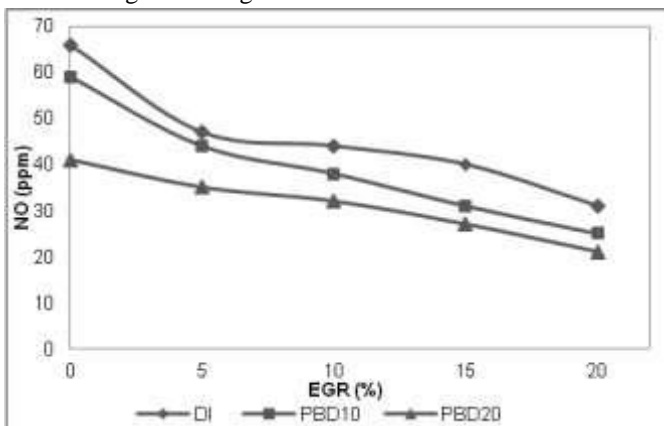


Fig.7: Comparison of NO with EGR

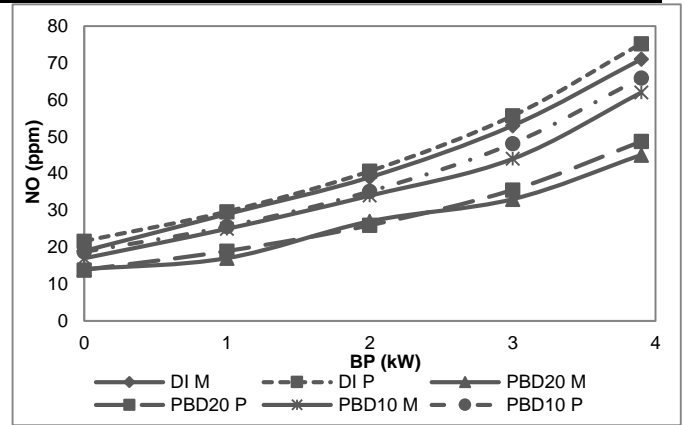


Fig.8: Measured and Predicted NO of Diesel and PBD20 with 0% EGR

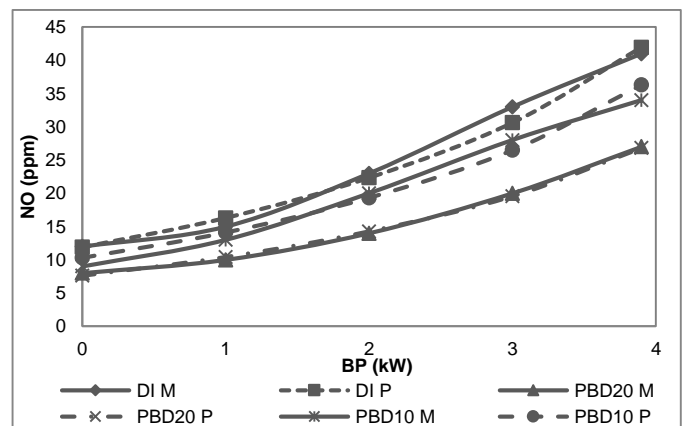


Fig.9: Measured and Predicted NO of Diesel and PBD20 with 15% EGR

D. Carbon Monoxide (CO)

Fig. 10 indicates CO variation with brake power for diesel, PBD10 and PBD20 with 0% EGR. CO emissions are found to be lower for bio-diesel blends compared to diesel with and without EGR. CO levels increases as EGR rate increases for all three fuels [10, 15, 17, 18]. The deficiency of oxygen with the increase in EGR % can be attributed to the rapid growth of CO. However, the excess oxygen content in bio-diesel blends can compensate for the oxygen deficient operation under EGR as a result of which bio-diesel blends maintain a lower CO than diesel at a fixed EGR level. Dissociation of CO₂ to CO at peak loads where high combustion temperatures and comparatively fuel rich operation exists, can also contribute to higher CO emissions. The CO emission of an engine depends on oxygen content and temperature of the combustion chamber. The non linear regression equation for predicting CO emission is given in equation (6).

$$\ln(\text{CO}) = 178 + (0.0741 W) + (0.0318 \text{ EGR}) - (0.000949 \text{ CV}) + (166 \text{ FD}) \quad (6)$$

In statistical analysis R² value of CO is 89.3% which is not adequate. This is because of the unpredictable trend in CO emission curves. The comparison of measured and predicted CO emission for diesel, PBD10 and PBD20 with 10% and 20% EGR rate are shown in Fig.11 and Fig. 12.

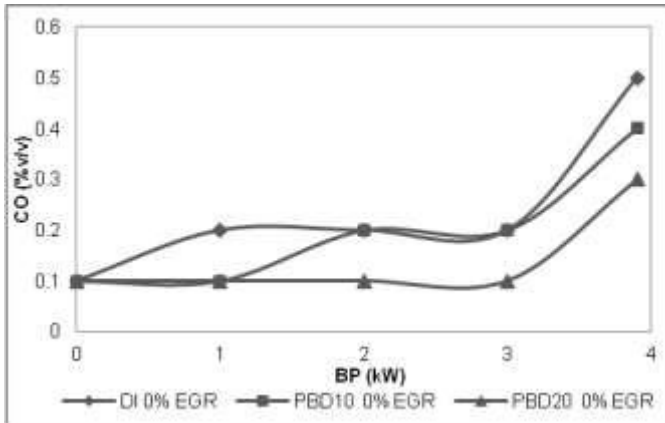


Fig.10: Comparison of CO (0% EGR)

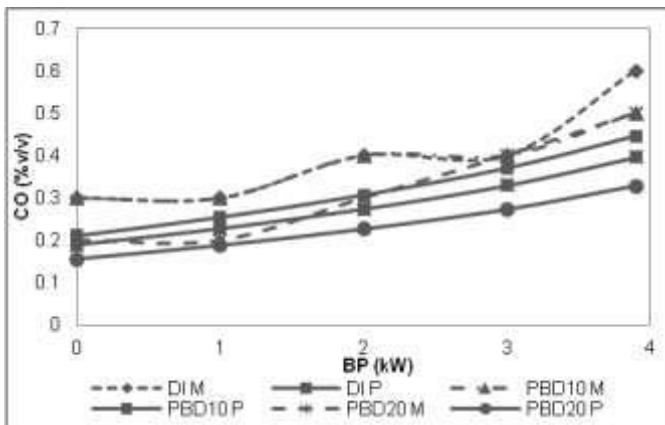


Fig. 11: Measured and Predicted CO of Diesel and PBD20 with 10% EGR

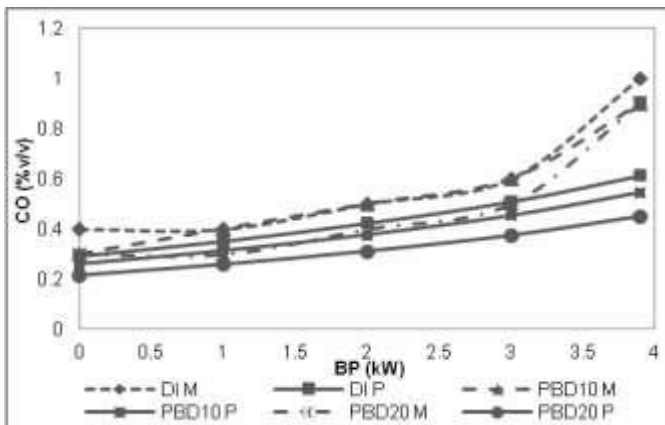


Fig.12: Measured and Predicted CO with 20% EGR

E. Smoke Emission

The smoke opacity of the exhaust gas is measured to quantify the particulate matter present in the exhaust gas. Figure 13 and figure 14 shows smoke variation with various EGR levels at no load and full load condition respectively. Higher smoke opacity of the exhaust is observed when the

engine is operated with EGR compared to without EGR [3, 10, 12, 15, 17]. The variations in the smoke opacity level at high loads are higher compared to that at lower loads. EGR reduces availability of oxygen for combustion of fuel, which results in relatively incomplete combustion and increased formation of particulate matter. Smoke emissions are lower for bio-diesel blends compared to diesel at all load conditions irrespective of EGR level. PBD20 shows 25.75%, 13.5% average reduction in smoke compared to diesel fuel and PBD10 respectively. This is presumably due to good mixture formation and presence of oxygen in bio-diesel blends. The non linear regression equation for predicting CO emission is given in equation (7).

$$\ln(\text{smoke}) = 23.2 + (0.171 W) + (0.0307 \text{ EGR}) - (0.00004 \text{ CV}) - (23.0 \text{ FD}) \quad (7)$$

The comparison of measured and predicted smoke emission vs EGR% for diesel, PBD10 and PBD20 at 25% load condition is shown in figure 15. Up to 15% EGR predicted and measured smoke are comparable for all three fuels. But at 20% EGR the variation is high, because at higher EGR level the oxygen deficiency inside the cylinder increases further which results in complete combustion and increased smoke emission.

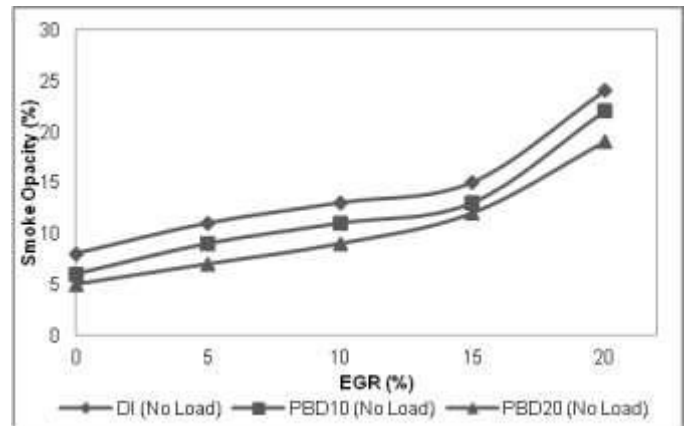


Fig.13: Comparison of smoke opacity with EGR (No load)

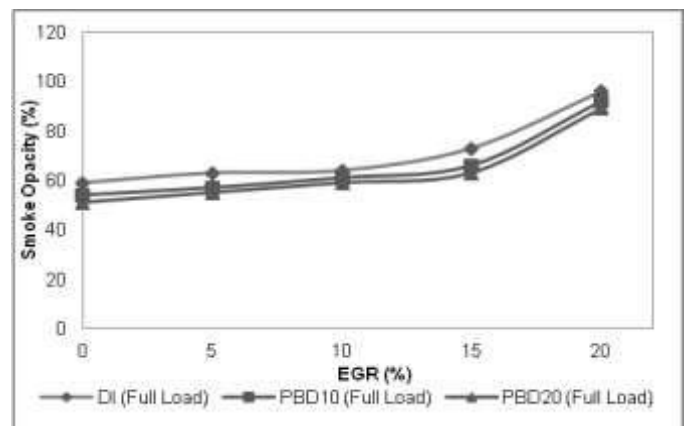


Fig. 14: Comparison of smoke opacity with EGR (Full load)

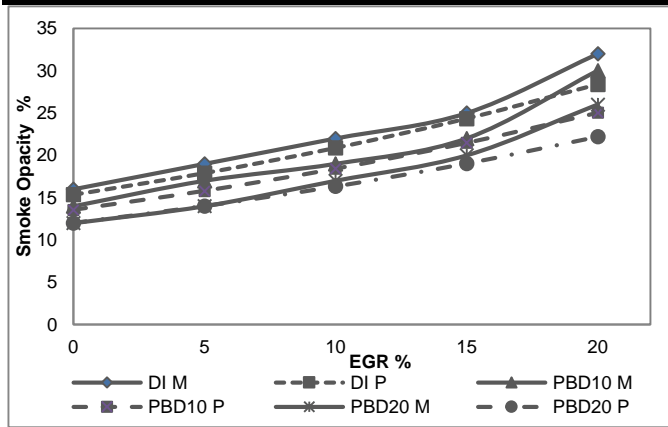


Fig.15: Measured and Predicted smoke opacity (25% load)

IV. CONCLUSION

A four stroke water cooled single cylinder direct injection diesel engine was run successfully using Diesel and Pongamia Bio-diesel blends (PBD10 and PBD20) as fuel for various proportions of EGR. The performance and emission characteristics have been analyzed and compared to baseline diesel fuel. The following conclusions are made with respect to the experimental and modeling results,

1. BTE of bio-diesel blends are found to be comparable with diesel, at all loads with and without EGR. At full load BTE of diesel, PBD10 and PBD20 are 34.76%, 34.27% and 34.03% with no EGR. The optimum EGR for the maximum BTE and the minimum BSFC is found to be 15%.
2. NO emission decreases with the increase in the percentage of EGR, but at a particular EGR percentage, NO decreases with the increase in the % of bio-diesel in the bio-diesel blend.
3. CO emissions are found to increase with the increase in the percentage of EGR. However at a particular EGR percentage, with the increase in the % of bio-diesel CO are found to decrease.
4. The increase in smoke at lower loads are insignificant with the increase in the percentage of EGR while at full load it also increases considerably with the increase in the percentage of bio-diesel.
5. Increasing EGR percentage beyond 15% can reduce NO further, but it will increase CO and smoke emission which is not acceptable. However the bio-diesel blends show lower emissions than diesel at a particular EGR percentage.
6. Multivariate non linear regression analysis is carried out to model the performance and emission parameters. Statistical analysis of these equations gives R^2 almost nearer to 0.95 except CO. Predicted values were compared with experimental data.

7. The performance and emission characteristics of diesel engine using similar fuel blends and EGR rates can be predicted without any expenses for experimentation with a correlation coefficient (R) in the range of 0.89-0.97.

REFERENCES

- [1] P. Brijesh, and S. Sreedhara, "Exhaust emissions and its control methods in compression ignition engines: a review", International Journal of Automotive Technology, Vol. 14, No. 2, pp. 195-206 (2013), doi: 10.1007/s12239-013-0022-2.
- [2] Abd-Alla, G.H, "Using exhaust gas recirculation in internal combustion engines: A review", Energy Conversion and Management, Volume 43, Issue 8, May 2002, Pages 1027-1042.
- [3] Zheng, M., Reader, G.T., Hawley, J.G., "Diesel engine exhaust gas recirculation - A review on advanced and novel concepts", Energy Conversion and Management, Volume 45, Issue 6, April 2004, Pages 883-900.
- [4] Bobade S.N. and Khyade V.B. "Detail study on the Properties of Pongamia Pinnata (Karanja) for the Production of Biofuel", Research Journal of Chemical Sciences, Vol. 2(7), 16-20, July (2012).
- [5] K. Sureshkumar and R. Velraj, "Performance and Characteristics Study of the Use of Environment Friendly Pongamia Pinnata Methyl Ester in C. I. Engines", Journal of Energy & Environment, Vol.5, May 2007.
- [6] Dembris A., "Biodiesel fuels from vegetable oils via catalytic and non-catalytic supercritical alcohol transesterification and other methods", A Survey Energy Conservation and Management, 44, 2093-2109 (2003).
- [7] Ladommatos, N., S.M. Abdelhalim, H. Zhao, and Z. Hu, "The Dilution, Chemical, and Thermal Effects of Exhaust Gas Recirculation on Diesel Engine Emissions - Part 1: Effect of Reducing Inlet Charge Oxygen," SAE Paper 961165, International Spring Fuels and Lubricants Meeting, Dearborn, Michigan, 1996.
- [8] Ladommatos, N., S.M. Abdelhalim, H. Zhao, and Z. Hu, "The Dilution, Chemical, and Thermal Effects of Exhaust Gas Recirculation on Diesel Engine Emissions - Part 2: Effects of Carbon Dioxide," SAE Paper 961167, International Spring Fuels and Lubricants Meeting, Dearborn, Michigan, 1996.
- [9] Ladommatos, N., S.M. Abdelhalim, H. Zhao, and Z. Hu, "The Dilution, Chemical, and Thermal Effects of Exhaust Gas Recirculation on Diesel Engine Emissions - Part 3: Effects of Water Vapor", SAE Paper 971659, International Spring Fuels and Lubricants Meeting, Dearborn, Michigan, 1997.

- [10] K. Venkateswarlu, B. S. R. Murthy, V. V. Subbarao, K. Vijaya Kumar, "Effect of exhaust gas recirculation and ethyl hexyl nitrate additive on biodiesel fuelled diesel engine for the reduction of NO_x emissions", *Front. Energy* 2012, 6(3): 304–310, doi:10.1007/s11708-012-0195-9.
- [11] S.C. Hill, L. Douglas Smoot, "Modeling of nitrogen oxides formation and destruction in combustion systems", *Progress in Energy and Combustion Science* 26 (2000) 417–458.
- [12] Agarwal AK, Singh SK, Sinha S, Shukla MK. "Effect of EGR on the exhaust gas temperature and exhaust opacity in compression ignition engines", *Sadhana* 2004; 29:275–84.
- [13] Wade RW., "Light duty NO_x-HC particulate trade-off", SAE No. 800335; 1980.
- [14] Heywood JB. "Internal combustion engines fundamentals", India, Tata McGraw Hill Education Pvt. Ltd., ISBN 10: 1259002071, 2011.
- [15] Deepak Agarwala, Shrawan Kumar Singha, Avinash Kumar Agarwal, "Effect of Exhaust Gas Recirculation (EGR) on performance, emissions, deposits and durability of a constant speed compression ignition engine", *Applied Energy* 88 (2011) 2900–2907, doi:10.1016/j.apenergy.2011.01.066.
- [16] Ronald E. Walpole, Raymond H. Myers, Sharon L. Myers and Keying Ye "Probability and statistics for engineers and scientists", Prentice Hall, UK, ISBN 10: 0-321-62911-6, 2002.
- [17] Nitin Shrivastava, Dr. S.N. Varma, Dr. Mukesh Pandey, "A Study on Reduction of Oxides of Nitrogen with Jatropha Oil Based Bio Diesel", *International Journal of Renewable Energy Research*, Vol.2, No.3, 2012.
- [18] V. Pradeep, R.P. Sharma, "Use of HOT EGR for NO_x control in a compression ignition engine fuelled with bio-diesel from Jatropha oil", *Renewable Energy* 32 (2007) 1136–1154, doi:10.1016/j.renene.2006.04.017.

A Phenomenon of Low-Alloy Steel Distribution Transformation Parameters at Cyclic Loading in Low-Cyclic Area

Shipachev A., Nazarova M.

Department of OGTS, Mining University, Russia, St. Petersburg

Abstract— Following on from the results of measurements of hardness, magnetizing force and the speed of ultrasonic longitudinal waves of 09G2S steel samples at various cyclic operating time values, there is a phenomenon of transformation from the normal law of speed distribution of these parameters in power-mode distribution. It shows the submission of the behavior of metal as a complex system to the theory of the self-organized criticality.

Keywords— Hardness, low-alloy steel, low-cycle loading, distribution, ultrasonic longitudinal waves.

I. INTRODUCTION

In the initial state of the metal (before the application of cyclic loads), its various structural parameters (mechanical, magnetic characteristics, velocity of ultrasonic waves, etc.) characterizing the structure of the material obey, as a rule, the normal distribution law. When investigating the cyclic damage of a metal, it is assumed that the laws of distribution of these parameters remain unchanged. Metal parts working in the machine, are a system in terms of different approaches. First, it is a system in terms of the existence of hierarchical levels of deformation and destruction, according to V. A. Panin [1]. Secondly, the presence of heterogeneities of local macrovolumes, comparable with grain sizes, having different local strength characteristics, causes a redistribution of stresses, deformations, energy in the volume of the metal between these microvolumes of the parts in an optimal way in accordance with the principles of synergetic. Thirdly, it is a system of "basic" metal and metal of the surface layer, which interact, carrying out information-energy exchange [2].

II. TRANSFORMATION OF STRUCTURE PARAMETERS

If we regard the metal parts as a system, it is logical to assume that when it approaches the limit state, it will undergo certain changes. To be exact - the changes characteristic of any complex system as it approaches a critical state or a catastrophe. It can be assumed that in this case the transformation of the distribution laws of

parameters takes place, characterizing the attainment of the limiting state of a metal as a complex system. According to the theory of self-organized criticality [3, 4], the system's achievement of a limiting, critical state means a change in the laws of the distribution of its characteristic parameters, a transition to a power law of distribution. In our case, this can be the transformation of the normal distribution law of the structural parameters of the macrovolumes of a metal into a power law. During the statistical processing of measurements of structural parameters, this transformation is not taken into account. A priori, it is assumed that the distribution law does not change in both the initial and limiting states of the material.

III. INDENTATIONS AND EQUATIONS

According to the theory of self-organized criticality [3, 4], the system's achievement of a limiting, critical state means a change in the laws of the distribution of its characteristic parameters, a transition to a power law of distribution. In our case, this can be the transformation of the normal distribution law of the structural parameters of the macrovolumes of a metal into a power law. During the statistical processing of measurements of structural parameters, this transformation is not taken into account. A priori, it is assumed that the distribution law does not change in both the initial and limiting states of the material. As a result of the analysis of a large body of data on natural and man-made disasters (earthquakes, floods, major accidents at industrial enterprises and transport, etc.), as well as shocks in economic, in particular, financial areas (stock crashes, default, market dynamics modeling of goods, etc.), the basic regularities inherent in these phenomena were determined, and a theory of self-organized criticality was created. The power law of the probability distribution (SSD) of probabilities when approaching the limiting state (a statistical image of catastrophic behavior) is a distinguishing feature of many complex systems [2]. The power distribution law has a probability density of the form

$$f(x)=x^{-(1+\alpha)}. \quad (1)$$

This law is an implication of Pareto distribution for which a distribution function is

$$F(x) = \begin{cases} 1 - x^{-\alpha}; & x \geq 1; \\ 0 & x < 1; \end{cases} \quad 0 < \alpha < 1. \quad (2)$$

We carried out studies of the transformation of the statistical laws of hardness distribution HB, magnetic field strength H, and the speed of ultrasonic longitudinal waves V during the cyclic operating time of 09G2C steel in the low-cycle fatigue region. These studies and their subsequent statistical processing were carried out with the aim: 1. To obtain sets of uniform data of ultrasonic wave velocity measurements in the working zone along the thickness of the sample, with a fixed cyclic operating time. 2. Conduct a statistical test of statistical hypotheses based on Pearson's criterion on the distribution of the general set both in accordance with the normal law and in accordance with the power law. 3. Determine which hypotheses about the distribution laws (normal or power law) are more acceptable in accordance with the Pearson criterion (for a given level of significance) for different values of the cyclic operating time of the samples. 4. To investigate whether the phenomenon of transformation of the normal law of velocity distribution of ultrasonic waves has a power law in the course of cyclic operating time up to destruction (this proves that the behavior of a metal as a complex system in a critical state close to destruction can be described by catastrophe theory). Investigation of fatigue life in the low-cycle region was carried out under cyclic elastoplastic loading. To increase the reliability of the results obtained, the study used samples of a thickness that correlated with the actual dimensions of the apparatuses of chemical production. Samples for tests on low-cycle fatigue were made according to GOST 25502-79 from two plates of sheet metal welded by automatic welding under a layer of flux. The direction of cutting samples along the rolling was chosen from the loading conditions of the products and the technology for obtaining the material. The specimens were loaded on the original fatigue testing machine according to the scheme of pure symmetrical bending. The control of the size of the deflection was carried out with the aid of a special device with a dial gauge. Hardness measurements were made by ultrasonic hardness tester UZIT-3. The principle of operation of the device is based on the dependence of the resonance frequency of a magnetostrictive rod with a diamond pyramid at the end embedded in the surface of the controlled article with a specified force from the area of contact of the diamond with the surface of the article. The strength of the magnetic field was measured by a flux-probe flaw detector FP. Measurements of the propagation velocity of ultrasonic longitudinal waves were performed

using a 36 DL Plus ultrasonic thickness gauge from Panametrics with a D-709 separate-converting transducer at each predetermined level of fatigue damage accumulation. Beforehand, a 6 × 5 mm grid was applied to each sample, and in each cell, thickness measurement was carried out using a micrometer. The method of statistical processing consisted of the following stages.

A set of uniform data of measurements of the velocity of ultrasonic waves was transformed into a variational series. The variational series is necessary for constructing an empirical distribution. The values of the intervals were chosen in such a way that the total number of intervals was not less than 7-8. The intervals were chosen to be equal. Further, all calculations were carried out in the Microsoft Excel software.

The arithmetic mean of the variational series was found

$$\bar{x} = \frac{\sum_{i=1}^m x_i n_i}{n}, \quad (3)$$

where n – total number of measurement data, n_i – number of measurements taken in the interval, m – number of intervals.

Dispersion of variation row was found (not shifted)

$$s^2 = \frac{\sum_{i=1}^m n_i (x_i - \bar{x})^2}{n - 1} \quad (4)$$

and mean square deviation

$$s = \sqrt{s^2}. \quad (5)$$

The analytic expression for the normal distribution law (Gauss' law) was determined from the found parameters of the variational series \bar{x} and s .

$$f(x) = \frac{1}{s\sqrt{2\pi}} e^{-\frac{(x-\bar{x})^2}{2s^2}} \quad (6)$$

Theoretical probabilities p_i were found for the random variable x (measured data) to fall into the i -th interval (equal to the theoretical frequencies of the intervals (n_i/n) from expression (6) under the assumption of a normal distribution law. Then the corresponding theoretical frequencies of the intervals np_i were found.

The value of Pearson's criterion (criterion "Chi-square") was calculated by the formula

$$\chi^2 = \sum_{i=1}^m \frac{(n_i - np_i)^2}{np_i}. \quad (7)$$

For the selected significance level α , which was assumed to be 0.05 and the number of degrees of freedom

$$k = m - r - 1,$$

where r - the number of parameters determining the distribution (for the normal distribution $r=2$), the critical

value of the criterion was determined $\chi^2_{\alpha;k}$. The values of the empirically determined value of the criterion χ^2 and the corresponding critical value $\chi^2_{\alpha;k}$ of it were compared. If $\chi^2 \leq \chi^2_{\alpha;k}$ or $\chi^2_{\alpha;k} - \chi^2 \geq 0$, the hypothesis of the normal distribution does not contradict the experimental data (that is, it is accepted), but if $\chi^2 > \chi^2_{\alpha;k}$ or $\chi^2_{\alpha;k} - \chi^2 < 0$, then the hypothesis is rejected (not accepted) at a given level of significance α or reliability $\gamma = 1 - \alpha$.

The difference $\chi^2_{\alpha;k} - \chi^2$ can serve as an indicator of the closeness of the empirical distribution of a random variable to the theoretical distribution under consideration. The greater the value of this difference, the closer the empirical distribution to the theoretical one being considered, and vice versa.

The acceptability of the power law of distribution was found

$$f(x) = Cx^a, \quad (8)$$

Where a and c are the parameters, $x > 0$, for the empirical variational series, or, in other words, whether it is possible to accept the hypothesis of the distribution of random variables (measurement data) in accordance with the power law. Since the power distribution is symmetric with respect to the mean (mean arithmetic variation series \bar{x}), only half can be investigated, for example, the region lying to the right of \bar{x} . It is assumed that it is legitimate to transfer the values of \bar{x} lying to the left of \bar{x} , in the range of values lying to the right of \bar{x} , symmetrically relative to \bar{x} . That is, if $x_i < \bar{x}$, then the new, "corrected" value of x_i will be equal to $x_i' = 2\bar{x} - x_i$. Or, more conveniently, you can simply combine the intervals lying at the same distance from \bar{x} , and sum up the corresponding empirical frequencies of these intervals. This unification operation was carried out for all the variational series found.

IV. MEASUREMENT PARAMETERS APPROXIMATION DIAGRAMS

To ensure a high-quality product, diagrams and lettering must be either computer-drafted or drawn using India ink Point diagrams of empirical frequencies were constructed on the basis of "combined" variational series. Further, in each diagram a curve was constructed - the trend line corresponding to the power approximation, and parameters a and C were found for this power curve, which correspond to the parameters of the corresponding

regression equation. In Fig. 1, for example, the dependence of empirical frequencies on the speed of ultrasonic longitudinal waves of the samples after operating 2500 cycles is an approximation of the power law of distribution. Figure 1 shows, as an example, a connection of empiric frequencies and ultrasonic wave speed of the samples after 2500 cycles loading – power law distribution approximation.

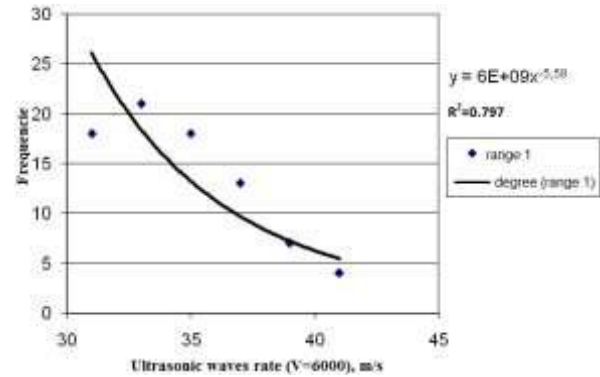


Fig. 1: Ultrasonic wave rates empiric frequencies power approximation of samples after 2500 cycles of loading

From dependence (8), substituting the corresponding parameters of a and C , the theoretical frequencies in each interval were determined.

The value of Pearson's criterion (criterion "Chi-square") was calculated by the formula (7). In this case, the significance level of a was also assumed to be equal to 0.05 and the parameter r in calculating the number of degrees of freedom was assumed equal to 2, since the power distribution also has two parameters.

In a similar manner to that described in point 7, a comparison was made between the values of the empirically determined value of the criterion χ^2 and its corresponding critical value $\chi^2_{\alpha;k}$.

Figure 2 shows the diagram of the hardness HB relative to the relative cyclic damage, where N_p is the number of destruction cycles, N_i is the number of cycles for a given loading stage.

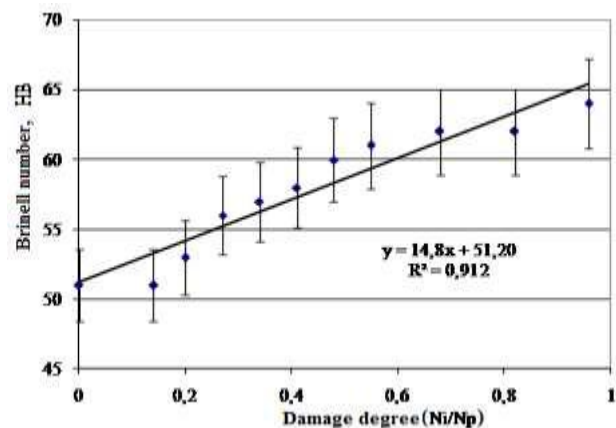


Fig. 2: Brinell number (HB) dependences of deterioration degree

Figures 3, 4, 5 demonstrate the dependence difference $\chi^2_{\alpha;k} - \chi^2$ of loading cycles for hardness HB, ultrasonic waves speed V and magnetizing force correspondingly.

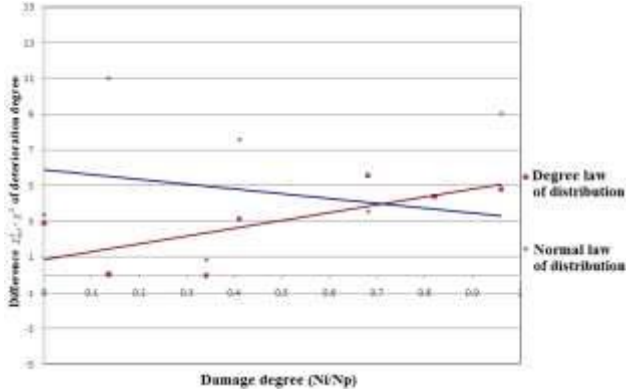


Fig. 3: Dependence the average difference $\chi^2_{\alpha;k} - \chi^2$ of deterioration degree, hardness HB

For each set of homogeneous measurement data on one face of the sample after a certain cyclic operating time, the differences $\chi^2_{\alpha;k} - \chi^2$ were found, respectively, to test the hypotheses of the normal and power distribution laws.

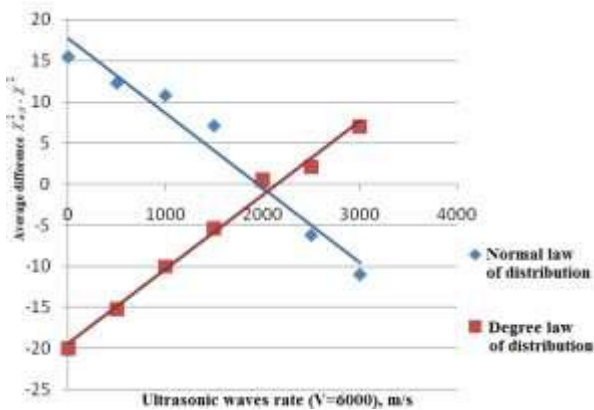


Fig. 4: Dependence of the average difference $\chi^2_{\alpha;k} - \chi^2$ of deterioration degree, ultrasonic waves speed V

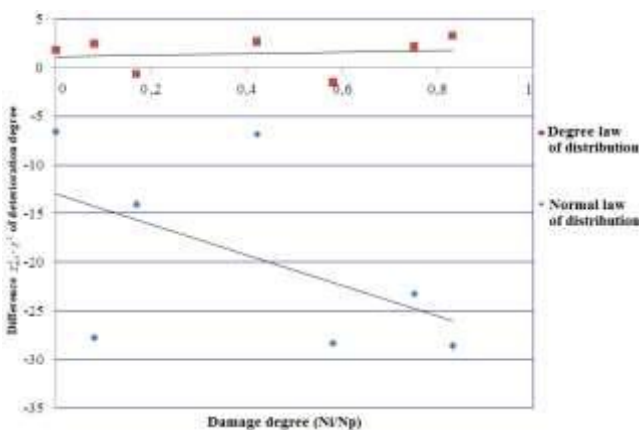


Fig. 5: Dependence of the average difference $\chi^2_{\alpha;k} - \chi^2$ of deterioration degree, magnetizing force

On pictures 3-5 it can be seen that the difference $\chi^2_{\alpha;k} - \chi^2$ when compared with the normal distribution law decreases, but when compared with the power distribution law increases.

V. CONCLUSION

It shows that at during cyclic loading an empiric distributions of steel physical and mechanical parameters is less correspond to normal distribution law, but more corresponds to power distribution law. The aerie higher the abscissa axis on the diagram mean the assumption of distribution law. An aerie lower means rejection of distribution law. In other words, a tendency of normal into power law distribution transformation have a place at cycling loading.

On the base of experimental results and literature sources [2, 3] we come to a conclusion that we have special case - a multiplicative process, which defines the value of α parameter much more than 2.

REFERENCES

- [1] Kuzeev I.R., Naunkin Y.A., Savicheva Y.S., Popova S.V. Poverhnoct I poverhnostnye yavleniya – Ufa: Neftegazovoye delo, 2008 – 144 p.
- [2] Panin V.A., Lihachev B.A., Grinyaev Y.V. Strukturnye urovni deformatsii tvorydyh tel. – Novosibirsk, Nauka, 1990 – 240 p.
- [3] Upravlenie riskom: risk, ustoychivoe razvitiye, sinergetica – Mocsow, Nauka, 2000 – 431 p.
- [4] Malinetskiy G.G., Podlazov A.V., Kuznetsov I.V. Sinergetica I prognoz bedstvii I katastrof / Prikladnaya sinergetica – II: Sbornic nauchnyh trudov – Ufa: UGNTU, 2004. – Volume 1, p 73-104.

Forecasting Particulate Matter Concentrations: Use of Unorganized Machines

Yara de Souza Tadano¹, Hugo Valadares Siqueira¹, Thiago Antonini Alves¹, Manoel Henrique de Nóbrega Marinho²

¹Federal University of Technology – Paraná, Ponta Grossa/PR, Brazil

Email: yarataadano@utfpr.edu.br, hugosiqueira@utfpr.edu.br, thiagoaalves@utfpr.edu.br

²Polytechnic School of Pernambuco, Pernambuco University, Recife/PE, Brazil

Email: marinho75@poli.br

Abstract— Air pollution is an environmental issue studied worldwide, as it has serious impacts on human health. Therefore, forecasting its concentration is of great importance. Then, this study presents an analysis comprising the appliance of Unorganized Machines – Extreme Learning Machines (ELM) and Echo State Networks (ESN) – aiming to predict particulate matter with aerodynamic diameter less than 2.5 μm ($PM_{2.5}$) and less than 10 μm (PM_{10}). The databases were from Kallio and Vallilla stations in Helsinki, Finland. The computational results showed that the ELM presented best results to $PM_{2.5}$, while the ESN achieved the best performance to PM_{10} .

Keywords— air pollution, artificial neural networks, particulate matter.

I. INTRODUCTION

Air pollution has always been an environmental issue studied worldwide. Therefore, its prediction comprises an important topic, mainly due to its impact on human health. Among urban air pollutants, particulate matter (PM) has been considered one of the most harmful ones, as it is related to hospital admissions for respiratory and cardiovascular problems, and even death [1, 2, 3]. Then, PM concentration forecasting is of great interest to government plans and to warn population regarding events of severe pollution levels.

Therefore, the present study aims to show a brief comparative analysis of artificial neural networks performance, the well-known Unorganized Machines – Extreme Learning Machines (ELM) and Echo State Networks (ESN) – on predicting particulate matter with aerodynamic diameter less than 10 μm (PM_{10}) and particulate matter with aerodynamic diameter less than 2.5 μm ($PM_{2.5}$). The database comprises Helsinki, Finland, air pollution from two distinct stations, Kallio and Vanilla from 2001 to 2003.

II. PREDICTOR MODELS

The Extreme Learning Machines (ELM) and the Echo State Networks (ESN) – collectively known as Unorganized Machines (UMs) – are artificial neural networks architectures characterized by a simple training process allied to good results [4]. The most important characteristic of these networks is their hidden layer stands untrained, allowing them to train only the output layer in a minimum mean square error sense, which confers a very fast adjust process to the networks [5].

The ELM, proposed by Huang *et al.* [6], are feedforward networks, quite similar to the traditional Multilayer Perceptron (MLP) [7]. The authors proved by a constructive approach that the output error of a signal could always be reduced inserting a new neuron in the hidden layer of a feedforward network. A condition have to be respected: the activation function of these neurons needs to be differentiable. By means of a rigorous mathematical demonstration, the authors proved that the structure have generalization capability and are universal approximators. Then, to predictions tasks, the ELM may present adequate results even to unknown input data, when it is trained. The most common way to adjust the output layer weights is the application of the Moore-Penrose pseudoinverse operation, which guarantees the best solution, by means of a deterministic solution [5].

Unlike the ELM, the ESN are recursive networks endowed by feedback loops of information. It means some output responses are reinserted in the network input, generating an intrinsic memory. This characteristic may be good to solve problems in which the samples present temporal dependence. The ESN were proposed by Jaeger [8] and, as the ELM, are universal approximators with generalization capability [8, 9].

The main difficulty in classic recurrent neural networks application is the training process, as it is necessary to apply nonlinear optimization techniques. This procedure may lead to instability, local convergence and, in general, it has high computational cost. As mentioned, in the ESN,

the intermediate layer weights – called dynamic reservoir – remains unadjusted. The theoretical element that guarantees the presence of memory is the echo state propriety, which means the most recent historic of inputs rules the internal dynamic of the reservoir. The immediate consequence is the weights of this layer may be previously defined. Then, the adjustment process can be limited to the output layer training, in the same way of the ELM case [8].

III. METHODOLOGY

The data preprocessing is very important to the direct application of the neural networks. For this, the padronization described in Equation (1) is applied [10]:

$$z_i = \frac{d_i - \bar{d}}{\sigma}, \quad (1)$$

where, $i = 1, \dots, N$ is the index of each sample, \bar{d} is the sample mean and σ is the standard deviation. The new series, z , are stationary with zero mean and standard deviation equals to one. The used lags were defined by preliminary tests and the lags selected are 2, 3, 4, 5, and 9, to PM₁₀ and, 1, 2, 4, 8, 9, and 10, to PM_{2.5}.

The adopted performance metrics were the Mean Square Error (MSE) and the Mean Absolute Percentage Error (MAPE), presented in Equations (2) and (3), respectively [10]:

$$MSE = \frac{1}{N} \sum_{n=1}^N (d_n - y_n)^2, \quad (2)$$

$$MAPE = \frac{100}{N} \sum_{n=1}^N \left| \frac{d_n - y_n}{d_n} \right|, \quad (3)$$

where, N is the number of samples, y_n the n -th data predicted and d_n the desired response to the respective predicted data.

IV. COMPUTATIONAL RESULTS

The prediction of PM₁₀ and PM_{2.5} concentrations were held to Helsinki, Finland. To model and predict PM time series, the most common method comprises a weighted combination of the same variable observed data. The database consists of daily data from 2001 to 2003 to Kallio and Vallila Stations [11]. These stations are located in regions with distinct characteristics. Kallio is an urban background and Vallila is located in city downtown with influence of traffic. It means, population around Kallio station is less exposed to air pollution than Vallila ones, which are severely exposed to it.

The computational results considered the forecasting with horizon of one-step ahead, and they are presented in Table 1, which shows the average of 30 simulations. The metrics used to evaluate the performance of the neural networks are MSE and MAPE to real domain (in the magnitude of the original data), and only MSE to padronized data. The label “NN” is the number of neurons in the intermediate layer of the neural networks that reached the best performance. The “K” label is related to Kallio station and “V” one is to Vallila station. The first observation is that there is no direct relation between performance and number of neurons (processor units). The ESN used always less neurons than the ELM. Interestingly, to PM₁₀ forecasting, the ELM achieved the best performance, while to PM_{2.5}, the opposite was verified, the ESN showing the best prediction. It may indicate which type of neural network – feedforward or recursive – is more suitable to solve the task. It is important to observe that the Friedman’s test [12] was performed to analyze the statistical significance of the results. The p -values found were close to zero, which allows assuming the hypothesis that changes in the predictor lead to distinct results.

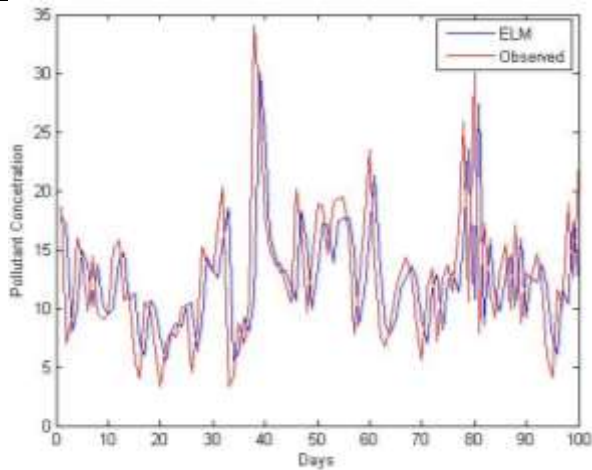
Table.1: Mean Square Error (MSE) and Mean Absolute Percentage Error (MAPE) of computational results to PM₁₀ and PM_{2.5} using ELM and ESN to Kallio (K) and Vallila (V) stations

Metrics		ELM	ESN	ELM		ESN
K-PM ₁₀	NN	120	3	K-PM _{2.5}	10	3
	MSE padron.	0.0052	0.0057		0.0065	0.0046
	MSE	33.1995	36.5808		21.1057	14.8165
	MAPE	32.5936	34.7290		42.7161	37.8863
V-PM ₁₀	NN	70	3	V-PM _{2.5}	70	3
	MSE padron.	0.0029	0.0034		0.0046	0.0033
	MSE	55.0645	64.0550		22.6697	16.4340
	MAPE	33.6415	43.3059		39.9475	35.7573

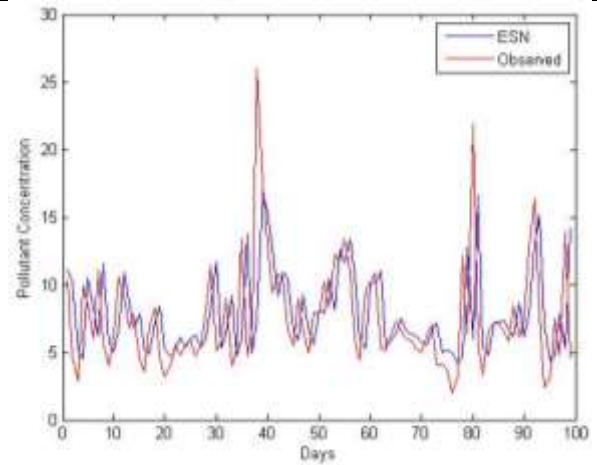
NN – number of neurons in the intermediate layer.

Figure 1 presents the forecasting results in comparison to the observed data to the best cases found. It shows the results to PM₁₀ from Kallio (a) and Vallila (b) stations and to PM_{2.5} from both stations (c, d), respectively. It is

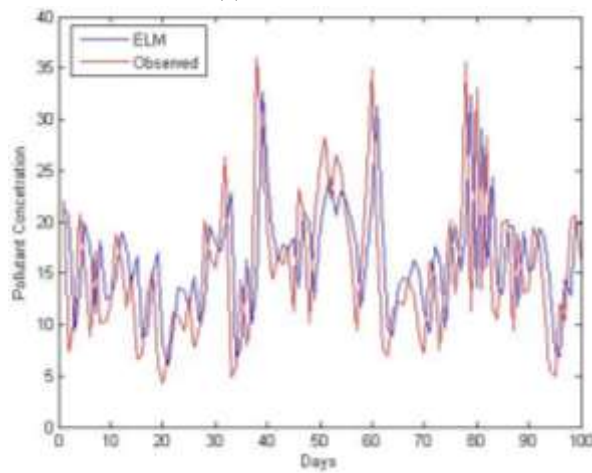
possible to observe that ELM and ESN fitted well to the observed data.



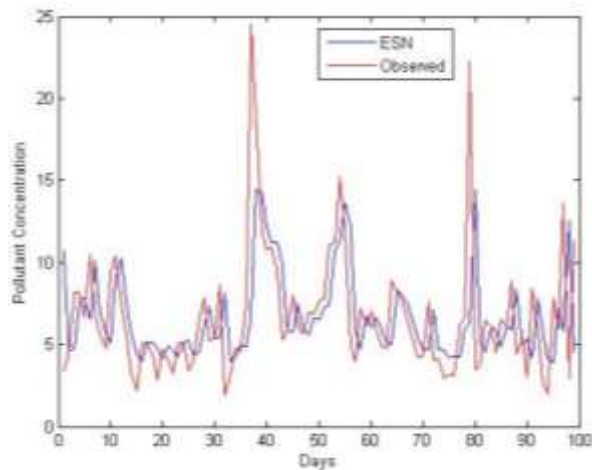
(a) Kallio and PM₁₀



(d) Vallila and PM_{2.5}



(b) Vallila and PM₁₀



(c) Kallio and PM_{2.5}

Fig. 1: Best predictions achieved by the unorganized machines in [$\mu\text{g}/\text{m}^3$]

V. CONCLUSIONS

The main reason to use ELM and ESN architectures is the good results in forecasting problems described in the literature, allied to a simple and efficient training process. The computational results showed that the ELM achieved the best performances to predict PM₁₀ concentrations, while the ESN showed better results to PM_{2.5}. These results could assist government with prediction tools that could help with mitigating measures. New researches can be done using regularized ELM and ESN with nonlinear output layers and, even applying variable selection techniques can increase the general performance of the models.

REFERENCES

- [1] J.P. Langrish, X. Li, S.F. Wang, M.M.V. Lee, G.D. Barnes, M.R. Miller, F.R. Cassee, N.A. Boon, K. Donaldson, J. Li, L. Li, N.L. Mills, D.E. Newby, and L.X. Jiang, "Reducing personal exposure to particulate air pollution improves cardiovascular health in patients with coronary heart disease," *Environ. Health Perspect.*, vol. 120, pp. 367-372, March 2012.
- [2] C.F. Wu, Y.R. Li, I.C. Kuo, S.C. Hsu, L.Y. Lin, and T.C. Su, "Investigating the association of cardiovascular effects with personal exposure to particle components and sources," *Sci. Total Environ.*, vol. 431, pp. 176-182, August 2012.
- [3] Y.S. Tadano, H.V. Siqueira, and T. Antonini Alves, "Unorganized machines to predict hospital admissions for respiratory diseases" in *Proceedings of Latin American Conference on Computational Intelligence (2016)*.

- [4] L. Boccato, E.S. Soares, M.M.L.P. Fernandes, D.C. Soriano, and R. Attux, "Unorganized machines: from Turing's ideas to modern connectionist approaches," *Intern. J. of Nat. Comp. Research*, vol. 2, pp. 1-16, October 2011.
- [5] H.V. Siqueira, L. Boccato, R. Attux, and C. Lyra, "Unorganized machines for seasonal streamflow series forecasting," *Int. J. of Neural Systems*, vol. 24, pp. 1430009.1-1430009.16, February 2014.
- [6] G.-B. Huang, G.-Y. Zhu, and C.-K. Siew, "Extreme Learning Machine: theory and applications," *Neurocomputing*, vol. 70, pp. 489-501, December 2006.
- [7] S. Haykin, *Neural Networks and Learning Machines*, 3rd ed., New York: Prentice-Hall, 2008.
- [8] H. Jaeger, *The Echo State Approach to Analyzing and Training Recurrent Neural Networks*, Bremen: German Nat. Res. Center for Inf. Tech., Tech. Rep. GMD Report 148, 2001.
- [9] A.M. Schäfer, and H.G. Zimmermann, "Recurrent neural networks are universal approximators," *Int. J. of Neural Systems*, vol. 17, pp. 253-263, August 2007.
- [10] G.E.P. Box, G.M. Jenkins, G.C. Reinsel, and G.M. Ljung, *Time Series Analysis: Forecasting and Control*, 5th ed., New York: John Wiley & Sons, 2015.
- [11] D. Voukantsis, K. Karatzas, J. Kukkonen, T. Räsänen, A. Karppinen, and M. Kolehmainen, "Intercomparison of air quality data using principal component analysis, and forecasting of PM₁₀ and PM_{2.5} concentrations using artificial neural networks, in Thessaloniki and Helsinki," *Sci. Total Environ*, vol. 409, pp. 1266-1276, March 2011.
- [12] I.R. Luna, and R. Ballini, "Top-down strategies based on adaptive fuzzy rule-based systems for daily time series forecasting," *Int. J. of Forecasting*, vol. 27, pp. 1-17, July 2011.

Separation of Sediment Contents and Water from Crude Oil of Khurmala and Guwayer Oil Fields in Kurdistan Region by using Centrifuge Method

SaimaJadoon¹, Arif Malik²

^{1,2}Institute of Molecular Biology and Biotechnology, The University of Lahore, Lahore, Pakistan.

¹Saima.jadoon95@gmail.com

²arifuaaf@yahoo.com

Abstract—The present research paper is aimed at determining water and sediment contents in crude oil by using centrifuge method in laboratory in which ASTM D 4007-02 is used to analyze the samples. Furthermore, water and sediment contents in crude oil should be removed because for custody transfer process purchasers prefer to pay only for crude oil and want to minimize the quantity of water and sediment contents in crude oil. Presence of water and sediment contents in crude oil creates problems such as corrosion of equipment when dealt in oil industry along with the problem of oil viscosity. We examined sixteen samples. Four samples were taken from Guwayer oil site area and remaining four from Khurmalla oil site area. These samples were analyzed properly at MNR laboratory in Kurdistan Region-Iraq. The crude oils is considered as the best if it contains less water and sediment content and the vice versa is for the worst quality of crude oil. The method is easy and sharp to check the quantity of sediments and water in crude oil samples in lab and this quantity helps to tell the quality of crude oil.

Keywords—Crude Oil, Sediment content, Centrifuge method, Guwayer and Khurmala, Kurdistan region.

I. INTRODUCTION

Crude oil is naturally occurring underground mixture which mainly contains hydrocarbons with some compounds of Oxygen, Sulphur and Nitrogen. Crude oil is known as petroleum in which petros comes from Greek word meaning rock or stones and oleum comes from Latin language meaning oil. Crude oil and its byproducts are commonly used for fuel purposes and sometimes in medicines. It is regarded as a viscous liquid which contains sediment contents and water. However sometimes one or both are not present in crude oil. In case if both are present then it becomes necessary to remove sediment contents and water from crude oil because it leads to corrosion of

equipment when dealt in oil industry besides effecting he quality of crude oil. It is worth to mention that the properties of crude oil are seriously effected in the presence of sediment content and water. Crude oil is considered to be the best if it is completely free or has very little amount of water or sediment contents Furthermore, the determination of sediment contents and water quantity is important to measure true net volumes of actual oil content in custody transfers, taxation, sales and exchanges. In addition, crude oil is also known as black gold in the world because in many ways our daily life activities heavily depend on crude oil. There are some known techniques which are in practice to determine water and sediment contents in crude oil. The centrifuge method is one of these techniques which is used to determine water and sediment contents in crude oil precisely in both, field and in laboratory.

Determining water and sediment content in crude oil either on site or inside laboratory is essential to custody transfer operations. The centrifuge method can be used on site and gives very accurate results if completed properly. The centrifuge method can also be used in side laboratory but handling or transporting samples may become more critical. (Williams,1990).

API (American Petroleum Institute) gravity is a unit which is used to rank the value of crude oil. The relationship between API gravity and density of crude oil are inversely related. More details about the relationship between API gravity, density and classification of crude oil (light, medium, heavy, and extra heavy) are shown in (Table 1). (Papavinasam, 2014).

1.1 Hydrocarbons

Basically, hydrocarbons are chemical species consisting only of hydrogen and carbon atoms. In addition, hydrocarbons occur naturally beneath the earth surface and are formed when organic matter such as the remains of animals or plants are compressed beneath the earth for a

long period of time at a very high temperature and pressure. Hydrocarbons may exist under the earth surface either as gas or as liquid. However, liquid hydrocarbons are known as a crude oil, and gaseous hydrocarbons are known as natural gas. There are several kinds of hydrocarbons that are classified chemically but with respect to oil industry, there are three types which are more relevant here: Alkanes, aromatic compounds, and cycloalkanes. (Papavinasam, 2014).

1.2 Centrifuge machine

It is a machine that is used to separate or determine sediment content and water in crude oil (Figure 1), in which the separations appear as lines and can be seen easily. The machine consists of four cone-shaped tubes which reads from 0 mL to 50 mL. Moreover, the separation lines usually start from water at the bottom to oil at the top of tubes and between water and oil contents of sediment as shown in (Figure 2).



Fig.1: Centrifuge Machine



Fig.2: Cone-Shaped Tube

II. METHODOLOGY

In this part, Chemical and instrumental methods are used to separate sediment contents and water from crude oil. The centrifuge machine which known as (ASTM D 4007-02) was used and the processes were carried out in the laboratory of MNR (Ministry of Natural Resources) Kurdistan, Iraq. All of samples were analyzed in laboratory. Prior to analyze, the samples should be mixed properly to bring it back to its original state because maybe the sample has been separated into layers while transported to laboratory. (Williams, 1990) .Each of these samples is

analyzed by centrifuge technique which contains 25 mL of crude oil and 25 mL of Toluene with 4 or 5 drops of a demulsifier in centrifuge tubes, after heating water in beaker till the temperature reaches to 60 Celsius degree. The centrifuge tubes should be put in beaker of hot water with temperature of 60° C. After that, the temperature of crude oil samples reaches to 60°C and all centrifuge tubes are put in a centrifuge machine. Finally, each of these sixteen samples are separated from water, sediment contents and oil by measuring (or reading) from centrifuge tubes, and the separation lines between each component (sediment, water and oil) can be seen easily.

III. RESULTS AND DISCUSSION

Sixteen samples of crude oil (eight of them from Khurmalla and eight from Guwayer wells) were tested. After centrifugation of samples the data was obtained by measuring (or reading) the tubes level of each component in mLs. Water and sediment content appear below the tubes if present in crude oil. The first sample of crude oil is called "Slop (Khurmalla)". Sediment content in this sample is nil, which means sediment content is not present in the sample. Water content is noted as 0.05 mL in Slope (Khurmalla) sample. The total sediment content and water in this sample is found to be 0.05 mL and the rest is crude oil. (Shown in Table 2)

Table.1: Shows the result of crude oil samples after centrifugation at 60 C°.

No	Samples (Mean of four)	Sediment content (mL)	Water (mL)	Total Water and Sediment Content (mL)	Crude oil (mL)
1	Slop (Khurmalla)	Nil	0.05	0.05	99.95
2	Crude oil (Khurmalla)	Trace	5.2	5.2	94.8
3	Guwayer-3 well	1.0	0.3	1.3	98.7
4	Guwayer-2 well	12.5	12.5	25	75

Note: Each sample is the mean of four samples of same place.

The quality of first sample was found very good because the amount of water and sediment content is very less, corrosion does not occur while transporting due to low or no water and sediment content. The percentage of free

crude oil is 99.95 mL with green color, which is very good to be sold in a high quality.

The second sample collected from Khurmalla oil field known as "Crude oil (Khurmalla)" was also analyzed in a similar way. Sediment content in this sample after reading through centrifuge tubes is traced in minute quantity. Despite having trace sediment content in the sample, 5.2 mL water was also found in the sample. In conclusion, the total sediment content and water in this sample is 5.2 mL and the rest is crude oil. (Shown in table 1).

The third sample collected from Guwayer oil site known as "Guwayer-3 well" was also analyzed. Water found in this sample in this sample after centrifugation is about 0.3 mL and sediment content of 1 mL as per readings of centrifuge tubes. The total sediment content and water is noted 1.3 mL and the rest which is about 98.7 mL is crude oil (Shown in table 1).

The fourth and last sample collected from Guwayer oil site known as "Guwayer- 2 well" was also tested in a similar way. Water in this sample after centrifugation can be read as 12.5 mL and sediment content was found to be 12.5 mL. The total sediment content and water in this sample is 25 mL and the rest which is 75 mL is crude oil free of water and sediment. (Shown in table 1)

The difference in elevation is so clear due to high amounts of water and sediment content in crude oil. Sediment content is 12.5 mL and water is also 12.5 mL and they are in the same level. The total sediment content and water becomes double (25 mL) and the line rises up. At the end, free crude oil rises up and reaches up to 75 mL. This sample is definitely the worst one due to high amounts of water and sediment content and corrosion might occur if not handled properly.

The percentage of this sample is totally different from other samples. There are huge amounts of water and sediment contents in crude oil of Guwayer-2 well. The purple color of crude oil without water and sediment content contains 75 percent of this sample. The blue color is water which is 12.5 percent and the red color is due to sediment content which is 12.5 percent of this sample of crude oil. The green color showing total sediment content and water is 25 percent of Guwayer-2 well crude oil sample. The quality of this crude oil is the worst one if compared with other three samples.

IV. CONCLUSION

To sum up, the Centrifuge method has been used to separate the water and sediment content from crude oil in laboratory. The results thus obtained are more accurate than the results obtained through other methods used for the separation of sediment contents and water from crude oil. Significant difference has been noticed between the samples collected from two different oil fields. In addition,

the worst sample of crude oil containing more water and sediment content is named as Guwayer-2 well and the best sample containing less water and sediment content in crude oil in this process is named as Slop (Khurmalla). As experienced from the procedure, the crude oils are considered as the best if they contain less water and sediment content and the vice versa is for the worst quality of crude oil. Therefore, to transport the crude oil through pipe lines, it is necessary to reduce the amount of water and sediment content from the crude oil in order to prevent corrosion.

REFERENCES

- [1] P. Hajivand and A. Vaziri, "OPTIMIZATION OF DEMULSIFIER FORMULATION FOR SEPARATION OF WATER FROM CRUDE OIL EMULSIONS", *Brazilian Journal of Chemical Engineering*, Vol. 32, No. 01, pp. 107 - 118, January - March, 2015
- [2] P R Bose, "Method for Recovering Bitumen from Tar Sand", San Francisco, Calif, 25221, 1979.
- [3] C.S.Shetty, "DEMULSIFICATION OF WATER IN OIL EMULSIONS USING WATER SOLUBLE DEMULSIFIERS", *J. DISPERSION SCIENCE AND TECHNOLOGY*, Vol.13, No2, pp.121-133, 1992.
- [4] K A Clark, *The K. A. Clarck Volume, "A collection Papers on the Athabasca Oil Sands.* Edmonton, Research Council of Alberta, 1963.
- [5] T P Clarke, "Oil Sands Hot Water Extraction Process", Alberta, Canada 1979.
- [6] Clarkson, "Oil Sand Separation" Gloucester 1999.
- [7] D. U. J, Chemical treatment of emulsion problem in crude oil. *Journal of Petroleum and Gas Engineering* Vol. 3, No7, pp. 135-141, 2012.
- [8] F Zhang, "DEMULSIFIER FOR SEPARATION OF LIQUID OBTAINED IN CHEMICAL FLOODING OF OIL LAYERS", *Chemistry and Technology of Fuels and Oils*, Vol. 46, No.2, 2010.
- [9] Gordon, "Understanding Unconventional Oil", Washington, D.C: 1779 Massachusetts Avenue, NW.
- [10] H. A. Faris, "The Performance of Toluene and Naphtha as Viscosity and Drag Reducing Solvents for the Pipeline Transportation of Heavy Crude Oil. *Petroleum Science and Technology*, 2015.
- [11] J Williams, "Accurate BS and W Testing Important For Crude-Oil Custody Transfer", Richardson, Tex.: Oryx Energy Co. 1990.

Call Blocking Probabilities Reduction of Channel Assignment in Mobile Communication Systems

Mohamed Abdelghader Morsi¹, Dr. Amin Babkir A.Alnabi², Dr. Ashraf Gasim Alsid³

¹P.G. Student, Department of Communication Engineering, Engineering College, El. Neelain University and spectrum Engineer at National Telecommunication Corporation (NTC), Planning & Studies & Research Department, Head of Future Trends, Sudan.

²Associate Professor, Alneelain University, Sudan.

³School of Electronic Engineering, College of Engineering, Sudan University of Science & Technology, Sudan.

Abstract— In wireless mobile communication systems, the radio spectrum is limited resource. However, efficient use of such limited spectrum becomes more important when the two, three or more cells in the network become hot - spot. The use of available channels has been shown to improve the system capacity. The role of channel assignment scheme is to allocate channels to cells in such way as to minimize call-blocking probability or call dropping probability and also maximize the quality of service. Different channel allocation schemes are in use for mobile communication systems, of which the Hybrid channel allocation (HCA) a combination of Fixed and Dynamic channel allocation schemes (FCA and DCA respectively) was effective. In this paper, the performance of three different channel allocation schemes FCA, DCA and HCA will be analytically compared and the results are presented.

Keywords— HCA, DCA, FCA, call blocking probability, channel allocation, hotspot.

I. INTRODUCTION

Technological advances and rapid development of handheld wireless terminals have facilitated the rapid growth of wireless communications and mobile computing. Taking ergonomic and economic factors into account, and considering the new trend in the telecommunications industry to provide ubiquitous information access, the population of mobile users will continue to grow at a tremendous rate. Another important developing phenomenon is the shift of many applications to multimedia platforms in order to present information more effectively.

The tremendous growth of the wireless/mobile user population, coupled

With the bandwidth Requirements of multimedia applications, requires efficient reuse of the scarce radio spectrum Allocated to wireless/mobile communications. Efficient use of radio spectrum is also important from a cost-of service point of view, where the number of base

stations required to service a given geographical area is an important factor. A reduction in the number of base stations, and hence in the cost of service, can be achieved by more efficient reuse of the radio spectrum. The basic prohibiting factor in radio spectrum reuse is interference caused by the environment or other mobiles. Interference can be reduced by deploying efficient radio subsystems and by making use of channel assignment techniques.

In the radio and transmission subsystems, techniques such as deployment of time and space diversity systems, use of low noise filters and efficient equalizers, and deployment of efficient modulation schemes can be used to suppress interference and to extract the desired signal. However, co-channel interference caused by frequency reuse is the most restraining factor on the overall system capacity in the wireless networks, and the main idea behind channel assignment algorithms is to make use of radio propagation path loss characteristics in order to minimize the carrier-to-interference ratio (CIR) and hence increase the radio spectrum re-use efficiency. The focus of this article is to provide an overview of different channel assignment algorithms and compare them in terms of performance, flexibility, and complexity. We first start by giving an overview of the channel assignment problem in a cellular environment and discuss the general idea behind major channel allocation schemes. Then we proceed to discuss different channel allocation schemes within each category. Here we made an simulation comparison of FCA, DCA, HCA in terms of blocking probability versus traffic load.

II. CALL BLOCKING PROBABILITY

Several metrics can be used to evaluate and compare the performance of the proposed algorithm. The call blocking probability is defined as the ratio of the number of new calls initiated by a mobile host which cannot be supported by existing channel arrangement to the total number of new

calls initiated. Call blocking probability (P_b) is given by the ratio of “number of calls lost by the system” to “the total number of new calls initiated”.

III. FIXED CHANNEL ASSIGNMENT

In the FCA strategy a set of nominal channels is permanently allocated to each cell for its exclusive use. Here a definite relationship is assumed between each channel and each cell, in accordance to co-channel reuse constraints.

The total number of available channels in the system C is divided into sets, and the minimum number of channel sets N required to serve the entire coverage area is related to the reuse distance ‘ s ’.

$N = (1/3)^2$, for hexagonal cells.

Here s is defined as D/R_a , where R_a is the radius of the cell and D is the physical distance between the two cell centers [5]. N can assume only the integer values 3, 4, 7, 9 . . . as generally presented by the series, $(i + j)^2 - i, j$, with i and j being integers [5, 7]. Figures 1(a) and 2(b) give the allocation of channel sets to cells for $N = 3$ ($0 = 3$) and $N = 7$ ($0 = 4.45$), respectively.

In the simple FCA strategy, the same number of nominal channels is allocated to each cell. This uniform channel distribution is efficient if the traffic distribution of the system is also uniform. In that case, the overall average blocking probability of the mobile system is the same as the call blocking probability in a cell. Because traffic in cellular systems can be non uniform with temporal and spatial Fluctuations, a uniform allocation of channels to cells may result in high blocking in some cells, while others might have a sizeable number of spare channels. This could result in poor channel utilization. It is therefore appropriate to tailor the number of channels in a cell to match the load in it by non uniform channel allocation or static borrowing. In non uniform channel allocation the number of nominal channels allocated to each cell depends on the expected traffic profile in that cell.

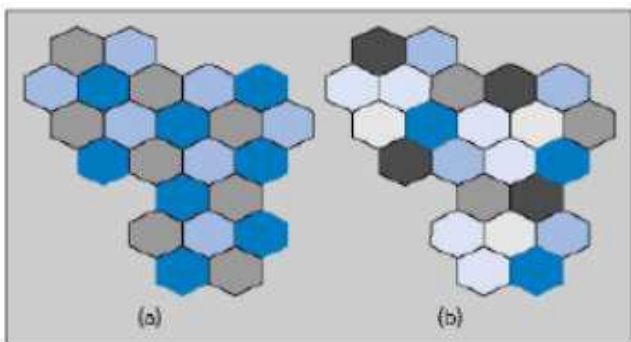


Fig.1: Allocation of channel sets to cells for $N = 3$ and $N = 7$ respectively

IV. DYNAMIC CHANNEL ASSIGNMENT

Due to short-term temporal and spatial variations of traffic in cellular systems, FCA schemes are not able to attain high channel efficiency. To overcome this, DCA schemes have been studied during the past 20 years. In contrast to FCA, there is no fixed relationship between channels and cells in DCA. All channels are kept in a central pool and are assigned dynamically to radio cells as new calls arrive in the system. After a call is completed, its channel is returned to the central pool.

In DCA, a channel is eligible for use in any cell provided that signal interference constraints are

Satisfied. Because, in general, more than one channel might be available in the central pool to be assigned to a cell that requires a channel, some strategy must be applied to select the assigned channel. Based on information used for channel assignment, DCA strategies could be classified either as call by- call DCA or adaptive DCA schemes. In the call-by-call DCA, the channel assignment is based only on current channel usage conditions in the service area, while in adaptive DCA the channel assignment is adaptively carried out using information on the previous as well as present channel usage conditions.

V. COMPARISON BETWEEN FCA AND DCA

In general, there is a trade-off between quality of service, the implementation complexity of the channel allocation algorithms, and spectrum utilization efficiency. Under low traffic intensity, DCA strategies perform better. However, FCA schemes become superior at high offered traffic, especially in the case of uniform traffic. In the case of non uniform traffic and light to moderate loads, it is believed that the DCA scheme will perform better due to the fact that under low traffic intensity, DCA Uses channels more efficiently than FCA. In the FCA case channels are pre assigned to cells, so there are occasions when, due to fluctuation in traffic, calls are blocked, even though there are channels available in adjacent cells. In addition, a basic fact of telephone traffic engineering is that a server With capacity C is more efficient than a number of small ones with the same total aggregate capacity. That is, for the same average blocking probability a system with high capacity has higher utilization. FCA schemes behave like a number of small groups of servers, while DCA provides a way of making these small groups of servers behave like a larger server. Then it is observed that in Fig. 2, with low traffic intensity DCA uses channels more efficiently than FCA because of flexible channel assignment and shows good performance. But with high traffic intensity, DCA

does not show better performance Than FCA as stated above.

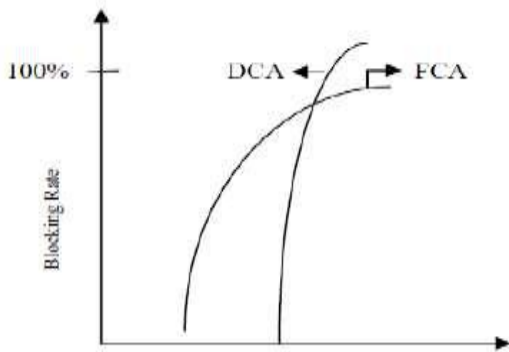


Fig.2: Traffic intensity and blocking rate.

A summary of the comparison between the fixed channel allocation schemes and dynamic channel allocation schemes is given in table (1):

Table.1: Comparison between the fixed channel allocation schemes and dynamic channel allocation schemes

FCA	DCA
Performs better under heavy traffic.	Performs better under light/moderate traffic.
Low flexibility in channel assignment.	Flexible allocation of channels.
Maximum channel reusability.	Not always Maximum channel reusability.
Sensitive to time and spatial changes.	Insensitive to time and spatial changes.
Not stable grade of service per cell in an interference cell group.	Stable grade of service per cell in an interference cell group.
High forced call termination probability.	Low to moderate forced call termination probability.
Suitable for large cell environment.	Suitable in micro-cellular environment.
Low flexibility.	High Flexibility.
Radio equipment covers all channels assigned to the cell.	Radio equipment covers the temporary channels assigned the cell
Low computational effort	Moderate to high call set up delay
Low call set up delay	No frequency planning
Complex. Labor intensive frequency planning	Moderate to high implementation complexity
Low implementation complexity	Centralized, decentralized. Distributed control depending on the scheme

VI. NON UNIFORM PROBABILITY DISTRIBUTION

6.1. Poisson distribution

Historically, the term process has been used to suggest the observation of a system over time. In our example with the copper wire, we showed that the Poisson distribution could also apply to intervals such as lengths. Figure (2.6) provides graphs of selected Poisson distributions. It is important to use consistent units in the calculation of probabilities, means, and variances involving Poisson random variables. The following example illustrates unit conversions.

For example, if the average number of flaws per millimeter of wire is 3.4, then the average number of flaws in 10 millimeters of wire is 34, and the average number of flaws in 100 millimeters of wire is 340.

If a Poisson random variable represents the number of counts in some interval, the mean of the random variable must equal the expected number of counts in the same length of interval.

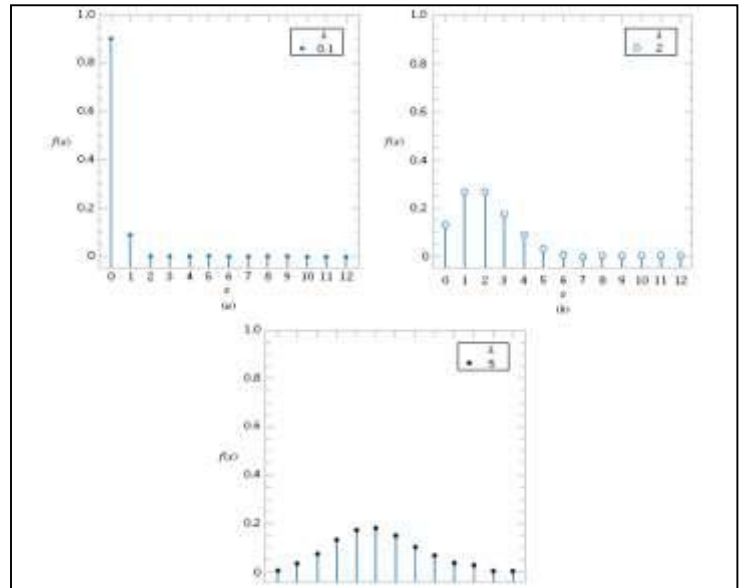


Fig.3: Poisson distribution for selected values of parameters.

VII. HYBRID CHANNEL ASSIGNMENT

Hybrid channel assignment schemes are a mixture of the FCA and DCA techniques. In HCA, the total number of channels available for service is divided into fixed and dynamic sets. The fixed set contains a number of nominal channels that are assigned to cells as in the FCA schemes and, in all cases, are to be preferred for use in their respective cells. The second set of channels is shared by all users in the system to increase flexibility. When a call requires service from a cell and all of its nominal channels are busy, a channel from the dynamic set is assigned to the call. The channel assignment procedure from the dynamic

set follows any of the DCA strategies described in the previous section. Variations of the main HCA schemes include HCA with channel reordering and HCA schemes where calls that cannot find an available channel are queued instead of blocked. The call blocking probability for an HCA scheme is defined as the probability that a call arriving to a cell finds both the fixed and dynamic channels busy.

Performance evaluation results of different HCA schemes have been compared. Theoretical study has done for an HCA scheme with Erlang-b service discipline for uniform size and shape cells where traffic is uniformly distributed over the whole system. The measure of interest is the probability of Blocking as the load increases for different ratios of fixed to dynamic cells. For a system with fixed to dynamic channel ratio 3: 1, the HCA gives a better grade of service than FCA for load increases up to 50 percent. Beyond this load HCA has been found to perform better by case study... A similar pattern of behavior is obtained from the analysis where the HCA scheme employed uses the FA DCA scheme and Erlang-c service discipline (calls that cannot find an available channel are queued instead of blocked). In addition, the HCA scheme with Erlang-c service discipline has lower probability of blocking than the HCA scheme with Erlang-b service discipline. In order to simplify the analysis of HCA we approximate the call blocking probability as a product of random pool as fixed channel allocation blocking probability and non random pool as dynamic channel allocation blocking probability. In comparison with all those channel allocation schemes in terms of call blocking probability HCA performs better results by using hotspot notification and central pool. The main advantage of central pool is that when new call arrives in hotspot cell automatically a channel is assigned to that call from central pool as long as traffic in the cell goes to normal level. Channels in central pools are accessible to hotspot cells. HCA plays a major role to minimize call blocking probability and effects positively on performance of system due to increased tracking capacity. HCA designs to take advantages of both FCA and DCA. An attempt is made to reduce call blocking probability by using hotspot notification.

VIII. HCA ALGORITHM

It consists of two phases

- Channel acquisition phase
- Channel release phase

8.1 Channel Acquisition Phase

Set level ($L = 0$) at the beginning to indicate that the channel request can be accommodated from the first group (A) and there is no hot-spot cell in the network.

1. When a mobile host wants to initiate a call, it has to send a channel request on the control channel to its related base station.
2. If the base station has an available channel from first group (A), it will assign a channel to mobile host.
3. If no channel from the first group (A) is available, then base station updates the value of (L) as shown in Fig (4).

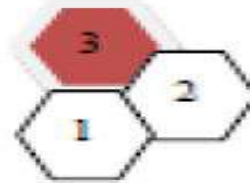


Fig.4: Cell no.3 is hot-spot cell, $L=1$

$$L = L + 1$$

$$L = 0 + 1 = 1$$

$$L = \max(L, M)$$

4. The base station then sends a request to borrow a channel from the central pool located at MSC. It also includes the current value and maximum value of (L).

8.2 Channel Release Phase

1. The MSC, on receiving channel request from the base stations assign up to the (L) channels if available from dynamic pool.
2. When the base station successfully acquires channel from the dynamic pool at MSC, it also adds a channel to its temporary pool (T).
3. When a call terminates on a channel at a mobile host, the base station needs to find out which type of channel the call belonged to.
4. If channel is belonged to dynamic pool at MSC the base station estimates current level of hot-spot (h) in the cell as shown in Fig (5):

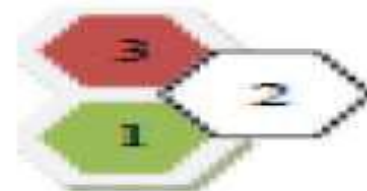


Fig.5: Estimation of current hot-spot level (h), cell no.1 and 3 hot-spot cells, $h=2$

5. If ($h \leq L$) meaning that the congestion in the cell is same or easing, the base station checks its temporary pool (T) and retains up to (h) channels in random order and all the remaining channels in (T) are returned back to MSC.

6. If $(h > L)$ meaning that the congestion in the cell is getting worse, the channel is retained in the cell. The channel is not returned back to MSC.

7. If MSC is unable to assign even one channel, the call will be blocked.

IX. SIMULATION

9.1 Simulated result of FCA:

$$B = A^2/2 / (1+A+A^2/2) \dots \dots \dots (1)$$

The resultant performance curve in this case plotting the blocking probability 'B' versus load Intensity of traffic by using above formula.

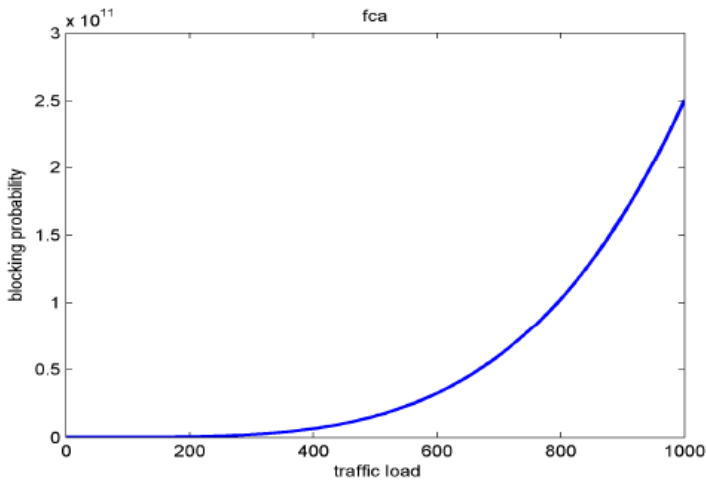


Fig.6: blocking probability Traffic Load of FCA

9.2 Theoretical result of HCA:

The blocking probability (Pb) in HCA is given by as Eq 2:

$$P_b = \frac{\frac{A^N}{N!}}{\sum_{k=0}^N \frac{A^k}{k!}} \dots \dots \dots (2)$$

Where A is given by $A = \lambda/\mu$, which is successive call time arrivals. In which, λ is the call arrival rate per second, μ is average call departure rate of users per second, and N is number of channels in the system

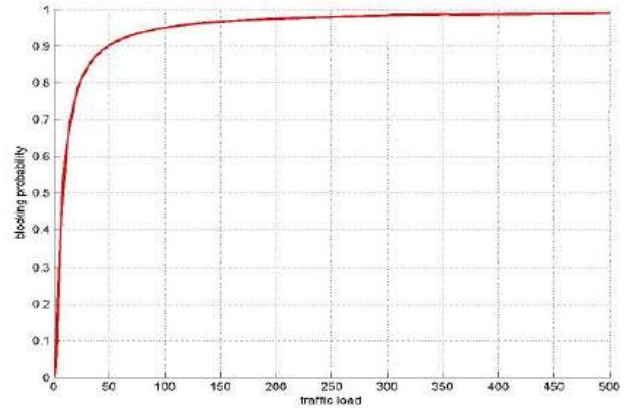


Fig.7: blocking probability traffic load of HCA

9.3 Simulated result of HCA:

The simulation result is shown in Fig. 7, HCA simulates with dynamic pool, and MSC does not have fixed number of channels. There is no fixed relationship between channels and cells. It keeps changing randomly within the range (here it is 50). This simulation scenario, for channel allocated from pool due to the lack of channels in the hot-spot has. Therefore, MSC has less channels to lend to other base stations. This indirectly simulates the effect of hot-spot in the Network.

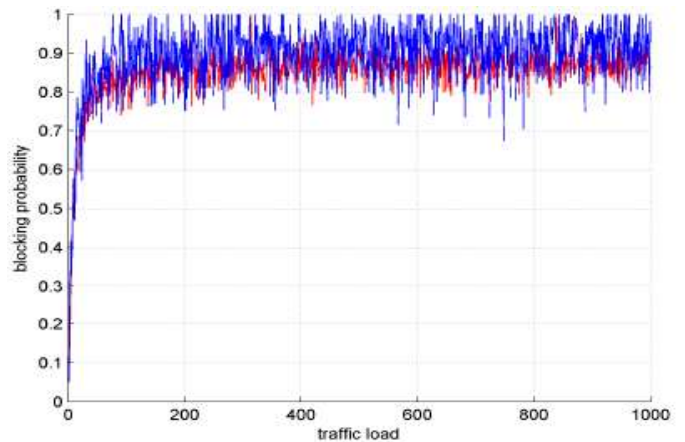


Fig.8: Simulated blocking probability traffic load of HCA.

X. SIMULATION TOOL

In order to evaluate the performance of channel assignment schemes we simulate the FCA, DCA, and HCA in terms of blocking probability versus traffic load by using MATLAB.

XI. CONCLUSION

The Channel Assignment is very important process and the channel Assignment Algorithm mechanism should be related to the traffic types and customer distribution. The HCA has Avery good performance for traffic load less than 200 erlang.

REFERENCES

- [1] P.M.PAPAZOGLU1, 3, D.A.KARRAS2, R.C.PAPADEMETRIOU3, Improved Integral Channel Allocation Algorithms in Cellular Communication Systems Enabling Multimedia QoS Services, **October 2008**.
- [2] Kanagasabapathy A A, Franklin A A, Murthy C S R. An adaptive channel recon_guration al-Gorithm for multi-channel multi-radio wireless mesh networks [J]. IEEE transactions on wireless Communications, **2010**, 9(10): 3064-3071.
- [3] Rincy George and Jude Hemanth, Application of an Optimization Algorithm for Channel Assignment in Mobile Communication, **2011**.
- [4] P.Ravi and P.Jesu Jayarin, Optimal Channel Allocation Mechanism to Improve the QoS in Wireless Networks, **2012**.
- [5] Swati Sonavane1 and Dr. R, and R. Sedamkar2, Improved Channel Assignment Scheme in Cellular Mobile Communication, October **2012**.
- [6] Y. Ryu, "A Buffer Management Scheme for Mobile Computers with Hybrid Main Memory and Flash Memory Storages", IJMUE, vol.7, no.2, (**2012**), pp. 235-240.
- [7] Seong-Hoon Lee1 and Byung-Tae, an Intelligent Channel Allocation Mechanism, **2013**.
- [8] Arafat Abu Mallouh1 and Christian Bach2, Dynamic Channel Allocation in Cellular Networks, **2013** Innovative Space of Scientific Research Journals.
- [9] G. Arul Dalton, Dr. T. Jeba Rajan, and Dr. K. Siva Sankar, an Optimized Channel Assignment Strategy for Wireless Cellular Networks, **2013**.
- [10] Mohamed Abdelghader Morsi1, Ashraf Gasim Elsid Abdalla2, and Mohammed Abaker3, Adaptive Hybrid Channel Assignment (AHCA) Algorithm, **Feb 2015**.
- [11] Mohamed Abdelghader Morsi1, Amin Babkir A.Alnabi2 and Ashraf Gasim Alsid3, New Adaptive Channel Assignment Scheme for Cellular Network, **April 2015**.

AUTHOR[S] BRIEF INTRODUCTION

Mohamed Abdelghader Morsi is Research in the level of PhD, Faculty Engineering, Alneelain University, Khartoum, Sudan. He received Master of Science (Msc) in Telecommunication Engineering degree in 2010, from Sudan University, Sudan. He Received Bachelor Degree in Electronic Engineering (Computer), from University of Technological Science, Khartoum, Sudan.

Research interests are Mobile & Satellite Networks .He Spectrum Engineer in NTC (National Telecommunication

Corporation), Planning & Studies & Research Department, **Head of Future Trends**, Khartoum, Sudan.

Dr.Amin Babkir Associate professor in telecommunication Engineering Also he is Associate Professor, Alneelain University, He got his PhD from Alneelain University and Msc from Khartoum University. He got his B.Sc. in electronic engineering Khartoum University. He is published more than 200 technical papers and supervised more than 150 Ph.D. and Master Students.

Dr.Ashraf Gasim Elsid Abdalla, Associate professor in telecommunication Engineering and researcher in space technology center in future university. Khartoum, Sudan. Also he is academic members of electronic department in college of engineering, Sudan University of science and technology. He was a former lecturer and researcher in many Malaysia Universities; UKM, UPM, UIA and MMU. He got his Ph.D. and M.Sc. from National university of Malaysia 2001 and 1996 in electrical and electronic system. He got his B.Sc. in electronic engineering from technical university of Budapest 1993. His research focus on Mobile and satellite communication. He published more than 100technical papers

And supervised more than 100 Ph.D. and Master Students.

Khalid Qasem Mohamed Alborahy, received the B.Sc degree in Electronic Engineering (major of telecommunications) from Sudan University of Science and Technology (SUST), Khartoum, Sudan, in 2007 and M.Sc. degree in Telecommunication Engineering from Sudan University of Science and Technology, Khartoum, Sudan, In 2010. Currently he is doing his PhD research in telecommunication engineering at the faculty of Engineering, Department of Electrical and Electronic Engineering, University of Khartoum (U of K), Khartoum, Sudan. His research interests are in wireless communications, including mobile broadband, 4G, 5G, heterogeneous networks, channel assignment, handover, integrated wireless networks, and next generation.

Notion, Essence and Evaluation of the use of Information Technologies in the Economy of Metallurgical Industry

Ghomrani Mohammed El Amine¹, Pavel B. Boldyrevskii²

¹Graduate student of mathematics and natural sciences department, Lobachevsky State University of Nizhny Novgorod – National Research University, Nizhny Novgorod, Russian Federation

²Professor, Head of mathematics and natural sciences department, Lobachevsky State University of Nizhny Novgorod – National Research University, Nizhny Novgorod, Russian Federation

Abstract— This article describes the main aspects of the use of IT technologies in the economy of the metallurgical industry, the Author emphasized the relevance of the study based on the current state of the Russian economy and the prospects of this direction. The article reveals the problems of assessing the possibilities of using IT technologies in the economy. And offered some solutions, which is of practical value.

Keywords— *IT-technologies, metallurgy, metallurgical industry, evaluation methods, industry.*

I. INTRODUCTION

The successful development of companies in the metallurgical industry of Russia which along with the fuel and energy sector is an important part of the domestic economy, it is currently impossible without the creation of a modern IT infrastructure. Using an arsenal of tools, the company considered both optimizes their business processes, which, in the final analysis, lead to a decrease in the level of operating costs. In the struggle to preserve the results achieved and increase its share in the global market enterprise in metallurgy industry systematically carry out the introduction of advanced technologies in both production and management [6]. The relevance of this study lies in the fact that those companies within the industry, which carried out the launch of modern production facilities Parallel with the introduction of modern information systems, according to the scientific community, will be able to take in the near future the leading position in the market.

The term "information technology" should be understood set of production processes, methods, and software and hardware tools that are integrated into the process chain, ensuring the collection, processing, storage, distribution and display of information in order to reduce the complexity of the processes used information resources, improve their efficiency and reliability [1, C.111].

Bringing the above-mentioned concept of the economy of metallurgical industry it should be understood by IT - use of information technology in the economy of the metallurgical industry, which includes the collection, processing, transmission and storage of large amounts of economic data in the sector in question [3, C.183].

Among the factors shaping the modern trends in the use of IT technology in the metallurgical industry experts are the following:

- Technological growth of market relations and the process of globalization of activity, i.e. participation of enterprises in the metallurgical industry in the global commodity chains, which makes it necessary to improve the quality of the processed information. The competitiveness of the enterprise in question depends largely on how the material resources, but to a greater extent on the availability of advanced means of communication links with partners and customers, the volume of each company staff accumulated industry knowledge and professional skills, as well as opportunities in their intensive use;
- Sustainability and profitability of the business in the relevant field are largely determined by the speed of response to the changing needs of the end user. Claiming success requires industries subject faster than their competitors restructure its internal organization in order to maintain readiness to meet the emerging needs of the client;
- Information requirements from the standpoint of accuracy, completeness, relevance and timeliness requirement supplemented its effective use at all levels of management. There is a tendency to integrate both services, and enterprise information systems into a single field with the aim of continuing to ensure economic

management of information about the position of the direct current affairs, as well as the opportunities available in the relevant market.

In our turn, the nature of the use of IT technology in the industry is the processing of information economic plan in the industry, which takes place on specific and pre-laid algorithms that including you must be able to competently use, but above all, we should understand their purpose and the correct meaning. Storing this information may be produced in different amounts and different types of media. Thus, communication can be performed at a sufficiently long distance in a short time.

In addition, a number of researchers are not groundless believes that today, "the world of thin technologies begins to rule the world of machines, that is the world of reality" [4]. In this context, the importance of acquiring the word "start" that can serve as a hint of some great opportunities of using IT technologies. In this aspect, a number of difficulties.

Assume that the cost estimate is performed in several stages, namely:

- A comparative analysis of IT spending in the whole group of companies in the metallurgical industry,

which involves calculation of the following indicators:

- At the IT costs that can be calculated as a percentage of income;
- The proportion of employees of IT services in the total staff number of employees of the enterprise;
- The number of PCs per 1 employee of the IT department;
- PC software personnel by 100%.

However, these figures do not allow to fully assessing the possibility of using IT technologies in the industry, as it does not contain complete information on the economic activity of the enterprise or group of enterprises relevant industry. If you give a more precise wording, this method takes into account only the costs [5, C.62].

The author Pergunova O.V "Assessment of the development and use of information and telecommunication technologies at the metallurgical enterprises of the Orenburg region" proposed approach to each of the enterprises of the industry individually, using individual assessment methods (see. Table 1) [2, c.250].

Table.1: Methods of evaluating the effectiveness of the use of ICT

methods of assessment	positive sides	negative sides
Traditional financial methods(Return on investment, Economic value Added, Total cost of ownership, Total Economic impact, Rapid economic justification)	1) Methods, on the basis of a classic financial analysis and profitability concepts operate net present value internal rate of return. 2)The effect of the application of information technology in the form of estimated cash equivalent.	Methods are based on a comparison of income and expenditure, so it is important assess as the outgoing cash flows (costs). Incoming and (profit) .methods allow us to estimate the cost side and the quantity. Incoming cash flows to determine practically impossible.
probabilistic methods(Real Options Valuation, Applied information economics)	The ability to assess the probability of occurrence of risk and new possibilities with the help of statistical and mathematical models.	Impossiblein today's economic environment to accurately predict changes in technical and economic indicators of the enterprise.
Qualitative methods(Balanced scorecard, information economics, portfolio management, It scorecard)	1) The ability to link the assessment of the effectiveness of IT projects with the corporate strategy of the company. 2) Range of textures that characterize the effectiveness of IT remains with the specialists, which allows taking into account the specifics of the enterprise.	1) For self-development of the system performance is significantly affected by the subjective opinion of specialists. 2) The absence of the fundamental principles of prioritization of key performance indicators.

As can be seen from the table given, the three main types of methods: qualitative, probabilistic and traditional financial valuation techniques. Each method has its advantages and disadvantages. Some methods for evaluating the ability to provide for the prediction of certain changes in technical and economic parameters of the enterprise, while others do not allow the relevant forecasts. Thus, the assessment of the possibilities of using IT technologies in the economy, the metallurgical industry is difficult, as there is no single, universal approach in the assessment.

The author of this article believes that in order to assess the feasibility of introduction of IT technologies necessary to the existence of a single differentiated system of indicators. Given the isolation of the enterprises need their unit to the appropriate group, depending on the volume of production. It is expected that the wider range and greater production volumes, the more important these enterprises play in the IT technology, respectively, the number of such enterprises should be a great indicator.

The procedure for the calculation of indicators for assessing IT consists of the following steps: a) selection of the initial array of indicators (egg, the presence of the PC, PC upgrade, PC software employees, the number of computers connected to the global and local networks); b) on the basis of the indicator index, which can be determined by dividing the achieved value baseline X_i to basic / standard value X_{bi} ; g) the calculation of the integral indicator of the use and development of information technology resources in an industrial plant or a group of industrial enterprises in the industry.

To optimize the calculations necessary to develop a national IT platform, allows you to enter the initial data, followed by the construction of charts and predictions.

Thus, IT-technology, used in the metallurgical industry will reduce the risks for individual companies and provide optimal operation in the economic crisis.

REFERENCES

- [1] Valko D.V Information technology as a kind of economic activity // Interdisciplinary dialogue: current trends in social, humanities, natural and technical sciences. - 2014. - №1. - S. 210 - 217.
- [2] Pergunova O.V Assessment of the development and use of information and telecommunication technologies at the metallurgical enterprises of the Orenburg region // Basic Research. - 2012. - №6-1. - S. 249-253.
- [3] Romaseva Y.A Metallurgy today // New Science: From the idea to the result. - 2017. - № 1-2. - S. 182-185.
- [4] Modern metallurgy beginning of the new millennium / collection of scientific papers /

Ministry of Education and Science of the Russian Federation, Lipetsk state. Technical Univ, Novolipetsk metallurgy; [The Editorial.: A/K Pogodaev (prev.), and others.]. - Lipetsk. - 2011. - Vol 2.

- [5] Demesinov T.J. Development methods of outsourcing commercial system in metallurgy enterprises // Bulletin of the University of Turan. - 2011. № 1 (49). - S.59-63.
- [6] The Russian Newspaper // Access: <https://rg.ru/2016/11/07/kak-it-tehnologii-primeniaiutsia-na-metallurgicheskikh-predpriatiiah.html>

Performance Evaluation and Study of Routing Protocols: MANET vs VANET

Annu¹, Ms. Reema²

Dept. of Computer Engineering, SKITM, Haryana, India

Abstract— In the recent years the number of vehicles on road increases at high speed. A lot of road accidents and traffic congestion emerges. So to control it vehicular ad-hoc network came in picture. In the last few years many protocols were proposed to route the packets efficiently and correctly. But no one was capable of routing the packets in case of cross links. So, a protocol named GEOCROSS was proposed. The introduction of MANETs, VANETs, their routing protocols, protocol structure of VANET, how broadcasting takes place in VANET, how information is disseminated in VANET and VANET communication & routing protocols like vehicular collision warning communication (VCWC), vehicle heading based routing protocol (VHRP) and GEOCROSS routing protocol will be discussed in this paper.

Keywords— MANET, VANET, routing protocols.

I. INTRODUCTION

MANET is a self-configured wireless ad-hoc network of mobile nodes. The MANET organization depends upon the location of nodes, their connectivity, their service discovery capability & their ability to search and route messages using nearest nodes or nearby nodes. The properties of MANETs are data routing abilities, neighbor discovery for data reception and transmission, variable routing paths, flexible network architecture, no access point requirement, peer-peer connectivity, limited wireless connectivity range, data caching saving and aggregation and requirement to solve exposed or hidden terminal problem.

VANET belongs to wireless communication networks area. VANET is the emerging area of MANETs in which vehicles act as the mobile nodes within the network. The basic target of VANET is to increase safety of road users and comfort of passengers. VANET is the wireless network in which communication takes place through wireless links mounted on each node (vehicle) . Each node within VANET act as both, the participant and router of the network as the nodes communicates through other intermediate node that lies within their own transmission range. VANET are self organizing network. It does not rely on any fixed network infrastructure. Although some fixed

nodes act as the roadside units to facilitate the vehicular networks for serving geographical data or a gateway to internet etc. Higher node mobility, speed and rapid pattern movement are the main characteristics of VANET. This also causes rapid changes in network topology .

VANET is a special type of MANET, in which vehicles act as nodes. Unlike MANET, vehicles move on predefined roads, vehicles velocity depends on the speed signs and in addition these vehicles also have to follow traffic signs and traffic signals. There are many challenges in VANET that are needed to be solved in order to provide reliable services. Stable & reliable routing in VANET is one of the major issues. Hence more research is needed to be conducted in order to make VANET more applicable. As vehicles have dynamic behavior, high speed and mobility that make routing even more challenging.

VANET routing protocols history starts with traditional MANET protocols such as AODV (Ad hoc on Demand Distance Vector Routing) and DSR (Dynamic Source Routing) . AODV and DSR have been considered efficient for Multi hop wireless ad hoc networks.

II. BASIC CONCEPTS AND BACKGROUND

Ad-hoc networks are self-organized, wireless and decentralized systems that form temporary networks. Wireless technology is becoming the dominant one because of mobility, accessibility and flexibility in information dissemination. Cellular phones, wireless internet like Wi-Fi, satellite televisions etc. are well known applications of wireless technologies. It is a well growing area for research. The two main reasons of rapid growth of mobile computing are lower prices and higher data rates.

MANET (Mobile ad hoc network) is an infra-structure less IP based network of mobile and wireless machine nodes connected with radio. In operation, the nodes of a MANET do not have a centralized administration mechanism. It is known for its routable network properties where each node act as a “router” to forward the traffic to other specified node in the network. MANET (Mobile ad hoc network) is a temporary self organizing system formed by a collection of nodes, which are connected with wireless links. In the

network, nodes may be disappeared or new nodes may be appeared over the time due to node mobility.

Ad Hoc Networks

A wireless ad hoc network is a multi hop network that is a collection of mobile or sometimes stationary nodes connected with bandwidth constrained wireless links i.e. every node should have wireless interfaces and thus have their own transmission ranges, forming a decentralized ad hoc network. Laptop computer or Personal Digital Assistance (PDA) can be the example of the nodes in a wireless ad hoc network. A node can leave the network or

enter into the network whenever it wants. There is no central administration and for that, each node forwards packets according to a routing protocol. A node in an ad hoc network is a host as well as a router. An ad hoc network is a network capable of adjusting itself in the change of routing topology in time. If any route is disturbed by the link failure or something, the station calls a route discovery function to find out an alternative route and forward the packet in the way of that route. To find out the way, a packet should be forwarded. Different routing protocols are available but only one protocol should be fixed before the network becomes operational.

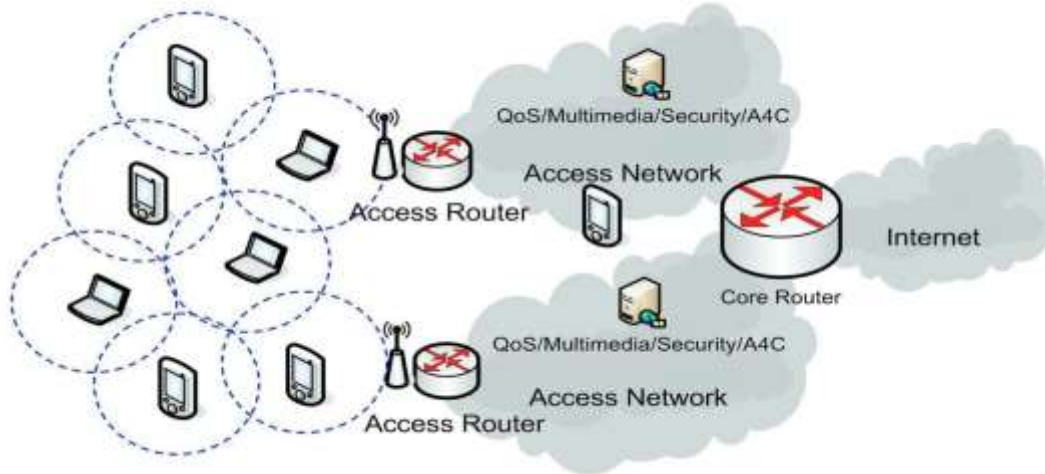


Fig.1: Ad-hoc network architecture

In the figure 2, a typical ad hoc network with three participating nodes is shown, where node1 cannot send packets directly to the node3 because they are not in the same transmission range. Node1 first sends the packet to node2 and node2 acts as a router, forwards the packet to node3 as they are on the same transmission range. There is no central administration and according to the figure 2, it is a clear that change of node mobility changes the routes.

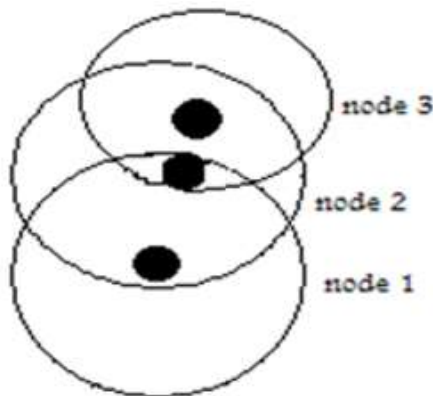


Fig.2: A Typical Ad hoc Network

Types of MANET

There are different types of MANETs including:

- InVANETs – Intelligent vehicular ad hoc networks make use of artificial intelligence to tackle unexpected situations like vehicle collision and accidents.
- Vehicular ad hoc networks (VANETs) – Enables effective communication with another vehicle or helps to communicate with roadside equipments.
- Internet Based Mobile Ad hoc Networks (iMANET) – helps to link fixed as well as mobile nodes.

MANET Characteristics

- In MANET, each node act as both host and router. That is it is autonomous in behavior.
- Multi-hop radio relaying- When a source node and destination node for a message is out of the radio range, the MANETs are capable of multi-hop routing.

- Distributed nature of operation for security, routing and host configuration. A centralized firewall is absent here.
- The nodes can join or leave the network anytime, making the network topology dynamic in nature.
- Mobile nodes are characterized with less memory, power and light weight features.
- The reliability, efficiency, stability and capacity of wireless links are often inferior when compared with wired links. This shows the fluctuating link bandwidth of wireless links.
- Mobile and spontaneous behavior which demands minimum human intervention to configure the network.

- All nodes have identical features with similar responsibilities and capabilities and hence it forms a completely symmetric environment.
- High user density and large level of user mobility.
- Nodal connectivity is intermittent.

VANET : VANET is the short form of Vehicular Adhoc Network. It is subclass of network of MANET type.

The routing protocols of MANET are not feasible to be used in the VANET network. If they are used then also they will not be able to deliver required throughput as it has fast changing adhoc network.

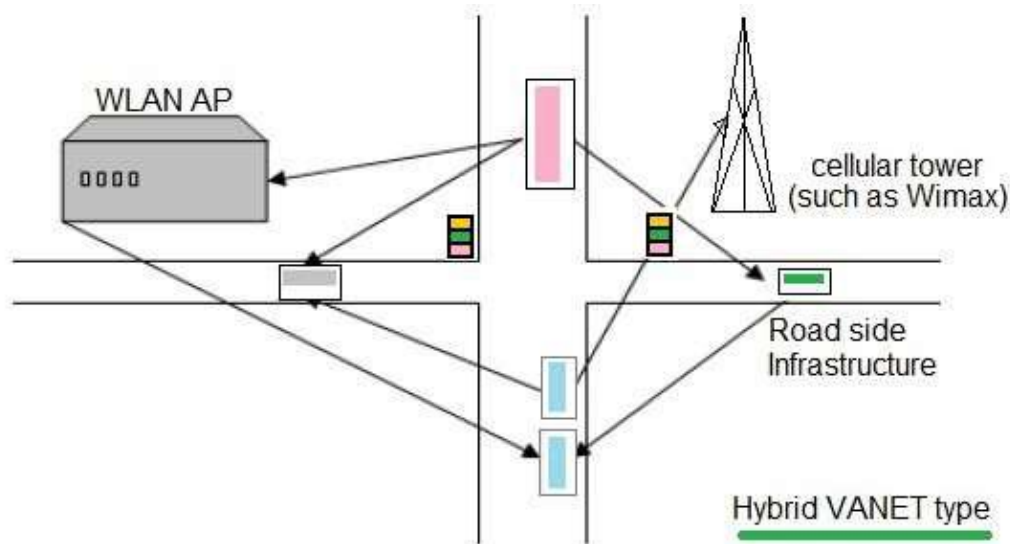


Fig.3: combination of both infrastructure and adhoc networks

In VANET, the communication nodes are moving on pre-defined roads as finalized initially.

The VANET architecture consists of three type of categories as mentioned below:

- cellular and WLAN network
- Pure Ad hoc (network between vehicles and fixed gateways)
- hybrid(combination of both infrastructure and adhoc networks), as shown in figure.

In the first type, fixed gateways and WiMaX/WiFi APs are used at traffic junctions to connect with the internet, to obtain traffic information and used for routing. The VANET nodes are not subject to storage and power limitation. Vehicular Ad hoc Network (VANET) is a subclass of mobile Ad Hoc networks (MANETs). These

networks have no fixed infrastructure and instead rely on the vehicles themselves to provide network functionality.

These networks offer several benefits to organizations of any size. While such a network does pose certain safety concerns but this does not limit VANET's potential as a productivity tool. GPS and navigation systems can benefit, as they can be integrated with traffic reports to provide the fastest route to work.

III. PROPERTIES OF AD-HOC ROUTING PROTOCOLS

The properties that are desirable in Ad-Hoc Routing protocols are:

- Distributed operation: The protocol should be distributed. It should not be dependent on a centralized controlling node. This is the case even for stationary networks. The dissimilarity is that the

- nodes in an ad-hoc network can enter or leave the network very easily and because of mobility the network can be partitioned.
- ii). Loop free: To improve the overall performance, the routing protocol should assurance that the routes supplied are loop free. This avoids any misuse of bandwidth or CPU consumption.
- iii). Demand based operation: To minimize the control overhead in the network and thus not misuse the network resources the protocol should be reactive. This means that the protocol should react only when needed and should not periodically broadcast control information.
- iv). Unidirectional link support: The radio environment can cause the formation of unidirectional links. Utilization of these links and not only the bi-directional links improves the routing protocol performance.
- v). Security: The radio environment is especially vulnerable to impersonation attacks so to ensure the wanted behavior of the routing protocol we need some sort of security measures. Authentication and encryption is the way to go and problem here lies within distributing the keys among the nodes in the ad-hoc network.
- vi). Power conservation: The nodes in the ad-hoc network can be laptops and thin clients such as PDA's that are limited in battery power and

therefore uses some standby mode to save the power. It is therefore very important that the routing protocol has support for these sleep modes.

- vii). Multiple routes: To reduce the number of reactions to topological changes and congestion multiple routes can be used. If one route becomes invalid, it is possible that another stored route could still be valid and thus saving the routing protocol from initiating another route discovery procedure.
- viii). Quality of Service Support: Some sort of Quality of service is necessary to incorporate into the routing protocol. This helps to find what these networks will be used for. It could be for instance real time traffic support.

IV. ROUTING PROTOCOLS IN VANET

The routing protocols of VANETs fall into two major categories of topology-based and position-based routing. There are many advantages and disadvantages of these routing protocols. We explore the motivation behind their design and trace the evolution of these routing protocols and analyze their efficiency with respect to MANETs as there are countless numbers of routing protocols [9, 14, 15] developed in MANETs, but they do not apply well to VANETs which represent a particularly challenging class of MANETs. They are distributed, self-organizing communication networks as described before.

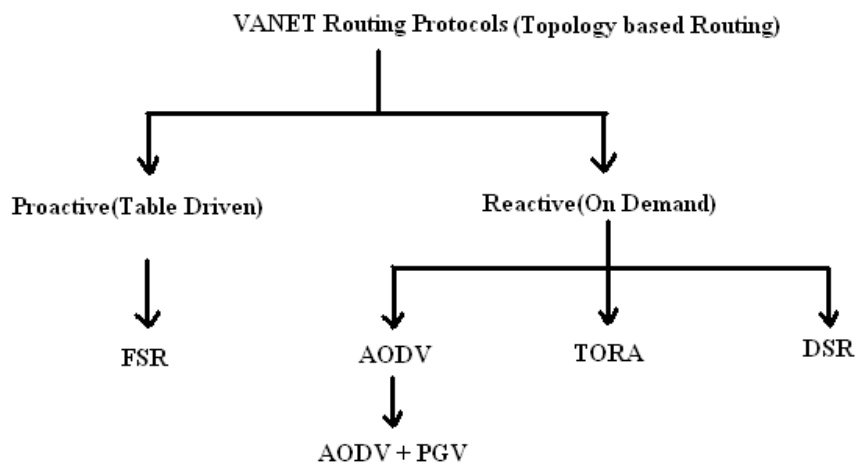


Fig.4: Classification of VANET Routing Protocols

The detailed coverage of relevant routing protocols and their impact on overall VANET architecture is incomplete without discussion of VANET topics and applications. The different types of VANET architectures can be as shown above in the figure. There are a number of MANET routing

protocols and surveys written on them, we will therefore only restrict our attention to MANET routing protocols used in the VANET context. Broadcast routing is frequently used in VANET for sharing, traffic, weather and emergency, road conditions among vehicles and delivering

advertisements and announcements. Broadcasting is used when messages need to be disseminated to the vehicles beyond the transmission range when multi hops are used.

V. CONCLUSION

The study of the various routing protocols considered under MANET and VANET on the basis of their architectures and their performance analysis provides that the protocols which are feasible for a MANET will be feasible in the VANET too but their performance varies with varying traffic conditions and densities. If we look for the best out of the existing protocols then we find that the Reactive protocols will be the best if we want to use the same set of rules in both the VANET and MANET. Moreover AODV results to be the best among the various reactive protocols for both MANET and VANET based on previous research works and studies.

REFERENCES

- [1] Different Routing Techniques in VANET from,"personal.psu.edu/ akb5073/routing_protocol.pdf".
- [2] Larry L. Peterson and Bruce S. Davie," Computer networks- A system approach", San Fransisco, Morgan Kaufman Publishers Inc. ISSN 1-55860-368-9.
- [3] C. Lochert, B. Scheuermann, and M. Mauve, "A survey on congestion control for mobile ad hoc networks," *Wireless Communications and Mobile Computing*, vol. 7, no. 5, pp. 655–676, 2007.
- [4] N. Wisitpongphan, O. Tonguz, J. Parikh, F. Bai, P. Mudalige, and V. Sadekar,
- [5] "On the Broadcast Storm Problem in Ad hoc Wireless Network," in *IEEE Wireless Communications*, to appear.
- [6] Deshmuk R., Ambhaika A., " Performance Evaluation of AODV and DSR with Reference to Network Size", *International Journal of Computer Applications* (0975 – 8887), Volume 11– No.8, December 2010.
- [7] Elizabeth M. R. and Chai-Keong T., "A review of current routing protocols for ad hoc mobile wireless networks", Technical report, University of California and Georgia Institute of Technology, USA, 1999.
- [8] Gerla M., Hong X., Pei G.. "Fisheye State Routing Protocol (FSR) for ad hoc networks", IETF Draft, 2001.
- [9] Helbing, D., Hennecke, A., Shvetsov, V., Treiber, M. (2002), "Micro and Macro simulation of Freeway Traffic," *Mathematical and Computer Modelling*, vol. 35, no. 5/6, pp. 517-547, 2002.
- [10] Jaap S., Bechler M., Wolf L. , "Evaluation of Routing Protocols for Vehicular Ad Hoc Networks in City Traffic Scenarios," *Proceedings of the 5th International Conference on Intelligent Transportation Systems (ITS) Telecommunications*, June, 2005.
- [11] Jetcheva J.G., Hu Y.C., PalChaudhuri, S., Saha, A.K., Johnson, D.B., "Design and evaluation of a metropolitan area multitier wireless adhoc network architecture," *Mobile Computing Systems and Applications*, 2003. *Proceedings. Fifth IEEE Workshop on* , vol., no.pp. 32-43, 9-10 Oct. 2003.

Power Factor Correction Using Bridgeless Boost Topology

Sachin Saini¹, Piyush Sharma², Dheeraj Kumar Dhakad³, Love Kumar Tripathi⁴

^{1,2,3}Department of Electrical Engineering, SS College of Engineering, Udaipur, Rajasthan, India

⁴Research Scholar, SITE, Udaipur, India

Abstract— Power quality is becoming a major concern for many electrical users. The high power non linear loads (such as adjustable speed drives, arc furnace, static power converter etc) and low power loads (such as computer, fax machine etc) produce voltage fluctuations, harmonic currents and an inequality in network system which results into low power factor operation of the power system. The devices commonly used in industrial, commercial and residential applications need to go through rectification for their proper functioning and operation. Due to the increasing demand of these devices, the line current harmonics create a major problem by degrading the power factor of the system thus affecting the performance of the devices. Hence there is a need to reduce the input line current harmonics so as to improve the power factor of the system. This has led to designing of Power Factor Correction circuits. Power Factor Correction (PFC) involves two techniques, Active PFC and Passive PFC. An active power factor circuit using Boost Converter is used for improving the power factor. This thesis work analyzes the procedural approach and benefits of applying Bridgeless Boost Topology for improving the power factor over Boost Converter Topology. A traditional design methodology Boost Converter Topology is initially analyzed and compared with the Bridgeless Boost topology and the overall Power Factor (PF) can be improved to the expectation. Method of re-shaping the input current waveform to be similar pattern as the sinusoidal input voltage is done by the Boost converter and the related controls that act as a Power Factor Correction (PFC) circuit. Higher efficiency can be achieved by using the Bridgeless Boost Topology. In this paper simulation of Boost Converter topology and Bridgeless PFC boost Converter is presented. Performance comparisons between the conventional PFC boost Converter and the Bridgeless PFC Boost Converter is done.

Keywords— THD, Power Factor Correction (PFC), PFC Boost Converter, Bridgeless PFC Boost Converter.

I. INTRODUCTION

In this paper the power factor correction of a system using Bridgeless Boost Topology. Power Factor is an important performance parameter of a system and improving power

factor is very much essential for the better and economical performance of the system. If the power factor of a system at a given power requirement is poor, then large value of Volt-Amperes or large amount of current is required by the system which is drawn from the supply. Hence it is seen that various measures are taken to improve the power factor of a system. The use and study of a Boost Converter Topology for the Power Factor Correction is described. It also describes the use and study of Bridgeless Boost Topology for power Factor Correction. The basic purpose of a Power Factor Correction circuit is to make the line current follow the waveform of the line voltage so that the input to the power supply becomes purely resistive and hence to improve the power factor. Bridgeless Boost Topology is used in the Power Factor Correction circuit to improve the power factor. The paper shows the study and analysis of power factor of a system by doing simulations on MATLAB (R2009a) Software using full wave rectifier in the beginning. After studying and analyzing the input current and voltage waveforms and the power factor of the system using Rectifier circuit, the Boost Converter is introduced in the circuit and then analyzed its effect in improving the power factor of the system. Then Bridgeless Boost Topology is implemented which gives better results and improved power factor.

II. POWER FACTOR

Power factor can be defined as the ratio of active or real power to the apparent power.

$$\text{Power Factor} = \text{Real Power} / \text{Apparent Power} \quad (1)$$

$$\text{power factor} = P \div (V_{rms} \times I_{rms}) \quad (2)$$

Where V_{rms} Root Mean Square Voltage of Load I_{rms} Root Mean Square Current of Load If the load is purely resistive, then the real power will be same as $V_{rms} \times I_{rms}$. Hence, the power factor will be unity. And if the load is not purely resistive, the power factor will be below unity. Assuming an ideal sinusoidal input voltage source, the power factor can be expressed as the product of two factors, the distortion factor and the displacement factor, as given

$$PF = K_d K_\theta \quad (3)$$

The distortion factor K_d is the ratio of the fundamental RMS current to the total RMS current. The displacement factor, K_θ , is the cosine of the displacement angle between the fundamental input current and the input voltage fundamental RMS current.

$$K_d = \frac{I_{1rms}}{I_{rms}} \quad (4)$$

$$K_\theta = \cos\theta_1 \quad (5)$$

Where the fundamental component of the line is current, is the total line current and is the phase shift of the current fundamental relative to the sinusoidal line voltage. The distortion factor is close to unity, even for waveforms with noticeable distortion; therefore, it is not a very convenient measure of distortion for practical use. The distortion factor is uniquely related to another figure of merit; the total harmonic distortion (THD).

$$THD = \sqrt{\frac{I_{rms}^2 - I_{1rms}^2}{I_{1rms}^2}} \quad (6)$$

$$K_d = \sqrt{\frac{1}{1+THD^2}} \quad (7)$$

Power factor correction circuits are developed so that the power factor is improved which means it tries to make the input to a power supply behave like purely resistive. This is done by trying to make the input current in response to the input voltage, so that a constant ratio is maintained between the voltage and current. This would ensure the input to be resistive in nature and thus, the power factor to be 1.0 or unity. When the ratio between voltage and current is not constant i.e. the load is not purely resistive, or the input to the power supply is not resistive, then the input will contain phase displacement and harmonic distortion, both of which will severely affect and degrade the power factor [1,2].

$$Kp = \frac{1}{\sqrt{1+(THDi)^2}} \quad (8)$$

$$THDi = \frac{\sqrt{\sum_{n=2}^{\infty} I_{n rms}^2}}{I_{1rms}} \quad (9)$$

III. EFFECTS OF HARMONICS

The non-linear loads result in production of harmonic currents in the power system. These harmonics in turn result in various undesirable effects on both the distribution network and consumers.

In transformers, shunt capacitors, power cables, AC machines and switchgear, they cause extra losses and overheating leading to their premature aging and failure.

In a three-phase four-wire system, excessive current flows in the neutral conductor. This is due to odd triple-n current harmonics (triple-n: 3rd, 9th, 15th, etc.) and eventually they cause tripping of the protective relay due to overheating of the neutral conductor. By interaction with the system components resonances take place in the power system. This

causes huge increase in amplitude of peak voltages and RMS currents [3]. The line voltage that gets distorted due to the harmonics may affect other consumers connected to the electricity distribution network. The power factor gets reduced. Due to this the active power that is available is less than the apparent power supplied. Other effects include - telephone interference, extra audio noise, cogging and crawling of induction motors, errors observed in metering equipments.

IV. STANDARDS FOR LINE CURRENT HARMONICS

For limiting the line current harmonics in the current waveform standards are set for regulating them. One such standard was IEC 555-2, which was published by the International Electro-technical Committee in 1982. In 1987, European Committee for Electro-Technical Standardization – CENELEC, adopted this as an European Standard EN 60555-2. Then standard IEC 555-2 has been replaced by standard IEC 1000-3-2 in 1995. The same has been adopted as an European standard EN 61000-3-2 by CENELEC. Hence, these limitations are kept in mind while designing any instrument. So that there is no violation and the negative effects of harmonics are not highly magnified [4].

V. CONVERTER TOPOLOGY

Boost Converter

It is a type of power converter in which the DC voltage obtained at the output stage is greater than that given at the input. It can be considered as a kind of switching-mode power supply (SMPS). The inductor has this peculiar property to resist any change of current in them and that serves as the main principle which drives a boost converter. The inductor acts like a load (like resistor) when it is being charged and acts as a source of energy (like battery) when it is discharged

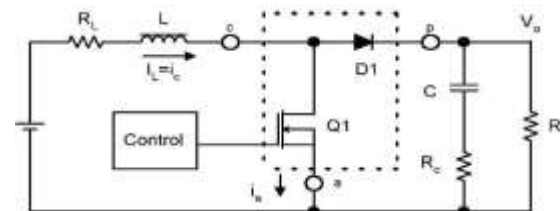


Fig.1: Boost converter

The input current and the inductor current are the same. Hence as one can see clearly that current in a boost converter is continuous type and hence the design of input filter is somewhat relaxed or it is of lower value.

Among different PFC topologies, the single switch conventional PFC is the most widely used topology because of its simplicity. The circuit topology is shown in Figure 2. A Conventional Boost PFC is considered to be the best choice for designing the power stage of the active power factor corrector. The boost converter can operate in two

modes, continuous and discontinuous. The conventional input stage for single phase power supplies operates by rectifying the ac line voltage and filtering with large electrolytic capacitors. This process generates a distorted input current waveform with large harmonic content. Thus, the resulting power factor is very poor. The reduction of input current harmonics and high power factor operation are important requirements for power supplies. In these applications, ac-dc converters featuring almost unity power factor are required.[5]

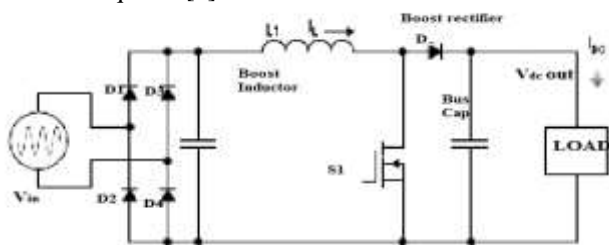


Fig.2: Conventional PFC boost converter

The technique usually employed to correct power factor of single-phase power supplies consists of a front-end full-bridge diode rectifier followed by a boost converter. The circuit is constructed by an uncontrolled diode-bridge rectifier and a Boost DC/DC stage. By adjusting Boost converter duty cycle, input current shape can be controlled and meets the current harmonic standard requirement.

Bridgeless Boost Topology

The basic Bridgeless PFC converter is shown in figure 3. Comparing to the traditional most popular Boost type PFC this smart concept improves PFC's efficiency by removing the bridge rectification system in front of it. Compare to the conventional Boost PFC the most important advantage of it is that it doesn't need four line frequency diodes operating as voltage rectifier.

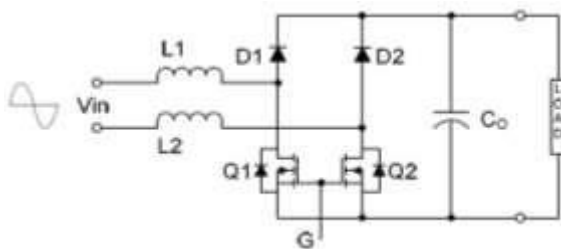


Fig.3: Bridgeless Boost Topology

VI. CONTROL TECHNIQUE OF CONVERTER

Converter provides a regulated dc output voltage under varying load and input voltage conditions. The converter component values are also changing with time, temperature and pressure. Hence, the control of the output voltage should be performed in a closed-loop manner using principles of negative feedback. There are many control techniques discussed below [6-8].

Peak current control

In the basic scheme of the peak current controller the switch is turned on at constant frequency by a clock signal, and is turned off when the sum of the positive ramp of the inductor current (i.e. the switch current) and an external ramp (compensating ramp) reaches the sinusoidal current reference. This reference is usually obtained by multiplying a scaled replica of the rectified line voltage v_g times the output of the voltage error amplifier, which sets the current reference amplitude. In this way, the reference signal is naturally synchronized and always proportional to the line voltage, which is the condition to obtain unity power factor.

Advantages

- Constant switching frequency.
- Only the switch current must be sensed and this can be accomplished by a current transformer, thus avoiding the losses due to the sensing resistor.
- No need of current error amplifier and its compensation network.
- Possibility of a true switch current limiting.

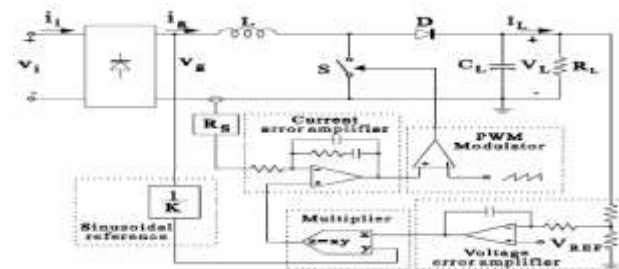
Disadvantages

- Presence of sub harmonic oscillations at duty cycles greater than 50%, so a compensation ramp is needed.
- Input current distortion which increases at high line voltages and light load and is worsened by the presence of the compensation ramp.
- Control more sensitive to commutation noises.

The input current distortion can be reduced by changing the current reference wave shape, for example introducing a dc offset or by introducing a soft clamp. Moreover, if the PFC is not intended for universal input operation, the duty-cycle can be kept below 50% so avoiding also the compensation ramp.

Average Current Mode Control

Another control method, which allows a better input current waveform, is the average current control represented in Figure 4.



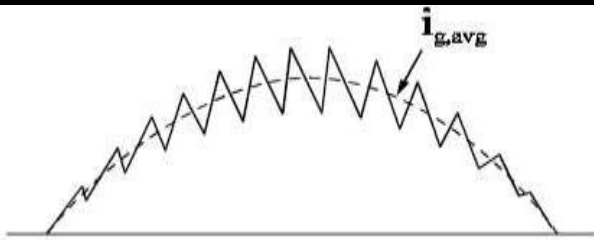


Fig.4: Average current control scheme

Here the inductor current is sensed and filtered by a current error amplifier whose output drives a PWM modulator. In this way the inner current loop tends to minimize the error between the average input current i_g and its reference. This latter is obtained in the same way as in the peak current control. The converter works in CICM, so the same considerations done with regard to the peak current control can be applied [9-12].

Advantages

- Constant switching frequency.
- No need of compensation ramp.
- Control is less sensitive to commutation noises, due to current filtering.
- Better input current waveforms than for the peak current control since, near the zero crossing of the line voltage, the duty cycle is close to one, so reducing the dead angle in the input current.

Disadvantages

- Inductor current must be sensed.
- A current error amplifier is needed and its compensation network design must take into account the different converter operating points during the line cycle.

Hysteresis Control

In this type of control two sinusoidal current references are generated, one for the peak and the other for the valley of the inductor current. According to this control technique, the switch is turned on when the inductor current goes below the lower reference and is turned off when the inductor current goes above the upper reference, giving rise to a variable frequency control. Also with this control technique the converter works in CICM.

Advantages

- No need of compensation ramp.
- Low distorted input current waveforms.

Disadvantages

- Variable switching frequency.
- Inductor current must be sensed.

In order to avoid too high switching frequency, the switch can be kept open near the zero crossing of the line voltage so introducing dead times in the line current .

The boost converter input current is forced to be proportional to the input voltage waveform for power factor correction. Feedback is necessary to control the input current. The average current mode control (ACMC) technique is applied.

VII. SIMULATION AND RESULTS

Firstly, simulation of Full bridge rectifier is done. For Full Bridge rectifier circuit, RLC load has been used and the variations in the input and output voltages and currents and the amount of distortions present in them. Further, improvement of power factor is taken care of in the successive circuits. First Conventional Boost Topology is simulated and power factor is improved up to an extent then the Bridgeless Boost Topology is simulated for getting better and improved power factor.

Full Bridge Rectifier

The Full Bridge Rectifier is shown in figure 5. The corresponding AC input voltage and output voltage waveforms are shown in figure 6. DC input current is shown in figure 7. DC output current is shown in figure 8. FFT Analysis of Full Bridge Rectifier is shown in figure 9 having a THD of 28.32 %.

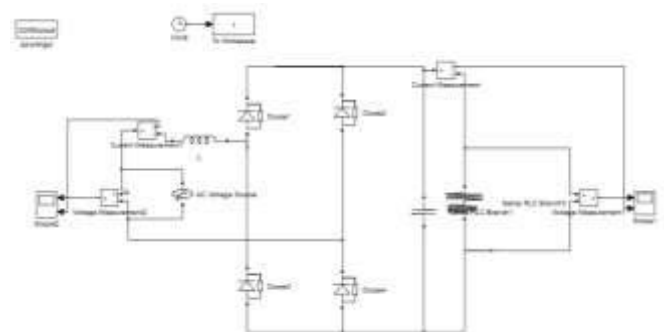


Fig.5: Circuit diagram of Full Bridge Rectifier

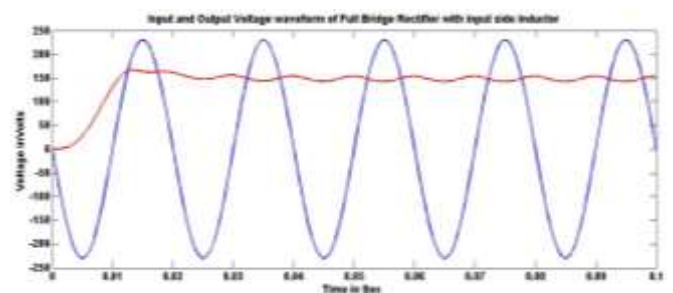


Fig.6: Input Voltage and Output Voltage waveform of Full Bridge Rectifier

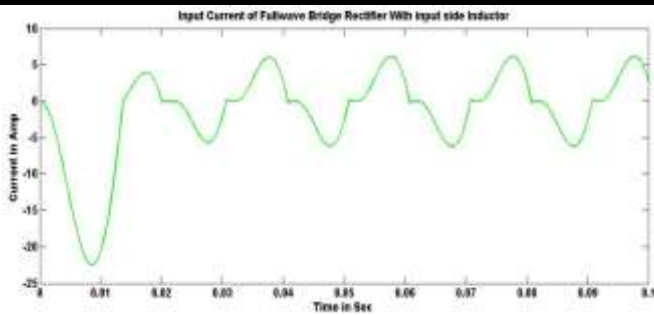


Fig.7: Input Current waveform of Full Bridge Rectifier

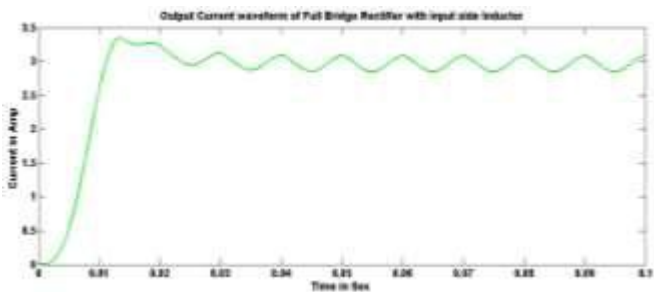


Fig.8: Output Current waveform of Full Bridge Rectifier

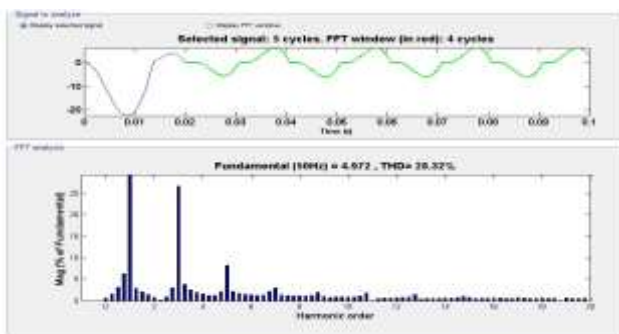


Fig.9: THD of Full Bridge Rectifier

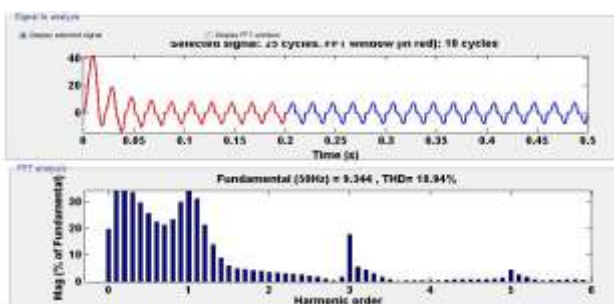


Fig.10: Closed Loop Conventional Boost PFC

The closed loop conventional boost converter is shown in figure 9. The corresponding AC input voltage and current waveforms are shown in figure 10. DC output voltage is shown in figure 11. DC output current is shown in figure 12. FFT Analysis of closed loop Conventional Boost Converter is shown in figure 13 having a THD of 18.84%.

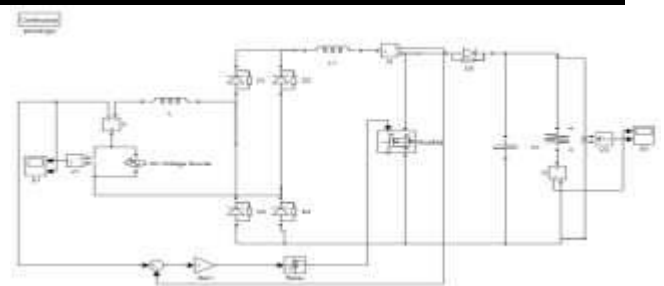


Fig.11: Closed Loop Conventional Boost PFC

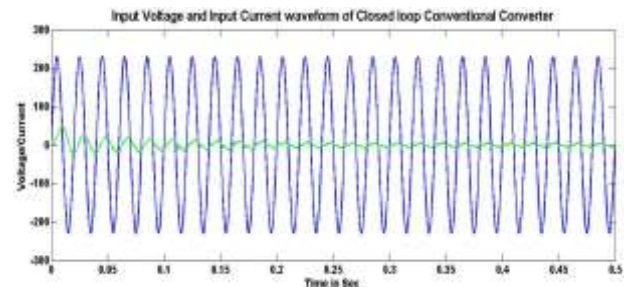


Fig.12: Input Voltage and Current waveform of Closed loop Conventional Boost PFC

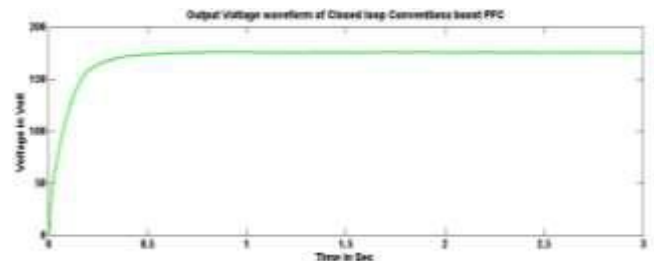


Fig.13: Output Voltage waveform of Closed loop Conventional Boost PFC

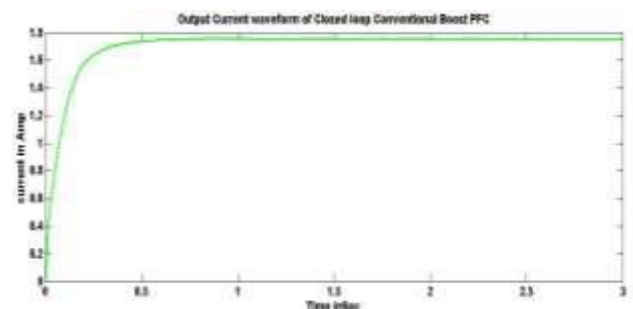


Fig.14: Output Current waveform of Closed loop Conventional Boost PFC

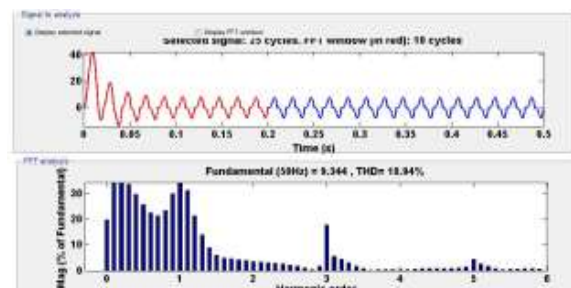


Fig.15: FFT Analysis of Conventional Boost Converter

Bridgeless Boost PFC

The Bridgeless boost PFC converter is shown in figure 14. The corresponding AC input voltage and current waveforms are shown in figure 15. DC output voltage is shown in figure 16. DC output current is shown in figure 17. FFT Analysis of Bridgeless boost PFC Converter is shown in figure 18 having a THD of 5.44 %.

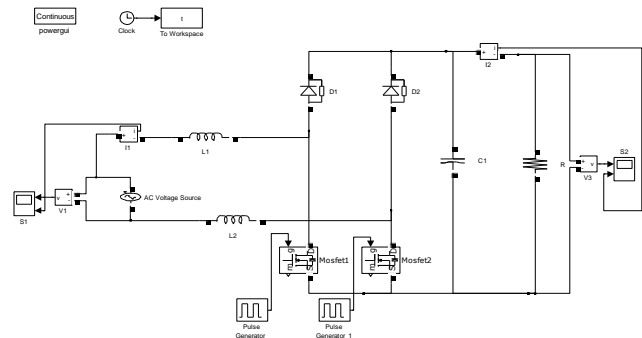


Fig.16: Bridgeless Boost Topology

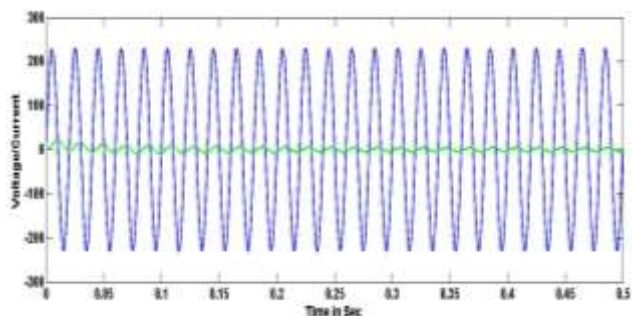


Fig.17: Input Voltage and Output Voltage waveform of Bridgeless Boost Topology

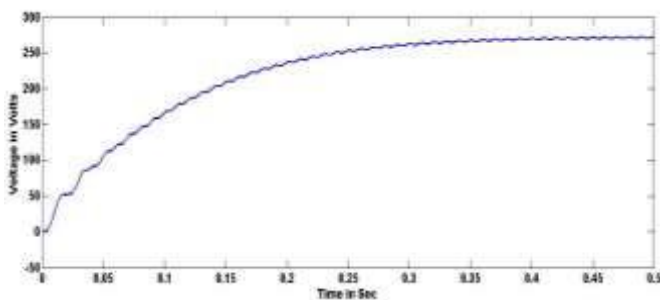


Fig.16: Output voltage waveform of Bridgeless Boost Topology

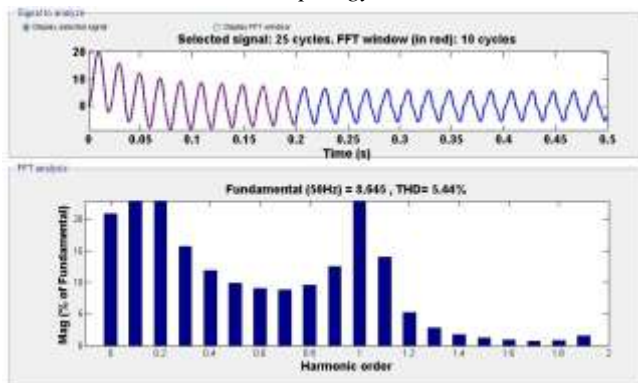


Fig.18: Output Current waveform of Bridgeless And FFT Analysis of Bridgeless Boost Topology

TABLE I.

PFC Converter	Conventional PFC	Bridgeless PFC
Slow Diode	4	0
Fast Diode	1	2
Switch (MOSFET)	1	2
Conduction Path On/Off	2 slow diode and 1 MOSFET/ 2 slow diode and 1 fast diode	1 diode and 1 MOSFET/ 1 MOSFET and 1 diode

VIII. CONCLUSION

The distortion produced in the line current in the electronic devices used for industrial and domestic applications due to harmonics and phase displacement caused by the non-linearity can be nullified by implementing bridgeless boost topology. A Conventional PFC Boost Converter is simulated. The Bridgeless PFC Boost Converter is simulated and compared to the Conventional PFC Boost Converter, generally, improves the power factor. The simulation studies indicate that the power factor is nearly unity by employing Bridgeless PFC Converter. Bridgeless PFC Converter has advantages like reduced hardware, high performance and better power factor.

REFERENCES

- [1] Prasuna, P.Vijaya.; Rao, J.; Rama, V. G.: Lakshmi, Ch. M. (2012). Improvement in Power Factor & THD Using Dual Boost Converter. *International Journal of Engineering Research and Applications (IJERA)*, 2, 2368 - 2376.
- [2] Bhattacharya, S.; Divan, D.; Banerjee, B. (1993). Control and reduction of terminal voltage, total harmonic distortion (THD) in a hybrid series active and parallel passive filter system. *IEEE PESC*, 779-786.
- [3] Spangler, J. & Behera, Anup. (1993). A comparison between hysteretic and fixed frequency boost converters used for power factor correction. *IEEE PESC*, 281 - 286.
- [4] Zhang, J.; Jovanovic, M. M.; Lee, F.C. (1999). Comparison between CCM Single-Stage and Two-stage Boost PFC converters. *IEEE Applied Power Electronics Conference and Exposition*, 1, 335-341.
- [5] Karaarslan, A. & Iskender, I. (2011). The analysis of ac-dc boost pfc converter based on peak and hysteresis current control techniques. *International Journal on Technical and Physical Problems of Engineering*, 3(7), 100-105.

- [6] Rashid, M.H. (2006). Power Electronics Handbook: Devices, Circuits, and Applications. *Academic Press*, 19, 525-530.
- [7] Rahim, N.A.; Selvaraj, J.; Krismadinata, C. (2007) Hysteresis Current Control and Sensorless MPPT for Grid-Connected Photovoltaic Systems. *Proc. IEEE ISIE*, 572-577.
- [8] Karaarslan, A. & Iskender, I. (2011). The Analysis Of Ac-Dc Boost PFC Converter Based On Peak And Hysteresis Current Control Techniques. *International Journal on Technical and Physical Problems of Engineering (Ijtpe)*, 3(7), 1-7.
- [9] Dhaked, D.K. & Lalwani, M. (2017). A Review Paper on a D-FACTS Controller: Enhanced Power Flow Controller. *International Journal of Advances in Engineering and Technology (IJAET)*, 10(1), 84-92.
- [10] Tayal, V.K.; Lather, J.S.; Sharma, P.; Sinha, S.K. (2014). Power system stability enhancement using fuzzy logic based power system stabilizer. *Proceedings of the Third International Conference on Soft Computing for Problem Solving, Advances in Intelligent Systems and Computing, Springer*, 258, 55–68.
- [11] Paliwal, S.; Sharma, P.; Sharma, A.K. (2015). Dynamic Stability Enhancement of Power System Using Intelligent Power System Stabilizer. *Proceedings of Fourth International Conference on Soft Computing for Problem Solving, Advances in Intelligent Systems and Computing, Springer*, 258, 571–583.
- [12] Singh, S.; Sharma, P.; Varshney, A.; Kumar, A. (2015). Speed Control of Multilevel Inverter-Based Induction Motor Using V/F Method. *Proceedings of Fourth International Conference on Soft Computing for Problem Solving, Advances in Intelligent Systems and Computing, Springer*, 258, 231–243.

Boundary Detection in 2-D and 3-D Wireless Sensor Networks

Aditi Pandey, Ranjana Thalore

Department of ECE,CET, Mody University, Lakshmangarh, India

Abstract—In order to track and detect continuous natured objects in wireless sensor networks, large number of sensor nodes are involved. These continuous objects like bio-chemical diffusions, forest fires, oil spills usually spread over larger area. The nodes that sense the phenomena need to communicate with each other for exchanging the information and also send sensing information to sink, possibly by passing through many intermediate nodes. In this paper, we have reviewed boundary detection in 2-D wireless sensor networks as well as in 3-D wireless sensor networks. A comparative study between the both has also been shown. The various challenges encountered in 3-D wireless sensor networks have also been discussed.

Keywords— *Boundary detection, Delaunay Triangulation, Event Boundary, Network Boundary.*

I. INTRODUCTION

Boundary detection plays a crucial role in information fusion and dissemination in 2D and 3D Wireless Sensor Network (WSN) applications such as target tracking, plume tracking, forest fires, animal migration, underwater WSNs and surveillance applications. It is also often important for self-organization of networks. A network has a specific embedding and can have three different types of boundaries which the scheme presented in this paper aims at detecting.

First is network's outer boundary which consists of a unique subset of nodes. Second is an inner boundary. The last type of boundary is an event boundary. For example events such as mobile targets or forest fires have highly dynamic event boundaries while an underground chemical plume may have boundaries that change gradually over time.

Currently available boundary detection schemes that have been targeted exclusively at 2D networks can be broadly categorized as physical information-based and topological/connectivity information-based [2][5] schemes. The former uses physical position of nodes to identify the boundary while the latter uses topological/connectivity information of the network. Physical domain schemes rely on node location or physical position information obtained using localization algorithms or GPS. Providing nodes with GPS is

expensive and infeasible for many applications. Localization based on parameters such as RSSI/time delay is error-prone even for 2D networks of modest size, is susceptible to interference, multipath and fading, which makes it impractical in many environments. Future sensor networks may have thousands or even millions of sensors, and hence distributed strategies that do not accumulate errors, and scalable in cost and complexity are of significant interest.

An alternative approach is connectivity based boundary detection [19-20]. A connectivity domain description of a network can have more than one valid embedding (configurations) [20] in physical domain, even though only one of them corresponds to the physical network. The actual embedding is one out of the many, but identifying the correct embedding solely based on the connectivity information is challenging. Hence, connectivity information based boundary identification captures a union of boundary nodes in every embedding. As a result the actual set of boundary nodes is a subset of it which leads to identifying a band of nodes as boundary nodes [20]. Due to such difficulties there is no connectivity based approach available to identify boundaries on 3D surfaces to the best of our knowledge.

Boundary detection in connectivity domain requires two steps:

- (1) Identifying the correct embedding, and
- (2) Detecting boundary.

A novel two step connectivity based approach for boundary detection is proposed. It produces highly accurate results by overcoming the ambiguity of network boundary due to multiple embedding in connectivity domain. It uses a Virtual Coordinate System (VCS) to generate a Topology Preserving Map (TPM) that identifies the correct physical embedding. In VCS, a subset of nodes is selected as anchors. Then all the nodes in the network including anchors estimate their shortest path hop distance to the anchors and use those values as virtual coordinates. Number of anchors is the cardinality of the coordinates. TPM is simply a map of the original network, in the original physical dimensionality, in which the neighbourhood is preserved. 2D topology preserving map (TPM) generation based on virtual coordinate system

(VCS) is discussed in [2]. The technique does not involve measuring signal strengths or time delays, which are costly and often impractical to implement in large scale networks.

Emerging technologies point to many applications for such networks. For example, an oil pipeline, a boiler or a bridge that needs to be monitored for corrosion, temperature distribution, or structural integrity. Tiny nano-sensors capable of wireless communication and minimal computation capability can be deployed in massive quantities on their surfaces.

II. BOUNDARY DETECTION

1. Detection of Event Boundary

The research on boundary detection started from the estimation and localization of events in sensor networks. The spatially distributed sensors usually report different measurements in respond to an event. For instance, in case of fire, the sensors located in the fire are likely to be destroyed (and thus resulting a void area of failed nodes), while the sensors close to the fire region measure higher temperature and smoke density than the faraway sensors do. Boundary detection is to delineate the regions of distinct behavior in a sensor network [1].

Achieving accurate detection of event boundary is challenging because the sampling density is limited, the sensor readings are noisy, the delivery of sensor data is unreliable, and the computation power of individual sensors is extremely low [1], [2]. To this end, a series of studies has been carried out to explore efficient information processing and modeling techniques to analyze sensor data in order to estimate the boundary of events [1]–[5].

Due to unavoidable errors in the raw sensor data, these approaches do not yield precise boundary. Instead, they aim at a close-enough estimation that correctly identifies the events frontier, based on either global or local data collected from a set of sensors.

2. Detection of Network Boundary

Besides the research discussed above that is mainly from the data processing perspective, interests are also developed to precisely locate the boundary of the network based on geometric or topology information of a wireless network. Noise in sensor data is no longer a concern here because such boundary detection is not based on sensor measurement. Nevertheless, various challenges arise due to the required precision of the required boundary, especially in networks with complex inner boundary (i.e., “holes”) or in high-dimensional space.

Most proposed network boundary detection algorithms are based on 2-D graphic tools. For example, Voronoi

diagrams are employed in [6] and [7] to discover coverage holes in sensor networks. Delaunay triangulation is adopted in [8] to identify communication voids. In contrast to [6]–[8] that exploit sensor locations, other two distributed algorithms are proposed in [9] by utilizing distance and/or angle information between nodes to discover coverage boundary.

In [10], an algebraic topological invariant called homology is computed to detect holes. The algorithm is generally applicable to networks in any dimensional space. However, it is a centralized approach, and there is significant challenge to decentralize its computation as pointed out in [10]. In [11], the isosets (each of which consists of nodes with the same hop distance to a beacon node) are identified. The disconnection in an isoset indicates the boundary nodes of holes. Multiple beacons can be employed to locate the boundary nodes at different directions of a hole. This approach does not guarantee to discover the complete boundary of every hole. Higher accuracy can be achieved if more beacons are employed or when the network is denser. Reference [12] introduces a deterministic algorithm for boundary detection. It searches for a special subgraph structure, called m-flower, which is bounded by a circle. Once an m-flower is identified, the algorithm can subsequently find the boundary nodes through a number of iterations of augmentation of the circle. However, not every graph has an m-flower structure. Therefore, the algorithm may fail especially when the nodal density is low. In [13], a shortest path tree is built to find the shortest circle, which is then refined to discover the tight boundaries of the inner holes.

All of the network boundary detection approaches discussed above are developed for networks in 2-D space. Except for [10], which is centralized, none of them can be readily applied to 3-D networks since higher-dimension space introduces significant complexity in searching for boundaries, and many topological and geometrical tools cannot be extended from 2-D to 3-D.

III. COMPARISON BETWEEN 2-D AND 3-D WSN

A wireless sensor network is built upon a large number of low cost sensor nodes. Although a two-dimensional (2D) planar setting is assumed in most earlier studies on wireless sensor networks, there have been increasing interests in deploying sensors in three-dimensional (3D) space for such applications as underwater reconnaissance and atmospheric monitoring [1]– [12]. While the third dimension appears irrelevant to network communication and management protocols at the first glance, surprising challenges are observed in efforts to extend many 2D networking techniques to 3D space.

This work focuses on boundary detection in 3D wireless sensor networks. Boundary is a key attribute that characterizes a sensor network, providing salient information for understanding environmental data and for efficient operation of the network itself, especially in geographic exploration and monitoring tasks. Due to the lack of precise nodal deployment and the nondeterministic sensor failures and channel dynamics, many wireless sensor networks exhibit substantial randomness, with their final formations heavily dependent on underlying environment. Consequently, the boundaries are often unknown before network deployment, calling for distributed and autonomous algorithms for efficient boundary detection.

1. Challenges in Connectivity-Based 3D Boundary Detection

Let's first look back upon the development of boundary detection algorithms in wireless sensor networks, which offers a full-spectrum understanding of the boundary detection problem and the limitation of existing boundary detection solutions.

2. Boundary Detection in 2D Sensor Networks

The problem of boundary detection has been extensively studied in 2D wireless sensor networks, covering the detection of event boundaries and network boundaries. Events are reported according to sensor readings. A sensor is called an event sensor if it detects the target event based on its measurement (e.g., high temperature and smoke density upon a fire). An event sensor declares itself on the event boundary if it has non-event sensors in its neighbourhood. While the basic idea appears straightforward, event boundary detection is challenging, due to limited sampling density, noisy sensor readings, lossy data delivery, and low computation power of individual sensors [13], [14], calling for efficient information processing and modeling techniques to analyze sensor data, in order to estimate the boundary of events [13]–[17].

The detection of network boundary is to locate the outmost nodes in a sensor network, irrespective of sensor data or events. Without the facilitation of neighbouring sensor readings, a sensor node depends on geometric or topological information to determine if it is on a boundary. The geometry-based approaches require the knowledge of location or distance for localized boundary detection [18], [19]. On the other hand, the topology-based schemes achieve location/distance-free by exploiting topological characteristics of the network [20][22].

3. Hurdles to Extending Topology-Based Schemes to 3D
Topology-based boundary detection is intrinsically challenging in 3D wireless sensor networks, because higher dimension space introduces significant complexity in searching for boundaries and many topological tools cannot be extended from 2D to 3D, rendering none of the available topology based schemes [19]–[20] readily applicable for distributed and autonomous boundary detection in 3D sensor networks.

For example, the fundamental group persevering (FGP) transformation is adopted in [20] to produce a reduced topology graph with all holes preserved. It can effectively identify fine-grained boundaries, but the transformation and further refinement techniques are usable on 2D plane only.

The algorithm in [22] exploits the fact that, on a 2D plane with holes, the branches of a shortest path tree belong to different homotopy types, which cannot be continuously deformed from one to another. Thus two paths with distinct homotopy types are connected to form a circle around an inner hole, which is further refined to discover tight boundaries. However, similar concept no longer holds in 3D, where the shortest paths around a hole are homotopy equivalent. Similarly, the m-flower structure employed in [20] is effective in 2D only.

In [20], isosets are identified for boundary detection. An isoset consists of nodes with the same hop distance to a beacon node. The disconnection in an isoset indicates a boundary.

While similar ideas can be applied in 3D, it becomes nontrivial to test disconnections in 3D isosets, and moreover the scheme does not guarantee to discover complete boundaries.

Finally, a whole detection algorithm based on homology is proposed in [20]. It is generally applicable to networks in any dimensional space, but it is a centralized approach and there exists significant challenge to decentralize its computation.

4. 3D Open Research Challenges

Although the sensor nodes are located in a 3D environment in real UWSNs and AANETs applications, most of the existing studies assume 2D wireless network topology structures. The characteristics of the physical layer affect the design of the other layers and the overall 3D wireless ad hoc and sensor networks performance directly. So a key research is required in the physical layer and antenna propagation for 3D environments. Another challenge is the MAC layer which faces link breakage and poor quality due to the high mobility and longer distances between nodes of the 3D networks. There are very few studies available in the area of MAC

layer in 3D environment. Therefore, 3D UWSNs and AANETs call for efficient research on testbeds and directional antennas. Furthermore, location estimation of the nodes and sharing of information are vital issues for directed antenna based MAC layers, and they are more challenging for AANETs especially because of highly mobile nodes, such UAV.

As discussed previously that routing is one of the most challenging issues for 3D UWSNs and AANETs due to the unique 3D wireless networks characteristics, the existing 3D wireless networks routing solutions are limited and have a lot of drawbacks. LOS communication is essential for collaborative coordination and collision avoidance between the nodes of UWSNs and AANETs. Thus, developing novel routing algorithms that can support LOS communication and manage huge traffic is still an open issue. Reliability is a critical issue for 3D wireless ad hoc and sensor networks transport layers. 3D applications use different types of data such as target images, acoustic signals, or video captures of a moving target. These applications require different high levels of reliability. Such reliability is not fulfilling with the existing transport layer protocols.

During the packet delivery in AANETs, the changes of aircraft trajectory will affect the accuracy of routing protocol. Thus, the accuracy of aircraft mobility is very important because all traffic advisories are based on the current state estimates of the aircraft. Clearly, a major challenge in aircraft tracking is thus to provide accurate state estimates of aircraft. However, it is difficult to obtain precise aircraft state estimates when the aircraft changes a flight mode. Due to high speeds nodes, the 3D network is highly dynamic with constantly changing topology. Furthermore, a severe bandwidth constraint occurs in the network, due to the high volume of data that needs to be transfer in a limited allocated spectrum.

IV. CONCLUSION

With the growing 3D applications, new 3D UWSNs (Underwater Wireless Sensor Networks) and AANETs (Airborne Ad Hoc Networks) have been developed and deployed in recent years. Due to the distinctive features of 3D wireless ad hoc and sensor networks and the complex deployment environment in 3D ocean spaces and sky spaces, various efficient and reliable 3D communication and networking protocols have been proposed. In this paper, 2D wireless sensor networks, 3D wireless sensor network, boundary detection and issues related to 2D and 3D networks have been surveyed as a separate network family for efficient communication. Furthermore, we present an overview of the challenges faced during

boundary detection in 3-D wireless sensor networks. We have a strong belief that more promising developments and significant improvements of 3D wireless networks will be achieved in the near future. This will greatly enhance human's abilities in investigation and manipulation of the 3D environment.

REFERENCES

- [1] R. Nowak and U. Mitra, "Boundary estimation in sensor networks: Theory and methods," in *Proc. IPSN*, 2003, pp. 80–95.
- [2] M. Ding and X. Cheng, "Robust event boundary detection and event tracking in sensor networks—A mixture model based approach," in *Proc. IEEE INFOCOM*, 2009, pp. 2991–2995.
- [3] K. Chintalapudi and R. Govindan, "Localized edge detection in sensor fields," in *Proc. 1st IEEE Int. Workshop Sensor Netw. Protocols Appl.*, 2003, pp. 59–70.
- [4] S. Duttgupta, K. Ramamritham, and P. Ramanathan, "Distributed boundary estimation using sensor networks," in *Proc. IEEE MASS*, 2006, pp. 316–325.
- [5] M. Ding, D. Chen, K. Xing, and X. Cheng, "Localized fault-tolerant event boundary detection in sensor networks," in *Proc. IEEE INFOCOM*, 2005, pp. 902–913.
- [6] G. Wang, G. Cao, and T. L. Porta, "Movement-assisted sensor deployment," in *Proc. IEEE INFOCOM*, 2004, pp. 2469–2479.
- [7] A. Ghosh, "Estimating coverage holes and enhancing coverage in mixed sensor networks," in *Proc. 29th Annu. IEEE Int. Conf. Local Comput. Netw.*, 2004, pp. 68–76.
- [8] Q. Fang, J. Gao, and L. J. Guibas, "Locating and bypassing routing holes in sensor networks," in *Proc. IEEE INFOCOM*, 2004, pp. 2458–2468.
- [9] C. Zhang, Y. Zhang, and Y. Fang, "Localized algorithms for coverage boundary detection in wireless sensor networks," *Wireless Netw.*, vol. 15, no. 1, pp. 3–20, 2009.
- [10] R. Ghrist and A. Muhammad, "Coverage and hole-detection in sensor networks via homology," in *Proc. IPSN*, 2005, pp. 254–260.
- [11] S. Funke, "Topological hole detection in wireless sensor networks and its applications," in *Proc. DIALM-POMC*, 2005, pp. 44–53.
- [12] A. Kroller, S. P. Fekete, D. Pfisterer, and S. Fischer, "Deterministic boundary recognition and topology extraction for large sensor networks," in *Proc. ACM-SIAM SODA*, 2006, pp. 1000–1009.

- [13] W. Cheng *et al.*, “Underwater localization in sparse 3D acoustic sensor networks,” in *Proc. IEEE INFOCOM*, 2008, pp. 798–806.
- [14] H. Zhou, S. Xia, M. Jin, and H. Wu, “Localized algorithm for precise boundary detection in 3D wireless networks,” in *Proc. ICDCS*, 2010, pp. 744–753.
- [15] F. Li, J. Luo, C. Zhang, S. Xin, and Y. He, “UNFOLD: Uniform fast on-line boundary detection for dynamic 3D wireless sensor networks,” in *Proc. MobiHoc*, 2011, pp. 141–152.
- [16] H. Jiang, S. Zhang, G. Tan, and C. Wang, “CABET: Connectivity-based boundary extraction of large-scale 3D sensor networks,” in *Proc. IEEE INFOCOM*, 2011, pp. 784–792.
- [17] H. Zhou, H. Wu, and M. Jin, “A robust boundary detection algorithm based on connectivity only for 3D wireless sensor networks,” in *Proc. IEEE INFOCOM*, 2012, pp. 1602–1610.
- [18] A. Kröller, S.P. Fekete, D. Pfisterer, and S. Fischer, “Deterministic boundary recognition and topology extraction for large sensor networks,” *Proc. of 17th Annual ACM-SIAM Symposium on Discrete Algorithms, SODA 06*.
- [19] S. Olga, S. Robert, G. Matthias, CSC and M. P. José, “On boundary recognition without location information in Wireless Sensor Networks,” *Proc. of 7th Int. Conf. on Information Processing in Sensor Networks*, April 22-24, 2008., pp:207-218.
- [20] S. Funke and N. Milosavljević, “How much geometry hides in connectivity? — Part II,” in *Proc. ACM-SIAM SODA*, 2007, pp. 958–967.
- [21] Hongyu Zhou, SuXia, Miao Jin, and Hongyi Wu, “Localized and Precise Boundary Detection in 3-D Wireless Sensor Networks,” in *Proc. IEEE INFOCOM*, 2014.
- [22] Dulanjalie C. Dhanapala, Anura P. Jayasumana and Sahil Mehta, “On Boundary Detection of 2-D and 3-D Wireless Sensor Networks”, in *IEEE Globecom 2011*.

A Review of Various Routing Protocols in VANET

Rajashree Dutta, Ranjana Thalore

Department of ECE, CET, Mody University, Lakshmangarh, India

Abstract—Vehicular Ad Hoc Networks (VANET) is a subclass of Mobile ad hoc networks which provides a distinguished approach for Intelligent Transport System (ITS). VANET's provide communication between vehicles moving on the roads. Many protocols have been adopted to serve different topology and scenarios. We introduce and review Position based Routing Protocols, Broadcast based routing protocols, Multicast/Geocast routing protocols, Cluster based routing protocols. The survey of routing protocols in VANET is very essential and necessary for smart ITS. This paper also discusses the advantages / disadvantages and the applications of the above mentioned routing protocols for vehicular ad hoc networks. The challenges and perspectives of routing protocols for VANET's are finally discussed.

Keywords– Delay-bounded routing, MANET, Routing protocols, VANET.

connect mobile devices using wireless channels. It is used to supply each device to ceaselessly maintain the information required to correctly route traffic [1]. Apart from the safety applications, VANET's broadcast valuable, real-time information to the users such as transit systems, weather information, mobile e-commerce, internet access and other multimedia applications. [5][6] Routing in Vehicular Ad hoc Networks is a challenging task due to the unique characteristics of the network such as high mobility of nodes, dynamically changing topology and highly partitioned network. [2] The performance of routing protocols depends on various internal factors such as mobility of nodes and external factors such as road topology and obstacles that block the signal. [3] This demands a highly adaptive approach to deal with the dynamic scenarios by selecting the best routing and forwarding strategies and by using appropriate mobility and propagation models.

I. INTRODUCTION

MANET (mobile ad hoc network) is a network that has no infrastructure and it has the ability to configure itself to

II. ROUTING PROTOCOLS IN VANET

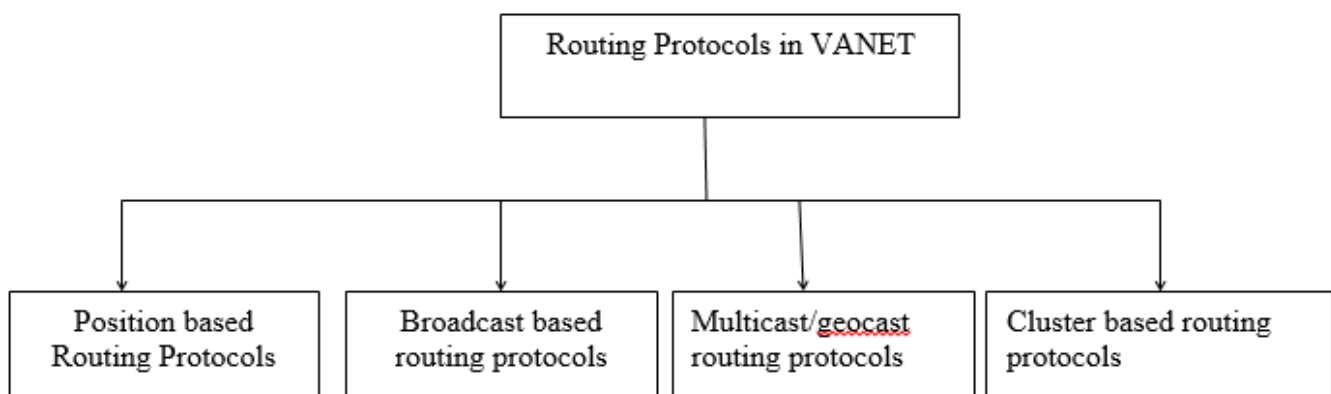


Fig. 1: Routing Protocols in VANET

Vehicle to Vehicle data transfer is one of the main challenges within the design of VANET because it needs to design a dynamic routing protocol. [4] Routing in traditional MANET is different to the VANET routing because of extremely dynamical topologies. Routing in VANET can be classified into following major categories:

1. Position based Routing Protocols

In position based protocols, the routing decisions are based on geographic position of the vehicles. [7][9] This does not require establishment or maintenance of routes, but requires location services to determine the position of the destination. Some of the commonly used location services include Global Position System (GPS), DREAM

Location Services (DLS), Reactive Location Services (RLS) and Simple Location Services (SLS).[1] With the advancement of GPS based location services, position based routing protocols are gaining importance.

PROS:

- Good performance in highway environment
- Need of global route not required.
- With high mobility in environment stability increases.

CONS:

- It needs global positioning system position (GPS).
- GPS device stop working in tunnel.
- Location server sometime goes into deadlock state.

2. Broadcast based routing protocols

This is the most commonly used routing protocol in VANETs, particularly in safety related applications.[7] In broadcast mode, a packet is sent to all (even unknown or unspecified) nodes in the network and in turn each node re-broadcasts the message to other nodes in the network. Flooding is a prominent technique used in broadcast routing protocols. [8] However, blind flooding results in broadcast storm problem. A broadcast storm can overload the limited channel capacity, causing channel congestion that reduces communication reliability.[2] Broadcast routing is frequently used in VANET for sharing, traffic, weather and emergency, road conditions among vehicles and delivering advertisements and announcements.[6] The various Broadcast routing protocols are BROADCAST, UMB, VTRADE, and DV-CAST.

PROS:

- Since packet is delivered via many nodes so the packet transmission is reliable.
- Minimize overhead by occurrence of broadcast storms

CONS:

- Consume the large amount of network bandwidth.

3. Multicast/geocast routing protocols

Multicast routing enables dissemination of messages from single source to a group of starting point nodes of

interest.[5][7] Geocast routing is basically a location based multicast routing, which aims to deliver information from a source node to all other nodes within a specified geographical region called a Zone of Relevance (ZOR). A Zone of Forwarding (ZOF) is demarcated, inside which the packets are directed instead of simply flooding the packets everywhere in the network. In Geocast routing vehicles outside the ZOR are not alerted to avoid unnecessary hasty reaction. [5][6] Geocast is considered as a multicast service within a specific geographic region. It normally defines a forwarding zone where it directs the flooding of packets in order to reduce message overhead and network congestion caused by simply flooding packets everywhere [1].

PROS:

- Reduced network overhead and congestion.
- Reliable packet delivery in highly dynamic topology.

CONS:

- Packet transmission delay due to network disconnection.

4. Cluster based routing protocol

Clustering in vehicular ad hoc network can be defined as the virtual partitioning of the dynamic nodes into various groups. [1][9][10] A group of nodes identify themselves to be part of a cluster. A special node, designated as cluster-head is responsible for routing, relaying of inter cluster traffic, scheduling of intra-cluster traffic and channel assignment for cluster members. Cluster based routing is preferred in clusters. [5] A group of nodes identifies themselves to be a part of cluster and a node is designated as cluster head will broadcast the packet to cluster. Good scalability can be delivered for large networks but network delays and overhead are experienced when forming clusters in highly mobile VANET. In cluster based routing virtual network infrastructure must be created through the clustering of nodes in order to provide scalability [1].

PROS:

- It has good scalability of large networks.
- Delays in highly dynamic networks.

CONS:

- Network overhead is increased.

III. COMPARISON BETWEEN VARIOUS ROUTING PROTOCOLS

Table.1: Comparison of various routing protocols based on different parameters.

Protocols	Position Based Protocols	Broadcast Based Protocols	Geocast Based Protocols	Cluster Based Protocols
Prior Forwarding Method	Heuristic method	Wire less multi hop Forwarding	Wire less multi hop Forwarding	Wireless Multi hop Forwarding
Digital Map Requirement	No	No	No	Yes
Virtual Infrastructure Requirement	No	No	No	Yes
Realistic Traffic Flow	Yes	Yes	Yes	No
Recovery Strategy	Carry & Forward	Carry & Forward	Flooding	Carry & Forward
Scenario	Urban	Highway	Highway	Urban

IV. CONCLUSION

Conniving effective routing protocols for VANET is one of the biggest challenges to be addressed in order to leverage the benefits of the VANET technology in day-to-day life. Performance of routing protocol for VANET's depends drastically on the mobility of nodes, vehicular density and several external factors such as driving environment; [4] But a universal routing solution for all the VANET's application scenarios may not be practical; we need to design specific routing protocol and mobility model to fulfill the specific QoS requirements of each application[1][5].

This paper reviews the literature concerning four most common protocols Position based Routing Protocols, Broadcast based routing protocols, Multicast/geocast routing protocols, Cluster based routing protocols, that are used to route data between communicated vehicles in VANET.[7] This work comes to address how a routing protocol performs in high node density VANET for different mobility models.

Position based routing contains class of routing algorithm. [8][9] They share the property of using geographic positioning information in order to select the next forwarding hops. Broadcast routing is frequently used in VANET for sharing, traffic, weather and emergency etc.[1] Multicast routing enables dissemination of messages from single source to a group of destination nodes of interest. In Geo cast routing vehicles outside the ZOR are not alerted to avoid unnecessary hasty reaction. Cluster based routing is preferred in clusters.

REFERENCES

- [1] Rakesh Kumar, Mayank Dave, "A Comparative Study of Various Routing Protocols in VANET", IJCSI International Journal of Computer Science Issues, Vol. 8, Issue 4, No 1, July 2011 ISSN (Online): 1694-0814, pp 643-648.
- [2] Venkatesh, AIndra, R Murali, "Routing Protocols for Vehicular Adhoc Networks (VANETs): A Review", Journal of Emerging Trends in Computing and Information Sciences Vol. 5, No. 1 January 2014 ISSN 2079-8407, pp 25-43.
- [3] Yun-weilin, Yuh-shyanchen, Sing-ling lee, "Routing protocols in Vehicular Ad Hoc Networks: a Survey and future perspectives", National Science Council of the R.O.C. Under grant nsc-97-2221-e-305-003-my3, pp 02-19.
- [4] Komal Mehta, Dr. L. G. Malik, Dr. Preeti Bajaj, "VANET: Challenges, Issues and Solutions", 2013 Sixth International Conference on Emerging Trends in Engineering and Technology 978-1-4799-2560-5/13 \$31.00 © 2013 IEEE DOI 10.1109/ICETET.2013.18, pp 64-66.
- [5] Surmukh Singh, Poonam Kumari, Sunil Agrawal, "Comparative Analysis of Various Routing Protocols inVANET", 2015 Fifth International Conference on Advanced Computing & Communication Technologies 2327-0659/15 \$31.00 © 2015 IEEE DOI 10.1109/ACCT.2015.113, pp 315-319.
- [6] Surmukh Singh, Sunil Agrawal, "VANET Routing Protocols: Issues and Challenges", Proceedings of 2014 RA ECS UIET Panjab University Chandigarh, 06 – 08 March, 2014 978-1-4799-2291-8/14/\$31.00 ©2014 IEEE, pp 205-210.

- [7] Venkatesh, Indra. A ,Murali. R, “Vehicular AdHoc Networks (VANETs): Issues andApplications”, Journal of Analysis and computation, Vol. 8, No. 1, 2012, pp.31-46.
- [8] A. K. Saha and D. B. Johnson, “Modeling mobility for vehicular ad hoc networks,” ACM International Workshop on Vehicular Ad Hoc Networks (VANET), Oct. 2004, pp.91-92.
- [9] H. Safa, H. Artail, and R. Shibli, “An Interoperability Model for Supporting Reliability and Power-Efficient Routing in MANETs,” International Journal of Ad Hoc and Ubiquitous Computing (IJAHUC), vol. 4, no. 2, 2009, pp.71-83.
- [10] S. Corson, and J. Macker, “Mobile Ad Hoc Networking (MANET): Routing Protocol Performance Issues and Evaluation Considerations,” RFC editor, 1999. S. Corson, and J. Macker, “Mobile Ad Hoc Networking (MANET): Routing Protocol Performance Issues andEvaluation Considerations,” RFC editor, 199

Assessment of Quality of Groundwater in Certain Villages nearby Krishna River, Krishna District, Andhra Pradesh, India

V. Rajesh^{1*}, R. L. N. Charyulu², B. V. Ravi Kumar², B. Prasanna Kumar³

¹Department of Chemistry, V. R. Siddhartha Engineering College (Autonomous), Vijayawada-7, Andhra Pradesh, India

²Department of Mathematics, V. R. Siddhartha Engineering College (Autonomous), Vijayawada-7, Andhra Pradesh, India

³Department of Environmental Sciences, Andhra University, Visakhapatnam-3, Andhra Pradesh, India

Abstract— In the present study, the quality of groundwater samples was evaluated in terms of certain water quality parameters. The 24 groundwater samples were collected from the villages located along the Krishna river in Krishna district of Andhra Pradesh. Nine most significant quality parameters were determined for all the water samples collected. Water quality index values were calculated by incorporating data of quality parameters in to mathematical equations. Based on the water quality index values, the quality of water is assessed. From the results, it is found that all the water samples are of good quality and suitable for drinking/domestic purpose.

Keywords— Water quality index, Krishna river, Groundwater, Krishna district, Villages.

I. INTRODUCTION

It is believed that groundwater is polluted to a lesser extent when compared with any surface water. This is the reason for usage of groundwater for several applications including domestic, agricultural and industrial purposes. But, groundwater has also been polluted gradually because of natural and anthropogenic activities including continuous dumping of waste water from industries and domestic sewage and it is continuously becoming harmful for human health. Water resource management involves several aspects including study of water quality of groundwater at different intervals of time. However, it is difficult task to study and evaluate for larger number of samples. Further, each sample has several parameters and each parameter is very significant in assessing the suitability of water for a particular purpose [1]. The complexity in water quality assessment is mainly due to complexity of parameters that significantly affect water quality, and the large variability of parameters used to indicate the quality of water resources [2].

In order to minimize the complexity in expressing water quality, a dimensionless number was proposed, by name water quality index (WQI). Using WQI, it is possible to indicate quality of water in a simple form by the aggregation of the measurements of the selected parameters. Considering the easiness of the use of WQI and their scientific basis, WQIs became important and popular tool for the assessment of water quality of water bodies [3]. WQI attempts to provide a mechanism for presenting a cumulatively derived numerical expression defining a certain level of water quality [4]. There are several reports in literature in which WQI was determined in order to assess the quality of water at different places and different sources [5-13]. The present investigation of the quality of groundwater from various villages of Krishna district of Andhra Pradesh state has been carried out, based on the above background. All the 24 groundwater samples were collected from the villages located adjacent to the river. For each sample of groundwater, nine quality parameters were determined from which water quality index was calculated. Based on the WQIs, the water quality status of each location is presented.

II. MATERIALS AND METHODS

In order to determine water quality indices, the groundwater samples were collected from 24 sampling locations, all of them being in villages located adjacent to the Krishna river in Krishna district of Andhra Pradesh, India. The map indicating the selected villages and the sampling locations are shown in Fig. 1. The names of the locations with the corresponding sample numbers are listed in Table 1. The samples were collected in clean brown glass bottles with all the necessary precautions. All the chemicals used belong to AR grade purity.

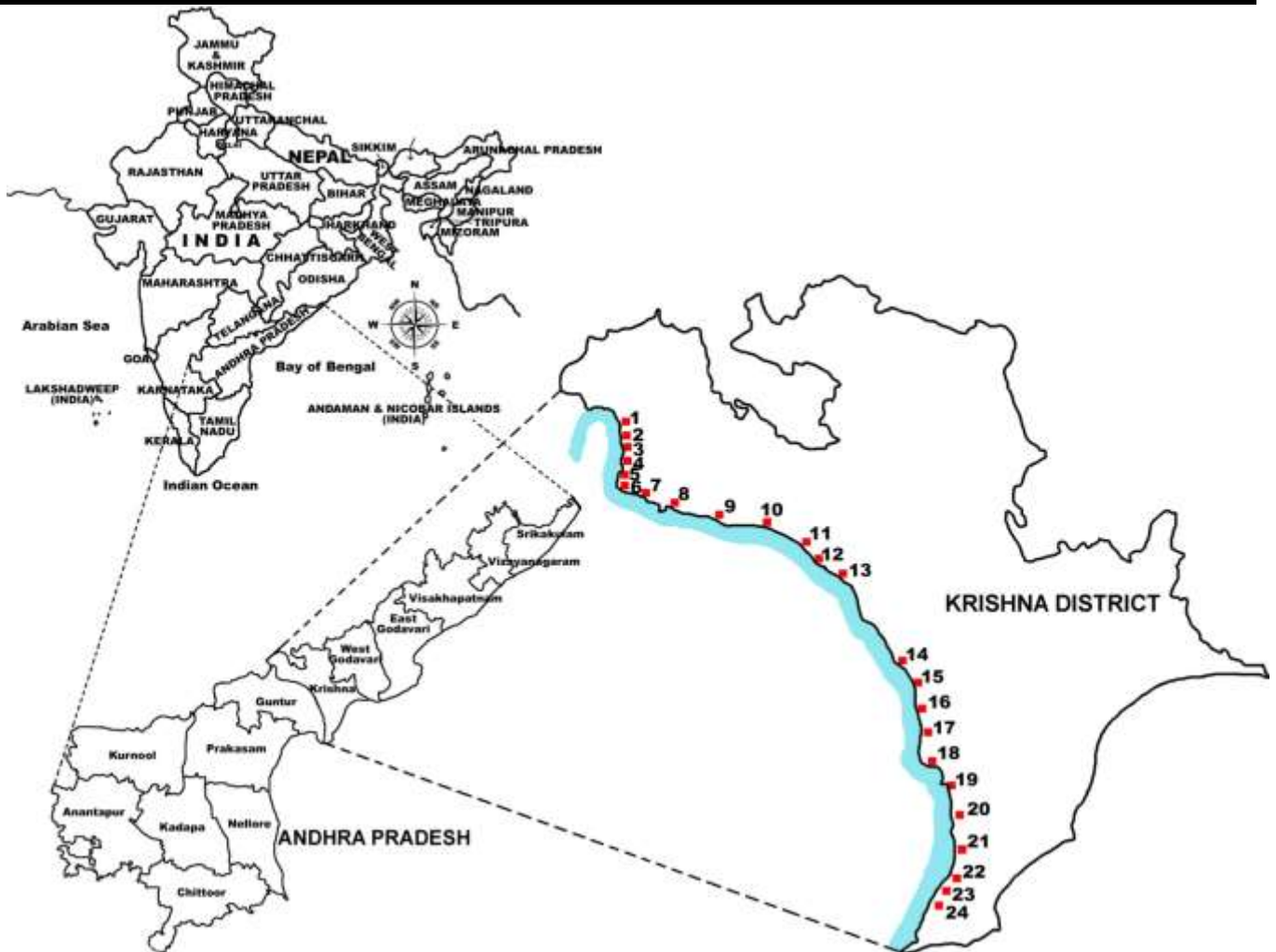


Fig.1: Map indicating the location of sampling sites

Table.1: Names of sampling villages and corresponding sample numbers

Name of village	Sample number	Name of village	Sample number	Name of village	Sample number	Name of village	Sample number
Vedadri	01	Kodavatikallu	07	Surayapalem	13	Bhadrirajupalem	19
Katrenipalle	02	Veladi	08	Kasaranenivaripalem	14	Devarapalli	20
Ramanapeta	03	Chevitikallu	09	Madduru	15	Iluru	21
Ustepalle	04	Damuluru	10	Royyuru	16	Inapuru	22
Kasarabada	05	Ferri	11	Vallurupalem	17	Srikakulam	23
Pokkunuru	06	Tummalapalem	12	Thotlavalluru	18	Nimmagadda	24

Table.2: Water quality parameters, their units and analytical methods/instruments used

Parameter	Analytical method/ Instrument	Parameter	Analytical method/ Instrument
Chlorides (Cl ⁻) (mg/L)	Volumetric – Argentometry	Electrical conductivity (EC) (μS/cm)	Digital conductivity meter
Total alkalinity (mg/L)	Volumetric – Neutralization	Dissolved oxygen (DO) (mg/L)	Winkler’s method
Total hardness (mg/L)	Volumetric – EDTA method	Turbidity (NTU)	Nephelometer
Total dissolved solids (TDS) (mg/L)	Gravimetric method	Fluorides (F ⁻) (mg/L)	SPADNS method–UV-vis spectrophotometer
pH	Digital pH meter		

Double distilled water was used for preparation of the solutions and reagents. The water samples were analysed for various water quality parameters as per the standard procedures [14, 15] given in Table 2. The experimental values of water quality parameters were compared with the standard values recommended by the Indian Council for Medical Research (ICMR) and Bureau of Indian Standards (BIS) [16] given in Table 3. In order to calculate water quality index, 9 important parameters such as chlorides, total alkalinity, total hardness, total dissolved solids, dissolved oxygen, pH, electrical conductivity, turbidity and fluoride concentration were selected. The subindex (q_i) corresponding to i^{th} parameter is a number reflecting the relative value of this parameter in water with respect to its standard permissible value. q_i value is obtained from the following expression [13].

$$q_i = 100 \times [V_i - V_o] / [S_i - V_o]$$

q_i = subindex for the i^{th} water quality parameter
 V_i = Estimated value of the i^{th} parameter at a given sampling location
 S_i = Standard permissible value of the i^{th} parameter
 V_o = Ideal value of the parameter in pure water
 (For pH and DO, $V_o = 7.0$ and 14.6 mg/L respectively, and for all other parameters $V_o = 0$)
 Unit weight was calculated by a value inversely proportional to the recommended standard value S_i of the corresponding parameter [13].

$$W_i = k / S_i$$

W_i = Unit weight for the i^{th} parameter
 S_i = Standard value for the i^{th} parameter
 k = Proportionality constant
 Finally, the overall water quality index was calculated by aggregating the subindex with the unit weight linearly [13].

$$WQI = \sum q_i W_i / \sum W_i$$

Table.3: Standard values of drinking water quality parameters, recommending agencies and unit weights

Parameter	Standard value	Recommended by	Unit weight
Chlorides	250 mg/L	ICMR/BIS	0.00260
Alkalinity	120 mg/L	ICMR	0.00542
Hardness	300 mg/L	ICMR/BIS	0.00217
TDS	500 mg/L	ICMR/BIS	0.00130
DO	5.0 mg/L	ICMR	0.12998
pH	6.5-8.5	ICMR/BIS	0.07646
EC	300 μ S/cm	ICMR	0.00217
Turbidity	5.0 NTU	BIS	0.12998
Fluorides	1.0 mg/L	BIS	0.64992

III. RESULTS AND DISCUSSION

The physicochemical parameters for all the groundwater samples are listed in Table 4. From the Table, it can be stated that the quality parameters namely fluorides, turbidity, pH and DO are within the permissible standard limits described by ICMR and BIS. The other variables namely chlorides, alkalinity, hardness, TDS and electrical conductivity are found to exceed the limits. The presence of very low levels of suspended and colloidal impurities in all the water samples is inferred by the extremely low turbidity values even compared with the maximum permissible limit of 5.0 NTU. Conductivity of water is said to be a direct function of its TDS [17]. Thus, it is an index to the total concentration of soluble salts in water [18]. In the present study, electrical conductivity of groundwater samples varied between 359 μ S/cm and 2570 μ S/cm. The TDS values are in the range 357-3024 mg/L, while the permissible limit of TDS is 500 mg/L. A few samples are found to contain very high levels of TDS and EC. As far as TDS and EC are concerned, the water is not preferable for drinking purpose. High TDS values in groundwater affect people who are suffering from kidney and heart diseases [19].

Concentration of chloride was observed to be within the permissible limit of 250 mg/L in most of the stations. It was found to exceed the limit at locations 9, 10 and 11. Soil porosity and permeability have important role in increasing the chloride concentration [6]. Fluoride limit as per the ICMR and BIS are 1.0 mg/L, while it is 1.5 mg/L as per the WHO standards [20]. The concentration of fluoride in the study area is found to be less than 1.0 mg/L. Total alkalinity values of all the samples are found to exceed the limit of 120 mg/L. The high alkalinity of groundwater sample is due to release of ions like hydroxide, carbonate and bicarbonate from carbonate-rich soils, limestone, sedimentary rocks as well as domestic solid waste [21]. Hardness is one among the important water quality parameters. Its excess beyond the above limit causes gastrointestinal irritation [22]. The total hardness values were found to be within the limit of 300 mg/L at 17 locations, while the higher values were obtained at remaining 7 locations. Table 4 also infers that the variables like chlorides, alkalinity, TDS and EC are extremely high when compared with the standard values in case of the samples 9, 11 and 19. The water quality index (WQI) values and corresponding water quality status [12] are shown in Table 5. The WQI values obtained for all the water samples in the present study are shown in Fig. 2. The figure shows that three water samples (from Katrenipalle, Kasarabada and Kasaranenivaripalem) exhibited WQI less than 25 indicating that these samples are of excellent quality and suitable for domestic purpose [12]. The water samples

from Royyuru and Devarapalli have the WQI value of 25.1 and hence they also can be treated suitable for domestic usage. The samples from the villages namely, Ramanapeta, Veladi, Chevitikallu, Ferri, Tummalapalem, Madduru, Inapuru and Srikakulam exhibited WQI values in the range 27-30, which indicates that these groundwater samples are also of good quality. However, the remaining 11 water samples were found to exhibit WQI values from 30 to 40. As per the standards, these

samples are also good in quality and can be used for domestic purpose. The highest value of WQI (= 36.8) was exhibited by the groundwater sample of Pokkunuru village. The sample from the station, Mullapadu exhibited the WQI value of 36, which indicates the water as good quality water. The higher value of WQI for the water at this station is due to higher values of many parameters namely EC, TDS, hardness, chlorides, etc.

Table.4: Physicochemical parameters of groundwater samples collected at 24 sampling locations

Sample no.	[Cl ⁻]	Alkalinity	Hardness	TDS	DO	pH	EC	Turbidity	[F ⁻]
1	105	189	226	743	6.9	7.89	450	0.45	0.28
2	88	254	228	588	6.7	7.05	540	0.56	0.11
3	134	298	367	358	7.9	7.55	823	0.49	0.18
4	113	214	245	593	7.3	7.55	928	0.78	0.27
5	117	196	252	584	7.7	7.23	506	0.84	0.14
6	109	281	275	778	7.1	7.89	750	0.37	0.29
7	158	232	317	804	8.0	7.9	954	0.58	0.27
8	122	291	198	829	7.7	8.11	1089	0.64	0.13
9	369	225	503	3024	7.2	7.3	2570	0.17	0.17
10	287	321	355	672	7.5	7.81	556	0.68	0.22
11	295	371	256	1736	7.9	7.59	1425	0.15	0.19
12	186	288	381	955	6.8	7.23	870	0.46	0.21
13	144	267	245	812	7.4	7.58	1046	0.74	0.22
14	98	214	266	692	7.5	7.46	856	0.39	0.15
15	77	295	175	394	7.1	7.49	359	0.25	0.19
16	129	198	371	813	6.9	7.44	888	0.94	0.12
17	95	352	229	357	6.5	7.89	412	0.81	0.25
18	119	331	274	952	6.8	7.29	1566	0.68	0.21
19	138	591	295	1354	5.9	8.33	1197	0.93	0.10
20	128	348	298	542	7.8	7.86	546	0.24	0.13
21	98	268	311	881	8.0	8.23	1222	0.82	0.25
22	110	378	293	555	7.7	8.44	814	0.62	0.12
23	94	597	176	619	7.4	8.59	572	0.97	0.09
24	74	319	238	452	7.3	8.15	511	0.54	0.26

Table.5: Water quality index (WQI) range and corresponding water quality status [12]

WQI range	Water quality status	WQI range	Water quality status
0 – 25	Excellent water quality	51 – 75	Poor water quality
26 – 50	Good water quality	76 – 100	Very poor water quality
> 100	Unsuitable for drinking purpose		

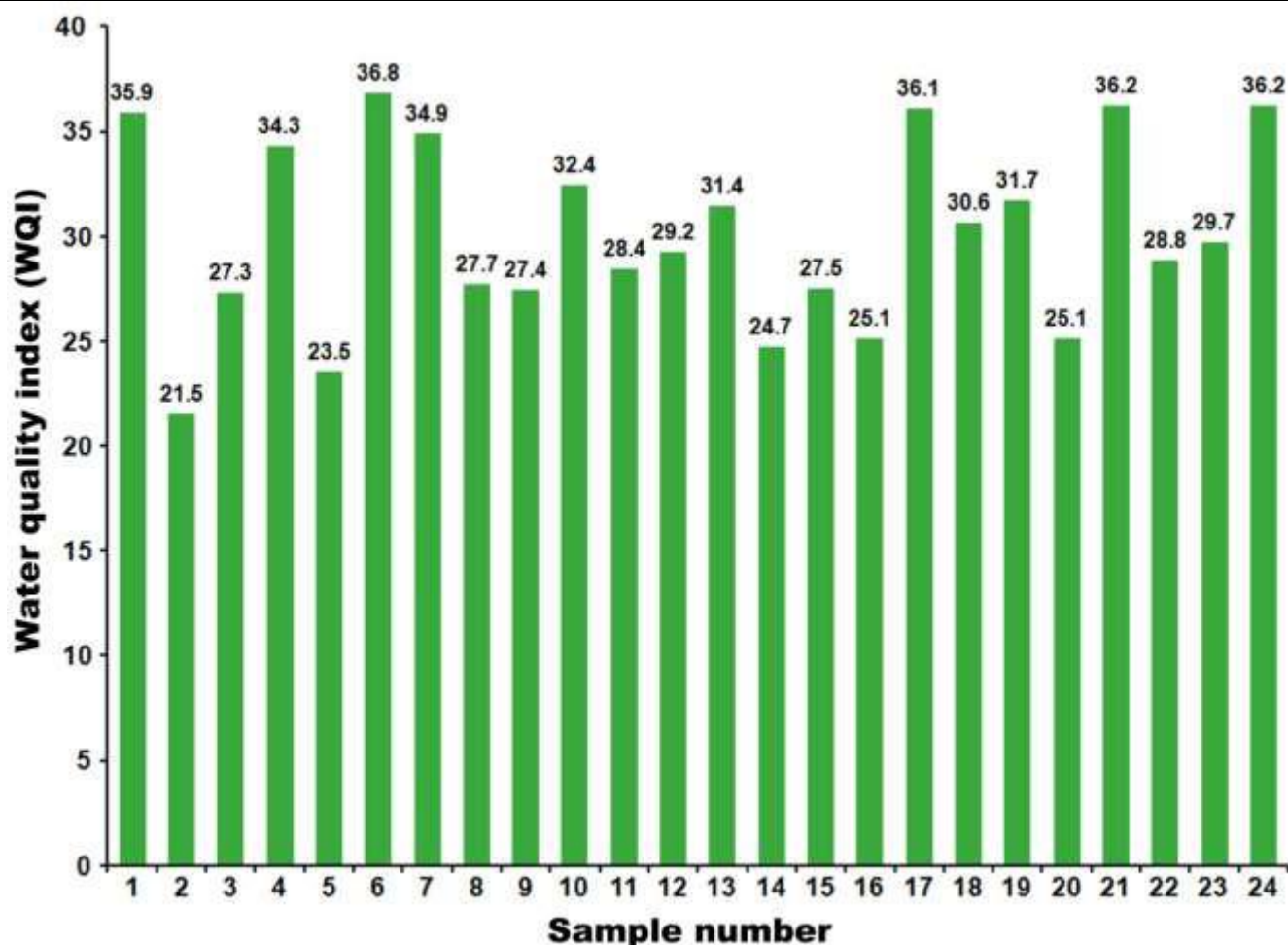


Fig. 2: Water quality index (WQI) values of groundwater samples

IV. CONCLUSIONS

1. The quality parameters viz., fluorides, turbidity, pH and DO are within the permissible standard limits described by ICMR and BIS.
2. The chlorides, alkalinity, hardness, TDS and electrical conductivity are found to exceed the limits.
3. Concentration of chloride was observed to be within the permissible limit of 250 mg/L in most of the stations. Total alkalinity values of all the samples are found to exceed the limit of 120 mg/L.
4. Chlorides, alkalinity, TDS and EC are extremely high when compared with the standard values in case of the samples at Chevitikallu, Ferri and Bhadrirajupalem.
5. The water samples from Katrenipalle, Kasarabada and Kasaranenivaripalem are of excellent quality and suitable for domestic purpose as inferred from very low values of WQI.
6. The groundwater sample from Pollunuru village has the WQI value of 36.8, which is highest value among all the water samples collected in the present study.

7. All the water samples considered in the present study are suitable for domestic/drinking purpose, as per the WQI values. However, it is desirable that the water samples containing very high values of TDS, hardness and EC may be treated before the water is consumed for drinking purpose.

ACKNOWLEDGEMENTS

The authors based on V. R. Siddhartha Engineering College, are thankful to the Management and Principal of the College for providing research facilities.

REFERENCES

- [1] C. A. Almeida, S. Quintar, P. Gonzalez and M. A. Mallea, "Influence of urbanization and tourist activities on the water quality of the potrero de los Funes River (San Luis-Argentina)", *Environ. Monit. Assess.*, vol. 133, pp. 459-465, 2007.
- [2] D. Chapman (UNESCO, WHO, and UNEP), *Water quality assessment*, London, Chapman & Hall, 1992.
- [3] A. D. Sutadian, N. Muttill, A. G. Yilmaz and B. J. C. Perera, "Development of river water quality indices –

- a review”, *Environ. Monit. Assess.*, vol. 188, article no. 58, 2016.
- [4] W. W. Miller, H. M. Joung, C. N. Mahannah and J. Garrett, “Identification of water quality differences in Nevada through index application”, *J. Environ. Qual.*, vol. 15, pp. 265-272, 1986.
- [5] K. Yogendra and E. T. Puttaiah, “Determination of water quality index and suitability of an urban waterbody in Shimoga Town, Karnataka”, in M. Sengupta and R. Dalwani, Editors: *Proc. Taal 2007: The 12th World Lake Conference*, pp. 342-346, 2008.
- [6] D. Sarala Thambavani and T. S. R. Uma Mageswari, “Water quality indices as indicators for potable water”, *Desalination and Water Treatment*, vol. 52, pp. 4772-4782, 2014.
- [7] S. Ramesh, N. Sukumaran, A. G. Murugesan, M. P. Rajan, “An innovative approach of drinking water quality index – A case study from Southern Tamil Nadu, India”, *Ecological Indicators*, vol. 10, pp. 857-868, 2010.
- [8] Shiow-Mey Liou, Shang-Lien Lo and Shan-Hsien Wang, “A generalized water quality index for Taiwan”, *Environ. Monit. Assess.*, vol. 96, pp. 35-52, 2004.
- [9] C. R. Ramakrishnaiah, C. Sadashivaiah and G. Ranganna, “Assessment of water quality index for the groundwater in Tumkur taluk, Karnataka state, India”, *E-Journal of Chemistry*, vol. 6, pp. 523-530, 2009.
- [10] A. A. Bordalo, R. Teixeira and W. J. Wiebe, “A water quality index applied to an international shared river basin: The case of the Douro river”, *Environ. Manage.*, vol. 38, pp. 910-920, 2006.
- [11] M. Vasanthavigar, K. Srinivasamoorthy, K. Vijayaragavan, R. Rajiv Ganthi, S. Chidambaram, P. Anandhan, R. Manivannan and S. Vasudevan, “Application of water quality index for groundwater quality assessment: Thirumanimuttar sub-basin, Tamilnadu, India”, *Environ. Monit. Assess.*, vol. 171, pp. 595-609, 2010.
- [12] C. Chatterjee and M. Raziuddin, “Determination of water quality index (WQI) of a degraded river in Asanol industrial area, Raniganj, Burdwan, West Bengal”, *Nature, Environment and Pollution Technology*, vol. 1, pp. 181-189, 2002.
- [13] D. Sarada Kalyani, V. Rajesh, C. L. Monica and S. Srinivasa Rao, “Assessment of quality of groundwater in parts of north-west mandals of Krishna district, Andhra Pradesh, India”, vol. 14, pp. 1-9, 2016.
- [14] “APHA, AWWA and WPCF standard methods for the examination of waters and waste waters”, 21st Edition, American Public Health Association (APHA), Washington, DC, 2005.
- [15] “Manual on water and waste water analysis”, National Environmental Engineering Research Institute (NEERI), Nagpur, India, 1986.
- [16] BIS Analysis of water and waste water, Bureau of Indian Standards, New Delhi, 1993.
- [17] C. C. Harilal, A. Hashim, P. R. Arun and S. Baji, “Hydro-geochemistry of two rivers of Kerala with special reference to drinking water quality”, *J. Ecol. Environ. Conserv.*, vol. 10, pp. 187-192, 2004.
- [18] B. K. Purandara, N. Varadarajan and K. Jayashree, “Impact of sewage on groundwater: A case study”, *Poll. Res.*, vol. 22, pp. 189-197, 2003.
- [19] S. Gupta, A. Kumar, C. K. Ojha and G. Singh, “Chemical analysis of ground water of Sanganer area, Jaipur in Rajasthan”, *J. Environ. Sci. Eng.*, vol. 46, pp. 74-78, 2004.
- [20] WHO (World Health Organization), *Water sanitation and hygiene links to health*, WHO Press, Geneva, 2004.
- [21] N. S. Rajukar, B. Nongbri, A. M. Patwardhan, “Water quality status of river Umkhrak at Shillong”, *Int. J. Environ. Prot.*, vol. 23, pp. 990-998, 2003.
- [22] ICMR, *Manual of standards of quality for drinking water supplies*, 2nd Edition, Special report series no. 44, Indian Council for Medical Research, New Delhi, India, 1975.

Experimental Study on Pervious Concrete: An Eco Friendly Concrete Pavement

Yogesh N. Sonawane

Assistant Professor, Department of Civil Engineering, R.C.P.I.T. Shirpur, Dist. Dhule, Maharashtra, India

Abstract— As a civil engineer and human being it's our prime duty prime to save environment, because lack of water absorption and air permeability of common concrete pavement, rain water is not entered in to the ground directly. It will reduce ground water table, plants are difficult to grow normally, difficult to maintain temperature and humidity of earth. To minimize such affects, the research on pervious concrete pavement widely done for road way application. In this study, determine compressive strength, porosity test on pervious concrete. The compressive strength is relatively low because of its porosity but at the same time we increase water absorption quality. Due to low strength we cannot be used as a road pavement. The pervious concrete can only be applied to footpaths, parking and where low strength is required.

Keywords— Compressive Strength, Pervious Concrete, Porosity etc.

I. INTRODUCTION

Now a day's concrete pavement are widely used to enhance comfort for all citizens. But at the same we want to study about environment, because lack of water absorption and air permeability of common concrete pavement, rain water is not entered in to the ground directly. It will reduce ground water table, plants are difficult to grow normally, difficult to maintain temperature and humidity of earth. Many advantages of pervious concrete are as follows –

1. The rain water quickly filtered in to the ground, so ground water table can increase.
2. As the Pavement is air permeable and water permeable, the soil underneath can be kept wet. It improves the environment of road surface.

Pervious concrete have holes that can cumulate heat. Such pavement adjust temperature and humidity of earth surface

II. APPLICATIONS OF PERVOUS CONCRETE

1. Pervious Concrete as a Road pavement (Foot path, Parking area)
2. Residential roads and driveways
3. Parking lots
4. Noise barriers
5. Slope stabilization

6. Swimming pool decks

III. HISTORICAL BACKGROUND

The initial use of porous concrete was in the United Kingdom in 1852 with the construction of two residential houses and a sea groyne. Cost efficiency seems to have been the primary reason for its earliest usage due to the limited amount of cement used. It was not until 1923 when porous concrete re surfaced as a viable construction material. This time it was limited to the construction of 2-story homes in areas such as Scotland, Liverpool, London and Manchester. Use of porous concrete in Europe increased steadily, especially in the World War II era.

IV. COMPRESSIVE TEST ON PERVIOUS CONCRETE

(A) Sample Preparations

Table. 1: Samples

Sample's	Size of Aggregate mm	Cement Kg	Coarse Aggregate Kg	Water Kg	Admixture(1 %Of Cement)
A	10	440	1720	156.97	-
B	20	531.42	1735.69	182.46	-
A _A	10	440	1720	156.97	4.4
B _B	20	531.42	1735.69	182.46	5.31

Where A & B is a sample without admixture

Where A_A& B_B is a sample with admixture

1. Compressive strength (Conventional)

Table.2

Sam ple	Size of Aggre gate	Compre ssive strength (7 days) MPa	Avg. Compre ssive strength (7 days) MPa	Compre ssive strength (28 days) MPa	Avg. Compre ssive strength (28 days) MPa
B	20 mm	15.2	14.06	20.1	19.53
B	20 mm	14		19.6	
B	20 mm	13		18.9	

2. Compressive strength Results of Pervious concrete

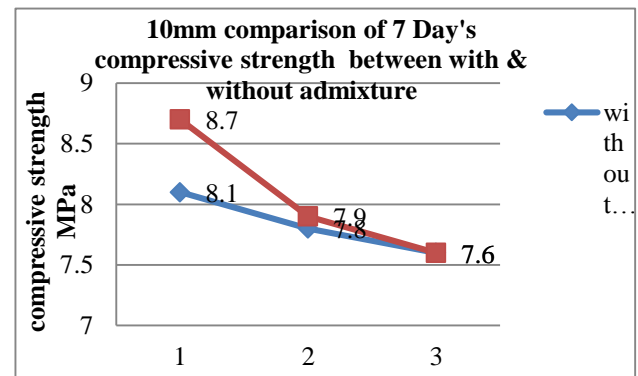
Table.3

Sam ple	Size of Aggre gate in mm	Compre ssive strength (7 days) MPa	Avg. Compre ssive strength (7 days) MPa	Compre ssive strength (28 days) MPa	Avg. Compre ssive strength (28 days) MPa
A	10	8.1	7.83	12.4	11.36
A	10	7.8		11.6	
A	10	7.6		10.1	
B	20	8.4	7.70	11.6	11.13
B	20	7.8		10.8	
B	20	6.9		11	
A _A	10	8.7	8.06	10.6	15.30
A _A	10	7.9		14	
A _A	10	7.6		15.3	
B _A	20	2.9	3.73	5.9	7.90
B _A	20	4.6		9.9	
B _A	20	3.7		7.9	

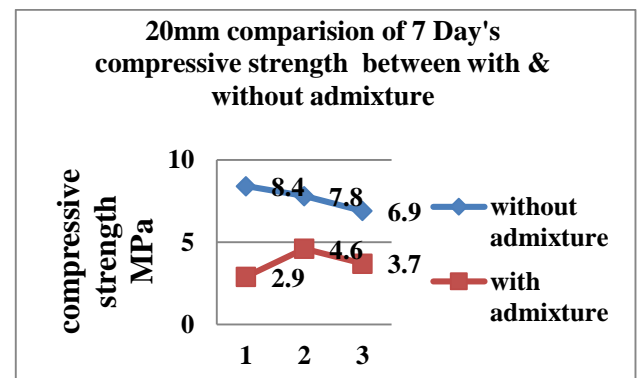


Fig. 1: Cube for Testing

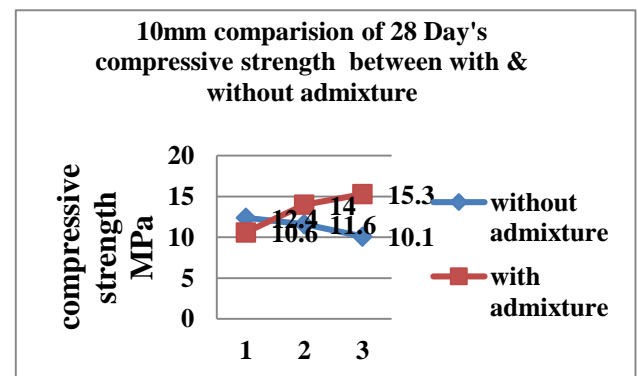
3. Results



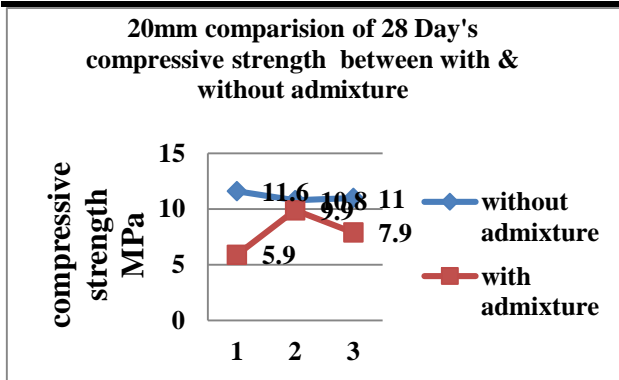
Graph 1: A and A_A Sample Compressive Strength at 7 days



Graph 2: B and B_B Sample Compressive Strength at 7 days



Graph 3: A and A_A Sample Compressive Strength at 28 days



Graph 4: B and B_B Sample Compressive Strength at 28 days

V. CONCLUSION

From results obtained following conclusion may are-

1. The pervious concrete is suitable only for low volume road pavement like foot path, parking slots. Due to voids in pervious concrete it is difficult obtained required compressive strength.
2. Using smaller size aggregate (10 mm) can enhance the compressive strength of pervious concrete than bigger size aggregate (20mm).
3. Compressive strength can be increase by using proper admixtures also.
4. Water absorption, abrasion resistance are good property of pervious concrete.
5. It is an eco friendly concrete material.

REFERENCES

- [1] Mr. V. R. Patil, Prof. A. K. Gupta, Prof. D. B. Desai, "Use Of Pervious Concrete In Construction Of Pavement For Improving Their Performance," IOSR Journal of Mechanical and Civil Engineering (IOSR-JMCE), PP: 54-56
- [2] Jing Yang*, Guoliang Jiang, "Experimental study on properties of pervious concrete pavement materials," Cement and Concrete Research 33 (2003) 381–386,
- [3] M. Harshavarthana Balaji, M. R. Amarnaath, R. A. Kavin, S. Jaya pradeep, "Design of Eco Friendly Pervious Concrete," International Journal of Civil Engineering and Technology (IJCIET), Volume 6, Issue 2, February (2015), pp. 22-29
- [4] Darshan S. Shah , Prof. Jayeshkumar Pitroda, Prof. J .J. Bhavsar, "Pervious Concrete: New Era For Rural Road Pavement," International Journal of Engineering Trends and Technology (IJETT) – Volume 4 Issue 8- August 2013, pp: 3495-3499
- [5] Rasiyah Sriravindrarah, Neo Derek Huai Wang, Lai Jian Wen Ervin, "Mix Design for Pervious Recycled Aggregate Concrete," International Journal of Concrete Structures and Materials, December 2012, Volume 6, Issue 4, pp 239–246

Optical and Thermal Performance Analysis of a Steady Spherical Collector with a Crescent-shaped Rotating Absorber

Thierry S. M. Ky¹, Boureima Dianda¹, Moktar Ousmane^{1,2}, Magloire Pakouzou¹, Sié Kam¹, Dieudonné J. Bathiebo¹

¹Laboratory of Renewable Thermal Energies, UFR-SEA, 03 BP 7021, University Ouaga I Pr Joseph KI-ZERBO, Burkina Faso.

²University of Agadez PO BOX 199 Niger.

Abstract— In this paper, optical analysis of spherical concentrator is made to determine the local and the global geometric concentration, as knowing the geometric concentration of a system can help predict what temperatures can possibly be obtained with it. This leads to conclude that spherical collectors may produce higher temperatures than parabolic trough, and they could even be sharply improved by using a mixt cylindrical and cavity (or flat) absorber.

A craft prototype of a steady spherical concentrator made with concrete and having a smooth inner surface mapped with mirror tape is presented. Its absorber is made with blacken steel sheets and shaped like a moon crescent to be aligned with the declination plan and to avoid motorization for the tracking of the sun from East to West. Experimental measurements lead to temperatures reaching 686°C on the curve of the least diffusion, and 252°C in the absorber oven-like reservoir. Overall, the results suggests higher potentialities of spherical collectors, which also show possibility of use with much reduced tracking system and less vulnerability to bad weather.

Keywords—Fixed Mirror Distributed Focus-FMDF, Mixt conical and cavity absorber. Optical analysis, Spherical collector, Solar Bowl.

I. INTRODUCTION

Cooking bread requires temperatures between 250°C and 300°C. To do so with solar systems, we need a concentrator that tracks the sun. Scheffler systems (Muniret *al.*, 2010[1]) are designed for developing countries as less heavy in care, and use hot air for cooking bread. Even so, Scheffler systems installed in Burkina Faso-West Africa had shown poor resistance to bad weather and a quite dependency to the daily presence of a mechanic to adjust the plant concentrators for tracking the declination.

A recent study made by Mahdi and Bellel 2014 [2] tends to suggest that hemispherical concentrator has interesting mean concentration ratio, because it is used for focusing in one spot. This also had been studied by Kyet *al.*, 2015 [3] who proposed the use of hemispherical concentrator to replace Scheffler systems. The geometric mean concentration of the hemispherical concentrator had been restudied to best locate the plan of the least diffusion and to determine the size of the cavity absorber to be disposed. For a record, the geometric mean concentration is advocated when the target is a flat or cavity absorber.

In this paper, we study the geometric concentration of a hemispherical concentrator and determine the size of the absorber to dispose along the axis of reflection. Knowing the geometric concentration of a system can help predict what can possibly be obtained as temperatures. Then, a prototype using crescent-shaped absorber is studied. That absorber is placed in the plan of declination so that it can be easily rotated for adjustment, and works without any motorized system for tracking the sun from East to West.

II. GEOMETRIC CONCENTRATION OF A HEMISPHERICAL CONCENTRATOR

The hemispherical concentrator does not focus on one point. It focuses on the axis parallel to the solar rays and passing through the center of the sphere. It is on this axis that an absorber (or receiver) needs to be placed (Fig.1). A study shows that the reflection position on the axis is obtained by the following formula (El-Refaie, 1987 [4], Ng *et al.*, 2012 [5], Bouguetaia, 2013 [6]),

$$Y(\phi, n) = \sqrt{1 - R^2} + (-1)^n \frac{\sin \phi}{\sin(2n\phi)} - R \cot(2n\phi) \quad (1)$$

With the ratio R equal the radius of the cylindrical axis of the absorber R_{aa} on the radius of the hemispherer r_s ,

$$R = \frac{R_{aa}}{r_s} \tag{2}$$

and ϕ_s the half-angle of the area of sun ray reflecting to the absorber from the concentrator. For a half-angle $\phi_s \geq 60^\circ$ the solar ray knows multiple reflections before reaching its target. It is however always projected along the axis. The number of reflections in relation to the angle of incidence of the ray was given by (Ng *et al.*, 1012. P.286, El-Refaie, 1987, P.167),

$$n = \left\lceil \frac{\phi - \sin^{-1} R}{180 - 2\phi} \right\rceil + 1 \tag{3}$$

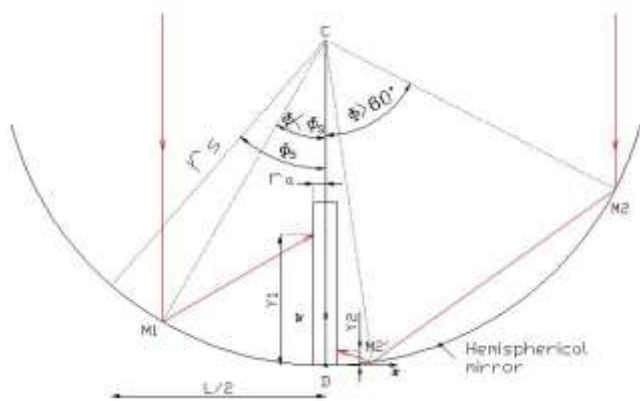


Fig. 1: Optical characteristics

One equation to determine R characterizing the cylindrical absorber to dispose on the concentrator axis (Ng *et al.*, 1012 P.286, El-Refaie, 1989),

$$R \geq \frac{4,65 \cdot 10^{-3} \sin(2n\phi) \left[(n-1) \frac{\sin(2\phi)}{\sin \phi} + \frac{\sin((2n-1)\phi)}{\sin(2n\phi)} \right]}{\sin(2n\phi) - (-1)^n 4,65 \cdot 10^{-3}} \tag{4}$$

We can perceive the desire to optimize the cylindrical absorber by taking into account the half angle $\theta_s = 4,65 \cdot 10^{-3}$ rad characterizing the radius of the optical image of the sun, and by adopting the maximum ratio of R where the optical image is widest. However, if we refer to the optical images formed along the axis, we find that the distance between the reflection point on the concentrator and the reception point on the absorber varies from $\frac{r_s}{2}$ to r_s (Fig.2).

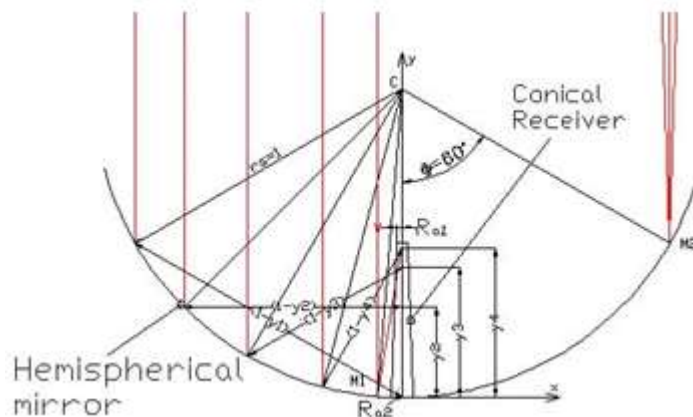


Fig. 2: Relation between R_a and y

- For an optimization of the absorber and by considering a change in its cross section according to the projection distance, it is found that the axis-shaped absorber must be in the form of a truncated cone with the bottom closed to the hemispherical surface and the top at the half-radius of the hemispherical concentrator. We obtain so the absorber characteristics as a truncated cone. This is also stated by Steward and Kreith 1975[7]. By considering the half angle of the sun image projection $\theta_s = 4,65 \cdot 10^{-3}$, we obtain:

- $R_{a1} = \frac{r_s}{2} \sin \theta_s$ the upper radius of the cone closed to the half-radius of the hemisphere.
- $R_{a2} = r_s \sin \theta_s$ the lower radius of the cone closed to the surface of the concentrator.
- $h = \frac{r_s}{2}$ the height of the cone.

An equation that expresses the absorber radius R_{aa} according to the optical image of the sun can be established as follows,

$$R_{aa}(\phi, n) = -r_s (-1)^n \frac{\sin \phi}{\sin(2n\phi)} \sin \theta_s \tag{5}$$

$R_{aa}(\phi, n)$ depends of $n(\phi)$. We must redefine $n(\phi)$:

2.1. Redefining $n(\phi)$:

$n(\phi)$ which is independent to $R_{aa}(\phi, n)$ can be written from (equation (3)),

$$n(\phi) = \text{Lower.round} \left\{ \left\lceil \frac{\phi}{180 - 2\phi} \right\rceil + 1 \right\} \tag{6}$$

2.2. Redefining $Y(\phi, n)$:

The optical image is proportional to the radius of the absorber since the optical spot covers the absorber. Fig.2 shows a relationship between R_{aa} and y .

$\frac{R_{aa}}{r_s} = (1 - y) \sin \theta_s$ for $y = \frac{Y}{r_s}$. So $Y(\phi, n)$ can be

defined using equations (5) and (6),

$$Y(\phi, n) = r_s \left[1 + (-1)^n \frac{\sin \phi}{\sin(2n\phi)} \right] \tag{7}$$

2.3. Definition of the geometric concentration $C_{g(Cir_3D)}$:

We will define a local geometric concentration (or local geometric concentration ratio) $C_{g(Cir_3D)}$ as the variation of concentration along the absorber for any half angle ϕ ; it is the concentration of a partial area projected to the corresponding partial area of the absorber. This will allow to determine the way temperature are distributed along the conical absorber.

We will also define a global geometric concentration $C_{g(Cir_3D)}$ as the concentration of an entire area of the concentrator to its entire corresponding absorber for an aperture half angle ϕ_s .

In the following optical study, we will consider the frontal area of the spherical concentrator always facing the sun and all the rays projected on the conical absorber. The landmark will be with the origin at the junction between the absorber and the concentrator and the y axis going toward the center of the sphere.

The local geometric concentration along the absorber $C_{g(Cir_3D)}$ is the interpolation of the ratios of the elementary surface of reflection from the hemispheric concentrator on the elementary surface of projection on the absorber. These surfaces may be defined as follows (Fig. 3):

* The elementary surface reflected by the concentrator,

$$S_{sph}(\phi_{i+1} - \phi_i) = \pi r_s^2 \left[\sin^2(\phi_{i+1}) - \sin^2(\phi_i) \right] \tag{8}$$

* The elementary surface of projection on the absorber using equations (5) and (7),

$$S_{rec}(\phi_{i+1} - \phi_i, n) = 2\pi \frac{R_{aa}(\phi_{i+1}, n) + R_{aa}(\phi_i, n)}{2} \left[Y(\phi_{i+1}, n) - Y(\phi_i, n) \right] \tag{9}$$

* The elementary (or local) geometric concentration is obtained using equations (8) and (9) as,

$$c_g(\phi_{i+1} - \phi_i, n) = \frac{S_{sph}(\phi_{i+1} - \phi_i)}{S_{rec}(\phi_{i+1} - \phi_i, n)}$$

and:

$$c_{g(Cir_3D)}(\phi_{i+1} - \phi_i, n) = \frac{1}{\sin \theta_s} \frac{\sin^2(\phi_{i+1}) - \sin^2(\phi_i)}{|A^2(\phi_{i+1}, n) - A^2(\phi_i, n)|}$$

$$\text{with: } A(\phi, n) = \frac{\sin \phi}{\sin(2n\phi)} \tag{10}$$

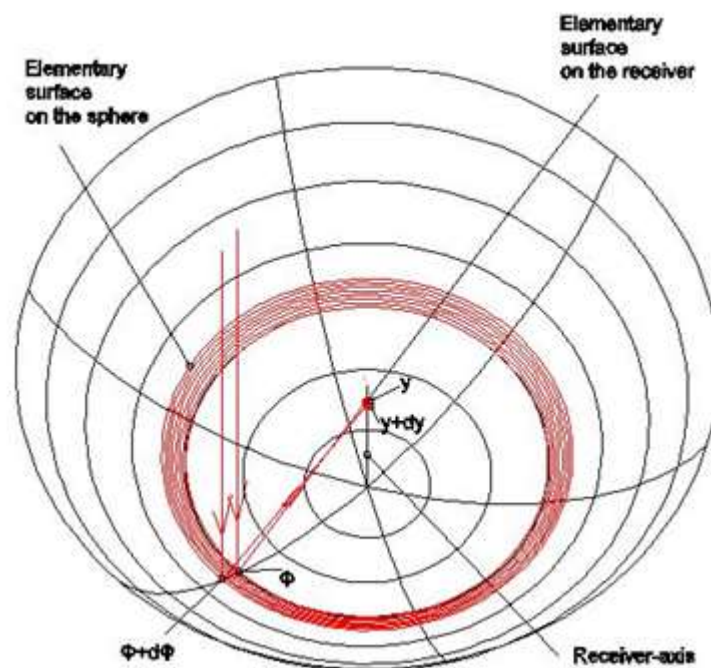


Fig. 3: Elementary surfaces for geometric concentration calculation

$C_{g(Cir_3D)}(\phi_{i+1} - \phi_i, n)$ is an algorithm that determines the geometric concentration in any location of the absorber (ie the local geometric concentration) as well as the global geometric concentration. The parameter i varies in the range $\phi \in [\theta_s; 90^\circ]$ depending on the chosen step of discretization (Fig.3).

We used MATLAB program to define a new function based on y (with $y = \frac{Y}{r_s}$ and $0 \leq y \leq 0,5 - \sin \theta_s$) rather

than ϕ , so the curve of the local geometric concentration along the absorber can be drawn (Fig.4).

The curves show a maximum of 860 reached for $\phi = \sin \theta_s$ (or $y \approx 0,5 - \sin \theta_s$) that progressively decrease to 76 (for $\phi = \sin \theta_s$ or $y \approx 0,08$). Then we notice multiple reflections.

Observations:

* Multiple reflections generate concentration peaks in the

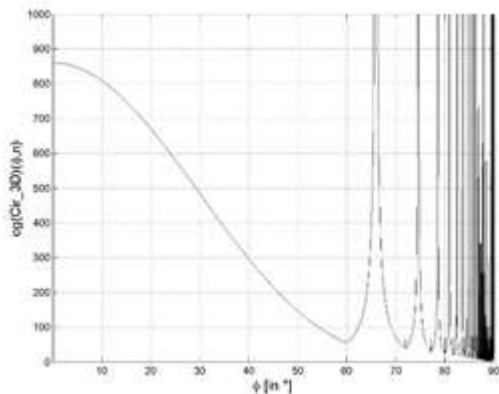


Fig.4: Curves of local geometric concentration along the absorber depending on Φ or y

* The second curve of Fig.4 is fairly concise in comparison with the optical concentration ratio values measured on a similar system in Texas (Stine *et al.*, 1986 [8]) (Fig.5). The curve of the Texas system, however, shows a rise of concentration near the contact zone between the concentrator and absorber. This is due to the superposition (overlapping) phenomenon of optical images of the sun generated by multiple reflections.

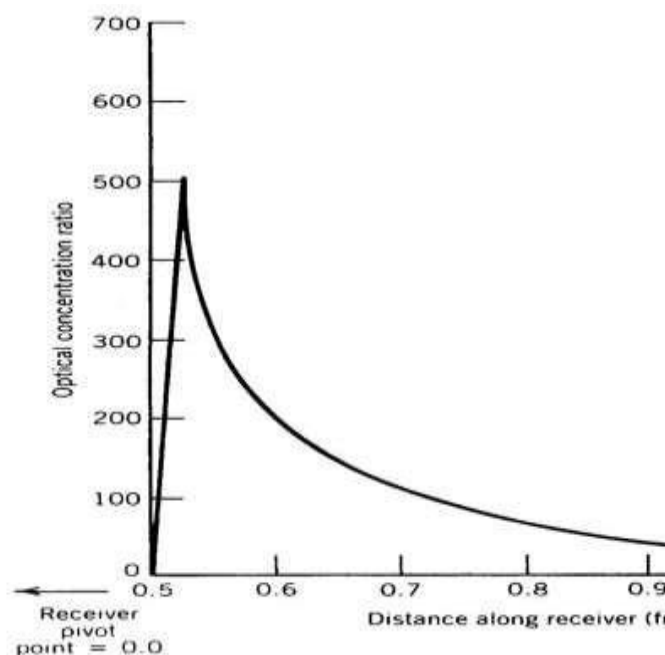
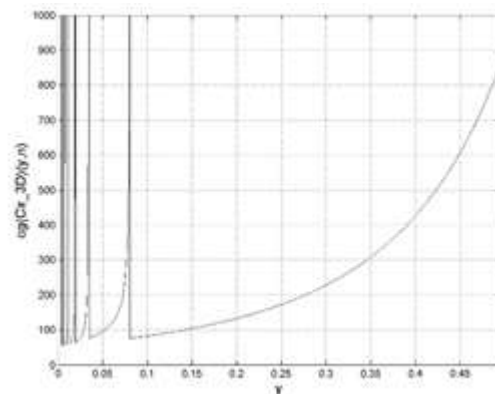


Fig.5: Flux distribution along the absorber of a FMDF collector. (Stine *et al.*, 1986)

Taking into account the superposition phenomenon will bring us to sum all local geometric concentrations depending on the number of reflections. Equation to use is,

vicinity of the lower end of the conical absorber, thereby creating a zone of heat very close to the surface of the concentrator.



$$c_{g(Cir_3D)}(y) = \sum_{j=1}^{2n-1} c_{g(Cir_3D)}(y, n(j)) \tag{11}$$

That gives the following curve using MATLAB program (Fig. 6).

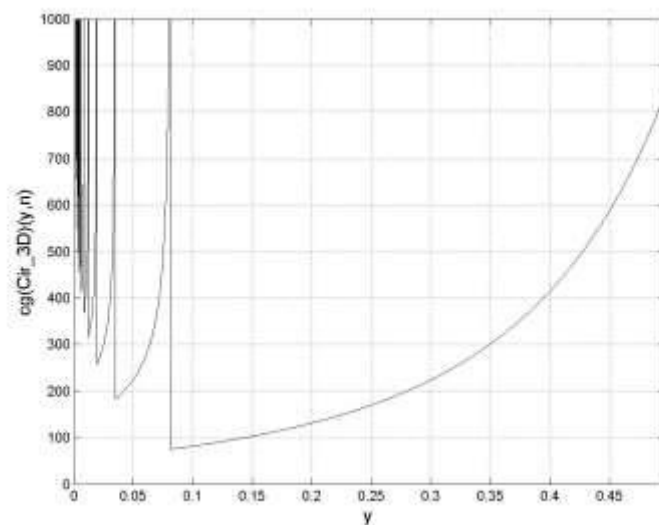


Fig.6: Local geometric concentration considering the superposition phenomenon

Studying the local geometric concentration allows to understand the way the absorber is used. Usually, the fluid flows from bottom to top, because it flows from the part with low local concentration (meanwhile lesser heat) to the part with higher concentration (higher heat). The FMDF absorber is also shaped as a cone and water inlet is from the lower part (Fig. 7).

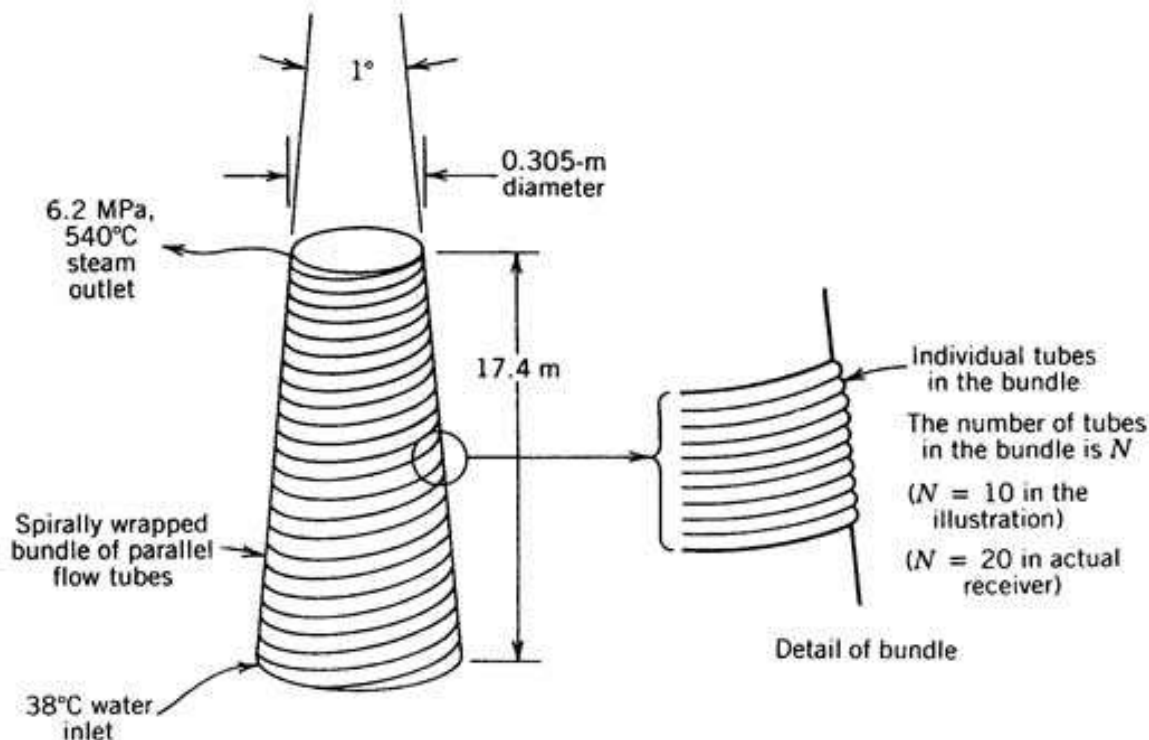


Fig.7: Schematic diagram of the absorber for FMDF collector. Courtesy of Santia National Laboratories. Built at Crosbyton-Texas-USA.

2.4. Linearization of the function $c_{g(Cir_3D)}(\phi_{i+1} - \phi_i, n)$

:
 Since all geometric concentrations are determined directly as a function of ϕ parameter, the function $c_{g(Cir_3D)}(\phi_{i+1} - \phi_i, n)$ can also be expressed likewise. This linearization is obtained for $n = 1$, ie by excluding the multiple reflections and focusing exclusively on the interval $\phi_s \in [0; 60^\circ]$ (or on the interval

$y \in [0; 0,5 - \sin \theta_s]$). We obtain the following functions as linearization of equation (10) with their plots (Fig.8),

$$c_{g(Cir_3D)}(\phi) = \frac{4}{\sin \theta_s} \cos^4 \phi \tag{12}$$

$$\text{and } c_{g(Cir_3D)}(y) = \frac{1}{4(y-1)^4 \sin \theta_s} \tag{13}$$

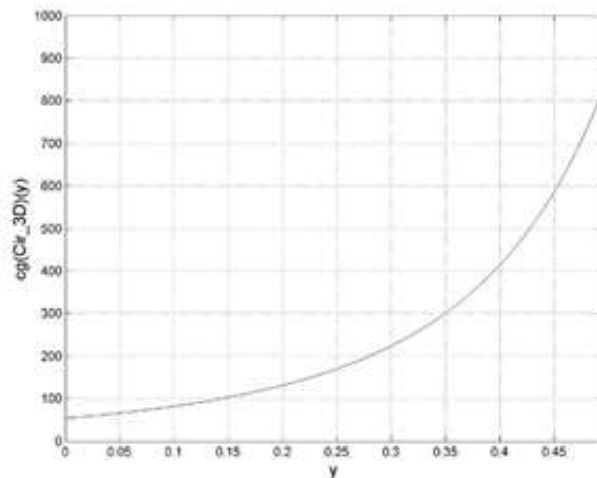
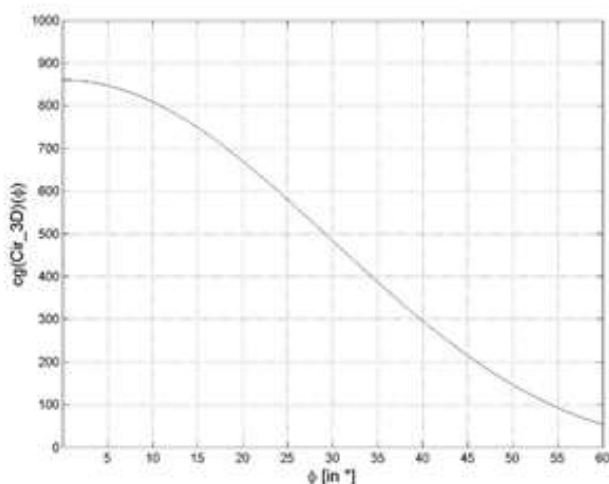


Fig. 8: Linearization of local geometric concentration depending on Φ and y

2.5. Validation domain for $c_{g(Cir_3D)}$:

This equation is meaningless for small values of ϕ . Indeed, the sunspot covers almost the entire surface of the absorber for these small values. However, it is very precise for the side rays. Moreover, the equation considers the homogeneous sunspot in one hand, and the juxtaposition effect of the sun rays rather than the superposition effect on the other hand. (Veynant, 2011) [9].

2.6. The global geometric concentration $C_{g(Cir_3D)}$.

The global geometric concentration (which is usually called geometric concentration) $C_{g(Cir_3D)}$ is determined by using the equation (10) and by fixing ϕ_i to 0° and ϕ_{i+1} to ϕ_s . The equation therefore becomes,

$$C_{g(Cir_3D)}(\phi_s) = \frac{4}{\sin \theta_s} \cos^2 \phi_s \text{ for } \phi_s \leq 60^\circ \quad (14)$$

This equation concretely shows the increase of the size of the conical absorber with the half angle ϕ_s till it reaches its limits to $h = \frac{r_s}{2}$ when $\phi_s = 60^\circ$ (Fig.9). Then, since the size of the absorber will not increase any longer while the projected area of the concentrator is still increasing and projecting towards the conical absorber, the equation (14) of the global concentration shifts to,

$$C_{g(Cir_3D)}(\phi_s) = \frac{4}{3 \sin \theta_s} \sin^2 \phi_s \text{ for } \phi_s > 60^\circ \quad (15)$$

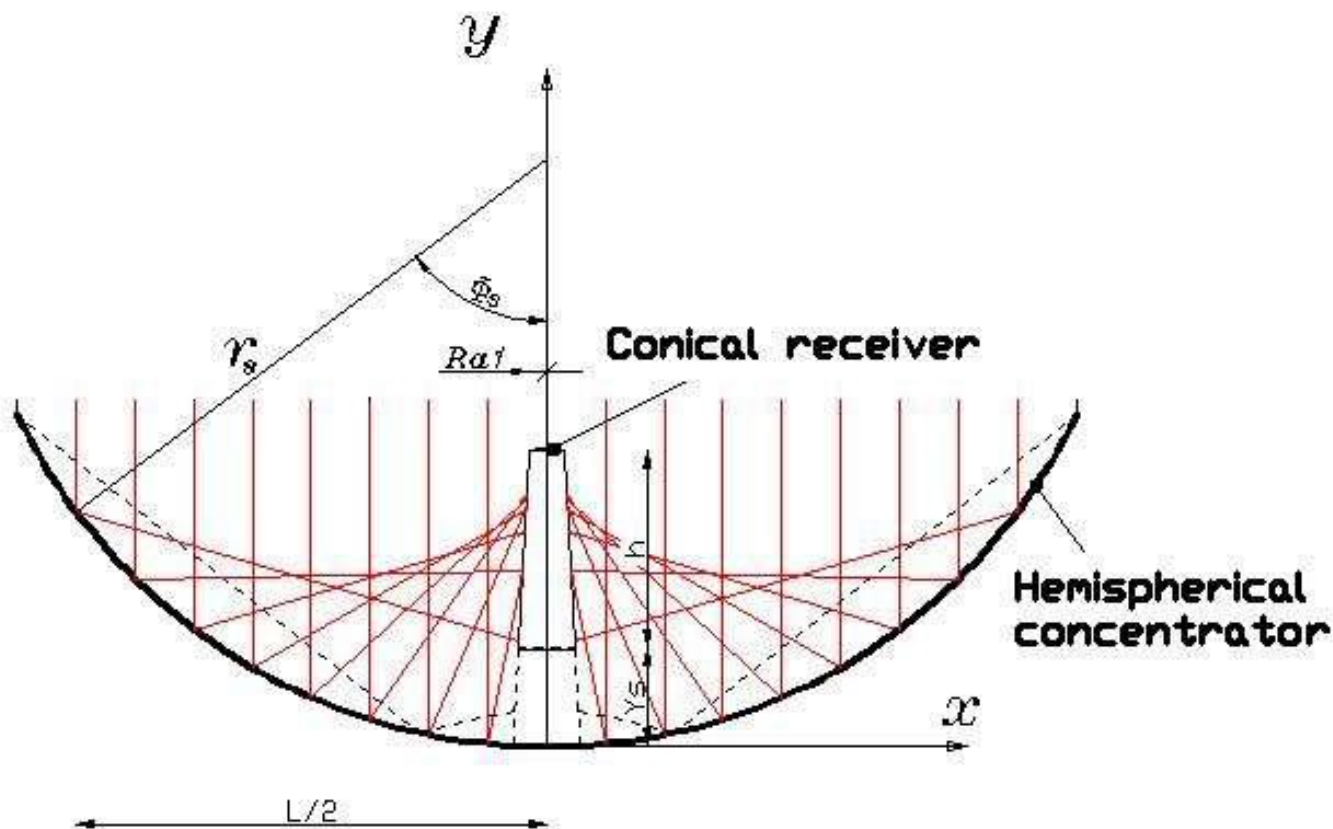


Fig.9: Concentrator projecting to its conical absorber. The wider the circle' radius ($L/2$), the higher the cone until $\phi_s = 60^\circ$ when h is maximum. Afterwards, multiple projections continue to reach the conical absorber.

The plot of equations (14) and (15) is given on the following fig. 10

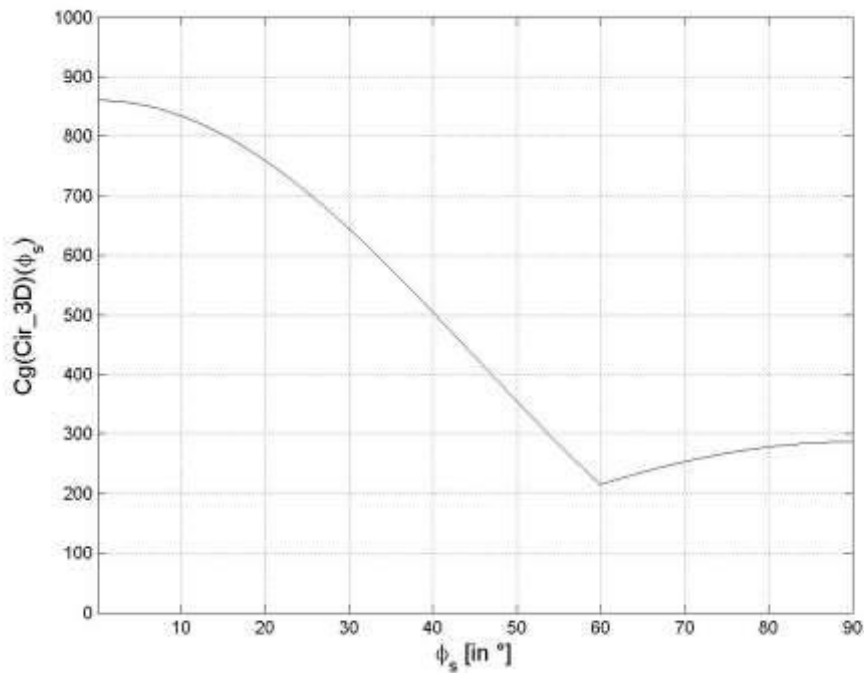


Fig. 10: Global geometric concentration depending on ϕ_s . With the increase of the size of the absorber, the geometric concentration sharply decreases from 860 to 215. Then since the absorber size no longer evolves, the geometric concentration increases to 287.

The global concentration can also be defined to express the change of the height h of the conical absorber by the equation:

$$C_{g(\text{Cir}_{3D})}(y) = \frac{1}{(1-y_s)^2 \sin \theta_s} \quad (16)$$

so setting $y_s = \frac{1}{2} - \frac{h}{r_s}$ leads to $C_{g(\text{Cir}_{3D})}\left(\frac{h}{r_s}\right) = \frac{1}{\left(\frac{1}{2} + \frac{h}{r_s}\right)^2 \sin \theta_s}$ with $\frac{h}{r_s} \in \left[\sin \theta_s; \frac{1}{2}\right]$ (17)

The plot of equation(17) is given on the following fig. 11:

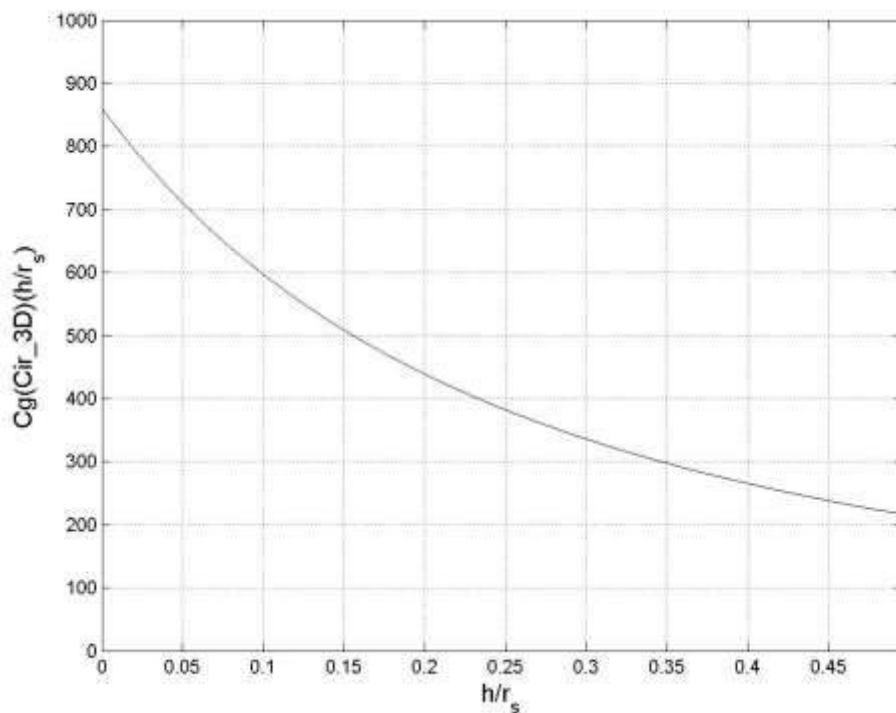


Fig. 11: Global geometric concentration depending on $\frac{h}{r_s}$. The conical absorber starts from $\frac{h}{r_s} = \sin \theta_s$. This is where the cone begins to grow while the geometric concentration is at its maximum (860). Then, the conical absorber has its full height at $\frac{h}{r_s} = 0,5$, and the geometric concentration had decreased from 860 to 215.

Multiple reflections are not taken into account in the equation (17) and fig. 11.

2.7. Real global geometric concentration of the system:

If the concentrator system studied above is designed using flat mirrors tiles of 5 cm x 5 cm for example, it is possible to introduce Δl , characterizing the linear dispersion caused by such tiles. Using equations (16) and (17), we obtain,

$$C_{g(Cir_{3D})}(\phi_s) = \frac{4}{\Delta l + \sin \theta_s} \cos^2 \phi_s \text{ for } \phi_s \leq 60^\circ \quad (18)$$

$$\text{and } C_{g(Cir_{3D})}(\phi_s) = \frac{4}{3(\Delta l + \sin \theta_s)} \sin^2 \phi_s \text{ for}$$

$$\phi_s > 60^\circ \quad (19)$$

Note: A dispersion is generally represented by a half-angle $\Delta \theta$. In this case, $(\Delta l + \sin \theta_s)$ should be replaced by $\sin(\Delta \theta + \theta_s)$ in the preceding equations (18) and (19).

2.8. Comparisons between hemispheric global geometric concentration $C_{g(Cir_{3D})}$ and geometric mean concentration $C_{gmed(Cir_{3D})}$.

From the previous results on the geometric concentration reachable for a parabolic trough (215), we can consider that using a hemispherical concentrator already guarantees a higher temperature in comparison with the parabolic trough. But when we also use the result of geometric mean concentration of a hemispherical concentrator known from previous publications (Kyet *et al.*, 2015, Bernard *et al.*, 1980[10]), we notice that for the values of angle ϕ_s below 23° (angle taken from the center of the sphere), a cavity (or flat) absorber is more suggested to be used, for the curve of geometric mean concentration is above that of the geometric concentration as we can see on fig. 12. This geometric mean concentration reaches a maximum at $\phi_s = 11^\circ$ to a value of 2.964. Actually, the hemispheric concentrator is one of the concentrators with a geometric mean concentration

higher than its geometric concentration. Beyond 23°, a use of conical absorber is compulsory.

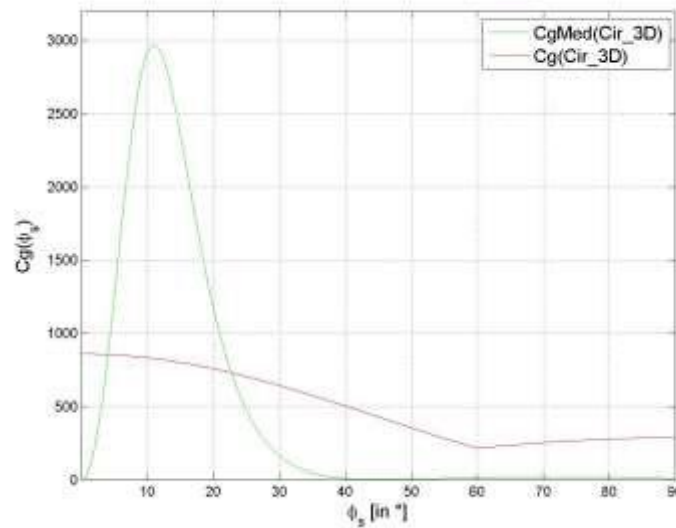


Fig. 12: curves comparing global geometric concentration and geometric mean concentration of a hemispherical concentrator. We see that $C_{gmed(Cir_3D)} \geq C_{g(Cir_3D)}$ for angle $\phi_s \leq 23^\circ$ suggesting the use of a cavity absorber in that zone. When beyond that value, it would be compulsory to use a conical absorber.

It is quite common to see a mixt use of cavity and conical absorber on the same hemispherical concentration system. That will be a good solution to optimize the system by having the fluid admitted from the lower inlet of a conical receiver to the upper outlet in a cavity absorber. The cavity absorber will best contribute if the area projecting into it has a half angle $\phi_{s1} < 23^\circ$ as shown in fig. 13. As a matter of fact, Sulaiman *et al.*, 1997 [11] used this particularity of FMDF collector to suggest a hybrid photovoltaic and thermal receiver to dispose.

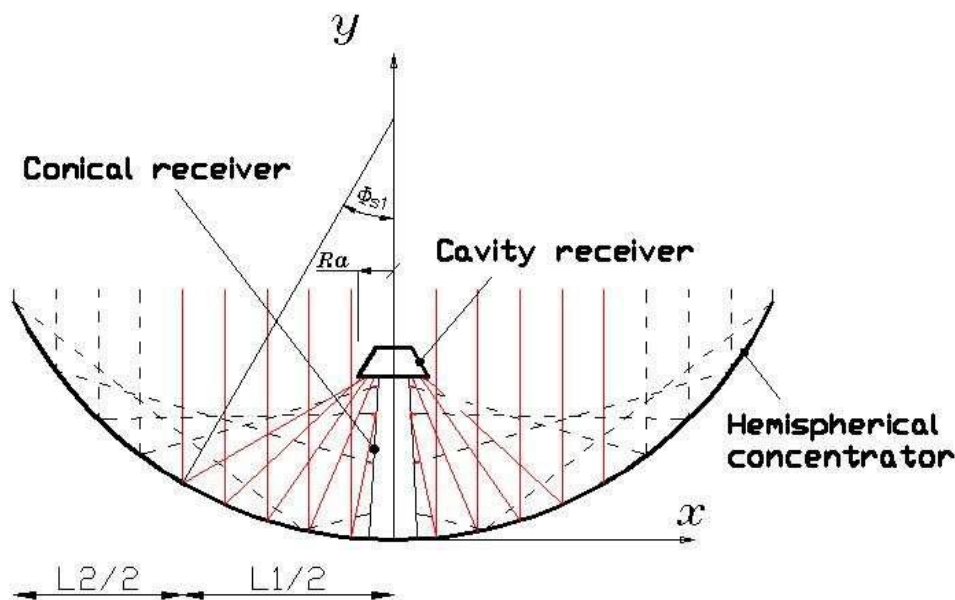


Fig.13: Hemispherical concentrator with a mixt conical and cavity absorber

III. THERMAL PERFORMANCE ANALYSIS ON A PROTOTYPE

The spherical concentrator was conceived with concrete to get a smooth inner surface. A taping film of mirror was used to get the reflective surface. The circular frontal area has a diameter of 1,14m. The sphere inner diameter is 1,18m (Fig. 14).



Fig.14: Image of the prototype - Concrete hemispherical concentrator with it moon crescent-like absorber.

The absorber is made of steel sheet painted in black. It has a closing reservoir, and we are concerned in having the air temperature inside the reservoir. The absorber has a lip at its bottom that is designed to be in the curve of the least diffusion, meanwhile, the bottom part of the reservoir receives sunlight as a plate corresponding to a geometric mean concentration with a half angle of 22°C (Fig.15).

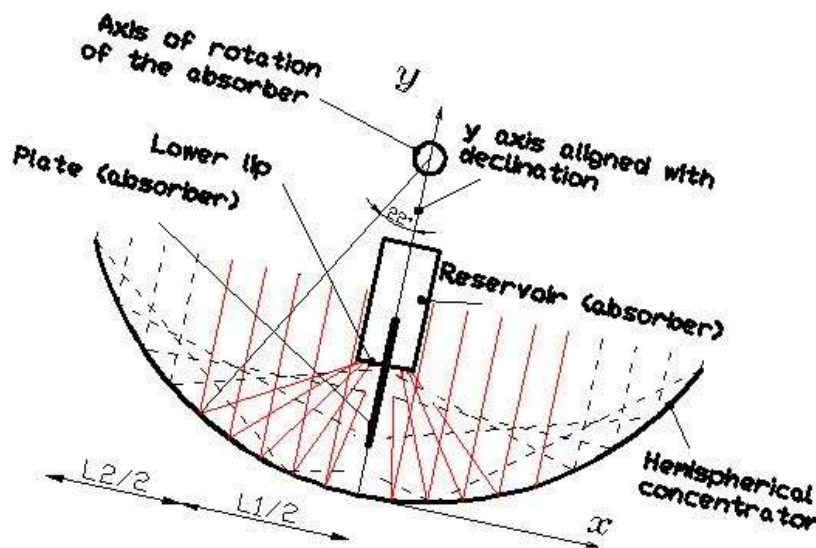


Fig.15: Schematic design of the prototype with its reservoir and plate absorber aligned in the declination plan.

There is also a plate in the middle that receives sunlight in the place of a conical absorber. After all, the absorber was design shaped like a moon crescent to be positioned in the plan of declination such that there will be no need to track the sun from East to West, and the tracking for the

declination is obtained by a rotation of the absorber along an axis passing through the center of the sphere.

3.1. Materials and methods.

Following materials and methods were used to get our results:

- A data logger type Midi LOGGER GL200A of GRAPHTEC brand.
- Probes A and B are placed against bottom lip of the receiver in both sides (North and South) to measure the temperature in the focal point. To do this, we follow the light spot indicating the reflection of the sun to search for the highest temperature. We follow the sun's path every 5 minutes.
- Probes C and D are placed inside the reservoir in both side East and West 10 cm from the closet. They will get the inner air temperature, so they are not in contact with any surface.

- Probe Amb. reports the ambient temperature.
- A type SL100 and brand KIMO solarimeter is used to measure solar radiation.

3.2. Results and discussions about the measurements of June 06, 2016:

The curves A and B (Fig. 16) grow progressively till 11.a.m. when they reach a pic of 686°C. This follows at some point the irradiation curve of the day which had an average of 750 W.m⁻² (Fig. 17). The curves of probes A and B not being continuous indicates the difficulty to get the focal points.

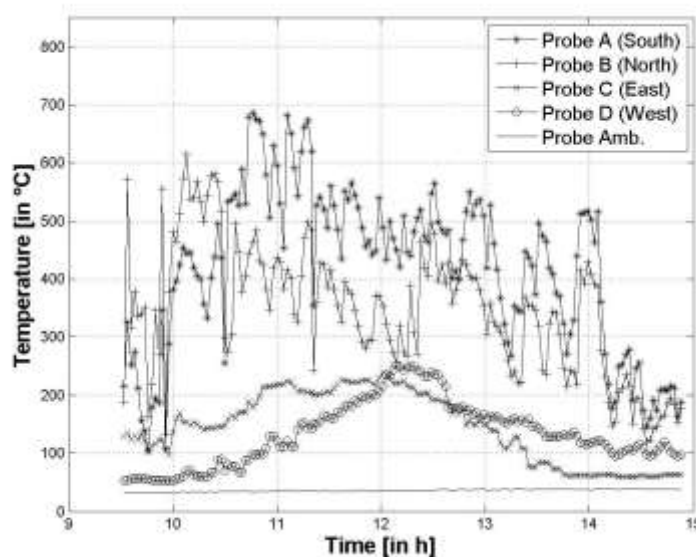


Fig.16: temperature curves on June 06, 2016.

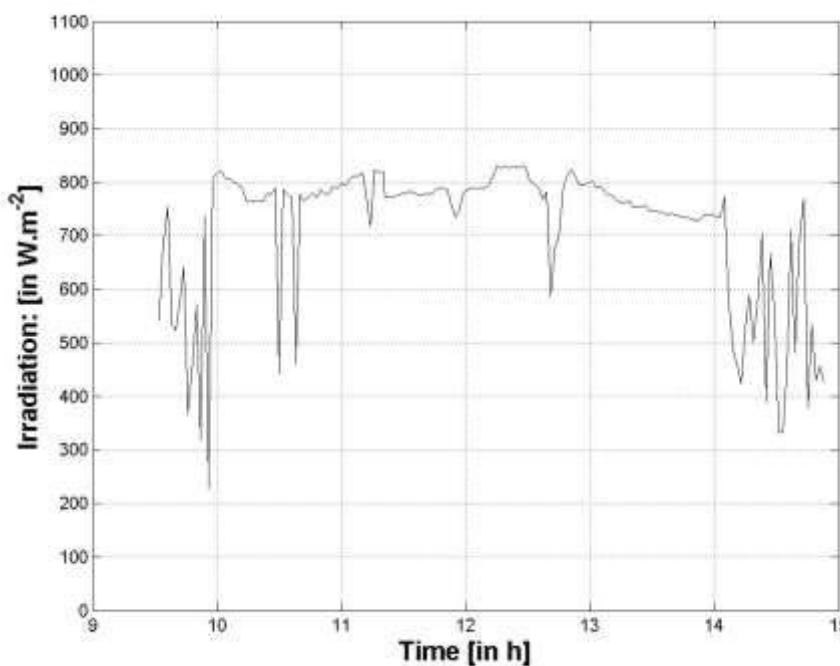


Fig.17: Irradiation curve on June 06, 2016.

Temperatures above 500°C are already reached around 9.30.a.m. and are also kept till 2.10.p.m, which allow us to state that if the absorber was perfectly aligned with the declination plan, temperatures well above 500°C will be maintained from 9.30 a.m. to 2.10 p.m.

Temperatures inside the absorber, considering maximum reached by probes C and D, are ranged between 97°C and 252°C. To some points, these temperatures could have been improved if the reservoir's North and South sides were better prepared to limit heat losses.

IV. CONCLUSION

We have made an optical analysis of a hemispherical concentrator, showing how the local concentration evolves along an axis absorber which is conical. A global geometric concentration curve had been also drawn for comparison with geometric mean concentration.

From this analysis, we notice that the geometric concentration of a hemispherical concentrator is always higher than that of a parabolic trough, telling us that the hemispheric system gives higher temperature than parabolic trough. Moreover, the hemispherical concentrator could do better if it is used with mixed conical and cavity (or plate) absorber with respect to the projection angles of the sunlightsizing the cavity.

From the prototype, high temperatures could be obtained with a hemispherical concentrator: 686°C maximum at the focal lip, and 252°C maximum for the air inside the absorber reservoir. This is still less than what was obtained by the Crosbyton courtesy in Texas-USA (540°C of steam generated by an only conical absorber), but suggests higher potentialities of hemispherical concentrators, which additionally show possibility of use with much reduced tracking system and less vulnerability to bad weather.

REFERENCES

- [1] Munir, A., Hensel, O. and Scheffler, W., 2010. Design principle and calculations of a Scheffler fixed focus concentrator for medium temperature applications. *Solar Energy* 84: 1490-1502.
- [2] Mahdi, K., Bellel, N., Development of a spherical solar collector with a cylindrical receiver. *Energy Procedia* 52 (2014) 438-448.
- [3] Ky, Thierry. S. M., Kam, Sié., Dianda, Boureima and Bathiebo, D. Joseph. Optical analysis of a hemispheric concentrator with a manual tracking system for the declination. *Global Journal of Pure and Applied Sciences*. Vol 21, 2015: 145-154.
- [4] M. F. El-Refai. Performance analysis of the stationary-reflector/tracking absorber solar collector. *Applied Energy*, 28 :163–189, 1987.

- [5] K. M. Ng, N. M. Adam, and B. Z. Azmi. Numerical simulation on the reflection characterization and performance of a solar collector - a case study of upm solar bowl. *Science and Technology*, 20 :283–298, 2012.
- [6] Nadia Bouguetaia. Contribution à l'étude et à la simulation d'un concentrateur cylindro-parabolique. Master's thesis, Université Constantine 1 Faculté Des Sciences Exactes, 2013.
- [7] Steward W. G. and Kreith F., Stationary concentrating reflector cum tracking absorber solar energy collector: optical design characteristics. *Applied optics*. Vol 14, No.7, 1975.
- [8] Williams B. Stine, Michael Geyer, and R. W. Harrigan. Solar energy systems design. *Solar Power System*, 1986.
- [9] François Veynandt. Congénération hélio thermodynamique avec concentrateur linéaire de fresnel : modélisation de l'ensemble du procédé. PhD thesis, Institut National Polytechnique de Toulouse (INP Toulouse), 2011.
- [10] R. Bernard, G. Menguy, M. Schwartz. Le rayonnement solaire, Conversion thermique et applications. Editions Tec-Doc, 1980.
- [11] M. Yusof Sulaiman, W. M. Hlaing Oo, Mahdi AbdWahab, Z. Abidin Sulaiman and K. Y. Khouzam. Conceptual design of a hybrid thermal and photovoltaic receiver of a FMDF collector. *Renewable Energy*, Vol. 12, No. 1, pp. 91-98, 1997.

Susceptibility Gene Prediction in Hereditary Disease Retinoblastoma

S. Sumathi¹, Dr. R. Dhaya², Dr. R. Kanthavel³

¹Research Scholar, Velammal Engineering college, Chennai, India

²Associate professor, Rajalakshmi Engineering College, Chennai, India

³Vice Principal, Rajalakshmi, Institute of Technology, Chennai, India

Abstract— Nowadays Bioinformatics, proteomics and Genomics are the most intriguing sciences to understand the human genome and diseases. Several hereditary genetic diseases like Retinoblastoma involve a sequence of complex interactions between multiple biological processes. With this paper, genetic similarities were found within a selected group of patient's DNA sequences through the use of signal processing tools. DNA, RNA and protein sequences have similarities in structure and function of the gene with their location. In this paper, we introduce a novel method using scoring matrix and wavelet windowing, for the integrative gene prediction. The proposed methods not only integrate multiple genomic data but can be used to predict gene location, gene mutation and genetic disorder from the multi-block genomic data. The performance was assessed by simulation.

Keywords— Gene, scoring matrix, WWM.

I. INTRODUCTION

Retinoblastoma is a malignant cancer of the increasing retinal cells caused in the majority cases by mutations in both copies of the RB1 gene. The RB1 gene is a tumor suppressor gene, located on the genetic material, chromosome 13q14 and is the first cloned human cancer gene. The gene codes for the tumor suppressor protein pRB, which by binding to the transcription factor E2F, inhibits the cell from entering the S-phase during mitosis. Latest facts about retinoblastoma suggests that post-mitotic cone precursors are uniquely sensitive to pRB depletion and may be the cells in which retinoblastoma originates. The occurrence and viability of retinoblastic cells may be more complex than suggested by simple loss of function of the RB1 alleles. Hereditary retinoblastoma demonstrate close relation of the gene for this cancer with genetic locus for esterase D. Data are presented here in support of the hypothesis that at least one disease, the retinoblastoma observed in children is caused by two mutational events.



Fig.1: Healthy eye



Fig.2: Retinoblastoma affected eye

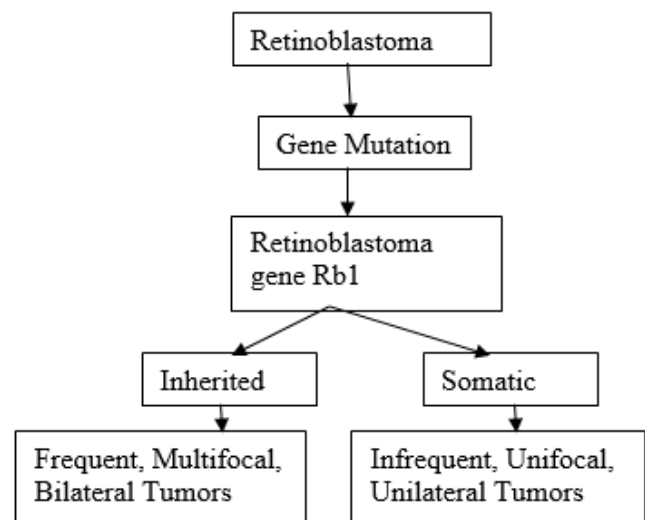


Fig.3: Flow graph of gene mutation in Eye

In 5% of retinoblastoma cases with germline mutations the ancestor history is positive. The risk for developing bilateral and multifocal retinoblastoma is high and the age of inception is around 15 months. The mean number of tumors is about 5 in the two eyes. The offspring of a parent with bilateral retinoblastoma have a 50% probability of developing a tumor and 50% possibility of inheriting the germline mutant allele. Reduced reentrance of 10 to 15% lowers the estimated occurrence of disease from 50% to 25%. Individuals who have mutations in both alleles somatically do not have a mutation in their germ cells and therefore usually transfer no tumor risk to their offspring.

II. DNA SEQUENCE

Deoxyribonucleic acid (DNA) and ribonucleic acid (RNA) are consisting of a nucleobases, a pentose sugar and a phosphate group. DNA nucleobases are Cytosine (C), Guanine (G), Adenine (A) and Thymine (T) and RNA nucleobases are Cytosine (C), Guanine (G), Adenine (A) and Uracil (U)^[1]. In recent years huge databases available for genetic information as open source which lead to a huge progress in bioinformatics; if a genetic sequences are known then this information could be a very important in early disease diagnosis, drug discovery for it.^[2] It leads to Biological sequence alignment a field of Bioinformatics and Computational Biology. It's aim analyzing similarities between DNA, RNA or protein sequences, to predict the genetic relationship between organisms and structural or functional relationships.

Each segment in DNA is called a gene. Genes control the protein synthesis and regulate most of the activities inside a living organism. All the genetic information is copied when a cell divides. When a change occurs in the base sequence of a DNA strand, it is called a mutation. These mutations can lead to diseases or the death of a cell.

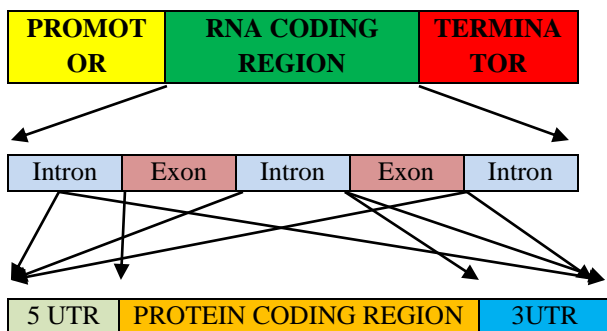


Fig.4: Gene structure

The numerical representation of DNA sequences becomes very essential as almost all DSP techniques require two parts: mapping the symbolic sequence into a numeric and calculating a kind of transform of the resultant numeric series [2]. Most of the numerical representations associate one numerical value to one position in the sequence using numerical values related to each nucleotide and, finally, reveal the existence or the nonexistence of a certain nucleotide in a specific position [3]. Another approach could be to include information about the number and type of repeated nucleotides to generate only one numerical value for each DNA subsequence which may be associated with a recur. This representation needs a mapping algorithm which use distances to determine similar subsequences and then evaluate a consensus sequence for these subsequences to generate candidates.

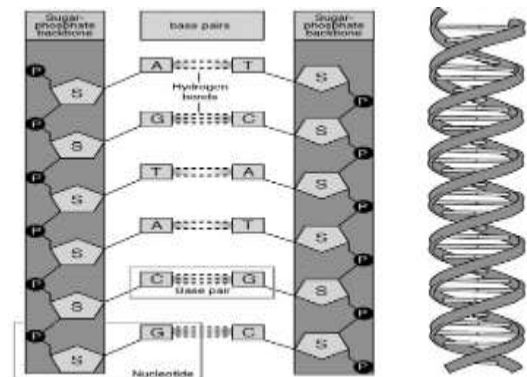


Fig.5: DNA Helical Structure

III. GENE PREDICTION

Gene Prediction refers to detect the locations of the protein-coding regions of genes in a lengthy DNA sequence. Signal processing techniques offer a huge guarantee in analyzing genomic data because of its digital nature. Signal processing analysis of bio-molecular sequences is stalled by their representation as strings of alphabet characters.

Table.1: Genetic code

	T(U)	C	A	G
T(U)	TTT Phe (F)	TCT Ser (S)	TAT Tyr (Y)	TGT Cys (C)
	TTC Phe	TCC Ser	TAC Tyr	TGC Cys
	TTA Leu (L)	TCA Ser	TAA Ter	TGA Ter
	TTG Leu	TCG Ser	TAG Ter	TGG Trp (W)
C	CTT Leu (L)	CCT Pro (P)	CAT His (H)	CGT Arg (R)
	CTC Leu	CCC Pro	CAC His	CGC Arg
	CTA Leu	CCA Pro	CAA Gln (Q)	CGA Arg
	CTG Leu	CCG Pro	CAG Gln	CGG Arg
A	ATT Ile (I)	ACT Thr (T)	AAT Asn (N)	AGT Ser (S)
	ATC Ile	ACC Thr	AAC Asn	AGC Ser
	ATA Ile	ACA Thr	AAA Lys (K)	AGA Arg (R)
	ATG Met (M)	ACG Thr	AAG Lys	AGG Arg
G	GTT Val (V)	GCT Ala (A)	GAT Asp (D)	GGT Gly (G)
	GTC Val	GCC Ala	GAU Asp	GGC Gly
	GTA Val	GCA Ala	GAA Glu (E)	GGA Gly
	GTG Val	GCG Ala	GAG Glu	GGG Gly

IV. NUMERICAL REPRESENTATION

The arithmetical depiction of a DNA sequence is given as a chain of integers derived from a unique graphical representation of the regular hereditary code. This numerical representation is appropriate for the quantitative analysis of the sequences.

4.1 LD matrix

LD matrix is used to calculate linkage disequilibrium values. "composite" for LD composite measure, "r" for R coefficient (by EM algorithm), "dprime" for D', and "corr" for correlation coefficient. The method "corr" is equivalent to "composite", when SNP genotypes are coded as: 0 – BB, 1 – AB, 2 – AA. Matrix elements adjacent to the main diagonal represent the extent of the line segments producing the line.

4.2 Transition matrix

Transition matrix is used for transitions from one kind of base to another. For a given DNA sequence 's' it can construct a 4x4 matrix $A = (t_{ij})$, where t_{ij} means the number of times a given base being succeeded by another in the sequence. A is called the transition frequency matrix of s. We can construct a matrix $P = (P_{ij})$ by dividing each element by the total of all entries in A. Such a matrix represents the relative frequency of all the possible types of transitions, and is called the transition proportion matrix of s. The initial mapping of DNA to binary which represents DNA with four binary indicator sequences showing the presence '1' and absence '0' of the relevant nucleotides at locations 'n'.

4.3 Complex representation

The complex representation is based on the assumption that coefficients of the four 3-D tetrahedron vectors representing each DNA letter are either +1 or -1. The dimensionality of the resultant bipolar representation can be condensed to two.

V. DSP TECHNIQUES

A. DFT

Fourier transform is used to detect the likely coding regions in DNA sequences, by computing the amplitude profile of this spectral component which is a sharp peak at frequency $f = 1/3$ in the power spectrum. The strength of the peak depends obviously on the repetition of gene. This gives relatively good results but it is dependent on DNA sequence and thus requires computation before processing of the mapping scheme for gene prediction. The DNA sequence to be generated from a white random process through an all

pole system and thus used Auto-Regressive modeling to replace Fourier analysis for exon prediction.

B. STFT

In non-stationary signals, The Short Time Fourier Transform (STFT) is an algorithm frequently used for the DFT-based spectral analysis. In the STFT, the time signal is divided into short segments and a DFT is calculated for each one of these segments. Spectrogram, a three dimensional graph called is obtained by plotting the squared magnitude of the DFT coefficients as a function of time.

C. DWT

The Discrete Wavelet Transform is a mathematical tool that can be used very effectively for non-stationary signal analysis. The DWT, for which an algorithm called Fast Wavelet Transforms (FWT) allows a very efficient calculation. Methods based on a modified Gabor-wavelet transform (MGWT) for the identification of protein coding regions also exists.

VI. WAVELET WINDOW METHOD

A Wavelet Transform Modulus Maxima (WTMM) is defined as a point (x_0, t_0) such that

$$|W_{x_0, t}| \leq |W_{x_0, t_0}|$$

when t belongs to either a right or the left neighbourhood of t_0 , and

$$|W_{x_0, t}| \leq |W_{x_0, t_0}|$$

when t belongs to the other side of the neighbourhood of t_0 . We describe maxima line, any connected curve in the scale space (x, t) along which all points are WTMM.

VII. RESULTS AND DISCUSSIONS

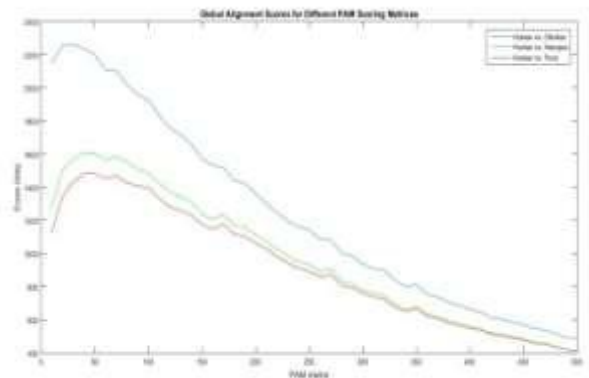


Fig.1: Best of DNA seq

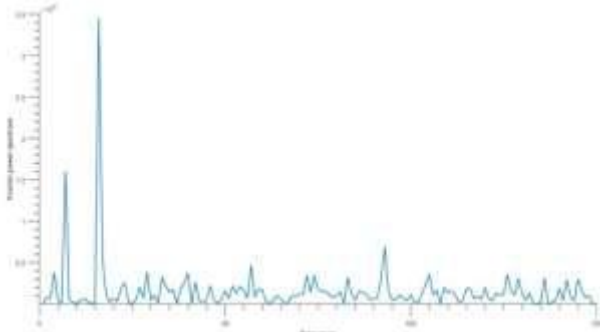


Fig.2: Fourier spectrum of DNA sequence

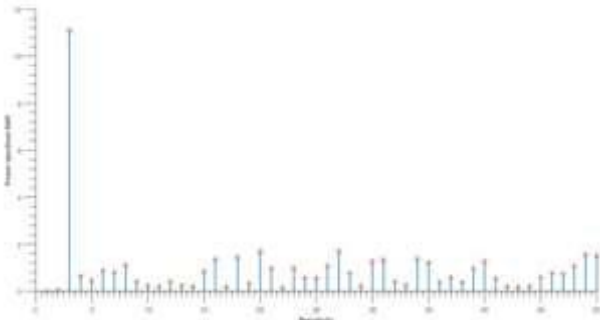


Fig.3: Power spectrum SNR of DNA sequence using WWM

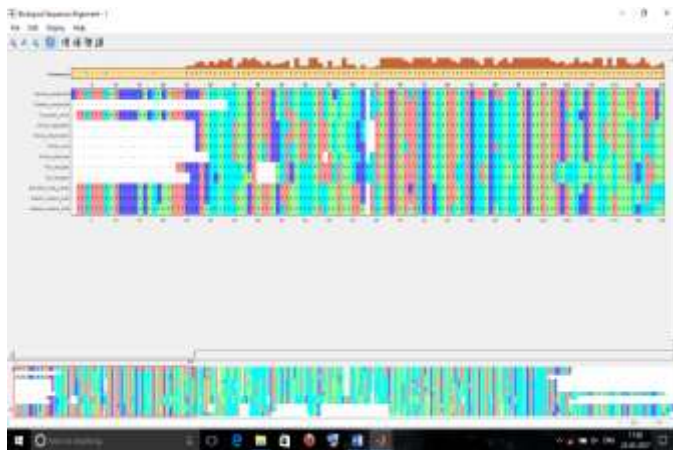


Fig.4: Spectrum analysis of normal and abnormal DNA sequence

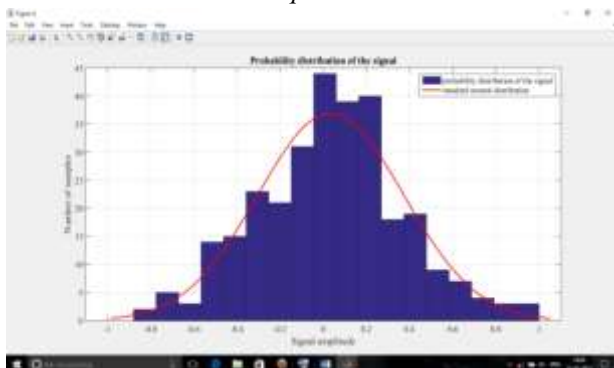


Fig.5: PDF of given sequence

VIII. CONCLUSION

In this work, a new analyzing wavelet window and scoring matrix method for the prediction of protein coding regions has been proposed. The wavelet window method can be applied to predict different coding regions of different lengths. The selection of the value of the window length has always been a problem in DSP based methods as it has an effect on the gene prediction. Future work can focus on integrating this technique to refine the predicted location of gene and protein coding regions.

REFERENCES

- [1] Asmaa G.Seliem, Wael Abou El-Wafa, etl., Parallel Smith-Waterman algorithm hardware implementation for ancestors and offspring gene tracer
- [2] Lim KG, Kwok CK, Hsu LY, Wirawan A., "Review of tandem repeat search tools: a systematic approach to evaluating algorithmic performance", Brief Bioinformatics, 2012, vol. 14, no. 1, pp:67-81.
- [3] Lorenzo-Ginori, J.V., Rodriguez-Fuentes, A., Abalo, R.G., Rodrigues, R.S., "Digital signal processing in the analysis of genomic sequences", Curr. Bioinformatics, 2009, 4, pp:28-40.
- [4] Pop, P.G., Voinea, A., "Representations Involved in DNA Repeats Detection Using Spectral Analysis", Studies in Informatics and Control, 2011, vol. 20, no. 2, pp:163-180.
- [5] V.I. Levenshtein, "Binary codes capable of correcting deletions, insertions, and reversals", Soviet Physics Doklady, 1966, 10, pp:707-10.
- [6] Deza, M.M., Deza E., Encyclopedia of Distances, Springer, 2009.
- [7] NCBI at <http://www.ncbi.nlm.nih.gov/genban/>
- [8] Alkan C, Ventura M, Archidiacono N, Rocchi M, Sahinalp SC, Eichler EE., "Organization and evolution of primate centromeric DNA from whole-genome shotgun sequence data", PLoS Comput Biol. 2007, Sep; 3(9), pp:1807-18.
- [9] D. Anastassiou, "Genomic signal processing," IEEE Signal Processing Mag., vol. 18, pp. 8–20, 2001.
- [10] D. Cohen, I. Chumakov, and J. Weissenbach. A first-generation physical map of the human genome. Nature, 698–701, Dec 1993.
- [11] T. Lengauer, editor. Bioinformatics - From Genome to Drugs, volume II: Applications of Methods and Principles in Medicinal Chemistry. Wiley-VCH Verlag, Weinheim, 2002.

- [12] K. Usdin The biological effects of simple tandem repeats: lessons from the repeat expansion diseases. *Genome Res*;18:1011–9, 2008.
- [13] F. Glutamine, repeats and neurodegenerative diseases: molecular aspects. *Trends in biochemical sciences*, 24(2), 58-63, 1999.
- [14] V. R. Chechetkin and A. Y. Turygin, “Search of hidden periodicities in DNA sequences,” *J. Theoretical Biol.*, vol. 175, pp. 477---497, 1995.
- [15] M. Buchner and S. Janjarasjitt, “Detection and visualization of tandem repeats in DNA sequences,” *IEEE Trans. Signal Process.*, vol. 51, no. 9, pp. 2280–2287, Sep. 2003.
- [16] D. Sussillo, A. Kundaje, and D. Anastassiou, “Spectrogram analysis of genomes,” *EURASIP J. Appl. Signal Process.*, vol. 2004, no. 1, pp. 29–42, 2004.
- [17] Zhou Zhi-min, Chen Zhong-wen, “Dynamic Programming for Protein Sequence Alignment”, *International Journal of Bio-Science and Bio-Technology*, Vol. 5, No. 2, pp. 141–150, April, 2013.
- [18] S. S. Ray, S. Ghosh, and R. Prasad, “Low-cost hierarchical memorybased pipelined architecture for DNA sequence matching”, *IEEE INDICON 2014*, pp. 1–6, 11-13 Dec. 2014.
- [19] S. Ghosh, S. Mandal and S. Saha Ray, “A scalable high-throughput pipeline architecture for DNA sequence alignment”, *IEEE TENCON 2015 IEEE Region 10 Conference*, Macao, pp. 1–6, Nov. 2015.
- [20] P. K Lala and J. Parkerson, “A CAM (Content Addressable Memory)- based architecture for molecular sequence matching”, *International Conference on Bioinformatics and Computational Biology*, Las Vegas, July 18–21, 2011.

Development of Automated Room Security System

Saksham Rastogi^{1*}, Rahul Das², Kriti³

Department of Electronics & Instrumentation, Galgotias College of Engg. & Tech, Greater Noida, Uttar Pradesh, India

Abstract—The work on “Development of automated room security system” using Microcontroller is a reliable circuit that takes over the task of security of a room very accurately. When somebody enters into the room then the count will be incremented by one and the set limit is checked, if the count is less than the set limit then the door opens and the person is granted access. When any one leaves the room then count will be decremented by one. If the total count exceeds the set limit then the buzzer is sound and the image of the person trying to enter the room is captured via a camera. The microcontroller does the above job. It receives the signals from the sensors, and this signal is operated under the control of software which is stored in ROM. 89s51 Microcontroller continuously monitor the sensors, an IR Sensor sends signal to the microcontroller, to increment or decrement the count accordingly. The system includes IR sensor, microcontroller, LCD, display, buzzer, camera and a 12v power is supplied to run the system. The system uses a compact circuitry built around 89s51 microcontroller programs are developed in Embedded C.

Keywords—89s51 microcontroller, Infrared sensors (IR sensors), LCD display, Embedded C.

I. INTRODUCTION

Concept of this project is very useful in all modern classrooms, auditorium, where we want to restrict the number of person to enter in the room. Just insert the maximum count and leave all the work for smart microcontroller system.

Microcontroller system not only display the total person in the room but also the maximum limit. As the limit is over connected door is closed and buzzer turns on for a time when any person tries to enters in the room. Add on feature of this project is to show the image of the person entering the room via a camera. Moreover there will be an automatic light detecting sensor as whenever a person is inside the room the lights and fan would be switched on automatically. There will be additional fire detector in order to detect fire for safety reasons. Logic behind this project is to count the total person entering and exiting from the room with the help of the infra-red interruption sensor. In this project we use 89s51 controller with one 2by 16 lcd and wire CCTV camera.

II. PROPOSED DESIGN

In this system, the traffic or agents or human follow a certain route or door or some threshold to enter into and to exit from the place. While entering to the system, there are two sensors are installed which are connected with each other via infra red network. While a visitor crosses the infrared bar or line, it is disconnected and at that time microcontroller increases its count by one. The count is shown on the lcd. When someone crosses the bar in opposite direction, the infrared line is again interrupted and then microcontroller decreases its count by one to signify that one visitor is entered and one is get away from the place.

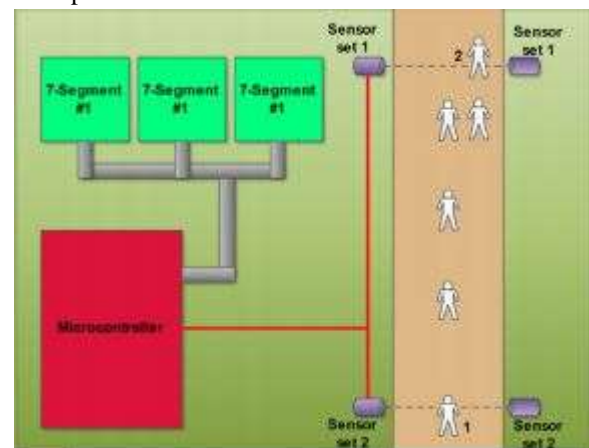


Fig.1: Block diagram of Bidirectional Visitor Counter

In the above figure, the person at place 1, first crosses the infrared line and when crosses, it breaks. The count is then shown on 7-Segment display like follows:



Fig.2: Count Increment

When person at place 2, crosses the infrared network or when the first person goes and breaks it, the count is decreased by one and the output is shown below:



Fig.3: Count Decrement

After the increment decrement of the counter there is automated light control system using IR Sensor and microcontroller .This system is designed by using two sets of IR transmitter and receiver. As the microcontroller receives the output from the IR sensor, the current value of the persons inside the room gets altered, and accordingly if the current value of the persons inside the room is greater than 0 then the lights and fan are turned on else the lights and fan are switched off.

An additional feature to ensure safety along with the security fire detector system is used .Here we use a thermistor, whose resistance is dependent on the temperature. The thermistor is connected to a voltage comparator, in case of fire the resistance of the thermistor decreases and the output of the voltage comparator goes active low. The microcontroller on receiving an active low signal from the comparator , activates the alarm and the door is opened.



Fig.4: Thermistor

III. BLOCK DIAGRAM

The following figure shows the block diagram for automated room security system, thereby giving a vivid sequence of the hardware parts connected.

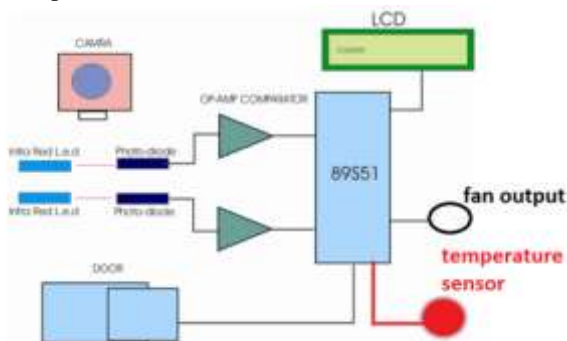


Fig.4: Block Diagram

IV. SOFTWARE IMPEMENTATION

For software realization in this research work, software named Keil is used. μ Vision4 incorporated improvement atmosphere that summarized a development supervisor, built capability, device design, editor and a grateful debugger. μ Vision4 is used to write down and assemble the programs via the apparatus. It could move the assembly language as well as C code into the hex file. . Keil software consists of the following: Linker Control File – It is a text file that μ Vision surpasses to the linker. The control file consists of all information, names of object files and library files to comprise in the output file. Map File – The map file is a listing file created by the linker. Project Target – In an assignment, a target is an executable program that is generated. A project may create an aim that runs on an 8051 family. Plans might be produced to build with no optimization and to make with entire optimization. Source File Group – In a scheme, a group is a number of source files that compose the project target. Although we may individually specify the toolset options for a file, a group lets us to apply the same options to a group of source files. The choice for a set might be various since the choice for the aim. Toolsets – A toolset consist of an assembler, compiler, linker, HEX converter, debugger and the other related tools for a picky device family like the 8051. Every tool or program in a toolset is dedicated to build mark code for a detailed family of chips. To guesstimate the software for correct method, the case was planned hooked on the microcontroller on the significant maturity board. Encoding of the microcontroller is accomplished via the Universal Programmer. It is a handy serial programmer. These accede to hexadecimal files to be burdened into the microcontroller. Mainly the microcontroller is planned by exterminating it since the hole on the board and bringing in it into the multi-pin hole on the programmer. Microcontroller next to with it's an assortment of edges rivet software to work on.



Fig.5: Flowchart

V. CIRCUIT DIAGRAM

The below shows the circuit diagram of the proposed system.

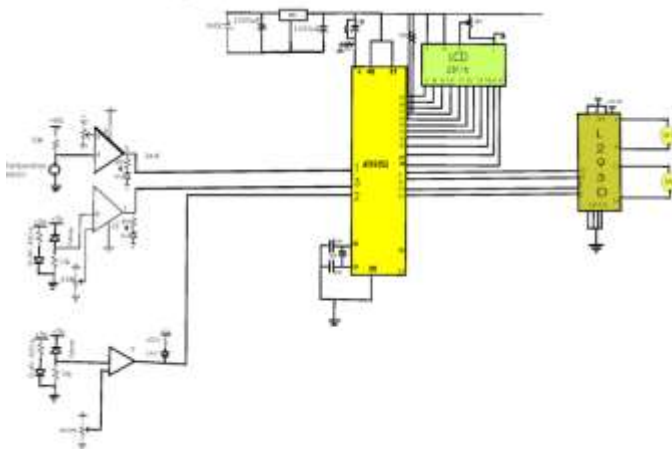


Fig.6: Circuit Diagram

The following are the hardware requirements:

1) **Microcontroller:** The AT89S52 is a low-power, high-performance CMOS 8-bit microcontroller with 8KBytes of in-system programmable Flash memory. The appliance is feigned using Atmel's high-density non-volatile memory skill and is companionable with the industry-standard 80C51

training set and pin out. The on-chip flare permits the program memory to be reprogrammed in-system or by a conventional non-volatile memory programmer. By combining a versatile 8-bit CPU with in-system programmable Flash on a monolithic chip, the Atmel AT89S52 is a powerful microcontroller which provides a highly-flexible and cost-effective solution to many embedded control applications. The AT89S52 provides the following standard features: 8K bytes of flash, 256 bytes of RAM, 32 I/O lines, Watchdog timer, two data pointers, three 16-bit timer/counters, a Six-vector two-level interrupt architecture, a full duplex serial port, on-chip oscillator, Down to zero frequency and supports two software selectable power saving modes: Low-power Idle and Power down Modes.



Fig.7: Microcontroller

2) **IR Sensor:** It is the device which is utilized to detect the nearness, nonappearance, separation of the protest or intrusion. There are two sections the IR photoelectric sensor named light transmitter and photoelectric receiver. IR sensor detects the question by utilizing infrared beams between light transmitter and photoelectric receiver. These sensors as 'non-normal eyes' are natural to the computerization innovation. These sensors are mounted in side design in the project. The working guideline of the utilized sensor is that when the beam transmitted by the producer is blocked or mostly reflected by the object, the bar recipient whereby makes a judgments and responds.



Fig.8: IR LED (Tx & Rx)

VI. WORKING OT THE PROJECT

Automated room security system is basically an automated movable barrier which is installed at the entry of an authorized room where unauthentic entry are restricted. The project is basically made with the help of AT89s52 microcontroller .In this gear mechanism is used followed by L293D motor driver and dc gear motor of 60rpmare used to

provide ease of opening as well as closing the door. In order to sense the presence of person bidirectional infrared sensor are used followed by the counter in order to count the presence of people inside the room and display the same with the help of LCD installed in the project. This system works on the principle of breaking an infrared beam of light, sensed by a photodiode. It consists of two transmitting infrared diodes and two receiving photodiodes. The first one is when someone coming in and the second one is used someone going out of the room. The photodiodes are connected to comparators, which give a lower output as soon as the beam is broken and high output when they are transmitting normally. Along with security optimum energy usage has also being done with the help of IR sensors counter. As light and fan will automatically start working as soon as it will sense any presence and will automatically switch off if no presence will be detected. Apart from this Thermistor NTC103 has being used for fire safety purpose, as soon as it will detect heat the automated door will open for easy and fast evacuation and a buzzer of 3v is switched on used for awareness purpose. To monitor the whole ongoing process a CCTV has also being used for surveillance thus ensuring more security.

VII. CONCLUSION

The framework proposed in this paper is presently under research for the improvement in future understanding. The most vital parts of the framework are the remote numbering and the forefront security. These two elements makes the framework idealize, also the cost will low as no expensive parts are utilized for the development of the framework.

VIII. FUTURE SCOPE

Keeping in mind the end goal to expand the security of this proposed mechanized room security framework the remote camera with GSM framework could be joined in which the unapproved people data would straightforwardly be send to the worry division ,subsequently expanding greater security.

REFERENCES

- [1] Ciubotaru-Petrescu, B., Chiciudean, D., Cioarga, R., & Stanescu, D. (2006), "Wireless Solutions for Telemetry in Civil Equipment and Infrastructure Monitoring", 3rd Romanian-Hungarian Joint Symposium on Applied Computational Intelligence (SACI) May 25-26, 2006.
- [2] Kalpakjian (2008), "Automation in Manufacturing. Manufacturing processes for Engineering Materials", 5th Ed.,

PearsonEducationhttp://nd.edu/~manufact/MPEM%20pdf_files/Ch14.pdf

- [3] Potamitis, I., Georgila, K., Fakotakis, N., & Kokkinakis, G. (2003), "An integrated system for smart-home control of appliances based on remote speech interaction", EUROSPEECH 2003, 8th European Conference on Speech Communication and Technology, Geneva, Switzerland, Sept. 1-4, 2003, pp. 2197-2200.
- [4] Zungeru, A.M. et al., (2012). Design and Implementation of a Low Cost Digital Bus Passenger Counter. Innovative Systems Design and Engineering, 3(4), pp. 29-41.

Advanced Image Processing Technique for Failure Analysis

Smt.Maya.V. Lakha¹, Dr.S.P.RajaManohar², Dr. K. ChennaKeshava Reddy³, Dr .Abdul Sattar⁴

¹Research Scholar, ECE dept. Jawaharlal Nehru Technological University Hyderabad, T.S. India.

²Supervisor, ECE dept. Jawaharlal Nehru Technological University Hyderabad, T.S., India.

³Co- Supervisor, ECE dept. Jawaharlal Nehru Technological University Hyderabad, T.S. India.

⁴ECE dept., Royal Institute of Technology, Chevella, Hyderabad, T.S. India.

Abstract—Failure patterns of mechanical components and materials can be observed by surface deformations. Preventive maintenance always minimizes the failure patterns and here is a method proposed which not only minimizes the failures but also analyses the life expectancy of such components and materials. Image processing using Matlab Tool Boxes is emerging as a perfect simulation platform and by writing simple codes one can see its effect which can be analyzed by ease. The paper proposes a robust image processing technique and is developed on Matlab platform.

Keywords—Light Interferometer, Non-Destructive Techniques, Optical NDT, Surface Deformation, SVD.

I. INTRODUCTION

Failure analysis is thought to be finite elemental analysis as far as mechanical components and materials are considered. Added to it is non-destructive technique which ways back to 1879 and since then the topics evolved into a necessity in industry for quality, quantity analysis and valuations. Nondestructive testing (NDT) is the process of inspecting, testing, or evaluating materials, components or assemblies for discontinuities, or differences in characteristics without destroying the serviceability of the part or system.

Today modern nondestructive tests are used in manufacturing, fabrication and in-service inspections to ensure product integrity and reliability, to control manufacturing processes, lower production costs and to maintain a uniform quality level. During construction, NDT is used to ensure the quality of materials and joining processes during the fabrication and erection phases, and in-service NDT inspections are used to ensure that the products in use continue to have the integrity necessary to ensure their usefulness and the safety of the public.

A four step process is usually popular in the field of Structural Health Monitoring and damage detection. The first three steps are connected and involve the detection of the presence, the location and the severity of damage, while the fourth step, related to the prediction of service life is usually a separate problem by itself.

Machine vision systems provide quality control and real-time feedback for industrial processes, overcoming physical limitations and subjective judgment of humans. In this paper, the image processing techniques for developing low-cost machine vision system for surface deformation inspection is explored. By developing image processing techniques, and minimal hardware, a low-cost flexible system is developed. The system acquires the image data and this image is processed and then a custom classification system algorithm accepts or rejects the mechanical element or material.

II. METHODOLOGICAL SURVEY

Non-Destructive Testing (NDT) [1] is defined as the determination of the physical condition of an object without affecting that object's ability to fulfill its intended function. Non-destructive testing techniques typically use a probing energy form to determine material properties or to indicate the presence of material discontinuities (surface, internal or concealed). The methods and techniques used in NDT measure physical properties or non-uniformity in physical properties of materials as well. Variations or non-uniformities in physical properties may or may not affect the usefulness of a material, depending upon the particular application under consideration. Nondestructive testing is the testing of materials, for surface or internal flaws or metallurgical condition, without interfering in any way with the integrity of the material or its suitability for service. The technique can be applied on a sampling basis for individual

investigation or may be used for 100% checking of material in a production quality control system. The common NDT methods are:

Visual and optical Testing: Visual inspection is particularly effective detecting macroscopic flaws.

Ultrasonic Testing: This technique is used for the detection of internal and surface (particularly distant surface) defects in sound conducting materials. The principle is similar to echo sounding.

Electromagnetic Testing: The main applications of the eddy current technique are for the detection of surface or subsurface flaws.

Thermographic Testing: Infrared Thermography is the science of measuring and mapping surface temperatures.

Radiographic Testing: radiography provides a permanent reference for the internal soundness of the object.

Liquid Penetration Testing: LPI is used to detect casting, forging and welding surface defects such as hairline cracks, surface porosity, leaks in new products, and fatigue cracks on in-service components.

Magnetic particle Testing: This method is suitable for the detection of surface and near surface discontinuities in magnetic material, mainly ferrite steel and iron.

Acoustic Emission testing: Used to measure small surface displacement of a material produced due to stress waves generated when the energy in a material or on its surface is released rapidly.

Magnetic Resonance Imaging Testing: medical imaging technique used in radiology to visualize internal structures of the body in detail.

Near-Infrared Spectroscopy: it is very useful in probing bulk material with little or no sample preparation.

Optical Microscope Testing: Purely digital microscopes are now available which use a CCD camera to examine a sample, showing the resulting image directly on a computer screen without the need for eyepieces.

The use of statistical pattern recognition dates from 1950s and, although it is not one of the main topics of image processing research, it provides an important background - especially in the area of automated visual inspection where decisions about the adequacy of the products have to be made constantly [2]. On the other hand, real industrial applications of texture description and recognition are becoming more and more common [3, 4]

During the last two decades, the improvement in image processing with microcomputers has caused non-contact measurement techniques to become more and more popular in the experimental mechanics community. Some full-field measurement techniques like moiré, interferometry or

photo elasticimetry were known and used beforehand. These techniques suffered however from the non-automatic processing of the fringe patterns they provided, leading to some heavy, boring and unreliable by-hand manipulations before obtaining relevant information in terms of displacement or strain. In the recent past, thanks to the dramatic advances in microcomputer and camera technology, many research groups devoted to optics, experimental mechanics or data processing have been developing suitable techniques based on the use of optical devices, digital cameras, algorithms and software's which automatically process images. These techniques directly provide displacement or strain contours onto specimens under testing. Temperature fields are also available thanks to infrared scanning cameras. Such measurements constitute in fact a new type of tool for researchers in mechanics of solids, which is especially interesting in the field of composite material characterization. Indeed, composites present some features like heterogeneities at different scales which render such full field measurements very attractive [5].

III. PROPOSED METHODOLOGY

One of the most important problems, perhaps the most urgent from the point of view of industry productivity and competitiveness, is automatic inspection. Early detection of defects in the production means lower costs and faster feedback on the production line in order to eliminate the causes of defects, overcomes physical limitations and subjective judgment of humans. In industry, zero defect quality is highly required in competitive markets. So, a very cost effective, high throughput and reliable quality inspection method is important in the industry.

The paper proposes a robust Image processing technique [6-12] wherein the image is acquired, preprocessed, features are extracted and then test images are classified as go or no-go decision based on comparison. The preprocessing step reduces the image to a processing compatible format and the most popular and robust Singular Value Decomposition Algorithm is used to extract the image features. Classification decision is based on the comparison with standard values which are served as thresholds. Near comparison is done by using the Euclidian distance.

The various steps and the block schematics are depicted as below:

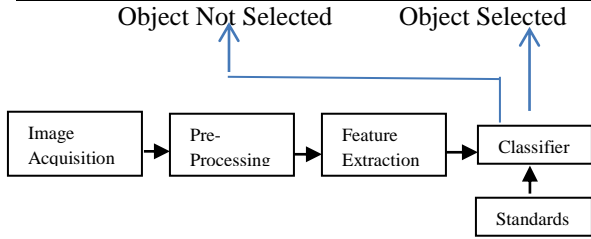


Fig. 1: Proposed system.

To acquire the image either Digital Camera or Phenomenon of Light Interferometer techniques are used. The image is then made processing compatible by reducing the size to 128x128 pixels, the color images are converted into gray and 3D images are converted into 2D image.

The feature Extraction Algorithm runs the Singular Value Decomposition Algorithm and calculates the S, U and V matrices. Comparing the weights of the object under test with the known weights of the standards performs identification. Mathematically, a score is found by calculating the Euclidian norm of the differences between the test and known set of weights, such that a minimum difference between any pair would symbolize the closest match. The classifier gives out select or reject as the output.

IV. ALGORITHM AND SIMULATION RESULT

Singular Value Decomposition (SVD) is statistical tool and found application in digital image processing since it is assumed that every image matrix is having a well-known SVD. It is based upon covariance matrix property to reduce image dimensions. The dimension of the data is reduced by finding a few orthogonal linear combinations of the original variables with the largest variance. The singular value decomposition is an outcome of linear algebra. It plays an interesting, fundamental role in many different applications. One such application is in digital image processing. SVD in digital applications provides a robust method of storing large images as smaller, more manageable square ones. This is accomplished by reproducing the original image with each succeeding nonzero singular value. Furthermore, to reduce storage size even further, images may approximate using fewer singular values [17- 20]

The singular value decomposition of a matrix A of m x n matrix is given in the form,

$$A = U\Sigma V^T \text{ ----- (1)}$$

Where U is an m x m orthogonal matrix; V an n x n orthogonal matrix, and Σ is an m x n matrix containing the singular values of A along its diagonal.

$$\sigma_1 \geq \sigma_2 \geq \dots \geq \sigma_n \geq 0 \text{ ----- (2)}$$

An SVD operation breaks down the matrix A into three separate matrices.

$$\begin{aligned}
 A &= U\Sigma V^T \\
 &= [u_1, \dots, u_n] \begin{bmatrix} \sigma_1 & & & \\ & \dots & & \\ & & \sigma_n & \\ & & & \dots \end{bmatrix} \begin{bmatrix} v_1^T \\ \vdots \\ v_n^T \end{bmatrix} \\
 &= [u_1, \dots, u_n] \begin{bmatrix} \sigma_1 v_1^T \\ \vdots \\ \sigma_n v_n^T \end{bmatrix} \\
 &= \sigma_1 u_1 v_1^T + \dots + \sigma_n u_n v_n^T \\
 &= \sigma_1 u_1 v_1^T + \dots + \sigma_r u_r v_r^T
 \end{aligned}$$

Because

$$\sigma_{r+1} \dots \sigma_n = \text{are equal to zeros.}$$

The center matrix known as the diagonal matrix which can be treated as a defect indicator.

For result simulation let us consider a mechanical object viz., tire with no surface deformation and one with deformation.

Case 1: Tire with no deformation:

Original Query Image



Fig. 2: Tire Image with no deformation

The algorithm classifies the query image as selected and generates its related Singular Values which are in close proximity with the standards

60.962	0	0	0	0	0
0	15.402	0	0	0	0
0	0	7.6051	0	0	0
0	0	0	6.7205	0	0
0	0	0	0	4.2795	0
0	0	0	0	0	4.0941

Fig. 3: Generated singular values for query image 1

Case 2: Tire with Deformation



Original Query Image

Fig. 4: Tire Image with deformation

The figure shows the tire with surface deformation and the SVD algorithm classifies it as not selected and generates its singular values which are far below the standards.

65.503	0	0	0	0	0
0	17.69	0	0	0	0
0	0	9.5787	0	0	0
0	0	0	7.5057	0	0
0	0	0	0	6.7604	0
0	0	0	0	0	4.8269

Fig. 5: Generated singular values for query image 2

V. CONCLUSION

Image processing aspects in this paper and in general are seen as pattern recognition problem. Much of the work on non-destructive techniques particularly in the area of failure analyses of mechanical or for that matter any industrial product is largely based on heavy testing equipment's or methods but, this paper proposes a more reliable and easy process through which one can assess the usefulness of the material or the element under question quickly. Light interferometry or shearography combined with Image processing can be useful for analyzing the mechanical aspects of the material or the elements.

REFERENCES

- [1] Fein, H. (1997), "Holographic Interferometry: Non-destructive tool". The Industrial Physicist, American Institute of Physics.
- [2] E. Davies, Machine vision: theory, algorithms, practicalities. Morgan Kaufmann, 2005.
- [3] M. Egmont-Petersen, D. Ridder, and H. Handels, "Image processing with neural networks - a review", Pattern recognition, vol. 35, pp. 2279-2301, 2002.
- [4] M. Sonka, V. Hlavac, and R. Boyle, "Image Processing, Analysis, and Machine Vision", Brooks/Cole Publ., 1999.
- [5] Michel Gre' diac, "The use of full-field measurement methods in composite material characterization: interest and limitations", Composites: Part A 35 (2004) 751-761, Elsevier.
- [6] Pan, B., Qian, K., Xie, H., Asundi, A. (2009), "Two-dimensional digital image correlation for in-plane displacement and strain measurement: A review. Measurement", Sci. and Tech., 20(6), 1-17.
- [7] Sutton, M.A. (2008), "Digital image correlation for shape and deformation measurements", Handbook of Experimental Solid Mechanics. New York: Springer.
- [8] Sutton, M.A., Orteu, J.J., Schreier, H.W. (2009). DIC, "Image Correlation for Shape, Motion and Deformation Measurements: Basic Concepts, Theory and Applications". New York: Springer, 83.
- [9] Giachetti, A. (2000), "Matching techniques to compute image motion". Image Vis. Comput., 18, 247-260.
- [10] Sutton, M.A., Orteu, J.J., Schreier, H.W. (2009). DIC, "Image Correlation for Shape, Motion and Deformation Measurements: Basic Concepts, Theory and Applications". New York: Springer, 95.
- [11] Chu, T.C., Ranson, W.F., Sutton, M.A., Peters, W.H. (1985), "Applications of digital image correlation techniques to experimental mechanics, Experimental Mechanics, 25(3), 232-244.
- [12] Glover, C., Jones, H. (1994), "Stress, strain and deformation in solids. Conservation Principles of Continuous Media". Texas: McGraw-Hill.
- [13] Guo, X., Liang, J., Xiao, Z.Z., Cao, B.B. (2014), "Digital image correlation for large deformation applied in Ti alloy compression and tension test". Optik, 125(18), 5316-5322.
- [14] Mathworks, Integral Image. (2012). mathworks.com/help/vision/ref/integralimage.html
- [15] McNeill, S.R., Sutton, M.A., Miao, Z., Ma, J. (1997), "Measurement of surface profile using digital image correlation", Experimental Mechanics, 37(1), 13-20.
- [16] K.R. Mak P. Peng and H.Y.K. Lau, "A real time computer vision systems for detecting defects in textile fabrics", IEEE International Conference on Industrial Technology, pp. 469-474, 2005.
- [17] Z. Hong, "Algebraic feature extraction of image for recognition", Pattern Recognition, 24 (1991) 211-219.
- [18] Y. Tian, T. Tan, Y. Wang, Y. Fang, "Do singular values contain adequate information for face recognition", Pattern Recognition 36 (3) (2003) 649-655.
- [19] J. Ye, "Generalized low rank approximation of matrices", in: Int. Confe. on Machine Learning, pp. 2004, pp. 887-894.
- [20] B. Le Roux and H. Rouanet, Geometric Data Analysis. New York: Sp

Electro-synthesized Conjugated Salen Polymer-Glassy Carbon as Hydrochromic Reflective Filter for Humidity Detection: Introduction of Humidity Optical Sensor

Mohammad Mahdi Doroodmand, Sina Owji

Department of Chemistry, College of Sciences, Shiraz University, Shiraz 71454, Iran.

*Corresponding Author: (M. M. Doroodmand) doroodmand@shirazu.ac.ir, Tel: +098-711-6137363, Fax: +098-711-2286008.

Abstract— A novel humidity optical sensor was fabricated based on adsorption of water vapor via the hydrochromic reflective filtration behavior of conjugated Salen polymer, immobilized on the surface of a glassy carbon (GC) electrode by cyclic voltammetry (CV). This process was attributed to the hydrophilic behavior of the electro-synthesized conjugated Salen-based polymer when contacting with water vapors especially during coordination with K^+ through the electro-synthesis process. Optical image of the hydrochromic reflective filter was considered as appropriate detection system for relative humidity (RH) sensing purpose. The mechanism of the change in the color intensity was evaluated via optical filtration of a white laser diode as polychromatic optical source via filtration by the conjugated polymer during its reflection from a smooth surface such as GC. The GC electrode therefore acted as both i) the working electrode during the electrochemical synthesis by CV, and ii) light reflector (mirror) during the light radiation. In this study the electrochemical and optical properties of the GC was compared to a graphite or metal electrode. Parameters such as linearity, rise/fall time, sensitivity, and selectivity of each the fabricated humidity optical sensor were evaluated. Also, dependency of humidity sensor to temperature was investigated. The intensity of the blue component was linearly increased over a wide range of RH between 5 - 80%. The fabricated optical sensor had improved detection limit (0.17% RH), standard saturated limit (>80% RH), accepted relative standard deviation (RSD= 3.6%, n=3), short rise time (~9.5 s compared to the commercial RH sensor), good linearity ($R=0.9971$) and maximum~7.5 % RH hysteresis. Effects of interferences such as H_2 , CO, CO_2 , NO_x , He, and volatile organic compounds (VOCs) were also considered. Results showed no noticeable interfering

effects. This sensor was applicable for selective and reliable detection of %RH in different environmental samples without having any significant interferences.

Keywords— *Electro-synthesis; Conjugated Salen polymer; Hydrochromic reflective filter; Humidity sensor.*

I. INTRODUCTION

Humidity quantity is considered as one of the most important scientific topics in different branches of fields such as food industry, biology, chemistry, medicine, drug delivery, agriculture, automobiles, etc. According to the literature, humidity detection methodology, relative humidity (RH), Dew/Frost point (D/F point) and “parts per million” (ppm) are the most common techniques [1]. RH is defined as the fractional pressure of water vapors in air that implies the saturated vapor pressure. This term is powerfully attributed to the moisture content (absolute humidity), temperature and pressure. The RH value is often adopted while the rate of water evaporation is significant. Dew point is also attributed to the temperature upon which water vapors are concentrated to the water. This term designates the quantity of RH. The higher the relative humidity, the smaller difference is existed between the dew point and the air temperature. The phrase “ppm”, as a new absolute measurement has widespread functions in industry, particularly for the trace moisture detection [2]. Among these units, RH that studied in this work, is commonly used with medium or ambient levels of the humidity. Consequently, powerful, economical, consistent, receptive and specific humidity sensors is very focal subject [3]. During the last decades, different sensing technologies based on change in the intensity of electromagnetic waves [4], or via recording the changes in the electrical properties such as impedance [5], capacity [6], or the frequency of

surface acoustic waves (SAWs) [7], inter-digitated circuit[8], electronic devices such as field effect transistors (FETs) [9-11], quartz crystal microbalance [12-15] and optical detection system [16], have been investigated for humidity detection and determination. However between these ranges of sensing methods, optical sensing has been selected in this study, because of its significant advantages such as improved detection system, fast response time, high sensitivity and its wide linear response [16].

In the fabrication of the optical sensing devices, often conductive polymers are adopted [6]. Briefly conductive polymers as metal conductive materials or semiconductors are selected as organic polymers that conduct electricity. These conductive polymers are fabricated using different chemical or electrochemical methods [3].

Among the introduced synthetic methods for the generation of conductive polymers, electro-synthesis is considered as selective techniques that often lead to have polymer with defined morphology and acceptable purity. Along with the introduced conductive polymers such as polyphenylenes, polypyrenes, polypyrroles, etc. [17], Salen-based polymer is considered as polymer with partial conductivity [18]. Based on the literature, a new electroactive and sometimes conducting polymers based on metal-Salen containing units has been prepared by electro-oxidation of mononuclear transition metals ion complexes and found to exhibit the electrochemical features of the metal system, associated with the reversible oxidation of the ligand [18]. However in spite of the great developments of the optical-based sensors, but to the best of knowledge no reliable humidity-based optical sensors have been introduced. This problem is probably attributed to some major challenges such as limited sensitivity of conductive polymer during interaction with water molecules, high cost of the general optical sensors, etc. To solve these problems hereby in this work, a simple method is introduced for fabrication of humidity sensor using electro-synthetic conductive polymer using Salen molecule.

II. EXPERIMENTAL

2.1. Reagents and Materials

All the chemical reagents were from their analytical grades. Inorganic salts such as KCl, NaCl and LiCl with >99% purity percentage were all from Merck Company. Analytical grades of non-aqueous solvents such as CH₃OH (purity: 99.9 %, GMW= 32.04 g mol⁻¹), C₂H₅OH (purity: 99.5 %, GMW= 46.07 g mol⁻¹), C₃H₈OH (purity: 99.5 %, GMW= 60.1 g mol⁻¹), DMF (purity: 99.8 %, GMW= 73.09 g mol⁻¹), DMSO (purity: 99.9 %, GMW= 78.13 g mol⁻¹),

and acetone (purity: 99.5 %, GMW= 58.08g mol⁻¹) were purchased from Merck company. Deionized water (conductivity: 1 micro-Zimens) was also adopted as water solvent. To synthesize the Salen monomer, salicylaldehyde (Analytical grade, purity: >99 %, GMW= 122.12 g mol⁻¹) and ethylene diamine (Analytical grade, purity: >99 %, GMW= 60.10 g mol⁻¹) were from the Merck company. Also potassium salts of Fe(CN)₆^{3-/4-} were from Merck company. The pH of the electrolyte was controlled using HCl (purity: 32.0 %, w/w, Merck), and NaOH (purity: >99 %, Merck).

2.2. Apparatus

The three-electrode system included GC as working electrode, Ag/AgCl (sat'd Cl⁻) as reference electrode and a Pt rode as counter electrode. The cyclic voltammetry (CV) was performed with a Potentiostat–Galvanostat, μAutolab type III. All the experiments were conducted at 25±2 °C. Also a fluorescence optical microscopy (model: CETI-Magnum T) was adopted for imaging the synthesized thin film polymer. Photographic images from the electrode surface were captured using a digital Camera (model: AGPtek, magnifying ratio: X 800). The morphology of the synthesized polymer was also evaluated using scanning electron microscopy (SEM, KYKY-EM3200). A chamber with 1500 mL volume was made of glass plates that assembled all the components of Humidity sensor system. This system included a reference humidity sensor (Model: Lutron GCH-2018), a glassy carbon (GC) electrode deposited polymer as probe, a thermometer, a tiny fan, an infra-red (IR) source (model: HG-IR1XYJ-F-1W), air input/output ports, and a camera for capturing the surface of the probe. All these components were assembled to a fixed position on the glassy chamber. The chamber was covered by a black coverage to prevent exposing the light in chamber. Required light was supplied for the imaging process by the camera.

2.3. Synthesis of Salen and Salen-Based Polymer

To synthesize the Salen, 200 mL dried ethanol was added to 0.10 mole (GMW= 122.12 g mole⁻¹, V=10.6 mL) of salicylaldehyde and stirred at room temperature according the procedure reported in Ref. [19]. After that 0.05 mole (V= 3.3 mL) ethylenediamine was slowly added. After about several seconds, a yellow precipitation was observed. To complete the reaction, the solution was stirred for ~30 min at room temperature. Then the temperature of the suspension was set to around zero temperature using an ice bath. The precipitation was then separated via filtration

through a paper filter (mesh: 300). The precipitation was then washed using 200 mL cooled ethanol-water (50% V/V) for three times. Finally the precipitation was dried at 50 °C using an oven.

To electro-synthesize the Salen-based polymer, the potential window was set from -1.0 to +2.25 V (vs. Ag/AgCl) at scan rate of 100 mV s⁻¹ on the surface of the GC as working electrode. This process led to have anodic polymerization process during observation of an anodic peak current at potential ~+0.70 V (vs. Ag/AgCl) during formation of complex between polymeric Salen and K⁺. Then during sweeping the potential to a negative potential such as (-1.0 V, vs. Ag/AgCl), three independent anodic peaks were observed at potential of ~ +0.5, +1.25 and +1.75 V (vs. Ag/AgCl), respectively during formation of conjugated Salen-based polymer on the surface of the GC electrode. Then the surface of the electrode was washed with distilled water and dried in air atmosphere. The modified electrode was finally adopted for evaluation of its application for the humidity sensing purpose.

2.4. Apparatus

Fig. 1 shows the schematic of the designed apparatus for humidity detection and measurement. To evaluate the capability of the electro-synthesized Salen-based polymer on the surface of the carbon electrode, a glass cubic cell with volume to around 1500 mL (dimension: 10×10×15 cm) was fabricated. Then the modified GC electrode was introduced from one side of the cell. Also from the opposite, side a white light LED, as well as a digital camera (model: AGPtek, magnifying ratio: X 800) were positioned with angle between 10-20° versus the GC carbon electrode. Also to remove the hysteresis of the GC electrode from any adsorption and diffusion of humidity, an IR light source was positioned next to the GC electrode to eliminate the memory effect. In addition, N₂ gas (purity: 99.995) was selected as solvent during making the humidity standard solutions. To introduce the humidity to the cell, an ultrasonic source was assembled in a glassy box for introduction of transmitted humidified air to the cell. The standard humidity solutions were also standardized using a Ref. humidity sensor (model: Lutron GCH-2018). To prevent arrival of the stray light, the cell was positioned in a dark room via painting the external surface of the glass cell with black color.

2.5. Procedure

Before starting the humidity detection process, the memory effect of the sensors was eliminated via radiation of the

Salen-based electrode system with the IR light for ~0.5 min. Also the space inside the glass cell was cleaned from any water vapor (humidity) via purging N₂ gas as inert gas solvent for ~ 1 min with flow rate of ~2 L min⁻¹. Then the humidifier (humidity generator) was turned on for essential time to introduce water aerosols to the glass cell by the use of N₂ as both gaseous solvent and carrier gas. The standardization of the standard humidity concentrations was achieved using the humidity Ref. sensor. After cooling the Salen-based GC support to the room temperature, the white light (optical source) was turned on and the optical changes in the color was imaged during filtration by the Salen-based GC support along 5 s time interval at ~ 25 °C temperature and ambient pressure as standard temperature and pressure (STP). After saving the optical images in a PC, the images were processed using Photoshop software (version: CC 16.1.2). The schematic of the analysis using the software has been shown in Sc hem. 1. For this purpose combination of the blue or green component of each image was selected as humidity measuring probe.

2.6. Real sample analysis

The reliability of this sensor was evaluated via analyses of different real samples such as the air atmosphere of the urban tunnel, lab air, automobile exhaust air, etc. For this purpose, each sample was accumulated in a plastic balloon (~2 L) using a membrane pump (model: Tornado AC580). After cleaning the glass cell as well as elimination of any probable memory effect from the previous analysis using the procedure reported in the previous section, each sample was introduced to the cell directly with ~1.0 L min⁻¹ flow rate for ~ 1 min time interval and the images were processed according to the recommended procedure.

III. RESULTS AND DISCUSSION

Salen is considered as the family of Schiff bases, derived from ethylenediamine and ortho-phenolic aldehydes (N, N'-ethyleneis(salicylideneiminato) Salen). In these polymers to enhance their electrical conductivity as well as to control their polarity, they are often coordinated with metal ion species such as Al, Ce, Co, Cu, Cr, Fe, Ga, Hg, Mn, Mo, Ni, and V [20]. This relationship often lead to have more conductive polymer, which is suitable for various catalytic purposes such as electro-catalyst in the electrochemical processes [21]. In these complexes, the conductivity is majorly attributed to the metal ion species, compared to the Salen monomer or polymer, which possessed small dielectric constant. In another word, the polarity of the Salen-based complex is promoted during coordination with

metal species [22]. All of these characteristics have made the current Salen-based sensors to be considered as metal-based sensors.

3.1. Electro-synthesis of Salen polymer, successive cyclic voltammetry

The continuous CV of Salen monomer during the electro-synthesis of Salen (0.04M) at potential ranging between -1.0 - +2.25 V and scan rate of 100 mV s⁻¹ has been shown in Fig. 2.A. As shown, observation of a strong peak in the first scan of potential at ~+0.70 V (vs. Ag/AgCl) was related to the anodic electro-synthesis of the Salen polymer. However, during the continuous CV from the second scan, significant decrease was observed in the peak intensity (anodic peak current). As clearly evaluated, the higher the number of cycles, the lower was the anodic peak intensity after the first CV cycle. This phenomenon was related to the non-conductivity of the synthesized Salen polymer. This problem has been considered as serious challenge for fabrication of various electrochemical probes during modification of the working electrode by Salen polymer. However to the best of knowledge from the earliest literature review, all the reports have focused on the use of metal/Salen instead of free Salen monomer [23]. This technique therefore led to have a conductive polymer via evaluation of the redox behavior of coordinated metal ions. But in this study for this first time it has been reported that, continuous CVs lead to have three independent anodic peaks. This observation clearly pointed to the effective role of the proposed procedure for formation of new type of Salen-based polymer using Salen as monomer.

3.2. Effect of solvent

Based on the literature, the electro-synthesis of Salen-based polymer was provided inside organic solvents such as DMF, DMSO, etc. The choice of organic solvent was based on the solubility of metal/Salen complex. In this study from one side, Salen monomer was adopted and from the other side the electrical charge enhanced its solubility inside partially polar solvents such as H₂O, alcohol, acetone, etc. Therefore, in this study it was focused on less toxic and greener solvents. In addition, higher polarity of these solvents simply decreased the ohmic potential of the electrolyte, resulting in the need of less positive electrical potential for the electro-synthesis of the conjugated Salen polymer. Effect of different solvent such as propanol, sulfolane, methanol, dimethyl formamide (DMF), acetone, ethanol, diethylether, 1-butanol, and isobutanol has been evaluated according to the CVs shown in Fig. 2.B. Some

solvents such as diethylether, 1-butanol and isobutanol did not produce a single-phase and transparent solution. Therefore acetone was selected as solvent during the electro-synthetic process.

As shown (Fig. 2.B), significant enhancements were observed in the anodic peak currents during using solvents such as CH₃OH, C₂H₅OH and acetone. More sensitive signals were observed when using acetone in comparison with alcohols. Therefore, acetone was selected as appropriate solvent. Based on the results, maximum sensitivity was evaluated at optimum ratio.

3.3. Effect of pH and ionic strength

Mixture of acetone:water as electrolyte from one side was miscible inside each other and from the other side provided the possibility to control the basicity and the ionic strength of the electrolyte. As explained no Salen-based polymer was generated under the acidic conditions due to the decomposition of the Salen monomer. Therefore, the optimization process was evaluated at different pH values between ~7 to above 13. Fig. 4 shows the CVs during the electro-synthesis using Salen (0.04 M) at 100 mV s⁻¹ scan rate at various pH values using different concentrations of KOH and HCl. Based on the results (Fig. 4), the higher the pH values, the

3.4. Kind and concentration of cation

To evaluate the effect of cations during the polymerization of Salen polymer, the effect of various cations such as K⁺, Na⁺, Li⁺, Ca²⁺, Ba²⁺, Mg²⁺, Al³⁺, etc. were evaluated in detail. Insoluble precipitations were observed during formation of complexes of Salen with Ca²⁺, Ba²⁺, Mg²⁺, Al³⁺, etc. As cations with two or three capacities were insoluble inside the solvent, therefore it was only focused on the cations with one capacity such as K⁺, Na⁺ and Li⁺. Fig. 5 shows the CVs during the electro-polymerization of polymer using Salen (0.04 M) at scan rate of 100 mVs⁻¹ at strong basic condition controlled using the same concentrations of each LiOH, NaOH and KOH under similar conditions. The sequence of sensitivity of the anodic peak currents were as follows: K⁺>Na⁺>Li⁺. Therefore, the higher the diameter of the cations, the more conductive polymer was synthesized. This effect was further evaluated via image processing the Salen polymer-modified GC electrode at an environment with ~40% humidity. Based on the images (Fig. 6), the same correction was observed between the color of the polymer with the atomic spectrum during analysis of K⁺, Na⁺ or Li⁺. Whereas no clear color was observed during narrowing the potential window ranging from -1.0 to 2.25 V (vs. Ag/AgCl). This

observation from one side pointed to the coordination of cations at the negative potentials and from the other side revealed the hydrophilicity of the synthesized Salen-based polymer. In this study due to the availability of KOH, this reagent was selected for controlling the pH of the electrolyte. This effect was again evidenced via addition of different concentrations of KCl. Further concentrations of K^+ were optimized during addition of different concentrations of KCl between 0.00 and 0.05 M as shown according to the CVs in Fig. 7. As shown, although the ionic strength of the electrolyte was high enough during setting the pH higher than ~13, but K^+ had enhancing effect on the sensitivity of the anodic peak current. Concentrations above 0.05 M KCl made a two-phase solution and precipitation. Therefore optimum concentration of KCl was estimated to 0.05 M.

3.5. Characterization of conjugated Salen-based polymer

Fig. 8.A shows the SEM image of the conjugated thin film. Based on the images, the thickness of the film was estimated to be 91 ± 1 nm. Consequently, besides the green nature of water, this effect was considered as another advantageous of the use of water as a fraction of electrolyte. Fig. 8.B shows the FT-IR spectra of the synthesized conjugated Salen-based polymer. However the same behavior was observed during evaluation of the FT-IR spectra of the synthesized Salen-based polymers at two reported scan rates, but observation of an absorption peak at frequency of ~ 1385 cm^{-1} pointed to the C=C bond of the benzene cycle [24], whereas formation of aliphatic C=C bond was evidenced according to the absorption peak positioned at ~ 1442 cm^{-1} , which were in good agreement with the vibrational frequencies estimated for the C=C based on Ref. [24].

Fig. 8.C shows the XPS spectra of free Salen and the electro-synthesized conjugated Salen-based polymer. Based on the XPS spectra of Salen, the sharp peak positioned at 284.8 eV was attributed to the C_{1s} of the C-C bond. Whereas the peak positioned to the 281.2 eV was related to the C_{1s} of the C=C bond. In addition, the C_{1s} of the C-N bond was positioned at ~ 288.3 eV. As clearly shown according to the XPS spectra of the synthesized conjugated Salen-based polymer, the peak related to the C-C bond was completely disappeared. Whereas the peak related to the C=C bond was majorly enhanced. In addition, major decrease was observed in the C-N bond that pointed to the formation of conjugated polymer that acted like a novel molecular wire through the electrochemical process.

3.6. Hydrophilicity of conjugated Salen-based polymer

As explained in detail, the formation of C=C bond in the Salen-based polymer led to have conjugated polymer that behaves as molecular wire. The schematic of the reactions during the formation of conjugated polymer has been shown in the Scheme. 2. In this study, UV-Vis. Spectroscopy was adopted to estimate the ratio of $\text{Metal}^+/\text{Salen}$ during formation of the complex.

According to the results, the ratio of K^+/Salen during formation of coordination compound between K^+ and Salen monomer was estimated to be 5.3: 1. Also the same results were estimated during analysis of other alkali meters such as Na^+ , K^+ and Li^+ . This result pointed to the great capacity of the Salen-based polymer for binding with the alkali species. Therefore, high hydrophobicity was expected for the conjugated Salen-based polymer during the electro-synthesis process. All these results clearly revealed the capability of the fabricated Salen-based polymer for playing role as suitable optical humidity sensor.

3.7. Figures of merit

The trace of the Salen-based optical sensor ranging from 0.0 to 93.0 % RH has been shown in Fig. 9. The same behavior was observed during reversing the humidity trend. Also Fig. 10 shows the linearity of the blue component vs. different %RH values. The results showed good linearity for the blue component (correlation coefficient, $R^2=0.9943$) from 5 to $\sim 80\%$ RH. The rate of the change in the humidity of the chamber was controlled for having enough time to stabilize the response of the sensor during sweeping the humidity. Based on comparison to the reference probe, 90% of maximum response time (t_{90} of reference sensor: ~ 8 s), the response time of the fabricated RH sensor was estimated to be 9.5 s. Also the recovery time of the sensor based on 90% of minimum response (t_{90}) was estimated to be below 10 s. Short rise time (~ 9.5 s) was also estimated for the fabricated optical humidity sensor. The hysteresis during rapid and alternative contacting the optical; RH sensor to 25 and 60 % RH, during at least 4 times was shown in Fig. 11. In this test the white laser was only used for removing the memory effect during each analysis. At this condition the temperature of the electrode surface was estimated to around 50 °C during maximum 60 s time intervals as the recovery time.

As was shown in Fig. 12, the results were compared with those related to the Ref. RH sensor. Minimum difference (less than $\sim 2\%$) was observed between these two RH sensors that revealed the acceptable behavior of the introduced RH sensor during sensing %RH at different

environments. The reproducibility of fabricated humidity sensor is also shown in Fig. 12 at ~20 and ~30 % RH, revealing relative standard deviation (RSD, repeatability) of 3.6 % (n=3) for fabricated optical sensor. Also the RSD% (reproducibility) during analysis of ~25 %RH during at least 4 replicate analyses was estimated to be ~4.0, revealing the acceptable reproducibility of the sensor for RH sensing purposes.

About this optical RH sensor, the stability was also evaluated. Linear stability was observed for the fabricated sensor during providing reverse changes between %RH and temperature ranging between 5.0 – 85% for RH and 15 – 50 °C for the temperature. At a fixed humidity (%RH~25%), there were no interferences by increasing the temperature up to 50 °C. In this study, detection limit was defined as three folds of the standard deviation of blank (dry air) to the calibration sensitivity. More improved detection limit was evaluated for the conjugated Salen-based polymer.

3.8. Interferences

The interference of different gases was investigated at room temperature. For this purpose, the humidity sensor was placed in the chamber and high enough value (such as 1000 parts per million) of foreign gases such as CO, CO₂, NO_x, CH₄, Ar, He, and volatile organic compounds (VOCs) as well as vapor of Acids Such as HCl were individually introduced to the cell in the 30.0±0.5% RH as standard RH solution. The results are shown in Fig. 13. No noticeable change in blue component clearly revealed the specificity of the fabricated sensor for reliable humidity sensing purpose. The RH behavior of the fabricated RH sensor has also correlated to the number of Salen layers grown on the surface of GC electrode via different successive (repetitive) CV mode up to ~ 20 sequential CV scans. Based on the results, the smoothest surface as well as maximum sensitivity (optical color changes) was observed only for the 10th layer. Therefore this layer was selected as optimum polymer layer.

Based on the results, acceptable sensitivity (color changes and softness) was observed during coating only 10 sequential polymeric layers of the Salen-based polymer. Therefore it was suggested to select this replicate layers during the fabrication of the RH sensor using the recommended procedure.

3.9. Proposed behavior

Based on the results, the probable behavior of the RH behavior of the fabricated sensor was attributed to the

filtration properties of conjugated Salen-based polymer. The evidences related to this claim are summarized as follows:

- The optical behavior of the sensor was function of some optical factors such as intensity of the light source as well as the radiation and reflection angles and the alignment of the light during the optical detections. Therefore the electro-synthesized Salen-based polymer seemed to be considered as "Hydrochromic Reflective Filter".
- The RH behavior of this sensor was strongly dependent to the smoothness of the surface on which the conjugated Salen-based polymer was grown by the electro-synthesis technique. To approve this effect, the RH responses of the sensor was compared to the graphite (i.d.: 0.2 cm) support under the similar condition. Based on the optical observation, the smooth behavior of the electrode support (GC electrode) was majorly effective on the sensitivity and homogeneity color of the sensor for RH detection. This result was considered as an important evidence for playing role as optical filter.
- The filtration property of the introduced polymer was also evidenced via introducing different %RH environments with gradient of ~5 %RH per second. As shown the color of the polymer was sequentially changed from orange color to violet color.

These results revealed the filtration behavior of the sensor during %RH sensing purposes. However this process could be approved via formation of some humidity perturbations simply by exhaling for several seconds. As clearly shown the filtration properties of the sensor were evidenced during introduction of different %RH values. Probable behavior of the color changing by absorbing the humidity on synthesized polymer could be due to the reflective index shift by change in polymer volume.

IV. CONCLUSIONS

A simple and low cost method has been introduced for fabrication of an optical humidity sensor using conjugated Salen-based polymer. The behavior of each humidity sensor in presence of humidity was studied. It can be concluded that, fabricated humidity sensor had acceptable detection limit (0.17 %), saturated limit (>80 % RH), the least relative standard deviation (RSD=3.0%), short rise time (~9.5 s) also the good enough linearity (R= 0.9971), compared to the RH sensors previously reported in the literature (Table 1). This type of conjugated polymer was adopted as an optical RH sensor. However this sensor partially suffered

form a little hysteresis (maximum ~7.5% RH). All in all, the results prove the capability of all studied samples particularly the Salen-based sensor as humidity sensor.

ACKNOWLEDGEMENT

The authors wish to acknowledge the support of this work to Shiraz University Research Council for kindly supporting this work.

REFERENCES

- [1] Y. Zhang, K. Yu, R. Xu, D. Jiang, L. Luo, Z. Zhu, Quartz crystal microbalance coated with carbon nanotube films used as humidity sensor, *Sens. Actuat. A: Phys.* 120 (2005) 142-146.
- [2] F. Sattarzadeh, M.M. Doroodmand, M.H. Sheikhi, A. Zarifkar, Fabrication of a Humidity Sensor Based on Chemical Vapor Deposition-Synthesized Single-Walled Carbon Nanotubes, *Sci. Adv. Mater.* 5 (2013) 557-565.
- [3] Z. Chen, C. Lu, Humidity sensors: a review of materials and mechanisms, *Sens. Lett.* 3 (2005) 274-295.
- [4] P.R. Somani, A.K. Viswanath, R. Aiyer, S. Radhakrishnan, Charge transfer complex-forming dyes incorporated in solid polymer electrolyte for optical humidity sensing, *Sens. Actuat. B: Chem.* 80 (2001) 141-148.
- [5] K. Zheng, Y. Zhou, L. Gu, X. Mo, G.R. Patzke, G. Chen, Humidity sensors based on Aurivillius type Bi 2 MO 6 (M= W, Mo) oxide films, *Sens. Actuat. B: Chem.* 148 (2010) 240-246.
- [6] Y. Sakai, Y. Sadaoka, M. Matsuguchi, Humidity sensors based on polymer thin films, *Sens. Actuat. B: Chem.* 35 (1996) 85-90.
- [7] M. Penza, G. Cassano, Relative humidity sensing by PVA-coated dual resonator SAW oscillator, *Sens. Actuat. B: Chem.* 68 (2000) 300-306.
- [8] X. Wang, O. Larsson, D. Platt, S. Nordlinder, I. Engquist, M. Berggren, X. Crispin, An all-printed wireless humidity sensor label, *Sens. Actuat. B: Chem.* 166 (2012) 556-561.
- [9] S.P. Lee, K.-J. Park, Humidity sensitive field effect transistors, *Sens. Actuat. B: Chem.* 35 (1996) 80-84.
- [10] A. Star, T.R. Han, V. Joshi, J.R. Stetter, Sensing with Nafion Coated Carbon Nanotube Field-Effect Transistors, *Electroanalysis* 16 (2004) 108-112.
- [11] J. Boyle, K. Jones, The effects of CO, water vapor and surface temperature on the conductivity of a SnO₂ gas sensor, *J. Electron. Mater.* 6 (1977) 717-733.
- [12] M. Neshkova, R. Petrova, V. Petrov, Piezoelectric quartz crystal humidity sensor using chemically modified nitrated polystyrene as water sorbing coating, *Anal. Chim. Acta* 332 (1996) 93-103.
- [13] L.-X. Sun, T. Okada, Simultaneous determination of the concentration of methanol and relative humidity based on a single Nafion (Ag)-coated quartz crystal microbalance, *Anal. Chim. Acta* 421 (2000) 83-92.
- [14] S. Mintova, T. Bein, Nanosized zeolite films for vapor-sensing applications, *Micropor. Mesopor. Mater.* 50 (2001) 159-166.
- [15] H.-W. Chen, R.-J. Wu, K.-H. Chan, Y.-L. Sun, P.-G. Su, The application of CNT/Nafion composite material to low humidity sensing measurement, *Sens. Actuat. B: Chem.* 104 (2005) 80-84.
- [16] T. Yeo, T. Sun, K. Grattan, Fibre-optic sensor technologies for humidity and moisture measurement, *Sens. Actuat. A: Phys.* 144 (2008) 280-295.
- [17] D. Kumar, R. Sharma, Advances in conductive polymers, *Europ. Polymer J.* 34 (1998) 1053-1060.
- [18] P. Capdevielle, M. Maumy, Redox and conducting polymers based on salen-type metal units; electrochemical study and some characteristics, *New J. Chem.* 16 (1992) 697-703.
- [19] H. Diehl, C.C. Hach, J.C. Bailar, Bis (N, N'-Disalicylalethylenediamine)-μ-Aquodnicobalt (II), *Inorganic Synthesis* 3 (2007) 196-201.
- [20] O. Fatibello-Filho, E.R. Dockal, L.H. Marcolino-Junior, M.F. Teixeira, Electrochemical modified electrodes based on metal-salen complexes, *Anal. Lett.* 40 (2007) 1825-1852.
- [21] P.G. Cozzi, Metal-Salen Schiff base complexes in catalysis: practical aspects, *Chem. Soc. Rev.* 33 (2004) 410-421.
- [22] L. Canali, D.C. Sherrington, Utilisation of homogeneous and supported chiral metal (salen) complexes in asymmetric catalysis, *Chem. Soc. Rev.* 28 (1999) 85-93.
- [23] F. Gao, J. Li, F. Kang, Y. Zhang, X. Wang, F. Ye, J. Yang, Preparation and characterization of a poly [Ni (salen)]/multiwalled carbon nanotube composite by in situ electropolymerization as a capacitive material, *Phys. Chem. C* 115 (2011) 11822-11829.
- [24] G. Socrates, *Infrared and Raman Characteristic Group Frequencies: Tables and Charts*, John Wiley & Sons, 2004.
- [25] A. Sun, Z. Li, T. Wei, Y. Li, P. Cui, Highly sensitive humidity sensor at low humidity based on the

- quaternized polypyrrole composite film, *Sens. Actuat. B: Chem.* 142 (2009) 197-203.
- [26] P.-G. Su, C.-P. Wang, Highly sensitive humidity sensor at low humidity based on the quaternized polypyrrole composite, *Flexible humidity sensor based on TiO₂ nanoparticles-polypyrrole-poly-[3-(methacrylamino)propyl] trimethyl ammonium chloride composite materials*, *Sens. Actuat. B: Chem.* 129 (2008) 538-543.
- [27] Y. Li, Y. Chen, C. Zhang, T. Xue, M. Yang, A humidity sensor based on interpenetrating polymer network prepared from poly(dimethylaminoethyl methacrylate) and poly(glycidyl methacrylate), *Sens. Actuat. B: Chem.* 125 (2007) 131-137.
- [28] P.-G. Su, C.-S. Wang, Novel flexible resistive-type humidity sensor, *Sens. Actuat. B: Chem.* 123 (2007) 1071-1076.
- [29] P.-G. Su, C.-L. Uen, In situ copolymerization of copolymer of methyl methacrylate and [3-(methacrylamino)propyl] trimethyl ammonium chloride on an alumina substrate for humidity sensing, *Sens. Actuat. B: Chem.* 107 (2005) 317-322.
- [30] P.-G. Su, L.-N. Huang, Humidity sensors based on TiO₂ nanoparticles/polypyrrole composite thin films, *Sens. Actuat. B: Chem.* 123 (2007) 501-507.
- [31] X. Lv, Y. Li, L. Hong, D. Luo and M. Yang, A highly water-resistive humidity sensor based on silicon-containing polyelectrolytes prepared by one-pot method, *Sens. Actuat. B: Chem.* 124 (2007) 347-351.
- [32] R. Sundaram, Comparative study on micromorphology and humidity sensitive properties of thick film and disc humidity sensors based on semiconducting SnWO₄-SnO₂ composites, *Sens. Actuat. B: Chem.* 124 (2007) 429-436.
- [33] C.-L. Dai, M.-C. Liu, F.-S. Chen, C.-C. Wu, M.-W. Chang, A nanowire WO₃ humidity sensor integrated with micro-heater and inverting amplifier circuit on chip manufactured using CMOS-MEMS technique, *Sens. Actuat. B: Chem.* 123 (2007) 896-901.

LEGEND TO THE FIGURES

Fig. 1. Schematic of the designed apparatus for humidity sensing process.

Fig. 2. CVs related to the electro-synthesis of conjugated Salen-based polymer using A) Salen monomer (0.04 M) in acetone as solvent and B) different solvents at 0.04 M Salen, pH >13, 0.04 M KCl and 100 mVs⁻¹ scan rate.

Fig. 3. Cyclic voltammetry showing the CVs of Salen (0.04 M) during using different ratios of acetone: water as solvent at pH>13, 0.04 KCl and 100 mVs⁻¹ scan rate.

Fig. 4. Cyclic voltammetry showing electro-synthesis using Salen (0.04 M) at 100 mV s⁻¹ scan rate and at different pH values using different concentrations of KOH and HCl.

Fig. 5. Cyclic voltammetry showing the effect of different cationic species (0.20 M) during the electro-synthesis of Salen-based polymer at 100 mVs⁻¹ scan rate and pH >13.

Fig. 6. Photographic image of electrosynthesized Salen-based polymer on the surface of GC electrode during using A) K⁺ and B) Na⁺ (0.04 M) at ~40% humidity.

Fig. 7. Cyclic voltammetry showing the effect of different concentrations of K⁺ on the electro-synthesis of Salen-based polymer at pH >13 and 100 mVs⁻¹ scan rate.

Fig. 8. Characterization of conjugated Salen-based polymer including A) SEM, B) FT-IR spectra and C) XPS spectra.

Fig. 9. Trace of RGB parameter vs. %RH.

Fig. 10. Linearity of blue component vs. different %RH values.

Fig. 11. Diagram representing the hysteresis of the fabricated RH sensor according to blue parameter.

Fig. 12. Reproducibility of fabricated RH sensor during contacting with 20 and 30 % RH.

Fig. 13. Effect of coexisting species on the performance of the Salen-based RH sensor during spiking into a standard %RH (50%).

Schem. 1. Proposed mechanism for the electrosynthesis of the conjugated Salen-based polymer.

Schem. 2. Proposed behavior of the conjugated Salen-based humidity sensor.

BIOGRAPHY OF AUTHORS

Mohammad Mahdi Doroodmand

Department of Chemistry, College of Sciences, Shiraz University, Shiraz 71454, Iran. Associate professor in analytical Chemistry. Experience: Analytical chemistry, Instrumentation Design, Synthesis of nanostructures, Bioelectrochemistry. Email address: doroodmand@shirazu.ac.ir, Tel: +098-713-6137152, Fax: +098-713-6460788.

Sina Owji

Department of Chemistry, College of Sciences, Shiraz University, Shiraz 71454, Iran. M.S. in analytical Chemistry. Experience: Analytical Chemistry, Detection and determination. Email address: s.owji@yahoo.com, Tel: +098-713-6137153, Fax: +098-713-6460788.

Fig. 1

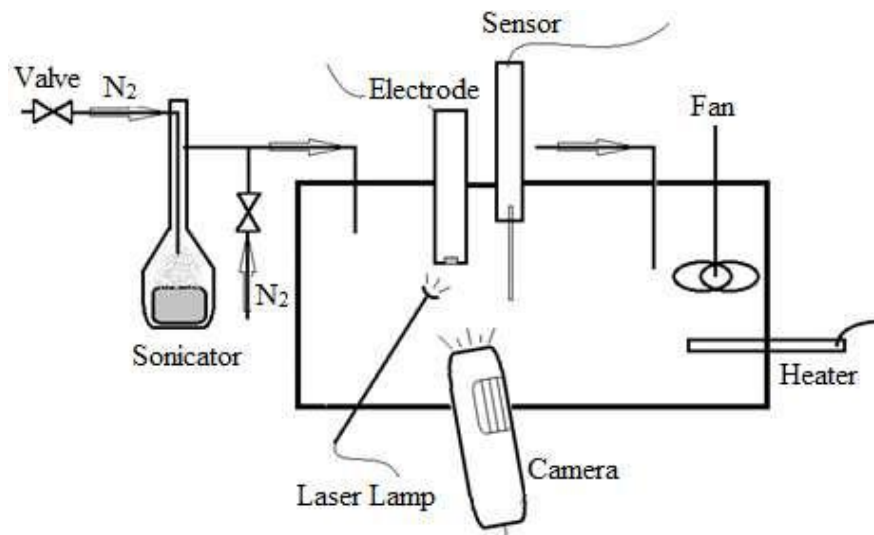


Fig. 2

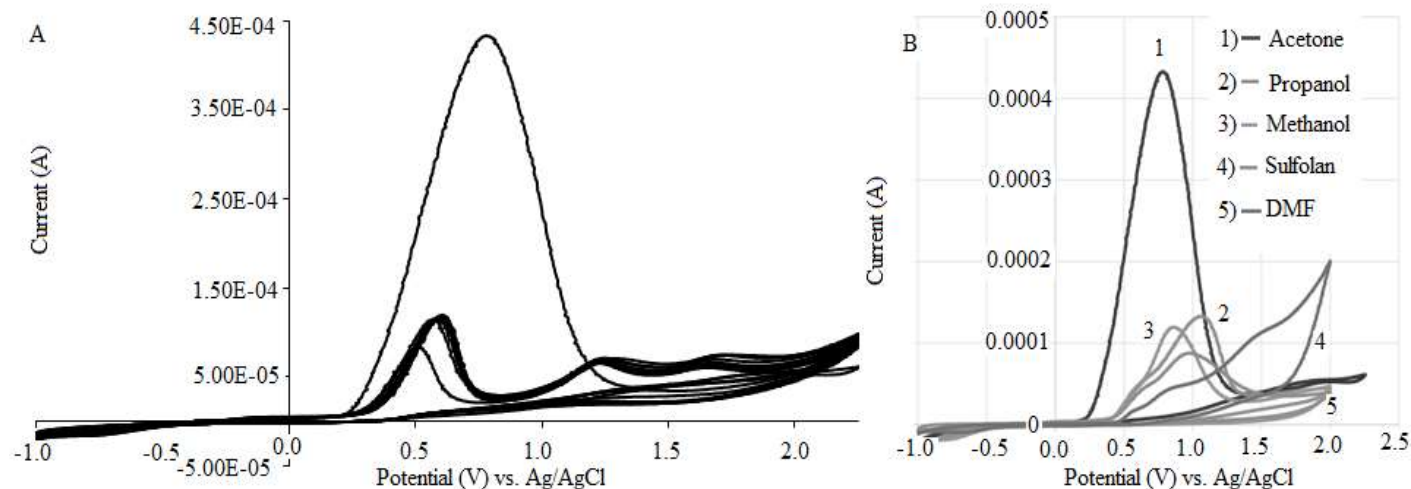


Fig. 3

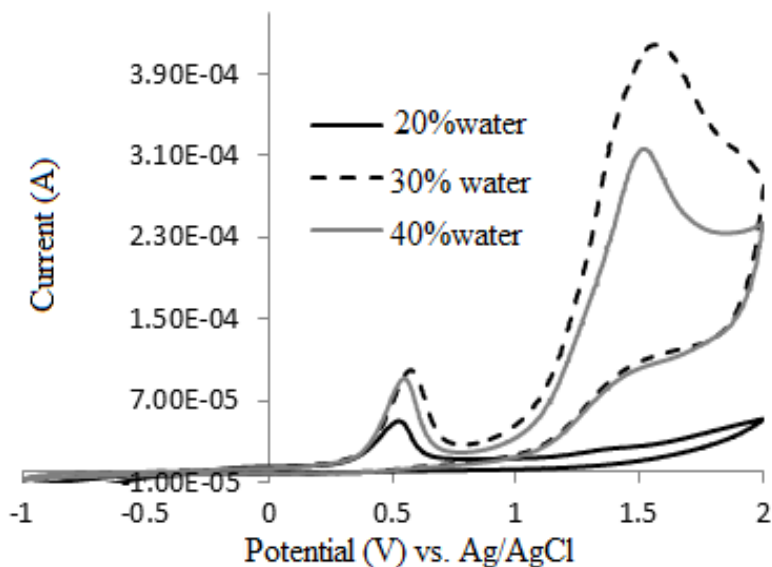


Fig. 4

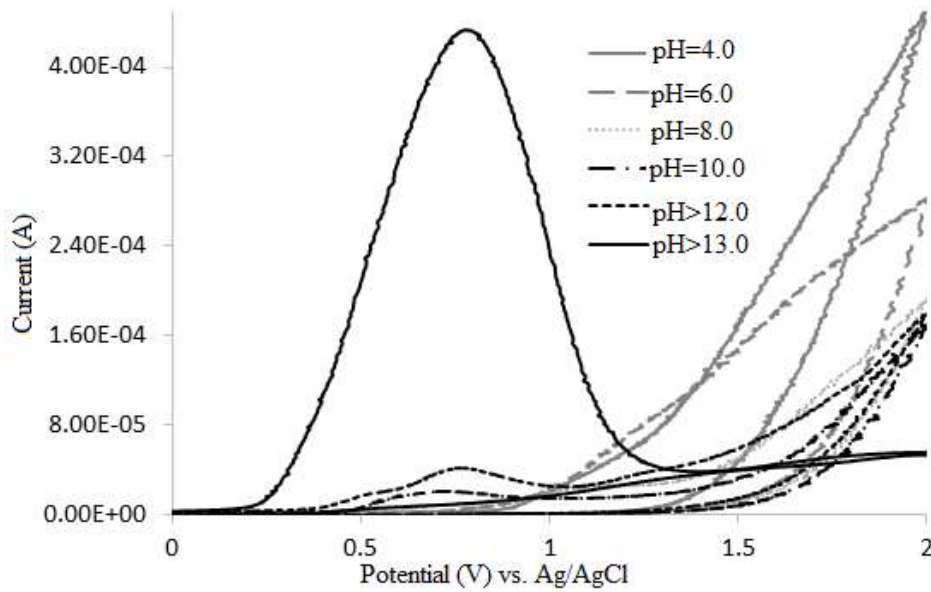


Fig. 5

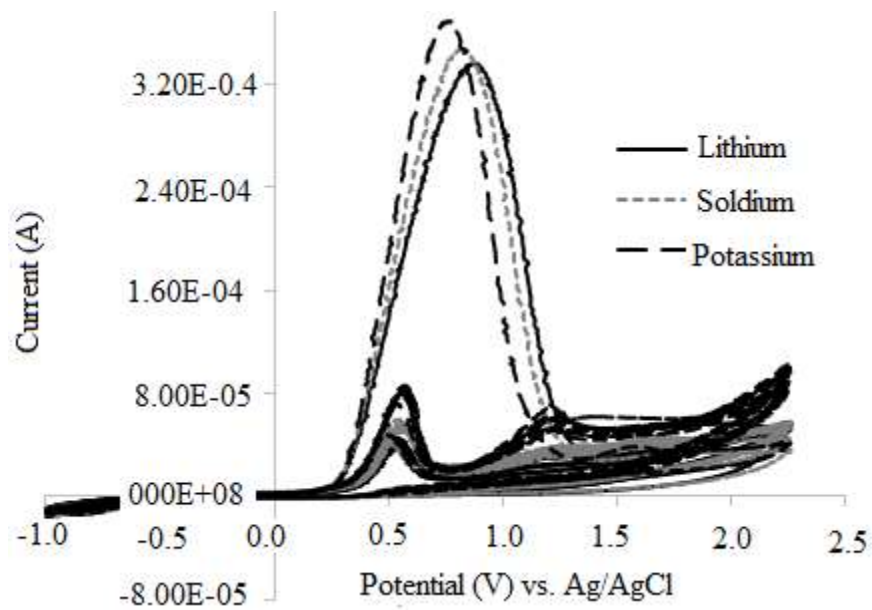


Fig. 6

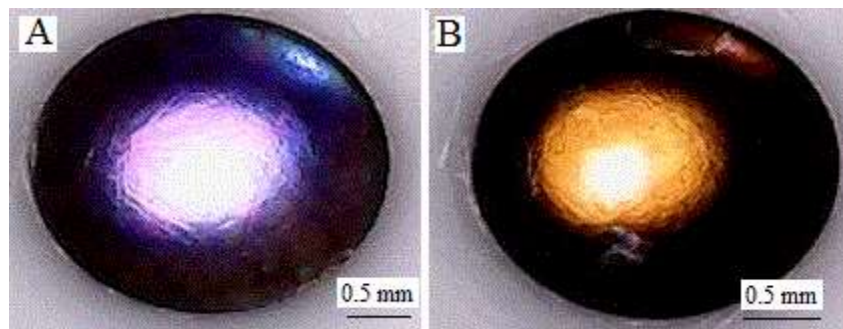


Fig. 7

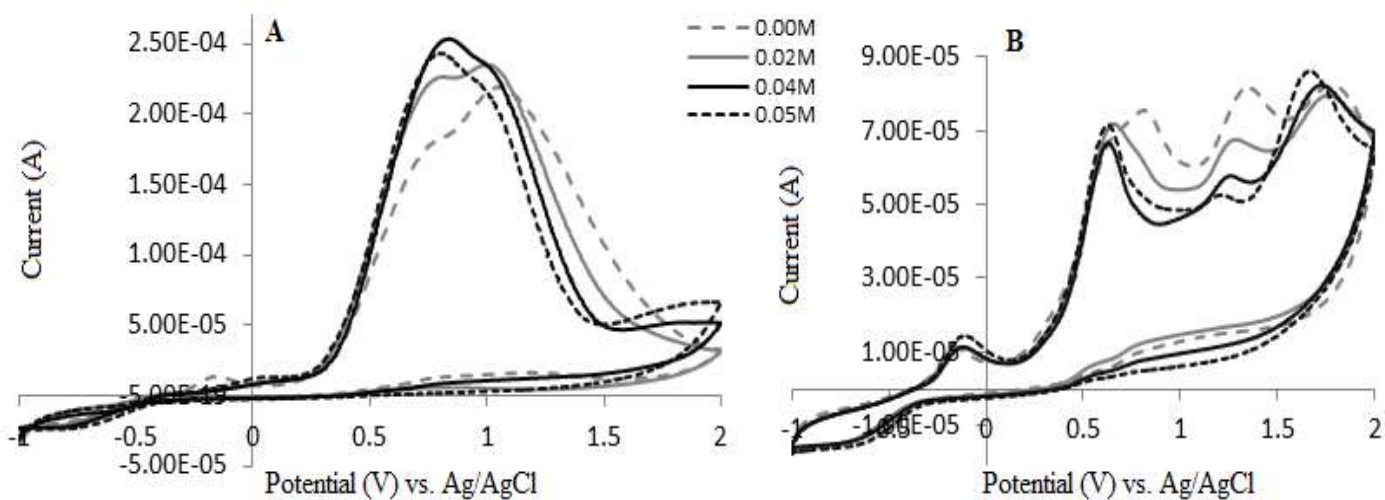


Fig. 8

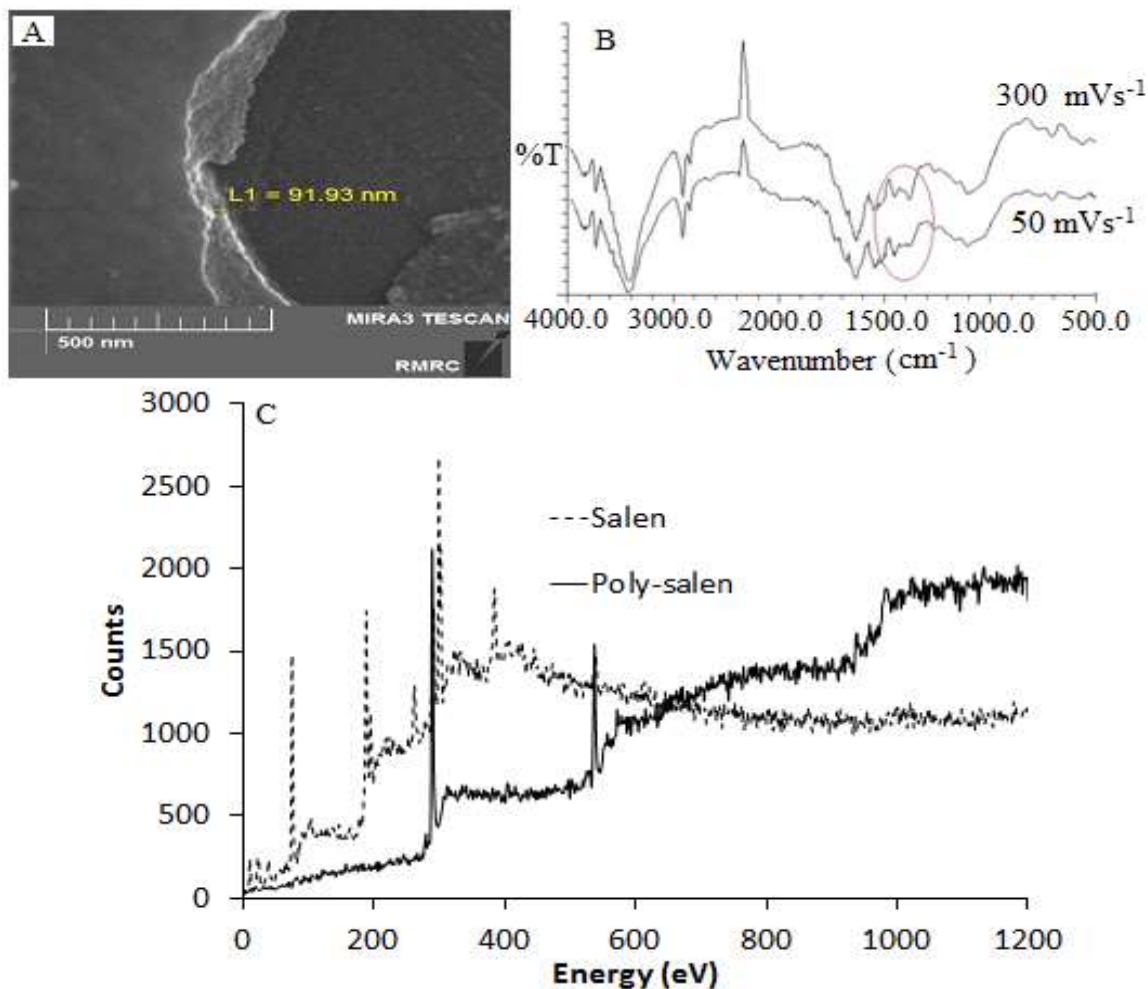


Fig. 9

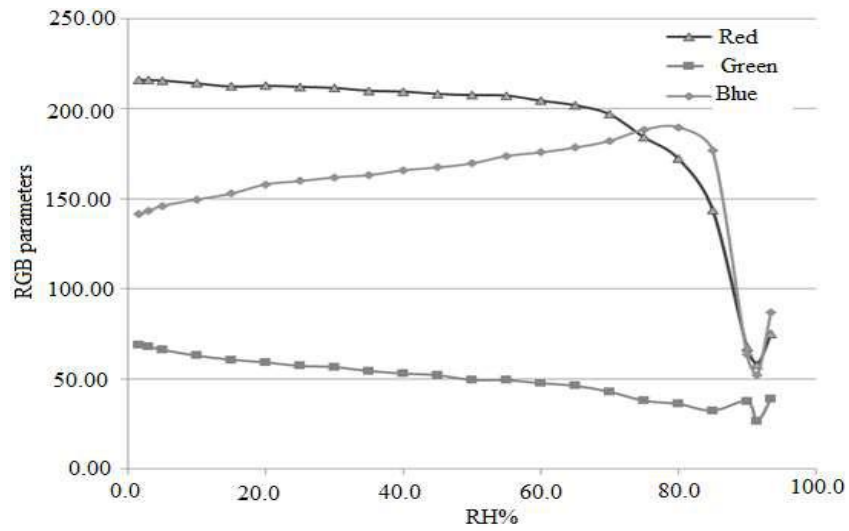


Fig. 10

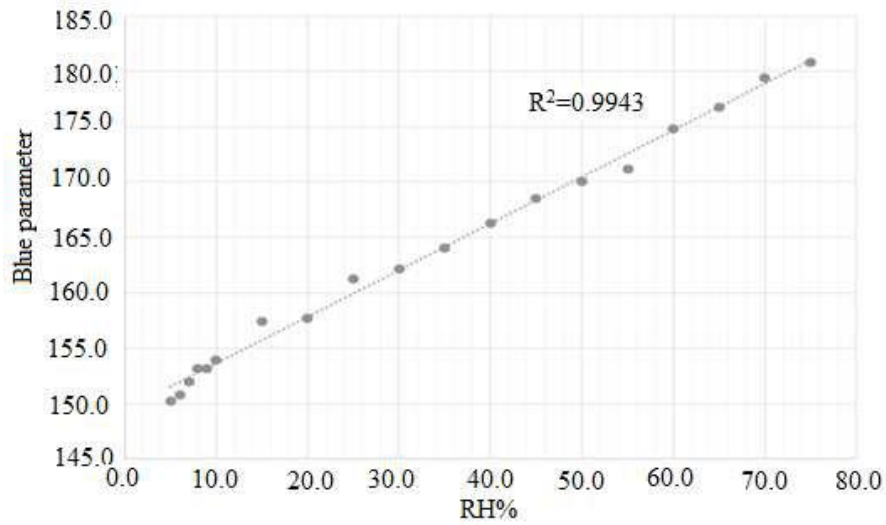


Fig. 11

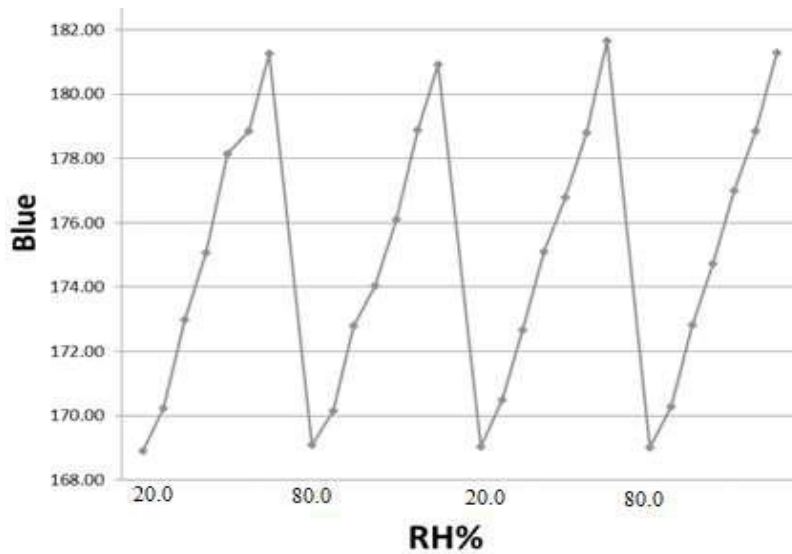


Fig. 12

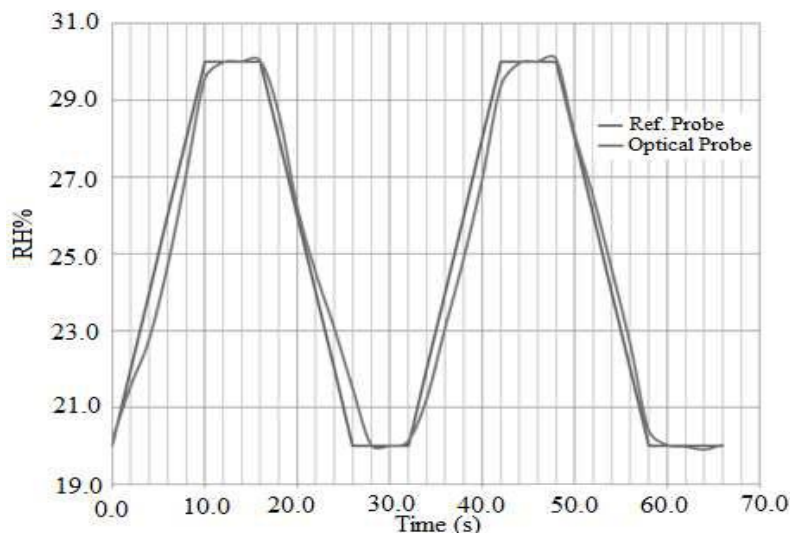


Fig. 13

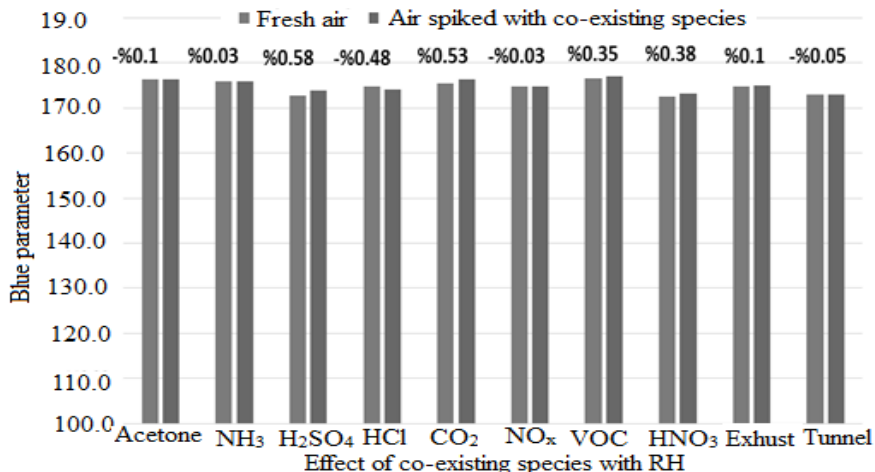
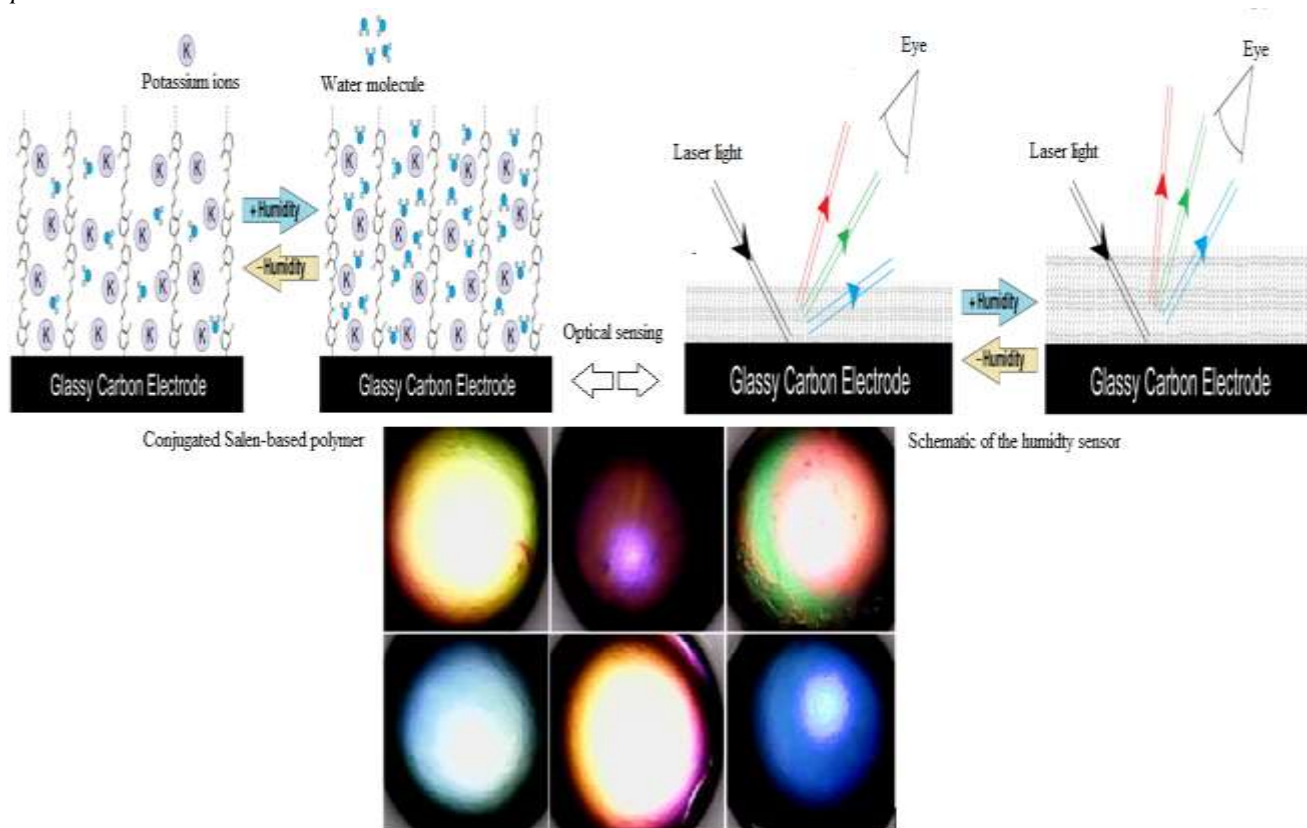


Table.1: Comparison between the fabricated sensors with previously reported RH sensors.

Parameter	Fabricated sensor	Previously reported Impedance-based RH sensors
Linearity (R)	0.9971	0.9916 [25], 0.9972 [26], 0.9894 [27], 0.9351 [28], 0.9315 [29], 0.9491[30]
Standard deviation ¹	3.0	0.1099[25]
Rise time (s) ²	9.5	41 [25], 30 [26], 45 [28], 30 [29], 40 [30], ~81.5 [31], 300 [32]
Recovery time (s)	10	120 [25], 45 [26], 20 [27], 150 [28], 8 [30], ~226 [31] , 390 [32]
Linear range (%RH)	5-80	11-95 [25], 30-90 [26], 20-97 [27], 10-90 [28, 29], 30-90 [30], 11-97 [31], 5-98 [32], 25-95 [33]
Hysteresis ³ (%RH)	7.5	6.1±0.7 [28], 5.8±0.6[29]

¹. The standard deviation was obtained by extraction in three replicate analyses.² Time interval needed for 90% of maximum response (t₉₀). ³. The differences between humidifying and desiccation processes in the range of 20-80%RH.

Graphical Abstract



Optical behaviors of the conjugated Salen-based filter during introduction of different humidity environments by the human exhaling. (Colors changes were randomly)

Energy Efficient MAC Protocols with Adaptive Duty Cycle for Wireless Sensor Networks

Kaushik Ghosh, Prashansa Choudhary

Mody University of Science and Technology, Lakshmanagarh, Rajasthan, India

Abstract— In Wireless Sensor Networks due to limited energy and resources it is very important to conserve energy and improve utilization of its resources by reducing latency. In this paper we focus on Medium Access Control protocols proposed to adapt towards more efficient use of energy and decreasing latency. We discuss how protocols like DMAC, T-MAC, DSMAC, AREA-MAC and adaptable CSMA/CA MAC work on sleep duration, decreasing idle listening and overhearing, and collision of packets. These protocols enhance their channel adaptation methods for varying traffic conditions, providing a tradeoff between various parameters like energy conservation, throughput, fairness and latency. Additionally we compare all these protocols based on their various assumptions and metric parameters. Finally, we discuss advantages and disadvantages of some of these protocols to provide an insight for their favorability under various environments.

Keywords— WSN, MAC Protocol, Energy.

I. INTRODUCTION

Sensors are used in almost every area of networking and monitoring these days. With advancement in the sensor technology they have found implementation in multifarious domains of technology for providing information about their environment. Its application varies from fields like traffic management, climate control, environment monitoring, wildlife conservation to health monitoring, defense systems, robotics, space exploration and many more. The need for communication with other sensors to aggregate and fathom useful results for the above mentioned applications, is addressed – Wireless Sensor Networks (WSN)[6]. Multiple small sensors monitor various parameters of their environment and form a network of their own i.e. WSN to report any update or change. These sensors have limited capabilities and resources like battery, computation power, memory etc. Thus, it becomes of cardinal importance to use these resources very efficiently and reduce wastage. Most important of all resources is battery, which is very hard to replace particularly in a large networks, hence it is of prime importance to reduce wastage of energy and also reducing latency of sensors to improve throughput and fairness of network as a whole.

These improvements are measured under various parameters defining the quality of network like energy, latency, throughput, fairness and scalability.

Energy: Networks heavily depend on the capabilities of the large number of sensors. These sensors have limited energy capabilities as changing the batteries frequently is not a feasible solution in large WSNs. This poses as a big problem where sensors need to interact with each other, transmit, receive, compute and even store data. Hence one of the highest priorities of MAC protocol schemes is to provide an energy efficient solution and thus minimize the cost.

Latency: The delay in transfer of data among sensors and base stations is called latency. In WSNs latency play very crucial role, especially in multiple applications which require data in real time and also in applications which require data in certain time frame for a fruitful result. For this, latency has to be minimized to make the system work under required time constrains.

Throughput: The success rate of message delivery is a very important constrain in various applications. Some applications like fire monitoring completely depend on throughput for being effective as they are triggered by even a single message. Hence it is very important to deliver the message and achieve a defined success rate to make system work.

Fairness: In high traffic networks especially there arises problem of achieving fairness in receiving data from all the sensors and acquiring medium access by sensors. If a node cannot access the medium then it deprives network of fairness as the node doesn't get equal opportunity for sending data.

Scalability: MAC protocol schemes proposed the need to adapt to scalable WSN system. WSN should be able to scale by adding more sensors in the system and function normally.

MAC layer provides protocols that are necessary for nodes to transmit data by providing channel access, so that nodes may interact without any interference. The protocols suggest the methods to achieve energy efficient way to transmit data and still achieve reduced latency, high throughput, fairness and scalability depending upon the application.

This paper has the following structure:

In Section II we are describing the problem addressed by the protocols to improve MAC layer to optimize energy usage of nodes, reducing latency and hence improving throughput. In section III we mention background study of previous work on Non-adaptable MAC protocol S-MAC. In IV section we describe T-MAC, DMAC, DSMAC and AREA-MAC CSMA/CA MAC protocol scheme and how the problems are addressed then in section V Comparison we discuss how these protocols rate with each other and finally in section VI we provide the Conclusion of our study of these protocols and the possible future work.

II. PROBLEMS

Sensors in a WSN need to conserve its resources to make the network more efficient. There are many problems we have to address to achieve that. These problems give overview of the concept addressed in the MAC Protocol scheme we are going to address. These problems are:

Idle Listening: The sensor nodes in WSN are not aware of the timing or schedule of other nodes for transmitting data. So to be prepared to listen to data from other nodes at any time, it keeps its radio on all the time. Due to lack of a definite schedule in basic MAC protocol, the sensor node ends up wasting large amount of its energy in idle listening. This problem can be seen with an example as mentioned in [1] as a node exchanges data with other nodes with frequency of one message per second and while it takes around 5 millisecond (ms) to transmit it, hence in total 10 ms for sending and receiving combined. While it spends rest 990 ms of the second waiting and idle listening for messages.

Collision: In WSN when two or more than two sensor nodes try to send data at the same time across same network or using same channel, collision occurs. The colliding packets are discarded and then they are sent again after certain period of time wasting more resources of network. Due to collision the performance of the network decreases, resulting in poor fairness, throughput and energy consumption hence it is one of the major problems that are to be addressed in WSN.

Overhearing: Because the radio of the sensors is ON most of the time, the node may receive messages that are not destined for it. This results in unnecessary wastage of computational and energy resources of nodes. The node could turn its radio OFF for this period of time and save energy and decrease the redundancy and computational time.

Protocol Overhead: MAC protocols provide functionality to sensors by sending control packets along with the data/message. These control messages mostly carry various information and message handling capabilities for

optimizing the MAC layer, but still these messages are excessive data that could be minimized and is considered as protocol overhead. By optimizing this protocol overhead we save packet size, computation, energy and also memory of the sensors.

III. BACKGROUND

To address the problems above we need to understand basic concept of non adaptable MAC protocols which is required to understand this paper. Sensor MAC protocol (S-MAC) is one of most popular non adaptable MAC protocol. As per [7] S-MAC is a non adaptable duty cycle MAC protocol. It makes use of four types of data packet. Synchronization packet (SYNC) was introduced in S-MAC and rest were introduced initially in MACA:

- RTS (Request To Send)
- CTS (Clear to Send)
- ACK (Acknowledgement)

As Fig. 1 explains, S-MAC divides its time period also known as the duty cycle in two parts: Active and Sleep. In sleep part it buffers all changes from its environment. When node reaches its active part it turns ON its radio and listens to all the data it is receiving. Sometime it involves idle listening or overhearing also. It will gather all the buffered messages and starts sending and receiving messages to and fro to other sensors nodes or to sink. All the sender nodes contend for acquiring the medium to send data to receiver. They do this by sending a RTS packet to the receiver. Receiver replies with CTS to the sender of first RTS it receives. All the nodes contending for sending data to that node, hear the CTS message if they are in range of radio of the sender node and get to know about the node that is cleared to send the message.

Apart from its significant improvement compared to formal MAC protocols without duty cycle, it has many problems that need to be addressed. High latency is prominent in non adaptable S-MAC because of the message arriving to sensor node during its sleep time is not acknowledged or replied to until node wakes up. Also the issue of high energy loss occurs because nodes waste energy during their wake up period of duty cycle by keeping radio ON for idle listening even when there is no data on the channel.

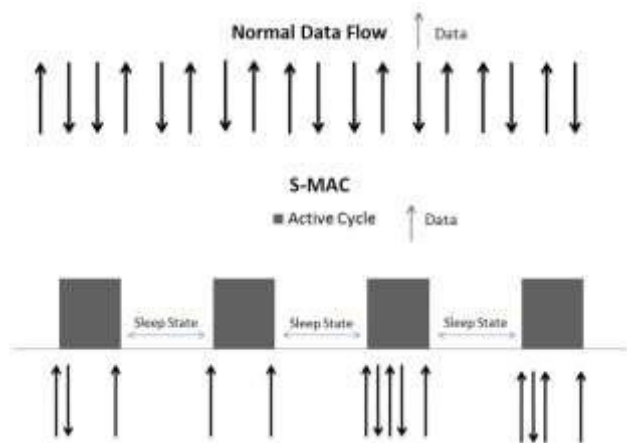


Fig.1: Normal Data Flow in MAC and S-MAC Duty Cycle Division

IV. ADAPTABLE MAC PROTOCOL

S-MAC were overcome by the new adaptable duty cycle MAC protocols. These protocols provided improved fairness, throughput, latency problem and energy efficiency by adapting their duty cycle to the load, to deadline of packet or by using low energy messages transmission etc. In the following section we will discuss basic principles of working of protocols, their environments and assumptions, their metrics, parameters, advantages and disadvantages to give a comparative study of adaptable MAC protocol:

A. T-MAC

Timeout MAC (T-MAC) is a contention based MAC protocol for WSN, where the nodes contend for data transmission to a node. It reduces energy consumption by adaptive active sleep duty cycle and hence reduce idle listening providing higher throughput and solves the problem posed in S-MAC called Early Sleep Problem.

The early sleep problem arises in case where one node wants to send data to second node, second wants to send packet to third and third wants send to fourth. In such case if first node wins medium contention and starts sending data to second then fourth node would remain active all the time as it is not aware of the transmission between first and second as it is out of hearing range of communicating nodes. While the third node would go to sleep, waking up at a later stage to contend again. Not being awake of both third and fourth node at same time drops the success probability of packet transmission to 50% per packet and even less for 2 or more packets. This problem is called as early sleeping problem.

As discussed in [1] when a new node joins the network, it starts listening through its radio waiting to receive any preexisting SYNC message to know the already working schedule of duty cycle among sensor nodes of WSN. If it receives any preexisting SYNC then it saves the schedule

and sets its own duty cycle accordingly and transmits its schedule along with the SYNC message. In case it fails to receive any SYNC packet within a particular time period, it generates its own schedule of duty cycle and transmits its own SYNC packet.

The sensor node which wants to send data to another node initialize by sending a RTS packet to the receiver node. If receiver doesn't reply, then it will retry by sending the RTS again two times.

As mentioned above, the nodes contend for sending message. All the nodes loosing in contention go to sleep to avoid wastage of energy to contend for the medium to send again at a later point of time. In the mean time the winner node starts transmitting the data as soon as it receives CTS. At the completion of data transmission the receiver node replies with ACK message. All the sleeping node wake up after sleep period and wait for a period called Contention Interval (C) to again send RTS message for contention. C increases when the traffic is higher and vice versa. Now to implement this, the sensor node has to decide minimum time after which it will go to sleep. For this [1] suggested TA – time for minimal listening before ending the active period and going to sleep, must be long enough to hear at least the start of the CTS packet. TA is always greater then sum of time interval C, Length of RTS packet (R) and Turnaround time (T) i.e. small interval between ending of RTS packet and beginning of CTS packet.

$$TA > C + R + T \tag{1}$$

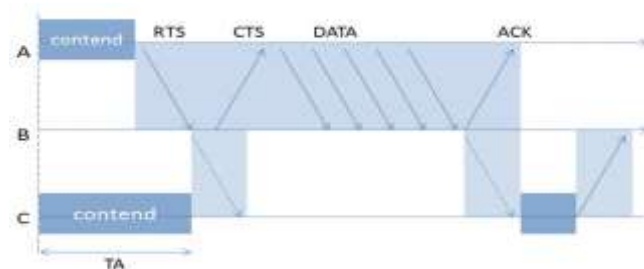


Fig. 2. T-MAC: A wants to send data to B and B to C. A wins contention, so B sends CTS to A. C overhears the CTS packet from B so it will go to sleep to wake up again in next contention period to contend.

T-MAC tries to solve the early sleep problem by using FRTS packets and Taking Priority on Full Buffers as mentioned in [1]. In FRTS packet solution, node posts a request to the future receiver node telling it to stay awake for transmission of data at a later stage in time. In another solution by [1], taking priority on full buffers, the nodes check for its buffers for sending and receiving. In case its receiving buffer is full, it prefers to send data then receiving, that means if it gets an RTS then instead of

sending a CTS it prefers to send a RTS of its own to avoid the before mentioned problem.

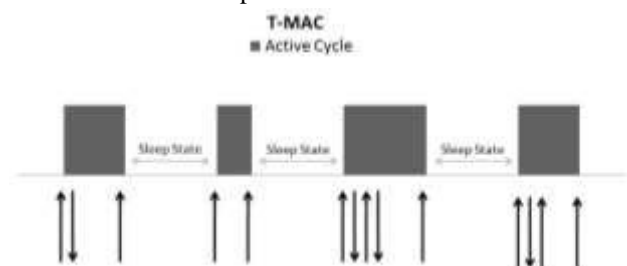


Fig.3: T-MAC with Data flow adaptable Sleep & Active states

As shown in Fig. 3, in the first Active cycle the data flow is average, so length of active cycle is also proportional. But in next Active cycle, data flow is decreased, resulting in a smaller active cycle. Similarly with the third Active cycle where data flow increases and the length of Active cycle also increases accordingly showing the adaptive changes in duty cycle of T-MAC protocol.

Advantages of T-MAC:

- adjust to data flow and hence improve energy efficiency
- Solution to early sleep problem

Disadvantage of T-MAC:

- Reduce throughput due to contention and fixed sleep cycle
- Adds Latency due to contention
- Add additional overhead for solving early sleeping problem while using FRTS

B. DMAC

According to DMAC mentioned in [2] DMAC is designed and optimized for data gathering sensor nodes tree topology in WSN. It addresses the energy, latency, throughput and fairness problems in WSN packet forwarding. As in [2] it also solves data forwarding interruption problem where the sleeping node halts the forwarding of packet. In this protocol the schedule of sensor node duty cycle depends on the depth of the node in the tree. In case there is more than one packet to send by the node below in tree topology, it proposes using More To Send (MTS) packets mechanism & Data Prediction Mechanism (DPM). DMAC is energy efficient for low load, if the load increases the latency in this protocol increases because of congestion among nodes. DMAC works on the assumption that the nodes are fixed sensors. It assumes the node topology as a tree structure. Duty cycle of node is divided into 2 parts: sleep and active. And active part is divided into sending and receiving. One active cycle is only long enough to transmit a packet to each hop. Nodes communicate with each other by

transmitting messages, but the nodes which are out of communication range are not aware of this message transmission so they go to sleep. These nodes cause interruption while data forwarding when the data needs to be communicated to any node out of the communication range of the nodes who were initially communicating. This problem is known as Data Forward Interruption.

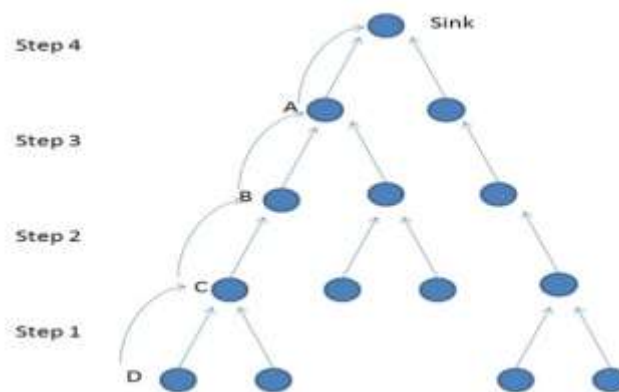


Fig. 4: Tree for data acquisition

DMAC solves this problem by Staggered Wake-up Schedule: In staggered wake up schedule the schedules of various nodes is staggered over the multihop path of data transmission. Now when the data is to be transmitted, the nodes wake up one by one to forward a packet to next hop and so on till it reaches the sink. In the Fig. 4, node D wants to send data to the sink. The route to send data is via C, B, A, i.e. D sends data to C which in turn forwards data to B which forwards data to A and A at the end sends data to Sink. According to staggered wake up schedule all the nodes in the route, i.e. C, B, A will be in active period of their duty cycle when their child needs to send data to them.

This solution also helps in reducing the sleep delay. The duty cycle is increased by only those nodes that are in the path of multihop from sender towards receiver. The receiving and sending periods for packets will be of same length μ that is enough to transmit and receive one packet. DMAC also reduces overhead by removing RTS/CTS and uses only ACK in comparison to T MAC. In ACK receiver tells the sender its willingness to be active in next slot.

In multihop chains, the nodes of WSN sometime need to send multiple data packets and to make sure its delivery [2] has used More to Flag, Data Prediction Techniques and More to Send.

More Data Flag: it is used to send more than one data packets in multihop environment. It asks nodes to increase their duty cycle after checking the more data flag. If it is active, the nodes sending more than one data packets are required to set this flag while sending and check for this

flag while receiving. Between every sending of acknowledgements after receiving packets there is time difference of at least 3μ .

Data Prediction: normally while sending data from multiple children to a parent, the parent node may go to sleep after the reception of data is complete from one child. While other child node of the same parent may have also data to send, and as the parent went to sleep since the other child didn't add a More Data Flag because its buffer is empty so it might have to wait till the parent wakes up. To avoid such problem parent node tries to predict the data coming from other child and hence it will sleep only for 3μ time period, and then wake up again, to see if its other child node has any data to send. In case there is no more data to send it will go back to sleep.

More to Send Packet: in condition where two nodes A and B of different parent want to send data to their respective parents and thus, contend; node A wins then neither node B nor its parent hold any active cycle in this interval then the node B can only send packet in the next sending slot, but its parents already goes to sleep which causes this node to wait for ACK from its parent but the parent doesn't receive any packet in its receiving slot. This causes data prediction scheme to fail here. Now to avoid this condition, More to send packet is used. It is used on any of the two conditions:

1. If channel was busy because other node was using it.
2. It receives from its child and packet with MTS flag already set

It removes MTS when any of 3 conditions hold true:

1. If buffer is empty
2. All requests from children for MTS are cleared
3. It sends request MTS to its parent before and has not send a clear MTS

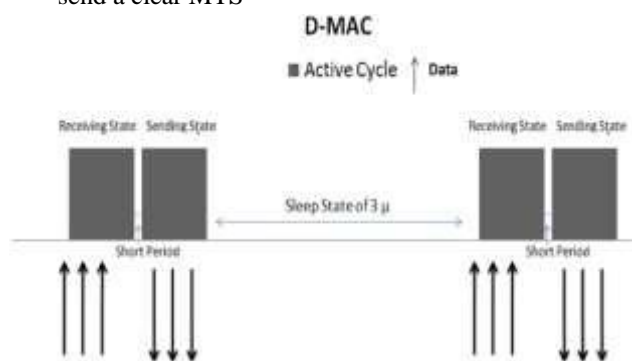


Fig. 5: DMAC Protocol

In the figure above, the node is receiving data initially. After completion of receiving it waits for a Short Period of time before starting to send data. It does so to avoid any collision or interference in packet transmission. After sending is completed it goes to sleep for a period of at least 3μ and repeats the process again.

Advantages of DMAC:

- DMAC reduces packet overhead by removing RTS/CTS and uses only ACK in comparison to T MAC
- DMAC increases the wake up time for its nodes in most of its scheme resulting in higher throughput/lower latency and higher energy efficiency.

Disadvantage of DMAC:

- DMAC is suggested for tree based topology of WSN and hence doesn't work in other topologies.
- Adds high overhead by using MTS Packet and More Data Flag.

C. DSMAC

According to [3] to manage the tradeoff between the performance and energy consumption DSMAC introduces dynamic duty cycles to adapt to variable changes in the energy consumption and latency. It alters the duty cycle and synchronizes with other nodes according to its duty cycle based on the packet load and energy consumed by nodes, and hence dynamically adapts for higher performance by the system by using less energy.

In [3] to manage according to the clock imparity SYNC messages are used by nodes. DSMAC uses SYNC in similar fashion to S-MAC. One node tries to listen to the network hoping to receive any existing wake up schedule of nodes, and adapt to the existing system. In case it does not over hear any schedule it creates it s own schedule and broadcasts the SYNC packets to other nodes to adapt to new schedule and broadcast their own SYNC packet. Every node maintains a local SYNC table to adjust its duty cycle according to load and energy consumption. Initially all sensors adopt a common service duty cycle. In comparison to S-MAC's SYNC it also contains the sender node's duty cycle in SYNC packet in DSMAC.

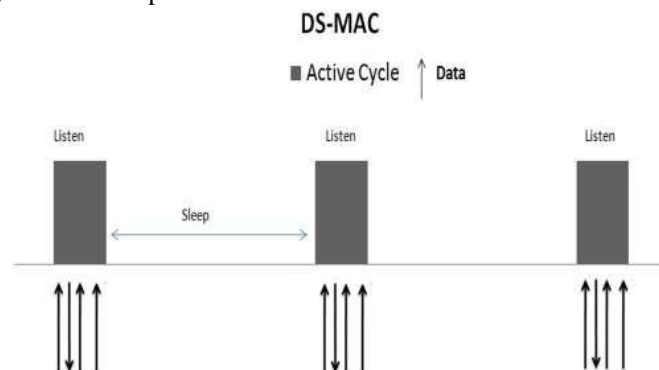


Fig.6: DSMAC for Low Load conditions

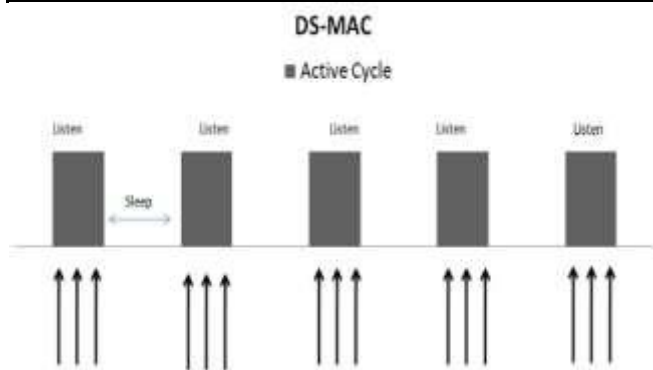


Fig.7: DSMAC for High Load conditions

All nodes adapt a common wake up schedule (Duty Cycle) at start. It uses following steps to alter its duty cycle:

1. When data packet is received, node measures the delay of packet based on the timestamp created by sender.
2. Receiving node adapts its duty cycle based on average delay, queue size and its duty cycle. It reduces its duty cycle if load is less and increases in higher load conditions.
3. It also adapts its duty cycle according to duty cycle of sender. After alteration it broadcasts its SYNC packet.

For a node if the load is low then sleep cycle would be longer as in Fig. 6 and for higher load smaller sleep cycle as in Fig 7.

Hence, by decreasing number of the active cycles of a node when the load on the node is low and increasing number of active cycles when the load is high, DSMAC manages a tradeoff between energy consumption and efficiency. Thus by following the 3 step mentioned above DSMAC adapts to varying load and provides an efficient way for increasing throughput and reducing latency.

Advantage of DSMAC:

- DSMAC is scalable as it does not affect the duty cycle of idle neighboring nodes.

Disadvantage of DSMAC:

- But it also introduces the overhead by adding timestamp to SYNC packet and delay for data packets like T-MAC.

D. AREA-MAC

AREA MAC provides a tradeoff between various parameters like latency, throughput, and energy consumption. As proposed by [4] it uses grid based wireless sensor network as a basic assumption for the AREA MAC Protocol. The nodes don't support any data aggregation or have any in-network capabilities. All nodes are fixed and know their locations regarding to their reference nodes and all nodes have a unique ID. It uses

LPL (Low Power Listening) mode with short preamble messages to reduce the latency and energy consumption and improve lifetime of sensor nodes. To increase the scalability of the system the nodes are kept completely independent of the sleep wakeup schedule of other nodes in network. Sender broadcasts a LPL with short preamble message with destination ID, when nodes wake up they will check for LPL with short preamble message, if there is any LPL with short preamble message they will check the destination id provided in the message.

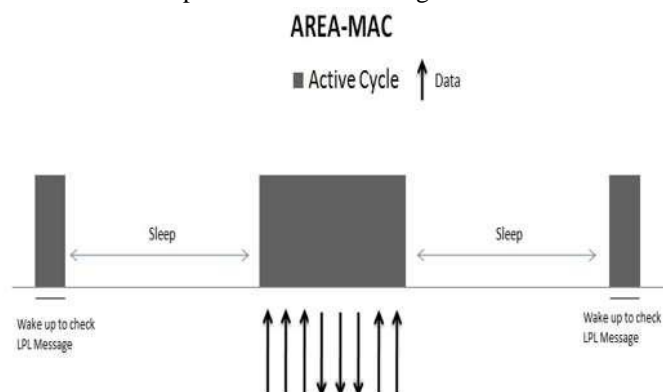


Fig.8: AREA-MAC

If the destination id matches to their ID, then an acknowledgement is sent immediately to the source node and if it doesn't then it goes back to sleep. Hence the sender node will know and stop sending any further LPL with short preamble message conserving the energy and it will start sending the data. If the node for the next hop is sleeping and sender wants to send data, it forcefully wakes up the suitable next hop neighbor, chosen on the basis of link cost metric and starts sending data and thus, provides real time support for nodes. The paper fails to provide details, how this action of forcefully waking up other nodes occur, which gives an abstract view of process.

In Fig. 8, the receiving node wakes up to check the medium for LPL with short preamble messages. It goes to sleep as no LPL with short preamble message was found for it. It wakes up after sleep cycle to check again and this time it receives LPL with short preamble message and finds it is addressed to it, so it sends back the ACK and starts transmitting data. After data transmission it goes to sleep and the cycle continues.

Advantages of AREA-MAC:

- Asynchrony: fully independent of sleep and wake up schedule of other nodes.
- Energy Efficient: Sender uses LPL approach where nodes wake up to check the data in channel and go back to sleep if there is no data for it.
- Adaptability: nodes adapt their duty cycles according to the requests received for data transmission.

Disadvantage of AREA-MAC:

- Works only in case of Grid based fixed network of sensors only, so the network cannot be dynamic in nature.
- All sensors are assumed to know location of sensors till next two hops which is a lot of overhead for sensors to store.

E. Adaptive CSMA/CA MAC

A novel adaptive CSMA/CA MAC protocols invented by Benazir and Manimaran [5], provides an insight for channel adaptation and load adaptation missing in various MAC protocols. It provides either low energy or low delay option for transmission of data for varying channel and load condition, providing low latency and high efficiency in successfully transmitting packet among nodes. It provides a metric of energy and delay in transmission of packets to decide the best message according to deadline

and energy requirement and modulation level to reduce delay and energy required at time of packet transmission. In [5] it proposes adaptive CSMA/CA MAC which uses Dynamic Modulation Scaling (DMS). In DMS we change number of bits per symbol while keeping the symbol rate constant. It uses the concept that a packet at with higher high modulation level can be sent at high energy while a packet with lower modulation level cannot. This results in a delay-energy tradeoff for each modulation level. It purports the theory that lower modulation is beneficial in some cases and in other higher may be beneficial. This allows us to develop a protocol that could sense and forward packet in either energy efficient way or delay efficient. Hence to adapt to real time networks and creates a tradeoff between the transmission delay and energy consumption during transmission.

TABLE I. COMPARISON TABLE

Protocol	Scheme Used	Timeliness	Scalability	Throughput (In Comparison to S-MAC being Lowest)	Assumed Environment	Adeptive To Change	Problem Solved
T-MAC	Adaptive Duty Cycle, Overhearing, FRTS	No	No	Low	General*	Good	Early Sleeping Problem
D-MAC	Converge Cast Communication	Yes	Yes	High	Tree	Week	Data Forwarding Interruption Problem
DS-MAC	Dynamic Duty Cycle Over S-MAC	Yes (But Partially)	No	Medium	General*	Good	Latency Problem
AREA-MAC	LPL With Short Preamble Messages	Yes	Yes	High	Grid	Good	Latency Problem
CSMA/CA	Energy-Delay matrix	Yes	Yes	High	General*	Best	Best Modulation Level Selection For Energy-Delay Pair

*General – No specific topology/environment assumed

To transmit a message successfully the probability of bit error is fixed to 10^{-6} . Thus, in the given case bit error probability is calculated and the minimum Sound to Noise Ratio (SNR) value is calculated for successful demodulation for each modulation level K. These values are used to calculate the transmission power for various K. This allows adaptive CSMA/CA MAC to cancel out those options of modulation level where transmission power is higher than the maximum transmission power of transmitter. With the help of transmission rate, transmission power per signal is calculated.

Now all the nodes in WSN who have any message to transmit in their buffer contend for medium to transmit packets and the winning node acquire the channel. The transmission power for messages is estimated for each value of K. If the transmission power is higher than the maximum transmission power of transmitter, then the corresponding values of K are discarded. It calculates the energy delay pair [E, D] for all K. For each node the Load

Index (LI) is calculated which describes the message load on a sensor in contention period and by varying deadlines for packets. Load index is thus inversely proportional to period of message and directly proportional to worst-case-transmission time. The calculated load index is to generate Energy-Delay Metric (M_i) using E_i normalized transmission energy consumption and D_i normalized transmission delay.

$$LI = \sum_{i=1}^m \frac{WCT_{xi}}{P_i} \tag{2}$$

$$M_i = \beta * E_i + \gamma * D_i \tag{3}$$

Where,

$$\gamma = 1/LI, LI \leq 1 \tag{4}$$

$$\beta = 1 - \gamma \tag{5}$$

Under current scenario of load on the channel, the minimum value of M_i represents the least energy and delay in message transmission for the modulation level i.

Advantages of adaptive CSMA/CA:

- Dynamically adapts to load by varying modulation level.
- Energy-Delay pair provides minimum delay and efficient energy usage for message transmission.

Disadvantages of adaptive CSMA/CA:

- Overhead of calculating and maintaining Energy-Delay pair metric.

V. COMPRESSION

TMAC is better than SMAC in context of energy saving for increasing load condition (byte/node). But the problem with TMAC is in case of providing real time data, as it doesn't change sleep cycle as node doesn't receive any data during part. Still TMAC proves to be very useful for solving early sleep problem.

DMAC provides better real time data than TMAC because it uses staggered wakeup schedule and hence provides higher throughput in comparison to SMAC and TMAC as well as solve data forwarding interruption problem. DMAC works on only tree topology based WSN, so it cannot be deployed on any other topology based WSN while SMAC and TMAC do not have any specific topology requirement. Due to the changes in the duty cycle that appear only after receiver node receives packet in condition of change in load on channel and packet delay measure by timestamp of packet, DSMAC doesn't provide real time data as efficiently as DMAC. In comparison to DMAC, DSMAC is not as much scalable because all the nodes have to adopt same duty cycle initially. But because there is no topological assumption in DSMAC, it can work on every topology of nodes in WSN.

In comparison to DSMAC, AREA MAC provides better real time data, higher throughput and is more scalable. But its application is applicable to only grid topology of WSN where all the nodes are fixed and aware of their location.

Adaptive CSMA/CA is comparatively better than AREA MAC because it considers an additional parameter for optimizing transmission, that is energy-delay metric, which provides a highly efficient energy consumption and high success ratio of data transmission by dynamically changing transmission power and rate via dynamic modulation scaling. Hence it provides highly real time data and throughput. Also because of no certain assumption about the topology of WSN, it is highly scalable.

VI. CONCLUSION

In our day today world WSN is being used extensively and our reliance is increasing on it every day. With the growing number of fields with deployment of WSN and criticality of WSN in those domains compels us to make them more efficient. With intensive research going on in this field,

MAC protocols in WSN have seen huge leaps of growth in recent times, making them more energy efficient, with low latency, high throughput, fairness and scalability. With the above discussion about MAC protocols like S-MAC, DMAC, DSMAC, AREAMAC, adaptive CSMA/CA MAC, we have provided a brief view of all these schemes, while describing their main improvements, working, and advantages. In this paper we described how S-MAC uses fixed duty cycles, T-MAC introduces adaptive duty cycles, DMAC introducing staggered wake up schedule, DSMAC using dynamic duty cycle, AREA MAC uses low power listening LPL with short permeable messages and how adaptive CSMA/CA gives concept of energy-delay metric to find best modulation level. Apart from all the advancement we have discussed in adaptive MAC protocols we believe there is room for a lot more research in this topic and many more schemes to discuss.

REFERENCES

- [1] T. van Dam and K. Langendoen. "An adaptive energy efficient MAC protocol for wireless sensor networks". In 1st ACM Conference on Embedded Networked Sensor
- [2] G. Lu, B. Krishnamachari, and C. S. Raghavendra, "An adaptive energy-efficient and low-latency MAC for data gathering in wireless sensor networks", in Proceedings of the 18th International Parallel and Distributed Processing Symposium (IPDPS '04), pp. 3091–3098, Los Alamitos, California, USA, April 2004.
- [3] P. Lin, C. Qiao, and X. Wang, "Medium access control with a dynamic duty cycle for sensor networks", in Proceedings of the IEEE Wireless Communications and Networking Conference (WCNC '04), vol. 3, pp. 1534–1539, March 2004.
- [4] P. Kumar, M. Gunes, Q. Mushtaq and B. Blywis, "A Real-Time and Energy-Efficient MAC Protocol for Wireless Sensor Networks", Proceedings of the 6th IEEE and IFIP International Conference on Wireless and Optical Communications Networks, 28-30 April 2009, pp. 1-5.
- [5] Benazir Fateh, and Manimaran Govindarasu "Energy-Aware Adaptive MAC Protocol for Real-Time Sensor". ICC, page 1-5. IEEE, (2011).
- [6] M. Tubaishat and S. Madria, "Sensor networks: an overview", IEEE Potentials, 22(2):20–23, April 2003.
- [7] W. Ye, J. Heidemann, and D. Estrin. "An energy-efficient MAC protocol for wireless sensor networks". In 21st Conference of the IEEE Computer and Communications Societies (INFOCOM), volume 3, pages 1567-1576, June 2002.

The Relationship between Cost-Volume Profit Management and Profitability in Private Organizations

Dr. Ghassan Farouk Ghandour

College of Financial & Administration-Department of Accounting & IT, Cihan University/ Sulaiymani, Kurdistan Region Government, Iraq.

Abstract— *The study showed that Phoenix academy employees staff with appropriate skills and experience, has the right number of staff purchase school items only when required, have measures to counter school defaulters, do not keep variable cost-volume profits below 30% of incomes, do not take staff for further training, outsource some staff and that the school gives allowances to staff. The study revealed that the school use sales maximization approach to profits they do aim at profit maximization, their profits do not grow steadily over the years, profits are considered basing on the revenues and investments and do not keep profits at 25% of revenues.*

Keywords— *unit, Cost-volume profit Management, Profitability, behavior, organization.*

I. INTRODUCTION

When you acquire supplies or services, you normally expect to pay a smaller price per unit as the purchase quantity increases. You expect contractors to have lower costs per unit as production quantity increases. This general expectation remains the same whether you are buying items specifically built for the Government or items that are mass-produced for a variety of commercial and Government customers. You can use cost-volume-profit analysis to analyze the natural relationship between cost, volume, and profit in pricing decisions. In cost-volume-profit analysis, you:

- Should consider only short-term operations. The short term may be defined as a period too short to permit facilities expansion or contraction or other changes that might affect overall pricing relationships.
- Assume that a straight line can reasonably be used in analysis. While actual price behavior may not follow a straight line, its use can closely approximate actual cost behavior in the short run.

- If purchase volume moves outside the relevant range of the available data, the straight-line assumption and the accuracy of estimates become questionable.
- If you know that product variable costs per unit are decreasing as quantity increases, consider using the log-linear improvement curve concept. Improvement curves are particularly useful in limited production situations where you can obtain cost/price information for all units sold.

Research problem

Cost-volume profit management in every organization determines the level of profitability. Phoenix Academy secondary school has restructured its control systems through credit risk controls and employing the required staff. Despite all the above efforts to minimize operational cost-volume profits, low profitability is still reported.

Research objectives

- i. To establish how cost-volume profits are managed in Phoenix Academy Secondary School.
- ii. To find out the profitability levels and trend registered in the school.
- iii. To establish the relationship between cost-volume profit management and profitability in the school.

Research importance

To establish whether cost-volume profit management affects the profitability levels of Phoenix Academy Secondary School.

Research Significances

Findings of the study will be of great importance to the following beneficiaries in the following ways.

- Phoenix Academy will be able to improve on the management of cost-volume profits as the study

findings will generate new ideas pertaining to cost-volume profit management.

- Business managers will benefit from the study by adopting best ways of cost-volume profit management in order to improve on their profitability levels

Research Methodology

Research design

In order to be consistent with the research objectives and questions in chapter one, cross sectional research and qualitative and quantitative research designs were used in order to collect the relevant data.

Research population

According to Krejcia and Morgan, the study population of Phoenix Secondary School consisted of 40 people, 15 being in Management, 20 on the teaching staff and 5 support staff.

Table.1: Showing the Study population.

Type of respondents	Number of people
Management	15
Teaching staff	20
Support/non teaching staff	5
Total	40

Source: Primary data

Sample size

The sample size of the study was 36 respondents from all the three sects.

Sampling methods

The study was based on stratified sampling method that enabled the collection of relevant data. The strata included; the teaching staff, management and the support staff.

Data collection methods

Questionnaires were the data collection tool used to extract the necessary data given the time constraint. They provide convenience with respect to time of respondents.

Sources of data

Data was collected from both primary and secondary sources.

- Primary sources

Primary data was collected from respondents concerned like those mentioned earlier.

- Secondary sources

Secondary data was collected from the original documents, books of accounts, the Board of Director’s reports and other relevant documents.

Data processing and analysis

Data collected was organized, sorted and checked for accuracy and completeness: Data was tabulated, interpreted and analyzed in line with the study objectives.

1. PRESENTATION, INTERPRETATION AND ANALYSIS OF THE FINDINGS.

1.1 Introduction

In this chapter, findings of the study are presented, interpreted and discussed in relation to the study objectives as follows.

1.2.1 General findings of the study

This includes findings relating to all parts of the questionnaires.

Table 1.2.1: Shows the response rate

Response	Frequency	Percentage (%)
Response	29	80.6%
Non-response	7	19.4%
Total	36	100%

Source: primary data survey question 1

From the table above, out of 36 respondents only 29 answered the questionnaires making a percentage of 80.6% respondents and 7 people did not return the questionnaire which brings a total of 19.4% non respondents. This implies that almost every sect of the school had interest on knowing how the school is performing.

1.2.2 Findings on personal data

Table 1.2.2: Showing the gender of respondents

Gender	Frequency	Percentage (%)
Male	17	58.6%
Female	12	41.4%
Total	29	100%

Source primary data survey question 2

From the table above, 17(58.6%) of the respondents were male while 12(41.4%) were female. This implies that majority of them belong to the teaching staff that is made up of the highest number. This is as a result of being a secondary school where most students tend to despise female staff and therefore the only option is employing more of the male staff.

1.2.3 Marital status of the respondents

Table 1.2.3: Shows the marital status of respondents in Phoenix academy secondary.

Marital status	Frequency	Percentage (%)
Married	23	79.3%
Single	4	13.8%
Others	2	6.9%
Total	29	100%

Source: primary data survey question 3

From the findings it is clear that majority of the respondents (79.3%) are the married people followed by single (13.8%) and the minority respondents (6.9%). This implies that since

married people in most cases are associated with family problems, they tend not to implement and follow the cost-volume profit controls put in place to minimize the problem of high cost-volume profit operations.

1.2.4 on the education levels of the respondents.

Table 1.2.4: Showing the education levels of the respondents

Education	Frequency	Percentage (%)
'A' Level	03	10.4%
Diploma	8	27.6%
Certificate	-	0%
Degree	15	51.7%
Others	03	10.4%
Total	29	100%

Source: primary data survey question 4

From the above table, the majority of respondents (51.7%) are graduates followed by Diploma (27.6%), A-level (10.4%), others (10.4%) and none of the respondents hold a certificate. This implies that the school has well educated staff and management. This probably means that the management just lack ways of goods implementation of their objectives.

1.2.5 Period worked for the school

Table 1.2.5: Showing number of years respondents have worked in the school.

Number of years	Frequency	Percentage (%)
Less than 2years	2	6.9%
2-5years	10	34.5%
More than 5years	17	58.6%
Total	29	100%

Source primary data survey question 5

The above table indicates that majority respondents are in the range of more than 5years followed by those from 2-5years and then less than 2years. This implies the school has the ability to contain its staff once recruited. This enables in the reduction of replacement cost-volume profits and cost-volume profits of inefficiency of performance of the staff.

1.2.6 Position held in the school

Table 1.2.6: Showing different positions held by respondents in the school.

Position	Frequency	Percentage (%)
Management	7	24.1%
Teaching staff	19	65.5%
Support staff	3	10.3%
Others	-	0%
Total	29	100%

Source: primary data survey question 6

The findings indicate that 7(24.1%) belong to management 19(65.5%) belong to the teaching staff, 03(10.3%) belong to the support staff and none belong to any other position. The teaching staff dominated the respondents because they dominate the sample size suggested followed by management and the support staff.

1.3 Findings on cost-volume profit management

The following information presents interprets and discusses the findings on cost-volume profit management of Phoenix Academy as the second part of the questionnaire.

1.3.1 Findings on the extent to which the respondents agreed or disagreed with the employment of staff with appropriate skills and experience

Table 1.3.1: Showing response on employment of staff with appropriate skills and experience

Extent of agreement	SA	A	N/S	D	SD	Total
Frequency	08	18	03	-	-	29
Percentage (%)	27.6%	62.1%	10.4%	-	-	100%

Source: Primary data survey question 7

From table 1.3.1: 08 (27.6%) strongly agree that the staff recruits has appropriate skills and experience, 18(62.1%) agree with the statement and 03(10.4%) are not sure of which staff recruited and none of the respondents disagreed and strongly disagreed with the statement. This pattern of response indicates that employee skills and experience is a prerequisite in the recruitment and selection of staff, in abide to try to reduce on the cost-volume profits of training.

1.3.2 Respondents on the right number of people employed in the school.

Table 1.3.2: Showing on the extent to which respondents agree or disagree with the employment of the right number of staff.

Extent of agreement	SA	A	NS	D	SD	Total
Frequency	06	18	03	01	01	29
Percentage (%)	20.7%	63.8%	10.3%	03.4%	01.7%	100%

Source: Primary data survey question 8

As observed from the table 1.3.2 about. 06(20.7) strongly agree, 18(63.8%) agree, 03(10.3%) are not sure 01(03.4%) disagree and 01(10.3) are not sure 01(3.4%) disagree and 01(1.7%) strongly disagree with the statement. This implies that Phoenix Academy tries to match its staff with work requirements and work hard in order to avoid over and

under capacity. Work overload and extravagant salary payments as well as under employment of staff is reduced.

1.3.3 Findings on the extent to which the respondents agreed or disagreed with the buy of school items only when they are headed.

Table 1.3.3: Showing the response on buying of school items only when they are needed.

Extent of agreement	SA	A	NS	D	SD	Total
Frequency	03	15	03	07	01	29
Percentage (%)	10.3%	51.7%	08.6%	25.9%	03.4%	100%

Source: Primary data survey question 9

According to the above table 04(10.3%) strongly agree, 15(51.7) Agree, 03(08.6%) not sure, 07(25.9%) disagree and 01(03.4%) strongly disagree with the above statement. This implies that the board is interested in applying just-in-time (JIT) approach in acquiring school properties in order to manage spending.

1.3.4 Findings on the extent to which the respondents agree or disagree with the proportionality of salary scale to the level of income.

Table 1.3.4: Showing response on proportionality of salary scale to the level of income

Extent of agreement	SA	A	NS	D	SD	Total
Frequency	-	02	12	05	10	29
Percentage (%)	-	6%	43.3%	17.2%	34.5%	100%

Source: Primary data survey question 10

From the table above, none strongly agreed with the statement that the salary scale of the school in proportional to the revenues, 02(6%) agreed, 12(43.3%) not sure, 05(17.2%) disagreed and 10(34.5%) strongly disagreed with the statement. This is due to the fact that majority of respondents are professionals whose salary scale is fixed and independent of the revenue levels and hence do not necessarily correspondent with it. Even for the non-professionals like the support staffs are held to be constant.

1.3.5 Measures to counter fees defaulters

Table 1.3.5: Showing the response on the presence of measures to counter fees defaulters in the school.

Extent of agreement	SA	A	N/S	D	SD	Total
Frequency	11	14	1	3	-	29
Percentage (%)	37.9%	48.3%	3.5%	10.6%	-	100%

Source: Primary data survey question 11

As observed from the above table 1.3.5 11(37.9%) strongly agreed with the statement, 14(48.3%) agreed, 01(3.5%) were not sure, 03(10.4%) disagreed and none strongly disagreed with the statement. The pattern of response stems from the fact that students are subjected to midterm exams whereby those with school fees balance are not allowed to sit them. This is according to the headmaster of the school, which according to him is enough to instill a sense of responsibility into students and parents regarding the in-time payment of school fees.

1.3.6 Findings on the extent to which the respondents agreed or disagreed with the outsourcing of some staff

Table 1.3.4: Showing response agreed or disagreed with the outsourcing of some staff

Extent of agreement	SA	A	N/S	D	SD	Total
Frequency	08	08	06	05	02	29
Percentage (%)	27.6%	27.6%	20.7%	17.2%	6.9%	100%

Source: Primary data survey question 12

As evidenced from table 1.3.6 above 08(27.6%) strongly agreed, 08(27.6%) agreed, 06(20.7%) were not sure, 05(17.2%) disagreed and 02(6.9%) strongly disagreed with the statement that the school outsource some staff. The outsourcing of staff pertains to the teaching staff especially during the end of the final year examinations for candidate classes to offer technical aspects to enable students perform better.

1.3.7 Findings on the extent to which the respondents agreed or disagreed with the keeping of variable cost-volume profits below 30% of income.

Table 1.3.7: Showing the responses on keeping variable cost-volume profits below 30% of income.

Extent of agreement	SA	A	N/S	D	SD	Total
Frequency	01	06	10	8	5	29
Percentage (%)	3.5%	20.7%	34.5%	27.6%	17.2%	100%

Source: Primary data survey question 13

Table 1.3.7: Above indicates that 01(3.5%) strongly agreed with the statement, 06(20.7%) agreed, 10 (34.5%) were not sure, 08(27.6%) disagreed and 05(17.2%) strongly disagreed with the fact that variable cost-volume profits are kept below 30% of the incomes. This kind of response seems to have resulted from respondents' failure to distinguish fixed cost-volume profits from variable cost-volume profits especially the support staff. It is also true

that the cost-volume profits are mostly constituted by fixed cost-volume profits and the variable cost-volume profits according to management are immaterial.

1.3.8 Findings on the extent to which the respondents agreed with the giving of allowances to staff.

Table 1.3.8: Showing the responses on the giving of allowances to staff.

Extent of agreement	SA	A	N/S	D	S D	Total
Frequency	10	12	05	02	-	29
Percentage (%)	34.5%	41.4%	17.2%	6.9%	-	100%

Source: Primary data survey question 14

Table 1.3.8 above shows that 10(34.5%) respondents strongly agreed with the statement, 12(41.4%) agreed, 05(17.2%) were not sure, 02 (6.9%) disagreed and no one strongly disagreed with the statement. This response is ideally based on the fact that only the teaching staff and management are entitled to such allowances and therefore the support staff was reluctant to consent hence uncertainty.

1.4 Findings on profitability

The following information presents, interprets and discusses the findings on profitability levels of the school.

1.4.1 Findings on the extent to which the respondents agreed or disagreed with the use of sales maximization approach to profits.

Table 1.4.1: Showing the response on the use of sales maximization approach to profits.

Extent of agreement	SA	A	N/S	D	SD	Total
Frequency	07	15	01	03	03	29
Percentage (%)	24.1%	51.7%	3.5%	10.4%	10.4%	100%

Source: Primary data survey question 15

From the above table, 07(24.1%) respondents strongly agreed with the statement 15(51.7%) agreed, 01(3.5%) were not sure, 03(10.4%) disagreed and 03 (10.4%) strongly disagreed with the statement. This pattern was derived from the fact that is the school’s intent to objectively lower the fees in order to attract a good number of students. According to the support staff the school has done a lot for the financially weaker parents to be able cover up their school dues.

1.4.2 Findings on the extent to which who agreed or disagreed with profit maximization as major objective of the school.

Table 1.4.2: showing the response on profit maximization as a major objective

Extent of agreement	SA	A	N/S	D	SD	Total
Frequency	10	08	02	06	03	29
Percentage (%)	34.5%	27.6%	6.9%	20.7%	10.4%	100%

Source: Primary data survey question 16

Table 1.4.2 above, indicates 10(34.5%) as strongly agree, 08(27.6%) agree, 02(6.9%) not sure, 06(20.7%) disagree and 03(10.4%) as strongly disagree with the statement. This is because profit maximization is ideally the opposite of sales maximization which the school decided to embark on and therefore one expected such results if there was some objectivity.

1.4.3 Findings on the extent to which the respondents agreed or disagreed with the inconsistency in the profits over the years.

Table 1.4.3: Showing the response on the inconsistency in the profits over the years.

Extent of agreement	SA	A	N/S	D	SD	Total
Frequency	16	09	03	01	-	29
Percentage (%)	55.2%	31%	10.4%	3.5%	-	100%

Source: Primary data survey question 17

The findings are evidenced from the table 1.4.3, 16(55.2%) strongly agreed, 09(31%) agreed, 03(10.4%) were not sure, 01(3.5%) disagreed and none of the respondents strongly disagreed with the statement. The implication is that due to changing economic climate such as inflation rates, students joining the school, cost-volume profits have been changing leading to inconsistency profits.

1.4.4 Findings on the extent to which respondents agreed or disagreed with the 25% target profit on revenue.

Table 1.4.4: Shows the response on 25% target profit on revenue.

Extent of agreement	SA	A	N/S	D	SD	Total
Frequency	02	05	20	02	-	29
Percentage (%)	6.9%	17.2%	69%	6.9%	-	100%

Source: Primary data survey question 18

As the table above exhibits 02(6.9%) strongly agreed, 05(17.6%) agreed, 20(69%) not sure, 02(6.9%) disagreed and none strongly disagreed implies that very few members of the school holding different positions are aware of the rate at which target profit is kept of the total revenue.

1.4.5 Findings on the extent to which the respondents agreed or disagreed with the steady growth of profits over the years.

Table 1.4.5: Showing the response on steady growth of profits over the years.

Extent of agreement	SA	A	N/S	D	SD	Total
Frequency	03	05	07	08	06	29
Percentage (%)	10.4%	17.2%	24.1%	20.6%	20.7%	100%

Source: Primary data survey question 19

As observed from table 1.4.5, 03(10.4%) strongly agreed with the statement that the school’s profits grows steadily over the years, 05 (17.2%) agreed, 07(24.1) were not sure, 08(27.6%) disagreed and 06(20.7%) strongly disagreed with the statement. This is based on the school’s past financial experience evidenced from the financial reports. Therefore according to management, profitability of the school has been in very bad position.

1.5. Cost-volume profit management and profitability relationship

The following information presents, interprets, and discusses the findings on cost-volume profit management and profitability of Phoenix Academy Secondary School.

1.5.1 Findings on the extent to which the respondents agreed or disagreed with the carrying out of cost-volume profit-volume profit analysis.

Table 1.5.1: Showing response on the carrying out of cost-volume profit-volume profit analysis

Extent of agreement	SA	A	N/S	D	SD	Total
Frequency	04	05	10	08	02	29
Percentage (%)	13.8%	17.2%	34.5%	27.6%	6.9%	100%

Source: Primary data survey question 20

Table 1.5.1 above shows that 04(13.8%) strongly agreed with the statement that the school carried out cost-volume profit volume profit analysis, 05 (17.2%) agreed, 10(34.5%) were not sure, 08(27.6) disagreed and 02(6.9%) strongly disagreed.

This is because of the nature of the business (Service business) which is not easy for the respondents to know

how to measure volume in such a business. That is why respondents shared a high degree of uncertainty.

1.5.2 Findings on the extent to which the respondents agreed or disagreed with profitability being mainly influenced by cost-volume profit management.

Table 1.5.2: Showing the response

Extent of agreement	SA	A	N/S	D	SD	Total
Frequency	06	12	04	04	03	29
Percentage (%)	20.7%	41.4%	13.8%	13.8%	10.4%	100%

Source: Primary data survey question 21

From the above 06(20.7%) strongly agreed, 12(41.4%) agreed, 04(13.8%) were not sure, 04(13.8%) disagreed and 03(10.4%) strongly disagreed with the statement that profitability is influenced by cost-volume profit management. Therefore in this case cost-volume profit management is the prime and basic platform for profit maximization hence the school should improve on cost-volume profit management for t to be profitable.

1.5.3 Findings on the extent to which respondents agreed or disagreed with minimizing cost-volume profits in order to maximize profits.

Table 1.5.3: Shows the response

Extent of agreement	SA	A	N/S	D	SD	Total
Frequency	07	08	04	06	04	29
Percentage (%)	24.1%	27.6%	13.8%	20.7%	13.8%	100%

Source: Primary data survey question 22.

The table above indicates that 07(24.1%) strongly agreed, 08(27.6%) agreed, 04(13.8%) were not sure, 06(20.7%) disagreed and 04(13.8%) strongly disagreed with the statement that cost-volume profits are minimized in order to maximize profits. This brings out the fact that cost-volume profit management and profitability are inversely proportional and therefore cost-volume profit management should be improved if profits are to be maximized.

1.5.4 Findings on the extent to which the respondents agreed or disagreed with the preparation of annual budgets to streamline profitability.

Table 1.5.4: Shows the respondents.

Extent of agreement	SA	A	N/S	D	SD	Total
Frequency	07	10	06	03	03	29
Percentage (%)	24.1%	34.5%	20.7%	10.4%	10.4%	100%

Source: Primary data survey question 23

As evidenced from table 1.5.4 above, 07(24.1%) strongly agreed with the statement that the school prepares annual budgets, 10(34.5%) agreed, 06(20.7%) were not sure, 03(10.4%) disagreed and 03(10.4%) strongly disagreed with the statement. This response was attained because all sectors of the school know that at every beginning of any academic year meetings are held to communicate such budget to the possible stakeholders.

1.5.5 Findings on the extent to which the respondents agreed or disagreed with profitability being independent of cost-volume profit management.

Table 1.5.5: Showing the respondents

Extent of agreement	SA	A	N/S	D	SD	Total
Frequency	04	04	02	10	09	29
Percentage (%)	13.8%	13.8%	6.9%	34.5%	31%	100%

Source: Primary data survey question 24

From the table above, 04(13.8%) strongly agreed 04(13.8%) agreed, 02(6.9%) were not sure, 10(34.5%) disagreed and 09(31%) strongly disagreed that profits are independent of cost-volume profit management. This is because all respondents are quite sure that a high cost-volume profit implies low profitability.

1.5.6 Findings on the extent to which respondents agreed or disagreed with stability in cost-volume profits causing stability in profits.

Table 1.5.6: Showing the extent of respondents

Extent of agreement	SA	A	N/S	D	SD	Total
Frequency	09	13	03	03	01	29
Percentage (%)	31%	44.8%	10.4%	10.4%	3.5%	100%

Source: Primary data survey question 25

From the table 1.5.6, 09(31%) strongly agreed, 13(44.8%) agreed, 03(10.4%) were not sure, 03(10.4%) disagreed and 01(3.5%) strongly disagreed that stability in cost-volume profits implies stability in profits. A vast majority of the respondents unanimously agreed that stability in cost-volume profit management can cause stability in profits though for Phoenix Academy it is still a nightmare for them to manage and maintain any of the two variables.

II. CONCLUSIONS AND RECOMMENDATIONS

2.1 Conclusions:

The study shows that managing cost-volume profits take into consideration a number of tools ranging from analytical, managerial and administrative, such tools can be

summarized as employing the right number of staff with appropriate experience, outsourcing of some staff, using just in time technique. From the previous Tables indicated that profitability is independent to cost-volume profit management and therefore there should be effective cost-volume profit management controls in order to earn profits.

2.2 Recommendations:

Phoenix academy should improve on its cost-volume profit management practices in order to foster profitability and therefore the following policies should be observed to reduce the above.

- Make profitability the prime cause of the existence of the school.
- Develop other pecuniary motivational technique to motivate staff other than the monetary benefits.
- Reduce as much as possible the allowances given to staff if they cannot scrap them off completely.
- Develop on the academic standard of the school to attract students so as to earn more.
- Carryout a systematic cost-volume profit-volume-profit analysis.
- Have deadlines for school defaulter so as to be able sustain operational cost-volume profits.

REFERENCES

- [1] Alan, P. (1989). Cost-volume profit and Management accounting. (3rd edition) Chapman publishing ltd.
- [2] Doll, J.P, and Orazem, F. (1984). Production economics. Theory and application. New York John Willey and Sons Ltd.
- [3] Drury Collin, (2000). Management and Cost-volume profit accounting (4th edition) London Chapman publishing Ltd.
- [4] Edward, J.Blocher, Kung, H. Chen and Thomas, W. Lin (2002). Cost-volume profit Management. A strategic emphasis. (International edition). London: Mc Graw Hill Irwin.
- [5] Horgren, T. Charles (1991). Cost-volume profit accounting: A managerial emphasis (7th edition) London: Prentice Hall.
- [6] Julius Kakulu (2001). Financial Management Kampala: Makerere University.
- [7] Kamukama Nixon Arinaitwe (2006). Cost-volume profit and Management Accounting (1st edition), Kampala.
- [8] Kamshad K (1996), Keys to profit Maximization.
- [9] Lopezi, Puchet, and Sanchet (2000) corporate profitability and the dynamics of competition in

emerging markets. San Antonio. TX: University of Missouri.

[10] Lucey, T. (1994) Cost-volume profiting 3rd edition: DP publishing.

[11] Pandey, I.M. (1995), Financial Management. PVT Ltd India: Vikas publishing House.